AN INVESTIGATION OF THE INTERACTION OF ROCK AND TYPES OF ROCK BOLTS FOR SELECTED LOADING CONDITIONS

Prepared for

UNITED STATES DEPARTMENT OF THE INTERIOR
BUREAU OF MINES

by

Rock Mechanics and Explosives Research Center
University of Missouri-Rolla

Final Report

on

USBM Contract No. H0122110

May 29, 1978

AN INVESTIGATION OF THE INTERACTION OF ROCK AND TYPES OF ROCK BOLTS FOR SELECTED LOADING CONDITIONS

Prepared for

UNITED STATES DEPARTMENT OF THE INTERIOR
BUREAU OF MINES

by

Rock Mechanics and Explosives Research Center
University of Missouri-Rolla

Final Report

on

USBM Contract No. H0122110

May 29, 1978

DISCLAIMER NOTICE

The views and conclusions contained in this document are those of the authors and should not be interpreted as necessarily representing the official policies or recommendations of the Interior Department's Bureau of Mines or of the U.S. Government.

50272-101

REPORT DOCUMENTATION PAGE	1. REPORT NO.	2.	3. Recipient's Accession No.

4. Title and Subtitle: An Investigation of the Interaction of Rock and Types of Rock Bolts for Selected Loading Conditions	5. Report Date: May 29, 1978 6.
7. Author(s): Charles J. Haas, Robert L. Davis, H. Dean Keith, and Wesley C. Patrick	8. Performing Organization Rept. No.
9. Performing Organization Name and Address: Rock Mechanics and Explosives Research Center, University of Missouri-Rolla, Rolla, Missouri 65401	10. Project/Task/Work Unit No. 11. Contract(C) or Grant(G) No. (C) H0122110 (G)
12. Sponsoring Organization Name and Address: Office of the Assistant Director-Mining, Bureau of Mines, Department of the Interior, Washington, D.C. 20241	13. Type of Report & Period Covered: Final Report 14.

15. Supplementary Notes

16. Abstract (Limit: 200 words) Rock bolts interact w/the surrounding rock to support coal mine roofs. Six aspects of these interactions were investigated. 1) A finite element analysis of the bolted mine roof structures including the effects of bedding planes, inclined fractures, lateral stress, & bolt type (expansion anchored & fully grouted). 2) Theoretical & experimental studies of a split ring forced into an undersized hole (split-set rock bolt) with elastic & plastic solutions. 3) Laboratory shear tests on resin-grouted bolts, expansion anchor bolts, split-set tubes, & fiberglass-resin pumpable bolts w/smooth & rough shear planes in limestone & shale rocks. 4) Laboratory creep tests on resin-grouted bars to determine the initial load bleedoff, creep under constant axial load, pull-out stiffness, & ultimate strength. 5) Field tests w/resin-grouted bolts instrumented w/strain gages & placed in the roofs of 3 coal mines. Roof sag stations were also installed in an attempt to relate bolt loading to vertical strata movements. 6) Critical review of existing design criteria for bolted coal mine roofs w/additional inputs gained from this investigation. The various design criteria have been stated in a step by step manner as used by a design engineer. Example problems are worked.

17. Document Analysis a. Descriptors

Rock bolts, coal mines, roof stability, ground control, rock mechanics

b. Identifiers/Open-Ended Terms

c. COSATI Field/Group

18. Availability Statement	19. Security Class (This Report): Unclassified	21. No. of Pages
	20. Security Class (This Page): Unclassified	22. Price

(See ANSI-Z39.18) See Instructions on Reverse OPTIONAL FORM 272 (4-77) (Formerly NTIS-35) Department of Commerce

FOREWORD

This report was prepared by the Rock Mechanics and Explosives Research Center, University of Missouri-Rolla, Rolla, Missouri, under USBM Contract No. H0122110. The contract was initiated under the Coal Mine Health and Safety Program. It was administered under the technical direction of the Spokane Mining Research Center with Mr. Juel Stears serving as the technical project officer. Ms Gladys Barrera was the contract administrator for the Bureau of Mines.

This final report is a summary of the work completed during the entire contract period from June 28, 1972 through January 27, 1978. This report was submitted by the authors on May 29, 1978.

The body of research presented in Chapters II through VII of this report was primarily performed and written by the following people:

Dr. H. Dean Keith, Co-investigator and Associate Professor of Engineering Mechanics - Chapter II.

Dr. Robert L. Davis, Co-investigator and Professor of Engineering Mechanics - Chapter III.

Dr. Charles J. Haas, Principal Investigator and Professor of Mining Engineering - Chapter IV.

Wesley C. Patrick, Graduate Research Assistant - Chapter V.

Chapter VI and VII were joint efforts of Dr. Haas and Mr. Patrick.

Professors other than the authors of this report who worked on various aspects of the project included:

Dr. George B. Clark who performed a comprehensive literature review on rock bolting theory and practice,

Dr. Ray N. Nitzsche who did some of the finite element work, and

Dr. Ernest M. Spokes who assisted in procuring shale blocks and in the theoretical analysis of bolted shear blocks.

Graduate students who contributed their talents to solving many of the problems encountered on this project and to the analyses of results are:

Janakkumar Dave
Richard L. Hoffmann
Wesley C. Patrick
Jack R. Strosnider

Appreciation is extended to Donald Foster, machinist, and Ed Harris, laboratory mechanic, who performed a large portion of the laboratory and field work on this project.

This report was typed by Melice Thrower and Betty Rotramel, secretaries in the Rock Mechanics and Explosives Research Center, and Vicki Hudgins, secretary in the Engineering Mechanics Department. Much of the drafting work for this report was performed by Makanvand Shahrokh.

The field investigation reported herein would not have been possible without the cooperation of the Hillsboro mine in southern Illinois and the Matthews No. 1 mine and Matthews No. 2 mine in Tennessee, all three mines of Consolidation Coal Company. Appreciation is extended to Emil Teisa, Assistant Mine Superintendent at the Hillsboro mine, and to Paul Miller, Chief Engineer at the Matthews mines.

Two strip coal mines cooperated in providing large blocks of shale for the test program. These were the Empire mine of the Pittsburgh and Midway Coal Company in western Missouri and the Captain mine of the Southwestern Illinois Coal Corporation in southern Illinois.

TABLE OF CONTENTS

LIST OF FIGURES

LIST OF TABLES

Chapter I

INTRODUCTION and SUMMARY

Introduction

Roof bolting as a primary method of roof control in underground coal mines is cost effective because the support components are relatively inexpensive and the operation has been mechanized to the point where the hole can be drilled and the bolt installed and tightened in a short time, like three to five minutes per bolt. The openings so supported are also free from obstructions such as posts so that equipment can be maneuvered.

Failure of the roof support system is an indirect cost of the bolting operation, although it is generally not considered as such. Roof failures lead to increased mining costs due to cleanup of roof falls, loss of production and equipment damage due to roof falls in critical areas. The dollar costs and human suffering due to injuries and deaths arising from roof falls are in themselves sufficient reasons for sound engineering of roof support systems.

This investigation of the interactions between rock bolts and the surrounding rock has been directed at understanding the support mechanisms and characteristics of expansion-anchor and resin-grouted roof bolts as used in coal mines. The investigation has involved laboratory, theoretical, and field work. The ultimate objective is to be able to design rock bolt support systems with some of the same confidence that is enjoyed in other engineering fields. This, of course, is a difficult task because of the generally unknown loads which bear on the mine structure and because of the variable nature of the rock properties and weakness planes in the rock.

Work on this contract has consisted of laboratory shear tests on various types of rock bolts used in coal mines; creep tests on resin-grouted steel bars; finite element analyses of single bolts, the bolted roof structures, and the friction rock stabilizer; and a field program where strain measurements are made at various points along resin-grouted bolts for a period of several months.

The currently accepted roof bolt design criteria which have application in coal mining are presented with example problems in Chapter VII. The research results presented herein are brought into the evaluation of these criteria whenever possible. Criteria for bolt type, length and spacing are needed by each mine engineer when he develops the roof control plan for his mine and also by MESA personnel when they evaluate the plan for approval or disapproval. Some of these decisions have become more difficult recently as additional bolting alternatives such as the resin-grouted bolts have been introduced into coal mine applications. The concept of distributed anchorage for fully grouted bolts and splitset tubes is a significant departure from the point anchorage of conventional expansion-anchor bolts. Much of the work reported herein is an attempt to explain and quantitatively evaluate

the capability of these various bolting systems to resist shear- and separation-type movements as occur in the roof structure.

This Final Report on U.S. Bureau of Mines Contract No. H0122110, An Investigation of the Interaction of Rock and Types of Rock Bolts for Selected Loading Conditions, summarizes the work reported in three Annual Reports on this contract (Refs. 1, 2, and 3), the work contained in a Ph.D. dissertation by Janak Dave (Ref. 4), and the work performed during the fourth contract year not reported elsewhere.

The following chapters each cover a specific area of investigation. These areas are now outlined and the principal conclusions stated.

Finite Element Analysis of Bolted Mine Roofs

Two dimensional finite element models were used to study two aspects of a bolted roof:

1. Axial symmetric models of the bolt and surrounding rock were used to determine the localized stress state in and around conventional and grouted roof bolts due to loads introduced at installation and bedding plane separation.

2. Plane strain models of a typical opening were used to determine the effects of bolts on the stability of a layered mine roof when bedding planes and in-situ lateral stresses are present. The stability of the bolted mine roof was assessed in terms of the stress distributions, roof deflections, and areas of tensile stress within the roof.

Roof bolts had no significant effect on stress distribution or roof deflection when the roof was continuous with no bedding planes. Bolts exerted more influence when bedding planes were present in the roof. Expansion-anchor bolts reduced the deflection of the roof with two bedding planes by 8.5 percent compared to the no bolt condition with similar lateral stresses. Bolts reduced, or in some cases closed, the separation between bedding planes. Preloaded anchor bolts reduced the deflection of the no tension rock roof about 12 percent.

Untensioned grouted bolts installed before face advance and initial settlement occurred exhibited compressive bolt loading along much of the bolt lengths when gravitational and overburden loads were applied. Such compressive bolt loading is thought to have an adverse effect on the initial roof stability, although the seriousness of this effect is not known. Compressive bolt loading did not occur when the untensioned grouted bolts were installed after the initial settlement had occurred. Also, favorable tensile bolt loading at a bedding plane occurred in the latter case.

The effect of lateral stresses on the stability of the roof is significant. The deflection of the roof subjected to low lateral stresses was higher than that subjected to high lateral stresses in all cases when horizontal bedding planes were present in the roof.

The volume of rock experiencing tensile stresses was much higher for low lateral stresses than high lateral stresses. However, the maximum octahedral shear stress was about two times higher for high-lateral-stress cases than for low-lateral-stress cases. This indicates that shear failure is more likely at the high lateral stresses.

The deflection of the roof increased as the number of bedding planes increased. The roof deflection for three bedding planes and no tension rock was about three times greater than for no bedding planes and competent rock.

The significance of the beam building effect was analyzed by considering two roof beams bolted together with preloaded anchor bolts. There was no significant amount of beam building, since there was separation between the beams over the center three-fourths of the span. The size of the bolts and preload required to close the separation completely was found to be impractical. The preloaded anchor bolts did, however, significantly increase the stability of the roof over the no bolt condition.

The commonly made assumption that roof beams deflect as though they are rigidly restrained on the ends was found to be invalid, particularly so in coal mine applications where the stiffness (Young's Modulus) of the supporting pillar of coal is much less than that of typical roof rock. As the corner of the pillar deforms downward under the overburden load the neutral axis at the end of the beam rotates through a relatively large angle causing the deflection curves to slope downward at the rib.

Split-Set Rock Bolt Analysis

Friction rock stabilizers (trade name Split-Set) are a new type of bolting mechanism used to stabilize rock structures. The split-set is formed by rolling a section of thin steel plate into a tube with a slit running its entire length. Split-sets may vary in length up to six feet and usually have about an inch and a half diameter, a tenth of an inch wall thickness, and a slit width of half an inch. The Split-Set is forced into a hole having a diameter approximately 1/8 in. less than the outside diameter of the undeformed tube. As a result, a radial pressure distribution is created between the split-set tube and the wall of the drill hole. The radial pressure distribution caused by the forced fit can be related, by the coefficient of friction between the split-set and the wall of the hole, to a force along the length of the tube. This force enables the split-set to support or reinforce the media into which it is driven.

A system of twelve equations has been developed for the elastic-plastic analysis of Split-Set roof bolts and these equations have been programmed for solution on the IBM 370/168 computer. Typical solutions have been presented in graphical form for comparison with experimental data. The results compare favorably for most of the Split-Sets tested provided the system parameters are properly specified. It appears that this analytical solution will be valuable to mining engineers since the solutions have been put in graphical form. Plots of the effects of the

various parameters (material strength, material strain-hardening, friction, thickness, radius, angle of contact) on the holding capacity of split-sets have been constructed and are presented in this report.

Shear Tests and Analysis

Shear displacements between roof layers and along fracture surfaces or other discontinuities are resisted by rock bolts which intersect such surfaces. That such displacements do occur is a fact fairly well known. Inspection of drill holes that have been in the roof for some time often reveals that the hole has been offset at one or more points some time after drilling.

The effectiveness of rock bolts in resisting this sort of movement has been determined with laboratory shear tests on full-scale rock bolts installed in blocks of rock.

The following parameters have been investigated in this program:

1. Bolt type

   a) conventional expansion-anchor type
   b) full column resin-grouted steel bars
   c) friction rock stabilizer
   d) fiberglass-resin (pumpable bolt)

2. Orientation of bolt relative to shear plane

   a) 0 degrees (normal)
   b) +45 degrees
   c) -45 degrees

3. Rock type

   a) limestone
   b) shale

4. Roughness of shear surface

   a) machine smooth
   b) rough fracture

5. Drill hole diameter

   a) 1 inch
   b) 1-3/8 inch

6. Normal pressure on shear surface

   a) σ_n = 25 psi

   b) σ_n = 250 psi

The orientation of the bolt relative to the shear plane had a pronounced effect on the shear resistance offered by the bolt. The bolt is most effective when it is inclined to the shear surface so that it tends to elongate as shear progresses. The bolt is quite ineffective when it is inclined the other way so as to experience axial compressive loading.

The shear strength of a bolted joint is the sum of that due to the bolt and that due to friction resulting from the in-situ normal stress on the shear plane. If this normal stress is high, say 250 psi or higher, the contribution of the bolt to the total shear strength is measurable, but not really significant from a practical point of view. If, however, the normal stress is low, say under 25 psi, the contribution of the bolt is quite significant and a designer would want to include the shear resistance of the bolt in his analysis.

Two major differences in shear behavior were observed between smooth and rough shear surfaces:

1) The interlocking of the asperities of the rough shear surface causes a high shear resistance for small shear displacements (less than 0.10 in.) but the coefficient of friction along the shear surface rapidly drops and approaches that for the initially smooth shear surface after approximately 2.5 in. of shear displacement.

2) The irregularities of the rough shear surface cause the shear joint to dilate rapidly as the shear progresses. This causes high tensile loading of a fully grouted bolt in the region near the shear surface. Anchorage failure along the grout annulus which was a problem when smooth drill holes were employed, was eliminated when the drill hole walls were rifled.

As noted above, the shear resistance of the bolted blocks is the sum of that due to the bolt and that due to the frictional strength along the shear surface due to the normal stress. The experimental data was then reduced to give the shear force resistance due to the bolt itself. This resistance is stated in terms of the resistance at small shear displacements (0.1 in.) and the maximum shear resistance, which in many cases is two or three times the resistance at small displacements. These tables of shear force values due to the bolt can then be easily used by the engineer to compare the effectiveness of various bolt types and the effect of bolt orientation relative to the shear surface. Tables are included for both smooth shear surfaces and rough fracture surfaces.

Creep Tests and Analysis

The laboratory creep test program for a full column resin-grouted bar was designed to determine the load distribution along the steel bar and the pull-out of the end of the bar as the bar is loaded for an extended period of time.

Loading is accomplished in three phases:

1. Load bleed-off from an initial load of 8,000 lbs for one month

2. Creep at a constant load of 8,000 lbs for one month

3. Creep at a constant load of 16,000 lbs for one month

The above load levels were used for 3/4 in. and 7/8 in. bars while load levels half as large as these were used on a few tests with 1/2 in. bars.

The load bleed-off phase simulates the load decrease with time which would occur underground if the grouted bolt is tensioned immediately after installation. Such tensioning occurs to some extent in the normal resin bolting operation in coal mines when the thrust of the bolting machine is applied to the bolt head to compress the roof strata while the resin hardens. When the thrust is removed there often remains a load of the order of 2,000 lbs on the bolt head. This load may be subject to bleed-off similar to that observed in the laboratory tests.

The creep loading at the two constant load levels simulates the long term time-dependent deformation and pull-out of the grouted bar caused by sustained loading in the roof.

Results indicate that: (1) a large percentage of an applied load bleeds off during the first 100 hours subsequent to bolt installation; (2) the amount of load bleed-off is a function of the grout annulus size and the bolt surface roughness; (3) retightening of grouted rock bolts reduces the magnitude and rate of the load bleed-off phenomenon; and (4) resin-grouted roof bolts provide a stiffer roof support system in that bolt elongation resulting from a given load, e.g., geologic post-tensioning due to strata movements, is much less for the resin-grouted bolts than for mechanically anchored systems.

Field Tests and Analysis

Instrumented roof bolts were installed in three coal mines, one in Illinois and two in Tennessee, to examine the reaction of resin-grouted bolts to geologic and mining stresses. Measurements of bolt strain at four locations along the grouted bars and strata displacements were made for three to six months in each mine. Measurements were usually made once a week during the first three months, and every two weeks thereafter. Borescope inspections for fractures in the roof strata were made at the beginning and at the end of the test period in the two mines in Tennessee.

In the Illinois mine the instrumented bolts were installed in the spaces between existing bolts of a normal bolting pattern. In the two mines in Tennessee the instrumented bolts were installed as members of the regular bolting pattern. Each configuration offers certain advantages and disadvantages. The first approach allows research personnel to operate under a protective canopy of other roof bolts. A history of lower apparent loads will be recorded, however, since the primary bolt pattern carries part of the load. The second approach offers the distinct

advantage of providing the exact load history that any bolt in that position would experience. The bolts must be installed more quickly when used in this configuration since support of the roof must be accomplished as soon as possible so normal mining activities may resume.

The principal conclusions about the behavior of full-column resin-grouted bolts under geologic loadings are as follows:

1. The practice of installing instrumented rock bolts and sag stations to evaluate the effectiveness of a bolting pattern provides data useful in selecting adequate roof support measures.

2. Installation of bolts commonly produces an initial tensile bolt load on the order of one ton.

3. The load distribution along a grouted bolt is nonuniform due to the nonuniform nature of loading following installation and the load transfer mechanism present with full-column anchorage.

4. Compressive loads may occur in a bolt given certain strata displacement histories. These loads may tend to weaken the lower roof strata, possibly inducing roof failure.

5. Strains in fully-grouted bolts cannot be directly related to measured vertical strata displacements because of complex strain distributions along the bolts and uncertainty of the location of the points (or zones) of load application to the bolt.

Roof Bolt Design Criteria

The problem facing the mine engineer, and the thrust of Chapter VII is the determination of the most effective roof support system for a given situation. Guidelines are given in Chapter VII to assist the mine engineer in selecting the type, length, orientation, and spacing of roof bolts to provide the safest, most cost-effective primary support system for his mine. This discussion presents a critical assessment of the most definitive, current research in roof support theory and practice related to multiple openings in bedded deposits having horizontal or near-horizontal orientations. Among the sources of information used in this assessment are publications from industrial and governmental sources, field information from mine personnel and the findings of four years of research under the current contract.

The theories which have been reviewed and presented in a step-by-step manner as required by a design user are as follows:

1. Continuous beam theory developed by Dr. Panek which includes the effects of friction between beams, suspension of thin beams by thicker ones, and the combined effects of friction and suspension.

2. Cracked beam theory developed by Dr. Wright which considers the stability of bolted and unbolted bedded roof strata intersection by one or more vertical joints.

3. Suspension of a layer of very weak or highly fractured rock from an overlying competent layer.

4. Keying of blocks of jointed rock to maintain stability by increasing the frictional strength along joint or fracture surfaces.

5. Arch formation and control which depends primarily on the in-situ stress field and the tensile, compressive, and shear failure characteristics of the roof rock.

6. Code of Federal Regulations which set forth in the form of law certain minimum requirements for roof control plans.

Each of the above criteria is applicable to certain situations, depending on the assumptions of the model. The arch concept and the Code of Federal Regulations probably have the greatest potential for application to all mining environments. The former requires finite element modeling and is for that reason probably the most difficult and expensive design tool presented herein.

Example problems are presented at the end of Chapter VII to illustrate the application of the various design criteria to typical geological conditions which exist in coal mine roofs.

Chapter II

FINITE ELEMENT ANALYSIS OF BOLTED MINE ROOFS

Introduction

The finite element method was used to analyze models which represent typical openings with rectangular cross-sections in mines using systematic room and pillar mining techniques. The stress states which occur in a bolted mine roof are always three-dimensional. However, many of the phenomena present can be studied by choosing appropriate two-dimensional models.

Two-dimensional models were used to study two distinctly different aspects of the bolted roof:

1. Axial symmetric models of the bolt and surrounding rock were used to determine the localized stress state in and around conventional and grouted roof bolts due to loads introduced when the bolts are installed and when bedding planes separate.

2. Plane strain models of a typical opening were used to determine the effects of bolts on the stability of a layered mine roof when bedding planes and in-situ lateral stresses are present.

The finite element computer program employed to analyze the models uses a quadrilateral element composed of four constant strain triangular elements to represent the continuum. The joint element developed by Ghaboussi, Wilson, and Isenberg (Ref. 5) was used to represent bedding planes. Point loads or simple truss (one-dimensional) elements were used to represent the bolts except when local stresses in the bolts and immediate surroundings were to be calculated. Then the bolts were modeled as a continuum. The initial stress method was used to include the nonlinear effects of the joints and no-tension rock material.

It must be remembered that the accuracy of any numerical method of stress analysis depends on the accuracy of the material properties input as data. Accurate material properties are very difficult to obtain for rock structures. Many characteristics of the mine environment, such as in-situ stress fields, may vary in different regions of the mine. Laboratory tests to quantitatively evaluate mechanical properties may not reflect the effects of weakness planes such as joints, bedding planes, and fractures induced by the mining activity. Moisture and its migration from the ventilation air into the rock has a strong effect on the elastic moduli and strength of shale, a typical roof rock in coal mines. Property data including the effects of moisture is not readily available. In the models analyzed average properties are used which do not correspond to a particular mine. They do, however, permit us to study the mechanisms by which bolts interact with the surrounding rock to support the mine roof.

The results from the model analyses are presented in tables and in plots of roof deflection and principal stress fields. The principal stress fields were plotted by drawing lines centered within each finite element whose lengths are proportional to the magnitude of the principal

stresses and whose directions coincide with the principal directions. An arrow at the end of the stress line indicates tensile stress. All conclusions were based on a study of these tables and plots.

Localized Stress State in Bolts and Surrounding Rock

The local initial stresses (those produced by installation) in the following types of installation were analyzed for a typical bolting pattern:

1. Fully grouted post-tensioned bolt

2. End grouted post-tensioned bolt

3. Conventional mechanical anchor bolt

4. Fully grouted pretensioned bolt (bearing plate and nut removed)

The axisymmetric models used to determine the local stress-state were selected by considering a typical roof bolt installation pattern as shown in Fig. 2-1a. The pattern is assumed to extend to infinity in all directions. A typical roof bolt is labeled A in Fig. 2-1a. The dashed lines indicate the intersections with the roof of planes of symmetry which pass in the vicinity of A. On each of the symmetry planes, material does not displace perpendicular to the planes. Thus, the rock surrounding bolt A is essentially constrained from radial movement with respect to A over the surface of a cylinder having a radius of one-half of the bolt spacing. The intersection of this cylinder with the plane of the roof is indicated by the circle shown. For points sufficiently far above the ends of the bolts, the loading from the bolts will appear to be uniform. Thus, the displacement of these points will be homogeneous and can be taken to be zero. The model which results from the above discussion is shown in Fig. 2-1b. Stress boundary conditions are added to the model to represent the various types of bolting installations. The steel bar and resin-grout were assumed initially to be in a stress free state as occurs when the grout sets up around an untensioned bar. Loading of the system was accomplished by post-tensioning the bolt with the subsequent application of a bearing plate and a nut. An example cross-section for a complete model is shown in Fig. 2-2. The detailed stress states for the four installations considered are presented in Refs. 1 and 2. In all installations the stresses are highly localized and decay very rapidly with distance into the rock.

This decay is seen in Fig. 2-3 which shows the distribution of load along a fully grouted post-tensioned steel bar. The load becomes negligible at approximately 10 hole diameters above the nut.

Similar reasoning was used to develop axisymmetric models for determining local stresses produced in fully grouted untensioned bolts by bedding plane separation. High stresses are localized in the bolt, grout, and rock just above and just below the separation. The bolt load is highest at the separation and decays with distance from the separation in a manner similar to that shown in Fig. 2-3.

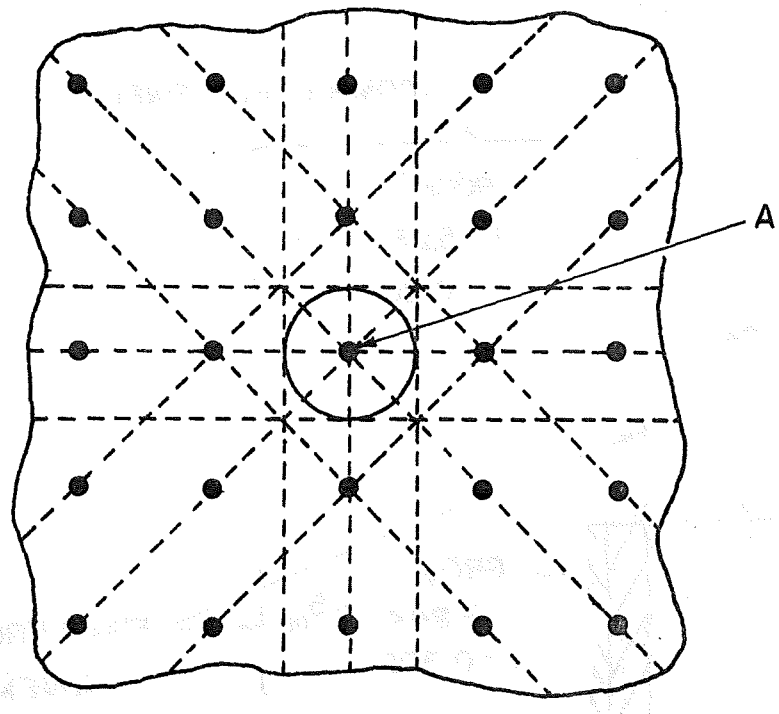

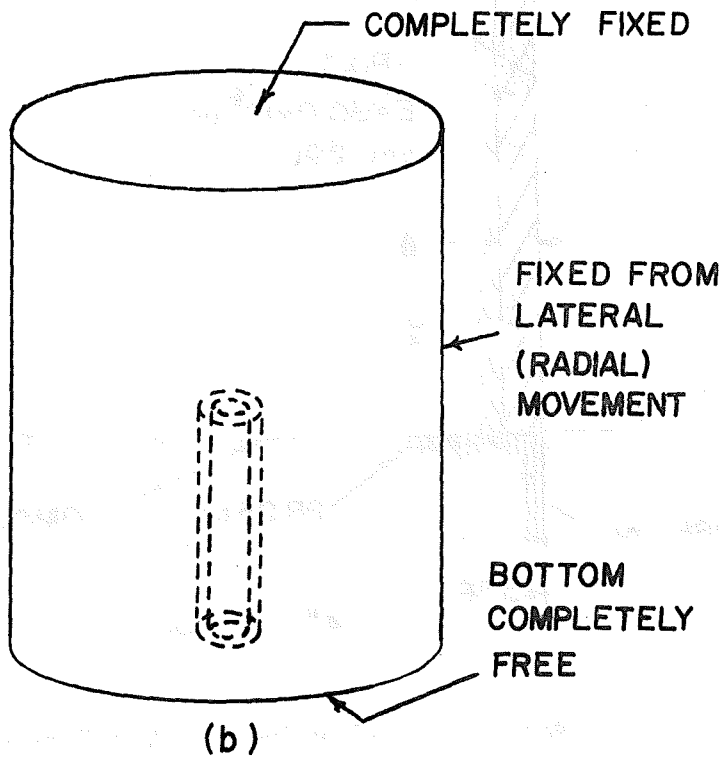

Fig. 2-1 Environment of a Typical Roof Bolt and the Resulting Boundary Conditions

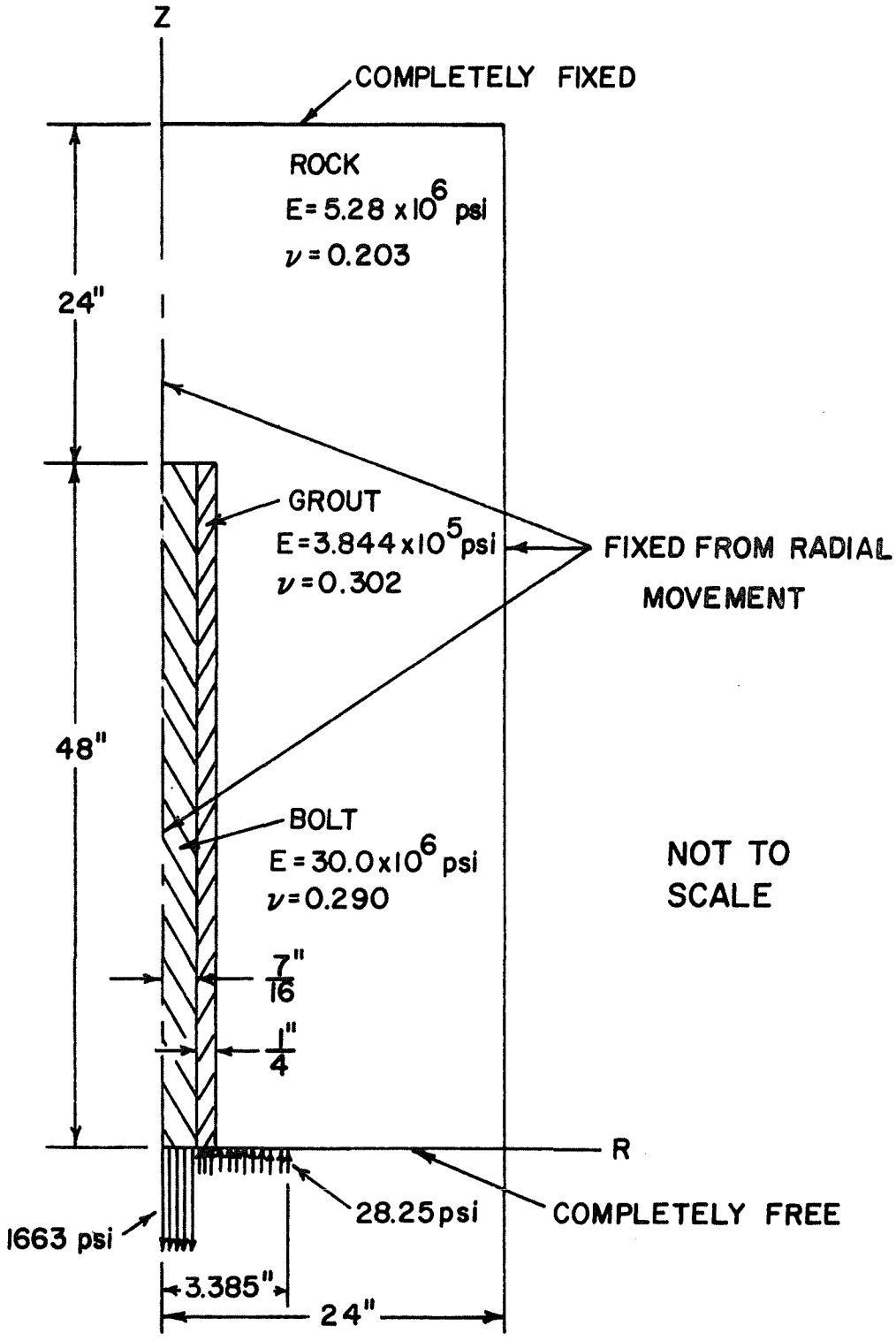

Fig. 2-2 Model of a Fully-Grouted Post-Tensioned Roof Bolt

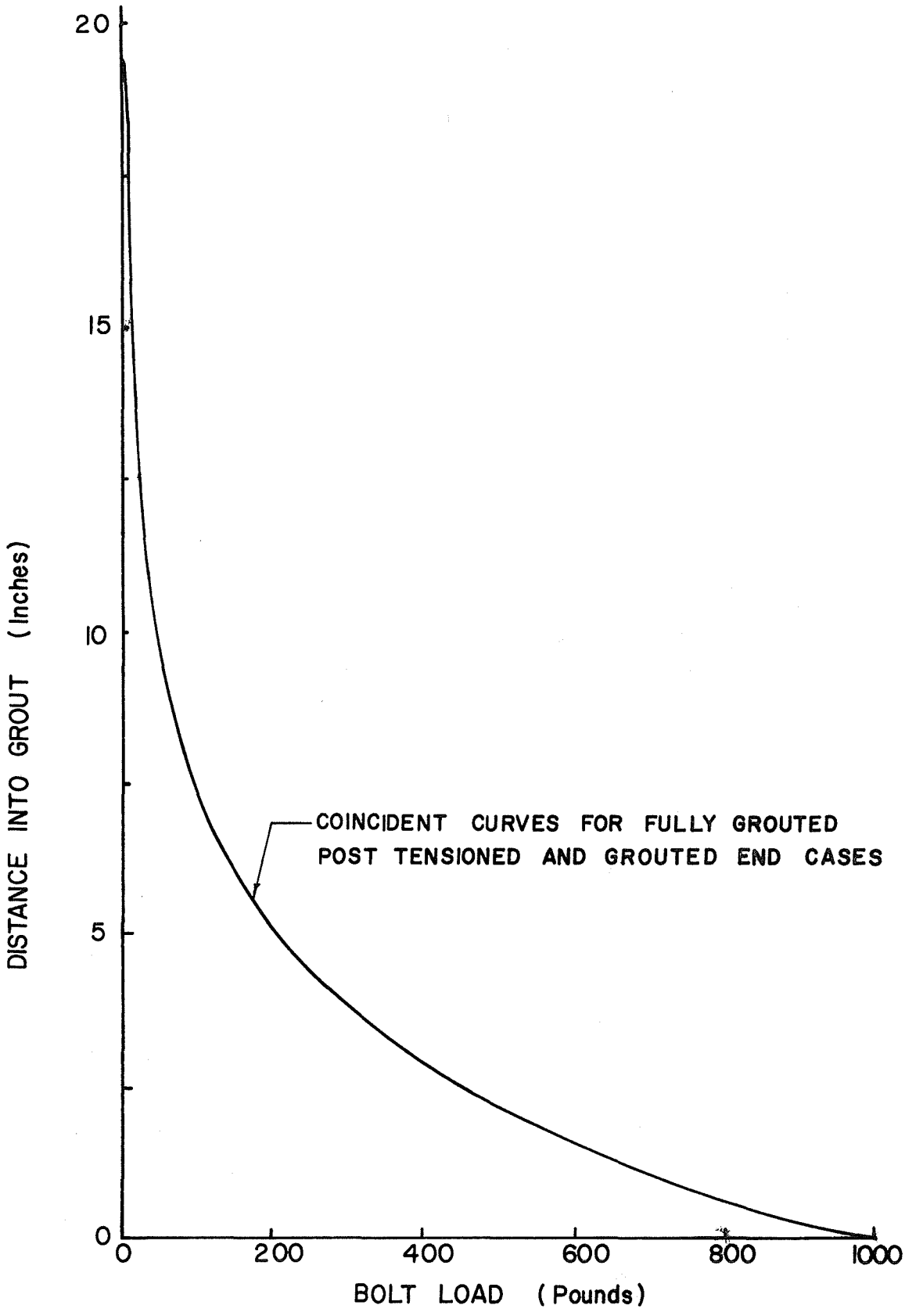

Fig. 2-3 Variation in Bolt Load with Distance into the Grout

The axisymmetric model was also used to study the effect of pretensioning a grouted bolt. In this case, a quick-set grout is used in the top part of the hole while a slow-set grout is used in the bottom portion. The nut is tightened against the bearing plate after the upper part of the grout has hardened, but before the bottom part has set.

The states of stress for the fully grouted pretensioned bolts were determined for the cases of nuts and bearing plates not removed, and the nuts and bearing plates removed. The variations of bolt load along the length of the bolt are also shown for the two cases by curves "a" and "b" in Fig. 2-4. The question naturally arises as to whether it is best to remove the bearing plates and nuts or to allow them to remain in their tightened state.

The relative stress states in the region around the bolt for the two conditions, with and without a bearing plate and nut, can be visualized by comparing curves "a" and "b" in Fig. 2-4. These curves are distributions of tensile bolt load and such tensile loads tend to pull the rock together and compress it. It is seen that removal of the nut and bearing plate reduces the bolt tension to zero or near so in the region near the hole collar. As a result, the vertical compressive stresses in the rock in this region are reduced and failure is more likely to occur.

In summary, this theoretical analysis shows that leaving the tightened nut and bearing plate on a pretensioned fully grouted rock bolt has a beneficial effect in stabilizing the rock near the hole collar, and that removing the nut and plate does not change the stress distribution far away, say, greater than 16 in. from the collar.

Effects of Rock Bolts on the Stability of Layered Mine Roofs

The purpose of this study was to determine the effects of various parameters such as bedding planes and in-situ lateral stress on the stability of a mine roof and how the stability is affected by the addition of rock bolts.

A. Selection of the Models

The models analyzed correspond to a typical mine with rectangular openings and systematic rooms and pillars. Fig. 2-5 shows a vertical cross-section of the general mine geometry and the region analyzed. Fig. 2-6 shows the corresponding plan view. Only half of the opening and pillar are analyzed because of the symmetry. The three different plane strain models analyzed are shown in Fig. 2-7. Each model had a 4 ft floor, 7 ft coal seam and 20 ft roof. Model A has no bedding planes. The different material layers are assumed to bond together. Model B has two bedding planes. Relative motion along the bedding planes is always possible. Model C has three bedding planes which form two slender rock beams between the planes. All bolts used with model C were such that they ended just below the top bedding plane so that no suspension effects from the overlying rock were present.

A uniform downward pressure of 500 psi was applied along the top of the model to simulate the effects of the overburden. Gravity loads were applied in all cases. No horizontal displacements at the midspan

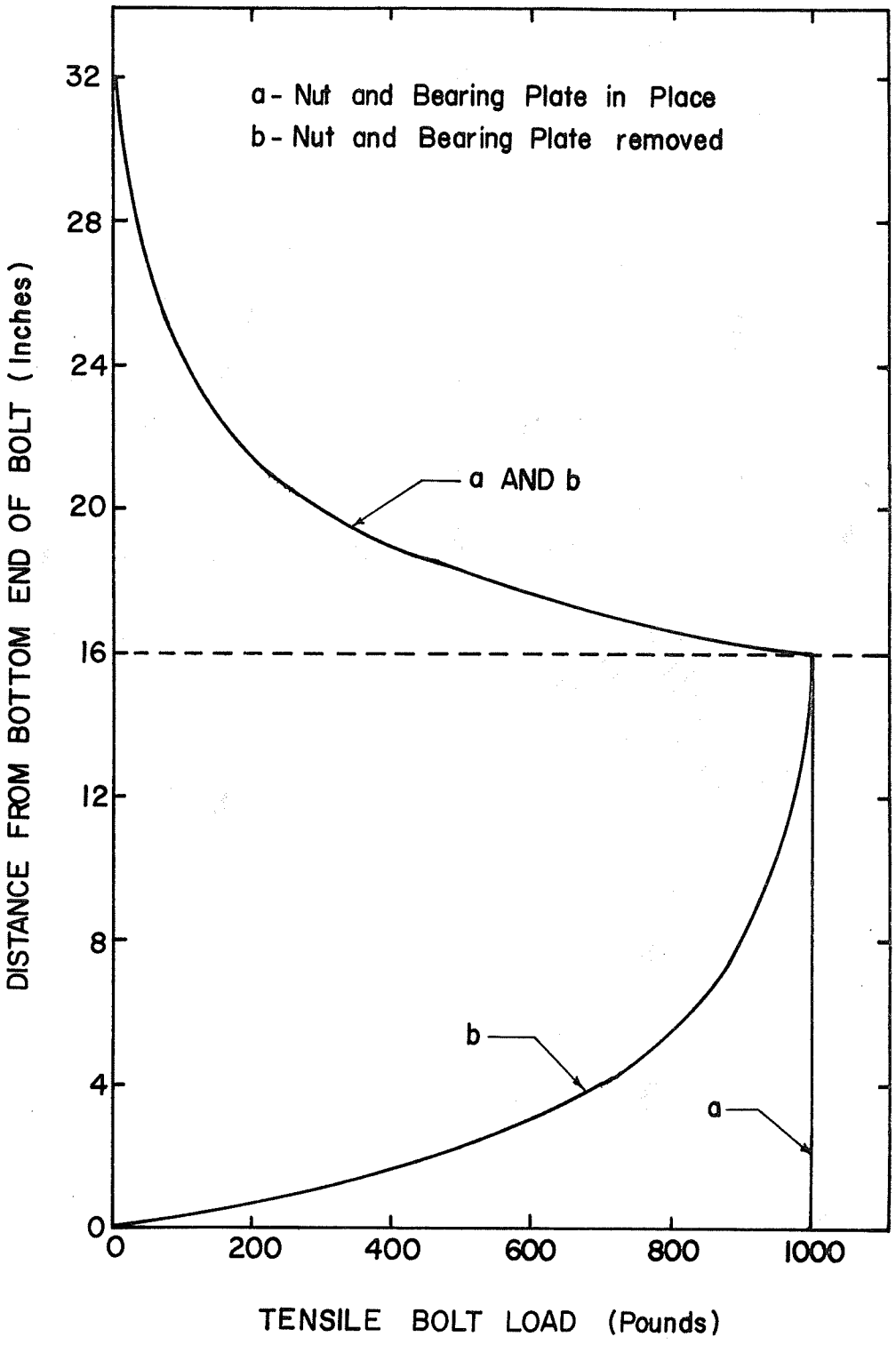

Fig. 2-4 Variation of Bolt Load with Distance from Hole Collar for Fully Grouted Pretensioned Bolts.

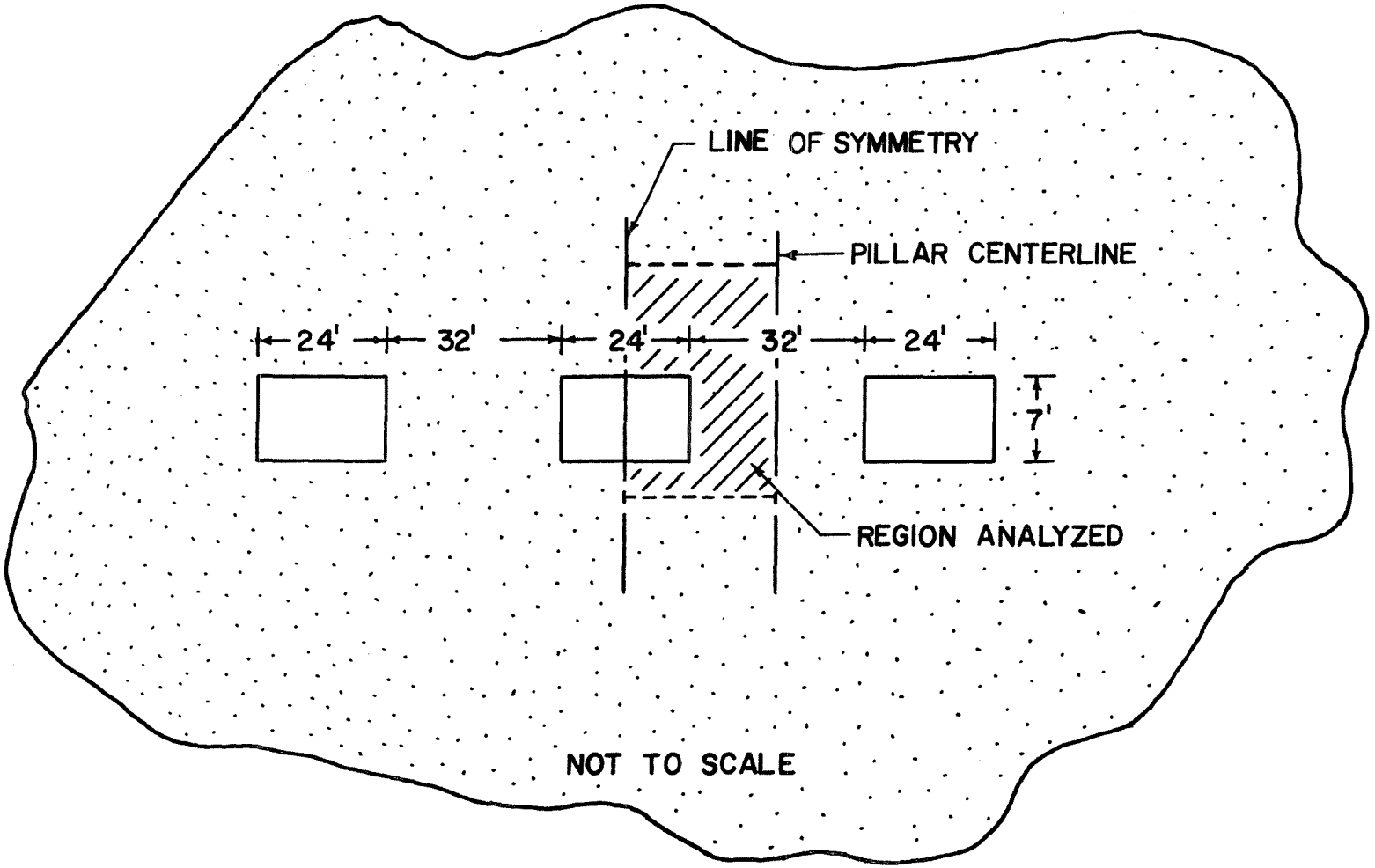

Fig. 2-5 Cross-sectional View Showing Opening and Pillars

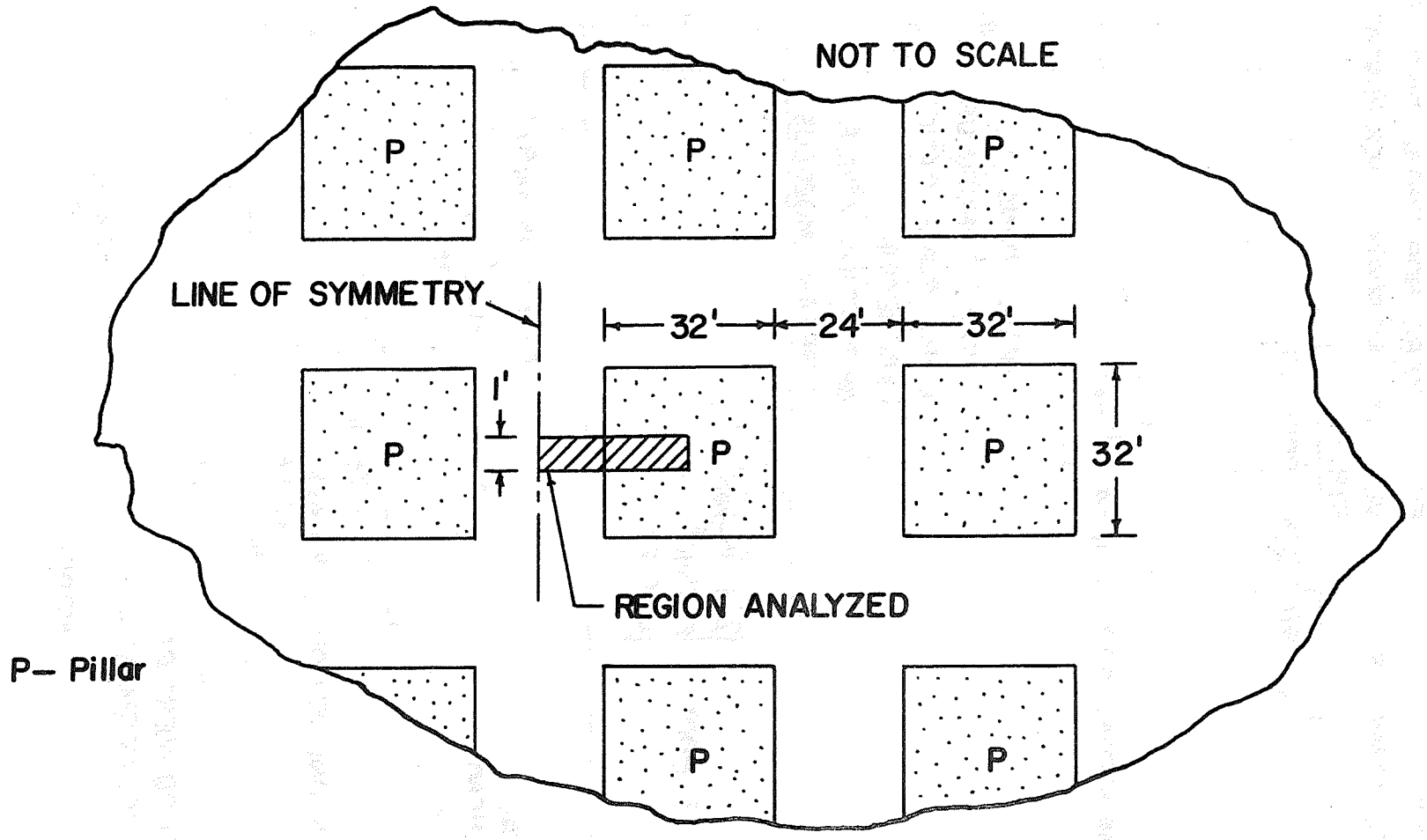

Fig. 2-6 Plan View Showing Rooms, Pillars and Region Analyzed

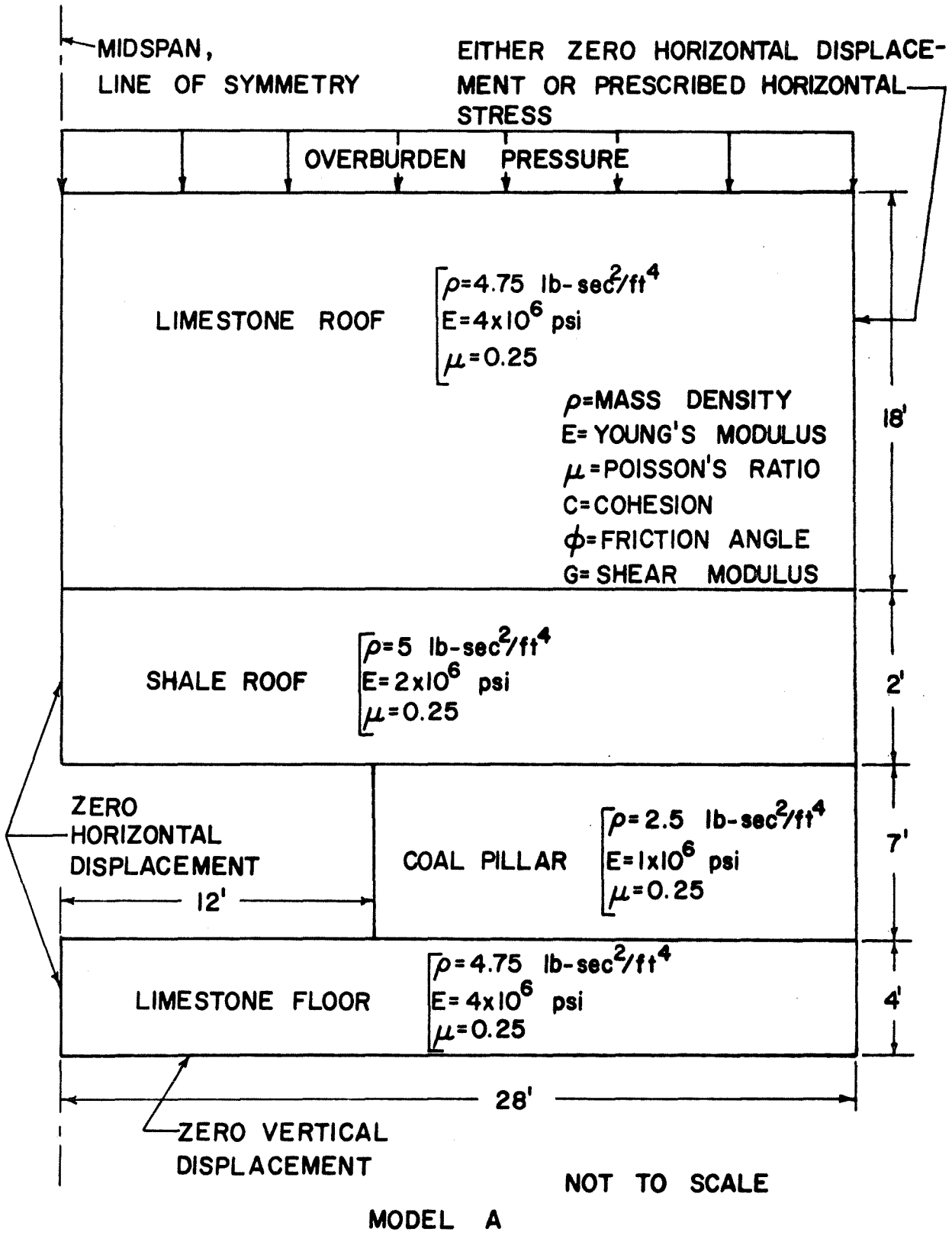

Fig. 2-7a Plane Strain Model of Mine Opening. No Bedding Planes

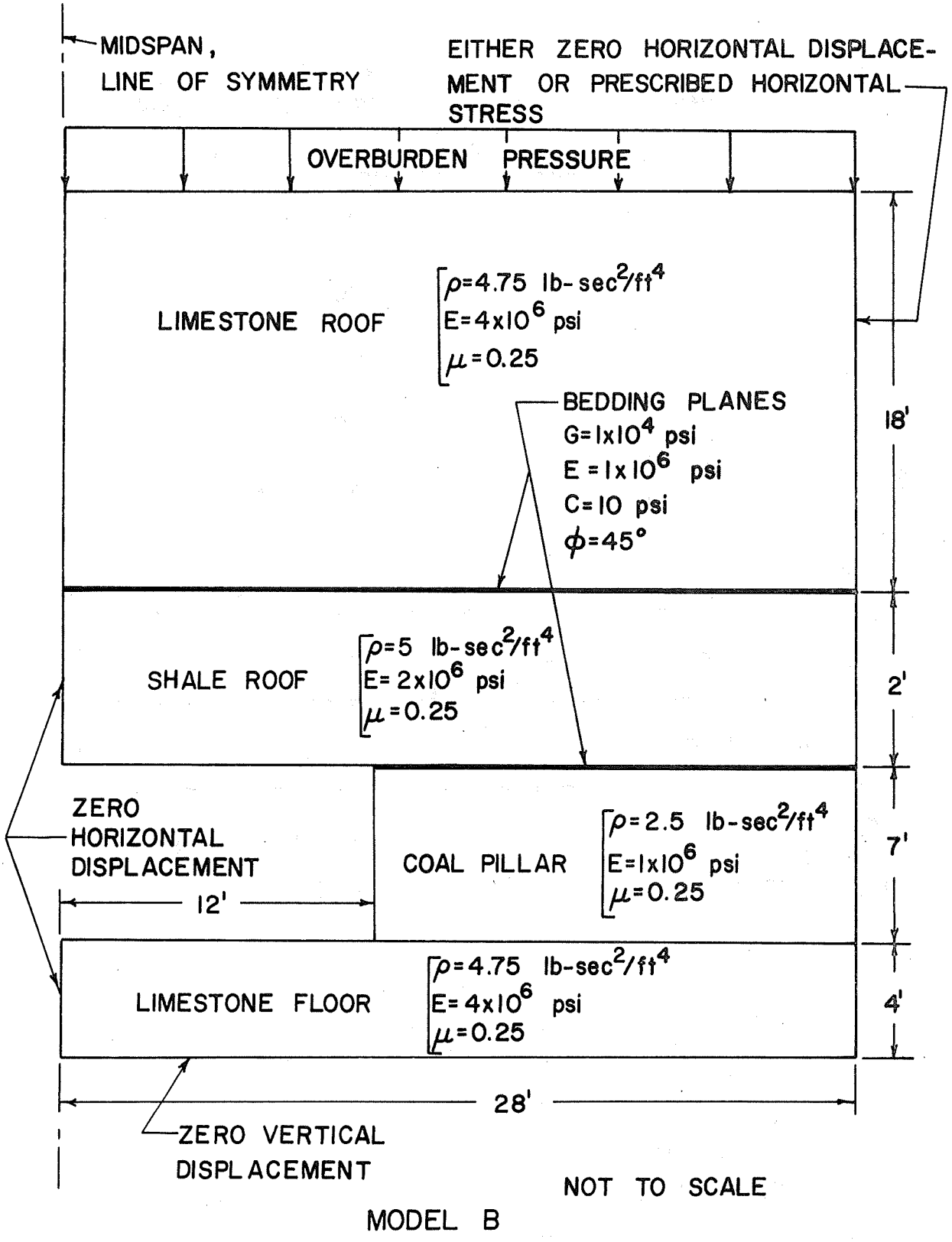

Fig. 2-7b Plane Strain Model of Mine Opening. Two Bedding Planes

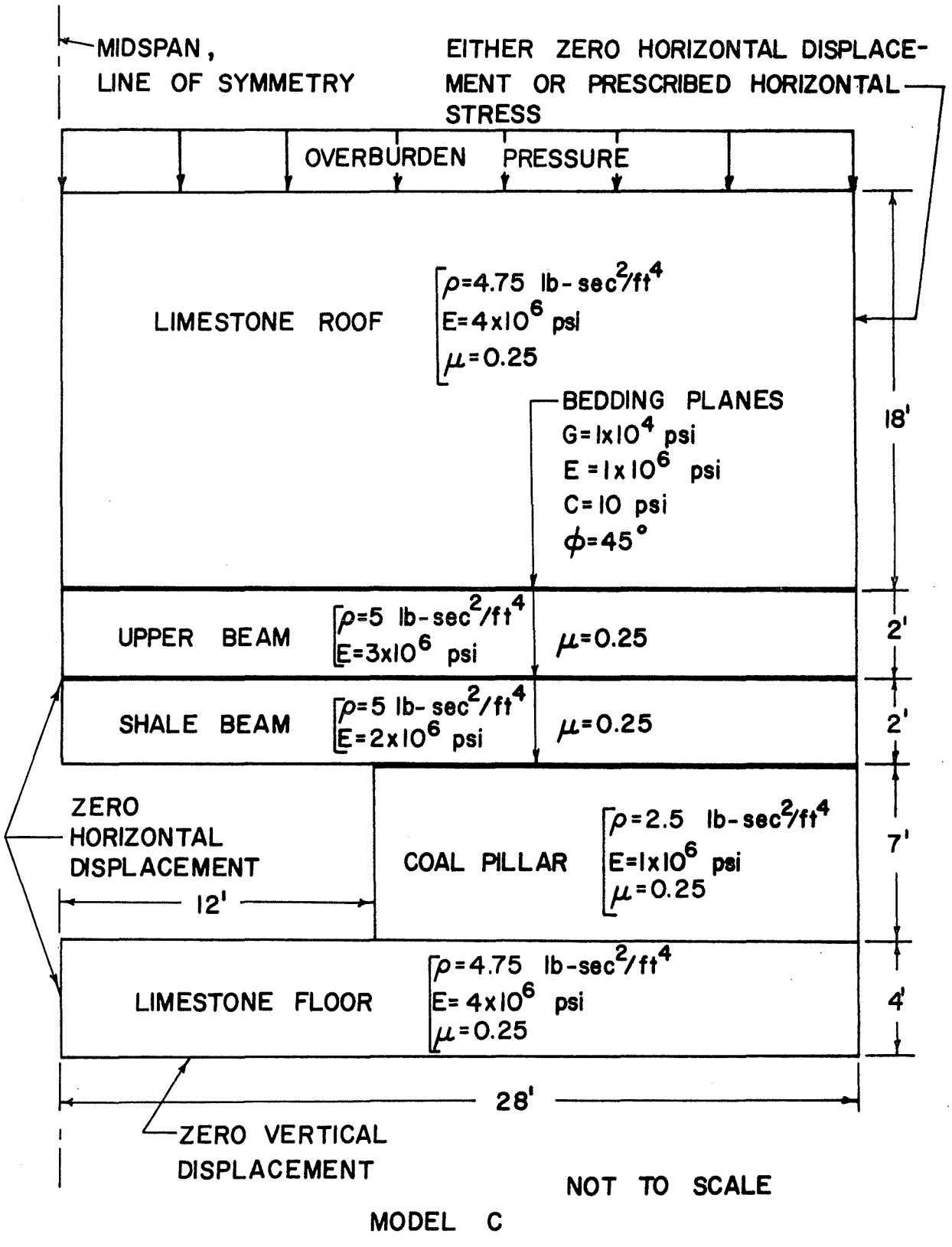

Fig. 2-7c Plane Strain Model of Mine Opening. Three Bedding Planes

were permitted because of the symmetry. All material properties were assumed to be isotropic.

Bolts, not shown in Fig. 2-7, were modeled in three different ways depending on their type and the loading situation. Grouted bolts were always modeled by a series of truss elements connected at all the nodal points along the bolt. This bonds the bolt to the surrounding rock along the entire length of the bolt. Conventional expansion-anchor bolts which load the rock at two points - at the anchor and bearing plate - were modeled as one truss element connecting the nut and anchor if it was necessary to consider the stiffness of the bolt. Otherwise, the preloaded anchor bolt was modeled by applying point loads at the anchor and bearing plate. The anchor bolt was connected to the rock at only two points. It was assumed that bolts were installed in a square pattern as shown in Fig. 2-1. To account for their effect in the 1 ft deep plane strain models shown in Fig. 2-6, the total bolt loads were changed to bolt load per foot of depth. When bolts were modeled by truss elements, their cross-sectional areas were reduced to area per foot of depth. The following bolt properties were used:

Nominal Bolt Diameter 5/8 in.

Young's Modulus 30×10^6 psi

Cross-Sectional Area of Bolt .2453 $in.^2$

Two types of boundary conditions were applied along the right boundary, pillar centerline, of the models. If there are several parallel openings, the right boundary of each model is essentially a plane of symmetry. For this condition the horizontal displacement along the boundary is zero. This boundary condition was used except when the effects of the free field horizontal (lateral) stresses were to be considered. When lateral stresses were included in the analysis, stress boundary conditions were applied along the right boundary. It was assumed that the free field stresses at a distance of two or three times the opening width from the opening are proportional to the vertical stress. Then the lateral stress distribution along the pillar centerline was calculated by analyzing a region which contained four openings. The geometry of the region is shown in Fig. 2-8. One example of the lateral stress distribution at the pillar centerline is shown in Fig. 2-9. Other cases are given in Ref. 4.

In some cases the rock is modeled as a no-tension material. This material is capable of sustaining compressive stresses but unable to support tension stresses. Such a material does not exist, but it is a close approximation to the behavior of randomly jointed rocks and other granular materials. Whenever any principal stress becomes tensile in the no-tension material, the material fails and the load in the direction of the tensile stress is transferred to the surrounding elements. An iterative computational scheme is employed until all tensile stresses have thus been reduced to zero.

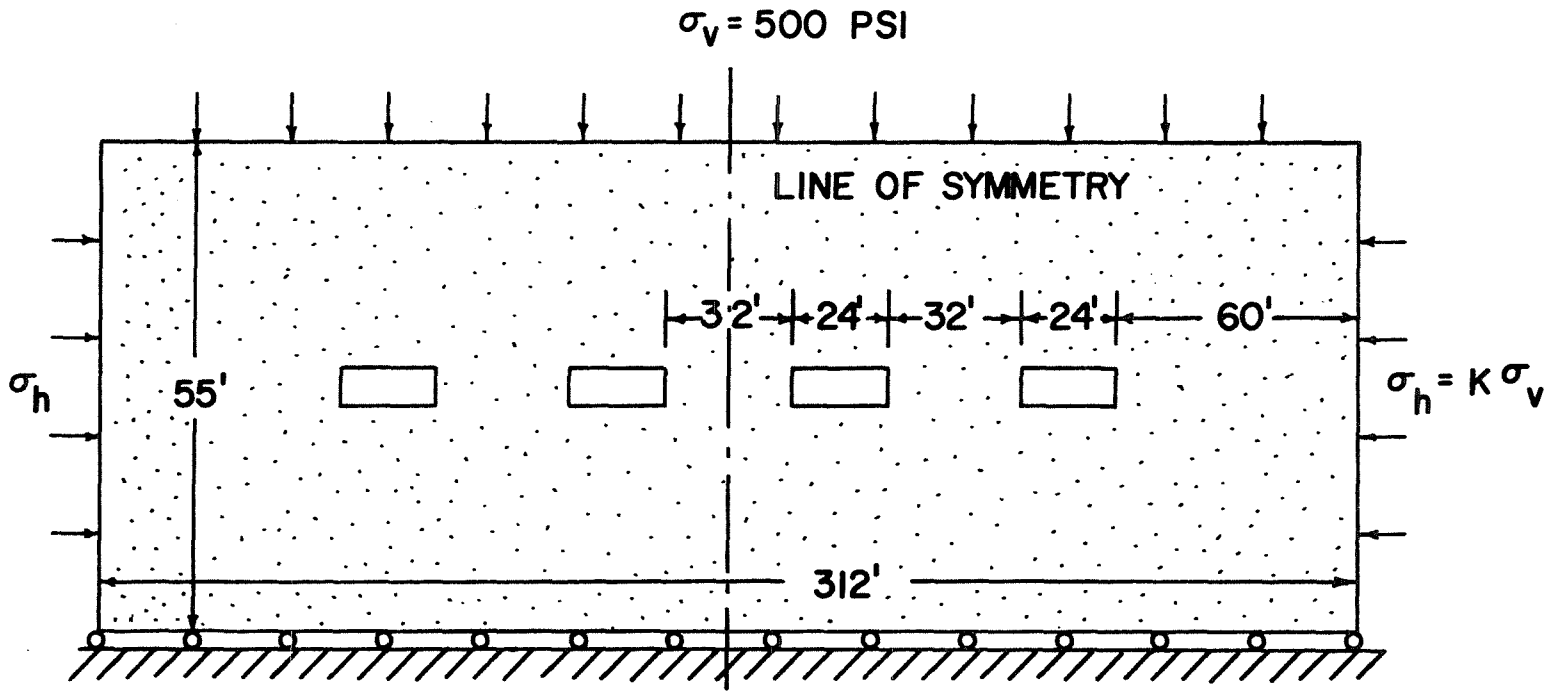

Fig. 2-8 Region Analyzed to Obtain Stress Distribution at Pillar Centerline

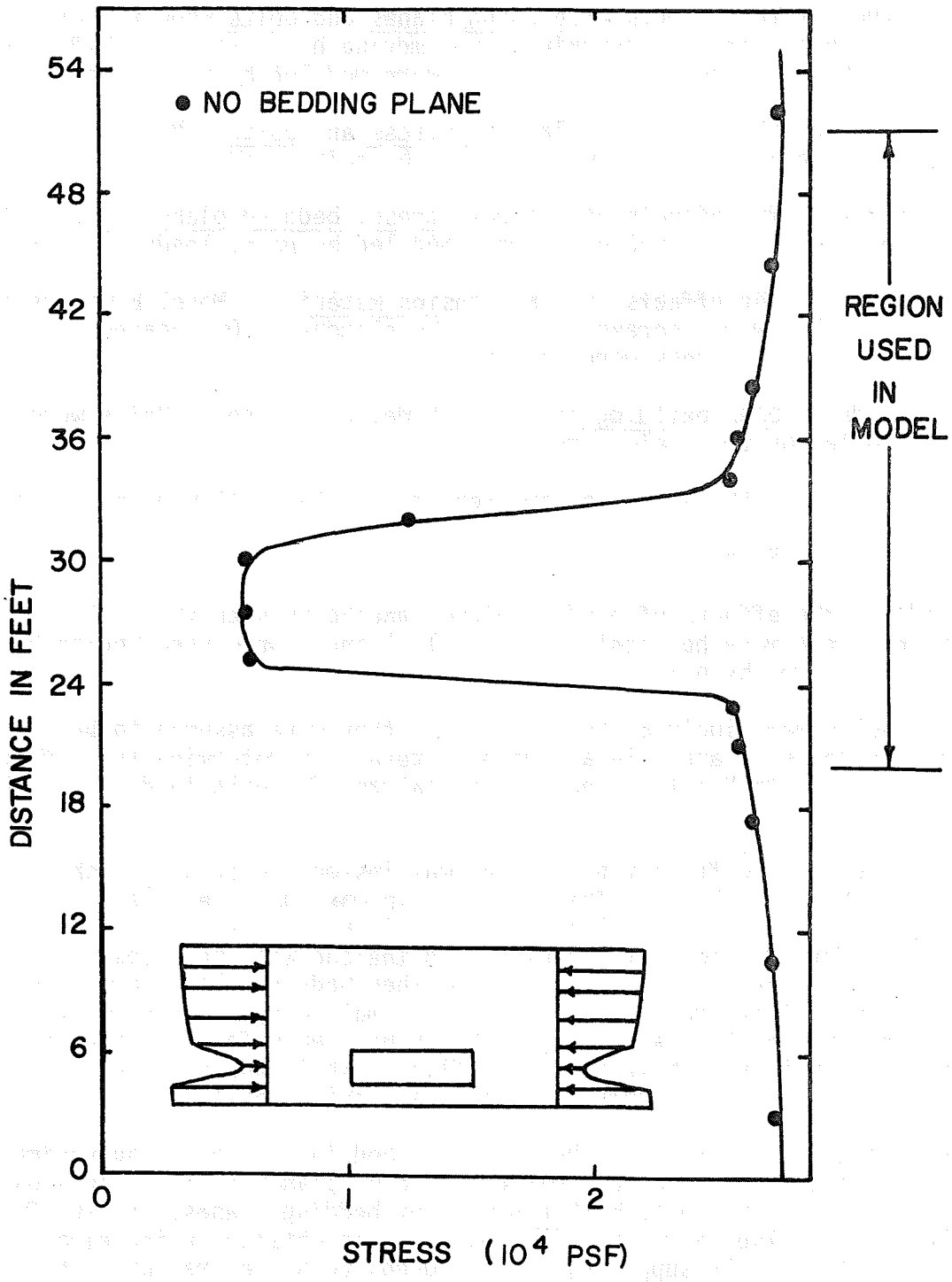

Fig. 2-9 Stress Distribution at Pillar Center Line for Low Lateral Stress without Bedding Planes

B. Results of Case Studies

The following five studies were performed:

1. Study of the effects of bedding planes and bolts when the pillar centerline is restrained from moving horizontally. Models A and B were used and anchor bolts were modeled by point loads.

2. Study of the effects of lateral stress and bolts. Model A was used and anchor bolts were modeled by point loads.

3. Study of the effects of lateral stress, bedding planes, and bolts. Model B was used and bolts were modeled by point loads.

4. Study of the effects of a no-tension material. Model B was used and bolts were represented by truss elements. Only cases with low lateral stress were analyzed.

5. Study of beam building effects. Model C was used. Bolts were modeled by truss elements.

The results of these studies are reported in the following paragraphs.

a. Case 1 - Study

Study of the effects of bedding planes and bolts when the pillar centerline does not move horizontally. Models A and B were used and anchor bolts were modeled by point loads.

When bolts were included in this study, they were assumed to be 4 ft long and spaced 4 ft apart in a square pattern. To determine the effect of bolt loads, both Models A and B were analyzed for bolt loads of 0, 10,000 and 20,000 lb.

The effects of different bolt loads was insignificant both with and without the bedding planes. The variation in maximum stress was less than 1 percent. All stress plots are given in Refs. 2 and 3. The deflection curves for the roof with no bolts and the one with bolt loads of 20,000 lb differ by less than 1.5 percent when bedding planes are present as well as when they are not included. The small effect of the bolts can be explained by the fact that the bolts have an effective load of only about 20 psi over their area of influence while the roof is subjected to a 500 psi overburden pressure and gravitational load.

The average deflection of the roof with bedding planes is approximately 6 percent greater than the roof without bedding planes. Fig. 2-10 shows the deflection of the roof, with and without bedding planes, for 10,000 lb bolt loads. It also shows the deflection curves obtained using elementary beam theory for simply supported and fixed-end (cantilevered at both ends) beams. The maximum deflection for a fixed-end beam is considerably less than the deflection calculated by the finite element analysis of Models A and B. In this case the maximum deflection for a simply supported beam is significantly greater than that calculated by the finite element analysis.

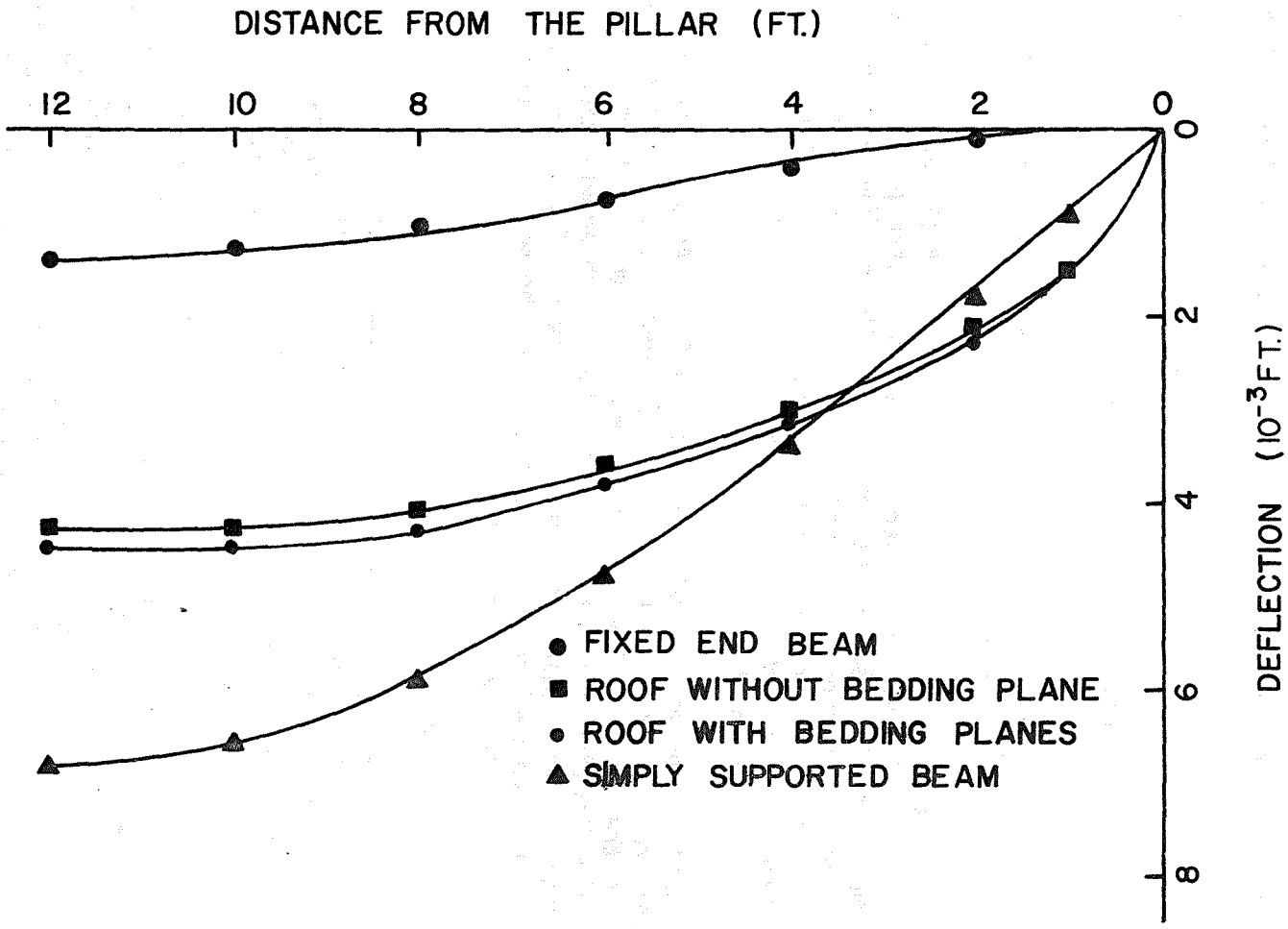

Fig. 2-10 Effect of Bedding Planes on Deflection of Mine Roof

b. Case 2 - Study

Study of the effects of lateral stress and bolts - no bedding planes. Model A was used and 4 ft long bolts were modeled by point loads.

To analyze the effects of lateral stresses, three distinct cases were considered. They were:

(2a) The free field lateral stress was assumed to be nonexistent.

(2b) The free field lateral stress was one-third of the vertical stress.

(2c) The free field lateral stress was three times greater than the vertical stress.

In most practical situations the free field stress falls between cases (2b) and (2c). Bolts were represented by concentrated point loads and were assumed to be in a square pattern. One, three, five and seven bolts across the opening represent spacings of 12 ft, 6 ft, 4 ft and 3 ft, respectively. The stress plots (given in Ref. 3) show that the area of the roof experiencing tensile stresses is much less when the lateral free field stress is high.

Roof deflections are summarized in Table 2-1. As shown in the table, the maximum roof deflection is 1.15 percent less for the high-lateral stress case than for the low-lateral stress case when no bolts are present. The deflection also decreases when bolts are added. However, the reduction is less than 1 percent in all cases. The bolts do not have any significant effect when the layers of the model are perfectly bonded along their contact surfaces.

c. Case 3 - Study

Study of the effects of lateral stress, bedding planes, and bolts. In all cases for this study, Model B which has bedding planes 2 ft above and parallel to the opening and along the roof-pillar interface was used. The 4 ft long bolts were modeled by point loads. Stress plots are given in Ref. 3 and roof deflections are summarized in Table 2-2.

The stress plots again indicate that the region of the roof experiencing tensile stresses is greatly affected by the lateral stresses. The size of the region is minimum for the high lateral stress and maximum for zero lateral stress. The general extent of these regions is illustrated in Fig. 2-11. The volume of rock in tension may be one of the most important factors influencing roof stability, since rock under tension is likely to fail and fall into the opening. To prevent this from happening the bolting system (type of bolt, length, and spacing) should be designed to support the rock in tension. This design could be based on diagrams such as shown in Fig. 2-11.

The weight of material supported would be the weight of rock in tension as determined from measurements of the area in tension as in Fig. 2-11. The proper bolt length would then be one which anchors above the tensile

Table 2-1

Effects of Lateral Stress and Bolts for No Bedding Planes

Lateral Stress	No. of Bolts	Deflection at Center 10^{-3} ft	% Change Due to Lateral Stress	% Change Due to Bolts
Low	None	4.23	--	--
High	None	4.1813	-1.15	--
Zero	None	4.2243	-0.1	--
Low	One	4.1971	--	-0.78
Low	Three	4.197	--	-0.78
Low	Five	4.198	--	-0.76
Low	Seven	4.198	--	-0.76

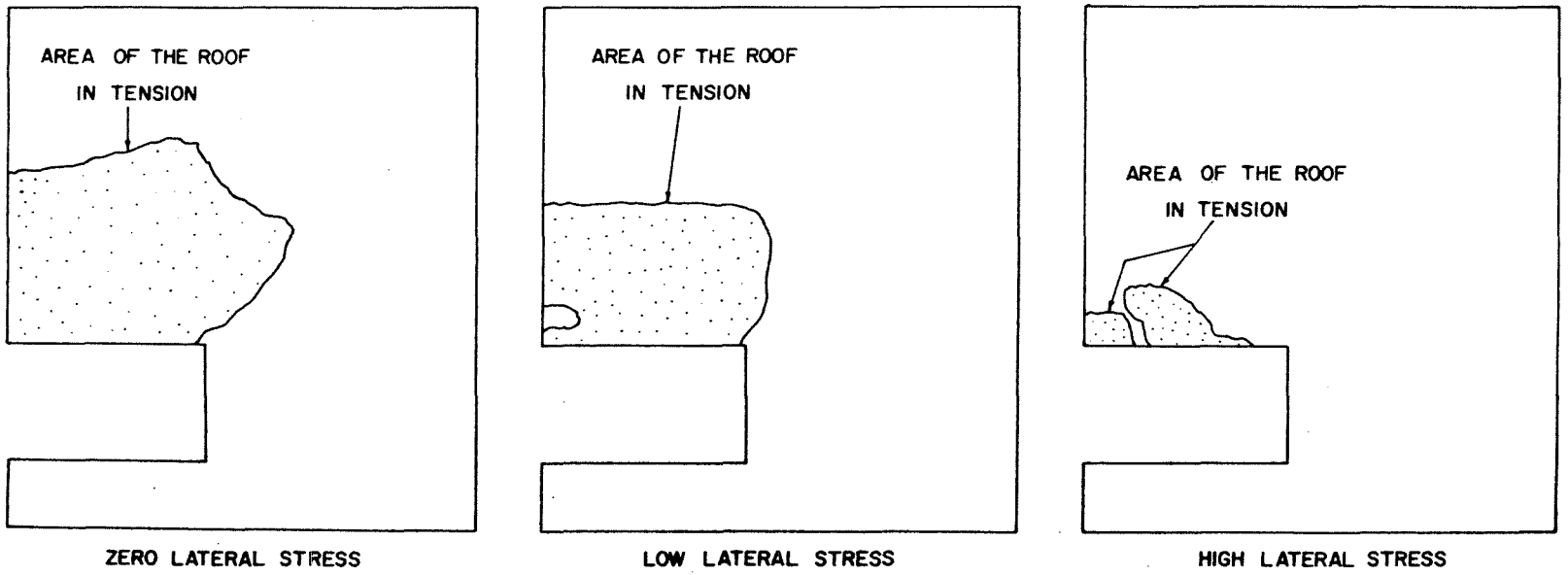

Fig. 2-11 Effect of Lateral Stresses on Area of the Roof in Tension for Two Bedding Planes

region. This would require bolts 10 to 12 ft long for the 24 ft wide openings with zero and low lateral stresses as shown in Fig. 2-11. The most common bolt lengths in practice are 4 and 5 ft. Seven- and nine-ft long bolts are commonly used in areas with exceptionally weak roof, however rarely in current practice are bolts used of sufficient length to reach above the tensile regions indicated for zero and low lateral stresses in Fig. 2-11.

As indicated in Table 2-2, high lateral stresses significantly reduce roof deflection. The maximum roof deflection is 7.16 percent less for the high lateral stress case than for the low lateral stress case. Bolts, preloaded to 15,000 lb, were also effective in reducing the roof deflection. The bolts reduced the maximum deflection of the roof by 8.54 percent for the low-lateral stress case and 4.41 percent for the high lateral stress case as compared with the corresponding no-bolt cases. Even though the bolts do not change the stress state significantly, they do affect the separation of the bedding planes. The bedding plane 2 ft above the opening was separated from the overlying massive rock all the way across the opening for both high and low lateral stresses when no bolts were used. It does not separate for the five and seven bolt cases, but does across a portion of the opening for the one and three bolt cases. Fig. 2-12 shows curves representing bedding plane separation for the various bolt spacings and low-lateral stress cases.

The fact that the pretensioned anchor bolts prevented separation of the immediate roof strata from the overlying massive rock is evidence that the bolts are contributing significantly to the support of the structure. One reason why it is so important to maintain contact between the strata is that the cohesion part of the shear strength between strata is lost when separations occur.

d. Case 4 - Study

Study of the effects of a no-tension material. Model B with two bedding planes was used. Only the low-lateral stress conditions was analyzed, since this approximates a common condition in the field. Bolts were represented by truss elements so that changes in bolt load could occur as the rock failed. The bolts were 11 ft long. Both grouted and anchor bolts were considered. Two bolting installations were modeled. In one the bolts were assumed to be installed close to the mine face so that nearly all roof deflection occurs after the bolts are installed as the face is advanced from the bolts. In the other situation the bolts were assumed to be installed sufficiently far from the face so that the roof deflection due to the overburden, gravity, and bedding planes had occurred before bolt installation. The only additional deflection is caused by the rock failing in tension regions.

Model B was analyzed with no bolts and the region in tension allowed to fail to establish baseline data. The stress distribution for this case is shown in Fig. 2-13.

Table 2-2

Effects of Lateral Stress and Bolts for Two Bedding Planes

Lateral Stress	No. of Bolts	Deflection at Center 10^{-3} ft	% Change Due to Lateral Stress	% Change Due to Bolts
Low	None	4.5885	--	--
High	None	4.26	-7.159	--
Zero	None	4.468	-2.626	--
Low	One	4.2739	--	-6.86
Low	Three	4.2081	--	-8.29
Low	Five	4.2073	--	-8.3
Low	Seven	4.1964	--	-8.54
High	One	4.1011	--	-3.73
High	Three	4.0968	--	-3.87
High	Five	4.101	--	-3.73
High	Seven	4.072	--	-4.41

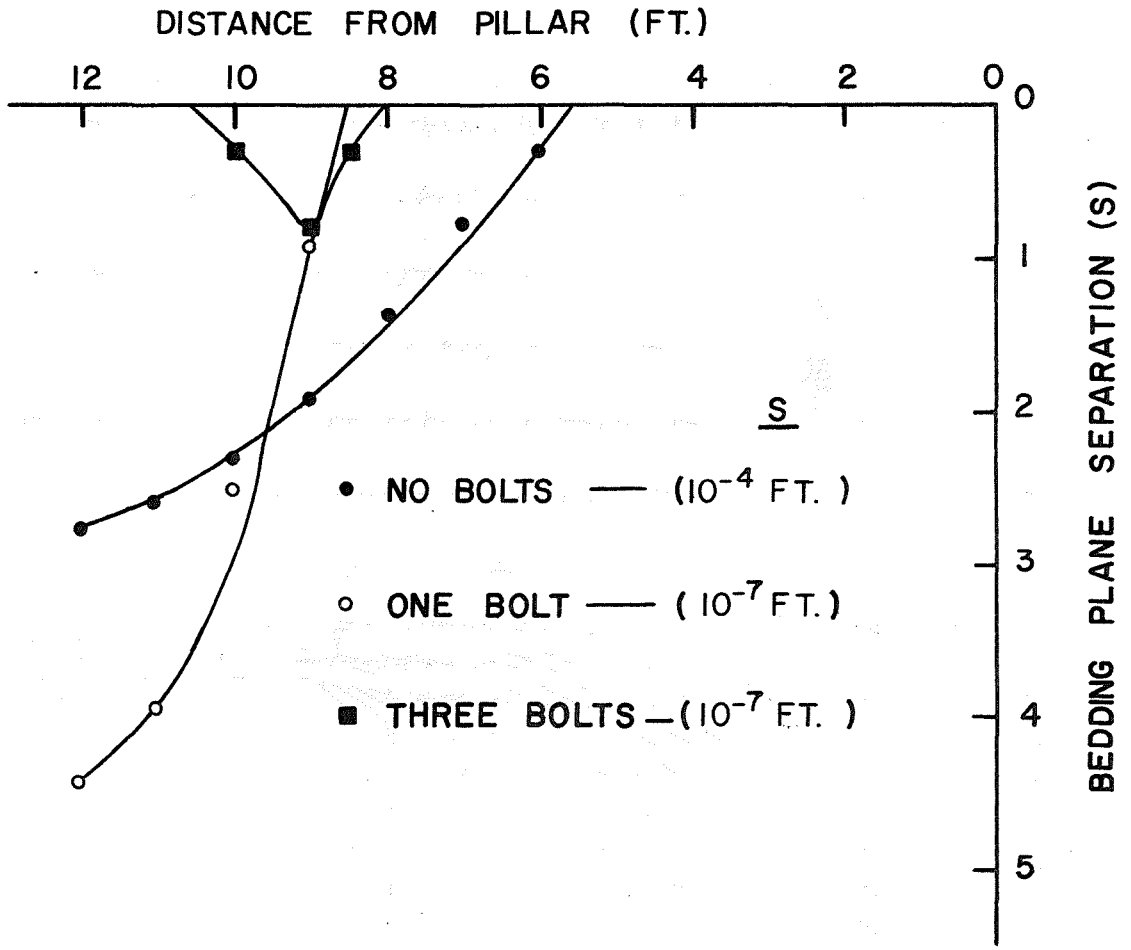

Fig. 2-12 Effect of Bolts (Point Loads) on Separation of Bedding Planes

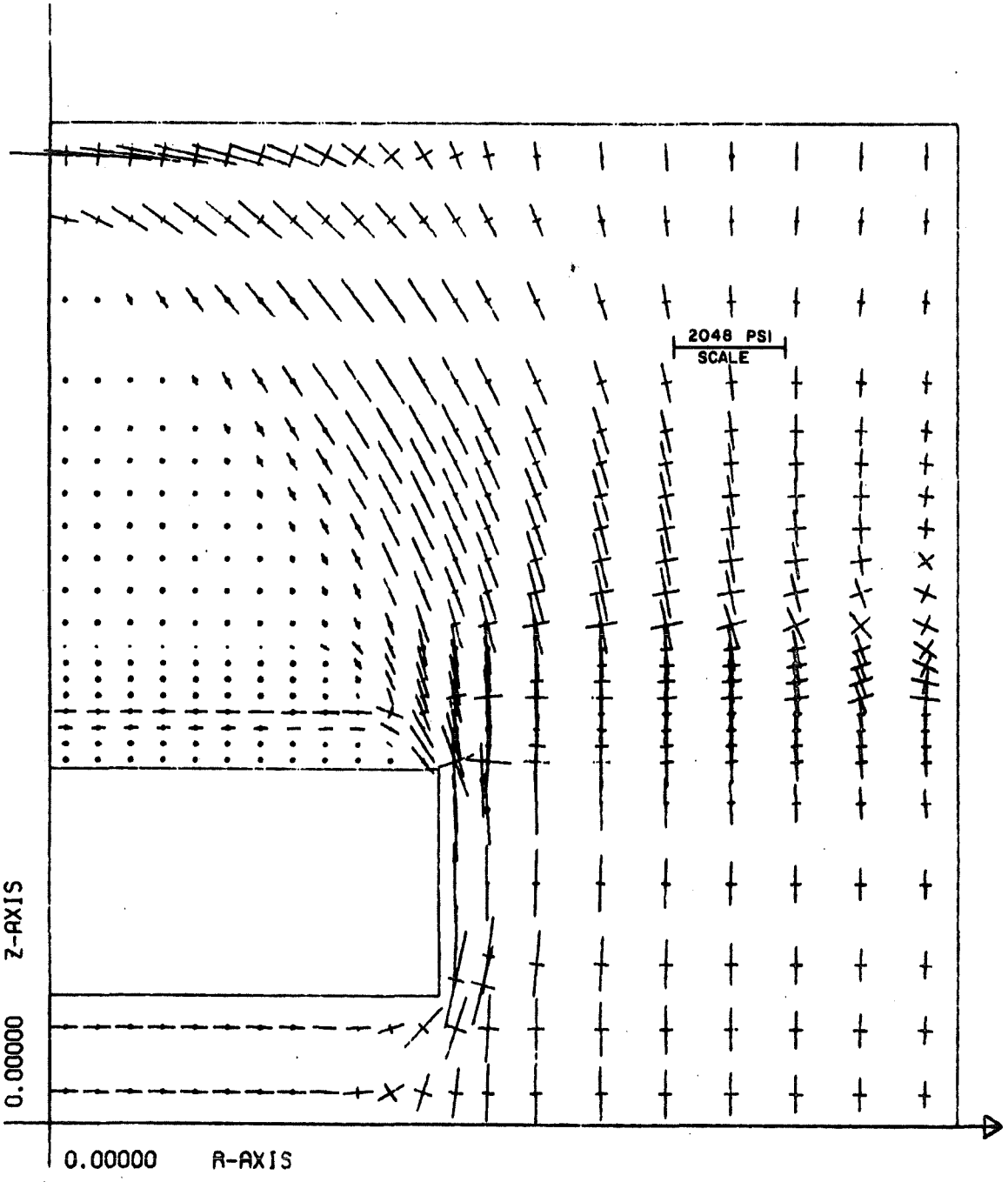

Fig. 2-13 Principal Stress Field for No-Tension Material and No Bolts

Grouted Bolts Installed Close to the Face

Seven grouted bolts were assumed to be installed close to the mine face with no initial tension. Fig. 2-14 shows the stress distribution before the rock in tension was allowed to fail and Fig. 2-15 shows the stresses after rock failure.

Comparison of Figs. 2-14 and 2-15 shows that the final size of the no-tension region when the material is allowed to fail is much greater than the region of initial tensile stress. This situation parallels that observed in the field when a roof fails progressively over a period of time until a stable arch forms.

The compressive stresses below the bedding plane in Fig. 2-13 indicates that favorable horizontal compressive stresses exist a short distance above the roof line even though the rock in tension has been permitted to fail when no bolts are present. However, these compressive stresses are not observed in Fig. 2-15 which shows the stress state for the bolted condition after rock failure. In this situation the bolted roof is apparently not as stable as the unbolted one. This conclusion is also supported by observing the stress distributions in the grouted bolts. Fig. 2-16 shows the stress distribution for a corner bolt (near the pillar) and the center bolt before and after the rock is allowed to fail as a no-tension material.

The case before tensile failure models the situation in which grouted bolts are installed with no initial stress in a completely stress-free roof. Gravity and overburden loads are applied and the roof deforms producing the stress distribution labeled "before no-tension failure" in Fig. 2-16. Before no-tension failure the lower portion of the bolt is in tension and the upper portion (above the bedding plane) is in compression. Since the grout is modeled by a perfect bond between the rock and bolt, the compressive strain in the rock is transferred to the bolt causing compressive stresses in the bolt. This phenomenon does not occur when point-anchor bolts are used.

The "after no-tension rock has failed" case starts with the case just described and allows the rock to fail progressively in tension. The rock can still support compressive and shear stresses. After the rock has failed, the compressive stresses in the center bolt has increased significantly.

Such axial compressive loading of fully grouted bolts is not interpreted as a favorable condition for roof stability. For example, if one passes a horizontal cutting plane through the bolt at some point, the resultant force on the end of the bolt remaining below the cutting plane is compressive, directed downward. Thus, the bolt would be attempting to push the lower part of the roof downward. This condition would not exist if the grouted bolt were sufficiently pretensioned before loading; however, pretensioning of fully grouted bolts is not done in coal mine applications.

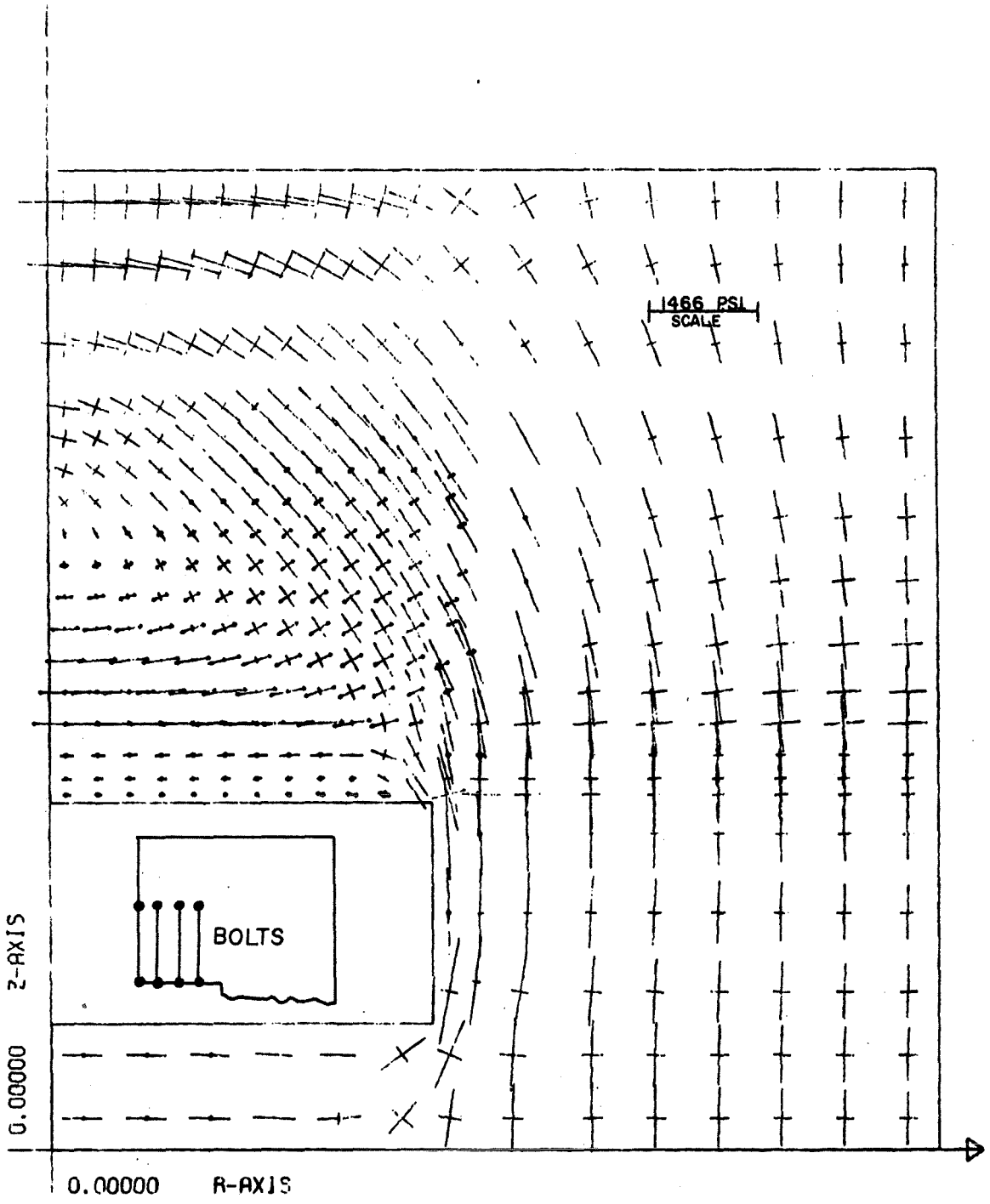

Fig. 2-14 Principal Stress Field for Seven Grouted Bolts

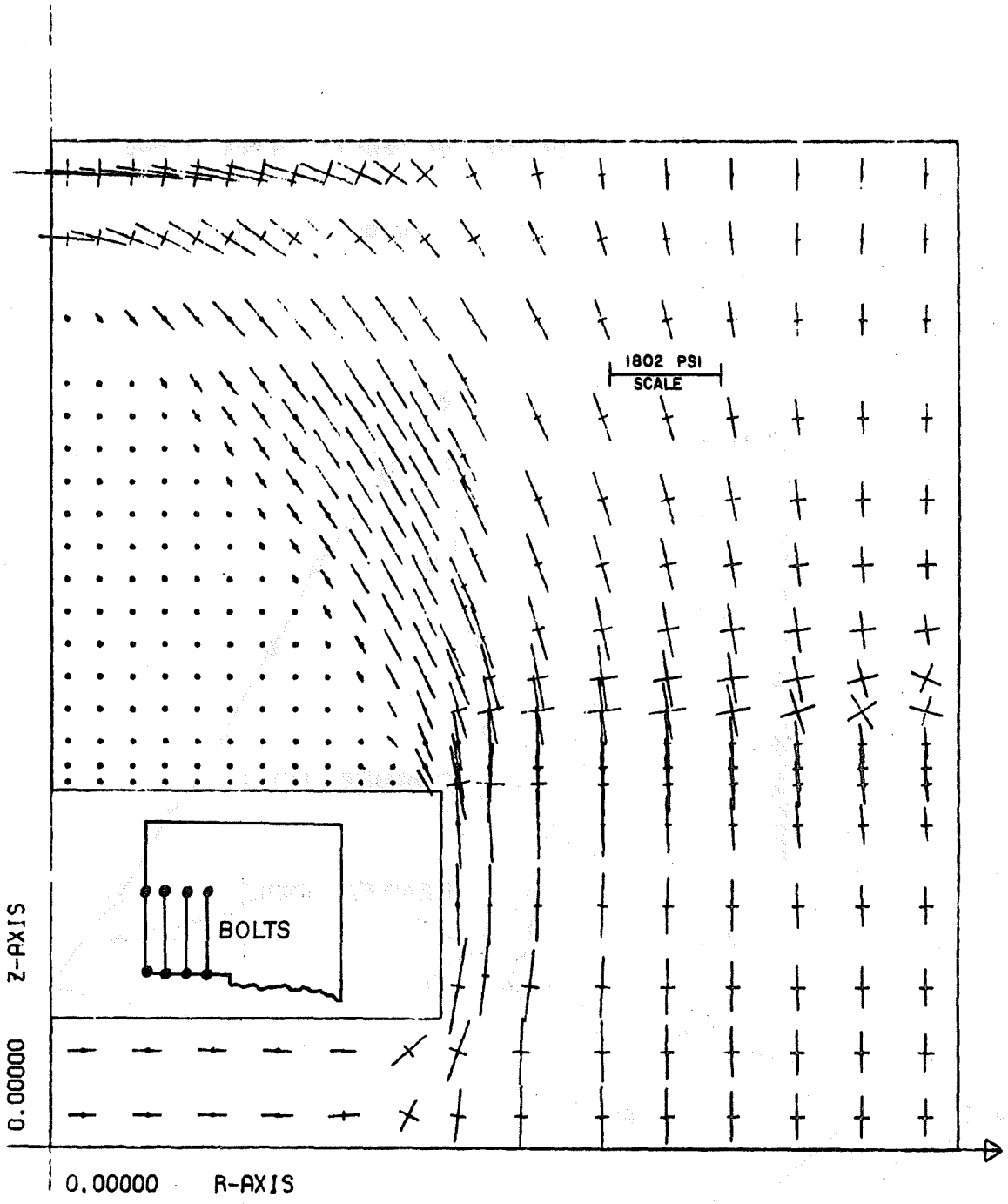

Fig. 2-15 Principal Stress Field for No Tension Material and Seven Grouted Bolts

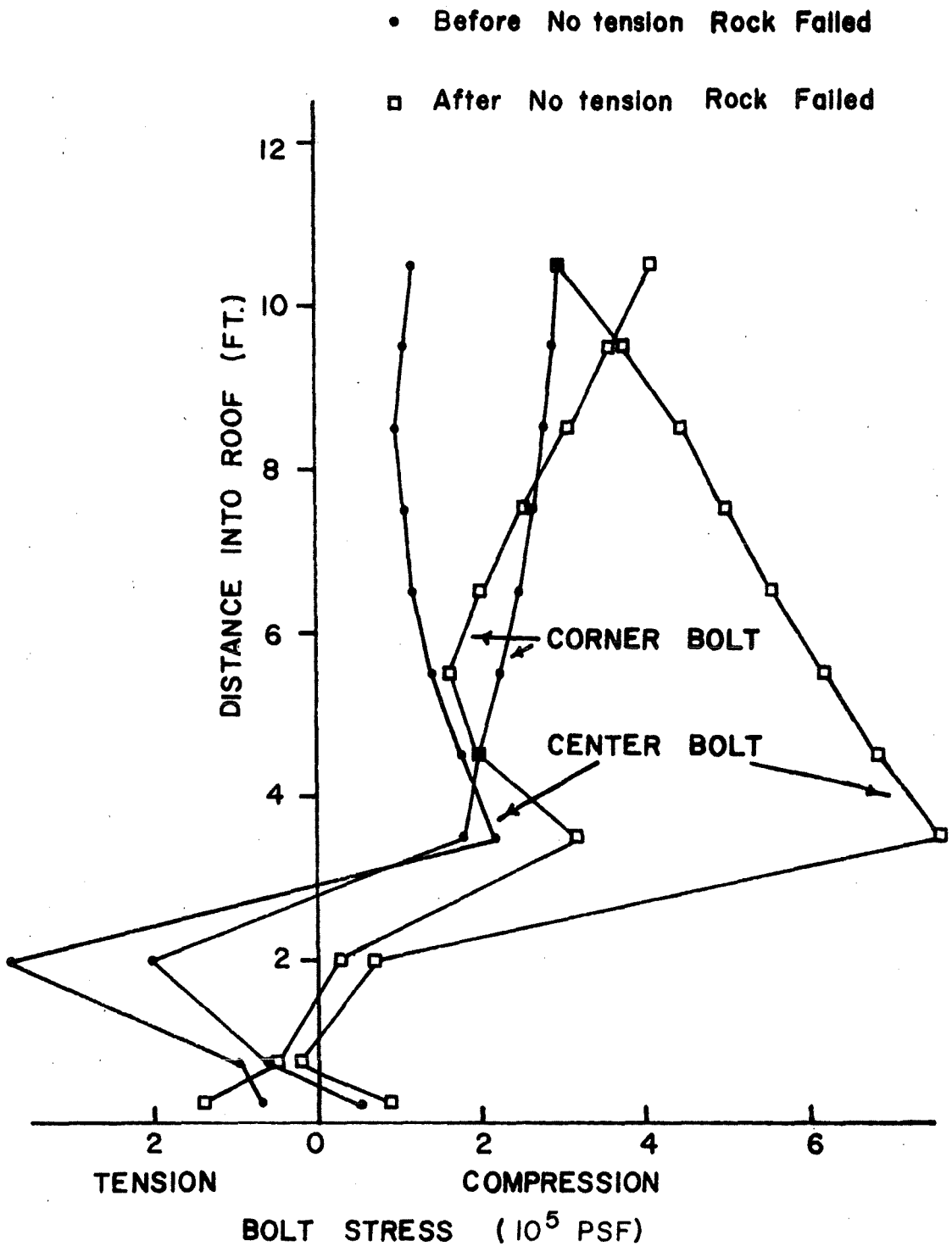

Fig. 2-16 Stresses Along the Length of Bolts Installed Before Initial Settlement

Anchor Bolts Installed Close to the Face

Seven anchor bolts with 15,000 lb preloads were assumed to be installed close to the face. The same loading program as for the grouted bolts described just above was applied. The maximum roof deflection was reduced by 12 percent from the no-bolt case. The preload in the center bolt decreased by 5 percent before the rock in tension was allowed to fail and decreased 11 percent more as the no-tension rock failed. These decreases in tensile bolt load indicate that the distance from the bearing plate to the point anchor decreases as the roof deforms under the gravitational load and then decreases additionally as the rock fails as a no-tension material. The tension loss in the anchor bolts is reflecting the same sort of rock movements which caused the compressive loading in the fully grouted bolts.

Grouted Bolts Installed Away from the Face

Model B was loaded with the overburden and gravity loads. Tensile and shear failures were allowed along the two bedding planes, but the rock in tension was not allowed to fail. This was done to model the initial settlement of the roof occurring before the bolts were installed. After the seven grouted bolts were installed, the bolt stiffness was included in the finite element model. The bolts were installed with no initial tension. The finite element program was run again with the displacement obtained from the first run as initial displacements. During the second run the rock in tension was allowed to fail. The resulting stress distribution is shown in Fig. 2-17. The compressive stresses below the bedding plane indicate that the roof is stable under these conditions. The bolt stresses are shown in Fig. 2-18. In this case high tensile stresses occur in the bolt at the bedding plane. However, the stress is low well above the bedding plane which indicates that this portion of the bolt is contributing little to the support of the roof.

e. Case 5 - Study

Study of beam building effects. Model C was used to determine if two separate slender beams connected by 4 ft long bolts behave as one beam under typical mine conditions. The bolts were modeled by truss elements. The low lateral stress situation was analyzed.

Fig. 2-19 shows the stress distribution without bolts and Fig. 2-20 shows the distribution with seven anchor bolts preloaded to 15,000 lb. The rock was not permitted to fail as a no-tension material in these cases. The stress distributions are nearly identical. Table 2-3 shows the horizontal stresses at various locations in the upper and lower beams for the two cases: with no bolts and with seven bolts. The stress variations along vertical lines are nearly linear at midspan and at 6 ft from the pillar. Near the pillar the stress variation is more irregular as expected. Comparison of the stresses with and without bolts shows that there are minor variations, but it is obvious that the bolt loads were not sufficient to "build" one thick beam from the two thin beams.

The stresses in Table 2-3 are all compressive rather than half tensile and half compressive as predicted by simple beam theory. The lack of tensile stresses is due to the compressive horizontal free field stress.

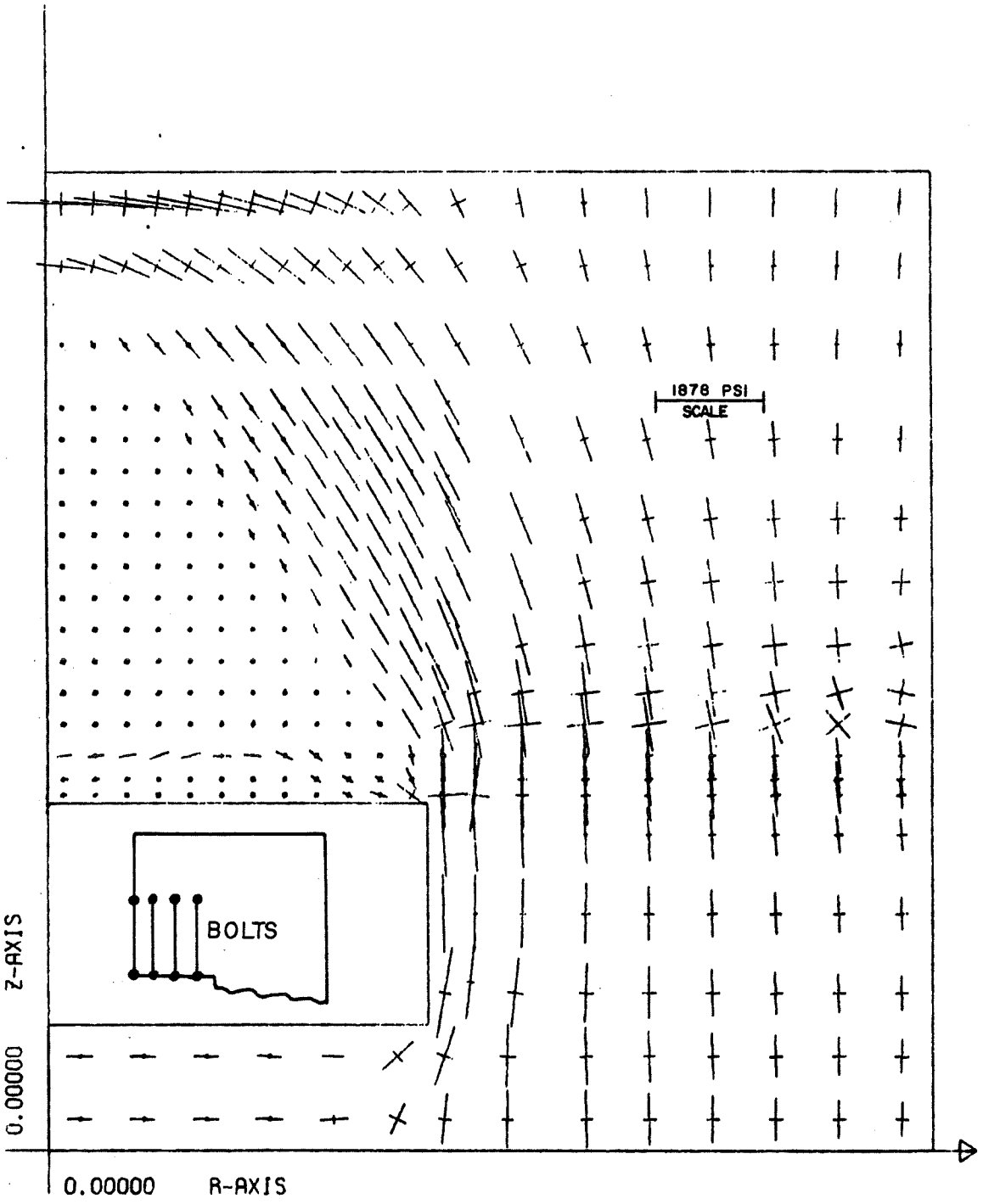

Fig. 2-17 Principal Stress Field for Seven Grouted Bolts Installed after Initial Settling

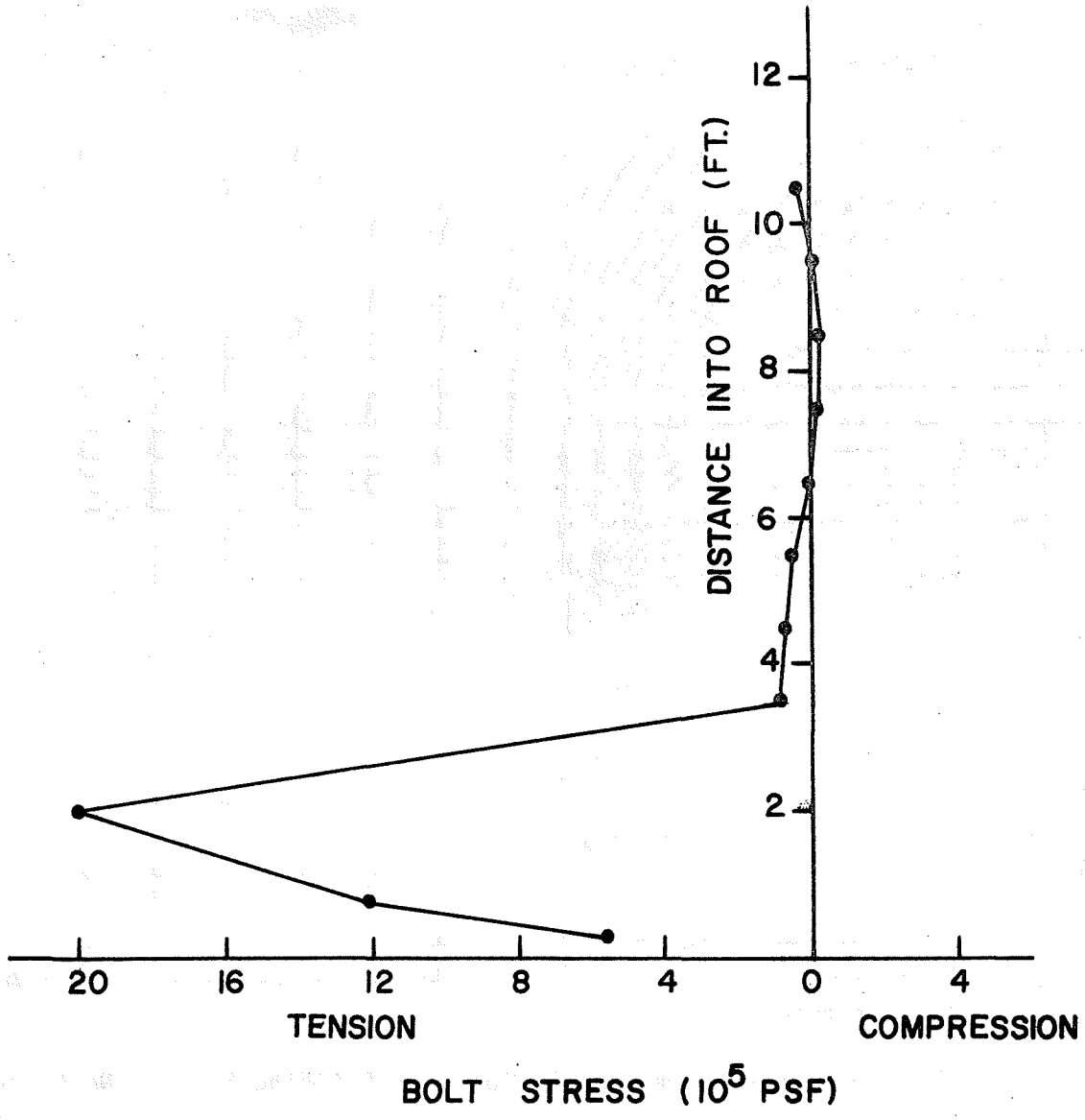

Fig. 2-18 Stresses along the Length of Center Bolt, Installed after Initial Settling, after No-tension Rock Has Failed

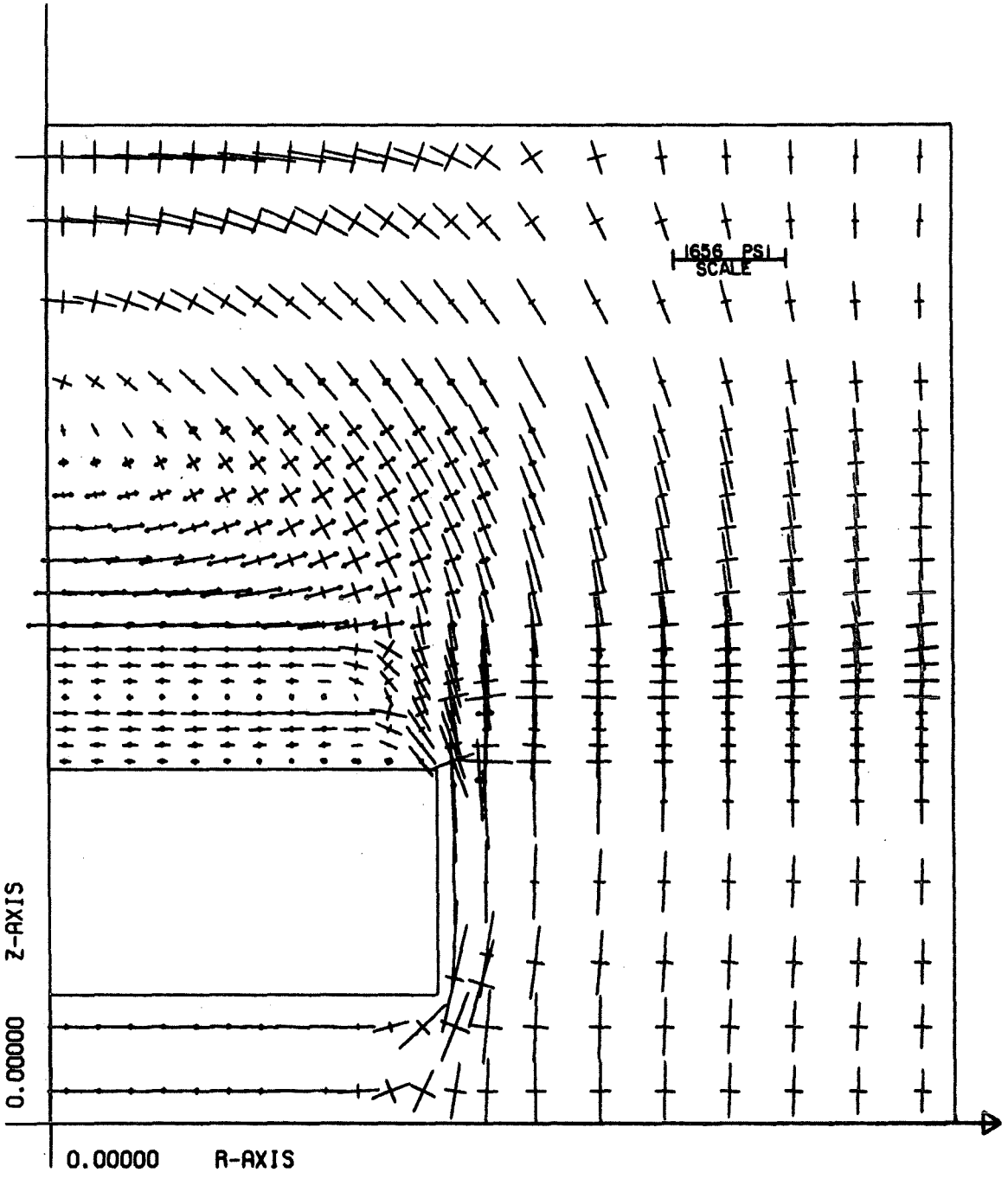

Fig. 2-19 Principal Stress Field for Beam Building Study: No Bolts

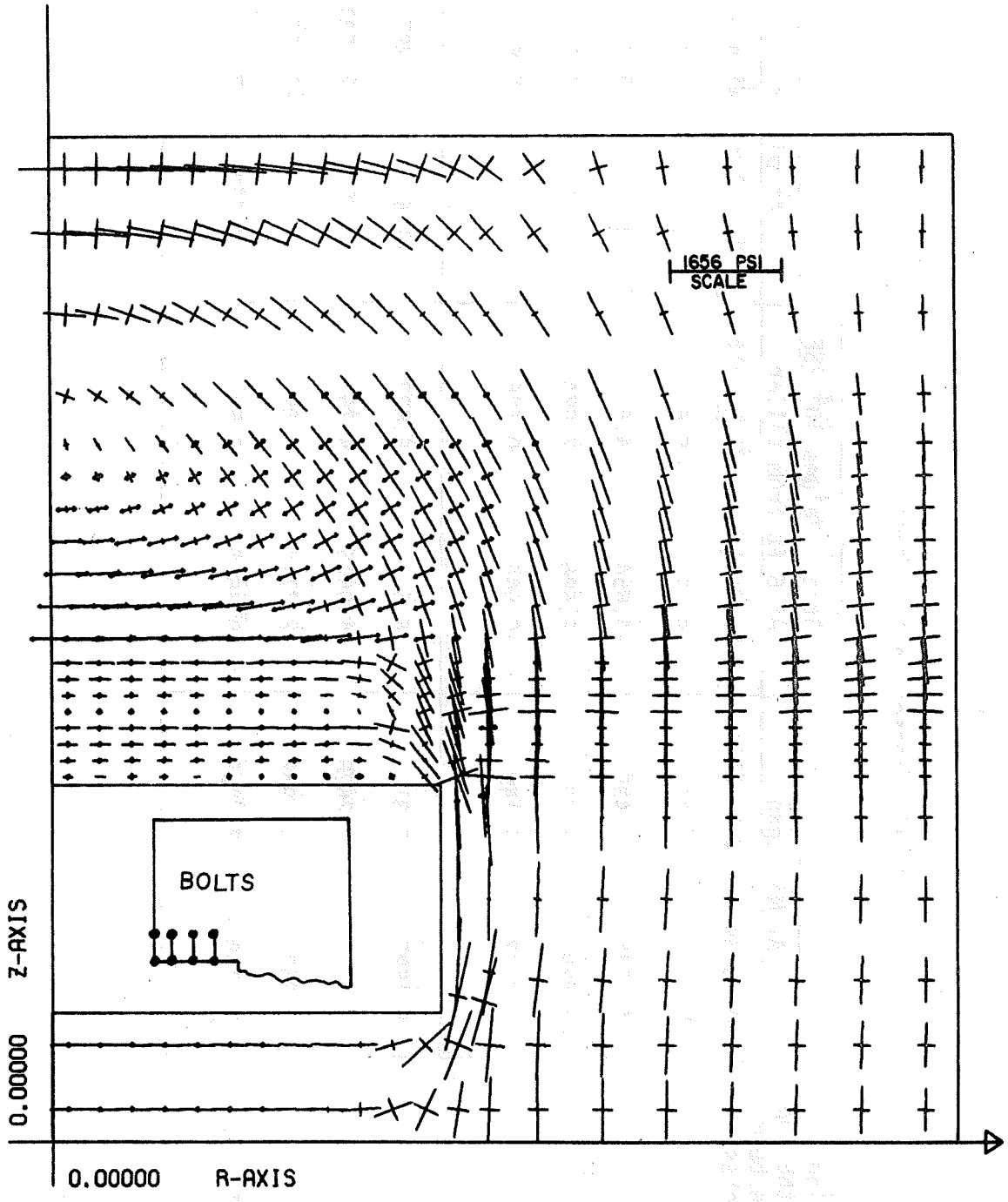

Fig. 2-20 Principal Stress Field for Beam Building Study: Seven Preloaded Bolts

Table 2-3

Flexural Stresses in the Beams

	Location from the top of the beam in inches	Stress Values 10^4 PSF					
		At Mid span		At 6 ft from pillar		At pillar	
		No Bolts	With Bolts	No Bolts	With Bolts	No Bolts	With Bolts
Upper Beam	3	-6.0017	-6.11	-6.72	-6.6	-2.925	-2.972
	9	-4.4185	-4.436	-4.654	-4.6	-3.7	-3.7
	15	-2.829	-2.79	-2.586	-2.624	-4.54	-4.5
	21	-1.2442	-1.149	-0.646	-0.646	-5.542	-5.5
Lower Beam	3	-5.1527	-5.319	-6.6	-6.823	-1.6	-1.287
	9	-4.21	-4.2628	-4.6925	-4.76	-3.08	-2.9531
	15	-3.257	-3.1962	-2.7714	-2.697	-4.7	-4.785
	21	-2.3158	-2.0869	-0.8616	-0.58	-7.023	-7.3365

The stresses in Table 2-3 reflect the combined effects of the beam bending and the lateral free field stress. If the lateral free field stresses were reduced, the regions of low compressive stress would probably become tensile and the high compressive stresses would be reduced. It is interesting to note that under these conditions that the region of highest tensile stress would occur in the bottom fibers halfway between the pillar and midspan. In contrast, elementary beam theory for fixed-end beams predicts that the highest tensile stresses occur in the top fibers of the beam at the pillar. Fig. 2-21 is a plot of bedding plane separation for the no-bolt and preloaded anchor-bolt situations. Two separations are shown, one between the two beams and the other above the upper beam. The plot shows that the bolts have negligible effect on the separation above the upper beam. The preloaded bolts did significantly reduce the magnitude of the separation between the beams but did not change the lateral extent of the separation. Calculations indicate that the size of bolt and preload required to completely close the separation between the bolts are impractical.

The rock in the tensile regions was also allowed to fail in the no-bolt and bolted situations. The stress distributions are given in Figs. 2-22 and 2-23, respectively. Fig. 2-22 indicates that the unbolted roof was not stable, but the compressive stresses above the roof in Fig. 2-23 indicated that the bolted roof was more likely to be stable. The stresses in the preloaded anchor bolts at various stages of loading are shown in Table 2-4 for competent rock and rock with no tensile strength. Failure was allowed only along the three bedding planes in the competent rock, while both the rock in tension and the bedding planes could fail in the no-tension case. The initial stress corresponds to the installed bolt tension of 15,000 lb. The columns labeled "after final iteration" are the bolt stresses after the failure had progressed to a stable configuration. As indicated by Table 2-4, the tensile stresses in the bolts increased as much as 18 percent as the failure progressed.

The roof deflection for the various cases is shown in Fig. 2-24. In each case the roof deflection is higher than that predicted by elementary beam theory for either a simply supported or a fixed-end beam. For earlier studies in which Model B with only one beam over the roof was used, the deflection curves from the finite element solution was between the fixed-end case and the simple support case. The additional bedding plane and the reduced constraint at the right boundary of the model increased the flexibility of the model at the pillar.

The effect of end support conditions was also demonstrated by analyzing the plane stress model shown in Fig. 2-25. This model is a prototype corresponding to the laboratory model, Series IV-B, studied by L. Panek (Ref. 6).

The prototype model was developed by satisfying the similarity requirements for scaling the model used in the series IV-B tests to typical mine size. One important difference between the model and prototype, however, is that the pillar support in the prototype was considerably less rigid than that in the series IV-B model. The physical models tested by Panek were rigidly clamped at the ends (pillars). Fig. 2-26 shows the roof deflection due to gravity loads (no bolts) calculated using the model in Fig. 2-25. The rotation of the lower beam at the edge

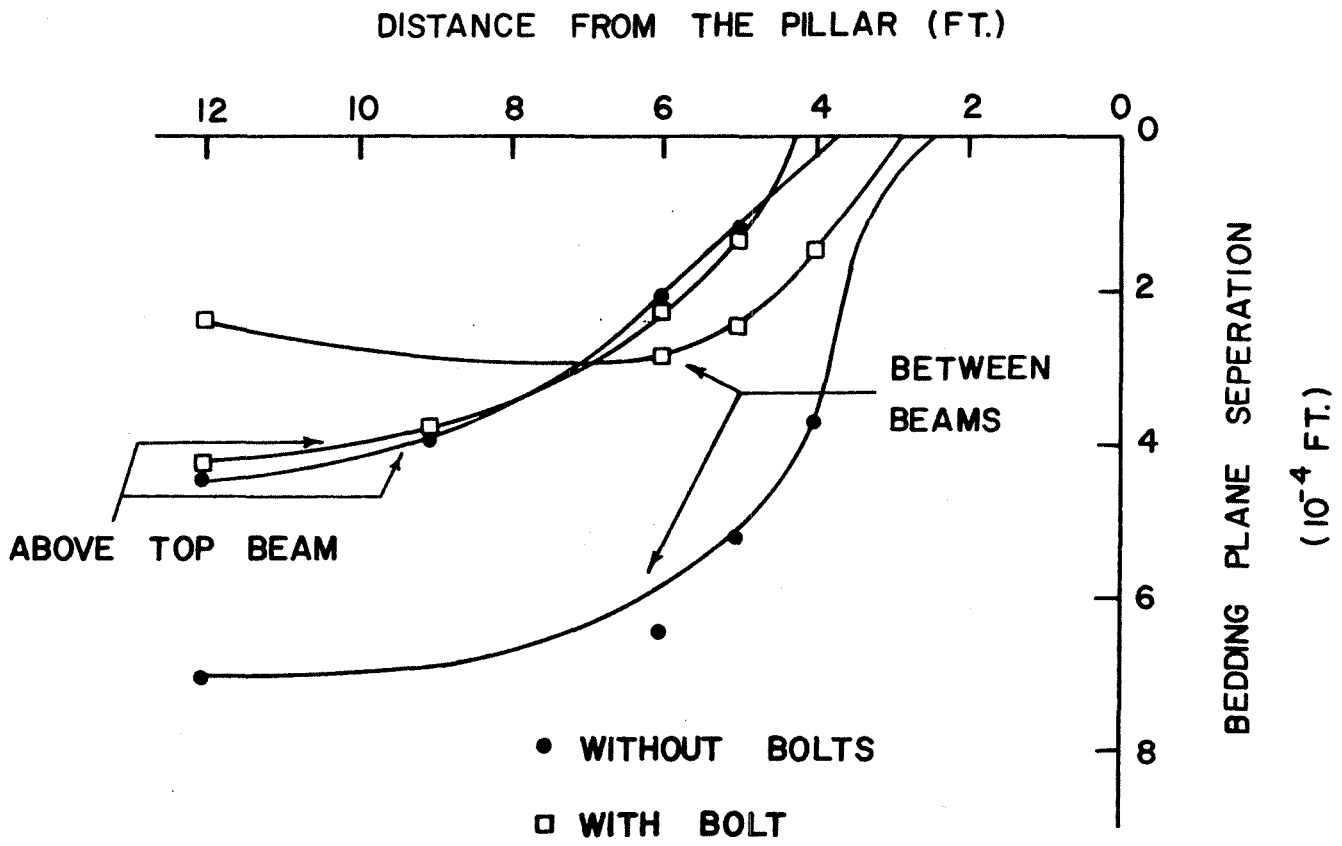

Fig. 2-21 Effect of Bolts on Separation of Bedding Planes

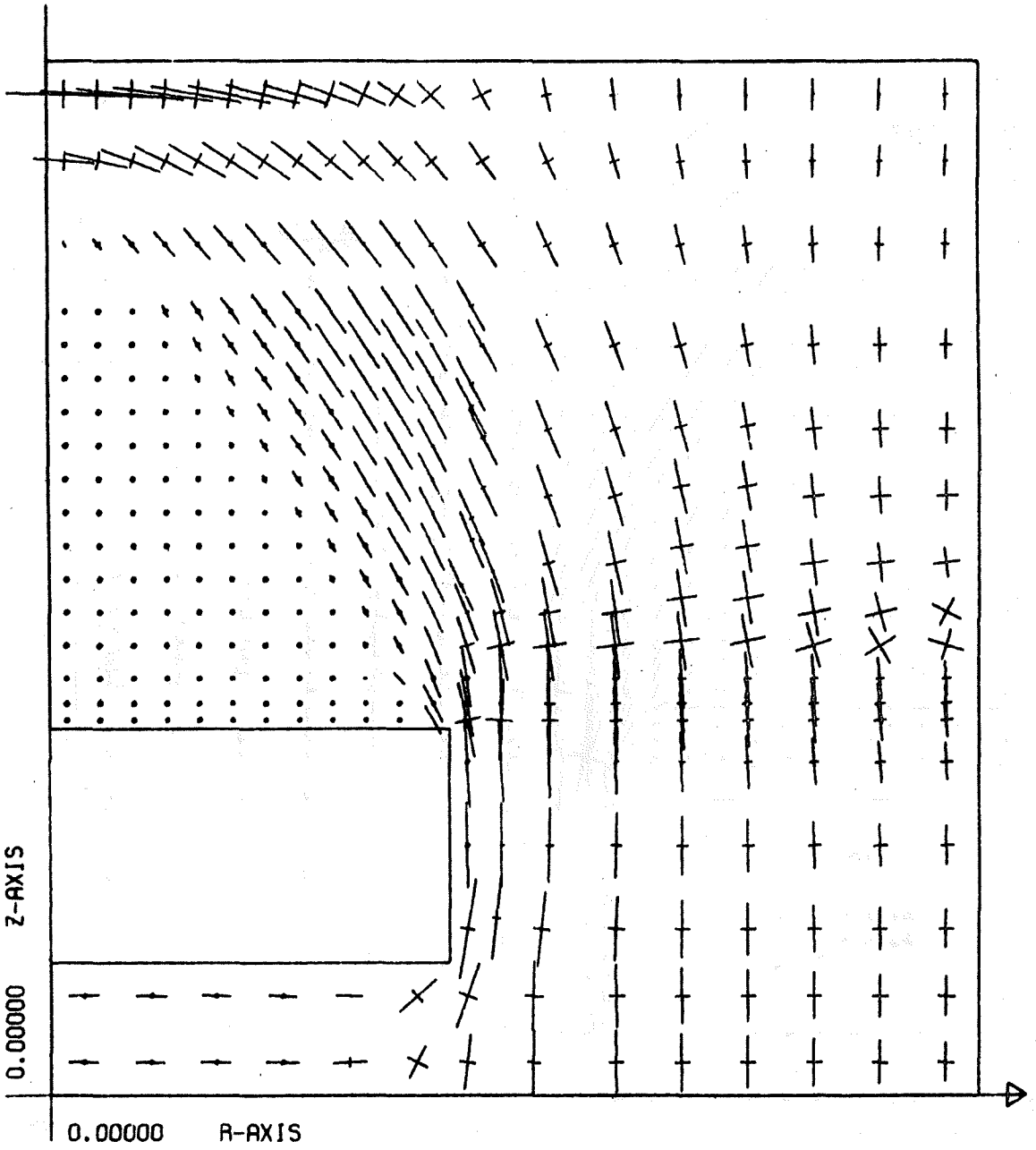

Fig. 2-22 Principal Stress Field for Beam Building Study: No-Tension Material and No Bolts

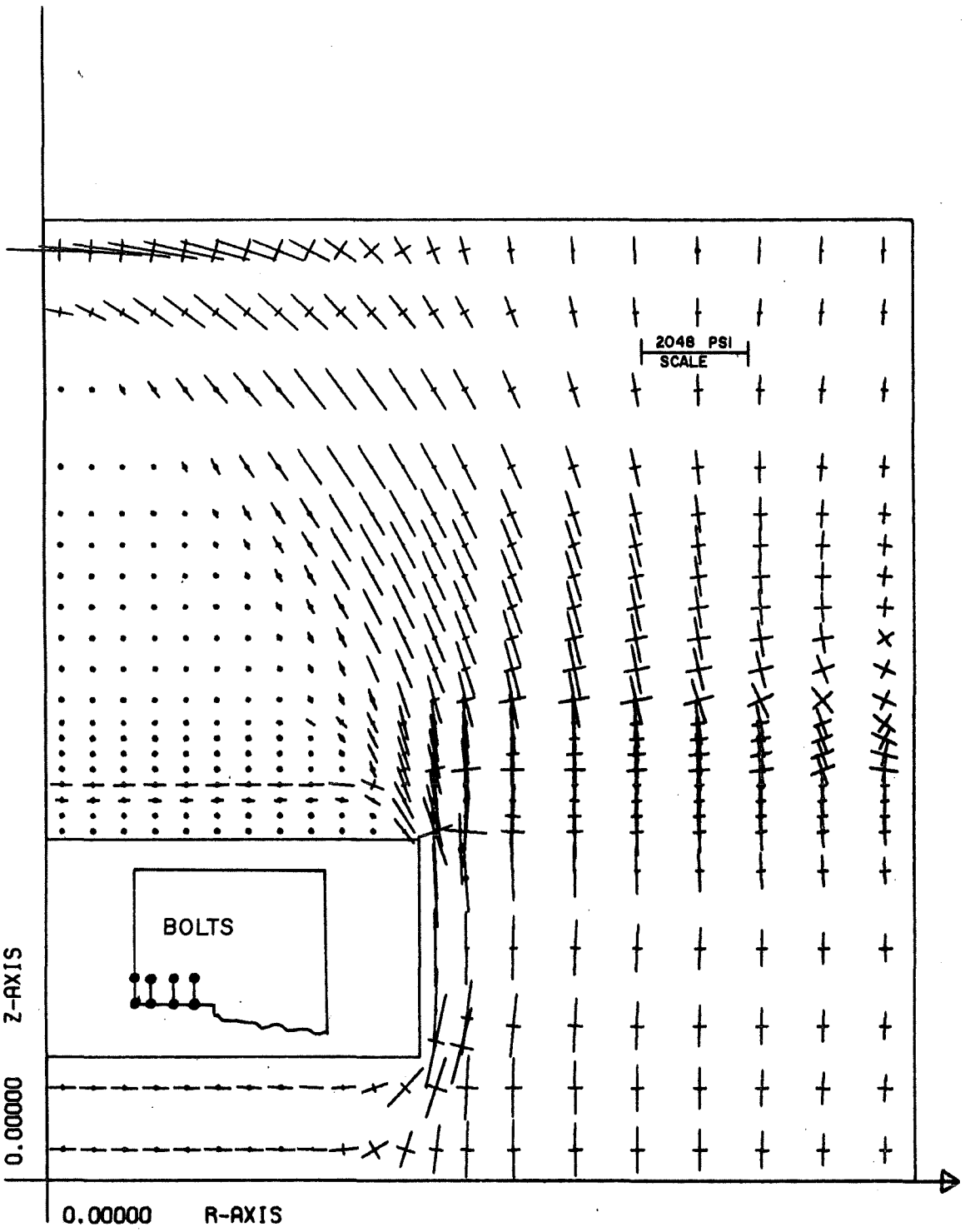

Fig. 2-23 Principal Stress Field for Beam Building Study: Seven Preloaded Bolts and No-Tension Material

Table 2-4

Variation of Stresses in Preloaded Anchor Bolts

Location of Bolt	Competent Rock Stress in 10^7 PSF					Rock as a No-Tension Material Stress in 10^7 PSF				
	Initial Stress	After first Iteration	% change	After final Iteration	% change	Initial Stress	After first Iteration	% change	After final Iteration	% change
Mid Span	0.88	0.898	2.05	0.986	12.0	0.88	0.898	2.05	1.038	18.0
9 ft from pillar	0.88	0.899	2.16	0.988	12.3	0.88	0.899	2.16	1.036	17.7
6 ft from pillar	0.88	0.902	2.5	0.977	11.0	0.88	0.902	2.5	1.009	14.7
3 ft from pillar	0.88	0.88	0.0	0.913	3.75	0.88	0.888	0.0	0.93	5.68

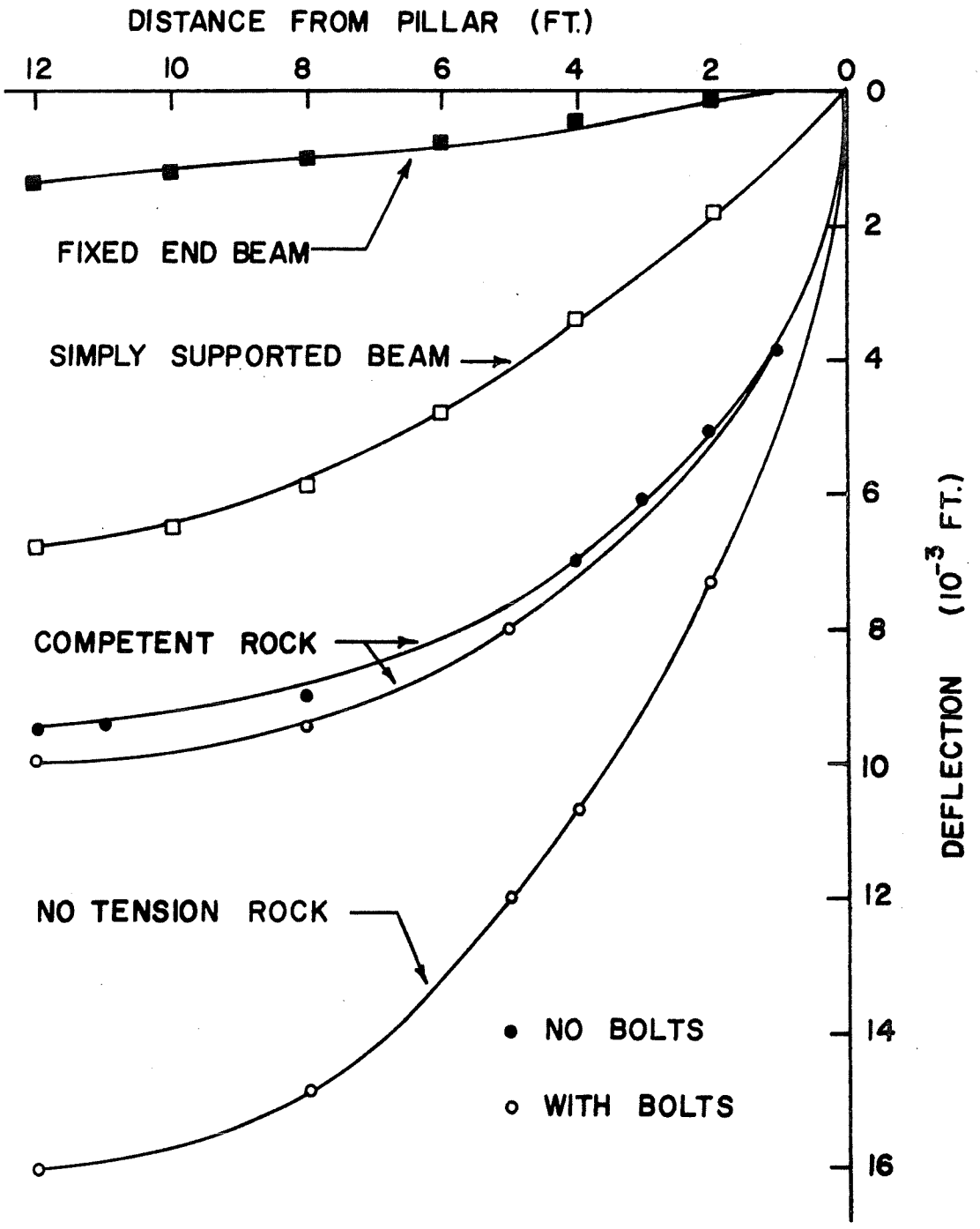

Fig. 2-24 Deflection Plots for Beam Building Case

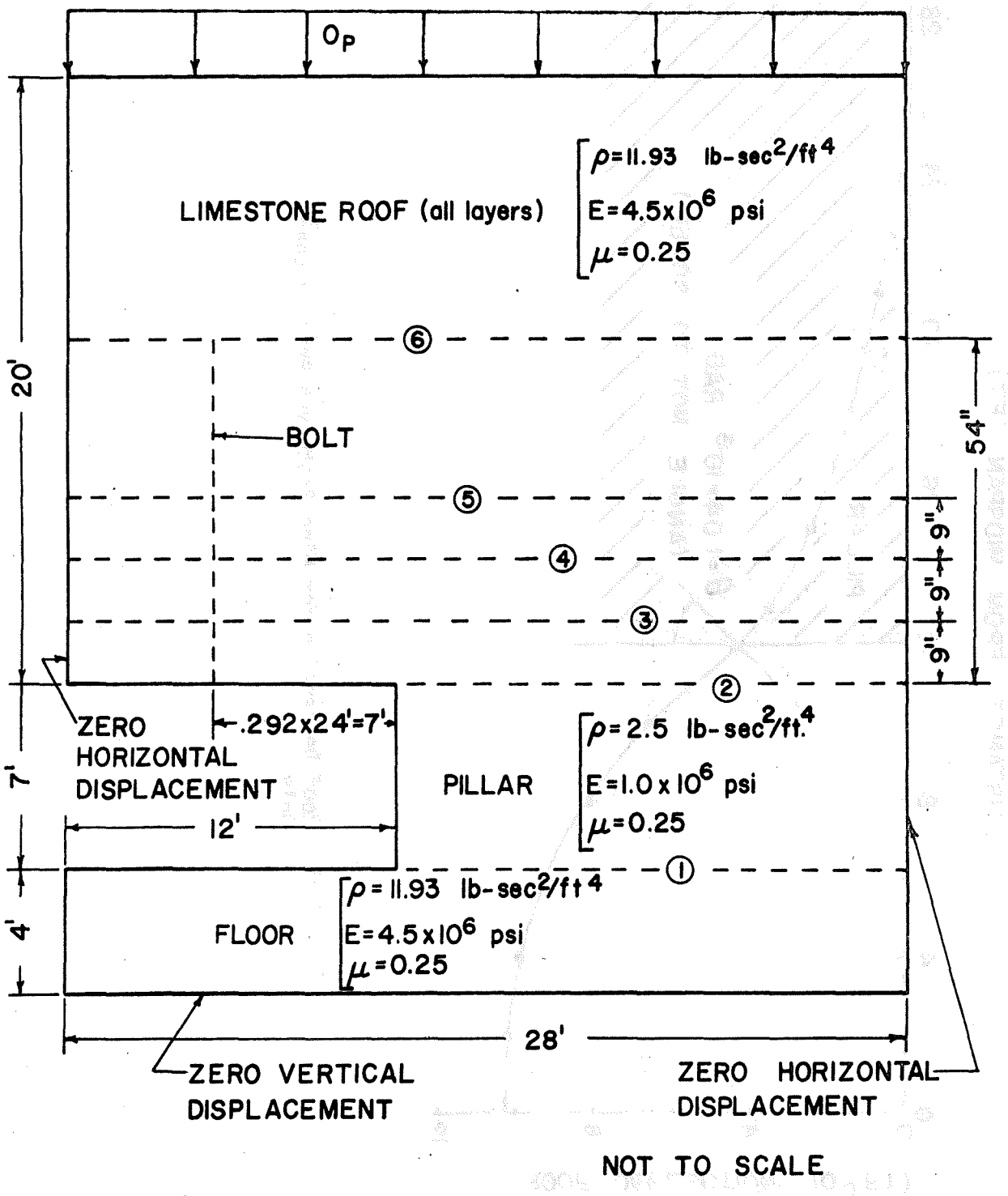

Fig. 2-25 Prototype Model of L. Panek Test Series IV-B.

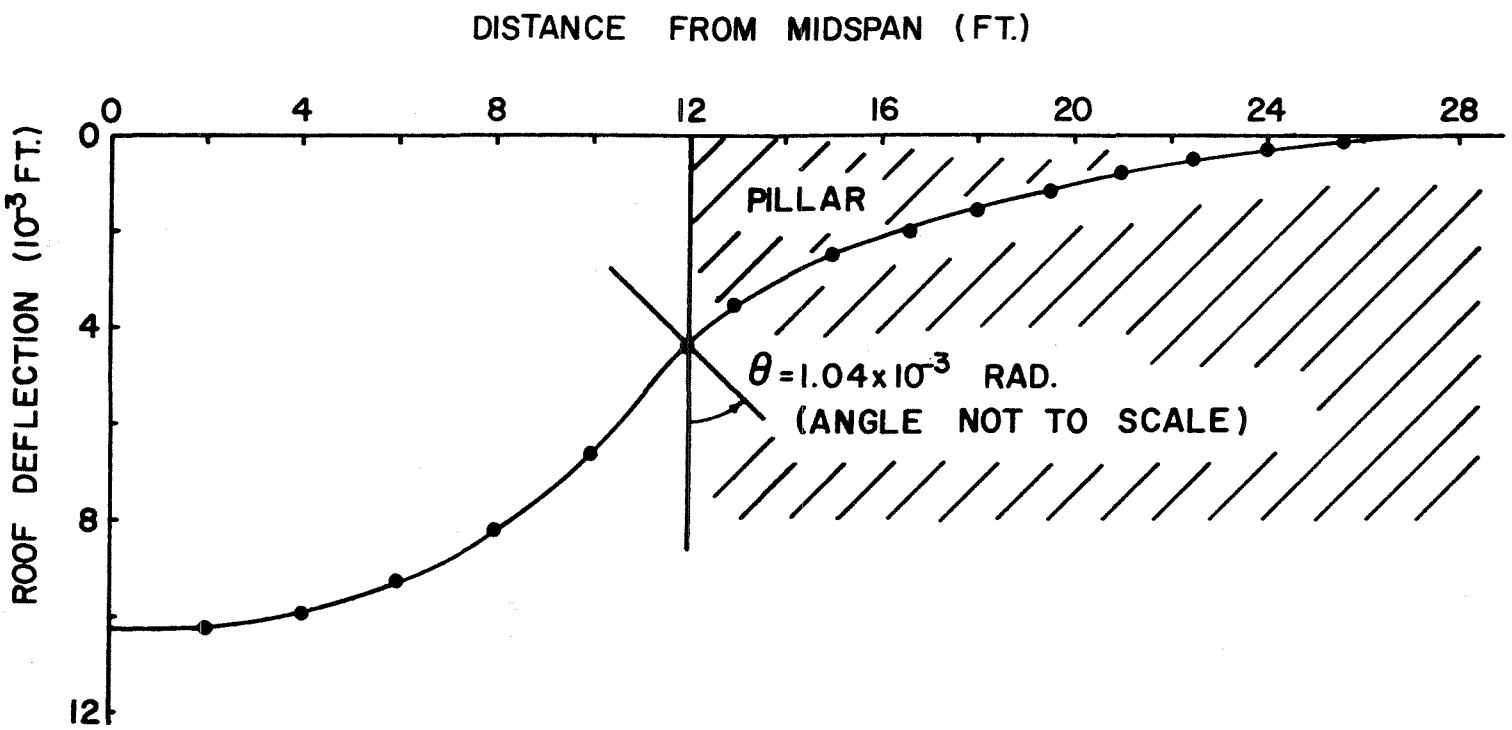

Fig. 2-26 Roof Deflection for Mine Prototype Gravity Load Only

of the pillar is 1.04×10^{-3} radian. The corresponding rotation of a simply supported, uniformly loaded (gravity load) beam is 7.28×10^{-3} radian. When the loading due to the overburden is applied, the rotation of the beam at the pillar increases significantly. For an overburden of 500 psi and no bolts, the rotation is 9.80×10^{-3} radian. Because of these large rotations at the pillar it is not correct to model the typical roof beam as a fixed-end beam.

Summary and Conclusions

Two-dimensional finite element models were used to study two aspects of a bolted roof:

1. Axial symmetric models of the bolt and surrounding rock were used to determine the localized stress state in and around conventional and grouted roof bolts due to loads introduced at installation and bedding plane separation. The stress distributions for these conditions are given in Refs. 1 and 2.

2. Plane strain models of a typical opening were used to determine the effects of bolts on the stability of a layered mine roof when bedding planes and in-situ lateral stresses are present. The stability of the bolted mine roof was assessed in terms of the stress distributions, roof deflections, and areas of tensile stress within the roof.

Roof bolts had no significant effect on stress distribution or roof deflection when the roof was continuous with no bedding planes. Bolts exerted more influence when bedding planes were present in the roof. Anchor bolts reduced the deflection of the roof with two bedding planes by 8.5 percent compared to the no-bolt condition with similar lateral stresses. Bolts reduced, or in some cases closed, the separation between bedding planes. Preloaded anchor bolts reduced the deflection of the no-tension rock roof about 12 percent.

Untensioned grouted bolts installed before face advance and initial settlement occurred exhibited compressive bolt loading along much of the bolt lengths when gravitational and overburden loads were applied. Such compressive bolt loading is thought to have an adverse effect on the initial roof stability, although the seriousness of this effect is not known. Compressive bolt loading did not occur when the untensioned grouted bolts were installed after the initial settlement had occurred. Also, favorable tensile bolt loading at a bedding plane occurred in the latter case.

The effect of lateral stresses on the stability of the roof is significant. The deflection of the roof subjected to low lateral stresses was higher than those subjected to high lateral stresses in all cases when horizontal bedding planes were present in the roof. The volume of rock experiencing tensile stresses was much higher for low lateral stresses than high lateral stresses. However, the maximum octahedral shear stress was about two times higher for high lateral stress cases than for low-lateral-stress cases. This indicates that shear failure is more likely at the high lateral stresses.

The deflection of the roof increased as the number of bedding planes increased. The roof deflection for three bending planes and no-tension rock was about three times greater than for no bedding planes and competent rock.

The significance of the beam building effect was analyzed by considering two roof beams bolted together with preloaded anchor bolts. There was no significant amount of beam building, since there was separation between the beams over the center three-fourths of the span. The size of the bolts and preload required to close the separation completely were found to be impractical. The preloaded anchor bolts did, however, significantly increase the stability of the roof over the no-bolt condition.

The commonly made assumption that roof beams deflect as though they were rigidly restrained on the ends was found to invalid, particularly so in coal mine applications where the stiffness (Young's modulus) of the supporting pillar of coal is much less than that of typical roof rock. As the corner of the pillar deforms downward under the overburden load the neutral axis at the end of the beam rotates through a relatively large angle causing the deflection curves to slope downward at the rib.

Chapter III

SPLIT-SET ROCK BOLT ANALYSIS

Introduction

Friction rock stabilizers, or split sets, are a new type of bolting mechanism used to stabilize rock structures. The split set (Fig. 3-1) is formed by rolling a section of thin plate into a tube with a slit running its entire length. Split sets may vary in length up to six feet and usually have about an inch and a half diameter, a tenth of an inch wall thickness, and a slit width of half an inch. When forced into a hole with a diameter smaller than its own, the split-set tube is forced to close inside the hole and a radial pressure distribution is created between the split-set tube and the wall of the hole. The radial pressure distribution caused by the forced fit can be related, by the coefficient of friction between the split set and the wall of the hole, to a force along the length of the tube. This force enables the split set to support or reinforce the media into which it is driven. One end of the split set is usually tapered to facilitate driving the split set into the undersized hole, while the other end is upset in order to support a bearing plate against the surface of the stabilized media.

Dr. J.J. Scott, inventor of the split set, has already established the potential of this new rock stabilizing technique in a report entitled "Friction Rock Stabilizers and Their Applications to Ground Control Problems" (Ref. 7). Promising field test results from Dr. Scott's report indicated a more detailed investigation of the split set mechanism should be conducted. Therefore the purpose of this research is to derive an analytical or numerical analysis to describe the split set mechanism and hopefully to provide some data or insight which will assist in the proper use of split sets in safe mine design.

Analysis

The first problem in analyzing the performance of the split-set roof bolt is determining the radial pressure distribution created by forcing the split set into an undersized hole. This radial pressure distribution is important since it can be related through a coefficient of friction to the maximum force available longitudinally between the split-set tube and the wall of the hole.

An energy method approach, curved beam theory, and the method of "Successive Elastic Solutions" were the techniques used in determining the radial pressure distribution.

A. Equilibrium Considerations

A free-body diagram of a typical cross section of a functioning split-set rock bolt is shown in Fig. 3-2. This diagram suggests that the radial pressure that is exerted on the split set by the surrounding geologic material acts only over a portion (given by the variable angle β) of the circumference, and that concentrated forces exist at the slit edge. The use of a variable area of contact between the split set and the hole is required since a portion of the split set falls naturally inside the hole.

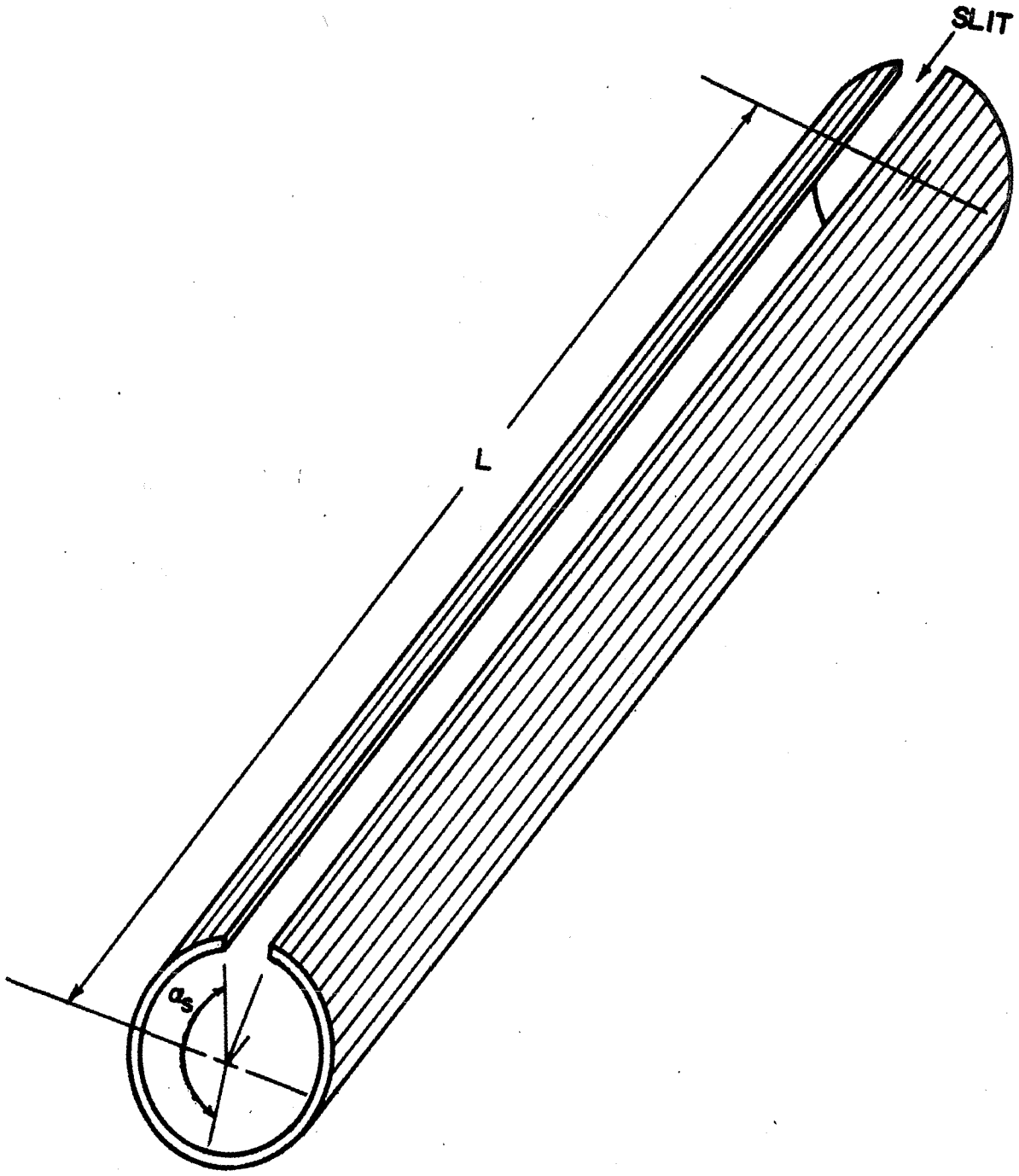

Fig. 3-1 Split-Set

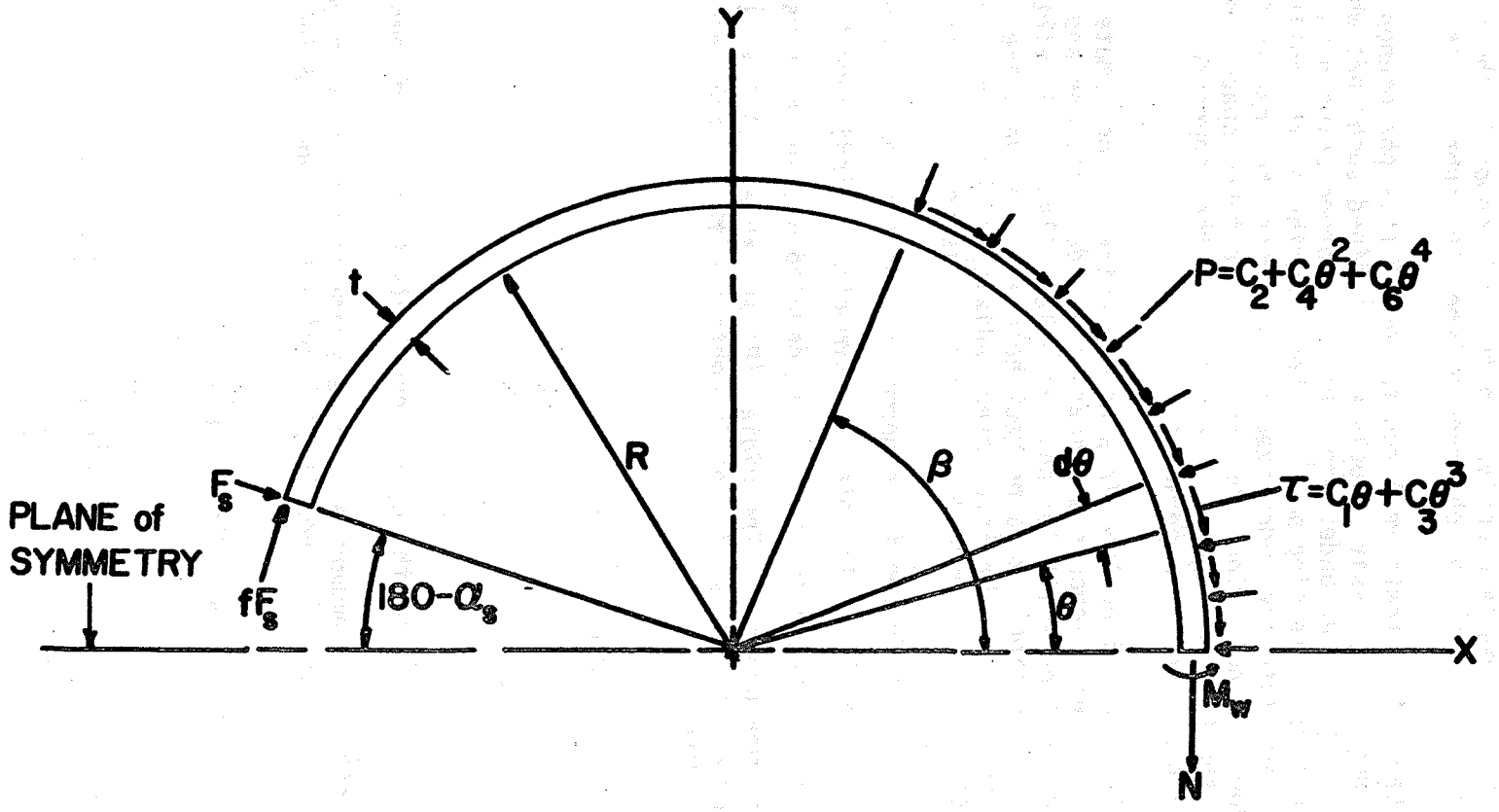

Fig. 3-2 Free-Body Diagram of a Split-Set

This phenomenon may be observed by rolling a piece of cardboard into the shape of a tube and placing it in the opening of a tin can or a coffee cup. If this experiment is executed, the cardboard tube will fit into the hole, making complete contact on the side opposite the slit. Approaching the slit, gaps will be observed between the tube and the wall of the hole.

Laboratory tests were run to see if this phenomenon applied to the split set. Compressive blocks were machined such that when they were placed together an undersized hole was formed between their mutual face. In a universal testing machine short lengths of the split-set tube were compressed into the undersized hole between the compressive blocks. Looking down the hole along the length of the tube, spaces were observed between the tube and the hole wall just as they appeared in the cardboard tube and coffee cup experiment.

It is realized that in some mines the geologic material (especially salt) will experience significant creep deformations and will close the gap between the split set and the hole. Also, it is virtually impossible to drill anything like a perfect hole in an actual mine, but the subsequent analysis utilizes the integrated radial pressures to determine the holding capacity and an average radial pressure is documented for easier reference.

The concentrated force normal to the slit edge is denoted by F_s, and the force-couple at the plane of symmetry is indicated by N and M_w, respectively. The angle to the slit is denoted α_s, and θ is used as a variable angular measurement. The radial (P) and shear (τ) tractions that act over the surface of the split set in contact with the hole are considered to be of the form

$$P = C_2 + C_4\theta^2 + C_6\theta^4$$
$$\tau = C_1\theta + C_3\theta^3 \qquad (3\text{-}1)$$

where $0 \leq \theta \leq \beta$ and the C_i are constants to be determined.

Setting the moment and force summations equal to zero for the free-body diagram of Fig. 3-2 gives the following three equilibrium equations.

$$M_w = fF_sR + NR + R^2L\left[\frac{1}{2}C_1\beta^2 + \frac{1}{4}C_3\beta^4\right] \qquad (3\text{-}2)$$

$$N = -fF_s\cos\alpha_s - F_s\sin\alpha_s - RL\left[\left(-C_1 + C_2 + 6C_3 - 2C_4 + 24C_6\right)\right.$$
$$\left. - \left(-C_1 + C_2 + 6C_3 - 2C_4 + 24C_6\right)\cos\beta - \left(-3C_3 + C_4 - 12C_6\right)\right.$$

(3-3)

$$\beta^2 \cos\beta - (C_6)\,\beta^4 \cos\beta + (C_1 + 2C_4 - 6C_3 - 24C_6)\,\beta \sin\beta + (C_3 + 4C_6)\,\beta^3 \sin\beta\Big]$$

$$F_s = \frac{RL}{f \sin\alpha_s - \cos\alpha_s}\Big[(-C_1 + C_2 + 6C_3 - 2C_4 + 24C_6)\,\sin\beta + (-3C_3 + C_4 - 12C_6)\,\beta^2 \sin\beta + (C_6)\,\beta^4 \sin\beta + (C_1 + 2C_4 - 6C_3 - 24C_6)\,\beta\cos\beta + (C_3 + 4C_6)\,\beta^3 \cos\beta\Big] \tag{3-4}$$

where R is the hole radius, f is the coefficient of friction, and L is length of the split set in contact with the hole.

B. Energy Methods

The constants (C_i) introduced in the surface loading Eq. (3-1) can be determined by specifying a set of appropriate displacement boundary conditions. The boundary conditions adopted for this analysis are:

$$\delta_{rotation} = 0 \quad @\ \theta = 0 \tag{3-5}$$

(no rotation at the plane of symmetry)

$$\delta_y = 0 \quad @\ \theta = 0 \tag{3-6}$$

(no deflection normal to the plane symmetry)

$$\delta_R = -\Delta R \quad @\ \theta = 0,\ \theta = \beta,\ \theta = \alpha_s \tag{3-7}$$

(radial deflection is consistent with the interference fit between the hole and the split set)

The deflection boundary conditions can be enforced by using Castigliano's theorem. Castigliano's theorem states that, "if external forces act on a member or structure which is subjected to deflections that are small and linearly related to the loads, the deflection, in the direction of any one of the forces, of the point of application of the force is equal

to the partial derivative with respect to the force of the total internal strain energy in the member". As will be shown later, a small portion of wall of the split-set experiences plastic straining during the loading process; however, the experimental data indicate that the load-deflection curve remains linear over the range of interest. Thus, the Castigliano theorem has been used to generate appropriate boundary conditions equations.

The first boundary condition (3-5) to satisfy is of the form

$$\delta_\theta = \frac{\partial U}{\partial M_w} = \int_0^\beta \frac{M}{EI} \frac{\partial M}{\partial M_w} R d\alpha + \int_\beta^\alpha \frac{M}{EI} \frac{\partial M}{\partial M_w} R d\alpha = 0 \qquad (3\text{-}8)$$

The moment (M) at an arbitrary section α is determined from Fig. 3-3 to be

$$\begin{aligned} M = {} & M_w - NR(1 - \cos\alpha) + F_n R(\cos\alpha \sin\xi - \sin\alpha\cos\xi) \\ & - R^2 L \int_0^\alpha \Big[P(\theta)\cos\theta \sin\alpha - P(\theta)\sin\theta\cos\alpha \\ & + \tau(\theta)\cos^2\theta - \tau(\theta)\cos\theta\cos\alpha - \tau(\theta)\sin\theta\sin\alpha \\ & + \tau(\theta)\sin^2\theta \Big] d\theta \end{aligned} \qquad (3\text{-}9)$$

where F_n is a dummy load applied at an arbitrary position ξ. Using the definitions presented in Eq. (3-1), Eq. (3-9) becomes, after integration,

$$\begin{aligned} M = {} & M_w - NR(1 - \cos\alpha) + F_n R(\cos\alpha \sin\xi - \sin\alpha\cos\xi) \\ & - R^2 L \Big[-A_4 + \tfrac{1}{2} A_3 \alpha^2 + \tfrac{1}{4} A_2 \alpha^4 + A_4 \cos\alpha \\ & + 2A_1 \alpha \sin\alpha \cos\alpha \Big] \end{aligned} \qquad (3\text{-}10)$$

where the constants A_i are defined as

$$\begin{aligned} A_1 &= C_4 - 12C_6 \\ A_2 &= C_3 + 4C_6 \\ A_3 &= C_1 - 6C_3 + 2C_4 - 24C_6 \\ A_4 &= C_1 - C_2 - 6C_3 + 2C_4 - 24C_6 \end{aligned} \qquad (3\text{-}11)$$

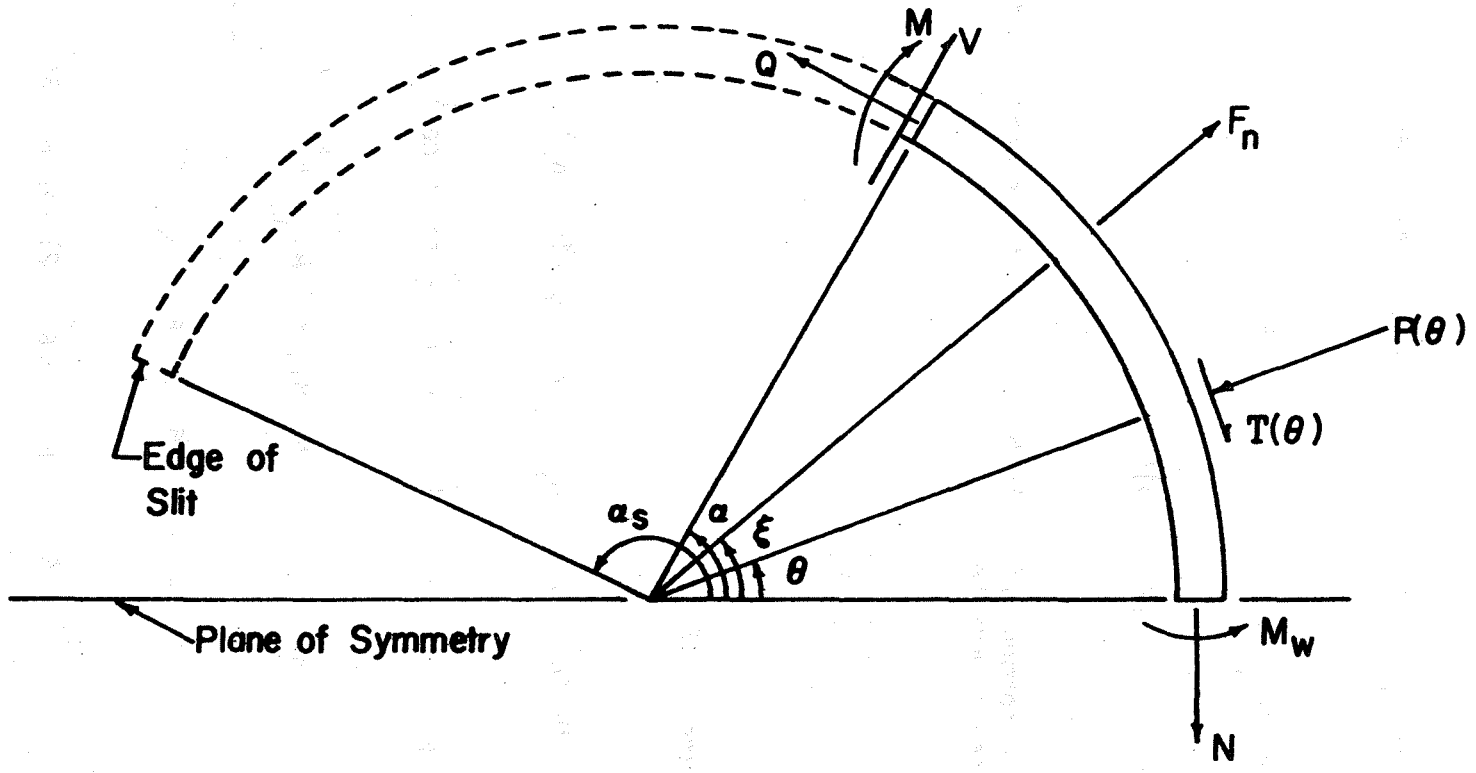

Fig. 3-3 Free-Body Section from a Split-Set

Combining Eqs. (3-8) and (3-9) gives the first boundary condition equation

$$M_w \alpha_s - NR (\alpha_s - \sin \alpha_s) - R^2L \left\{ \frac{1}{4} A_1 \left[(1 + 4\beta\alpha_s - 4\beta^2) \sin 2\beta \right.\right.$$

$$\left. - (2\beta) \cos 2\beta \right] + \frac{1}{20} A_2 \left[(5\alpha_s - 4\beta) \beta^4 \right] + \frac{1}{6} A_3 \left[(3\alpha_s - 2\beta)\beta^2 \right] \quad (3\text{-}12)$$

$$\left. + A_4 \left[-\alpha_s + \sin \beta + (\alpha_s - \beta) \cos \beta \right] \right\} = 0$$

Since the split set is deformed primarily by bending, the second boundary condition, Eq. (3-6), can be written as

$$\delta_y = \int_0^{\beta} \frac{M}{EI} \frac{\partial M}{\partial N} R d\alpha + \int_{\beta}^{\alpha_s} \frac{M}{EI} \frac{\partial M}{\partial N} R d\alpha = 0 \quad (3\text{-}13)$$

Combining Eqs. (3-10) and (3-13) yields

$$M_w (\sin \alpha_s - \alpha_s) + NR (\alpha_s - 2 \sin \alpha_s + \frac{1}{2} \alpha_s + \frac{1}{4} \sin 2 \alpha_s)$$

$$+ R^2L \left\{ A_1 \left[\frac{1}{4} \sin \beta - \frac{1}{4} \beta \cos \beta - \frac{2}{3} \beta \cos^3 \beta + \frac{2}{9} \sin \beta \cos^2 \beta \right.\right.$$

$$\left. + \frac{4}{9} \sin \beta + \beta (\alpha_s - \beta) \sin 2 \beta (1 - \cos \beta) \right] + \frac{1}{4} A_2 \left[\frac{1}{5} \beta^5 - \beta^4 \right. \quad (3\text{-}14)$$

$$\sin \beta + 12 (\beta^2 - 2) \sin \beta - 4\beta (\beta^2 - 6) \cos \beta + (\alpha_s - \beta)$$

$$\left. \beta^4 (1 - \cos \beta) \right] + \frac{1}{6} A_3 \left[\beta^3 - 6\beta \cos \beta - 3 (\beta^2 - 2) \sin \beta + 3\beta^2 \right.$$

$$\left. (1 - \cos \beta) (\alpha_s - \beta) \right] + A_4 \left[-\beta + 2 \sin \beta - \frac{1}{2} \beta - \frac{1}{4} \sin 2\beta \right.$$

$$\left. \left. - (1 - \cos \beta)^2 (\alpha_s - \beta) \right] \right\} = 0$$

The last three boundary conditions Eq. (3-7) can be formulated in a similar fashion to give

$$\frac{(\Delta R)\ EI}{R^2} = M_w(\sin\xi \sin\alpha_s + \cos\xi \cos\alpha_s - \cos\xi)$$

$$- NR\ (\sin\xi \sin\alpha_s - \cos\xi + \cos\xi \cos\alpha_s - \frac{1}{2}\alpha_s$$

$$- \frac{1}{4}\sin 2\alpha_s + \frac{1}{2}\sin^2\alpha_s) - R^2L\left\{2A_1\left[\frac{1}{3}\beta \sin\xi \cos^3\beta\right.\right.$$

$$- \frac{1}{9}\sin\xi \sin\beta \cos^2\beta - \frac{2}{9}\sin\xi \sin\beta - \frac{1}{3}\beta \cos\xi \sin^3\beta$$

$$- \frac{1}{9}\cos\xi \sin^2\beta \cos\beta - \frac{2}{9}\cos\xi \cos\beta + \frac{2}{9}\cos\xi$$

$$\left.+ \beta(\alpha_s - \beta) \sin\xi \sin\beta \cos^2\beta - \beta(\alpha_s - \beta)\cos\xi \sin^2\beta \cos\beta\right]$$

$$+ \frac{1}{4}A_2\left[\beta^4 \sin\xi \sin\beta - 12(\beta^2 - 2)\sin\xi \sin\beta\right.$$

Eqs. (3-15), (3-16), (3-17)

$$+ 4\beta(\beta^2 - 6)\sin\xi \cos\beta + \beta^4 \cos\xi \cos\beta$$

$$- 12(\beta^2 - 2)\cos\xi \cos\beta - 4\beta(\beta^2 - 6)\cos\xi \sin\beta - 24\cos\xi$$

$$\left.+ \beta^4(\alpha_s - \beta)\sin\xi \cos\beta - \beta^4(\alpha_s - \beta)\cos\xi \sin\beta\right]$$

$$+ \frac{1}{2}A_3\left[2\beta\sin\xi \cos\beta + (\beta^2 - 2)\sin\xi \sin\beta\right.$$

$$- 2\beta \cos\xi \sin\beta + (\beta^2 - 2)\cos\xi \cos\beta + 2\cos\xi$$

$$\left.+ \beta^2(\alpha_s - \beta)\sin\xi \cos\beta - \beta^2(\alpha_s - \beta)\cos\xi \sin\beta\right]$$

$$+ A_4\left[-\sin\xi \sin\beta + \cos\xi - \cos\xi \cos\beta + \frac{1}{2}\beta \sin\xi\right.$$

$$+ \frac{1}{4} \sin \xi \sin 2\beta - \frac{1}{2} \cos \xi \sin^2 \beta - (\alpha_s - \beta) \sin \xi \cos \beta$$

$$+ (\alpha_s - \beta) \cos \xi \sin \beta + (\alpha_s - \beta) \sin \xi \cos^2 \beta$$

$$- (\alpha_s - \beta) \cos \xi \sin \beta \cos \beta \Big] \Big\}$$

where Eqs. (3-15), (3-16), and (3-17) are generated by letting $\xi = 0$, β, and α_s, respectively.

C. Modified Winkler-Bach Equation

The strain distribution through the wall thickness of the split set has been determined by using curved beam analysis. The Winkler-Bach equation for curved beams has been modified to include plastic straining (ε^P) and axial (in-plane) loads N; hence, the normal strain (ε) distribution is given by the expression

$$\varepsilon = \left[\frac{R_i - R}{R} - \frac{N(R + R_i)}{EaR} - \frac{1}{a} \int \varepsilon^P \, da\right] \cdot \left(\frac{z}{1 + z}\right) \left[1 + \frac{1}{z} \left(\frac{y}{R + y}\right)\right] + \frac{1}{a} \int \varepsilon^P \, da + \frac{N}{Ea} \tag{3-18}$$

and the moment (M) at a typical section becomes

$$M = EaR \left[\frac{R_i - R}{R} - \frac{N(R + R_i)}{EaR} - \frac{1}{a} \int \varepsilon^P \, da\right] \left(\frac{z}{1 + z}\right) - E \int y \, \varepsilon^P \, da \tag{3-19}$$

where

R_i = initial split-set radius

E = Young's modulus

y = distance from centroidal axis

a = area experiencing normal strain (ε), a = Lt

L = length of split set

t = wall thickness

z = section property

$$z = -1 + \frac{R}{t} \ln \left[\frac{R + t/2}{R - t/2}\right]$$

D. Solution Procedure

The force (F) required to insert the split set into an undersize hole of radius R is

$$F = 2f\left[\int_0^{\beta} P\,(\theta)\, L\, R d\theta + F_s\right]$$

or, using Eq. (3-1)

$$F = 2f\left[RL(C_2\beta + \frac{1}{3}C_4\beta^3 + \frac{1}{5}C_6\beta^5) + F_s\right] \qquad (3\text{-}20)$$

Thus, the insertion, or holding, force can be found once the constants C_i, the half angle of contact β, and the force at the slit have been determined.

Before proceeding with a numerical solution, it will be advantageous to nondimensionalize the equations. This can be done by introducing the nondimensional variables as follows:

$$S = \frac{\sigma}{\sigma_o} \qquad \text{stress}$$

$$\varepsilon = \frac{\varepsilon}{\varepsilon_o} \qquad \text{total strain}$$

$$\varepsilon^P = \frac{\varepsilon^P}{\varepsilon_o} \qquad \text{plastic strain}$$

$$\eta = \frac{2y}{t} \qquad \text{distance from centroid}$$

$$m = \frac{E^P}{E} \qquad \text{strain hardening coefficient} \qquad (3\text{-}21)$$

$$R^* = \frac{R}{t} \qquad \text{radius}$$

$$\varepsilon_R = \frac{R_i - R}{R\varepsilon_o} \qquad \text{radial strain (interference)}$$

$$M^* = \frac{4M}{\sigma_o t^2 L} \qquad \text{moment at any section}$$

$$F^* = \frac{F}{RL\sigma_o} \qquad \text{insertion force}$$

$$N^* = \frac{N}{Ea\varepsilon_o} \qquad \text{in-plane force}$$

$$A_i^* = \frac{A_i}{\sigma_o} \qquad \text{constants}$$

$$C_i^* = \frac{C_i}{C_o}$$

$$z^* = z$$

where σ_o and ε_o are the material yield stress and yield strain, respectively, and E and E^P are the slopes of the stress-strain curve in the elastic and plastic regions, respectively.

The nondimensional strain and moment relations become

$$\varepsilon = \left[\varepsilon_R - 2N^* - \frac{1}{2}\int_{-1}^{1} \varepsilon^P d\eta\right] \cdot \left[\frac{z^*}{1 + z^*}\right] \cdot \left[1 + \frac{1}{z^*}\left(\frac{\eta}{2R^* + \eta}\right)\right] + \frac{1}{2}\int_{-1}^{1} \varepsilon^P d\eta + N^* \tag{3-22}$$

$$M^* = 4R^*\left[\varepsilon_R - 2N^* - \frac{1}{2}\int_{-1}^{1} \varepsilon^P d\eta\right]\left[\frac{Z^*}{1 + Z^*}\right] - \int_{-1}^{1} \eta\varepsilon^P d\eta \tag{3-23}$$

where

$$\varepsilon^P = 0 \qquad -1 \le \varepsilon \le 1$$

$$\varepsilon^P = (1 - m)(\varepsilon - 1) \qquad \varepsilon > 1$$

$$\varepsilon^P = (1 - m)(\varepsilon + 1) \qquad \varepsilon << -1$$

$$S = \varepsilon \qquad -1 \leq \varepsilon \leq 1$$

$$S = m(\varepsilon - 1) + 1 \qquad \varepsilon > 1 \tag{3-24}$$

$$S = m(\varepsilon + 1) - 1 \qquad \varepsilon < -1$$

$$Z^* = -1 + R^* \ln\left[\frac{R^* + 0.5}{R^* - 0.5}\right]$$

The nondimensional form of the boundary condition Eqs. (3-12), (3-14), (3-15), (3-16), and (3-17) are easily recognized, and the concentrated loading Eqs. (3-3) and (3-4), become

$$N^* = -f F^*_s R^* \cos\alpha_s - F^*_s R^* \sin\alpha_s$$

$$-R^* \left[-A^*_4 + A^*_4 \cos\beta - (A^*_1 - 3A^*_2 + 12 C^*_6)\beta^2 \cos\beta \right. \tag{3-25}$$

$$\left. -C^*_6 \beta^4 \cos\beta + A^*_3 \beta \sin\beta + A^*_2 \beta^3 \sin\beta\right]$$

$$F^*_s = \left(\frac{1}{f \sin\alpha_s - \cos\alpha_s}\right)\left[-A^*_4 \sin\beta + C^*_6 \beta^4 \sin\beta \right. \tag{3-26}$$

$$\left. + (A^*_1 - 3A^*_2 + 12C^*_6)\beta^2 \sin\beta + A^*_3 \beta \cos\beta + A^*_2 \beta^3 \cos\beta\right]$$

Equation (3-2) can be put in nondimensional form and solved explicitly for β to yield

$$\beta = \sqrt{\frac{-\left(\frac{C^*_1}{2}\right) \pm \left[\left(\frac{C^*_1}{2}\right)^2 + (C^*_3)\left\{\frac{M^*_w - 4fF^*_s(R^*)^2 - 4N^*R^*}{4(R^*)^2}\right\}\right]^{1/2}}{C^*_3/2}} \tag{3-27}$$

and, finally, the dimensionless insertion force (F^*) is

$$F^* = 2f\left[C^*_2\beta + \frac{1}{3}C^*_4\beta^3 + \frac{1}{5}C^*_6\beta^5 + F^*_s\right] \qquad (3\text{-}28)$$

The procedure for solving this system of equations is as follows:

(1) Assign values to the system parameters

f = coefficient of friction

R = radius of hole

R_i = initial radius of split set

t = wall thickness

E = Young's Modulus

α_s = angle to split

L = length of split set

I = second moment of area

a = area of section

σ_0 = yield stress

(2) Assign trial values for N^* and β.

(3) Calculate the strains from Eq. (3-22) as follows:

a) Assume to start that ε^P is zero for all values η.

b) Calculate ε for each value of η from Eq. (3-22).

c) If $-1 \leq \varepsilon \leq 1$ for all η, the strains are all elastic and this is the solution.

d) If $|\varepsilon| > 1$ for any value of η, use Eq. (3-24) to determine ε^P.

e) Use the values of ε^P computed in Step(d) with Eq. (3-22) to obtain better values for ε.

f) Repeat this process until convergence is achieved.

(4) Calculate M^* from Eq. (3-23).

(5) Solve the system of five boundary condition Eqs. (3-12), (3-14), (3-15), (3-16), and (3-17) for A^*_1, A^*_2, A^*_3, A^*_4, and N^*.

(6) Use the new value for N^* found in Step (5) and return to Step (2). Continue until N^* converges.

(7) Calculate F^*_s and C^*_6 from Eqs. (3-26) and (3-25).

(8) Calculate C^*_1, C^*_2, C^*_3, and C^*_4 from Eq. (3-11).

(9) Calculate β from Eq. (3-27) and return to Step (2). Continue until β converges.

(10) Calculate F* from Eq. (3-28).

A computer program has been written in accordance with the previous solution procedure, and a listing of the program is presented, with input instructions, in Appendix A. Plot routines have also been developed for graphically displaying the results and these routines are an integral part of the computer program.

Analytical Results

The iterative solution of Eq. (3-22) provides a distribution of the total normal strain through the wall thickness of the split-set tube. This distribution is presented in Figs. 3-4 and 3-5 for a family of interference values (ε_R) and for the specified values of α_s (one-half angle of the split-set cross section), R* (radius ratio R/t), and m (strain hardening coefficient). The corresponding normal stress (s) distribution is shown in Fig. 3-6.

The surface loadings, P and τ in Eq. (3-1), that the geologic media exerts on an installed split set are plotted in Fig. 3-7 for a family of ε_R (interference) values. The loading constants C_i are given in Table 3-1. Also presented in Table 3-1 are the numerical data for N*, M*, F^*_s, β, and the equivalent average radial pressure P* that is defined as

$$P^* = \left(\frac{1}{\sigma_o RL\alpha_s}\right) \left[\int_0^\beta P(\theta)\, LRd\theta + F_s\right]$$

or, from Eq. (3-28)

$$P^* = F^*/2\pi f \qquad (3\text{-}29)$$

The average radial pressure (P*) can be compared directly to the performance of the "Swell Bolt" which is a new roof bolt design now being investigated analytically.

The most important results of the split-set analysis are presented in Figs. 3-8, 3-9, 3-10, and 3-11. These are plots of the nondimensional insertion force as a function of radius ratio (R*) and the interference (ε_R). Thus, for a given split-set geometry (R, t, α_s, m, f, and σ_o are specified) the insertion, or holding force (F) can be calculated from the use of Figs. 3-8, 3-9, 3-10, or 3-11 and the relation $F = RL\sigma_o F^*$.

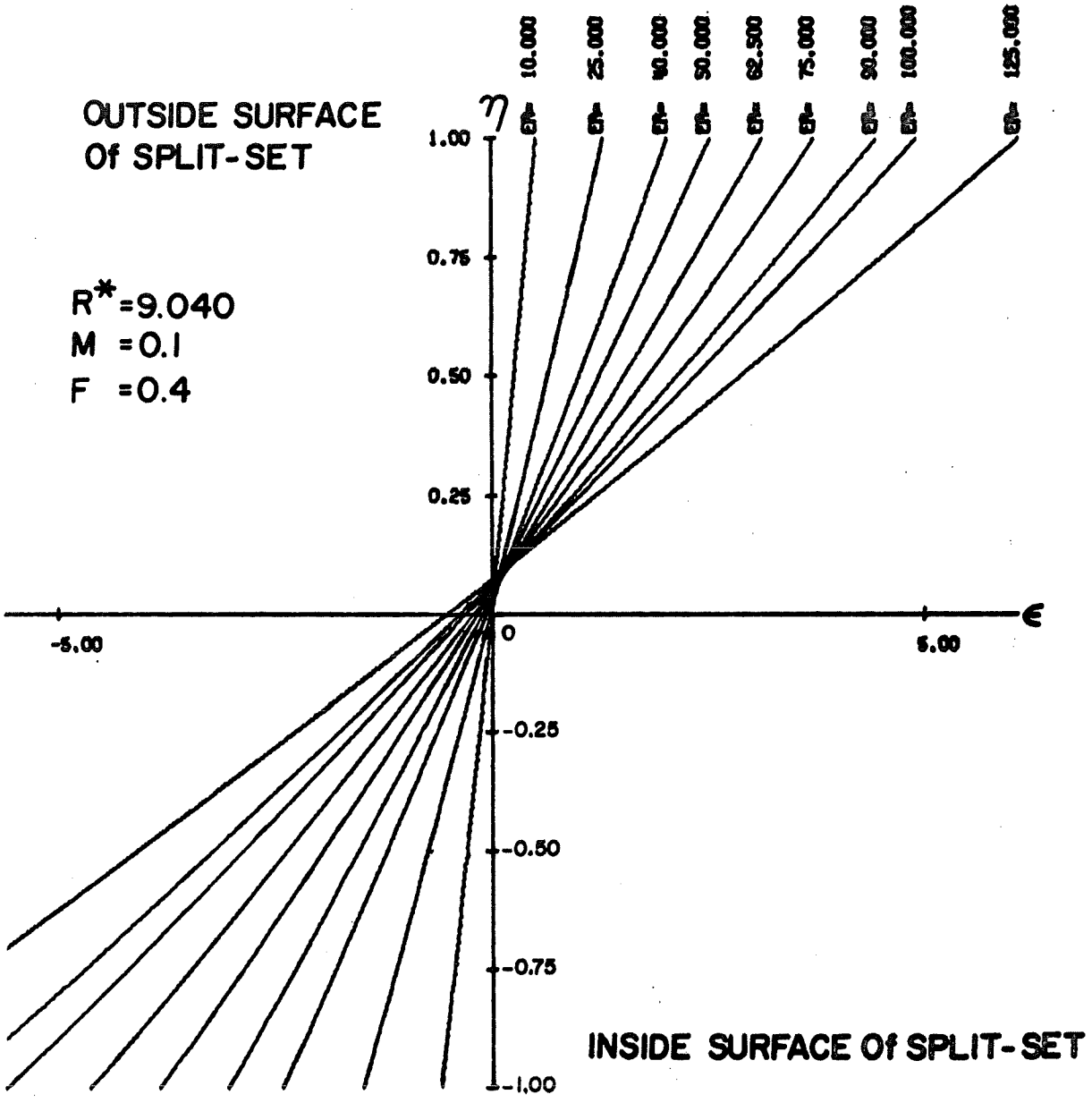

Fig. 3-4 Normal Strain Distribution Through the Split-Set Wall. Variable Interference (ER)

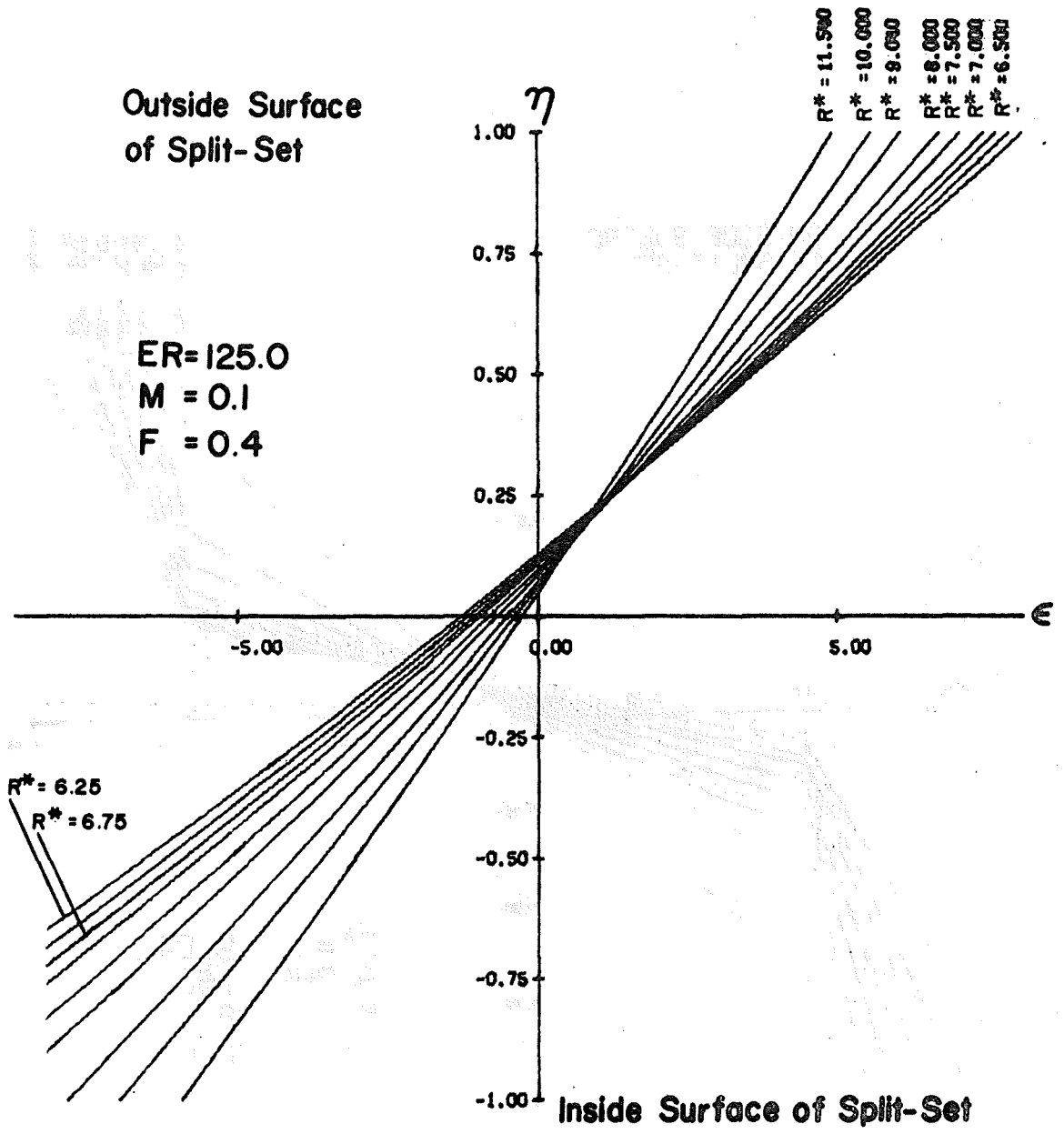

Fig. 3-5 Normal Strain Distribution Through the Split-Set Wall. Variable Radius Ratio (R*)

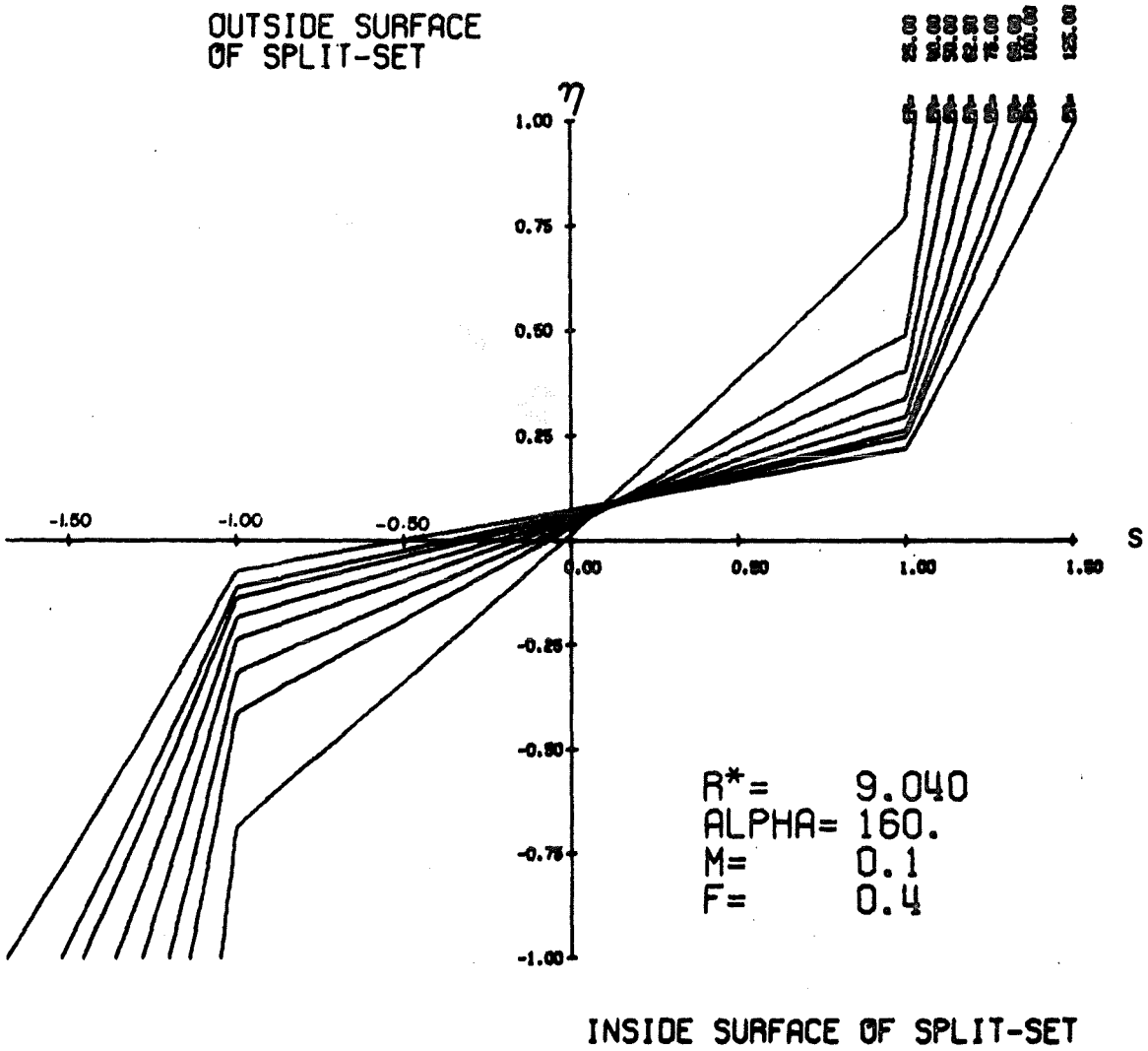

Fig. 3-6 Normal Stress Distribution Through the Split-Set Wall. Variable Interference (ER)

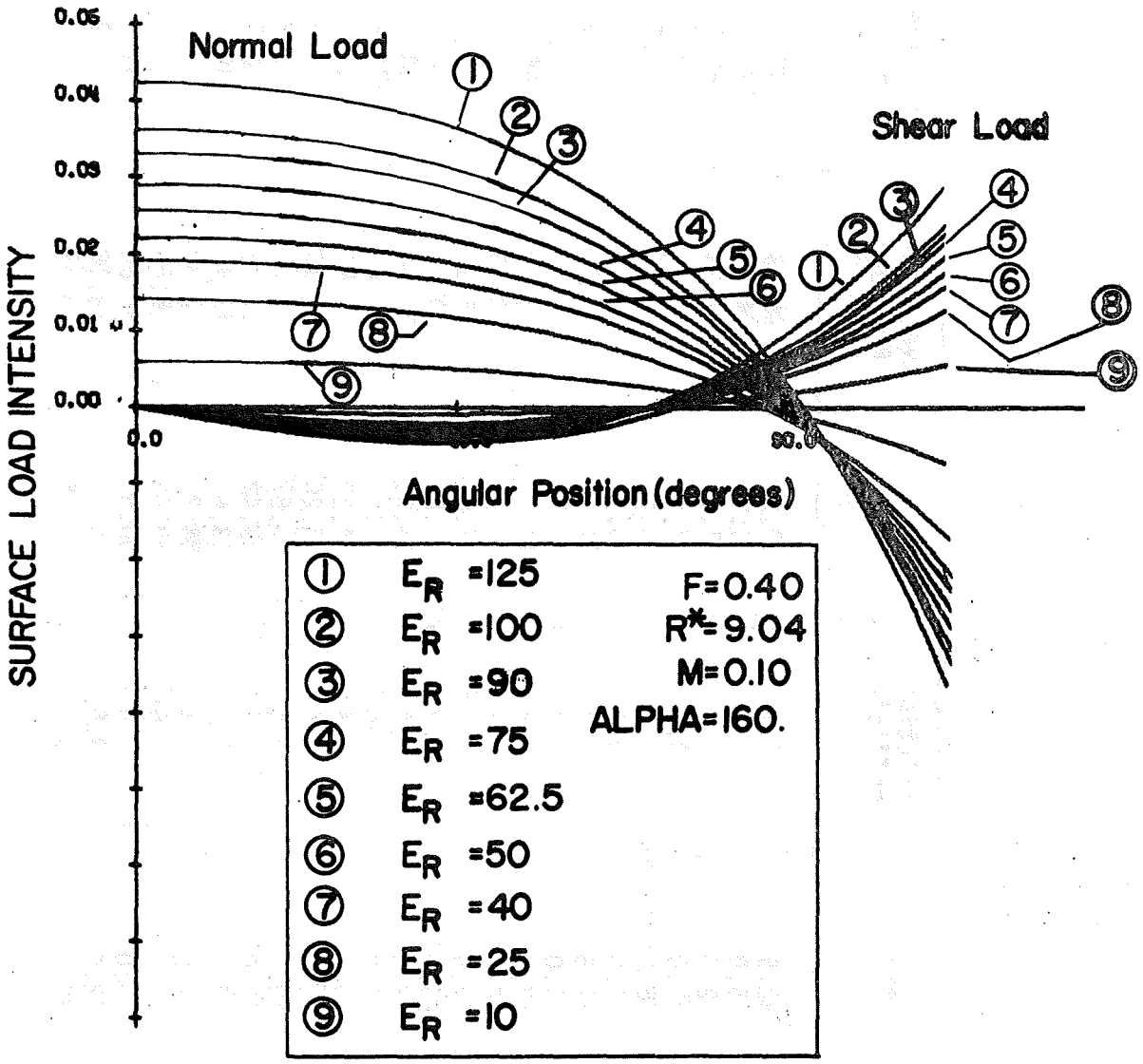

Fig. 3-7 Surface Loading

TABLE 3-1

Numerical Data for Split-Set Analysis

Case No.	Radius Ratio R*	Interference ε_R	Friction Coefficient f	Insertion force $F^* \cdot 10^3$	Ave. Radial Pressure $P^* \cdot 10^3$	In-Plane Force $N^* \cdot 10^3$	Moment M*
1	6.25	62.5	0.1	19.37	30.83	-137.7	1.22
2	6.25	125.0	0.1	34.24	54.49	-271.1	1.56
3	9.04	62.5	0.1	7.00	11.14	- 66.8	1.11
4	9.04	125.0	0.1	12.01	19.11	-130.5	1.35
5	11.54	62.5	0.1	3.60	5.73	- 41.5	1.04
6	11.54	125.0	0.1	6.05	9.63	- 80.5	1.25
7	6.25	62.5	0.2	41.28	32.85	-137.9	1.22
8	6.25	125.0	0.2	72.73	57.88	-271.3	1.56
9	9.04	62.5	0.2	14.94	11.89	- 66.9	1.11
10	9.04	125.0	0.2	25.55	20.33	-130.6	1.35
11	11.54	62.5	0.2	7.68	6.11	- 41.6	1.04
12	11.54	125.0	0.2	12.88	10.25	- 80.6	1.25
13	6.25	62.5	0.4	94.35	37.54	-138.2	1.22
14	6.25	125.0	0.4	165.1	65.69	-271.8	1.56
15	9.04	62.5	0.4	34.29	13.64	- 67.1	1.11
16	9.04	125.0	0.4	58.20	23.16	-130.9	1.35
17	11.54	62.5	0.4	17.67	7.03	- 41.7	1.04
18	11.54	125.0	0.4	29.42	11.71	- 80.8	1.25
19	6.25	62.5	0.6	163.6	43.40	-138.6	1.22
20	6.25	125.0	0.6	284.2	75.39	-272.5	1.56
21	9.04	62.5	0.6	59.69	15.83	- 67.3	1.11
22	9.04	125.0	0.6	100.5	26.66	-131.3	1.35
23	11.54	62.5	0.6	30.85	8.18	- 41.9	1.04
24	11.54	125.0	0.6	50.96	13.52	- 81.1	1.25

TABLE 3-1 (continued)

Case No.	Loading Constants for Equation (1)					Edge Force $F_s^* \cdot 10^3$	Contact Angle β
	$C_1 \cdot 10^3$	$C_2 \cdot 10^3$	$C_3 \cdot 10^3$	$C_4 \cdot 10^3$	$C_6 \cdot 10^3$		
1	-10.83	71.62	11.38	-18.02	-5.97	42.34	116.0153
2	-15.56	122.50	17.89	-28.85	-9.61	72.24	117.3649
3	- 4.43	26.48	4.45	- 6.95	-2.29	15.59	115.1222
4	- 6.07	43.65	6.64	-10.62	-3.53	25.80	116.6972
5	- 2.47	13.82	2.42	- 3.73	-1.22	8.08	114.4947
6	- 3.30	22.27	3.50	- 5.56	-1.84	13.16	116.1854
7	-12.69	70.93	11.20	-16.37	-5.81	44.32	115.9480
8	-18.59	121.40	17.58	-26.19	-9.36	75.56	117.3158
9	- 5.13	26.22	4.39	- 6.31	-2.23	16.29	115.0578
10	- 7.17	43.24	6.53	- 9.65	-3.44	27.04	116.6357
11	- 2.84	13.68	2.40	- 3.39	-1.19	8.44	114.4194
12	- 3.87	22.05	3.45	- 5.05	-1.79	13.76	116.1089
13	-17.03	69.33	10.81	-12.50	-5.46	49.03	115.7922
14	-25.62	118.80	16.86	-20.01	-8.79	83.35	117.1729
15	- 6.78	25.60	4.26	- 4.83	-2.10	18.12	114.8813
16	- 9.75	42.29	6.29	- 7.36	-3.23	29.83	116.4905
17	- 3.72	13.35	2.33	- 2.60	-1.12	9.40	114.2445
18	- 5.22	21.56	3.32	- 3.85	-1.69	15.26	115.9672
19	-22.47	67.33	10.33	- 7.63	-5.02	54.94	115.5926
20	-34.38	115.60	15.99	-12.29	-8.08	93.06	116.9990
21	- 8.86	24.83	4.09	- 2.94	-1.93	20.30	114.6641
22	-12.98	41.12	5.98	- 4.51	-2.97	33.33	116.3071
23	- 4.83	12.94	2.25	- 1.58	-1.03	10.54	114.0299
24	- 6.90	20.94	3.17	- 2.35	-1.55	17.06	115.7712

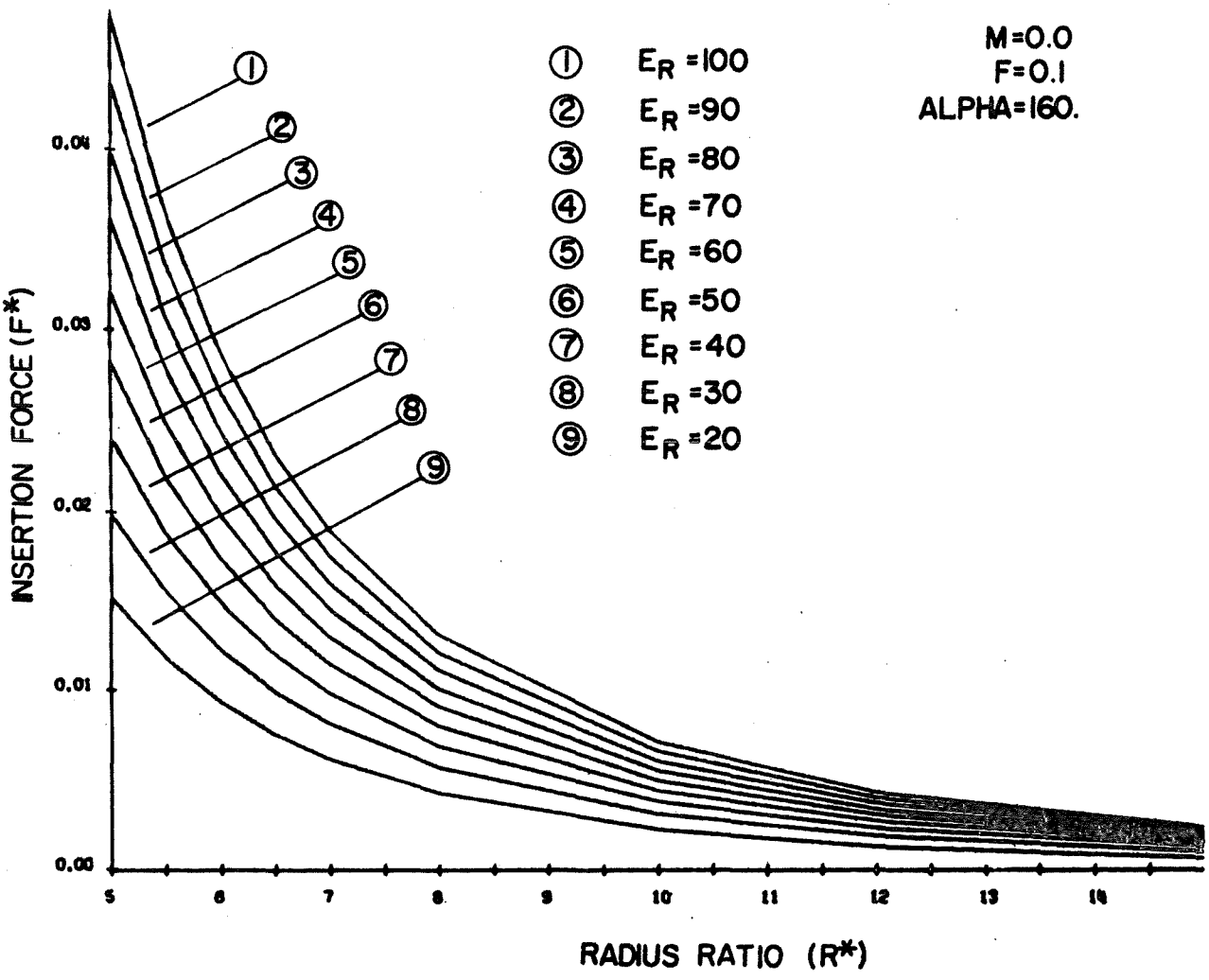

Fig. 3-8 Insertion Force.
Variable Interference (ER), Friction Coefficient of 0.1

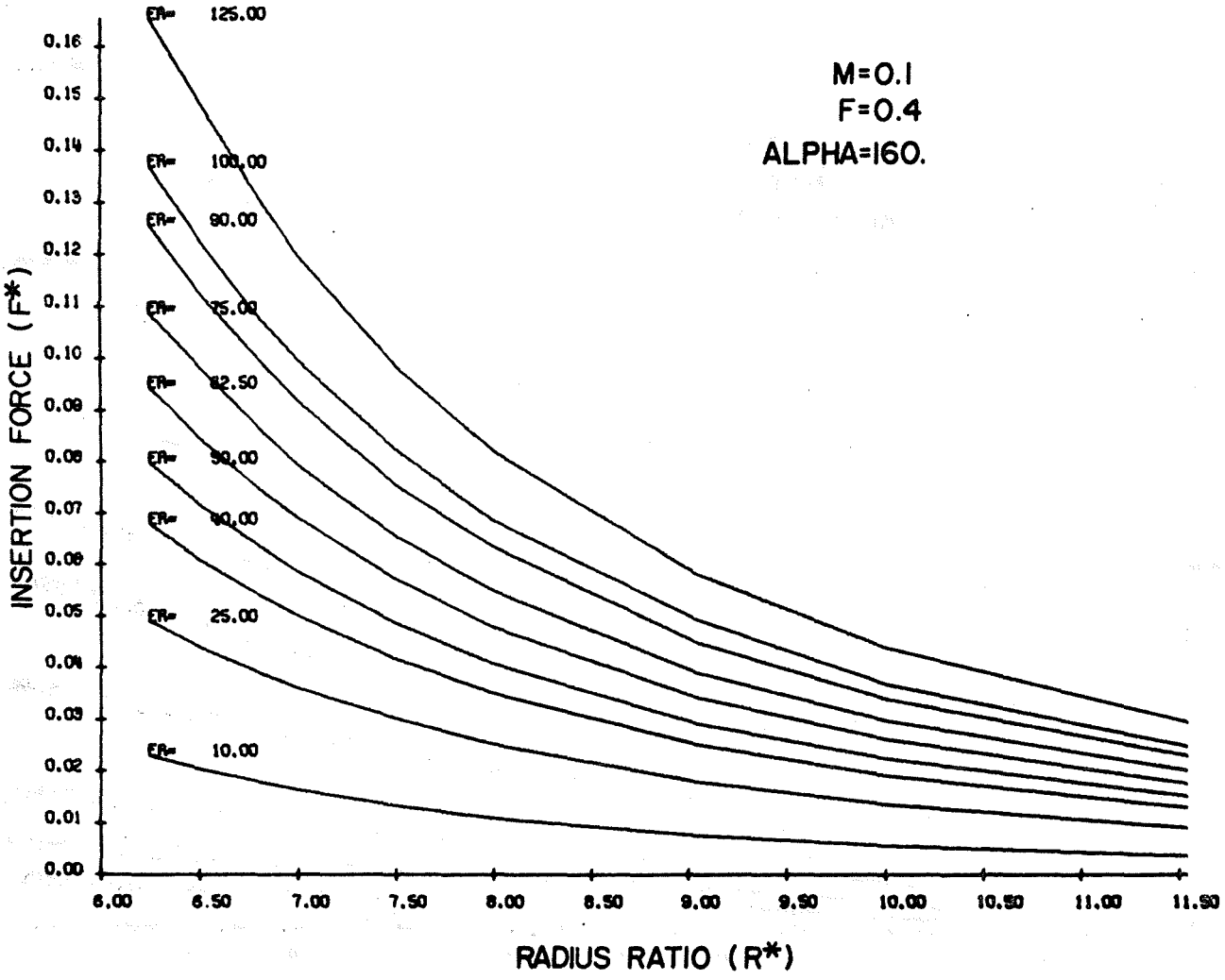

Fig. 3-9 Insertion Force.
Variable Interference (ER). Friction Coefficient of 0.4

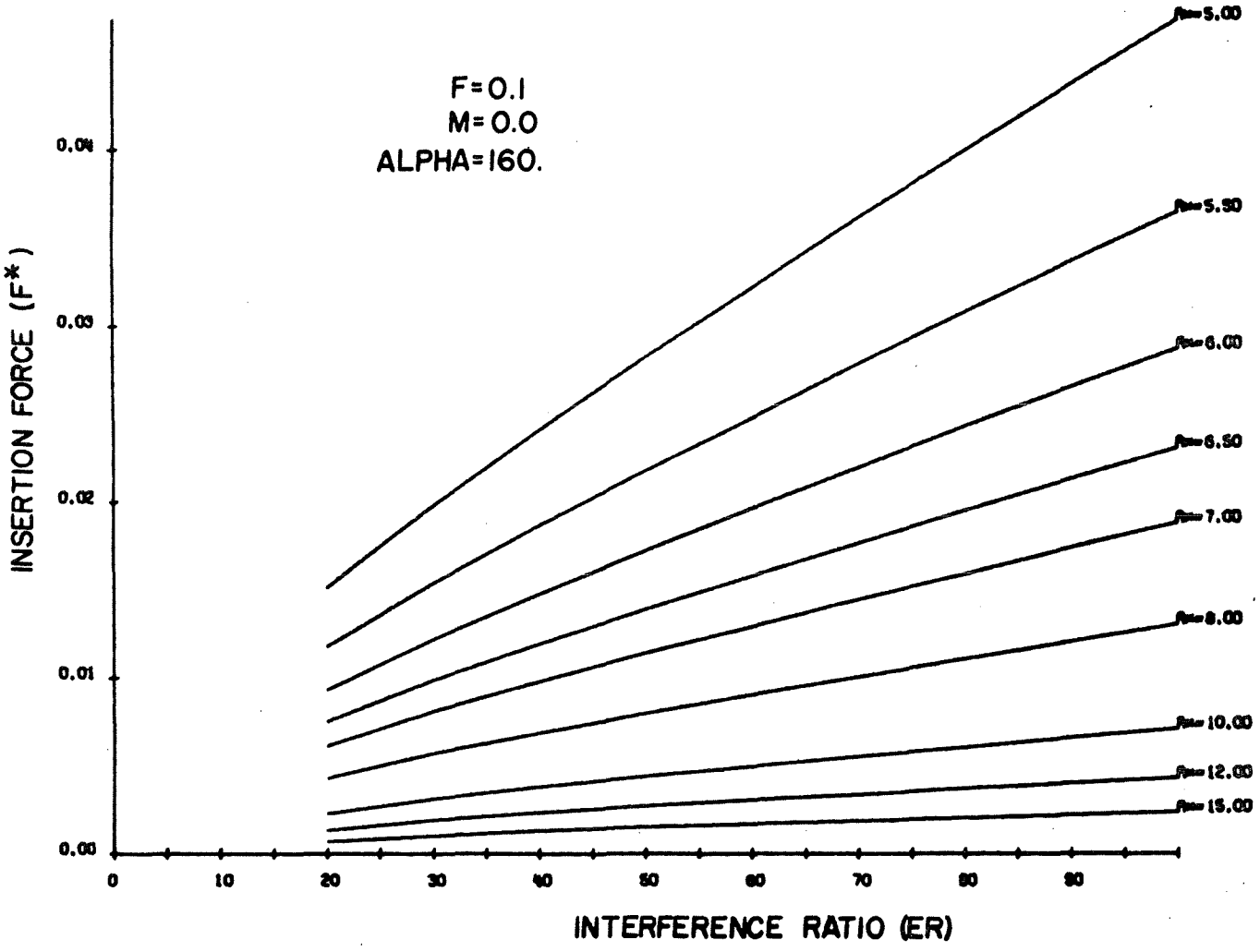

Fig. 3-10 Insertion Force.
Variable Radius Ratio (R*). Friction Coefficient of 0.1

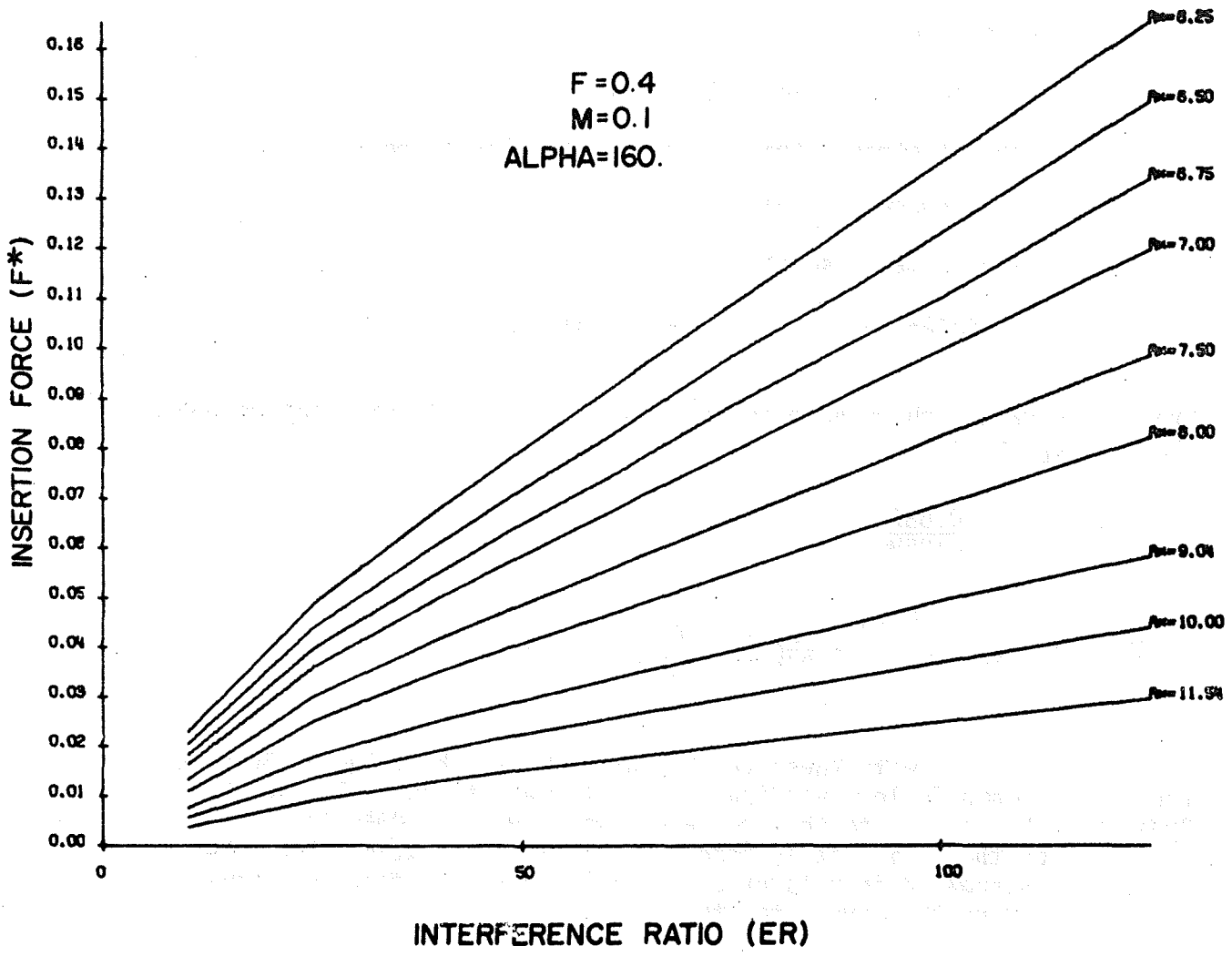

Fig. 3-11 Insertion Force.
Variable Radius Ratio (R*). Friction Coefficient of 0.4

To illustrate, consider a 1.5-inch diameter split set that is to be inserted into a 1.375 inch diameter drilled hole. The split set has the following geometric and material characteristics:

R_i = split-set radius - 0.750 in.

R = hole radius - 0.6875 in.

t = thickness - 0.0688 in.

L = length - 4 ft

α_s = half angle (see Fig. 3-1) - 160°

m = slope of stress-strain curve in the plastic region - 0.0

ε_o = yield strain - 0.00182 in./in.

σ_o = yield stress - 50,000 lb/in.^{2}

f = coefficient of friction between the split set and the rock - 0.1

From these values the nondimensional radius ratio (R*) and interference (E_R) or (ε_R) become

$$R^* = R/t = \frac{0.6875}{0.0688} = 10.0$$

$$(E_R) \text{ or } (\varepsilon_R) = \frac{R_i - R}{R_o} \quad \frac{0.750 - 0.6875}{(0.6875)(0.00182)} = 50.0$$

Entering Fig. 3-12 with these values, one selects the value of 50.0 on the abscissa and follows vertically to intersect the R* = 10.0 curve. Projecting horizontal to the ordinate gives a value 0.0044 for F*. If 24 inches of the split set is embedded in a layer of stable rock, and 24 inches is engaged in a layer of unstable rock, the force (F) available for holding the layers together is

$$F = RL\sigma_o F^* = (0.6875)(24)(50{,}000)(0.0044)$$

$$F = 3{,}630 \text{ lb}$$

Experimental Data

The most significant data available is that documented by Scott and shown in Table I of Reference 7. This data was collected in a mining environment and it represents the effects of a reasonable variation of the split-set parameters. Scott's data have been put in terms of the nondimensional parameters used in the analysis presented previously, and the results are documented in Table 3-2. The materials used by Scott were classified

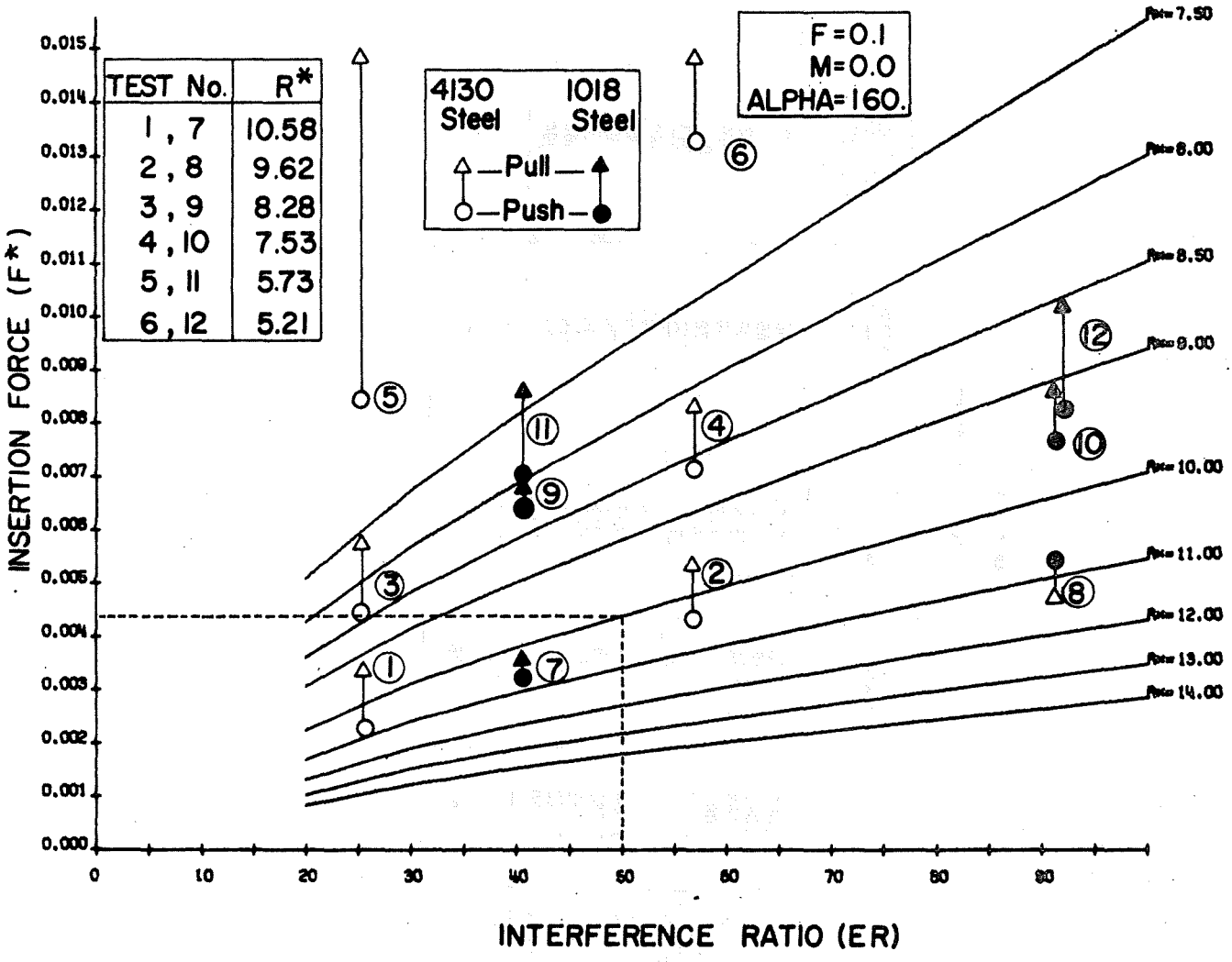

Fig. 3-12 Insertion Force.
Variable Radius Ratio (R*)

TABLE 3-2

Experimental Data for Split-Sets

Data Source	Test No.	Material	Hole Size	Wall Thickness	Radius Ratio R*	Interference ε_R	Average Insertion Force per inch F/L	Average Pull Force per inch F/L	Insertion Force $F^*.10^3$	Pull Force $F^*.10^3$
Scott[1]	1	4130 Steel	1.375	0.065	10.58	26.0	156	229	2.27	3.33
	2		1.250	0.065	9.62	57.2	266	330	4.26	5.28
	3		1.375	0.083	8.28	26.0	298	392	4.33	5.70
	4		1.250	0.083	7.53	57.2	439	514	7.02	8.22
	5		1.375	0.120	5.73	26.0	578	1014	8.41	14.75
	6		1.250	0.120	5.21	57.2	904	1013	13.15	14.74
	7	1018 Steel	1.375	0.065	10.58	41.6	136	149	3.17	3.47
	8		1.250	0.065	9.62	91.5	209	182	5.35	4.66
	9		1.375	0.083	8.28	41.6	276	294	6.42	6.84
	10		1.250	0.083	7.53	91.5	296	331	7.58	8.47
	11		1.375	0.120	5.73	41.6	299	366	6.96	8.52
	12		1.250	0.120	5.21	91.5	316	394	8.09	10.09
Strosnider[2]	min.	1018 Steel	1.375	0.083	8.28	41.6	130	90	3.02	2.09
	max.		1.375	0.083	8.28	41.6	150	120	3.49	2.79

as being 1018 and 4130 steel with assumed yield stresses of 40,000 psi and 60,000 psi, respectively. Strosnider (Ref. 3) tested a sample 1018 steel split set and found a yield stress of 62,500 psi and a strain hardening coefficient (m) of zero. Also, Byars and Snyder (p. 371, Ref. 8) indicate that 4130 steel has a yield stress of 100,000 psi. Thus, in reducing Scott's data (e.g., $F^* = F/RL\sigma_o$) yield stress (σ_o) values of 62,500 psi and 100,000 psi were used for 1018 and 4130 steel, respectively. Since the forming operation and heat treatment applied to the split set affects the yield stress, it is important that the designer know the actual value before attempting to estimate the holding capacity of a given split-set design.

Analytical curves of insertion force (F^*) versus interference (ε_R) and radius ratio (R^*) have been generated for a friction coefficient of 0.1 and a strain hardening coefficient of zero. These curves are presented in Figs. 3-12 and 3-13 with the experimental data of Scott's (Table 3-2). The analytical curves appear to agree well with the experimental data for values of R^* (radius ratio R/t) above 8.0 and for ε_R (interference values $\frac{R_i - R}{R\varepsilon_o}$) below 75. That is, for small thick-walled split sets, or for large interference fits between the hole and the split set, the analytical and experimental data may not be consistent. This is not considered to be a serious drawback to the analysis since all of the split sets being used in practice fall within the limits specified. Thus, the program presented in Appendix A should be quite useful for preparing analytical predictions of the holding capacity of various split-set designs.

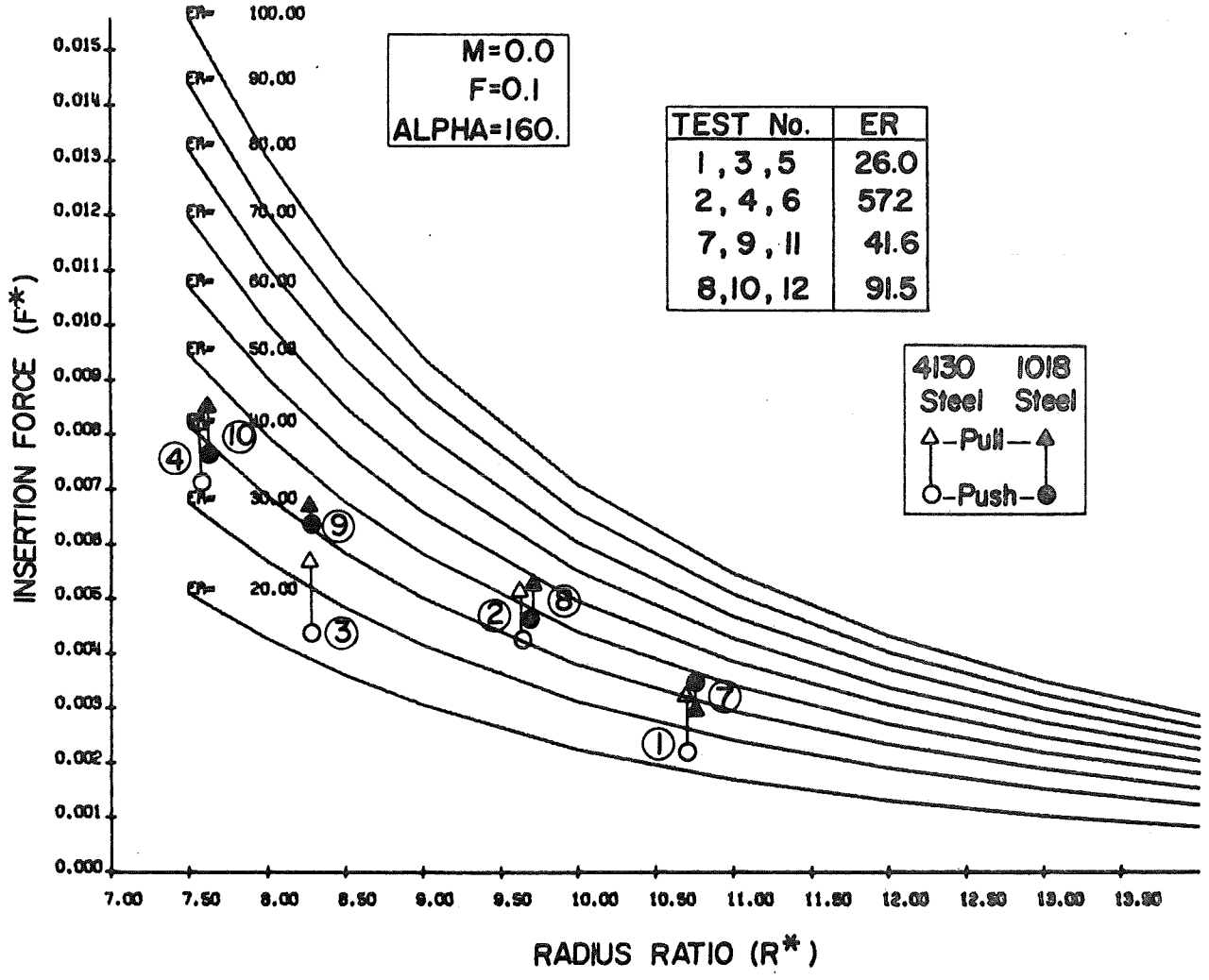

Fig. 3-13 Insertion Force.
Variable Interference (ER)

Chapter IV

SHEAR TESTS and ANALYSIS

Introduction

The resistance which rock bolts offer to shear movements along fracture planes and bedding planes in a mine roof has been suggested as one of the mechanisms by which bolts contribute to the support of the roof. That such displacements do occur is a fact fairly well known. Inspections of drill holes that have been in the roof for some time often reveal that the holes have been offset at one or more points some time after drilling. Resin grouted bolts are often cited as being better able to resist shear movement in the roof because the annulus around the steel bar is filled with grout whereas the sides of a conventional bolt will not contact the rock until a rather large shear displacement has occurred.

When this project began, there were no experimental data to support or refute the above arguments. A laboratory shear test program was therefore devised to evaluate the effectiveness of various types of bolts in resisting shear under various conditions which exist in-situ.

The case of a conventional bolt intersecting a shear surface was analyzed theoretically up to the point where the bolt begins to contact the rock. The magnitudes of the shear displacements between two elastic beams were also analyzed in an attempt to bracket the limits of shear displacements for elastic behavior of bedded mine roofs.

Theoretical Analysis - Conventional Bolts

This simplified analysis of shear resistance applies to conventional expansion-anchor type bolts intersecting shear planes in rocks. In this bolting system the body of the bolt does not fill the hole and thus a certain amount of shear movement may occur before the bolt makes contact with the rock. Changes in bolt load are also allowed to occur in the analysis as the bolt is stretched or shortened. Another approach to this problem made by Horino, et al., (Ref. 9) assumes that the bolts completely fill the hole such as is the case for fully grouted bolts, and that the bolt tension remains constant as deformation occurs.

The analysis considers two blocks of rock bolted together and sheared as shown in Fig. 4-1. The two blocks correspond to the laboratory shear test geometry and to the volume of influence of a typical bolt in a systematic bolting pattern.

The following assumptions referenced to Fig. 4-1, are made:

1. The blocks remain in uniform contact as the shear progresses, i.e., there is no rotation of either block.

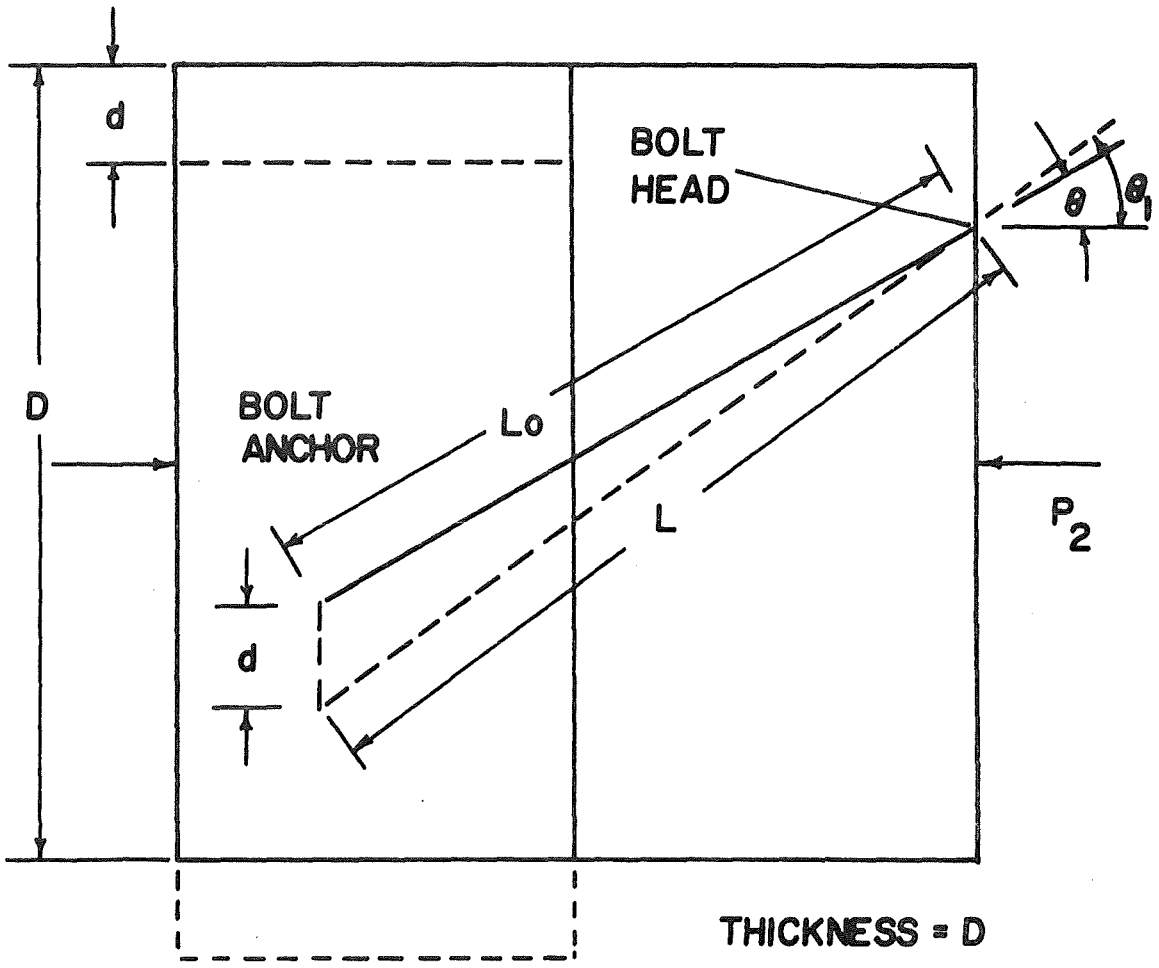

SOLID LINES – INITIAL POSITION
DASHED LINES – DISPLACED POSITION

Fig. 4-1 Geometry of Conventional Bolt Subjected to Shear Displacement

2. The normal load P_2 applied to the exterior of the blocks provides an average normal stress σ_n over the shear area D(D-d).

3. The coefficient of friction along the interface is constant.

4. The blocks of rock are rigid.

5. The bolt is linearly elastic up to the yield strength. Bolt load is constant for strains above the elastic limit.

6. The bolt anchor does not slip for tensile bolt loads.

7. The bolt will not support compressive loads since the anchor loosens.

8. The bolt has some installed tension when the shear displacement d is zero.

The average strength of the interface without a bolt is $\tau_o = \mu \sigma_n$ where μ is the coefficient of friction and σ_n is the average normal stress. The average shear stress when the bolt is installed is the sum of the stress required to slide the unbolted blocks and the stress required to overcome the additional resistance due to bolting.

The initial average shear stress with bolt for impending movement is given by

$$\tau_{ave} = \tau_o + \frac{\mu T_o \cos \theta + T_o \sin \theta}{A_s} \qquad (4\text{-}1)$$

where T_o = installed bolt tension

A_s = area in shear

θ = initial orientation of bolt.

When the shear displacement is increased to some value d, the distance from the anchor to the head is increased from L_o to L. This increase in length results in an increase in strain over the length of the bolt which will in turn result in increased bolt load up to the elastic limit. Above the elastic limit the bolt load is assumed to be constant. The orientation of the bolt also changes from θ to θ_1 during displacement d. The average shear stress at any displacement is then

$$\tau_{ave} = \tau_o + \frac{\mu T \cos \theta_1 + T \sin \theta_1}{A_s} \qquad (4\text{-}2)$$

where T = the bolt tension at displacement d

= 0 if compressive bolt loads are indicated

θ_1 = bolt orientation at displacement d

A_s = area in shear, D(D-d)

D = height and depth of the shear block

The new length of the bolt L is given by

$$L = \sqrt{d^2 + 2d\, L_o \sin\theta + L_o^2} \tag{4-3}$$

and the corresponding angle θ_1 is

$$\theta_1 = \arctan \frac{d + L_o \sin\theta}{L_o \cos\theta} \tag{4-4}$$

The tension T in the bolt is related to the bolt strain by

$$\begin{aligned} T &= E_b A_b (\varepsilon_o + \varepsilon_1) && \text{for } (\varepsilon_o + \varepsilon_1) < \varepsilon_y \\ T &= \text{yield load} = E_b A_b \varepsilon_y && \text{for } (\varepsilon_o + \varepsilon_1) > \varepsilon_y \end{aligned} \tag{4-5}$$

where E_b = Young's modulus for the bolt

A_b = cross-sectional area of the bolt

ε_o = axial strain induced by the initial torque applied to the bolt

ε_1 = increment of axial strain induced by shear displacement d

$$= \frac{L - L_o}{L_o}$$

ε_y = strain at onset of yielding.

It should be noted that Eq. (4-2) applies for either plus or minus values of θ_1. The tension T is non-negative so the frictional component $\mu T \cos\theta_1 / A_s$ will be positive for positive or negative values of θ_1. The tangential component of the bolt load, T sin θ_1, provides a positive contribution to the shear resistance for positive θ_1 and a negative contribution for negative θ_1.

The shear area, A_s, is equal to D(D-d) when blocks are sheared in the laboratory, however it would be equal to D^2 for shear of a typical bolt in a mine roof where the bolt spacing is square, D by D. The analysis which follows is in terms of the varying shear area D(D-d) since this corresponds to laboratory test situation.

Eq. (4-2) applies for shear displacements up to where the bolt begins to be sheared between the blocks. Beyond this point additional shear resistance is created by the direct shear effect on the bolt. This effect is not easily quantified by theory, even to a rough approximation, because large nonlinear deformation occur around the hole as the bolt is sheared, at least for the limestone and shale tested.

Eq. (4-2) was used to calculate theoretical curves of shear stress versus shear displacement for the conventional bolts and limestone rock and used in the experimental program. The properties and relevant dimensions are as follows:

L_o = 21.625 in. for θ = 0 degrees

= 27.625 for $\theta = \pm$ 45 degrees

$E_b = 28.65 \times 10^6$ psi

A_b = 0.2453 $in.^2$

ε_o = 1500 μ in./in.

Yield strength of bolt = 63,600 psi

$\varepsilon_y = 63{,}600/(28.65 \times 10^6) = 2220$ μ in./in.

The ratios of τ_{ave} to σ_n for shear tests on blocks of limestone without bolts were computed at shear displacements of 0.1, 0.5, 1.0, and 1.5 in. These ratios from 18 shear tests at the low normal pressure (σ_n = 25 psi) were averaged to obtain a coefficient of friction μ of 0.903. Similarly, the results from 16 tests at the high normal pressure (σ_n = 250 psi) were averaged to obtain a coefficient of friction of 0.871. The corresponding values of τ_o are 22.58 psi (for σ_n = 25 psi) and 217.7 psi (for σ_n = 250 psi).

The resulting theoretical curves of average shear stress versus shear displacement are shown in Fig. 4-2 for the two normal pressures, 25 and 250 psi, and three bolt orientations θ = 0, +45 and -45 degrees. The no-bolt curves are horizontal lines at 22.58 and 217.7 psi. The curves for -45-degree bolt orientation begin slightly below the no-bolt curves and follow along the no-bolt curves for displacements greater than 0.0586 in. In other words, the bolts loosen completely after only 0.0586 in. of displacement. On the other hand, bolts at +45 degrees experience rapid increases in tension with shear displacement until they yield at 0.0281 in. shear displacement. A more gradual increase in shear stress occurs for bolts oriented at 0 degrees with yielding occurring at 0.8207 in. shear displacement.

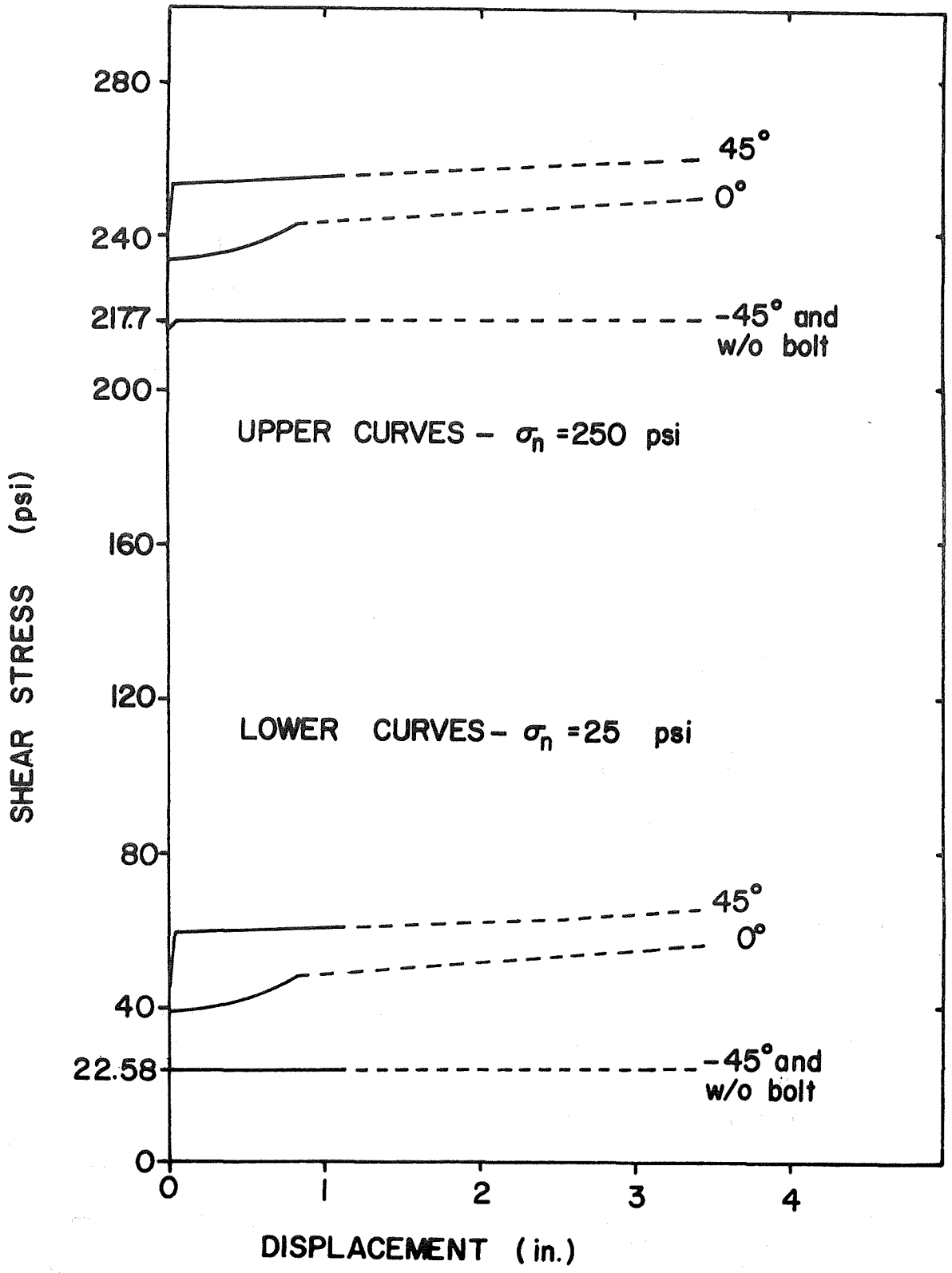

Fig. 4-2 Theoretical Relationship between Shear Stress and Shear Displacement for Conventional Bolts

It should be noted that the theoretical curves (with bolt) do not include the increase in shear resistance caused by direct shear of the bolt as interference develops between the bolt and the sides of the offset drill hole. This occurs when the shear displacement reaches 0.816 in. for the bolts oriented normal to the shear surface and 1.154 in. for the bolts inclined at +45 degrees and -45 degrees. Therefore one can expect the shear strengths to increase beyond those plotted in Fig. 4-2 for displacements greater than these values. The curves are thus shown dashed for displacements above the points of interference.

It is seen (Fig. 4-2) that bolts can be expected to contribute significantly to the shear strength at the low normal pressure of 25 psi for the 0-and +45-degree orientations since these curves are significantly above the curve for the unbolted joint. The increase in shear strength created by the bolts at the high normal pressure of 250 psi is not so significant, however, when compared to the strength of the unbolted joint. In other words, the relative importance of bolts in resisting shear is greater when the sliding blocks of rock are held together only slightly than when large normal pressures are present.

Shear Displacement Between Similar Roof Beams

The approximate magnitudes of the shear displacements which occur between roof beams under idealized conditions of homogeneity, continuity (no fractures), elastic behavior, and gravity loading were determined so that these magnitudes could be compared with those observed in the field and with those used in the shear test program.

The two gravity-load beams (Fig. 4-3) are assumed to have restrained ends and equal thicknesses. The beam material is linearly elastic with Young's modulus E being the same for both beams. It is also assumed that the frictional strength of the interface is zero.

The gravity loading is approximated by a uniformly distributed load per unit length of the beam q. The depth of beam normal to the plane of drawing (Fig. 4-3) is taken as one unit. The distributed load acting on each beam is therefore $q = \gamma t$, where γ is the unit weight of the material and t is the thickness of the beam.

Since the two beams have the same thickness and the same elastic properties and each is loaded by gravity, each beam will deflect the same amount and there will be no normal stress on the interface. The two beams will therefore deflect independently under the gravity load.

The deflection η at some point x along the length of either beam is given by the equation

$$\eta = \frac{q\,x^2}{24\,EI}(L - x)^2 \qquad (4\text{-}6)$$

where L = span of beam

and I = moment of inertia of the area of the cross section of one of the beams relative to its neutral axis.

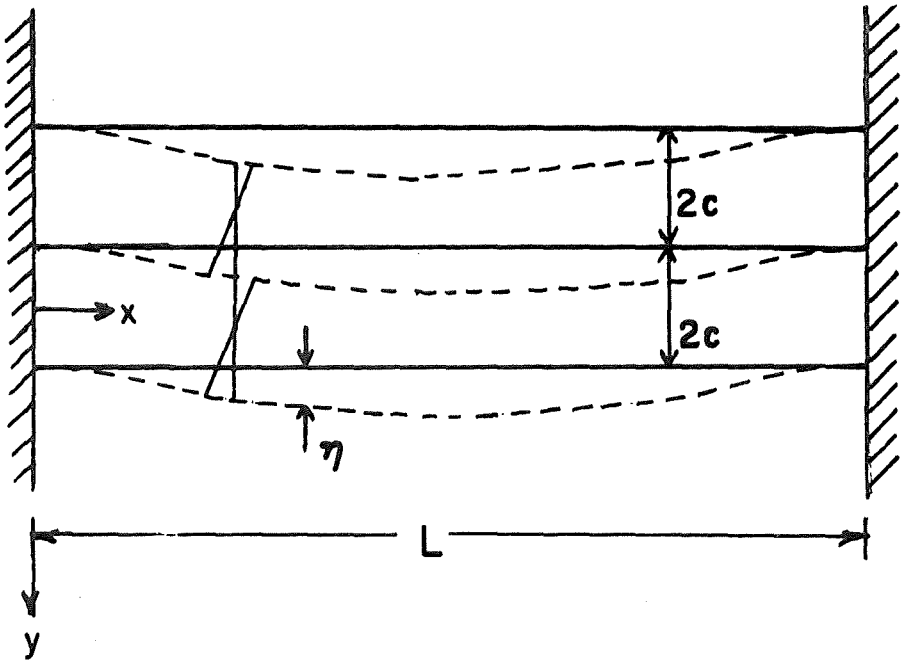

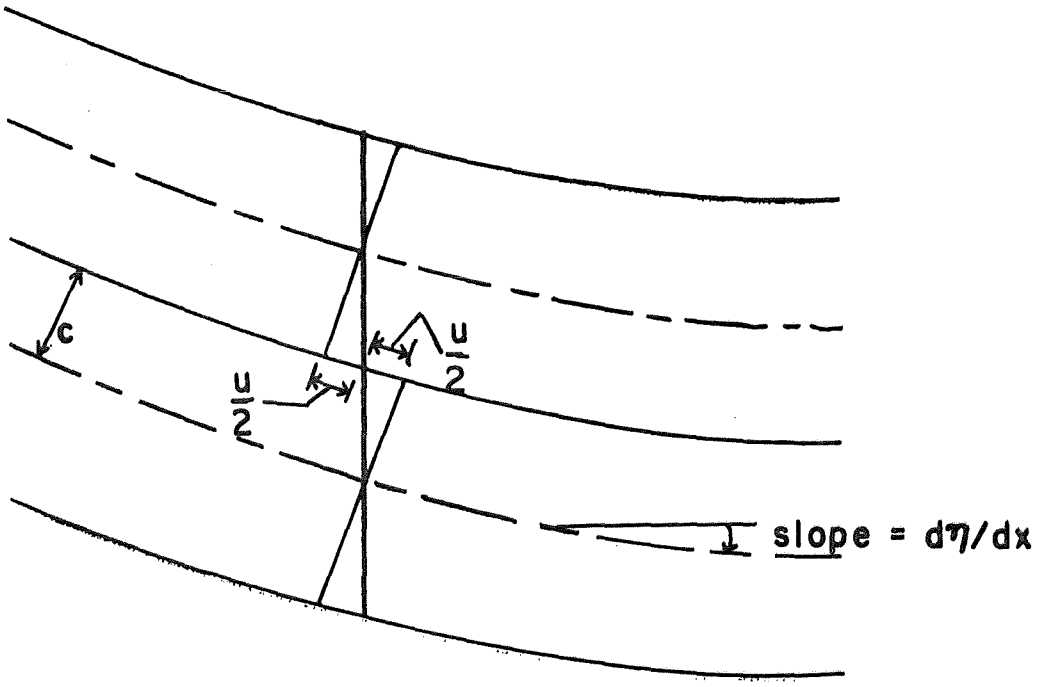

For small deflections

$$\frac{u}{2} = c\,\frac{d\eta}{dx}$$

Fig. 4-3 Shear Displacement between two Similar Beams Loaded by Gravity

For small deflections the horizontal displacement at the interface u/2 is given by

$$\frac{u}{2} = c \frac{d\eta}{dx} \tag{4-7}$$

The relative slip between the beams is twice the value of u/2, or

$$u = \frac{\gamma}{2Ec} (2x^3 - 3x^2L + xL^2) \tag{4-8}$$

The maximum value of u occurs at x = 0.211 L and x = 0.789 L. This maximum relative shear displacement between the two beams, u_{max}, is given by

$$u_{max} = \frac{0.04811\gamma L^3}{Ec} \tag{4-9}$$

An inspection of Eq. (4-9) reveals that the relative slippage between the two beams increases as the cube of the span L and is inversely proportional to the modulus and beam thickness. The unit weight γ does not vary greatly with rock type. The value of Young's modulus is usually within the range of 1×10^6 psi to 10×10^6 psi for roof rock in coal mines.

The magnitude of the maximum shear displacement between beams, u_{max} from Eq. (4-9), is plotted as a function of the roof span L in Fig. 4-4. Curves are plotted for five beam thicknesses (t = 0.2 ft, 0.4 ft, 1 ft, 2 ft, and 4 ft) and two moduli ($E = 1 \times 10^6$ psi and $E = 10 \times 10^6$ psi). The unit weight of the rock, γ , is assumed to be 150 lbs/ft^3. These curves show that the relative shear displacements between beams are small, in the order of 0.001 to 0.100 in. for the range of beam spans and beam thicknesses normally encountered in mining. A combination such as a 40 ft span with a 0.2 ft beam thickness and a low modulus of 1×10^6 psi would give a very large shear displacement from Fig. 4-19 of 0.385 in.; however, such a beam is so distorted that the analysis is not valid.

The assumptions of linearly elastic behavior and continuity throughout each beam were made in developing Eq. (4-9). Therefore, the range in shear displacements quoted in the above paragraph (0.001 to 0.100 in.) are what one could expect underground if the rock beams behave in an ideal elastic manner and there are no discontinuities such as joints or fractures present within the rock.

The magnitude of the shear displacement between beams should be considered when interpreting and applying the shear strength data presented in this chapter. The shear displacements for elastic behavior are small (0.001 to 0.100 in.) compared to the range of shear displacements (up to 3.0 in.) employed in the test program. This is not to say, however, that such large shear displacements do not occur in underground

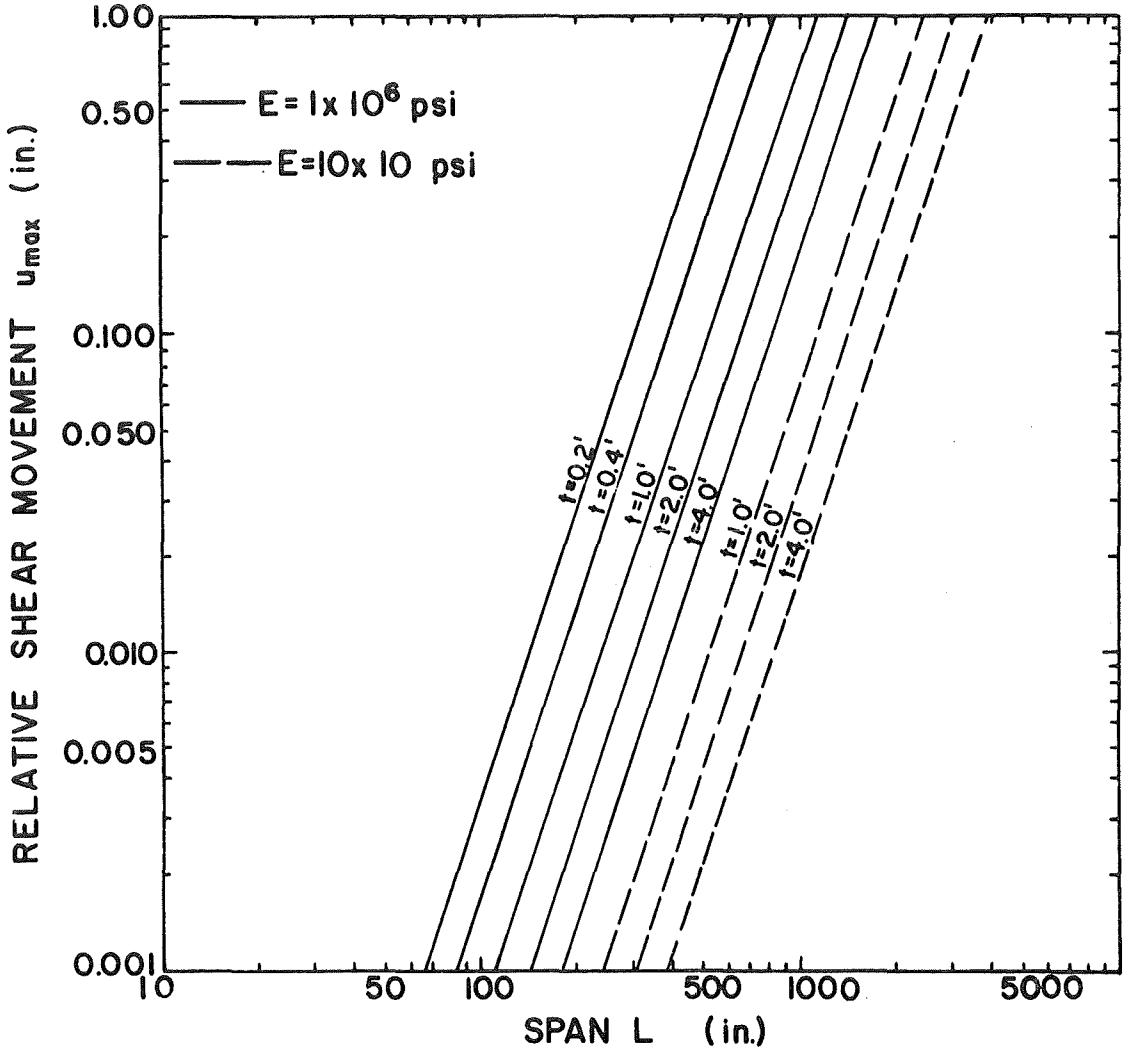

Fig. 4-4 Theoretical Shear Displacement Between Beams Versus Beam Length

situations. They do, in fact, occur as evidenced by offset drill holes sometimes observed in working ground. The rock in this case is not behaving as a continuous medium, but rather the ground forces are such that large discontinuous movements of blocks or slabs of rock occur.

Loading Equipment

The design of the shear test loading frame, shown in Fig. 4-5 (Ref. 1) is such that two blocks of rock 2 ft x 2 ft x 1 ft thick can be sheared past one another. The 2-ft x 2-ft interface (with a vertical orientation in Fig. 4-5) simulates a fracture or non-cohesive bedding plane. The blocks are bolted together with full-scale rock bolts of various types and which intersect the shear surface at different orientations.

The right-hand block of rock rests on a thick steel base and is against the right side plate, also made of steel (Fig. 4-5). Another steel plate is placed against the left face of the left block of rock. This plate is pressed against the left block by four hydraulic cylinders and horizontal tie rods between the two side plates symmetrically placed so as to provide a uniform normal pressure σ_n on the shear surface. During the shear test, the left block (and left side plate) is forced downward by a large hydraulic ram. The shear force, block displacements, and bolt strains are recorded at preselected increments of shear displacement as the test proceeds.

Displacements of the shear block relative to the rigid block were measured to determined the shear displacement, normal displacement (or dilatation), and tipping. The pull-out displacements of the bolt anchors or ends of the grouted steel bars were also measured. Axial bolt strains were measured at the shear plane and at 6 in. on either side of it (Fig. 4-6) for the three orientations tests, θ = 0, +45, and -45 degrees. The strain gage lead wires were potted in a small groove milled along the length of the grouted bar and were brought out through a small inclined hole drilled in the end of the bar.

The bolts were installed from the right side of the blocks (Fig. 4-6) for the normal orientation, from the upper right corner for the +45-degree orientation, and from the upper left corner for the -45-degree orientation.

Rock Blocks for Shear Tests

Both limestone and shale blocks were used in the shear tests. The limestone was the Indiana limestone from near Bedford, Indiana, and was chosen as the standard test rock in order to evaluate the various bolt types and the effects of varying the normal stress, bolt orientation, and roughness of the shear surface.

Two shale formations were included in the test program: the Dry Wood shale from western Missouri (near Asbury, Missouri) and the Interbedded shale from southern Illinois (near Butler, Illinois). It was not possible to obtain the necessary large blocks of shale from the roofs

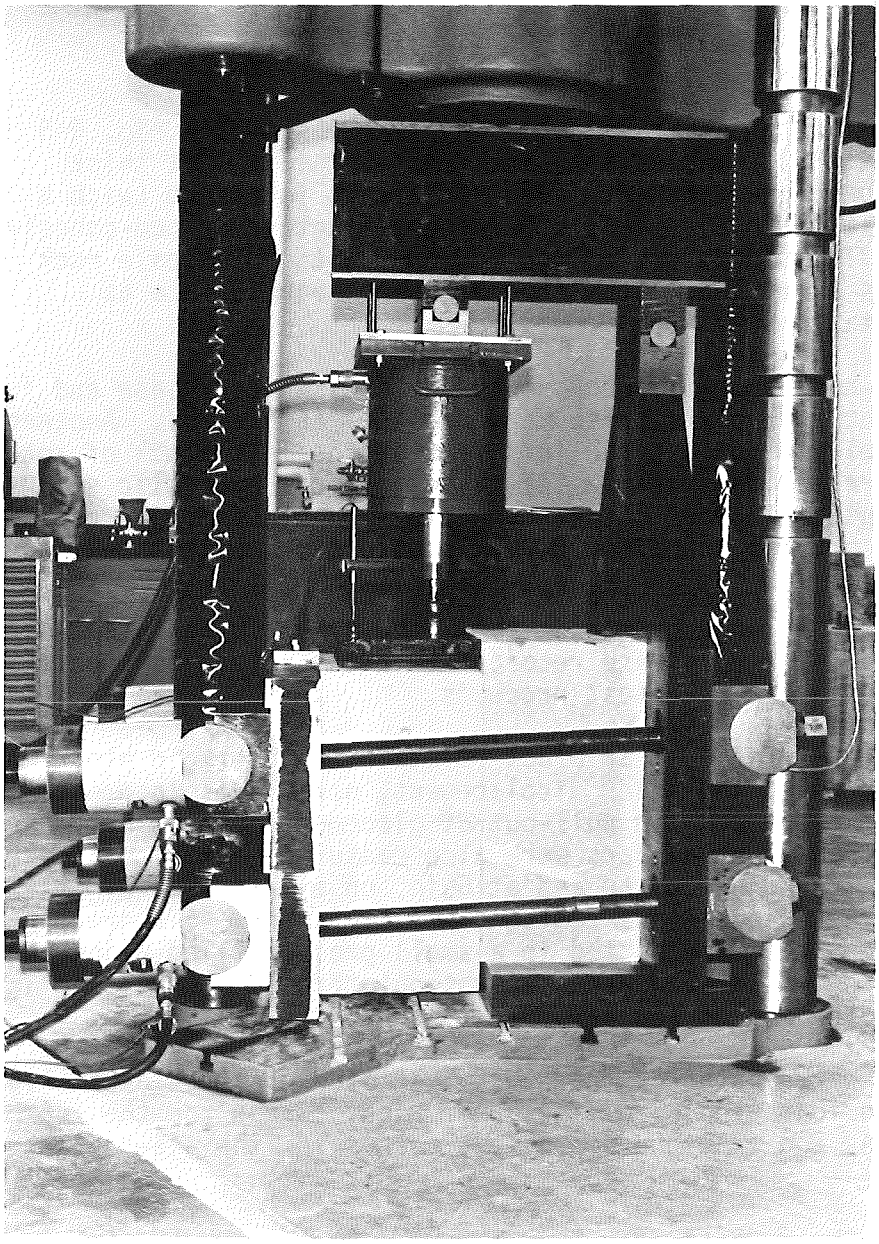

Fig. 4-5 Photograph of Shear Test System. Right-hand Block is Stationary while Left-hand Block is Sheared

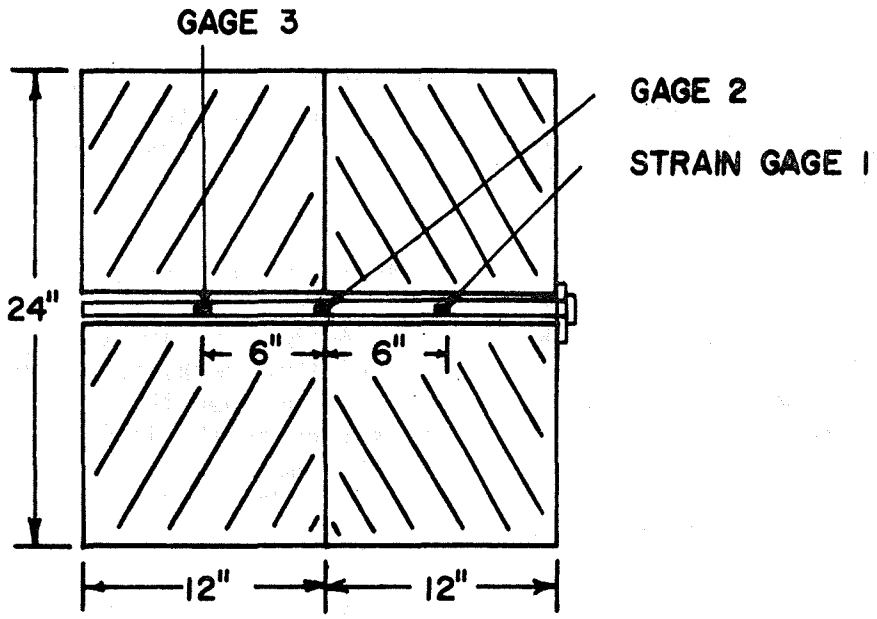

NORMAL BOLT, $\theta = 0°$

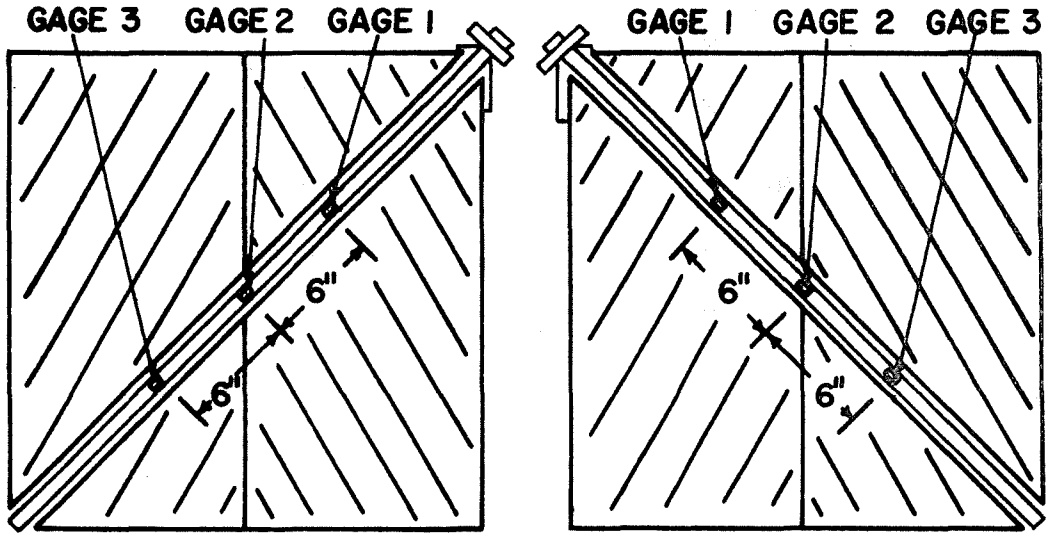

INCLINED BOLT, $\theta = 45°$ INCLINED BOLT, $\theta = -45°$

Fig. 4-6 Section through Shear Blocks Showing Strain Gage Locations

of underground coal mines so they were cut from large slabs of these shale formations uncovered by the stripping operation of coal mines at the two source locations. The slabs were hauled to custom stone plants who cut and finished the blocks.

A thorough search of operating coal mines in Missouri and Illinois revealed that these were the only two formations which could be classed as shale and still hold together well enough that test blocks could be cut from them. Deterioration of samples in the atmosphere and while sawing with water coolant limited the number of suitable formations to these two.

Detailed property data on the limestone and the two shales are given in the three annual reports (Refs. 1, 2, and 3). The average property values measured perpendicular to the bedding are given in Table 4-1. It is seen that the weakest of the three rocks is the Dry Wood shale, followed by the Indiana limestone, and then the Interbedded shale which is approximately three times as strong as the limestone. Such a high strength is not typical of shale; however, this rock had the pronounced layering typical of a shale and did deteriorate when exposed to outdoor weather for several weeks.

Table 4-1 Average Rock Property Values for Limestone and Shale

Property*	Formation		
	Indiana Limestone	Dry Wood Shale	Interbedded Shale
Uniaxial Compressive Strength, psi	9230	6410	28,170
Young's Modulus, 10^6 psi	4.88	1.85	9.70
Poisson's Ratio	0.181	0.208	0.302
Brazilian Tensile Strength, psi	739	658	1993
Apparent Specific Gravity, dry	2.31	2.57	2.80

*Values determined with axis of core perpendicular to bedding planes

The roughness of the shear surface is an important variable, so its effect was also studied. Two roughness conditions were considered: one in which the shear surface was first sawed and then smooth finished by either lapping or planing, and the other where a rough shear surface was created by splitting a larger block in half (Fig. 4-7) and using the rough fracture surface as "natural" shear surface. The term "natural fracture" is used to describe this rough shear surface since it simulates quite well the condition underground where shear occurs along fracture planes rather than smooth planar bedding planes.

The initial smoothness and flatness of the "smooth" machined shear surfaces were determined on a few representative samples by running a dial indicator over the surface and noting the movement of the pointer. Smoothness is reported in Table 4-2 as the variation in the indicator reading over 0.5 in., while flatness is defined as the variation over 24 in. The values of smoothness and flatness are close to the maximum values, although not all of the surfaces were actually studied. The truck load of limestone used in the tests in the first year of the contract was significantly smoother and more nearly flat. The smoothness on these blocks was ± 0.0008 in. over 1/2 in., and the flatness was ± 0.0030 in. over 24 in.

Table 4-2 Smoothness and Flatness of "Smooth" Shear Surfaces

Property	Rock Type		
	Indiana Limestone	Dry Wood Shale	Interbedded Shale
Smoothness over 1/2 in., in.	± 0.0028	± 0.0025	± 0.0060
Flatness over 24 in., in.	± 0.0214	± 0.0110	± 0.0224

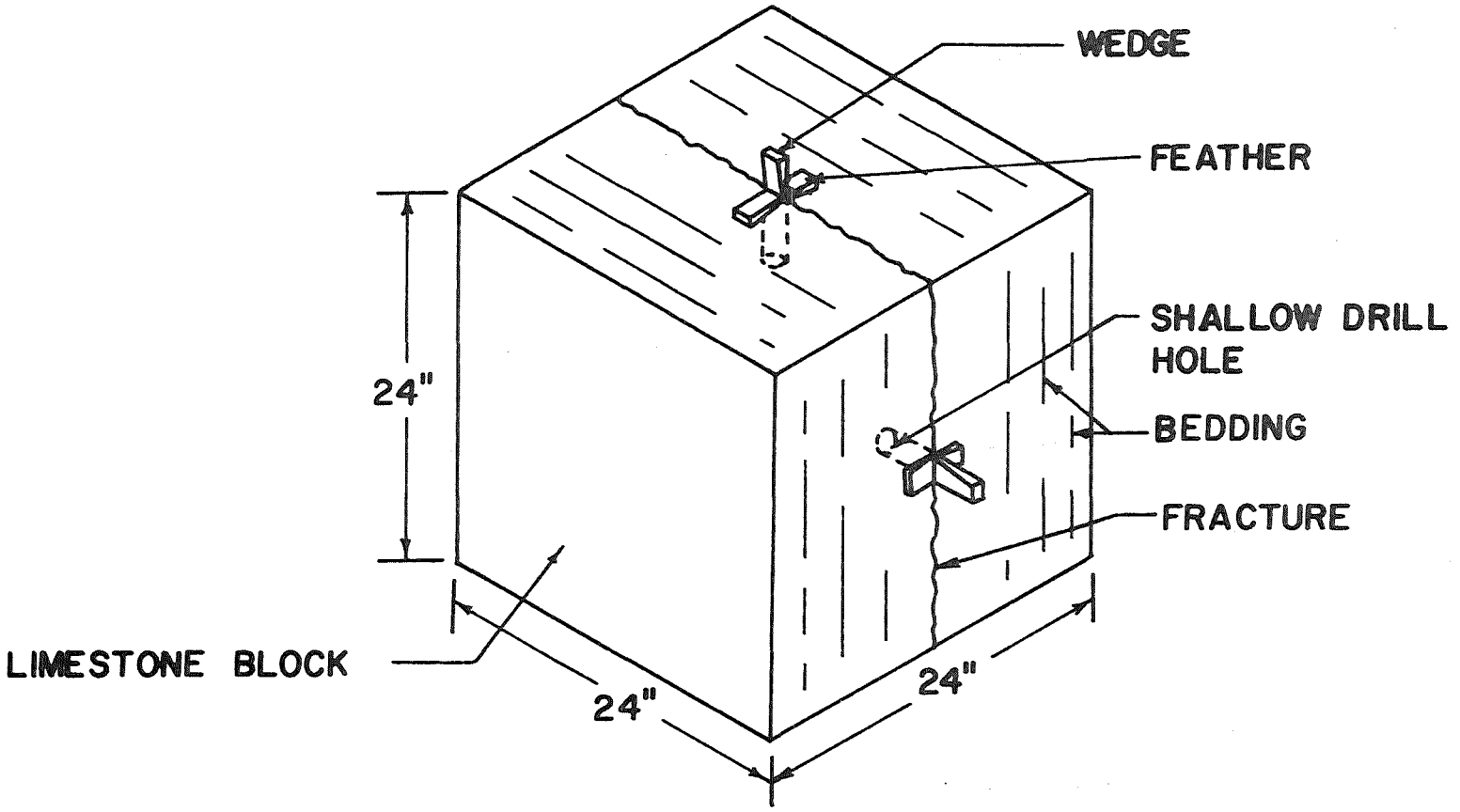

Fig. 4-7 Splitting Cube of Rock to Create "Natural" Fracture

The fracture surface profiles for the limestone blocks which were split apart to form the natural fracture shear surfaces were traced along grid lines spaced 2 in. apart. These profiles given in Refs. 2 and 3 show that the shear surfaces were very rough indeed. The fracture surface was created by tensile failure so it was initially free of rock powder or loose grains. The surface had small-scale and large-scale undulations as shown in Fig. 4-8. The deviations of the large-scale undulations from a plane (single amplitude) were often 1 in. or more. In a few cases, the heights of the humps (or depths of the depressions) were as much as 2 in. The roughness of the shear surface is an important factor because, as will be discussed later, the large-scale undulations cause the shear blocks to separate as the shear progresses, resulting in high tensile loading of a bolt intersecting the surface.

Two types of drill holes were used: a smooth hole drilled with a diamond core drill and a rifled hole drilled with a tungsten carbide rotary drag bit of the same type used for drilling roof bolt holes in coal mines. The only difference was that water circulation was used with the drag bits instead of air as in coal mines. Two hole diameters were employed, 1 and 1 3/8 in.

As will be discussed later, the roughness of the rifled drill holes greatly improves the anchorage capability of the fully grouted bolts.

Types of Bolts Tested

Several types of full-scale rock bolts were tested for shear resistance when installed in the rock shear blocks. The bolting materials were all commercial products and recommended installation procedures were followed except for a few exceptions which are noted.

The following types of bolts were employed:

1. Conventional expansion-anchor type. These bolts were Bethlehem Cat. No. 23-9, 5/8 in. nominal diameter, and were used with Bethlehem Type C-1 expansion anchors in 1 3/8 in. diameter holes.

2. Full column resin-grouted steel bars. Several combinations were employed:

   a) 7/8-in. nominal diameter reinforcing bars of grade-40 steel in 1 3/8 in. diameter holes with Celtite resin.

   b) 3/4-in. nominal diameter steel bar with the initial DuPont deformation pattern in 1-in. diameter holes with Fasloc resin.

   c) 3/4-in. nominal diameter steel bar with newer DuPont deformation pattern in 1-in. diameter hole with Fasloc resin. The new deformation pattern incorporates re-bar type deformations in addition to the longitudinal ribs and widely spaced angled beads on the earlier design.

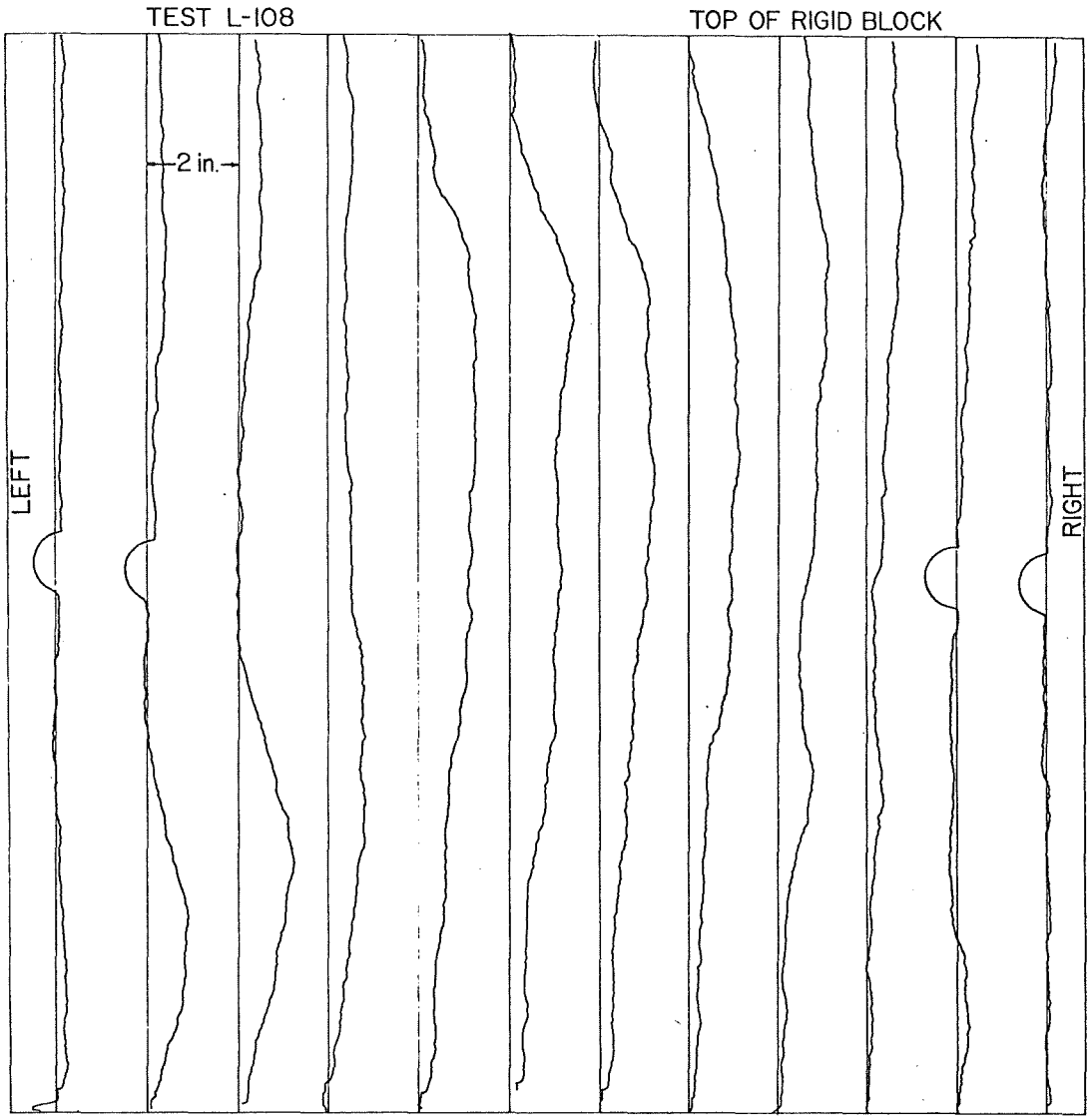

Fig. 4-8 Roughness Profile of Fracture Surface for Test L-108.

3. Friction rock stabilizer. These were made from mild steel tubing split longitudinally along one side. The outside diameters of the tubes before installation ranged from 1.49 to 1.51 in. and the wall thicknesses ranged from 0.092 to 0.100 in. The nominal hole diameter was 1 3/8 in.

4. Fiberglass-resin pumpable bolt developed by the U.S. Bureau of Mines. This bolt consists of a polyester resin, a catalyst, and fiberglass roving, with the mixed resin and catalyst being pumped into the drill hole after the fiberglass strands had been pushed to the bottom of the hole. These bolts were installed by U.S. Bureau of Mines personnel in shear test blocks sent to Salt Lake City, Utah. The nominal hole diameter was 1 3/8 in.

Shear Test Variables

The following variables have been investigated in the shear-test program:

1. Bolt type

   a) conventional expansion-anchor type
   b) full column resin-grouted steel bars
   c) friction rock stabilizer
   d) fiberglass-resin (pumpable bolt)

2. Tensioning of fully grouted bars

   a) untensioned
   b) post-tensioned
   c) pretensioned

3. Orientation of bolt relative to shear plane

   a) 0 degrees (normal)
   b) +45 degrees
   c) -45 degrees

4. Rock type

   a) limestone, Indiana
   b) shale, Dry Wood and Interbedded

5. Roughness of shear surface

   a) machined smooth
   b) rough fracture

6. Drill hole diameter

   a) 1 inch
   b) 1 3/8 inch

7. Normal pressure on shear surface

   a) σ_n = 25 psi

   b) σ_n = 250 psi

8. Roughness of drill hole

   a) drilled smooth with diamond core bit

   b) rifled after being drilled with a rotary drag bit

9. Length and quality of anchorage of grout column with fully grouted bolts

All of the above factors affect the shear resistance generated by rock bolts intersecting active shear planes in a rock mass. These effects will be illustrated by comparisons of the curves of shear resistance (stress) versus shear displacement. Most of the curves which follow are the average of two similar tests.

Except for the fiberglass bolts, axial strains were measured at three points along the length of each bolt. These strain data are presented in the three Annual Reports on this contract (Refs. 1, 2, and 3) and will be discussed herein only to the extent that the bolt strain measurements help to explain the shear behavior.

Experimental Results and Discussion

A. Tests on Expansion-anchor Bolts

Shear tests were performed on expansion-anchor type rock bolts to determine how well the theory proposed in the section "Theoretical Analysis - Conventional Bolts" in this chapter agrees with experimental results. Smooth machined rock shear surfaces were employed and the drill holes were diamond drilled so that they were straight and smooth. Three bolt orientations, θ = 0, 45, and -45 degrees, and two normal pressures, σ_n = 25 and 250 psi, were employed.

The test results are shown in Figs. 4-9 and 4-10 for the two normal pressures. The plots show both the theoretical and the experimental results. There is fairly good agreement between the theoretical and experimental curves in Fig. 4-9 for shear displacements up to 1.0 in. For greater displacements, the measured shear resistance was higher than that predicted by the theory. After interference developed between the bolt and the sides of the offset drill hole, additional shear resistance was mobilized by the direct shear of the bolt which was not accounted for in the theoretical development.

The sudden decreases in the 45-degree curves at around 2.0 in. of shear displacement are due to complete shearing of the bolt. After this point the shear resistance drops to the value with no bolt.

Conventional bolts at the 0-degree and +45-degree orientations in limestone at the low normal pressure, σ_n = 25 psi, (Fig. 4-9) provided

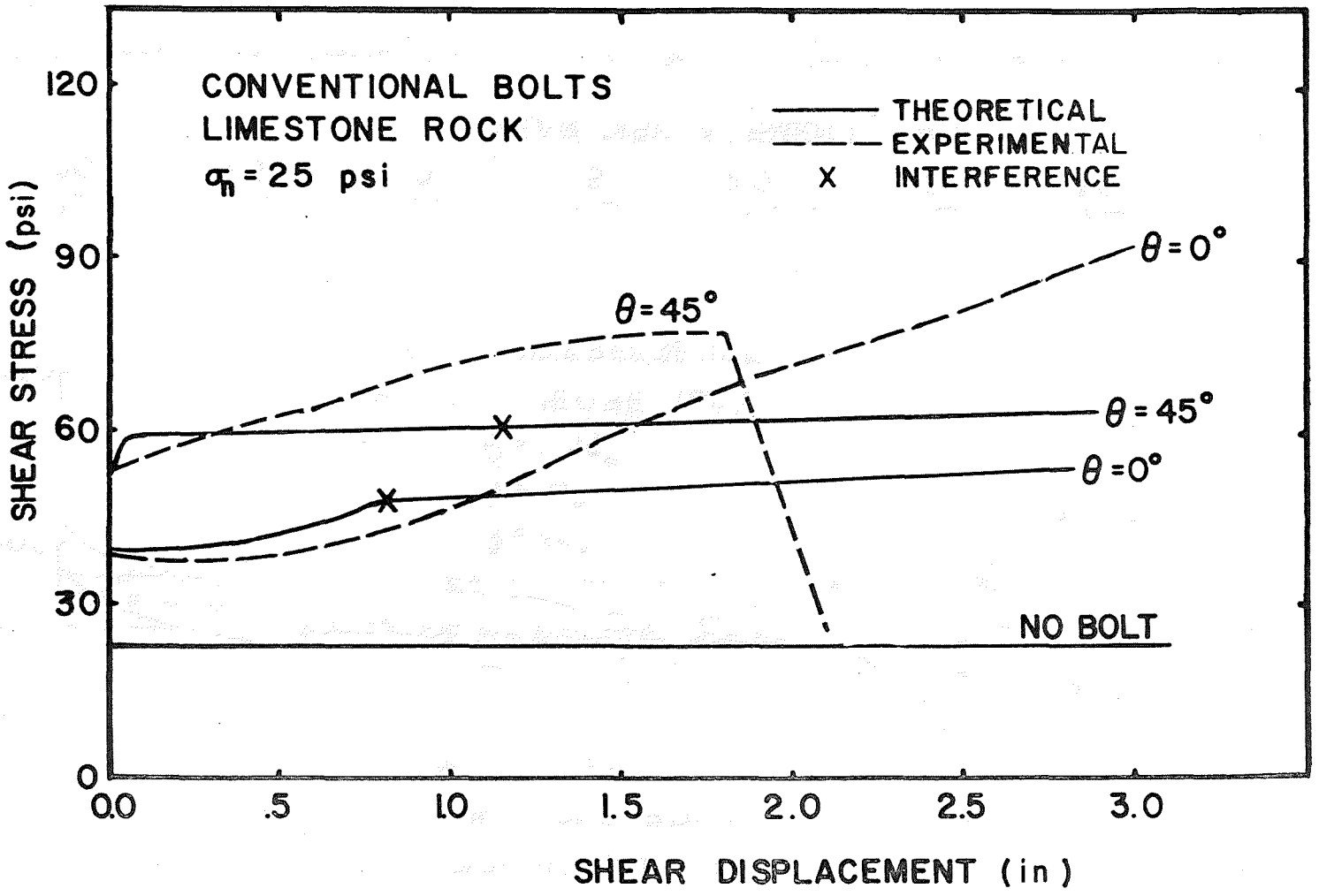

Fig. 4-9 Average Shear Stresses for Conventional Bolts in Limestone at Low Normal Pressure

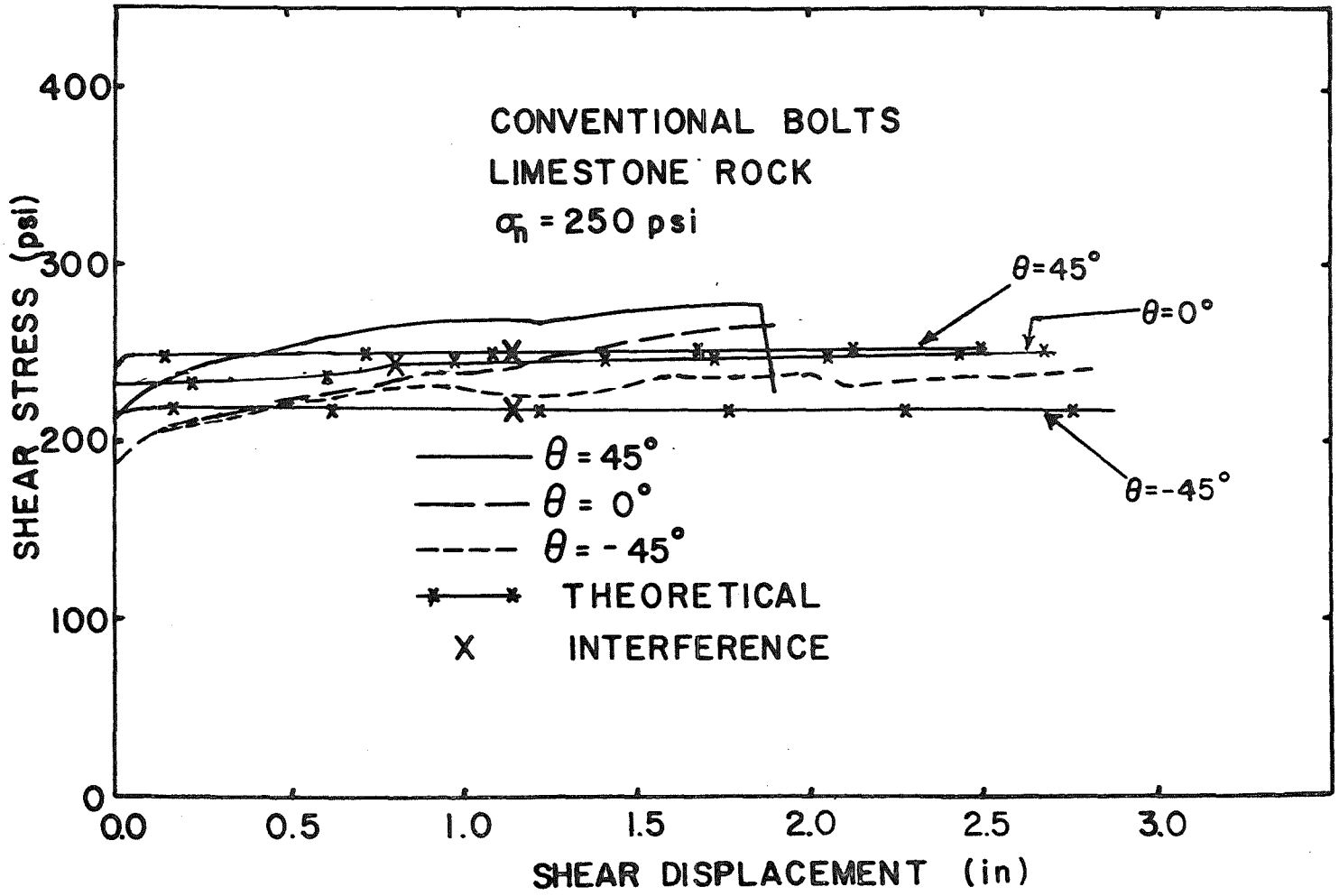

Fig. 4-10 Average Shear Stresses for Conventional Bolts in Limestone at High Normal Pressure

a significant increase in the shear resistance over the no-bolt case. More resistance was provided by the +45-degree orientation than the 0-degree one. It is seen that the shear resistance continues to increase, but not abruptly, after interference develops between the bolt and the sides of the hole.

At the higher normal pressure, σ_n = 250 psi, the conventional bolts in limestone (Fig. 4-10) contributed a much lower proportion of the total shear resistance. The component of friction due to the normal pressure was predominant. Nevertheless, the +45-degree orientation was found to be the most effective, the -45-degree one least effective, and 0-degree one in between.

B. Effects of Tensioning Grouted Rebars

The results of one definitive set of experiments to evaluate the effects of tensioning fully grouted bars and orientation of the bolt relative to the shear surface are shown in Fig. 4-11 for the low normal pressure (σ_n = 25 psi) and in Fig. 4-12 for the high normal pressure (σ_n = 250 psi). The rock shear surfaces in these tests were machined smooth initially and the holes were drilled with a diamond core bit. The bolts were 7/8-in. grade-40 re-bars with Celtite resin in 1 3/8-in. diameter holes. The grouted bars were installed after the shear blocks had been forced together by the preselected normal pressure. The untensioned bolts were simply installed and the resin allowed to harden without any type of tension being applied. The post-tensioned bolts were installed in the same manner as the untensioned ones; however, a nut and a bearing plate were applied to one end of the bar after the resin had hardened. Then a torque of 250 ft lb was applied to the nut, producing tension in the end of the bar. The tension was therefore induced after the grout had hardened.

Pretensioning of the grouted rebars was accomplished by placing some quick-set resin in the bottom of the hole and slow-set resin in the rest of the hole. The resin was mixed by rotation of the re-bar. After the quick-set resin had hardened but before the slow-set resin had hardened, a bearing plate and nut torqued to 250 ft lb were applied to the collar end of the bar. This put the length of bar within the slow-set resin in tension as this resin hardened. The nut was left in its tightened state during the shear test.

The horizontal curves labeled "no bar" are the shear resistances of the test blocks without any bolts present. The effect of the bolt in resisting shear is therefore reflected by the distance a curve is above the no-bar curve.

Fig. 4-11 shows that the orientation of the grouted bar is a much more significant factor in shear resistance than the state of tension in the grouted bar. The three highest curves (Fig. 4-11) are for the +45-degree orientation, followed by the three curves at 0 degrees, and the lowest curves being those at -45 degrees. The -45-degree orientation is seen to be quite ineffective as those curves are only slightly above the unbolted case.

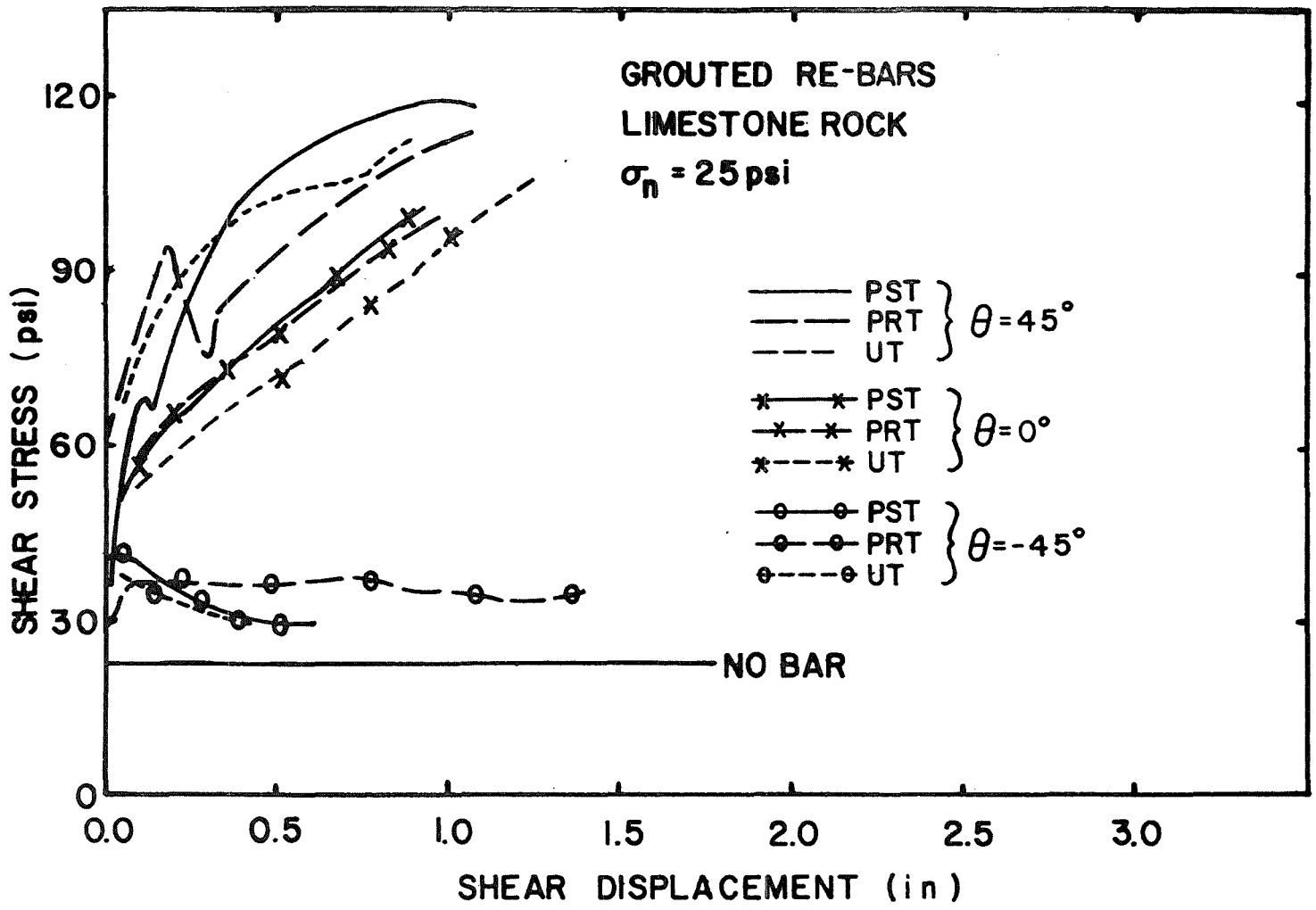

Fig. 4-11 Average Shear Stresses for Grouted Reinforcing Bars in Limestone at Low Normal Pressure. UT is Untensioned; PRT is Pretensioned: PST is Post Tensioned

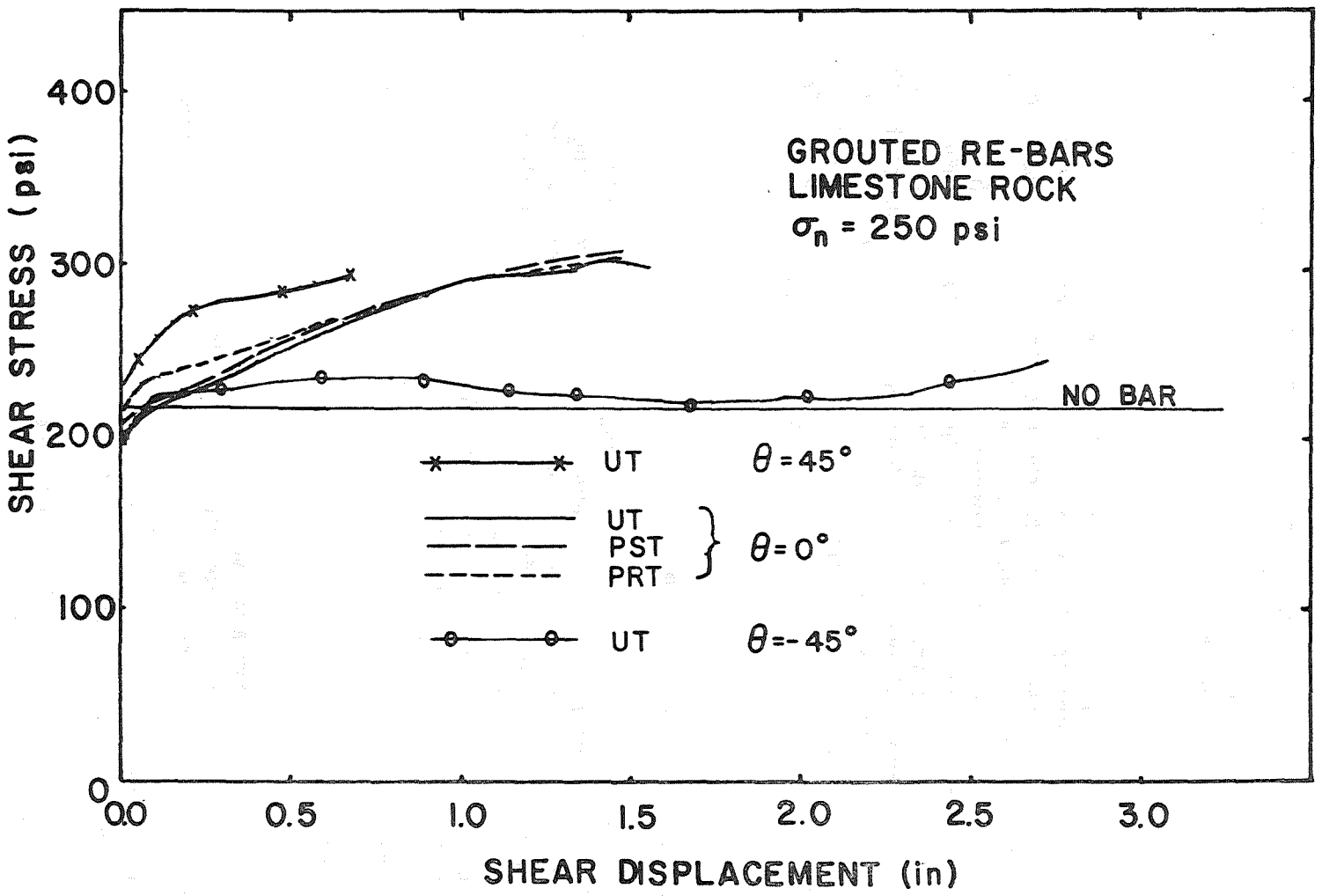

Fig. 4-12 Average Shear Stresses for Grouted Reinforcing Bars in Limestone at High Normal Pressure. UT is Untensioned; PST is Post Tensioned; PRT is Pretensioned

There is no conclusive indication in Fig. 4-11 that the state of initial tension (untensioned, post-tensioned, or pretensioned) affects the shear resistance of the grouted bolt system. One would not expect any difference between the untensioned and post-tensioned cases because the initial tension in the post-tensioned bar is highest near the nut and is nearly negligible at the shear surface 12 or more inches away. Reasoning would indicate that the pretensioned grouted bar would increase the shear resistance since in this case the initial bolt tension is high at the shear surface and tends to pull the shear blocks into tighter contact and increase the normal stress on the interface. The increase in normal stress on the shear surface would then increase the shear resistance. The experimental results in Fig. 4-11 did not indicate that this effect was significant, however.

The results for grouted re-bars at the high normal pressure (Fig. 4-12) indicate again that the grouted bolts increase the shear resistance, however the percent increase relative to the unbolted case is much less than it is for the low normal pressure (Fig. 4-11). The reason for this, of course, is that the higher normal pressure results in a higher frictional strength without a bolt. The total shear resistance of the bolted system is the sum of that due to the frictional strength developed as a result of the normal stress and the shear resistance induced by the bolt. Increasing the normal stress from 25 to 250 psi causes a nearly 10-fold increase in the first component of the shear resistance while the second component due to the bolt remains essentially constant. Thus the curves with bolts and without bolts are closer together in Fig. 4-12 than they are in Figure 4-11.

C. Effects of Bolt Type on Shear Resistance

Several different types of full-scale rock bolts were tested in order to evaluate the relative effectiveness of bolts in resisting shear movement in a rock mass. These comparative tests were performed with smooth machined rock shear surfaces. The drill hole diameters were all 1 3/8 in. except for the Fasloc system which utilized a 1-in. hole. The holes were all drilled with a diamond core bit except those for the Fasloc system and those for one group of tests on the split tube. These two exceptions were drilled with rotary drag bits which caused a considerable amount of rifling of the hole wall and the hole to be somewhat oversize. The specifications (diameter, material, etc.) of the various bolts are given in the section "Types of Bolts Tested" in this chapter.

The results of these comparative tests are given in Figs. 4-13 through 4-15 for the 0-degree, 45-degree, and -45-degree bolt orientations, respectively. These tests were all performed at the low normal pressure of 25 psi. A lesser number of tests performed at the -45-degree orientation showed that the bolt contributed very little to the shear strength of the bolted joint with that orientation.

Fig. 4-13 shows that the fully grouted Celtite system (7/8 in. bar in a 1 3/8-in. hole) was significantly more effective than the smaller Fasloc system (3/4-in. bar in a 1-in. hole). The Fasloc bolts did not shear off even though the shear displacement reached 3.25 in. The shear

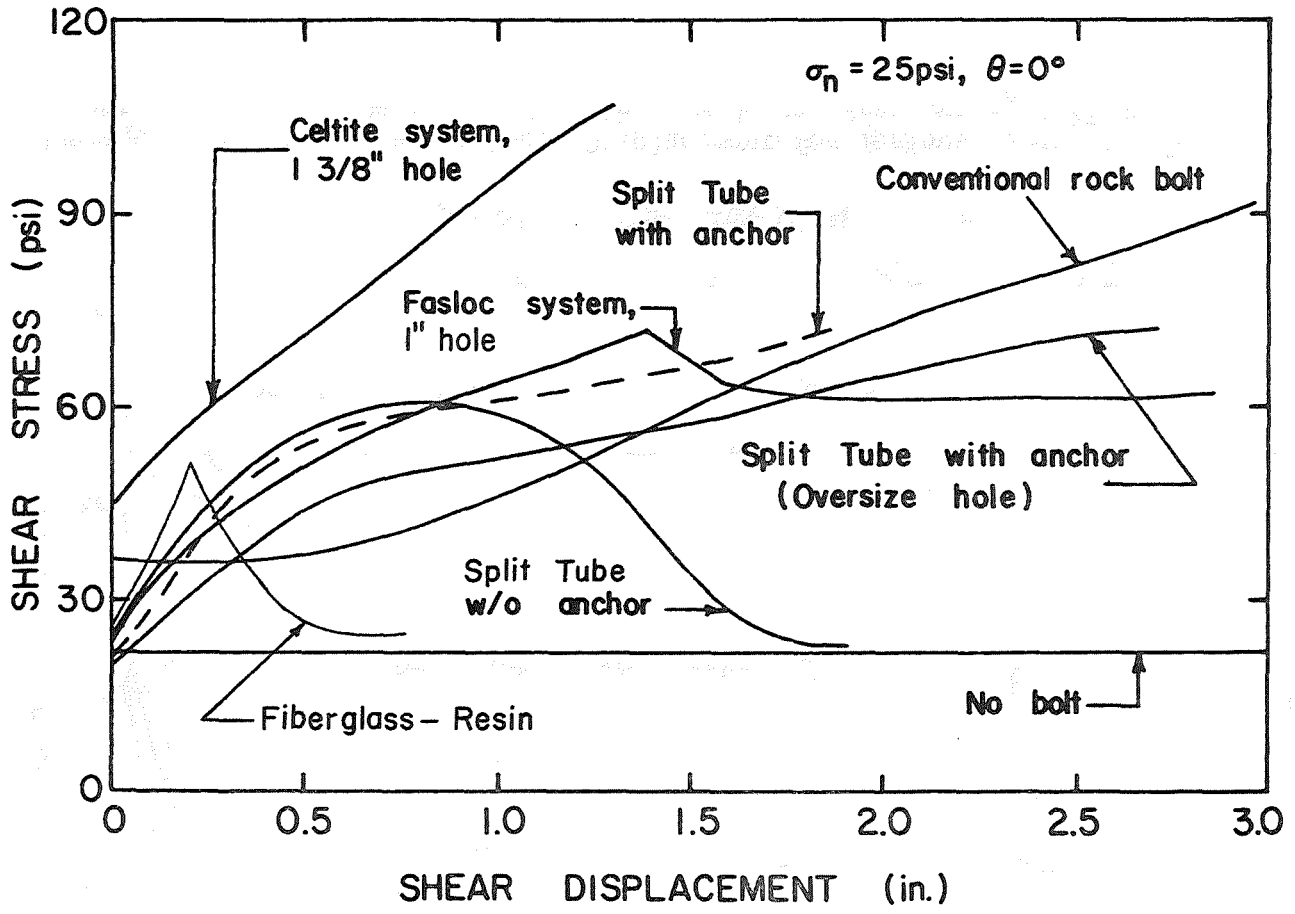

Fig. 4-13 Average Shear Stress Versus Shear Displacement for Various Types of Bolt Oriented at Θ = 0 Degrees and at the Low Normal Pressure σ_n = 25 psi.

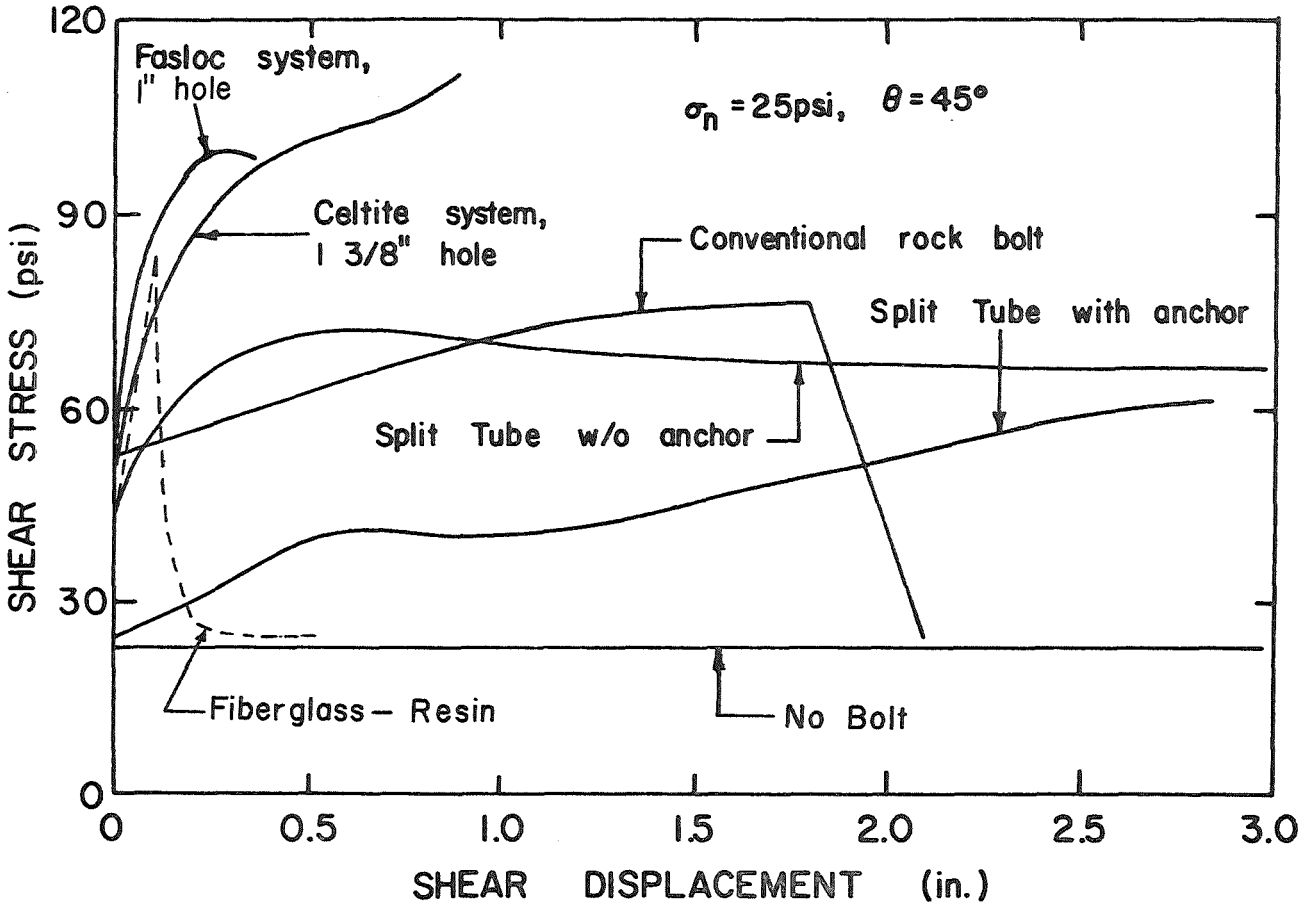

Fig. 4-14 Average Shear Stress Versus Shear Displacement for Various Types of Bolts Oriented at Θ = +45 Degrees and at the Low Normal Pressure σ_n = 25 psi

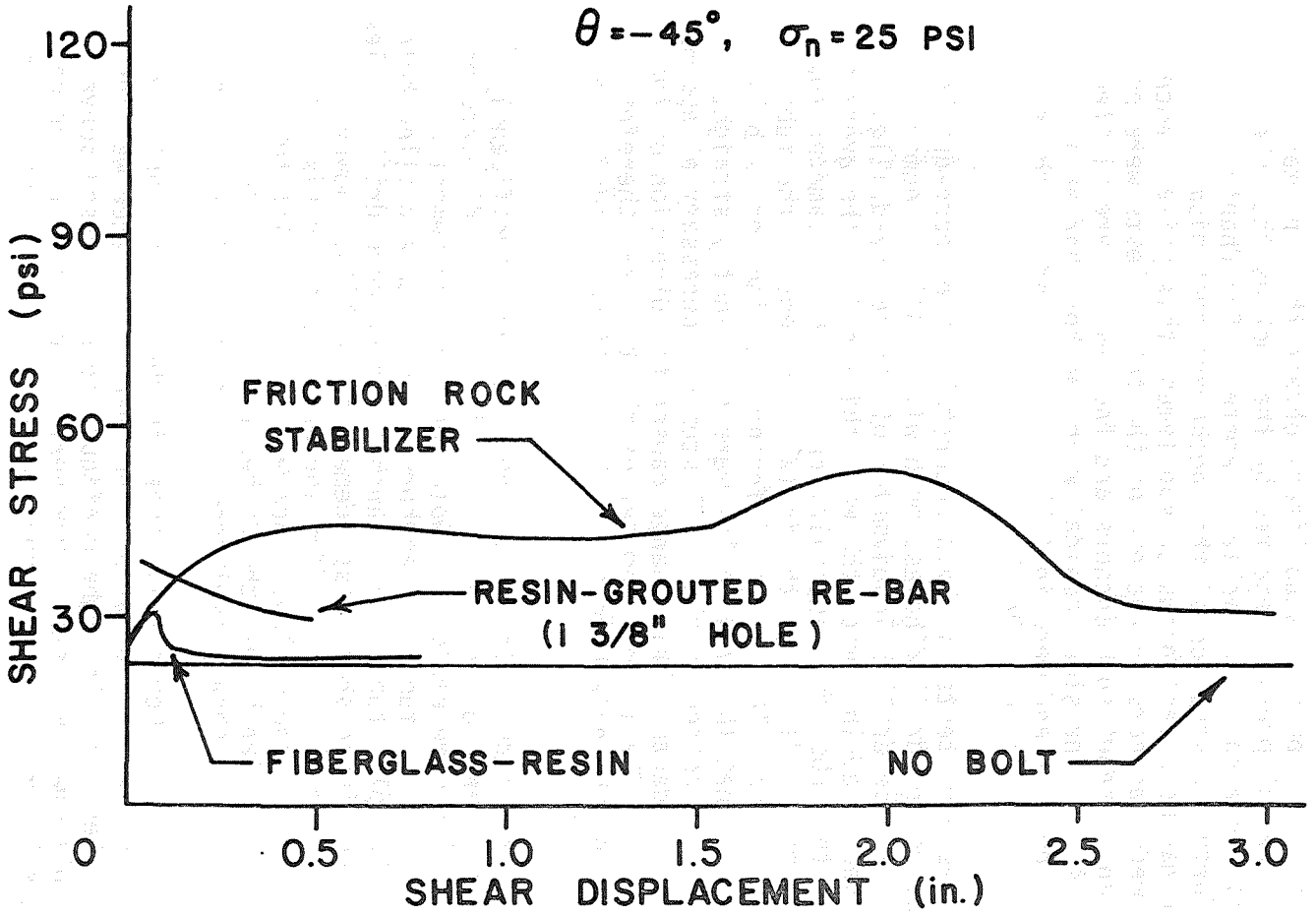

Fig. 4-15 Average Shear Stress versus Shear Displacement for Different Types of Bolts, θ = -45 Degrees

block split for the Celtite system when the shear displacement reached 1.3 in., so further data could not be obtained. The shear resistance of the Fasloc system was nearly constant, but dropping slightly, after 1.5 in. of shear displacement. This continued deformation of the bar was permitted because anchorage was lost. The ends of the bar pulled into the rock from 1 to 1.3 in. during the test. The 12 in. of anchorage failed despite the fact the drill holes were rifled.

Split tubes or friction rock stabilizers obtain their primary anchorage from the radial pressure exerted by the rock as the tube is forced into a drill hole having a smaller diameter. See Chapter 3 of this report for further discussion of this anchorage mechanism. In some instances it may be advantageous to supplement this primary anchorage with conical wedge anchors in the end of the tube. Tests were performed both with and without such anchors and the results are plotted in Figs. 4-13 and 4-14. The steel conical wedge anchors had an included angle of 10 degrees and were installed in both ends of the split tube with an estimated force of 3,940 lb.

The split tubes were tested in both accurately sized core-drilled holes and oversize rotary-drilled holes, both with 1 3/8-in. nominal bit sizes. The effective drill hole diameter of the rotary-drilled holes was determined by adding twice the wall thickness to the average inside diameter of the tube after installation. The hole diameter thus determined varied from 1.471 in. at the installation end of the tube to 1.402 at the other end. This large difference in diameter is believed to be due to the fact that the drill holes were not exactly straight all the way through. A change in the drill stem was necessary at approximately 18 in. of drill depth. This change caused the direction of the hole to vary slightly. The inside diameter of the tube was therefore less at the far end of the hole because of the additional interference caused by the crooked hole.

The anchors on the ends of the split tubes did not significantly affect the shear resistance during the first 1 in. of shear displacement when core-drilled holes were employed. Note the close agreement of the dashed curve (split set tube with anchors and with core-drilled holes) and the curve for the split tube without anchors (also core-drilled holes) in Fig. 4-13. For continued shear displacement above 1 in., however, the tubes with anchors continued to offer increasing shear resistance while the tubes without anchors slowly sheared off. The split tubes with anchors in core-drilled holes (the dashed curve in Fig. 4-13) sheared off gradually at a shear displacement of approximately 1.8 in.

The behavior of the anchored split tubes in the oversize holes was somewhat different as seen in Fig. 4-13. The shear resistance was less than that for the other two split tube configurations discussed above when the shear displacement was small; however, it continued to increase until the shear displacement reached approximately 3.0 in. at which time the tubes sheared off.

The detrimental effect of the oversize hole is also seen in the results for the 45-degree orientation plotted in Fig. 4-14 where the split tube with anchor in an oversize hole offered less shear resistance than did the unanchored tube in the proper size hole.

The reason for the smaller shear resistances with the split tubes in the oversize holes is that the optimum interference was not developed and therefore, the full friction anchorage was not mobilized. The core-drilled holes were near the proper diameter (1.375 in.); however, as pointed out earlier, the diameters of the rotary-drilled holes varied from 1.471 in. at the installation end to 1.402 in. at the far end of the hole. With an outside diameter of 1.494 in. for the tube before installation, the interference ranged from 0.023 in. to 0.092 in. as compared to 0.199 in. for a 1.375-in. diameter hole.

From a practical viewpoint, the lower shear resistance in the oversize holes indicates that the hole size must be controlled within some rather narrow range in order to achieve maximum anchorage. While the holes in these tests were as much as 0.096 in. oversize, they were drilled with the same type of rotary drag bit, 1 3/8 in. tungsten carbide, as are commonly used in coal mines. It is therefore recommended that the hole diameter and its variation as different lithologic units are drilled be considered when split-set tubes are employed for roof support.

For the 45-degree bolt orientation (Fig. 4-14) the Fasloc system in the 1-in. hole offered more shear resistance than did the Celtite system in the larger 1 3/8-in. hole. The reverse was true for the 0-degree orientation previously discussed. The holes in the tests with the Celtite system were smooth (core drilled) while those for the Fasloc tests were rotary drilled producing a rifled hole. It appears that the better anchorage achieved by the rifled hole caused the Fasloc system to perform better in this 45-degree orientation where the tendency of the bolt to pull out is much greater than it is for the 0-degree orientation.

The Fasloc bars sheared off at approximately 0.5 in. of shear displacement for the 45-degree bolt orientation. The split tubes with anchors continued to deform and slip in the holes until the shear displacement reached the experimental limit of the testing apparatus. The anchors had the effect of increasing the shear resistance for large shear displacements (greater than 1.5 in.) while the tubes without anchors showed a nearly constant shear resistance in this range of displacements.

The displacements of the ends of the Fasloc bars were small, less than 0.025 in. for the 45-degree bolt orientation, which indicates that the anchorages in the holes were very good indeed. The displacements of the ends of the split tubes were very large, approximately 1.0 in., which indicates that the conical anchors on each end of the tube were not effective. The wedge anchors were applied on the corners of the test blocks in the 45-degree bolt orientation and the rock was easily crushed in these regions.

The fiberglass-resin system was very effective for small shear displacements (less than 0.2 in.) in the +45-degree orientation (Fig. 4-14), less effective at the normal orientation (Fig. 4-13) and ineffective in the -45-degree orientation (Fig. 4-15). The reason for the better effectiveness in the +45-degree orientation is that the axial tensile loading of the bolt is greater in this orientation, and the fiberglass

is strong in tension. All of the fiberglass-resin bolts sheared as can be seen by the drop in shear stress to the no-bolt cases in Figs. 4-13 through 4-15.

D. Effects of Shear Surface Roughness on Shear Resistance

All of the shear tests discussed previously were performed with smooth machined rock shear surfaces. Such smooth shear surfaces were desirable in evaluating the effects of certain bolting variables such as type of bolt, inclination of bolt, and drill hole roughness. In practice, however, there are many situations in which the shear surfaces are rough rather than smooth. This in-situ roughness may vary over quite a wide range depending on the rock type, how the shear fracture plane developed, how much chemical alteration and fillings may have occurred, and how much shear movement may already have occurred.

One particular type of rough shear surface was investigated: that in which a solid limestone block is split in half with wedges as shown in Fig. 4-7. This resulted in quite a rough fracture surface as indicated by the typical fracture surface profile shown in Fig. 4-8. This rough fracture is herein referred to as a natural fracture because it simulates quite well a situation in freshly fractured rock underground.

The shear blocks with smooth machined shear surfaces were run through the shear test procedure twice, first without a bolt and then a second time with a bolt installed. Tests had shown that the repeated shear had little effect on the frictional strength of the smooth surfaces. This procedure had to be modified to allow for only one shear on the natural fracture because the asperities were quickly sheared off and the frictional characteristics greatly affected.

The measured shear resistance without any rock bolt present is shown in Fig. 4-16 for both the low and high normal pressures. The curves are characterized by a very rapid increase in shear resistance in the first 0.030 in. of shear displacement to reach a peak value, after which the shear resistance decreases quite rapidly until it approaches the curve for the smooth surface at approximately 2.5 in. of shear displacement. One can conclude therefore that the initial roughness and planarity of the shear surface has little effect on shear resistance for large displacements, say over 2.5 in., when the normal stress is held constant.

It should be pointed out, however, that the shear behavior for large displacements in an underground application may be quite different for smooth and rough undulating shear surfaces. The reason for this is that the normal displacement for an undulating surface is much greater than for a planar one. Larger normal stresses would be generated as the blocks moved apart in a partially restrained environment. The higher normal stress would then result in a higher shear resistance being generated by the undulating surface.

The no-bolt shear stress curves for lapped surfaces (Fig. 4-16) exhibit a different behavior. For these surfaces the shear resistance is low at small shear displacements and increases slightly as the shear proceeds.

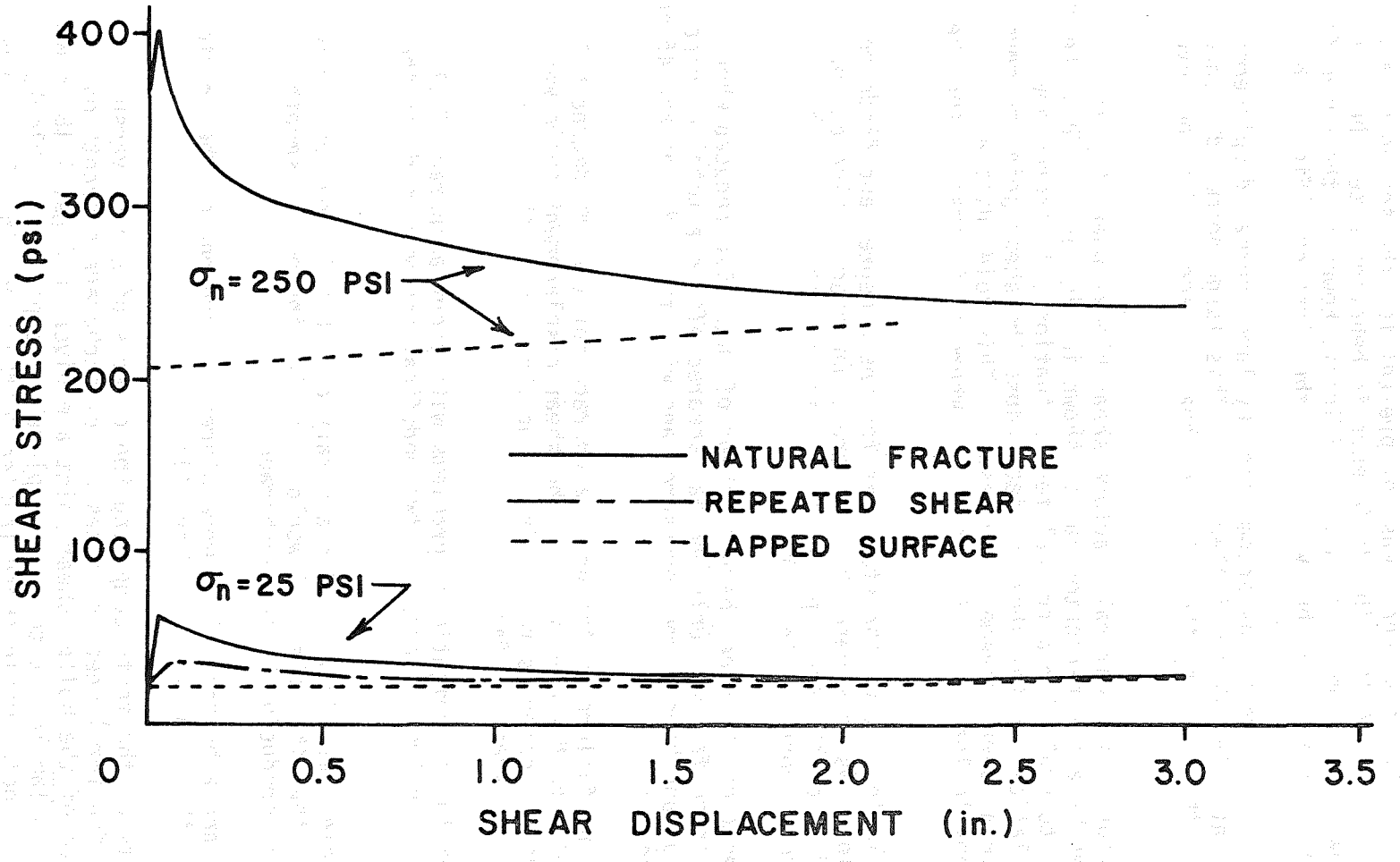

Fig. 4-16 Average Shear Stress versus Shear Displacement for Natural Fractures without Bolt

One no-bolt shear test on the natural fracture shear surface was repeated once to determine how much change in shear resistance would result from the repeated shear. The high initial shear resistance so characteristic of the first shear was not present for the second shear, as can be seen in Fig. 4-16. The difference in behavior after the first 0.2 in. of shear displacement was not significant; however, the curve for the second shear was slightly below that for the first one (Fig. 4-16).

The shear displacement was accompanied by large normal displacements, 0.3 to 0.6 in. at 3 in. shear displacement. This large normal displacement was due to the humps on the matching shear surfaces riding one over the other.

The behavior of the natural fracture shear blocks when they are bolted together by a resin-grouted bar is shown in Fig. 4-17. This sketch which is drawn to scale for a typical test situation illustrates how the large undulations of the shear surface cause the shear joint to move apart or dilate as shear movement progresses. This joint dilatation causes high tensile loading of the steel bar where it intersects the shear plane.

The tensile loading of the steel bar for the 0-degree and 45-degree bolt orientations was so severe that the grout anchorage failed on one side or the other of the shear plane for 7/8-in. diameter re-bar and 1 3/8-in. diameter core-drilled holes.

The tendency of the steel bars to shear off was also reduced when the grout anchorage failed. Only one bar sheared off in a total of nine tests at the low and high normal pressures and with the 0-degree and 45-degree bolt orientations.

There was no failure of the grout anchorage for the -45-degree bolt orientation. Due to the direction of the shear displacement there was a certain amount of compressive loading along the axis of the bar where it intersected the shear surface.

Because of the aforementioned problems with grout anchorage failure on the tests with natural fractures, two modifications were made in the test procedures.

1. The holes were drilled with a rotary drag bit instead of a core bit so that the hole wall would be rifled instead of smooth, thereby producing better anchorage.

2. A nut and a bearing plate were placed on each end of the grouted bar in the shear test configuration.

The results of the tests comparing the effects of smooth versus rough (natural fracture) shear surfaces and of anchorage strength on the shear resistance of the bolted shear joint are given in Figs. 4-18 through 4-20. The curves labeled "with bearing plate" also pertain to blocks with rifled drill holes while those labeled "without bearing plate" pertain to blocks with smooth core-drilled holes.

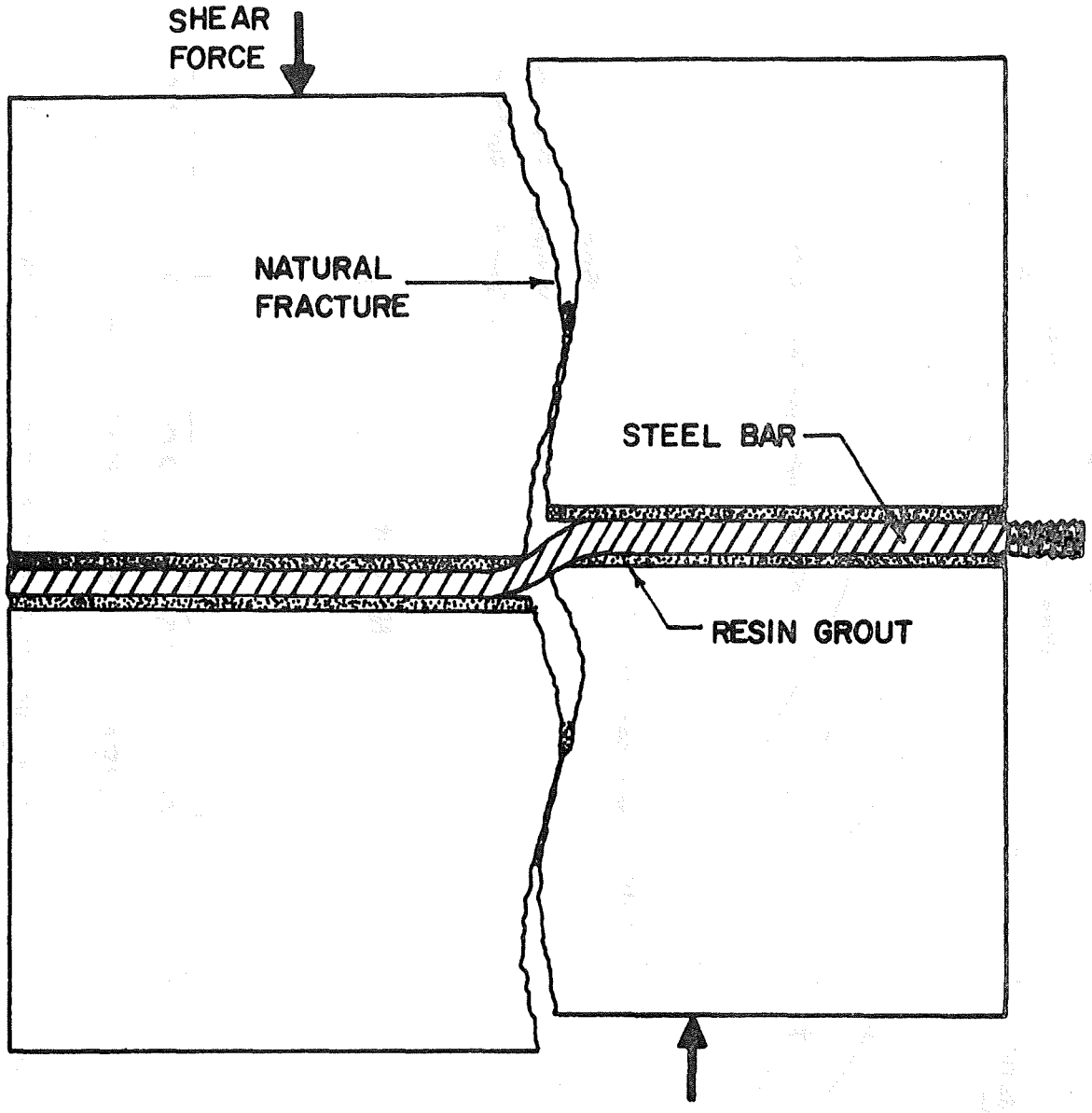

Fig. 4-17 Separation of Bolted Blocks with a Natural Fracture.

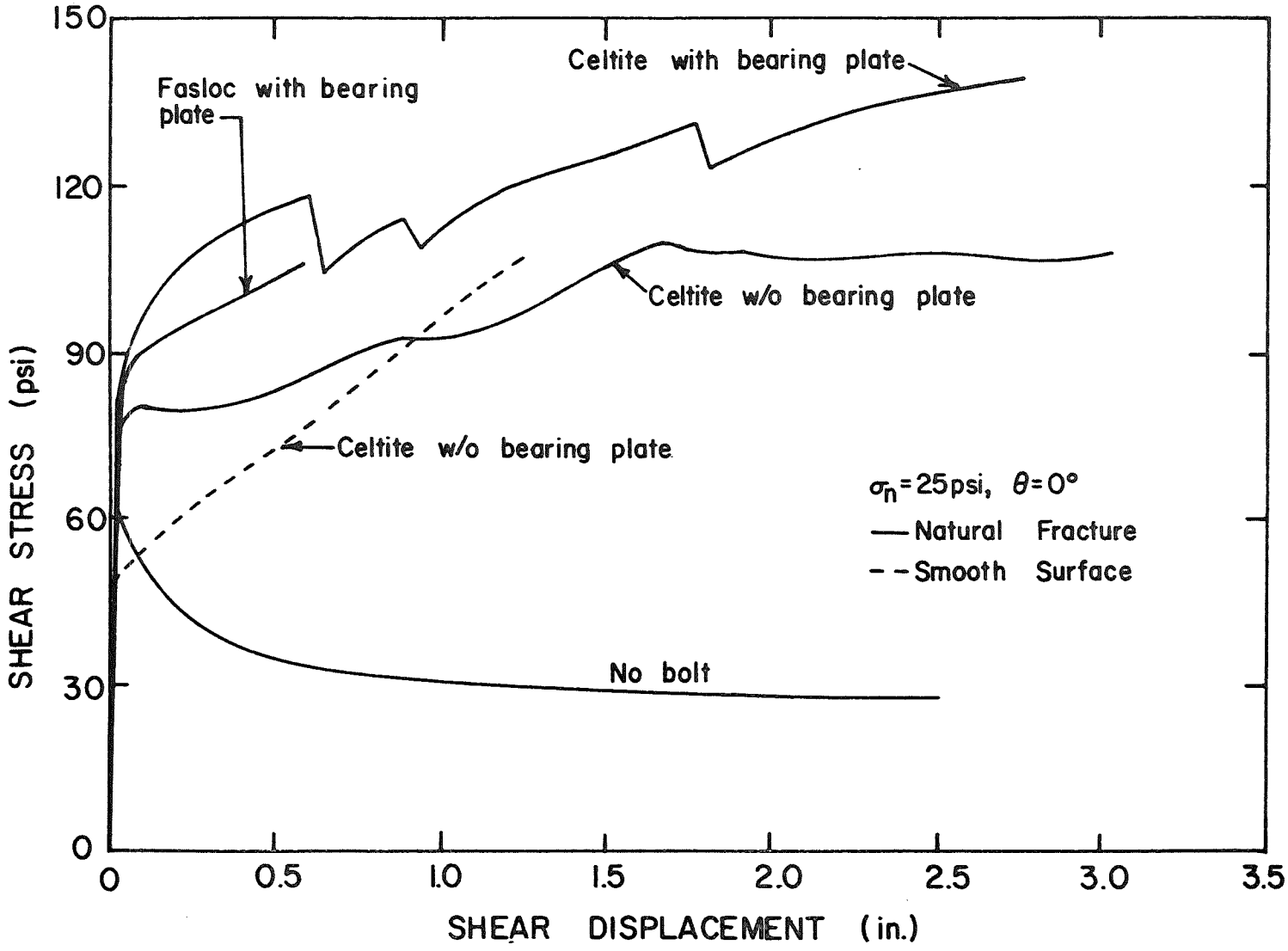

Fig. 4-18 Average Shear Stress versus Shear Displacement for Normal Bolts, Natural Fracture, and Low Normal Pressure

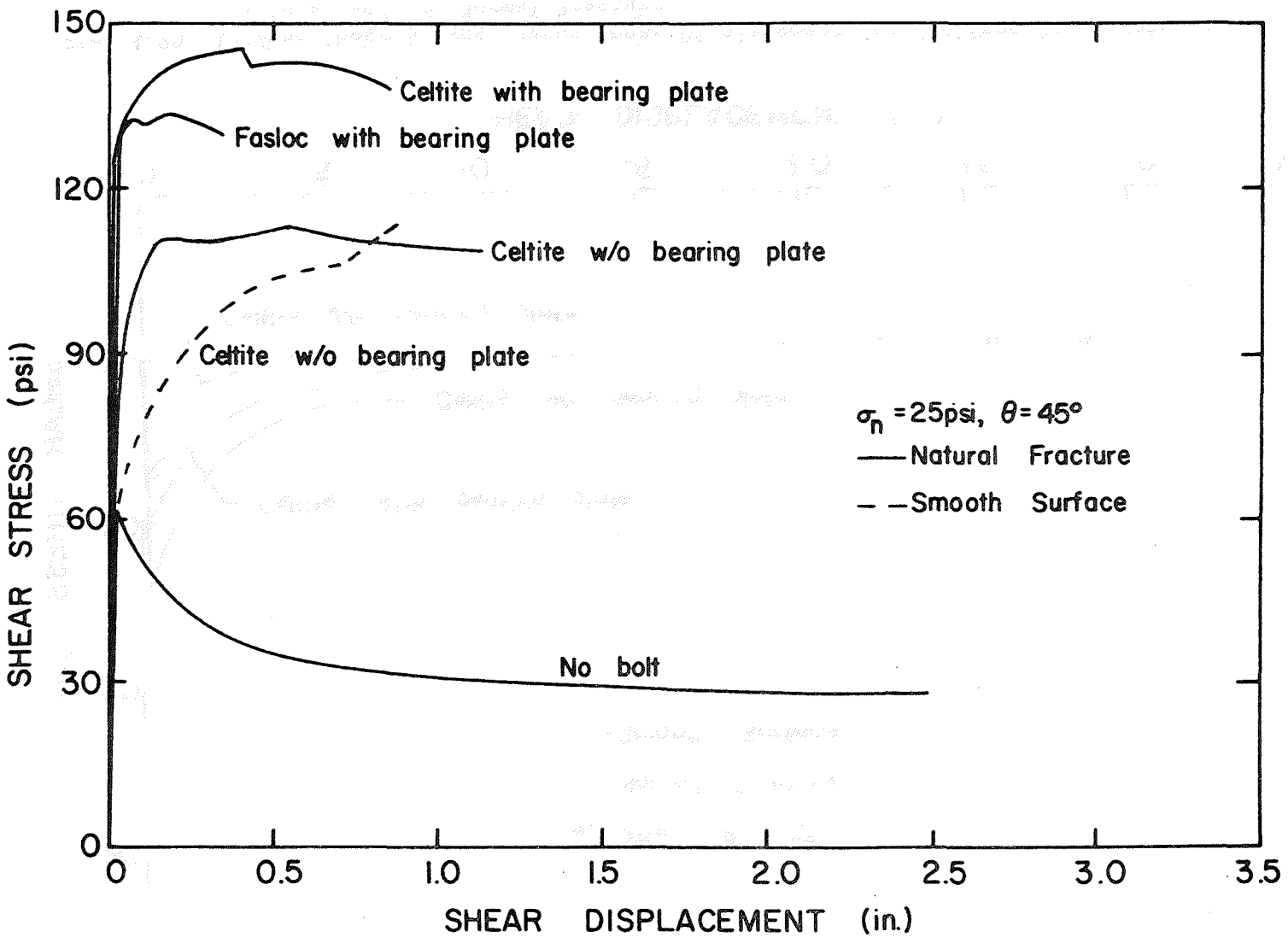

Fig. 4-19 Average Shear Stress versus Shear Displacement for Inclined Bolt, Natural Fracture, and Low Normal Pressure

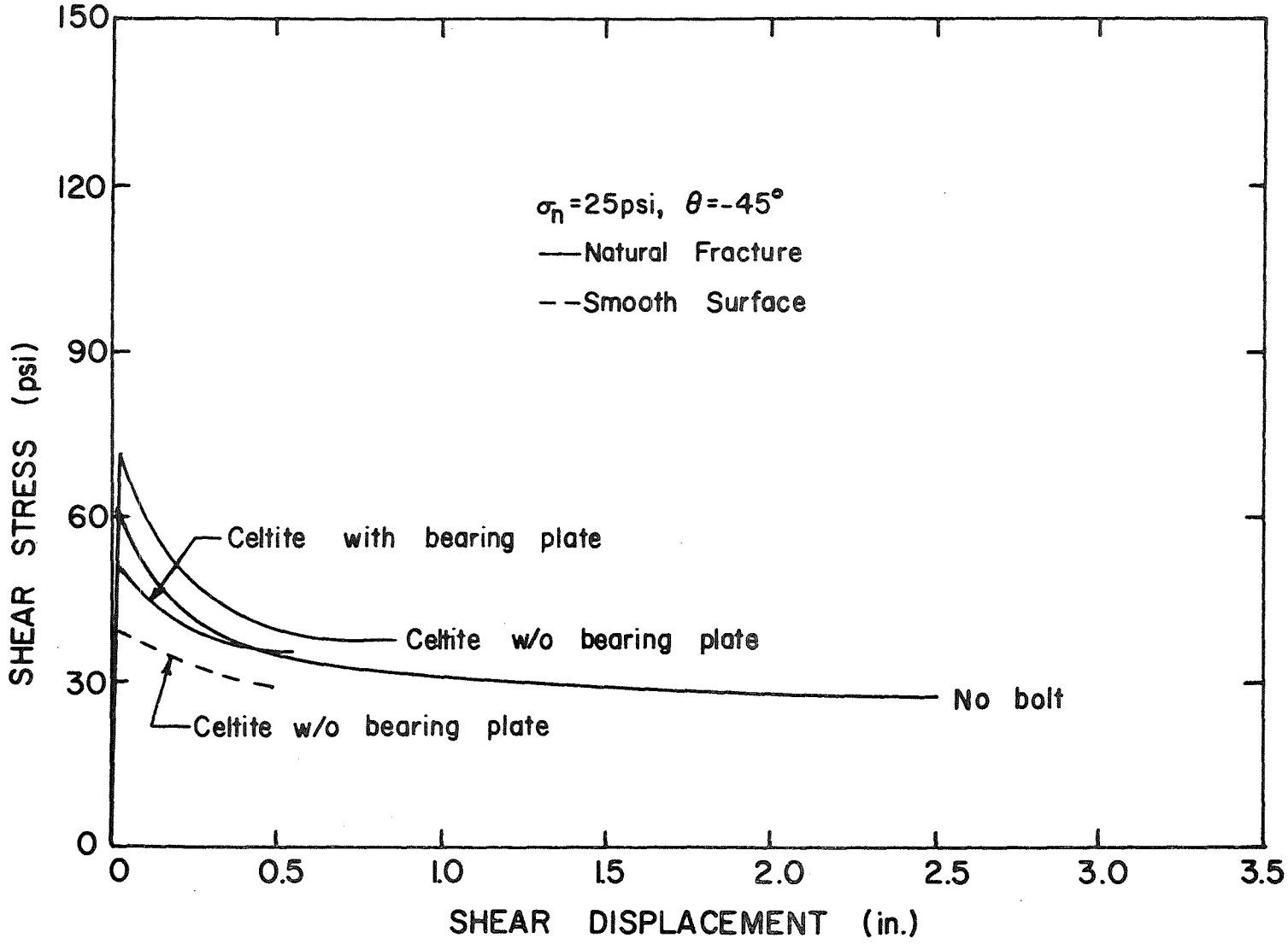

Fig. 4-20 Average Shear Stress versus Shear Displacement for Inclined Bolt, Natural Fracture, and Low Normal Pressure

When comparing the Fasloc and Celtite systems referred to in these graphs, note that the Celtite system is a 7/8-in. diameter re-bar in a 1 3/8-in. diameter hole with Celtite resin and the Fasloc system is a 3/4-in. DuPont design (new type) steel bar in a 1-in. diameter hole with Fasloc resin. Both bolt systems were installed according to the respective manufacturer's recommendations.

Fig. 4-18 for the 0-degree bolt orientation shows that the three curves for bolted natural fracture shear surfaces are nearly coincident for shear displacements up to approximately 0.1 in. The use of the bearing plate and rotary drilled holes did increase the shear resistance beyond that point, however, as can be seen by the upper two curves for the Celtite system. The Fasloc system was nearly as strong as the Celtite system, even though the hole and bar sizes were smaller for the Fasloc system.

The jagged appearance of the Celtite curve with bearing plate (Fig. 4-18) is due to fracturing of the shear blocks which fell apart into several pieces when the confinement was released. The bolts did not shear off in this case. The block split in one test and the bolt sheared in another test with the Fasloc system. The shear resistance decreased almost to the no-bolt condition after the bolt sheared. A major portion of the anchorage along the grout column was lost when the blocks of rock began to split and break apart. The exposed ends of the bars then began to pull into the rock as the shear displacement continued.

The average shear stress for the Celtite system in the 0-degree bolt orientation at a shear displacement of 0.1 in. increased from 79.5 to 98 psi when the bearing plate and rifled drill hole were employed. Also, the maximum shear stress for this system increased from 110 to 141 psi when the bearing plate and rifled hole were used. Thus, increasing the anchorage capability of the system did, in fact, increase the shear strength of the bolted joint. The 45-degree bolt orientation results in high tensile loading of the bar in the region of the shear surface. The increased tensile load has a normal component which tends to pull the blocks together and thus increase the frictional strength along the shear surface. In addition, there is an upward component of bolt load which helps resist the force producing the shear displacement.

The data for the 45-degree bolt orientation shown in Fig. 4-19 shows that the additional anchorage provided by the bearing plates and rifled holes increased both the initial shear resistance and the maximum shear resistance of the Celtite system. As in the 0-degree bolt orientation, the Fasloc system in the smaller hole (1 in.) was nearly as effective as the larger Celtite installation (1 3/8-in. holes). The steel bars sheared off in three of the four tests in the 45-degree bolt orientation at shear displacements ranging from 0.4 to 0.9 in.

The bearing plates and rifled holes increased the shear resistance at a displacement of 0.1 in. by 32 psi as compared to bars with unrestrained ends and with smooth drill holes in the 45 degree bolt orientation. The Fasloc system with 1-in. holes had essentially the same shear strength at d = 0.1 in., as did the Celtite system in 1 3/8-in. holes in the 45-degree orientation. The maximum shear resistance developed at shear displacements between 0.07 and 0.47 in. The curves of shear stress

versus shear displacement are typified by a rapid increase in shear stress with increasing shear displacement, followed by more or less constant stress until the bars sheared off, at which time the shear resistance drops to near the unbolted case.

The -45-degree bolt orientation is unfavorable for resisting shear movement because high loads are exerted on the rock forming the acute angle between the bolt and the shear surface. Because of this unfavorable geometry, the rock in this region is easily crushed which allows the bolt to bend. Axial compressive bolt loads are generated because the shear movement is such that the bolt tends to be shortened. There is no apparent reason that the curve "with bearing plate" in Fig. 4-20 should be lower than the one labeled "without bearing plate" for the -45-degree bolt orientation. As a practical matter, neither curve is significantly above the no-bolt curve, particularly when comparing these results with those in Figs. 4-18 and 4-19 where the bolted strength is much greater. High compressive bolt strains were measured at the shear surface. Smaller compressive bolt strains are observed at the other two gage locations 6.0 in. on either side of the shear plane. The exposed ends of the bars pushed out of the rock slightly as the shear displacement continued.

The bolts did not shear in the tests at the -45-degree bolt orientation. The rock blocks separated and the bolt was severely bent. The test was stopped when the left side plate on the test frame began to bear on the testing machine columns. Normal displacements of the shear blocks reached approximately 0.5 in.

E. Effects of Rock Type on Shear Resistance

All of the shear tests previously discussed were performed with Indiana limestone rock. This rock type is particularly useful for comparative tests because of its uniformity and limestone is a rock type commonly found in the roof bed sequence over a coal mine opening.

Two shales were also tested: Dry Wood shale from western Missouri and Interbedded shale from southern Illinois. The mechanical properties of the limestone and two shales are given in Table 4-1 and the smoothness and flatness of the machined shear surfaces are given in Table 4-2. The Interbedded shale was the strongest of the three rocks, with a compressive strength of 28,170 psi. The Indiana limestone had an intermediate strength of 9,230 psi and the Dry Wood shale had the lowest strength of 6,410 psi. These strength values apply to cores drilled perpendicular to the bedding planes.

The results of tests with conventional expansion-anchor bolts and Celtite grouted re-bars (7/8-in. diam. bar in 1 3/8-in. diam. hole) are given in Figs. 4-21 and 4-22 for the limestone and the Dry Wood shale. These tests were performed with the 0-degree bolt orientation and at the low and high normal pressures. The most significant difference between the two rock types was that the coefficient of friction (without a bolt) was much less for the Dry Wood shale than for the limestone (see Table 4-3). For this reason the curves for the shale are in each case displaced downward from the corresponding curves for the limestone.

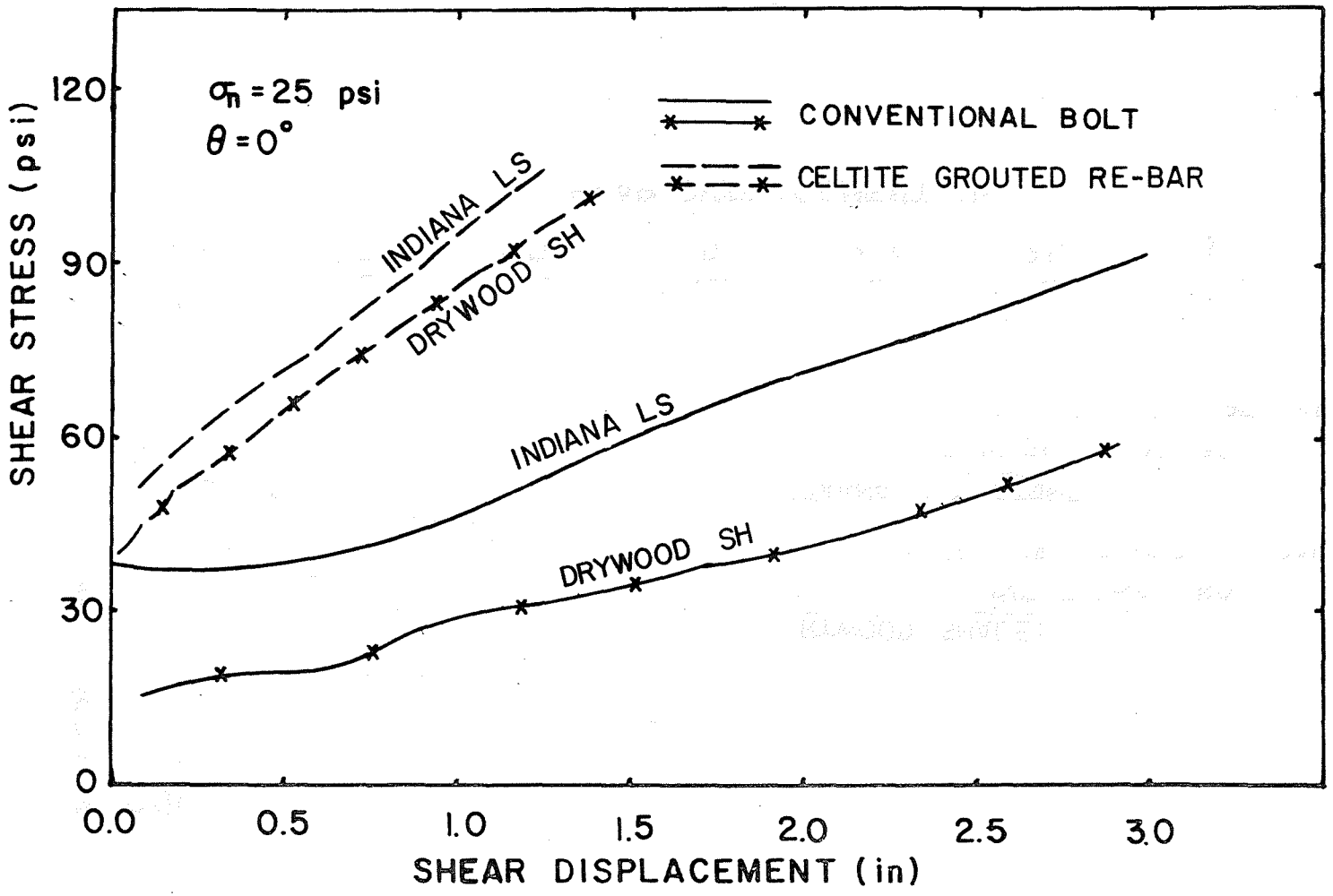

Fig. 4-21 Comparison of Shear Resistance for Limestone and Shale at Low Normal Pressure

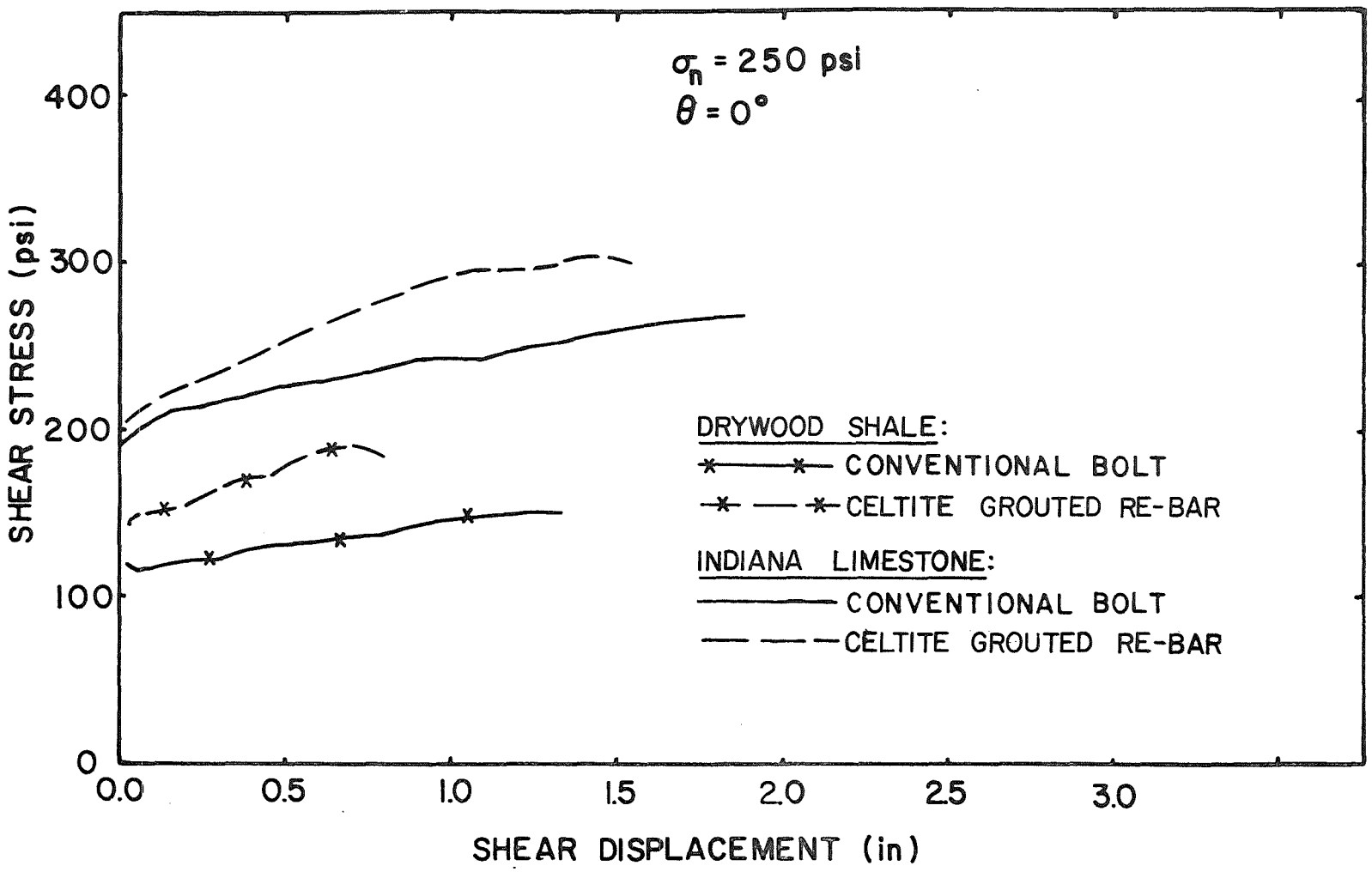

Fig. 4-22 Comparison of Shear Resistance for Limestone and Shale at High Normal Pressure

Table 4-3. Friction Properties of Various Rock Types at Low Normal Pressure, σ_n = 25 psi

Rock Type	Average Shear Stress, Without Bolt, psi	Coefficient of Friction
Indiana Ls	22.6	0.904
Dry Wood Sh	10.8	0.433
Interbedded Sh	20.0	0.800

The tests on the Interbedded shale were performed with the Fasloc system consisting of a 3/4-in. diameter bar in a 1-in. diameter rifled hole. The drill holes were core drilled 1 3/8-in. diameter for the Celtite system tests on the Indiana limestone and Dry Wood shale. The effectiveness of these two fully grouted bolting systems in the three rock types are compared in Figs. 4-23 and 4-24.

These curves show that the shear resistances were nearly the same for the Interbedded shale and the Indiana limestone even though different types of bolts and different hole diameters were employed. The tendency of the bolts to shear off rather than deform and crush the rock was greater for the Fasloc system. Rifled holes in this hard rock provided excellent anchorage so that the blocks would not separate as easily and thus would produce more of a direct shear on the bolt as the shear displacement occurred. Secondly, the harder rock would not crush as easily under the lateral loads imposed on the sides of the drill hole by the steel and grout column and thus would present a more rigid edge to shear the bolt.

The excellent anchorage of the Fasloc system in the Interbedded shale is also evident from the very small recorded pull-out of the bar ends which did not exceed 0.007 in., while the pull-out of the Celtite system with smooth holes in limestone exceeded 0.075 in.

F. Numerical Values of Shear Resistance

The graphs of shear stress versus shear displacement presented and discussed in the previous sections are based on the average shear stress over the shear area. The shear area A_s at some shear displacement d was determined from the equation

$$A_s = 24\ (24 - d)\ \text{in.}^2 \qquad (4\text{-}10)$$

since the initial contact surface between the shear test blocks was 24 by 24 in.

As seen from Eq. (4-10) the shear area decreased as the shear displacement increased. While this accurately describes the conditions in the test setup, such a decrease in area would not occur for a typical bolt in a systematic bolting pattern; the shear area would then remain constant as shear displacement increases.

For vertical bolts in a square pattern with a spacing D and with a horizontal shear plane, the shear area of influence for a given bolt is

$$A_s = D^2 \qquad (4\text{-}11)$$

In a general case the bolt may not be inclined to both the shear surface and the surface on which the bolt spacing D is laid out as shown in Fig. 4-25. The angle θ is the angle between the bolt and the normal to the shear surface. The angle ψ is the angle between the bolt and the normal to the surface of the opening on which the spacing D is measured.

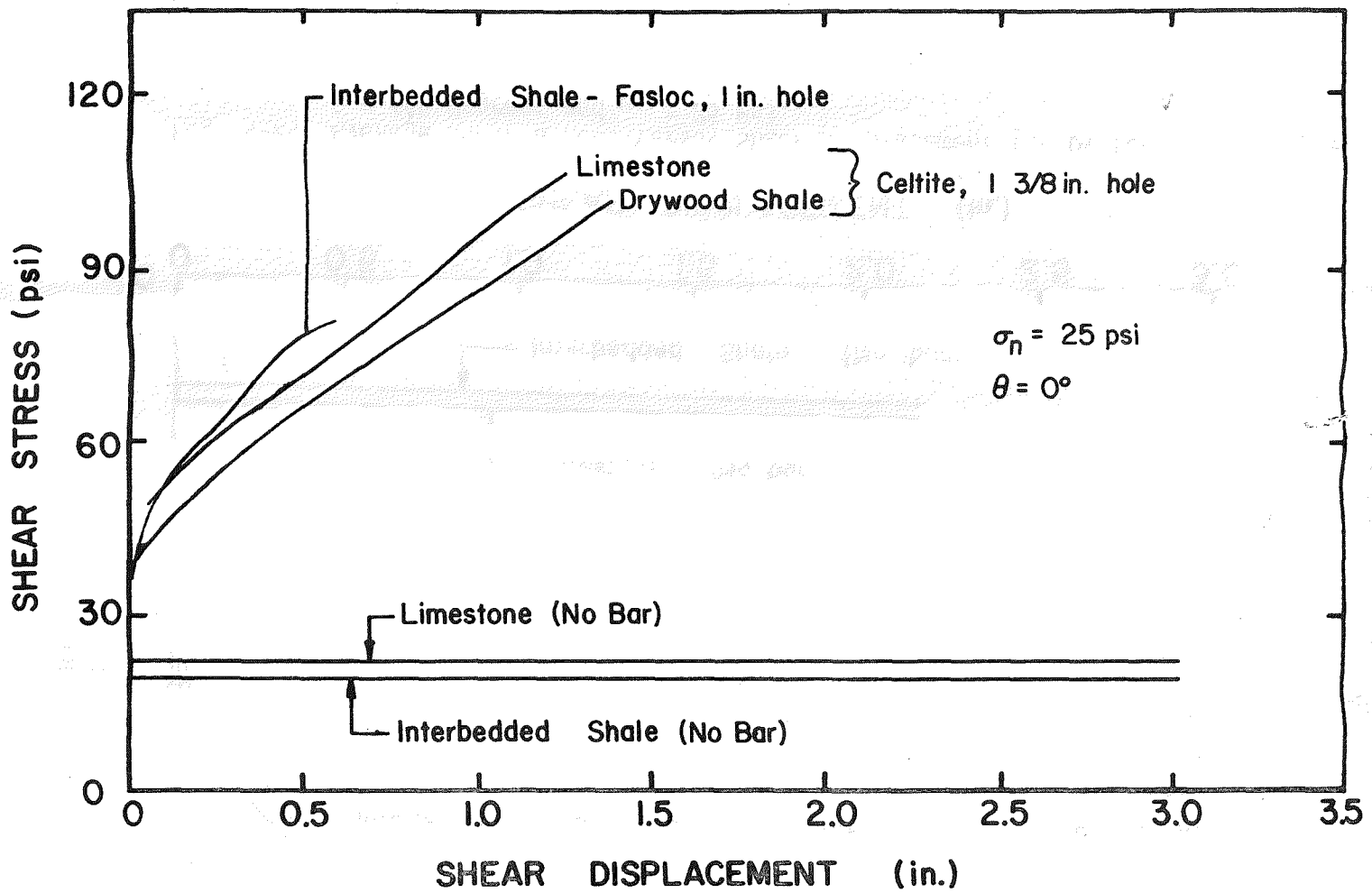

Fig. 4-23 Average Shear Stress Versus Shear Displacement for Different Rock Types, θ = 0 Degrees and σ_n = 25 Psi.

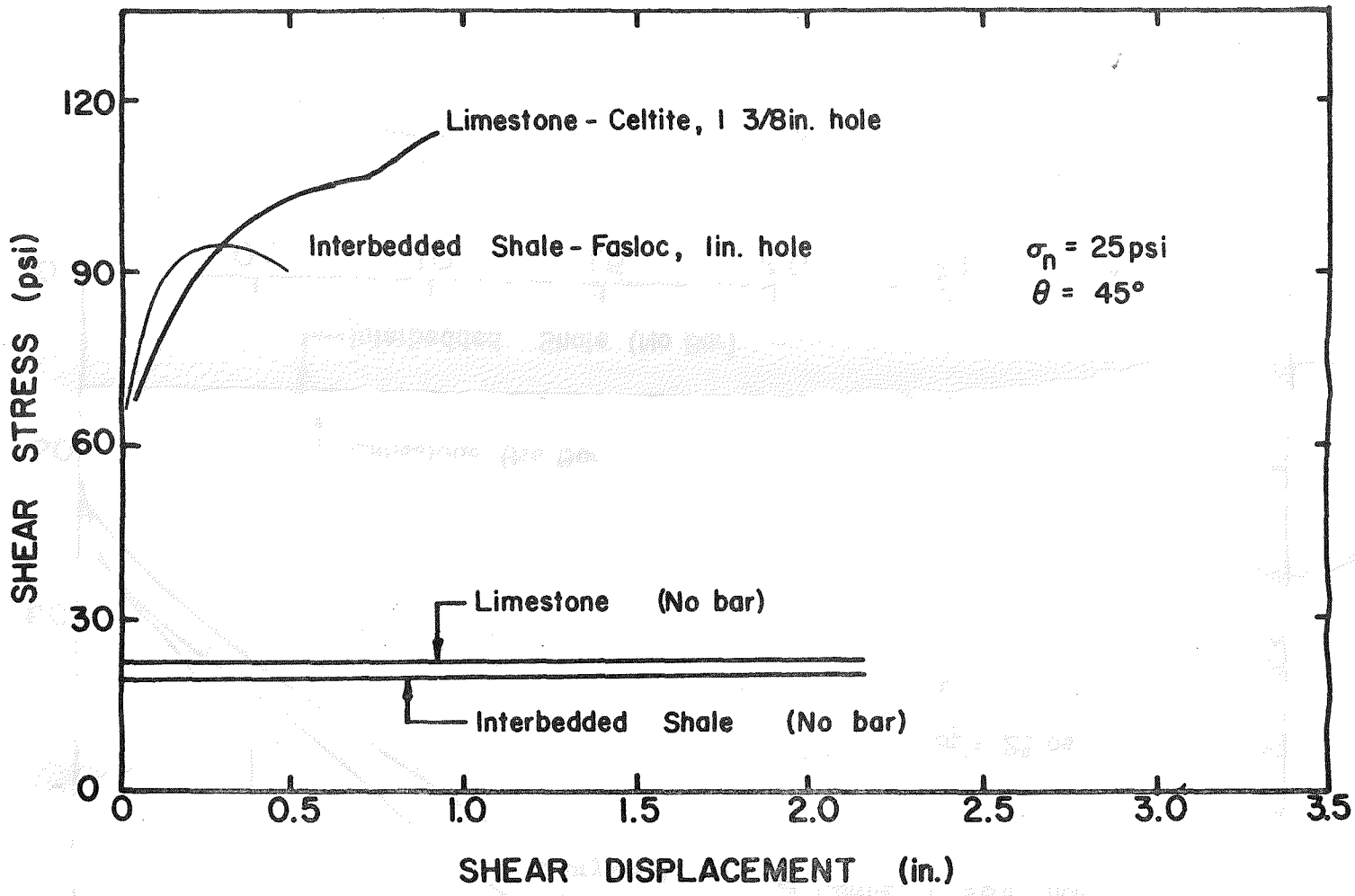

Fig. 4-24 Average Shear Stress Versus Shear Displacement for Different Rock Types, Θ = +45 Degrees and σ_n = 25 Psi.

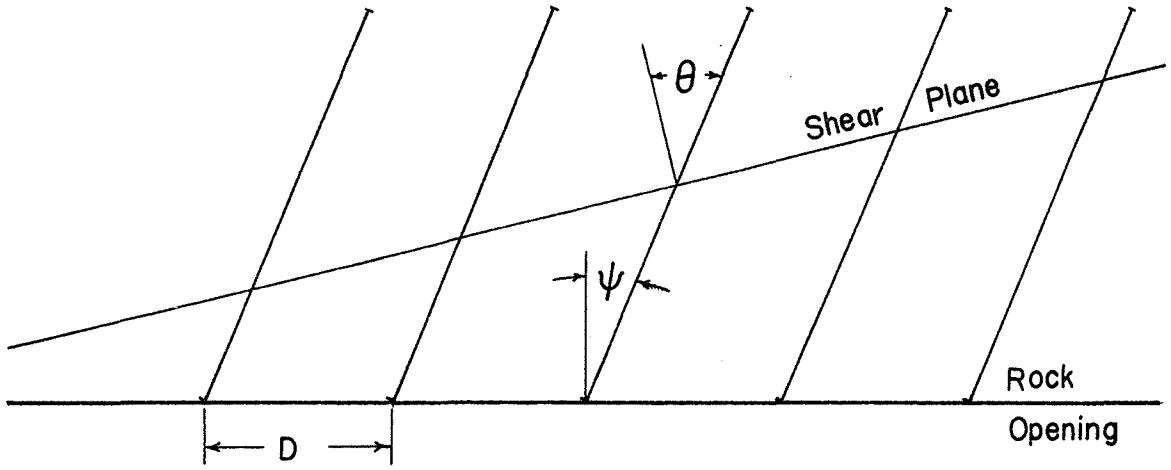

Fig. 4-25 Geometry of Inclined Bolts Intersecting a Shear Surface

The shear area of influence for a representative bolt is then given by the equation

$$A_s = \frac{D^2 \cos \psi}{\cos \theta} \qquad (4\text{-}12)$$

The shear resistance along the bolted shear surface is due to two contributions: that due to the frictional strength of the shear surface developed as a result of the normal stress and that due to the bolt. In order to apply the shear stress data in the previous curves to other bolt spacings it is necessary, therefore, to separate out the contribution due to the bolt. This has been done and the results are presented in Tables 4-4 through 4-6 as follows:

Table 4-4. Indiana limestone, smooth shear surface, θ = 0, 45, and -45 degrees σ_n = 25 and 250 psi

Table 4-5. Indiana limestone, natural-fracture shear surface, θ = 0, 45, and -45 degrees σ_n = 25 and 250 psi

Table 4-6. Dry Wood shale and Interbedded shale, smooth shear surface θ = 0, 45, and -45 degrees σ_n = 25 and 250 psi

In Tables 4-4 through 4-6 the shear resistance of the bolt in lbs is given for small shear displacements (d = 0.1 in.) and for the shear displacement at which the maximum shear resistance was generated. Within each bolt orientation, 0 = 0, 45, and -45 degrees, the values are listed in order of decreasing resistance at d = 0.1 in. Thus, the most effective installations will be at the top of the list in each category. The values for the low normal pressure (σ_n = 25 psi) are followed by those at the high normal pressure (σ_n = 250 psi). The values listed are the average of two test values in most instances.

G. Failures Associated with Shear Tests

Most of the previously described tests resulted in either the bolt (or reinforcing bar in the grouted-bar tests) shearing or the left shear block splitting. In several of the tests at the low normal pressure of 25 psi, particularly those with inclined bolts, the blocks separated to such an extent that the left side plate began to bear on the testing machine columns. In these instances it was necessary to stop the test at this point and the above mentioned failures did not occur.

Table 4-4 Shear Resistance of Rock Bolts in Indiana Limestone with a Smooth Shear Surface

Normal Pressure σ_n, psi	Bolt Orientation θ, degrees	Type of Bolt Installation	Type of Hole	Shear Force at d = 0.1 in. lbs	Max. Shear Force lbs	Displ. for Max. Shear Force, in.
25	0	Celtite system, post-tensioned	Smooth	21,800	48,000	1.617
25	0	Celtite system, pretensioned	Smooth	19,200	44,000	1.039
25	0	Celtite system, untensioned	Smooth	18,900	45,700	1.275
25	0	Fasloc system, (old), untensioned	Smooth	13,200	31,600	2.703
25	0	Fiberglass-resin, untensioned	Smooth	9750	18,900	0.250
25	0	Conventional, tensioned	Smooth	9470	33,100	3.126
25	0	Fasloc system, (new), untensioned	Rifled	8030	26,500	1.402
25	0	Split tube, without anchors	Smooth	8030	21,000	1.101
25	0	Split tube, with anchors	Smooth	4590	24,700	1.796
25	0	Split tube, with anchors	Rifled, oversize	3730	23,500	2.753

Table 4-4 (continued)

Normal Pressure σ_n, psi	Bolt Orientation θ, degrees	Type of Bolt Installation	Type of Hole	Shear Force at d = 0.1 in. lbs	Max. Shear Force lbs	Displ. for Max. Shear Force, in.
25	+45	Fasloc system, (new), untensioned	Rifled	39,600	46,100	0.303
25	+45	Fiberglass-resin, untensioned	Smooth	36,700	36,700	0.100
25	+45	Celtite system, pretensioned	Smooth	35,600	56,200	1.779
25	+45	Celtite system, untensioned	Smooth	32,700	52,000	1.016
25	+45	Celtite system, post-tensioned	Smooth	28,100	54,600	0.942
25	+45	Split tube, without anchors	Smooth	22,700	28,700	0.601
25	+45	Conventional, tensioned	Smooth	20,900	29,000	1.763
25	+45	Split tube, with anchors	Rifled, oversize	4880	17,900	2.766
25	-45	Celtite system, post-tensioned	Smooth	11,500	12,800	0.021
25	-45	Celtite system, pre-tensioned	Smooth	8890	10,600	0.807

Table 4-4 (continued)

Normal Pressure σ_n, psi	Bolt Orientation θ, degrees	Type of Bolt Installation	Type of Hole	Shear Force at d = 0.1 in. lbs	Max. Shear Force lbs	Displ. for Max. Shear Force, in.
25	-45	Celtite system, untensioned	Smooth	8890	10,500	0.052
25	-45	Split tube, without anchors	Smooth	8604	15,600	2.052
25	-45	Split tube, with anchors	Rifled, oversize	3440	12,600	3.211
25	-45	Fiberglass-resin, untensioned	Smooth	860	4680	0.530
250	0	Celtite system, pretensioned	Smooth	16,100	42,200	1.444
250	0	Celtite system, post-tensioned	Smooth	9750	41,400	1.457
250	0	Celtite system, untensioned	Smooth	6310	44,200	1.652
250	0	Conventional, tensioned	Smooth	-1430	17,600	2.401
250	+45	Celtite system, untensioned	Smooth	30,100	48,100	0.651

Table 4-4 (continued)

Normal Pressure σ_n, psi	Bolt Orientation θ, degrees	Type of Bolt Installation	Type of Hole	Shear Force at d = 0.1 in. lbs	Max. Shear Force lbs	Displ. for Max. Shear Force, in.
250	+45	Conventional, tensioned	Smooth	14,300	25,900	1.855
250	-45	Celtite system, untensioned	Smooth	9180	4410	2.875
250	-45	Conventional, tensioned	Smooth	-1150	910	2.901

Table 4-5 Shear Resistance of Rock Bolts in Indiana Limestone with Natural Fracture Shear Surfaces

Normal Pressure σ_n, psi	Bolt Orientation θ, degrees	Type of Bolt Installation	Type of Hole	Shear Force at d = 0.1 in. lbs	Max. Shear Force lbs	Displ. for Max. Shear Force, in.
25	0	Celtite system, untensioned	Rifled	28,300	58,300	2.699
25	0	Fasloc system, untensioned	Rifled	24,300	39,600	0.579
25	0	Celtite system, untensioned	Smooth	17,700	43,600	1.723
25	+45	Celtite system, untensioned	Rifled	51,200	60,600	0.634
25	+45	Fasloc system, untensioned	Rifled	46,900	53,100	0.300
25	+45	Celtite system, untensioned	Smooth	33,200	42,600	0.865
25	-45	Celtite system, untensioned	Smooth	6190	6430	0.090
25	-45	Celtite system, untensioned	Rifled	-2120	-114	0.250
250	0	Celtite system, untensioned	Smooth	21,800	59,300	2.544
250	+45	Celtite system, untensioned	Smooth	39,500	55,600	1.000

Table 4-6 Shear Resistance of Rock Bolts in Shale with Smooth Shear Surfaces

Normal Pressure σ_n, psi	Bolt Orientation θ, degrees	Type of Bolt Installation	Type of Hole	Shear Force at d = 0.1 in. lbs	Max. Shear Force lbs	Displ. for Max. Shear Force, in.
25	0	Dry Wood shale, Celtite system, untensioned	Smooth	21,200	50,400	1.434
25	0	Dry Wood shale, conventional. tensioned	Smooth	4880	20,800	2.951
250	0	Dry Wood shale, Celtite system, untensioned	Smooth	25,800	45,400	2.001
250	0	Dry Wood shale, conventional, tensioned	Smooth	4020	16,100	3.002
25	0	Interbedded shale, Fasloc system, untensioned	Rifled	19,200	35,700	0.667
25	+45°	Interbedded shale, Casloc system, untensioned	Rifled	39,300	44,100	0.286

The vertical splitting depicted in Fig. 4-26 was caused by the lateral force of the bolt or grouted reinforcing bar acting as a wedge against the sides of the drill hole and splitting the blocks apart.

The bolts were either sheared off completely during the test or were greatly deformed as they were loaded laterally by the sides of the drill hole as the shear load caused the holes to become offset. The tendency for the bolts to shear was greater at the high normal pressure than at the lower pressure. For example, in the tests performed on limestone blocks with smooth shear surfaces 4 out of 22 bolts and grouted reinforcing bars were sheared at the low normal pressure while 10 out of 17 were sheared at the higher normal pressure. At the low normal pressure the bolts and grouted reinforcing bar were often deformed between the blocks and actually forced the blocks to separate as shown in Fig. 4-27. At the high normal pressure, however, the blocks did not separate and the bolt or reinforcing bar experienced more of a direct shear as shown in Fig. 4-27. Crushing occurred in the surrounding rock to a depth of about 0.5 in. at both normal pressures since extremely high compressive loads were applied to the sides of the drill hole by the bolts and grouted reinforcing bars.

The sheared ends or portions of typical bolts and reinforcing bars are shown in Figs. 4-28 and 4-29. The bolt designated L-33 in Fig. 4-28 is typical of the conventional bolts sheared at the low normal pressure of 25 psi. The bolt is grossly deformed but did not shear. On the other hand, the conventional bolt from Test L-27 at the high normal pressure of 250 psi was sheared.

The reinforcing bar and grout annulus were recovered from Test L-13 (Fig. 4-28) at the high normal pressure. The bolt was sheared and the block split apart. The bar was flattened considerably and plastically deformed during the test. The deformation of a typical grouted reinforcing bar from Test L-3 at the low normal pressure is shown in Fig. 4-29. This bar did not shear. However, one of the shear blocks split at a shear displacement of approximately 1.3 in. which allowed the reinforcing bar and grout column to become exposed.

It was noted in several of the tests in which one of the shear blocks split away from the grouted reinforcing bar that the resin grout did not bond strongly to either the rock or reinforcing bar. In all cases the grout broke cleanly away from the rock or reinforcing bar. The reinforcing bars were also reasonably well centered in the holes even though there was no direct control over the position of the far end of the reinforcing bar during installation.

Effect of Bolt Spacing and Bolt Length on Shear Resistance

The theoretical equations developed in the section "Theoretical Analysis - Conventional Bolts" in this chapter have been applied to other bolt spacings and bolt lengths such as are typical in coal mine applications.

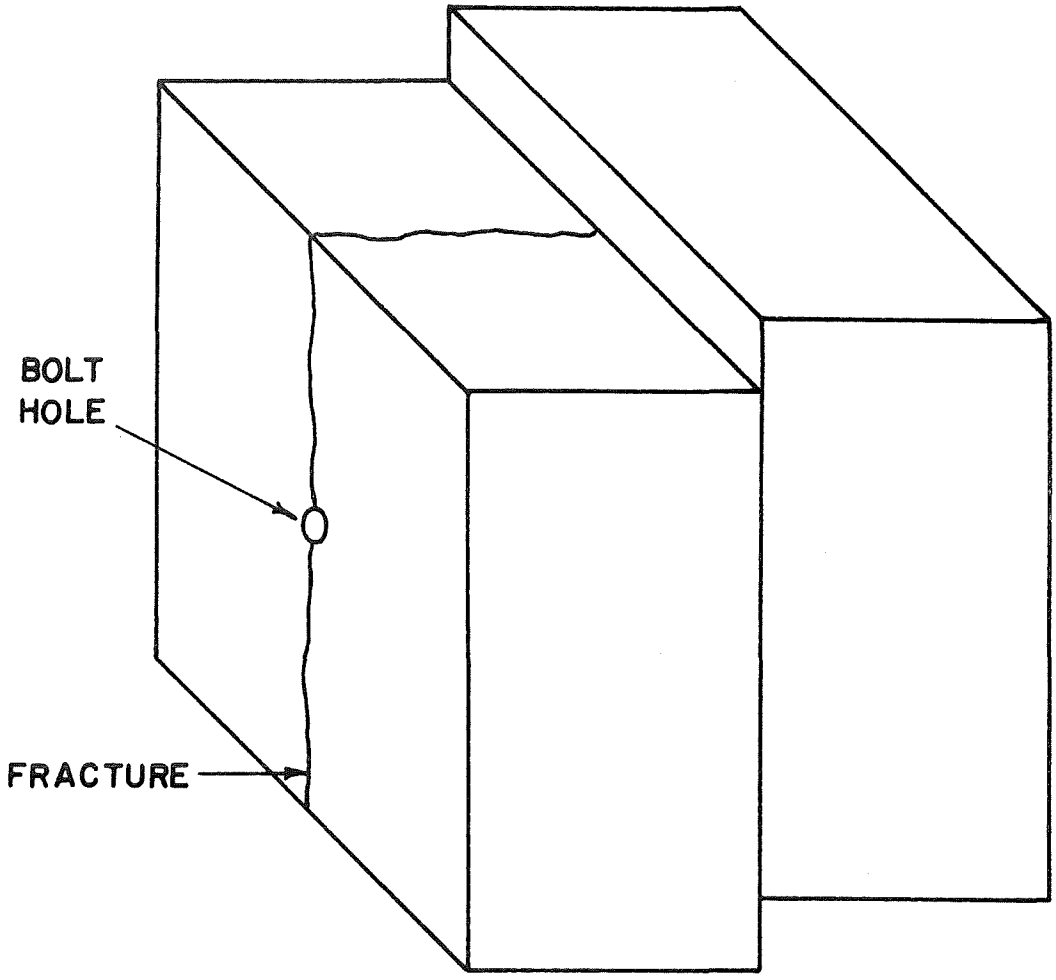

Fig. 4-26 Typical Block Splitting during Shear Tests

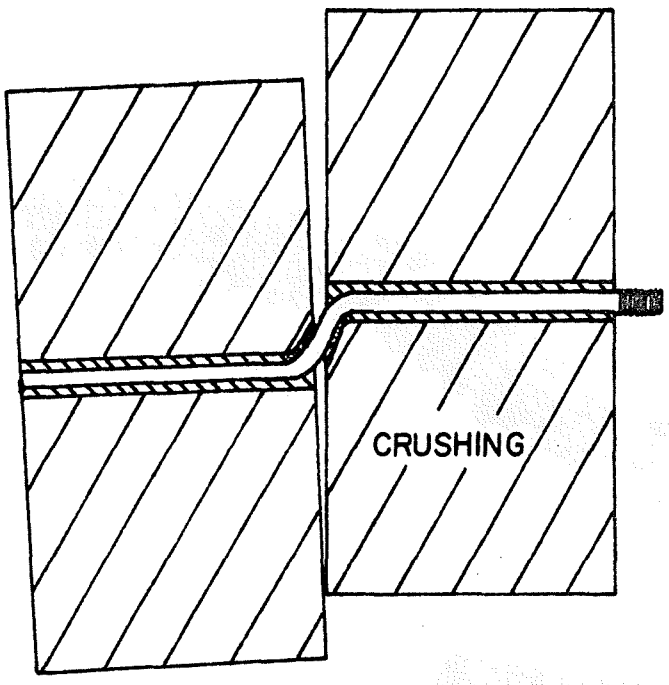

a) LOW NORMAL PRESSURE

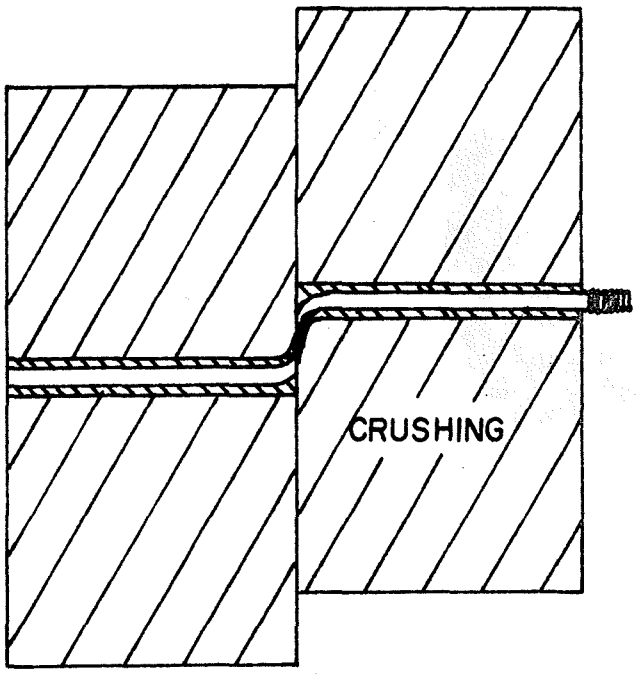

b) HIGH NORMAL PRESSURE

Fig. 4-27 Sections Through Shear Blocks Showing Typical Deformations and Failures

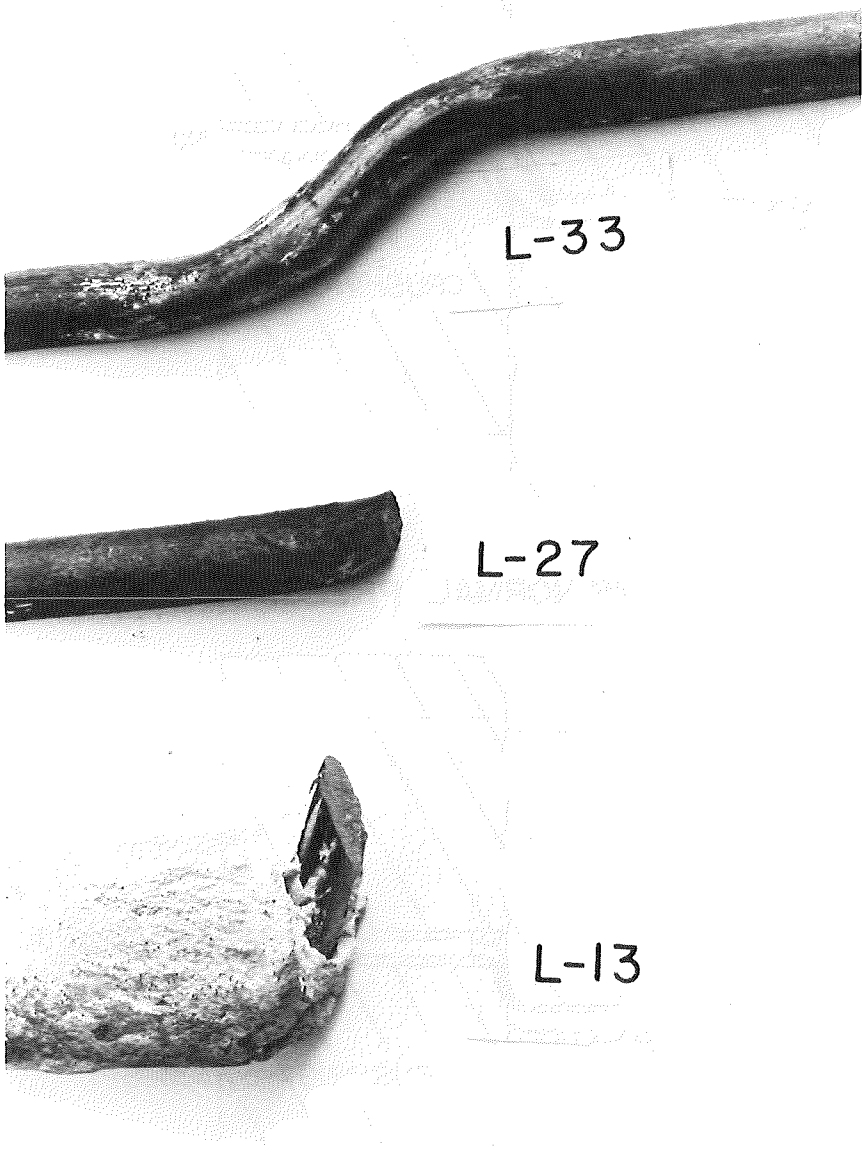

Fig. 4-28 Photograph of Sheared Bolts Recovered from Tests L-33, L-27, and L-13

Fig. 4-29 Photograph of Grouted Reinforcing Bar after Test L-3 at Low Normal Pressure

Eq. (4-2) restated here

$$\tau_{ave} = \tau_o + \frac{\mu T \cos \theta_1 + T \sin \theta_1}{A_s} \qquad (4\text{-}2)$$

was applied with the associated Eqs. (4-3) through (4-5) and with the following basic properties and dimensions for limestone rock and 5/8 in. conventional bolts:

Young's modulus for bolt = $E_b = 28.65 \times 10^6$ psi

Cross-sectional area of bolt = $A_b = 0.2453$ in.^{2}

Installation bolt strain = $\varepsilon_o = 1{,}500$ μin./in.

Yield strength of bolt = 63,600 psi

Yield strain of bolt = $\varepsilon_y = 2{,}200$ μin./in.

For the low normal pressure ($\sigma_n = 25$ psi) the coefficient of friction, μ, is 0.903; for high normal pressure (250 psi) the value of μ is 0.871. The corresponding values for τ_o are 22.58 psi and 217.7 psi.

The results of the calculations shown graphically in Figs. 4-30 through 4-33 do not include the increased shear resistance created by the direct shear action on the bolt as it is pinched between the offset drill holes. This effect becomes important for shear displacements greater than 0.816 in. for normal bolts and 1.154 in. for bolts inclined at ± 45 degrees (for 5/8-in. diameter bolts in 1 3/8-in. diameter holes). The shear stress curves are therefore shown as dashed lines for displacements greater than these values, indicating that the actual shear stress (including the direct shear of the bolt) is higher than what the curves indicate.

As can be seen from the graphs in Fig. 4-30 through 4-33, the spacing has a definite effect on the shearing stress. In the cases where θ = 0 degrees and θ = 45 degrees the shearing stress decreases with increased bolt spacing. On a relative basis the stress drop becomes less pronounced as the spacing increases. The shear area increases as the square of the bolt spacing and since the area is the divisor in Eq. (4-2) the shear contribution due to the bolt decreases inversely with the square of the spacing.

It is interesting to note that the decreases in shear stress with increased bolt spacing (at the same bolt orientation) for the high and low normal pressures, σ_n, are nearly identical. This is due to the fact that the contribution to the shear stress by the bolt [the second term in Eq. (4-2)] is a function of the shear area, A_s, and the coefficient of friction. On the other hand, the frictional stress, τ_o, is independent of the shear area. The above mentioned decreases in shear stress would be equal if the coefficients of friction, μ, were the same at the two

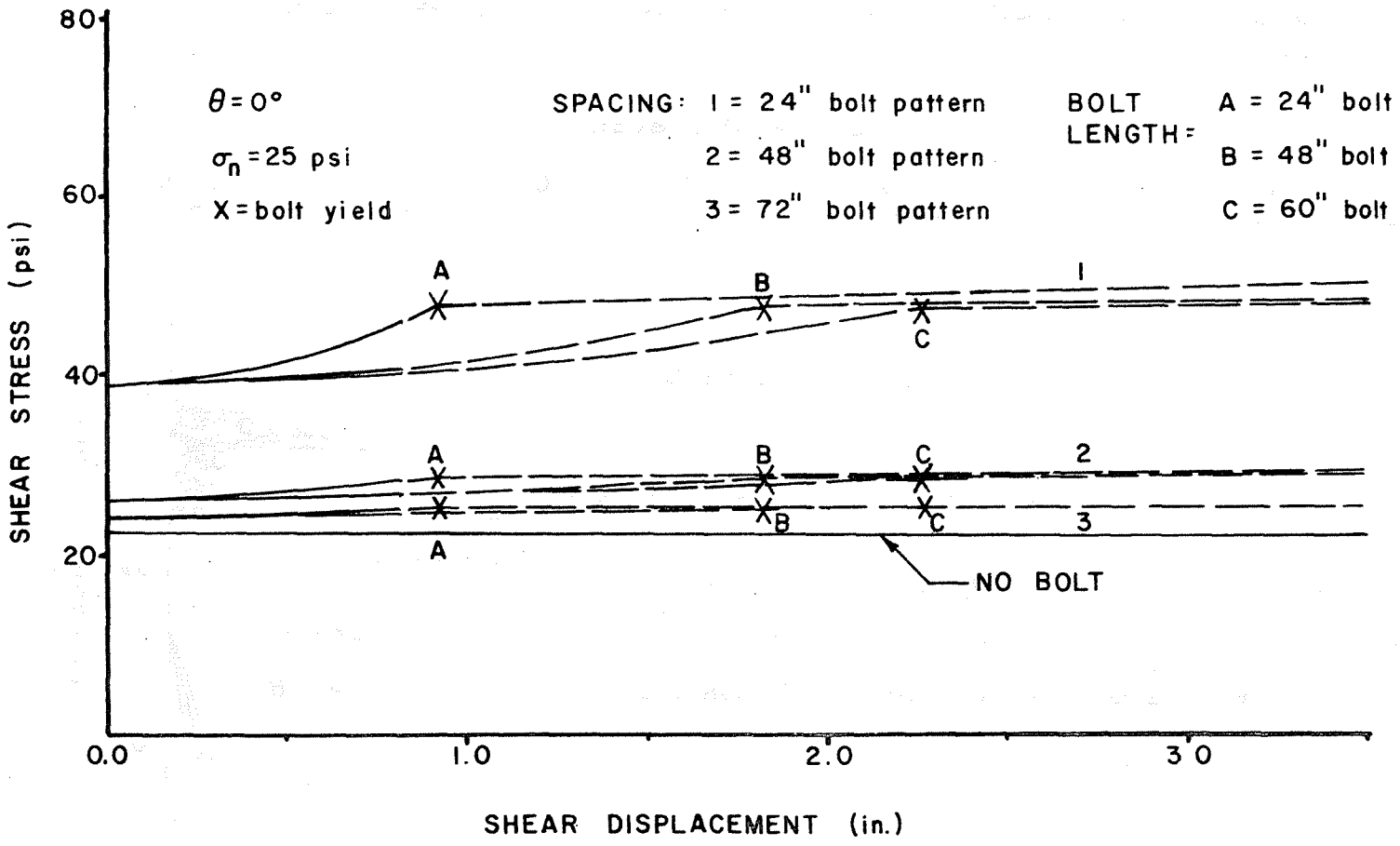

Fig. 4-30 Theoretical Curves of Shear Stress Versus Shear Displacement for Normal Bolts and Low Normal Pressure

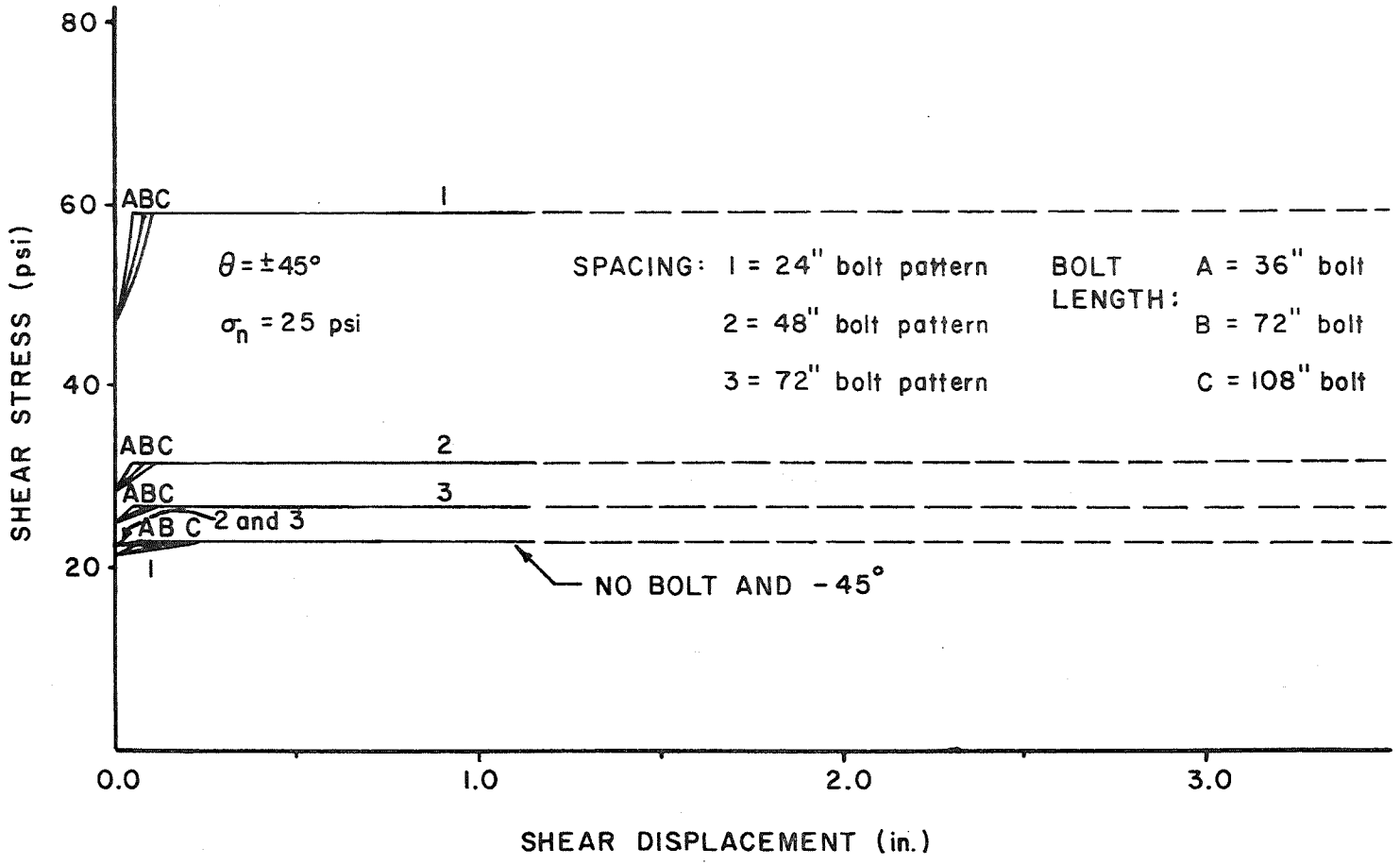

Fig. 4-31 Theoretical Curves of Shear Stress Versus Shear Displacement for Inclined Bolts and Low Normal Pressure

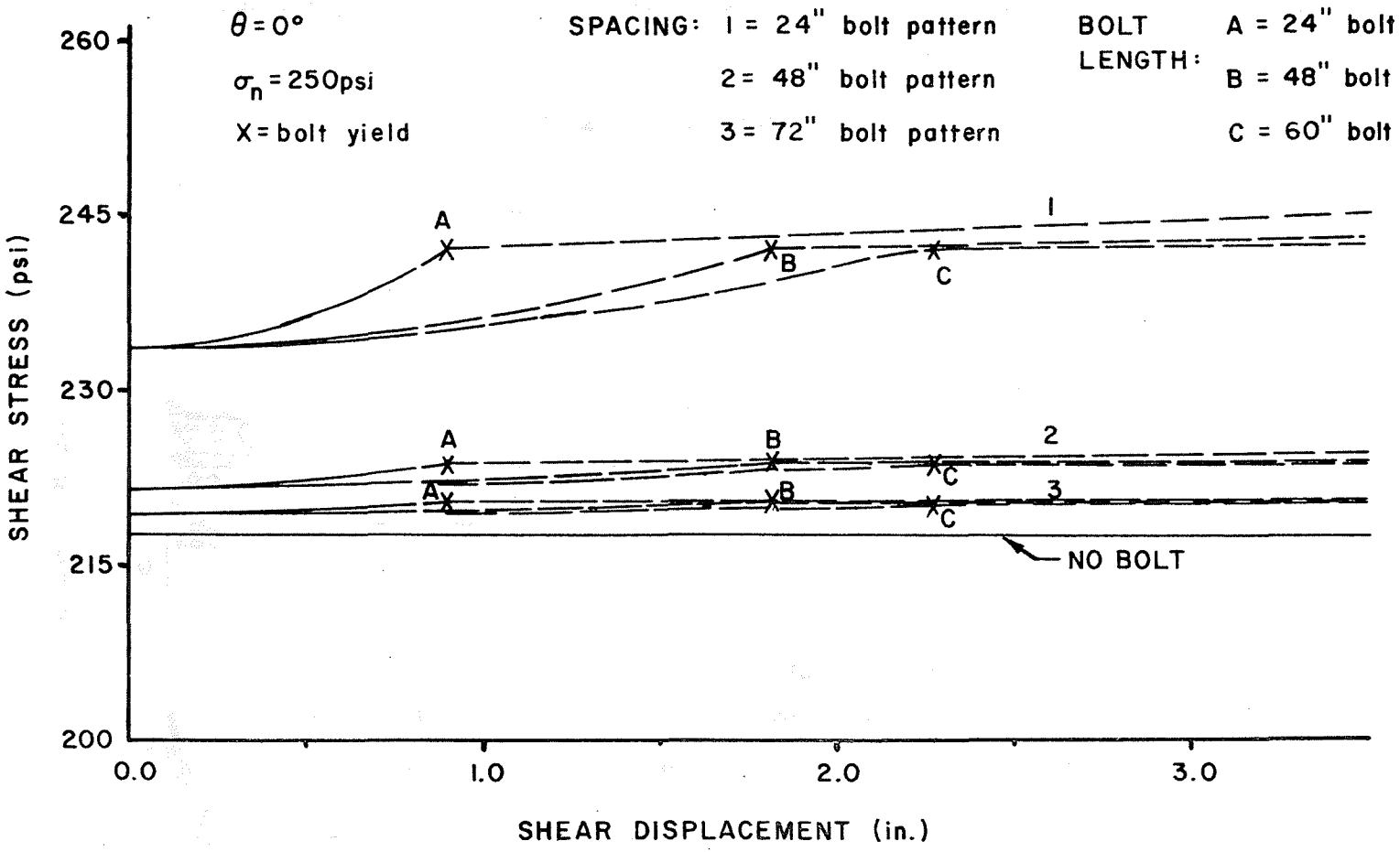

Fig. 4-32 Theoretical Curves of Shear Stress Versus Shear Displacement for Normal Bolts and High Normal Pressure

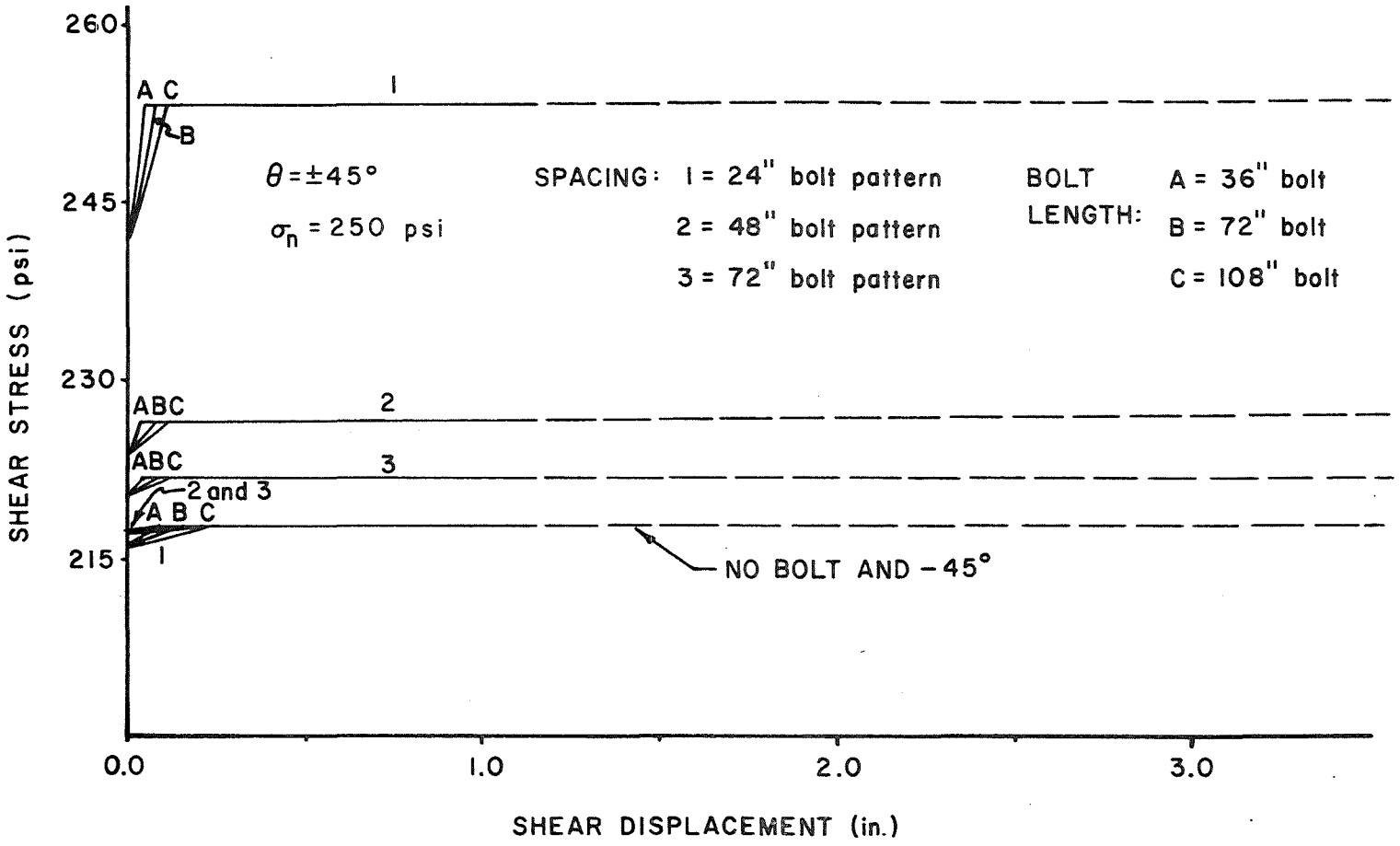

Fig. 4-33 Theoretical Curves of Shear Stress Versus Shear Displacement for Inclined Bolts and High Normal Pressure

normal pressures. In these calculations, the values of μ were 0.871 and 0.903 at the high and low normal pressures, respectively; thus, there is a slight difference in the drops in shear stress with increased spacing at the two normal pressures.

The apparent anomaly of the shear stress increasing with increases in spacing in the -45-degree case can be explained by an examination of Eq. (4-2). The component symbolized by $T \sin \theta_1$ is negative for negative angles and for these angles will cause a decrease in the total shear stress if the magnitude of $T \sin \theta_1$ is greater than $\mu T \cos \theta_1$. This effect is reduced when the shear area is increased.

The increase in shear resistance, $\Delta\tau$, caused by bolting is due in part to an increased normal stress, $\Delta\sigma_n$, on the shear surface which in turn increases the frictional stress since $\Delta\tau = \mu\Delta\sigma_n$. This quantity, $\Delta\sigma_n$, is caused by the initial bolt tension induced by torqueing the bolt and later by extension of the bolt. As the displacement increases, it causes increasing strain in the bolt; this in turn raises the tension in the bolt [Eq. (4-5)], which induces a larger shear stress [Eq. (4-2)]. The upward trend in the shear stress curve continues at an increasing rate until the yield strength of the bolt is reached. At this point the rate of increase drops sharply and a very gradual increase, due to change in θ_1, takes place. This effect is very apparent with normal bolts 24 in. long and spaced 24 in. apart as shown in Figs. 4-30 and 4-32.

As the bolt length increases, larger shear displacements are required to cause the bolt strain to reach its yield value. This effect is readily apparent in the top three curves in Fig. 4-32. The elastic portions of these curves have lesser slopes when the bolt lengths are long because the bolt extension is distributed over greater lengths.

For a given bolt length and orientation the shear displacement necessary to reach yield in the bolt is the same regardless of the normal pressure on the shear plane or the bolt spacing. For the normal bolt orientation, θ = 0 degrees, the displacements at the yield point are 0.911 in. for 24-in. bolts, 1.821 in. for 48-in. bolts, and 2.277 in. for 60-in. bolts. In the +45-degree orientation the displacements at the yield point are 0.037 in. for 36-in. bolts, 0.073 in. for 72-in. bolts, and 0.110 in. for 108-in. bolts. Bolts in the -45-degree orientation never reach the yield point since they lose tension as the shear displacement occurs. The initial shear resistance is in fact reduced below the no-bolt case for this bolt orientation.

Extrusion of Grout along Fracture Planes

The Celtite and Fasloc resin-grouted bolts were installed according to the manufacturer's recommendations for all of the tests reported herein. These recommendations differ in one important aspect. Celtite recommends that the bar be rotated as it is pushed into the hole thereby mixing and shredding the resin cartridge during penetration. The mixing is then continued by additional rotation for approximately 40 seconds after the

bar reaches the bottom of the hole. DuPont recommends that the Fasloc design bar be pushed to the bottom of the hole without rotation, and then the bar is to be rotated for approximately 20 seconds for mixing.

The Celtite bolts were installed with a 3/4-in. hand-held electric drill. Two men could provide sufficient thrust to push the 7/8-in. bar through the resin cartridges to a depth of 34 in., the length of the bolt for the 45-degree bolt orientation. The drill was rotating during installation in this case.

It was not possible to push the 3/4-in. DuPont bars through the Fasloc cartridges in 1-in. holes by hand without rotation. It was necessary to use hydraulic loading rams to push the Fasloc bars to the bottom of the hole. The rams were then removed, the electric drill attached, and the bar rotated for 20 seconds. It was necessary to use the Slo-Gel formulation of the Fasloc resin in order to allow sufficient time for the installation of the Fasloc system.

The force required to push the blunt ends of the 3/4-in. DuPont bars through the Fasloc resin cartridges in the 1-in. diameter holes was higher than expected. This force was approximately 1,300 lb when the bar had been pushed in 18 in. Part of this force is due to the pressure of the grout in the hole pushing on the cross-sectional area of the bolt. The remaining part of the force is due to friction of the grout surrounding the bar. As the bar moves into the hole, the grout moves outward toward the collar causing a frictional force which must be overcome for insertion. How the total force is divided between the pressure effect and the friction effect is not known; however, it was observed that considerable pressures were developed in the grout ahead of the bar as it was penetrating. Problems with leakage of the grout at the seal on the far end of the drill hole were difficult to overcome. Also, the grout usually pushed out along the shear surface, a phenomenon which was not observed when the bars were rotated during penetration.

The extent of the intrusion of the grout along the shear surface is shown by the dark coloration in Fig. 4-34, a photograph of the shear blocks in Test S-204 (shale). Here, the blocks have been opened up after the test to expose the sheared bolt. The diameter of the region is approximately 12 inches. A similar intrusion of grout occurred on some of the natural fracture tests, but generally the diameter of the region was less. It should be noted that the blocks were pushed together with an average normal stress of 25 psi as the bars were pushed in.

The extrusion of the grout from the drill hole into fractures, partings, and voids in the mine roof has important practical significance. First of all, the resin and catalyst are not mixed when they are extruded so there can be no bonding effect along the fracture or parting plane. Secondly, the pressures developed in the grout in a normal mine application are probably significantly higher than those developed in these laboratory tests. The depths of the holes in the mine are usually 4 to 6 ft, instead of the 2 ft in the laboratory tests, so the rate at which the bars are pushed in is much higher in the mine application. Third, when the ground is fractured and badly in need of support, this is the situation when the resin is most likely to be lost into the fractures and partings. In practice, the resin cartridges are designed so that there is

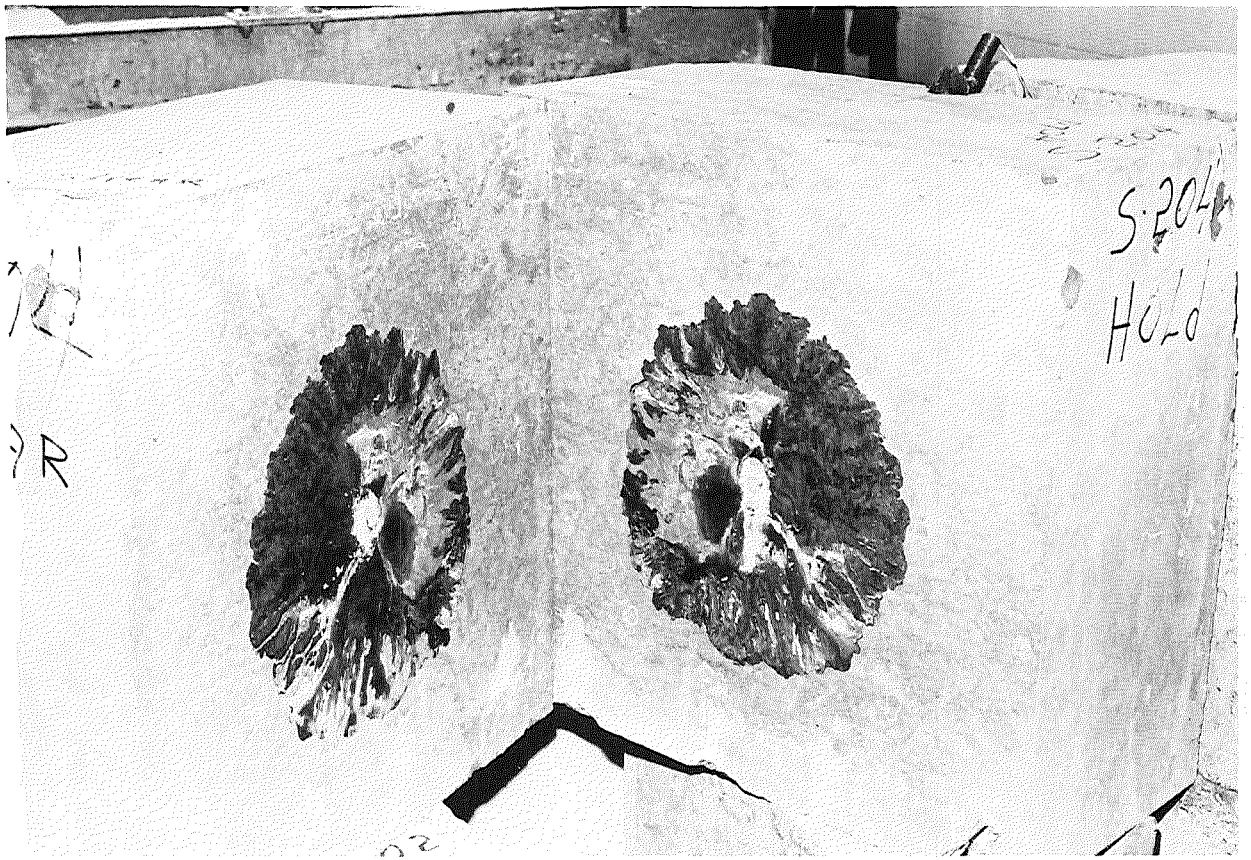

Fig. 4-34 Intrusion of Resin Grout along Shear Surface for Test S-204

an excess of resin in the hole to make up for some of these losses. An indicator that the holes are fully grouted is the extrusion of resin from around the hole collar as the bar is pushed in. If this visual evidence is seen, the installation is probably good. However, this visual verification is not always there because of the presence of the wood and steel bearing plates. What is insidious, therefore, is the fact that the grout may not have been visible because a major portion of it had been extruded into fractures in the roof. There is no obvious solution to this problem as long as the resin grout is placed in cartridges having a fixed volume. This is clearly an advantage to a pumpable grouting system which permits grout to be pumped in until the hole and voids are filled. The development of an inspection technique to evaluate the integrity of the grout column in place is therefore highly recommended.

Chapter V

CREEP TESTS and ANALYSIS

Introduction

Long term axial pull tests were performed on several sizes and types of resin-grouted bolts installed in three rock types to determine the strain (or load) distributions along the bolts and the pull-out characteristics under sustained loading for over three months. This information was then used to compare the effectiveness of the various bolt-resin configurations in resisting axial loads such as occur when two mine roof strata separate. Any creep or time-dependent behavior of the support system, steel bolt and resin, permits continued separation of the roof strata without substantially increasing the load on the bolt.

Nonlinear behavior of a resin bolt system may be due to several factors such as the composition of the component materials (rock, resin grout, and steel), the roughness of the drill hole and of the steel bolt, and the thickness of the resin-grout annulus. The latter is important for two reasons. First, if the annulus is too thick, the resin and catalyst may not mix properly during rotation of the bolt and therefore the resin will not set properly. Second, a thick grout annulus may allow more plastic deformation to occur in the grout because of its greater thickness.

The laboratory experiments described herein were designed so that the load distribution along a grouted bolt could be compared to that predicted by elastic time-independent analysis and to provide a measure of the creep (time-dependent deformation) associated with various bolt and resin combinations.

Creep Test Geometry and Loading Equipment

Eleven installation configurations were examined using a total of 33 bolts. Grade 40 reinforcing of 1/2-in., 3/4-in., and 7/8-in., diameter, and both the old style (smooth shank) and new style (corrugated shank), 3/4-in. diameter DuPont Fasloc bolts were employed (Table 5-1). Commercial polyester resins supplied by Celtite and DuPont for rock bolt applications were used.

It should be noted that not all of the test geometries are approved by the respective manufacturer of the components. These combinations were tested to examine the mixing problems associated with the large grout annulus and the resulting loss of effectiveness of the rock bolt.

Blocks of Indiana limestone 2 ft by 1 ft thick were obtained and drilled so that there were two creep-test installations in each block as shown in Fig. 5-1. Two blocks of an interbedded shale 2 ft by 2 ft by 1 ft thick were placed together to form a block approximately 2 ft on each side. Flat sawing the pieces allowed intimate contact of the surfaces. Five installations were made in this block (Fig. 5-2). The drill holes into which the grouted bolts were to be installed were 2 ft

Table 5-1

Description of Creep Test Installations.

Group Number	Installation	Nominal Bar Size (in.)	Bar Type	Hole Diameter (in.)	Resin Type	Rock Type
1	1-4, 10, 12	7/8	Re-bar	1-3/8	Celtite	Limestone
2	5, 6, 11	7/8	Re-bar	1-3/8	Fasloc	Limestone
3	7-9	3/4	Re-bar	1-3/8	Celtite	Limestone
4	13-15	3/4	Fasloc	1	Fasloc	Limestone
5	16-18	1/2	Re-bar	1	Fasloc	Limestone
6	CL19, CL20, CL21	3/4	Fasloc	1	Fasloc	Limestone
7	CL22, CL23, CL24	3/4	Re-bar	1	Celtite	Limestone
8	CS02, CS03, CS04	3/4	Fasloc	1	Fasloc	Anna Shale
9	CS01, CS05	3/4	Re-bar	1	Celtite	Anna Shale
10	CS08, CS09	3/4	Fasloc	1	Fasloc	Interbedded Shale
11	CS06, CS07	3/4	Re-bar	1	Celtite	Interbedded Shale

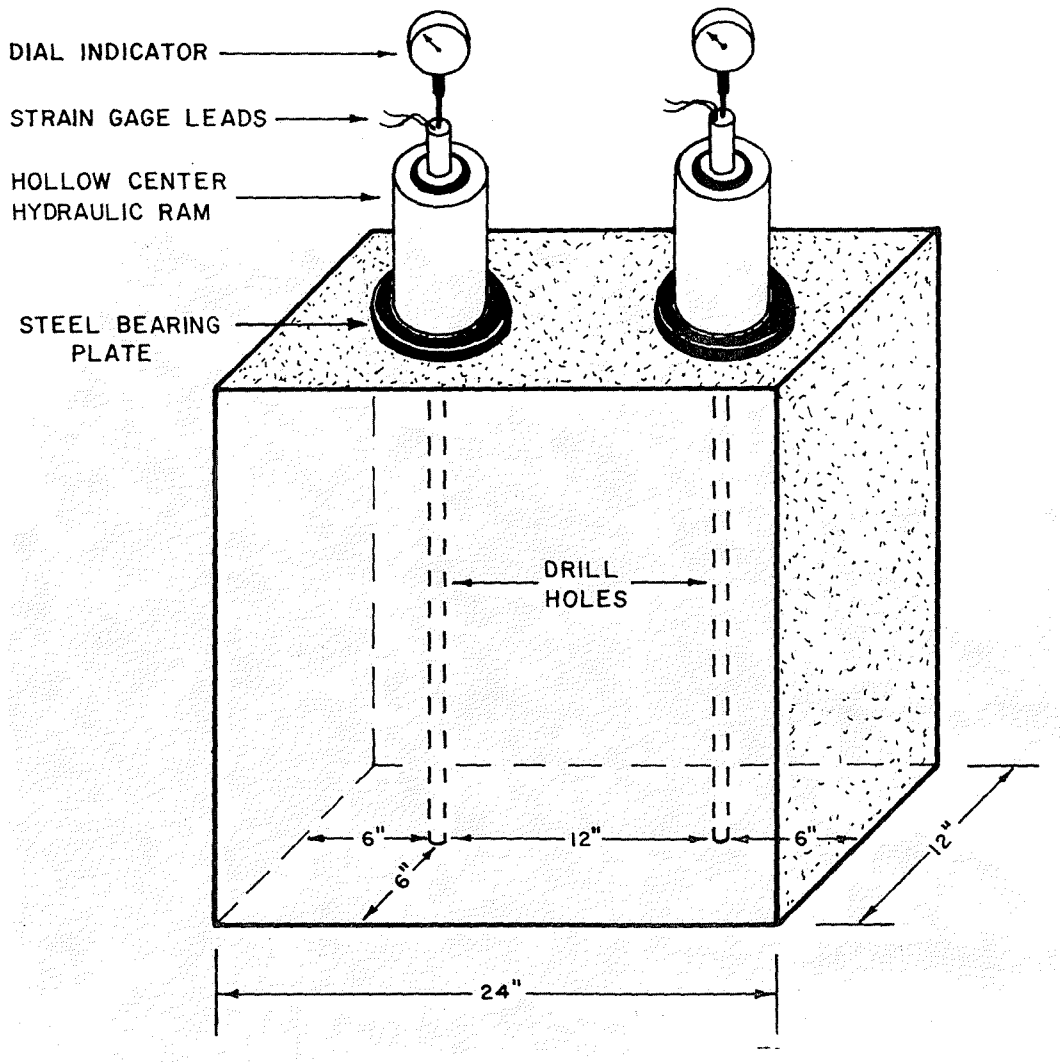

Fig. 5-1 Overall View of Creep Test Installation in Limestone Block

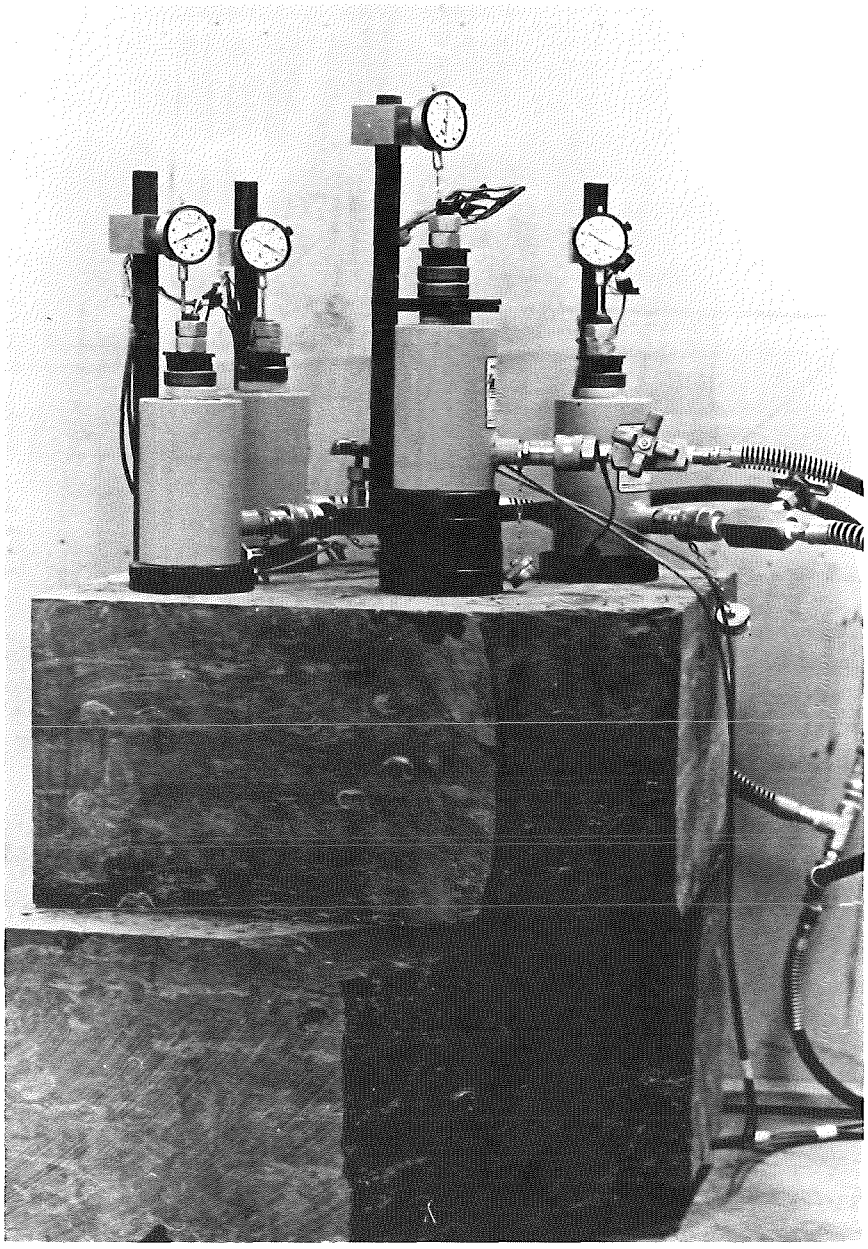

Fig. 5-2 Overall View of Creep Test Installation in Interbedded Shale Block.

deep and were drilled with 1-in. diameter rotary drag bits of the type commonly used in drilling roof bolt holes in coal mines. Water was used to remove the cuttings in the laboratory drilling instead of air vacuum as is used underground. A large irregular block of Anna shale approximately 5 ft by 3 ft by 1 1/2 ft thick was also obtained and drilled to accommodate five creep test installations (Fig. 5-3). Due to the moisture-sensitive nature of this shale, the cuttings were flushed with compressed air used in conjunction with a vacuum dust collector. Five flat test locations were prepared on the upper surface of the block with a belt sander. The surfaces of all drill holes were rifled and irregular which is thought to contribute to the anchorage mechanism. Each bolt was installed perpendicular to the bedding planes of the rock blocks.

Loading was accomplished by 20-ton capacity hydraulic loading rams which were pressurized by an air-driven hydraulic pump.

Four pairs of resistance strain gages were installed on each bar. The members of each pair of gages were connected in series and located on opposite sides of the bolt to provide bending compensation. Gages at 2, 5, and 12 in. within the grout column were used to determine the load distribution along the bar relative to the applied load, which was measured by a gage just outside the grout column (Fig. 5-4).

The strain gages were linked to a strain indicator through a precision switching unit. The three inactive arms of the Wheatstone bridge were 240 ohm precision resistors. Circuit stability was evaluated daily by substituting a 240 ohm precision resistor into the active arm of the bridge. Day to day variations usually did not exceed 7μ in./in.

Bolt-end displacement relative to the collar of the hole was measured with a dial indicator.

Installation and Loading Procedures

The procedures for installing the grouted bolts, loading them, and recording the bolt strains and displacements were critical in that it was desired to load the bolts shortly (10 minutes) after the resin grout had been mixed.

Several days prior to the creep tests, each bolt, already instrumented with strain gages, was loaded in tension in a testing machine and the strain in the uppermost gage (G1 in Fig. 5-4) was measured at preselected load increments. The determination of this load-strain relationship was necessary because of the reduced cross-sectional area at the gage location.

Just before the bolt was to be installed, the strain gage leads projecting from the end of the bolt were soldered to the ends of the cables leading to the switch unit. An "apparent" or "zero" strain reading was then taken for each gage. This reading was later subtracted from subsequent readings to give the actual strains in the bolt.

The strain gage leads were then unsoldered and the short leads folded up and placed in the hollow part of the adaptor used to connect the bolt to the chuck of an electric drill. Two insertion procedures were used. For Groups 1-5 the bolt was pushed through the resin with the drill rotating

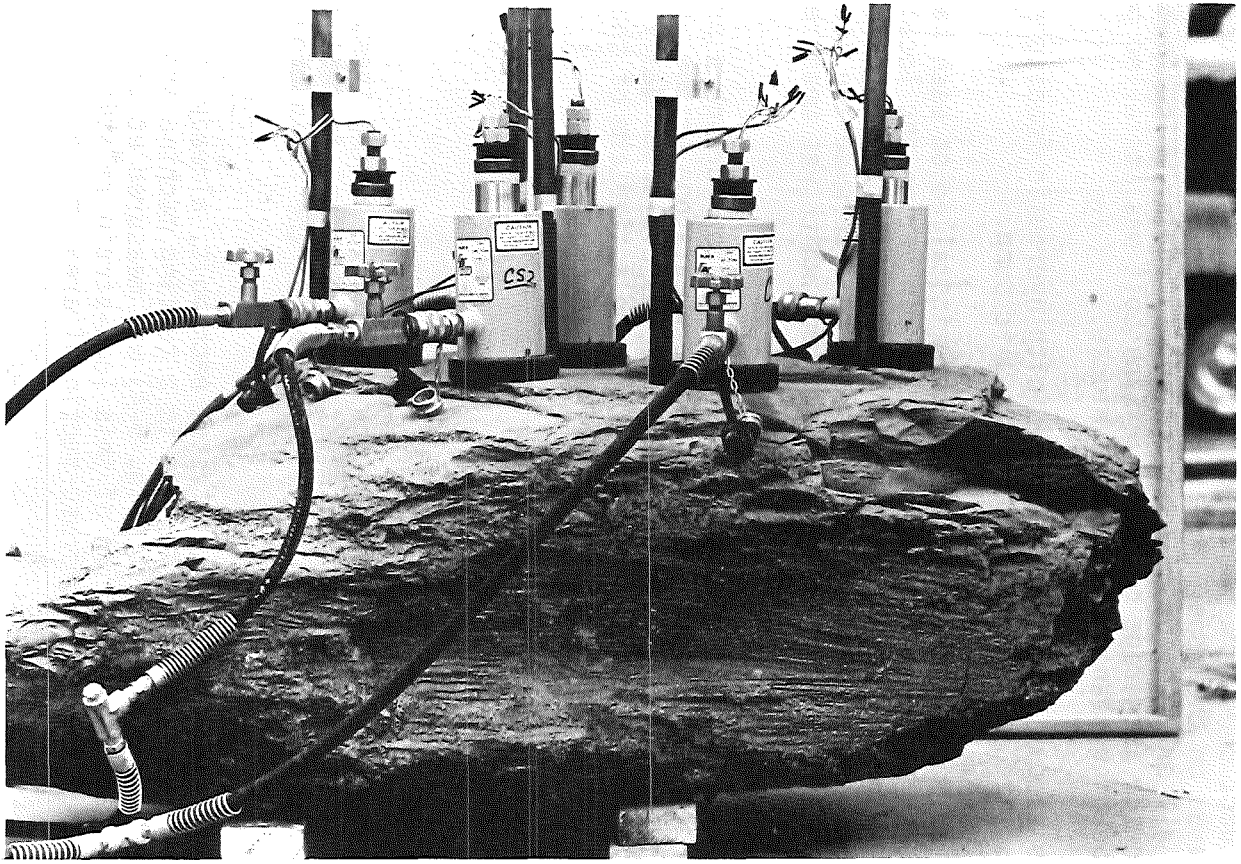

Fig. 5-3 Overall View of Creep Test Installation in Anna Shale Block.

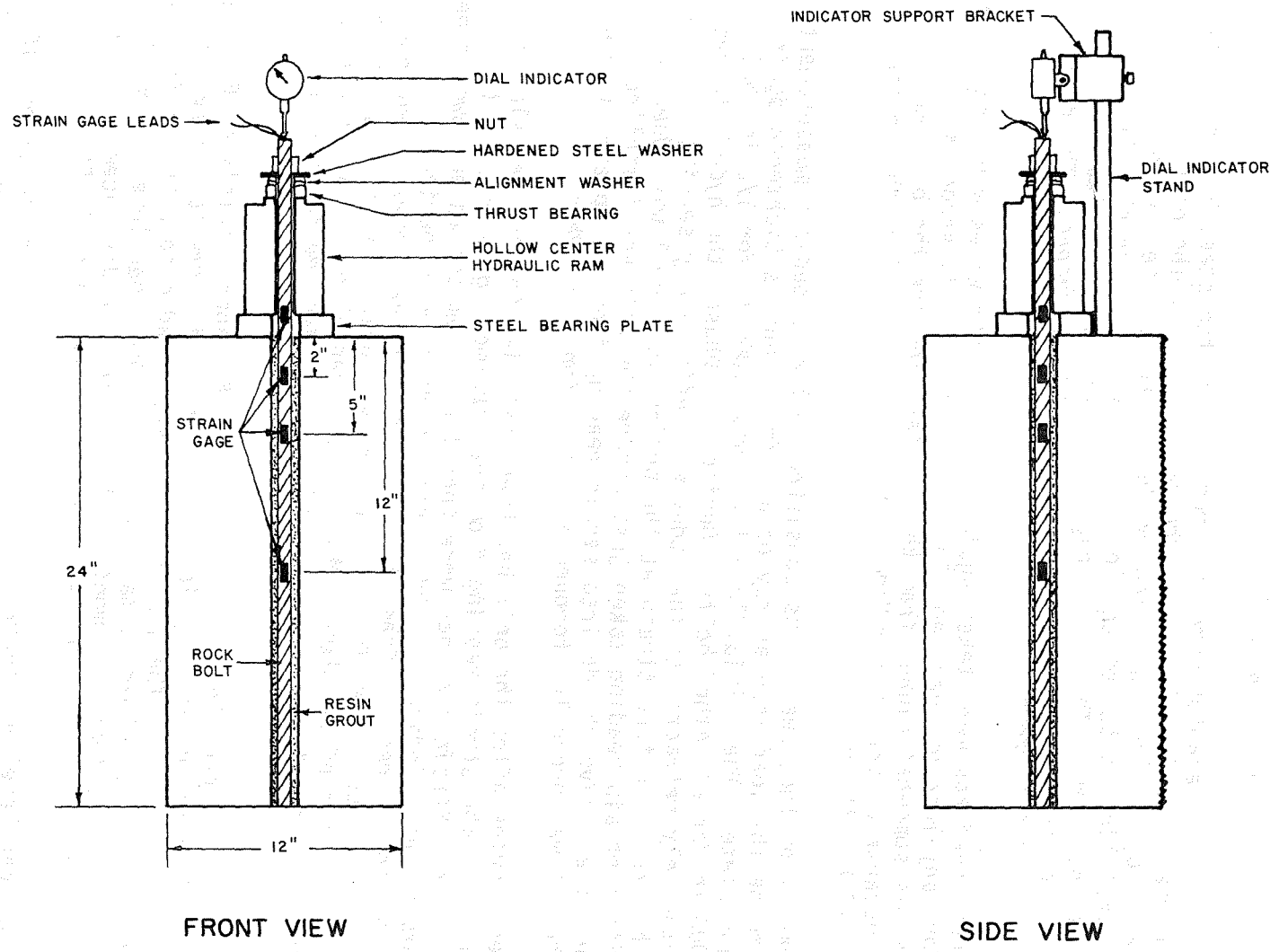

Fig. 5-4 Creep Test Installation Showing Strain-Gage Locations and Dial Indicator

whereas for Groups 6-11 the bolt was first pushed through the resin to the bottom of the hole with a pneumatic impact hammer and then rotated with the electric drill. Total mixing time after insertion of the bar was 30-40 sec for Celtite resin and 10-20 sec for Fasloc resin. Thorough mixing was rapidly followed by hardening of the grout as was noted by an increase in torque on the drill.

The drill and adaptor were then removed and the steel bearing plate and hollow ram were installed over the exposed end of the bolt. A thrust bearing, spherical alignment washer, hardened steel washer, and nut were installed on top of the loading ram which was completely retracted at this time. The strain gage leads were then resoldered to the cable and the dial indicator and bracket were attached. The dial indicator was set to zero.

Strain readings were taken again as soon as the wires were connected, but before any load had been applied to the bolt. This second set of readings was somewhat higher than the set taken before the bolt was installed because of the temperature increase resulting from the chemical reaction within the resin.

Phase I of the creep tests consisted of load bleed-off measurements to determine the load loss as may occur after a nut is tightened against a bearing plate. The initial load level was 4,000 lb for 1/2-in. bolts and 8,000 lb for all other bolts. During this phase, the hydraulic rams were completely retracted so that they were effectively serving as rigid spacer blocks. The true strain at the proper load level was added to the initial strain reading taken just before the bolt was installed. This sum, then, gave the desired strain reading from the uppermost gage when the nut was properly torqued at the beginning of Phase I.

Ten minutes after the bolt had been installed the nut was slowly torqued until the strain reading from the uppermost gage reached the proper value. Strain readings were then taken from the three lower gages and from the dial indicator. Additional readings were periodically recorded during the rest of Phase I. The time interval between readings was 10 minutes just after installation and was gradually increased to one day over a period of two days. Much of the load bleed off which did occur was during the first day so more readings were taken during that early period.

Phase I, a load bleed-off test, lasted for approximately 40-60 days. For Phase II pressure was applied to the hydraulic rams to achieve the initial load levels. (The 1/2-in. bolts were loaded to 3,540 lb instead of 4,000 lb due to a loading malfunction). These load levels were then maintained for at least one month. The strains and displacements were recorded periodically on the same schedule as described in Phase I.

The load level was increased to 5,890 lb on 1/2-in. bolts and 16,000 lb on the other bolts for Phase III. This load increase was accomplished stepwise in 2,000 lb increments with the dial indicator being read after each load increment. The axial pullout stiffness of each bar could then be evaluated after a correction for the stretch in that portion of the bar within the hollow ram was made. After the desired load level was

reached, the strains and displacements were again recorded at increasing time intervals ranging from ten minutes to one day for approximately one month.

Phase I - Load Bleed Off

Phase I testing began with the previously described installation of resin-grouted bolts and was in effect for 40-60 days. Decreases in load and bolt pullout were measured and recorded through the test period. This data was used to generate graphs depicting bolt strain as a function of time and load distribution along the bolts.

A. Load Bleed Off

A substantial loss of initially applied load was noted for all installations. This phenomenon is easily seen in the example graph (Fig. 5-5). Two important relations can be obtained from the graphs. First, the tensioning of the bar has progressively less effect deeper in the grout column. This is in general agreement with the elastic time-independent solution which assumed perfect bonding at the grout-rock and grout-bolt interfaces as described by Haas, et al., (Ref. 1). The grout serves as a medium for stress transfer from the bolt to the rock around it. Second, the bleed off slows to a negligible rate or ceases completely after approximately four days.

To quantify the amount of load bleed off, the percentages of load remaining ten minutes, one hour, one day, one week, and one month after installation were determined for each group of installations (Table 5-2). Comparing Groups 1, 7, and 11 with Groups 2, 6, and 10, respectively, it can be seen that the Celtite systems have somewhat more favorable bleed-off properties, showing 11 to 26 percent less load loss one month after installation. Groups 8 and 9 were not compared because the Anna shale was so weak the full load of 8,000 lb could not be applied. Thus, a quantitative comparison with the other installations would not be meaningful.

A comparison of Groups 2 and 5 indicates that bolt size, of itself, has some effect on load bleed-off characteristics. In these groups, bolt size and hole diameter were altered in such a way that annulus size was constant at 1/4 in. with the same resin type being used in each configuration. The 1/2-in. bolt lost 6.5 to 18.6 percent more load at various times during the test than did the 7/8-in. bolt.

Groups 1 and 3 had the same hole diameter and type of resin but different bolt sizes. Group 3, with the smaller bolt, had a slightly greater grout annulus than Group 1. Here, Group 1 shows up to seven percent less load loss than Group 3. Additional tests would be necessary to determine whether the smaller bolt size or larger grout annulus was responsible for the greater load bleed-off rate. Groups 3 and 4 cannot reasonably be compared for the effect of annulus size with constant bolt diameter since different bolt and resin types are utilized in the tests. These comparisons indicate that perhaps a combination of annulus size and grout/bolt contact area controls the load bleed-off characteristics of the systems.

It would seem reasonable that rock type would influence the bleed off characteristics of rock bolt installations. It is evident from comparing Groups 6 and 7 with Groups 8 and 9 and Groups 10 and 11 that the weak, highly fractured Anna shale was much less able to support the applied bolt load than were the limestone and interbedded shale.

Load bleed off is not peculiar to resin-grouted bolts. A similar phenomenon in mechanically anchored bolts was reported by Stefanko (Ref. 10). Stefanko examined the mechanisms of load loss and found that retightening aided in restoring and maintaining the required bolt tension. An extension of this research to resin-grouted bolts produced some interesting results. In this study, three groups of instrumented resin-grouted bolts were installed in blocks of limestone rock. The first group (A) consisted of four bolts installed in an approved manner and immediately loaded to 8,000 lb by torqueing a nut on the end of the bolt. The second group (B) consisted of two bolts which were installed, loaded, and subsequently reloaded by torqueing after an initial one-month load bleed-off phase. The third group (C) consisted of two bolts which were installed but not initially loaded. The resin was allowed to cure without load on the bolts for ten days, after which the bolts were loaded to 8,000 lb by torqueing (Table 5-3). Grade 40 7/8-in. diameter reinforcing bars with Celtite resin were placed in 1 3/8-in. holes for all eight installations.

A comparison of Groups A and B indicates the benefits obtained from retorqueing bolts subsequent to installation. It has been hypothesized (Ref. 3) that reloading was effective in reducing the load bleed off because the newly mixed grout, though hard to the touch, was not fully cured and thus could deform in a viscous manner when subjected to loading. The data obtained from Groups A and C tend to nullify this line of reasoning. The load bleed off of these groups was very similar throughout the experiment with the remaining loads after one month, differing by only 2.4 percent (Table 5-4). The load bleed-off mechanism associated with resin-grouted bolts is probably very similar to that of mechanical bolts. It is probable that some initial "seating in" at the resin-rock and resin-bolt interfaces is necessary before loads can be maintained by the bolt. This requirement may be a result of grout shrinkage or of readjustments in stress due to localized material failures at areas of stress concentrations.

Analysis of the data obtained from Group C indicated a relative compressive stress developed in the bolt which increased with increasing distance into the grout. Table 5-5 shows the total compressive strain at each gage location. Since the end of the bolt was free and the uppermost gage was outside the grout column, it may be concluded that the apparent compressive strain in this gage was due to thermal effects of the curing resin. Subtracting this strain from the strains at other gage locations provides an approximate measure of the shrinkage induced strains in the bolts.

It is clear now that substantial load bleed off occurs in resin-grouted bolts with the magnitude of the bleed off being dependent on the installation configuration. There is some question, however, as to whether or not initial and subsequent torqueing or loading of the resin-grouted bolts is necessary and beneficial in roof control applications. An examination of the theory and philosophy of full column resin-grouted bolting as a means of ground control should answer this question.

Table 5-3 Description of Test Installations

Group	Bolt Numbers	Nominal Bar Dia.	Nominal Hole Dia.	Resin Type	Loaded
A	CL1-CL4	7/8 in.	1 3/8 in.	Celtite	Immediately
B	CL10,Cl12	7/8 in.	1 3/8 in.	Celtite	Reloaded
C	CL25,CL26	7/8 in.	1 3/8 in.	Celtite	After 10 days

Table 5-4 Percentage of Load Remaining on the Bolt at Various Times After Installation

Group	Percentage of Load Remaining After				
	10 Minutes	1 hour	1 day	1 week	1 month
A	91.8	84.5	71.8	67.3	68.5
B	99.4	99.1	95.9	92.3	86.9
C	92.7	85.6	77.5	75.0	70.9

Table 5-5 Variation in Strain During Curing of Resin With No Applied Load (After 1 day)

Bolt Number	Depth of Gage Into Grout Column			
	0 in.	2 in.	5 in.	12 in.
CL25	-13μ in./in.	-21μ in./in.	-24μ in./in.	-44μ in./in.
CL26	-11	-20	-20	-28
Average	-12	-20	-22	-36

1. As was previously mentioned, theoretical and laboratory analyses indicate that the load induced at the end of a grouted bolt is transferred into the rock so that at 16 in. within the grout column virtually no load is present in the bolt. This would indicate that only surface loose is supported by the loading and that the loading has little effect on holding weak strata together if the bedding planes are, say, greater than 16 in. from the hole collar.

2. The laboratory test loadings were achieved by tightening a nut at the threaded end of a bolt. Another means of inducing load in the bolt is to apply the full thrust of the bolting machine upward against the bolt subsequent to mixing and prior to resin setup. This action compresses the strata and, after the resin is set and the bolter removed, induces tension in the bolt. According to Nitzsche and Haas (Ref. 11) loading the bolt in this manner would tend to hold weak strata together should a separation or plane of weakness occur between the ends of the grout column. It should also be noted, however, that if the upper end of the grout column occurs at or very near a plane of weakness, the compression induced by the bolting machine in the lower beds would produce a tensile force in the rock near the upper end of the bolt after the thrust was removed. The tensile force need not be large to produce failure along a plane of weakness so detrimental effects may occur as a result of using this method of installation. This mode of loading (applying thrust while resin sets) is also subject to bleed-off characteristics similar to those already described but there is no way of retightening this system after load bleed-off occurs because a head forged integral with the bolt, instead of a nut, is employed. Therefore, surface loose may not be given adequate support.

3. The practice of tightening grouted bolts may be a "throwback" from mechanical bolting procedures. In the latter, tensioning is necessary to remove some of the stretch from the system; stretch is present to a much lesser degree in the grouted bolts as will be shown in subsequent sections of this chapter. The tensioning also served to seat the anchor of the mechanical bolt, another action which is unnecessary with grouted bolts.

4. The grouted system is self-tightening and is advertised as such by some manufacturers. Should a bedding separation, joint, or other discontinuity begin to widen, tension is induced in the bolt providing the needed resistance to separation. Here again, this action is much different from the action of the mechanical bolt in a similar situation. In the latter, resistance to the separation is generated over the length of the bolt rather than over a few inches of effected length as in the grouted case. Under the same load a much greater elongation is allowed in the mechanical system, an action which allows further weakening of the strata.

5. If surface loose is to be supported, some preloading of the bolt would be beneficial to maintain control of surface material. This load need not be great, but only enough to support the weight of the immediate roof without allowing sag of a magnitude which would cause cracking and subsequent deterioration of the roof. For example, if bolts were installed on four-foot centers and six inches of coal were left below a fairly competent shale or limestone roof, the amount of material needing immediate support would be (4 ft) by (4 ft) by (0.5 ft) by

(85 lb/ft^3) = 680 lb. Since bolts are commonly loaded to about one ton by installation procedures, enough positive pressure would be available to resist movement of this immediate roof layer even if a large percentage of the load bled off. Furthermore, strata deflection would be small due to the inherent high stiffness of full-column anchorage (Ref. 3).

6. Yet another fact to consider is that while load bleed off is measurable in large magnitudes in the laboratory, post-installation strata movements in the mine tend to mask the phenomenon. It would seem reasonable, however, that the large load bleed off would be reflected in a lower stiffness coefficient for the installation resulting in somewhat larger deflections for a given load.

These six factors indicate that tensioning of the grouted bolt system is not essential to good strata control with the possible exception of support of loose surface material. Thus, retensioning also has limited application. The fact that the grouted system as presently available does provide good roof control and does not utilize retensioning is further support of this premise.

B. Bolt-Load versus Distance into Grout

A stepwise regression model was applied to the load versus distance-into-the-grout data from each installation type. The results of the statistical analysis indicated that only linear effects were significant above the 60 percent confidence level and that the linearity could be accepted with over 90 percent confidence. Based on this result, all subsequent data sets were modeled with a simple linear regression procedure using the least squares criterion.

The "confidence" in this case is a measure of the probability that there exists a linear relation between the dependent variable (load) and the independent variable (distance into the grout). Thus, if the model described is accepted with 90 percent confidence, it is implied that repeated samplings of load at various distances into the grout would produce data sets describable by the linear model 90 percent of the time.

The best curves obtained from these analyses were plotted. The data points were omitted for clarity of presentation. The theoretical curve for a 7/8-in. bar in a 1 3/8-in. hole obtained by Haas, et al., (Ref. 1) was expanded in scale and superimposed over the best lines. Analyses were performed at intervals of ten minutes, one hour, one day, one week, and one month during the load bleed-off phase. A typical graph is shown in Fig. 5-6.

The graphs show that, although the shape of the theoretical curve is not adhered to by the measured values of load; a point is reached where essentially no load is supported by the bolt. The mechanism of transfer of bolt load through the grout to the surrounding rock provides an explation of the high stiffness and effectiveness of resin-grouted bolts. The failure of data to assume the shape of the theoretical curves is due to the incompatibility of the assumptions of the finite element model and the properties of the laboratory test specimens.

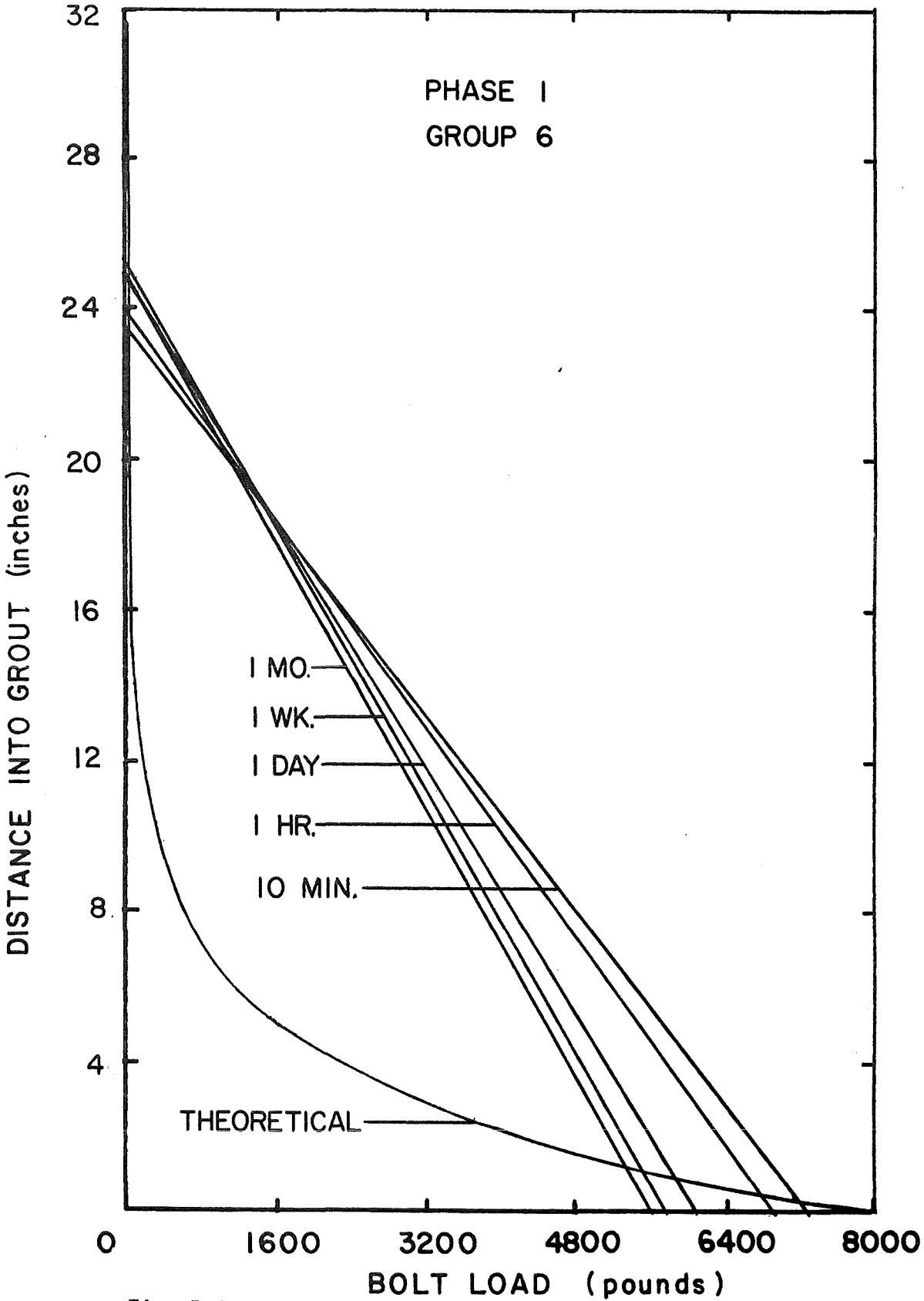

Fig. 5-6 Variations in Bolt Load with Distance into the Grout at Several Times During Phase I (Fasloc System in Limestone).

Phase II - Creep at Constant Low Loads

After the bolt load, as indicated by strain readings, had stabilized, the bleed-off portion of the creep tests was terminated. Using the hydraulic loading system described previously, the bars were reloaded. The bars of 3/4 in. and 7/8 in. diameters were loaded to 8,000 lb. The bars of 1/2 in. diameter were loaded to 3,540 lb. Two 7/8-in. diameter bars, Nos. 10 and 12, were not reloaded so that any further bleed off could be monitored. The stated loads were maintained at a constant level for the test duration of about 36 days. It should be noted that the minor fluctuations in bolt strain are due to the nature of the pumping mechanism used to maintain the constant load on these bolts. The "constant pressure" pump is activated by line pressure drops of approximately 50 psi. Some variation of strain is therefore present since the load was not maintained at a truly constant value.

The theoretical load-distance relations referred to earlier in this report were obtained using an assumption of perfect bonding at the rock-grout and grout-bolt interfaces. Locally complete and partial failures along the grout column can be detected in the data as adjacent gages reporting similar strain levels and as shifts in the load distribution along the bolt, respectively.

Complete shear failure or separation of the bond at either interface would put any gages within the zone of failure under essentially the same load since little load transfer to the surrounding rock could occur (Fig. 5-7). Failures of this type are evident in several installations as seen by similar loads at different gage locations in Fig. 5-8. (Refs. 2, 3).

The data in Table 5-6 indicate that the percentage of load carried by the bolt at each gage location at the end of Phase II is much greater than the theoretical values. Further, the percentage of the load at adjacent gages in some cases is comparable, indicating that little load transfer occurs between the two gage locations in these instances (Fig. 5-8). These factors support the idea that the mechanism of load distribution shift during Phase II is a cyclic one of progressive local failure followed by load redistribution which is followed in turn by local failure. This may be the mode of creep for the entire grout-bolt-rock system.

Graphs of bolt load versus distance into the grout were prepared as described for Phase I. At this low constant load, a time-dependent increase in depth of load penetration was noted in some installations (Fig. 5-9). During the first 30 days of Phase II, Groups 1, 3, 5, and 6 indicate 2 in. of penetration; Group 2, 4 in.; and Groups 4, 7, 10, and 11, essentially no change in depth of penetration. As the grout fails locally and creep occurs in the system, the load in the bolt must be carried to a greater distance into the grout to facilitate load transfer into the rock mass.

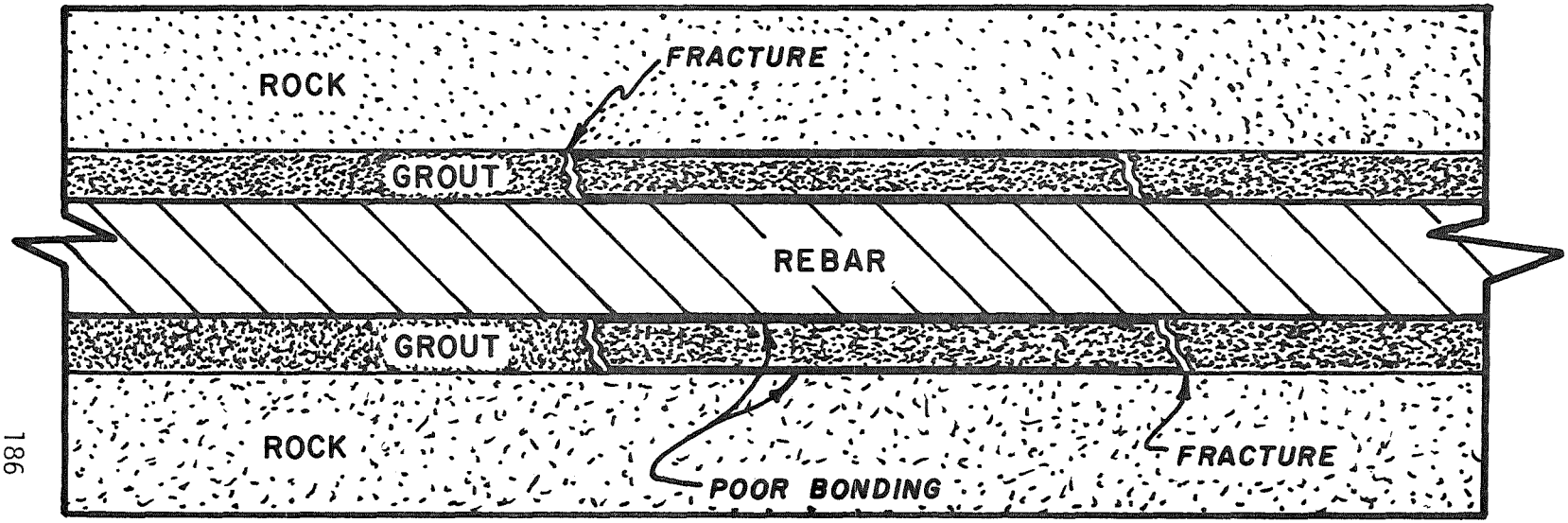

Fig. 5-7 Types of Grout Failures Responsible for the Load Distribution Shift and/or Reduction of Load Transfer to the Rock.

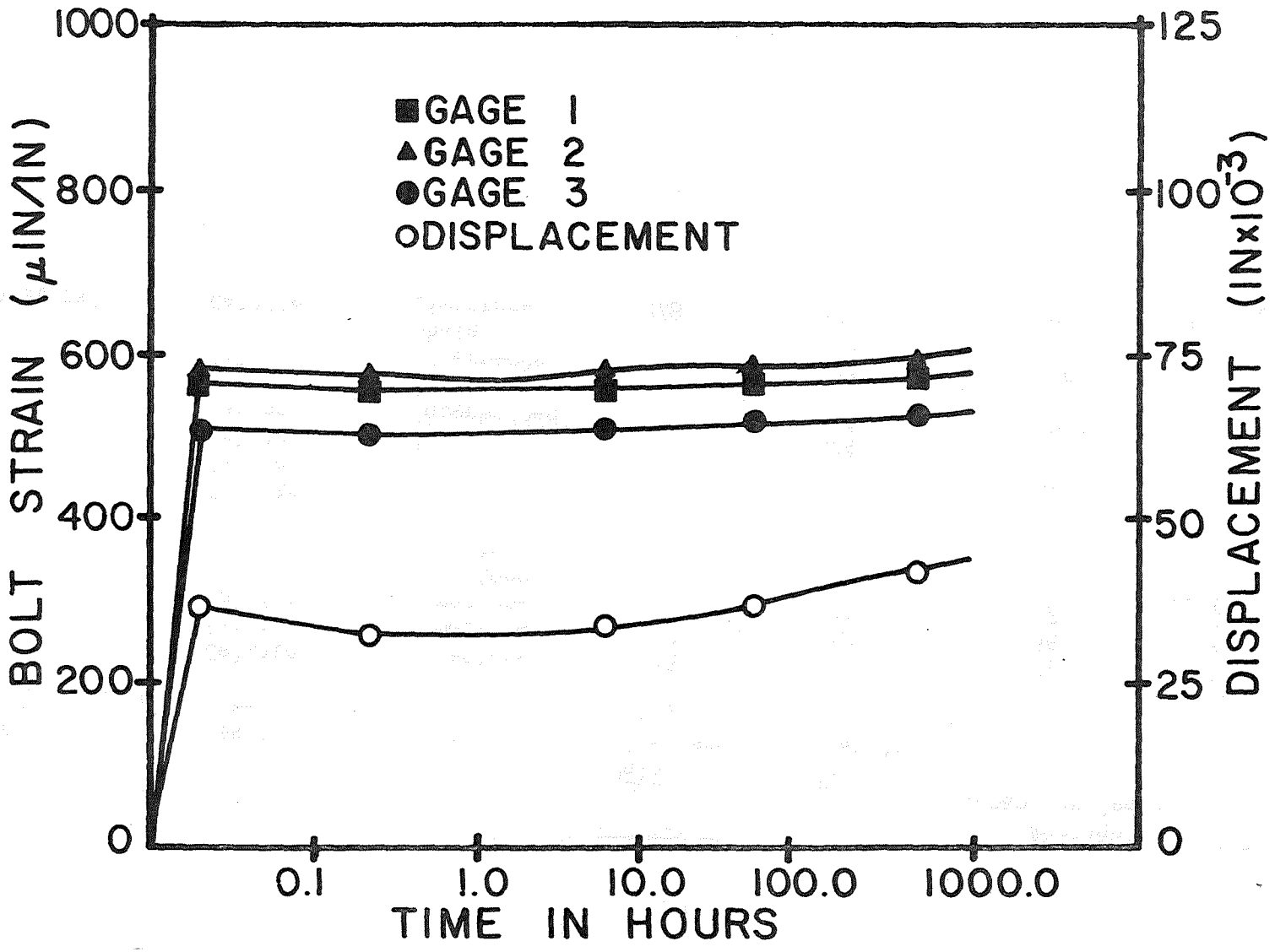

Fig. 5-8. Example of Gage Readings Indicative of Local Grout Failure (Installation CL14).

Table 5-6

Average Percentage of Load at Each Gage Location
(Phase II, 30 Days).

Group Number	Installation Description				Average Percentage of Load Carried at Location		
	Resin Type	Rock Type	Hole Diameter (in.)	Bar Diameter (in.)	G2	G3	G4
1	Celtite	Limestone	1 3/8	7/8	82.7	60.8	21.8
2	Fasloc	Limestone	1 3/8	7/8	96.3	86.4	55.7
3	Celtite	Limestone	1 3/8	3/4	82.1	77.9	45.8
4	Fasloc	Limestone	1	3/4	95.3	85.5	63.5
5	Fasloc	Limestone	1	1/2	91.3	69.6	21.6
6	Fasloc	Limestone	1	3/4	97.4	93.5	66.7
7	Celtite	Limestone	1	3/4	93.8	68.9	38.1
8	Fasloc	Anna Shale	1	3/4	NA	NA	NA
9	Celtite	Anna Shale	1	3/4	NA	NA	NA
10	Fasloc	Interbedded Shale	1	3/4	99.4	92.5	26.2
11	Celtite	Interbedded Shale	1	3/4	100.0	NA	27.8
Theoretical	Celtite	Limestone	1 3/8	7/8	48.0	16.0	2.8

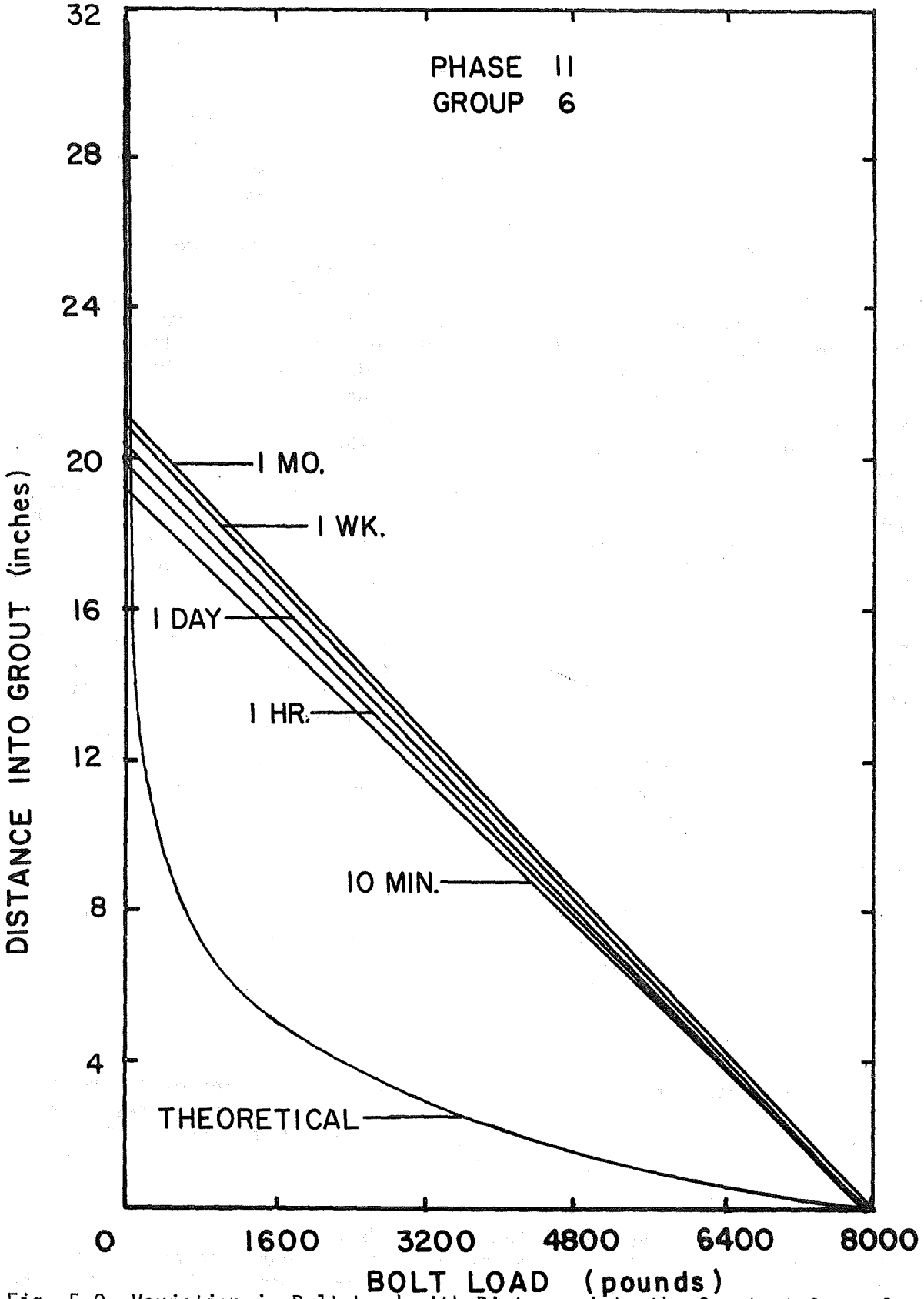

Fig. 5-9 Variation in Bolt Load with Distance into the Grout at Several Times During Phase II (Fasloc System in Limestone).

Phase III - Creep at Constant High Loads

The final phase of the creep testing program was initiated by increasing the load on the 7/8-in. and 3/4-in. bolts to 16,000 lb and by increasing the load on the 1/2-in. bolts to 5,890 lb. This portion of the tests was designed to provide information concerning creep and failure of grouted bolts at relatively high loads. The applied loads were approximately two-thirds of the yield load of the bolts. Measures of load transfer to the surrounding rock and the corresponding bolt load as a function of distance into the grout column were obtained.

The mechanisms of creep and localized failures described in Phase II continued to be evident in this phase of testing. Some installations showed very little increase in depth of penetration of load (Fig. 5-10), whereas others exhibited a more pronounced increase (Fig. 5-11). The penetration of load was deepest in Groups 2 and 4 where the lines obtained using bolt load and depth into grout data indicated that the applied load was not transferred within the length of the bolt used. In other words, the installations were no longer able to sustain the applied load. Steadily increasing displacements of the bolt heads under sustained load occurred in these installations (Fig. 5-12). Also to be noted is that all strain gages record approximately the same load. These three observations indicate complete installation failures. It should be noted, however, that bolts of greater length would not have completely failed but would have allowed fairly large strata displacements to occur.

A comparison of Tables 5-6 and 5-7 provides some interesting information. The percentage of load in the bolts at any given gage location either increased slightly or decreased slightly when the applied load was doubled. Although this observation is readily verified from theoretical analysis, it is in direct conflict with some engineers' concepts of how full-column anchorage works. The graphs of bolt load versus distance into the grout for Phases I and II may be similarly compared (Ref. 3). Here it is evident that the depth of load penetration was affected very little by a doubling of the applied load.

Installation Stiffness

The above discussion leads to the quantitative treatment of the stiffness of roof support systems. The change of length corresponding to a change in load on an elastic member can be expressed by a stiffness coefficient K such that

$$K = \frac{AE}{L} \qquad (5\text{-}1)$$

where E is Young's modulus, A is the cross-sectional area of the member, and L is the length of that member. The coefficient K is expressed as a load per unit length of elongation such as pounds per inch. This stiffness coefficient is analogous to the spring constant of axially loaded coiled springs.

After Phase II was completed, the loads on the grouted bolts were further increased in four increments with strain gage and displacement readings being taken immediately after each increment of load. The data

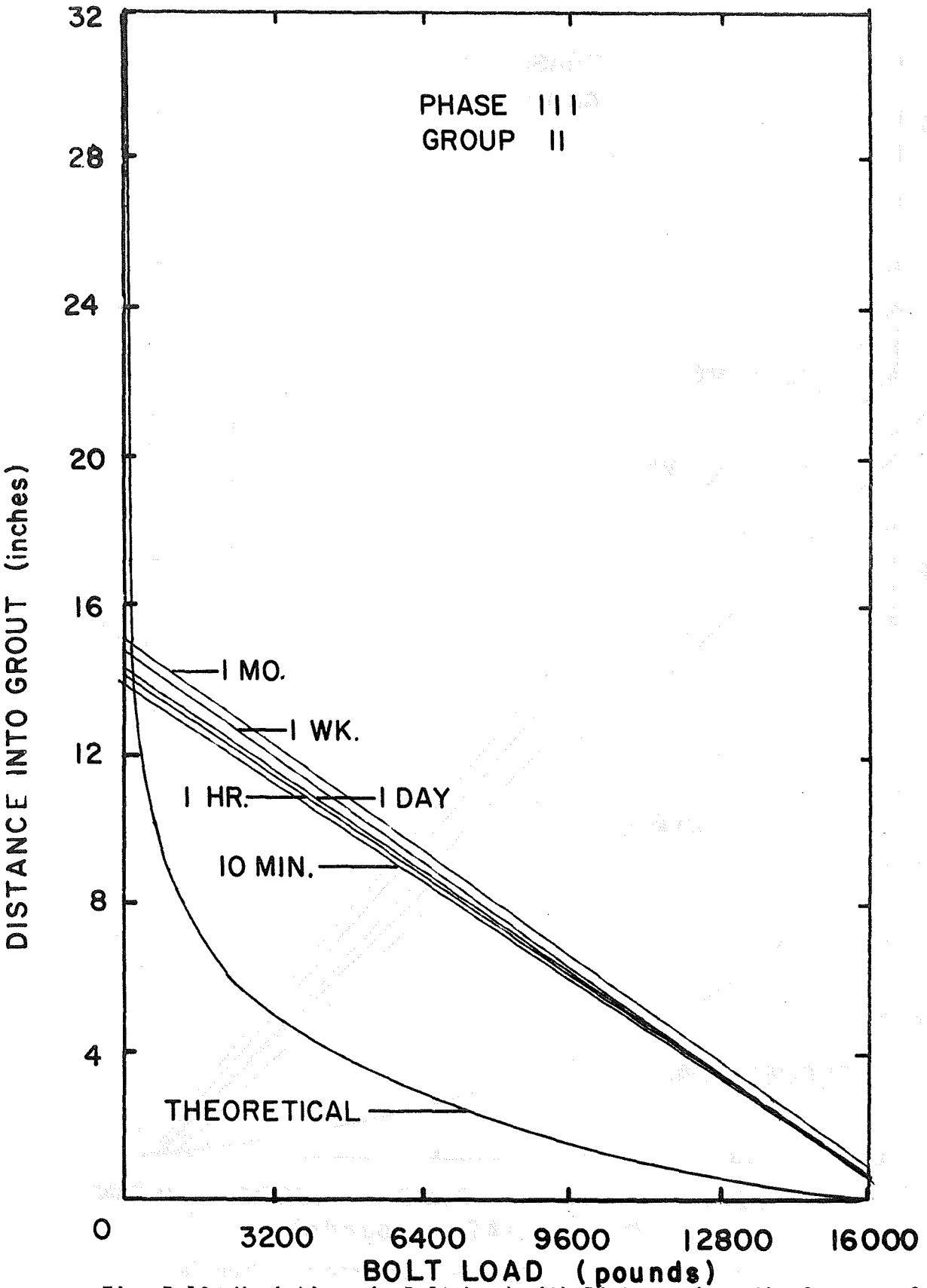

Fig. 5-10 Variations in Bolt Load with Distance into the Grout at Several Times During Phase III (3/4-in. Bar in a 1-in. Hole with Celtite Resin in Interbedded Shale).

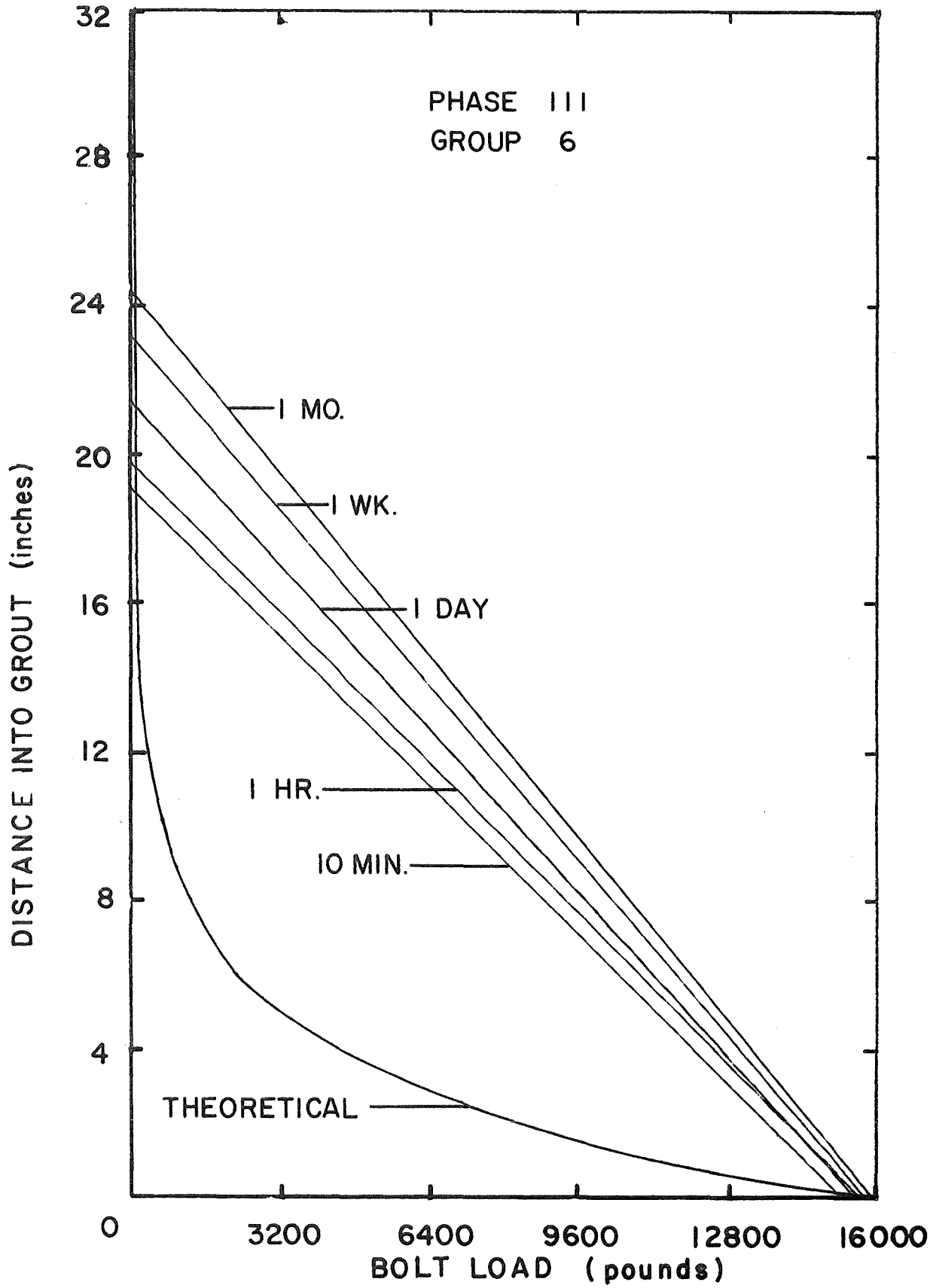

Fig. 5-11 Variations in Bolt Load with Distance into the Grout at Several Times During Phase III (Fasloc system in Limestone).

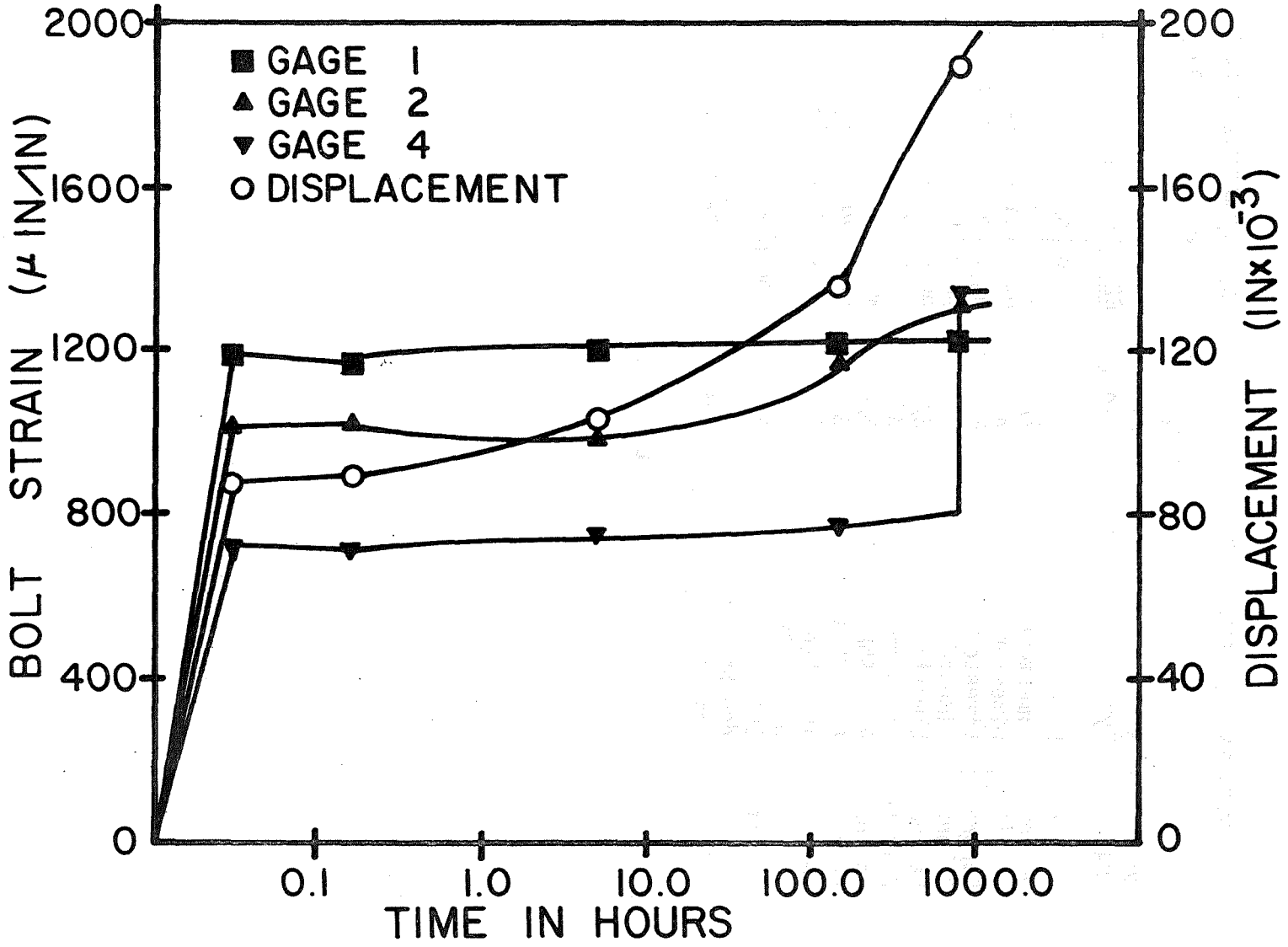

Fig. 5-12 Example of Total Installation Failure (Installation CL15).

Table 5-7

Average Percentage of Load at Each Gage Location
(Phase III, 30 Days).

Group Number	Installation Description				Average Percent Load Carried at Location		
	Resin Type	Rock Type	Hole Dia. (in.)	Bar Dia. (in.)	G2	G3	G4
1	Celtite	Limestone	1 3/8	7/8	80.9	58.5	20.6
2	DuPont	Limestone	1 3/8	7/8	96.6	85.5	59.4
3	Celtite	Limestone	1 3/8	3/4	86.7	71.5	45.5
4	DuPont	Limestone	1	3/4	96.1	84.6	66.0
5	DuPont	Limestone	1	1/2	96.9	81.4	32.2
6	Fasloc	Limestone	1	3/4	98.5	88.4	59.5
7	Celtite	Limestone	1	3/4	88.7	74.3	33.8
8	Fasloc	Anna Shale	1	3/4	NA	NA	NA
9	Celtite	Anna Shale	1	3/4	NA	NA	NA
10	Fasloc	Interbedded Shale	1	3/4	98.4	94.4	35.1
11	Celtite	Interbedded Shale	1	3/4	100.0	NA	24.1
Theoretical	Celtite	Limestone	1 3/8	7/8	48.0	16.0	2.8

obtained were used to determine a stiffness coefficient for each installation. The coefficient here is

$$K = \frac{\Delta P}{\Delta L} \qquad (5\text{-}2)$$

where ΔP is the change in load and ΔL is the change in displacement, corrected for that portion of the bolt extending up through the hollow part of the ram. The value of K is reported in pounds per inch.

The values of K for each group are given in Table 5-8. Theoretical coefficients for mechanical bolts are also supplied for comparison. These values were obtained using Eq. (5-1) above, with the assumption of perfect anchorage. It is of interest to note that while the stiffness of the mechanical bolts decreases inversely as the length, the stiffness of resin-grouted bolts is the same regardless of length. It is necessary only that the length of the grouted bolt exceed the depth required to provide complete load transfer to the surrounding rock, approximately 16 to 22 in. as determined by this investigation.

As can be seen in Table 5-8, grouted installations are much stiffer than their point-anchored counterparts. This observation substantiates the practice of installing untensioned grouted bolts. A very small rock movement would effectively "tighten" the grouted bolt whereas a relatively large elongation must occur under a load before an untensioned mechanical bolt would become "tightened" to the same degree, that is, equally resistant to further strata displacements.

A comparison of data for the various installations shows that the Celtite installations were considerably stiffer than Fasloc installations in similar rock types. Comparing the new style Fasloc system with the smooth shanked system previously available from DuPont (Ref. 2) shows an increased stiffness of 53 to 73 percent, depending on rock type, with the new system. As was discussed in the Second Annual Report, the smooth shanked Fasloc bars were not installed according to current methods recommended by the manufacturer. It should be emphasized that, in comparison with point-anchored rock bolts, both systems have very high stiffness coefficients.

Much has been said here about installation stiffness, the implication being that the stiffer the system is the better it is. Such is not the case. It would seem reasonable that a matching of rock-mass modulus and rock support modulus is desirable. Certain rock types such as salt, trona, and soft shales may allow relatively large plastic deformations prior to failure. These deformations would rapidly increase the load on a stiff support system causing failure of both the bolts and the supported rock. In this application a less stiff system of yieldable rock bolts or friction rock stabilizers may provide much better overall ground control. On the other hand, there are instances where prevention of any initial movement may produce a very stable opening whereas allowing relatively small movements could cause a loss of keying or interlocking of rock fragments which would lead to failure of the rock mass. These are items of concern to the engineer responsible for developing roof control plans.

Table 5-8

Comparison of Stiffness Influence Coefficients for Mechanical and Resin-Grouted Rock Bolts (Loading at Beginning of Phase III Creep Tests).

Group Number	Installation Description			Stiffness (K) of Grouted Bolts (1000 lbs/in.)	*Stiffness of Mechanically Anchored Bolts (1000 lbs/in.)		
	Resin Type	Hole Diameter (in.)	Bar Diameter (in.)	Group Average	Bolt Length 24 in.	48 in.	96 in.
1	Celtite	1 3/8	7/8	3130	752	376	188
2	Fasloc	1 3/8	7/8	1130	752	376	188
3	Celtite	1 3/8	3/4	1360	552	276	138
4	Fasloc	1	3/4	500	552	276	138
5	Fasloc	1	1/2	290	245	123	61
6	Fasloc	1	3/4	866	552	276	138
7	Celtite	1	3/4	1413	552	276	138
8	Fasloc	1	3/4	NA	552	276	138
9	Celtite	1	3/4	NA	552	276	138
10	Fasloc	1	3/4	766	552	276	138
11	Celtite	1	3/4	1423	552	276	138

*Note: Numbers in these columns are based on bolt diameters as listed in the column headed "Bar Diameter" and a Young's Modulus of 30 x 10^6 psi

Pull to Failure

After completion of Phase III, all installations were loaded until failure of either the bolt or the installation as a whole occurred. The bolts were individually loaded by 20-ton capacity, hollow hydraulic rams pressurized by an air-driven hydraulic pump. The failure loads of the installations are shown in Table 5-9.

It is interesting to note that the average failure load of each installation is substantially lower than the reported strength of the steel bolt used in the installation. The failures occurred due to stripping of the threads or brittle fracture at the root of one of the threads. Thus, the threads were the weak link in these systems. An important point to consider is that the Fasloc system (Groups 4, 6, 8, 10) does not utilize a threaded shank for mine use. The head of the bolt was removed and the shank was threaded to facilitate creep testing in the laboratory. It has been determined in laboratory tests that the standard forged head of the Fasloc bolt is at least as strong as the rest of the bolt (40,600 lb). This is not true of installation types which utilize a nut and plate on a threaded shank to secure the immediate roof. Running a thread cutter over the deformations of the reinforcing bar produces threads of poor quality and of obviously lower strength than the rest of the bolt.

Subsequent to installation failure, each test block was split longitudinally along the length of the grouted installation so that the grout column could be examined (Fig. 5-13). In Group 1, installations had zones of fractured grout 2 to 8 in. long from the collar of the hole downward. There was also some cratering in the surrounding rock. In the extreme case, the cratering extended 1 1/2 in. from the grout, resulting in a crater approximately 4 1/2 in. across. Sections of unshredded resin cartridge lined the lower 6 1/2 in. to 8 in. of two of the installations in Group 1. This material may provide a surface for slippage between the grout and the rock. Group 2 installations showed no cratering of the rock but the grout was fractured and broken for 4 to 7 in. down from the hole collar. Additional grout fractures were evident at 6 1/2 to 22 in. into the grout column. Group 3 exhibited grout fractures from 1 to 4 in. into the grout. No deeper fractures were present but the entire bolt and grout column was pulled approximately 1/16 in. out of the rock. There was some unshredded resin cartridge in this grout. Group 4 had extensive grout fracturing throughout the length of the grout column. Also, each installation had clumps of shredded plastic from the resin cartridges throughout the grout column. Group 5 had some fractured grout near the hole collar. The grout appeared to be very poorly mixed with the bottom 4 1/2 to 6 in. of each hole containing unsolidified resin. There were other zones of soft resin and clumps of unshredded plastic resin cartridge throughout the grout column. Group 6 had one visible fracture per installation at about 4 1/2 in. to 6 in. from the collar. The grout was well mixed with the exception of a few small pieces of shredded resin package. Group 7 was similarly well mixed. Small, shallow craters were noticed near the collars of two installations and the top 1 to 1 1/2 in. of grout was fractured. This fracturing was probably the result of high localized pressures due to loading.

Table 5-9

Average Failure Load for Full Column Resin-Grouted Rock Bolts

Group	Installation Description			Average Failure Load of Installation (lbs.)
	Resin Type	Hole Dia. (in.)	Bar Dia. (in.)	
1	Celtite	1 3/8	7/8	31,500
2	Fasloc	1 3/8	7/8	32,700
3	Celtite	1 3/8	3/4	36,800
4	Fasloc	1	3/4	27,000
5	Fasloc	1	1/2	7,900
6	Fasloc	1	3/4	29,300
7	Celtite	1	3/4	36,300
8	Fasloc	1	3/4	3,700*
9	Celtite	1	3/4	6,800*
10	Fasloc	1	3/4	30,000
11	Celtite	1	3/4	37,000

*The bolt did not break for Groups 8 and 9. See text for description.

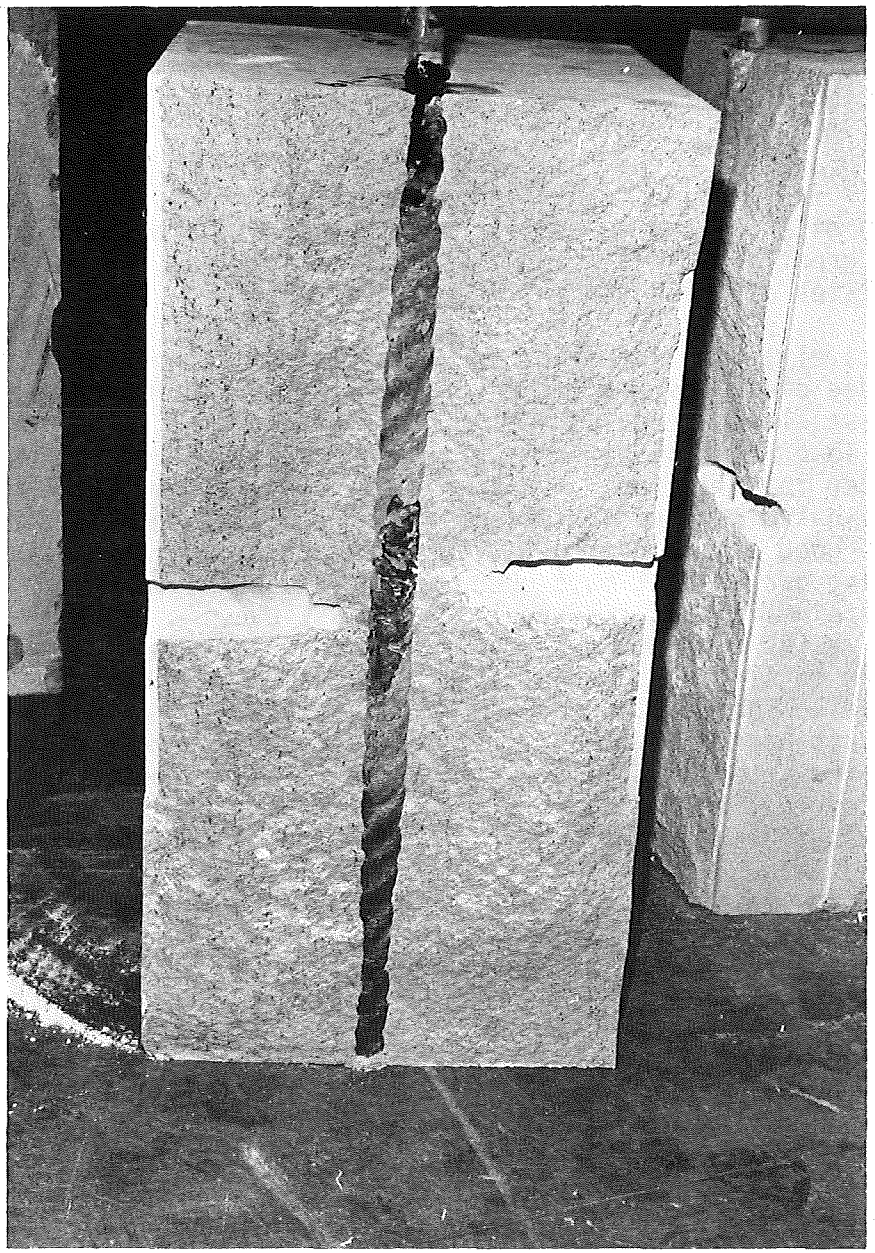

Fig. 5-13 Photograph of Limestone Block After Splitting Showing Exposed Grout Column. (Note the "rifled" appearance of the drill hole).

Groups 8 and 9 which were installed in the soft Anna shale exhibited an unusual failure. The bolt did not break for any of these installations. The bolt and most of the grout column were pulled from the hole, the only resistance to pull-out being interlocking of particles and frictional resistance along the grout-rock interface. The residual strength of these groups were 2,360 lb and 1,830 lb, respectively, after 6 in. of pull-out. This implies that in soft formations where the full strength of the bolt is not developed prior to slippage of the grouted bolt, there exists some residual installation strength. The residual strength is possibly a function of surface area of contact and surface roughness.

Groups 10 and 11 in the Interbedded shale performed much the same as Groups 6 and 7 in the limestone. There were voids in the upper 6 in. of grout in each of the Group 10 and 11 installations. In addition, the bottom 8 in. of grout in Installation CS09 was poorly mixed due to installation difficulties at the beginning of the test.

Qualitatively, the installations having zones of unhardened resin and/or shredded clumps of plastic cartridge material performed poorer than those installations having well mixed grout columns. The former exhibited more load bleed off per unit time and were, in general, less stiff than the latter installations. It is readily seen, then, that thorough mixing of resin and catalyst is essential to good long term anchorage and, therefore, to good strata control. Two factors are important here. First, the reinforcing bar or bolt must occupy a large enough volume of the hole to insure proper mixing of the grout. Previous investigations (Refs. 2, 12), as well as the current research, indicate that the optimum grout annulus is 1/8 to 1/4 in. Second, the resin must have a set-up time consistent with allowing good mixing and rapid installation. This suggests that there exist upper and lower limits on the set-up time. Although no research has indicated an optimum set-up time for the grout, the present study indicates that the rapid setting Fasloc resins (15 to 30 seconds) may not allow sufficient mixing of resin and catalyst if the bolt is not quickly pushed through the grout cartridges prior to any rotation of the bolt for mixing. Thus, in the mine, if roof bolting equipment is not in excellent condition, the mine manager should consider using a resin with a slightly longer set-up time to insure proper installation and, consequently, good strata control.

Conclusions

Several general conclusions can be advanced from the results of the creep tests described in the chapter.

1. A large load bleed off occurs during the first four or five days after bolt installation, with the majority of it taking place within the first day. This bleed off appears to be a function of grout annulus size and bolt surface roughness. A relatively thick grout annulus (1/8 to 1/4 in.) provides good load dissipation to the surrounding rock and a corrugated bolt allows less slippage at the grout-bolt interface, thereby improving anchorage characteristics.

2. Proper mixing of the resin grout along the entire hole length is essential to good strata control. The gel time of resins should be compatible with the bolt installation time as dictated by the condition of

equipment used and by the state of training of equipment operators. Resins with a variety of gel times are presently commercially available.

3. Load distributions, though not in complete agreement with elastic time-independent analyses, indicate that complete load transfer from bolt to rock occurs over a length of 14 to 22 in. of grout. This would indicate that post-tensioning would be effective only in supporting surface loose since only a few inches of material would be affected by the loading.

4. At constant loads, creep of the grouted bolt system is indicated by a progressive penetration of the load into the grout column. This penetration is believed to be the result of cyclic localized grout failure followed by load build-up and further localized grout failures.

5. The high stiffness of each resin-grouted installation tested substantiates the practice of installing these bolts untensioned. The stiffness of an installation becomes more important as bolt length increases since for point-anchored systems stiffness decreases in proportion to the length of the bolt, whereas the stiffness of full-column anchored systems is a constant, high value for bolt lengths greater than about 2 ft.

6. It is unlikely the high-stiffness installations have universal application. Certain soft formations which tolerate relatively large plastic displacements may be more readily controlled using less stiff, yieldable supports.

7. Resin-grouted bolts installed in soft formations possess some residual strength provided the strength of the steel bolt is not exceeded.

8. Three of the installation types tested should be viable roof support systems under most circumstances: the 7/8-in. reinforcing bar in a 1 3/8-in. hole with Celtite resin, the 3/4-in. reinforcing bar in a 1-in. hole with Celtite resin, and the 3/4-in. Fasloc bolt in a 1-in. hole with DuPont resin. The first should be used only where the additional strength of 7/8 in. of steel is needed since the cost of this system is considerably higher than that of the other two.

Chapter VI

FIELD TESTS and ANALYSIS

Introduction

As an extension of the study of the effects of various loadings on full-column, resin-grouted rock bolts, instrumented roof bolts were installed in three coal mines, one in Illinois and two in Tennessee, to examine the reaction of resin-grouted bolts to geologic and mining stresses. Observations of bolt strain and strata displacements were made for three to six months in each mine.

When designing the field tests, it was noted that two basic test configurations may be used to obtain the data necessary to evaluate the effectiveness of the resin bolts. First, the instrumented bolts may be installed in the spaces between existing bolts of a normal bolting pattern. Second, the instrumented bolts may be installed as members of the regular bolting pattern. Because of problems encountered in scheduling the installation of instrumentation, the first test configuration was used in the Illinois mine. The second configuration was used in both of the Tennessee mines, which were instrumented during the second year of field testing. Each configuration offers certain advantages and disadvantages. The first approach allows research personnel to operate under a protective canopy of other roof bolts. A history of lower apparent loads will be recorded, however, since the primary bolt pattern carries part of the load. The second approach offers the distinct advantage of providing the exact load history that any bolt in that position would experience. The bolts must be installed more quickly when used in this configuration since support of the roof must be accomplished as soon as possible so normal mining activities may resume. The required haste of installation increases the likelihood of damaging the instrumented bolts.

Field Test Geometry and Instrumentation

Two test sites were chosen in each of the three coal mines. The three operations employed continuous mining equipment in conjunction with shuttle car and belt haulage to remove the coal. The general mine plans for the operations were similar, however, the Tennessee operations required more flexibility in pillar layout due to varying geologic conditions (Table 6-1).

Instrumented bolts and sag stations were installed in Mine 1, Site 1, eight days after, and in Site 2, ten days after the room was mined and bolted. Installation of instrumentation in Mines 2 and 3 was carried out immediately following mining of the rooms.

The bolts used at each mine were of the type currently used in the roof control plan. Mine 1 used 3/4-in. diameter by 5-ft long, smooth shanked bolts of DuPont design in 1-in. holes with Fasloc resin. Mines 2 and 3 used 4-ft and 6-ft long bolts, respectively. These were the new DuPont 1-in. diameter corrugated bolts which were installed in 1 3/8-in. holes with Fasloc resin.

Table 6-1. Description of Test Sites

Mine	Test Site	Nominal Dimensions			Roof Rock
		Room Centers, ft.	Room Width, ft.	Coal Thickness, ft.	
Illinois (1)	1	70	20	7, (Herrin)	Anna shale overlain by Brereton limestone.
	2				Brereton limestone.
Tennessee (2)	1 and 2	40-100	20	4 1/2 (Jellico)	Gray shale with sand stringers overlain by sandstone (approx. 9-10 ft above roof line).
Tennessee (3)	1 and 2	40-100	20	4 1/2 (Jellico)	Gray shale with sand stringers overlain by sandstone (approx. 9-10 ft above roof line).

Each bolt was instrumented with four sets of electrical resistance strain gages (Ref. 2, Chapter 6). Each set of gages consisted of two axial strain gages which were mounted in diametrically opposite positions and were connected in series. In this manner, compensation for bending in the bolt was effected. Gage spacing was chosen to provide a record of load changes at the head of the bolt (outside the resin) and at three other locations along the bolt (Fig. 6-1). Mine 1 used 1/4-in. thick steel plates backed up by 2-in. thick oak boards and Mines 2 and 3 used 1/4-in. steel plates, only, to distribute the bolt loads to the roof strata.

The short strain gage lead wires which projected from the bolt head were attached to longer leads subsequent to bolt installation. In Mine 1, connection was made using crimping and conductive silver paint. Connections in Mines 2 and 3 were made with high quality eight-prong electrical connectors. All connections were wrapped with several layers of electrical tape to exclude moisture and dust and thereby prevent electrical leakage and shorting.

Each long lead consisted of a length of shielded Belden cable with a military specification connector on one end. A Wheatstone bridge type strain indicator was used to take the strain readings. The strain gages were connected to the strain indicator through a five-channel switch unit designed and built for the field test work. The switch unit contains the three 240-ohm precision resistors needed to complete the strain gage circuit. The first four channels of the unit were used to read the four sets of strain gages. In addition, a fourth precision resistor could be switched in on the fifth channel to provide a "standard" to check the stability of the strain gage circuitry.

Two types of instruments were used to measure relative strata displacements at four horizons. At Mine 1, stations measured vertical strata displacements at 1, 2, 4, and 6-ft horizons relative to an anchor point at the 15-ft horizon. Details of this type of sag station are shown in Fig. 6-2. At Mines 2 and 3, wire-type sag stations developed by the Mining Enforcement and Safety Administration (MESA) were employed (Fig. 6-3). These were anchored at 2, 4, 6, and 15-ft horizons in Mine 2 and at 1 1/2, 3, 6, and 12 to 13 1/2-ft horizons in Mine 3. Upper horizon locations varied in Mine 3 because of the presence of a hard sandstone strata. Benefits of this system are (a) movements of all four horizons are monitored from one hole reducing drilling time, and (b) the system is lighter and more compact than the previously described one. In addition, there is no discernible loss in accuracy with the MESA wire-type system, provided an adequate anchorage horizon is present and if sufficient care is taken when the dial indicator is set in place and read.

The measurement of strata displacements at different horizons is necessary since strata separated by bedding or fracture planes move downward at different rates. By delineating where the movements occur it is possible to correlate strata displacements with changes in bolt loads. In addition to the data collected using instrumented bolts and sag stations, further knowledge of roof behavior was obtained by borescope observations. Each test site in Mines 2 and 3 was borescoped immediately following installation of bolts and again at the close of the project to determine the location, orientation, and extent of open

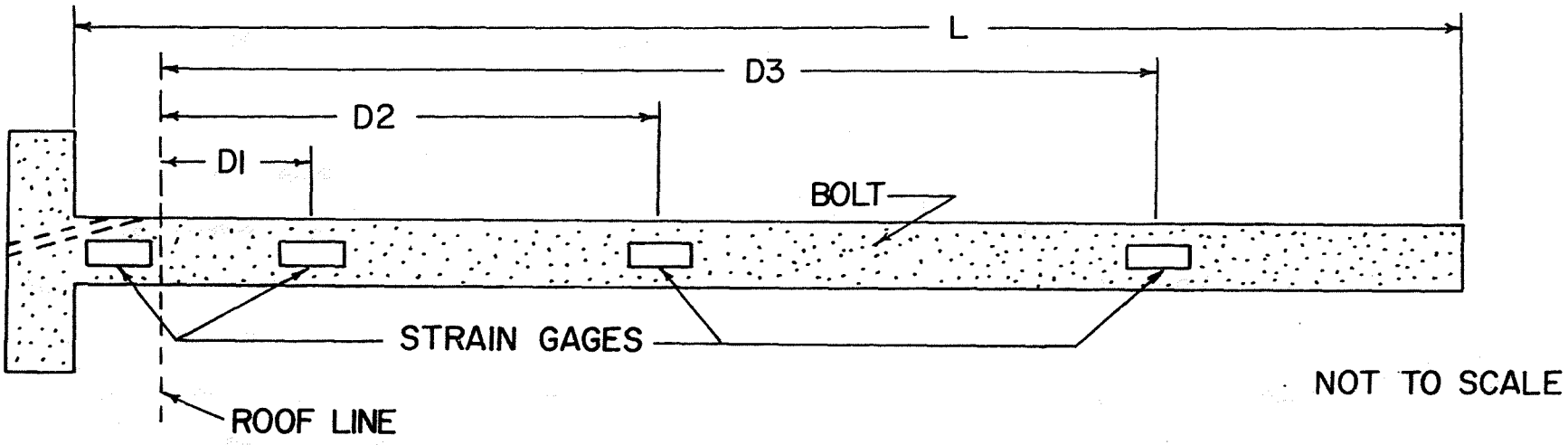

Mine No.	D1, in.	D2, in.	D3, in.	L, in.
1	6	18	36	60
2	6	18	36	48
3	6	24	54	72

Fig. 6-1 Locations of Strain Gages on Instrumented Rock Bolt.

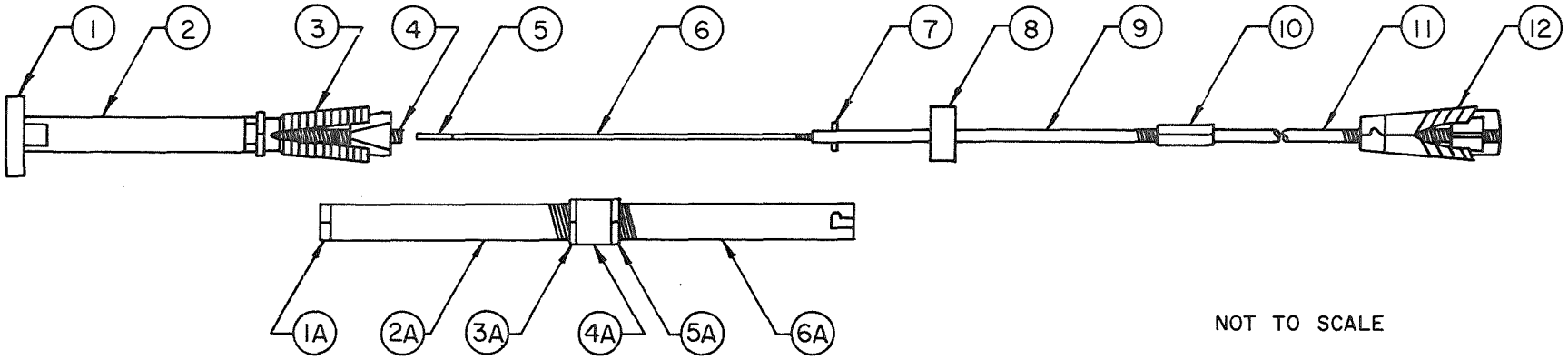

NOT TO SCALE

DEFORMETER			
1	3/8" X 1" X 2 1/2" stainless steel	9	5/8" roof bolt w/o head
2	3/4" X 36" black pipe	10	5/8" coupler
3	expansion shell (Bethehem Steel C-1)	11	5/8" roof bolt w/o head
4	5/8" X 4" hex. bolt NC	12	expansion shell (Ohio Brass)
5	1/4" dia. X 1" stainless steel		
6	1/4" X 43 3/4" mild steel rod		
7	1/4" X 1 1/16" hardened pin		
8	7/8" X 1 1/2" rubber bushing		

INSTALLATION TOOL	
1A	3/4" hex nut
2A	3/4" black pipe
3A	jamb nut
4A	3/4" pipe coupling
5A	jamb nut
6A	3/4" black pipe

Fig. 6-2 Detail Drawing of Roof Sag Indicator and Installation Tool

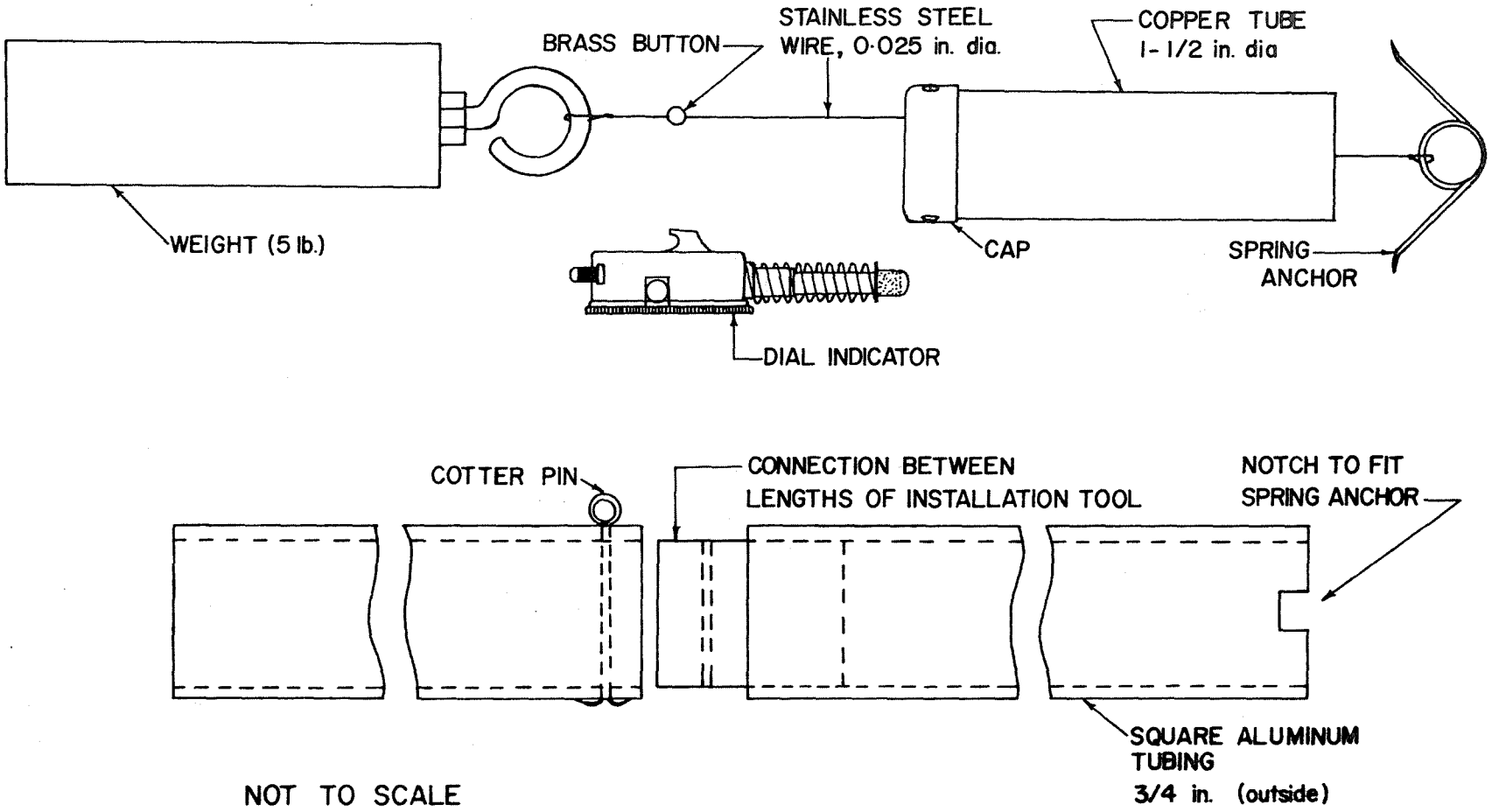

Fig. 6-3 Detail Drawing of MESA Wire-Type Sag Indicator and Installation Tool.

joints, fractures, and bedding surfaces. These borescope logs are presented in the Appendix. Scheduling conflicts, variable geology and nonuniform room dimensions resulted in a somewhat different test site geometry at each location (Figs. 6-4 to 6-9). At each site, however, the resulting cluster of instrumentation provided reliable bolt-strain and strata-displacement data for three to six months.

Installation Procedures

The problems encountered in laboratory testing are multiplied many times over when field tests are executed. In particular, the effects of the harsh mining environment on electrical and mechanical measuring devices must be acknowledged and countered if the maximum amount of valid data is to be obtained from a test site. The proper treatment of the bolt prior to and during insertion is important to ensure that a good installation is obtained which will provide much useful data. Even when proper care is exercised, many gages are destroyed as a result of mining activity at the test site.

Several days prior to the field tests, each bolt, already instrumented with strain gages, was loaded in tension in a testing machine and the strain in the gage nearest the bolt head was recorded. The determination of this load-strain relationship was necessary because of the reduced cross-sectional area at the gage location.

Just prior to the bolt installation, the short strain gage leads projecting from the end of the bolt were connected to the long Belden cable and connector. An "apparent" or "zero" reading was then taken for each gage. This reading was then subtracted from all post-installation strain readings to obtain the true strain in the bolt.

The short leads were then disconnected from the Belden cables and folded up. The bolt head was placed in a hollow-stem adapter which fit the roof bolting machine. The proper length of resin was placed in the previously drilled hole and the bolt was inserted and rotated approximately 20 seconds as is done during the regular bolting cycle. The full thrust of the bolting machine was then applied to the head of the bolt for approximately 30 seconds as the resin hardened. The resulting installation is shown in Fig. 6-10. The long cables were then permanently connected to the short leads.

The bolt-type sag stations were installed in 15-ft holes, 1 3/8 in. diameter. The portion of the installation which was to be anchored at the 15-ft horizon was inserted in the hole in sections, each section being tightened onto the next as installation progressed. Once this portion was in the hole, the anchor was tightened by means of the installation tool (Figs. 6-2, 6-11). The lower section was then inserted and tightened. The MESA wire-type sag stations were installed in 1 3/8-in. diameter holes drilled 12 to 15 ft deep, depending on the location of the hard sandstone strata. A short length of copper tubing was grouted into the bottom of the hole which was previously reamed to 1 3/4-in. diameter. Once the tube was securely in place, the spring anchors with wires attached were inserted to the proper horizon. The cap was then placed on the tube and small brass reference points were attached to each wire (Fig. 6-12). Initial readings were taken.

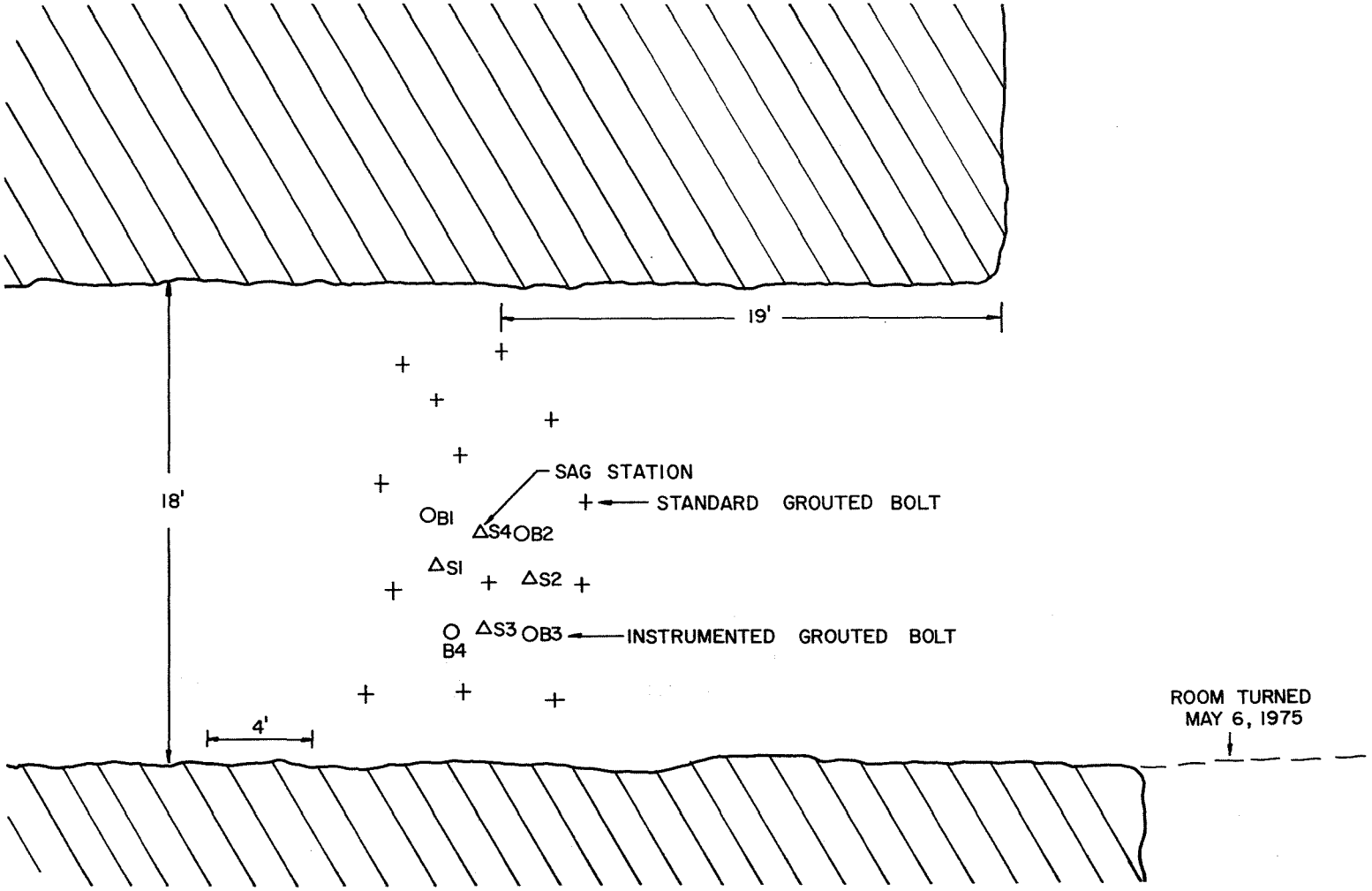

Fig. 6-4 Plan View of Test Site 1, Mine 1, in Shale Roof Showing Location of Instrumentation

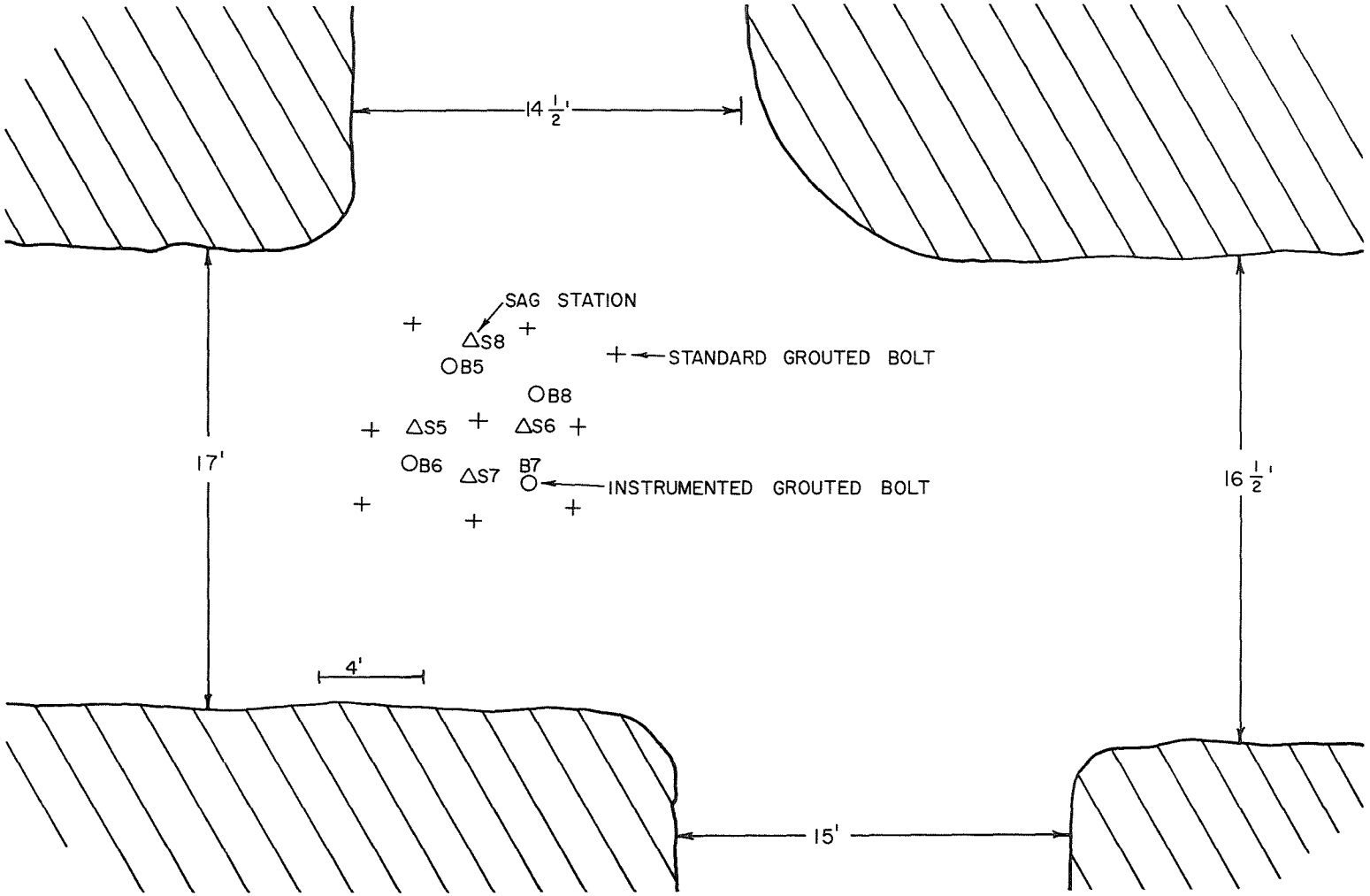

Fig. 6-5 Plan View of Test Site 2, Mine 1, in Limestone Roof Showing Location of Instrumentation.

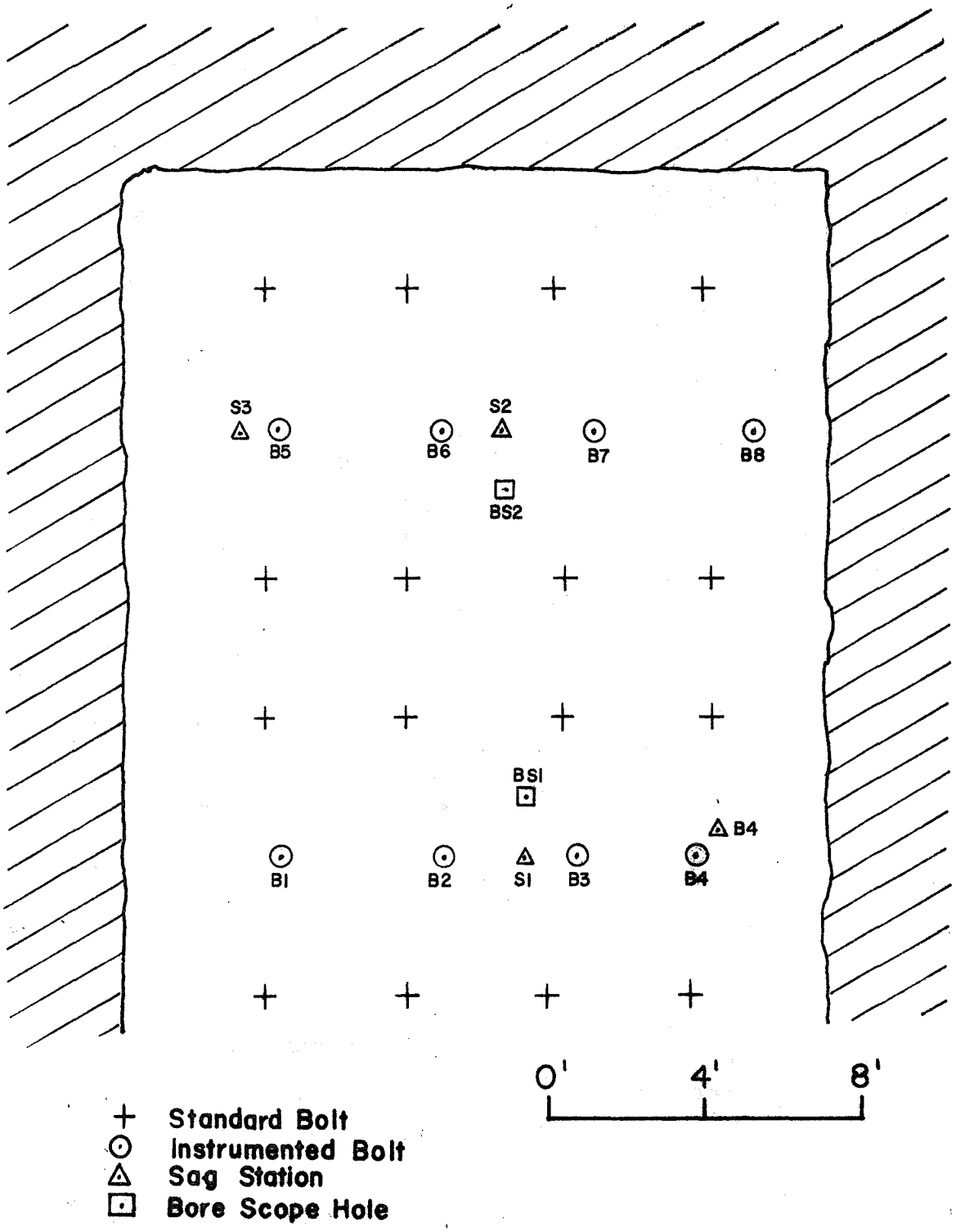

Fig. 6-6 Plan View of Test Site 1, Mine 2, in Shale Roof Showing Location of Instrumentation.

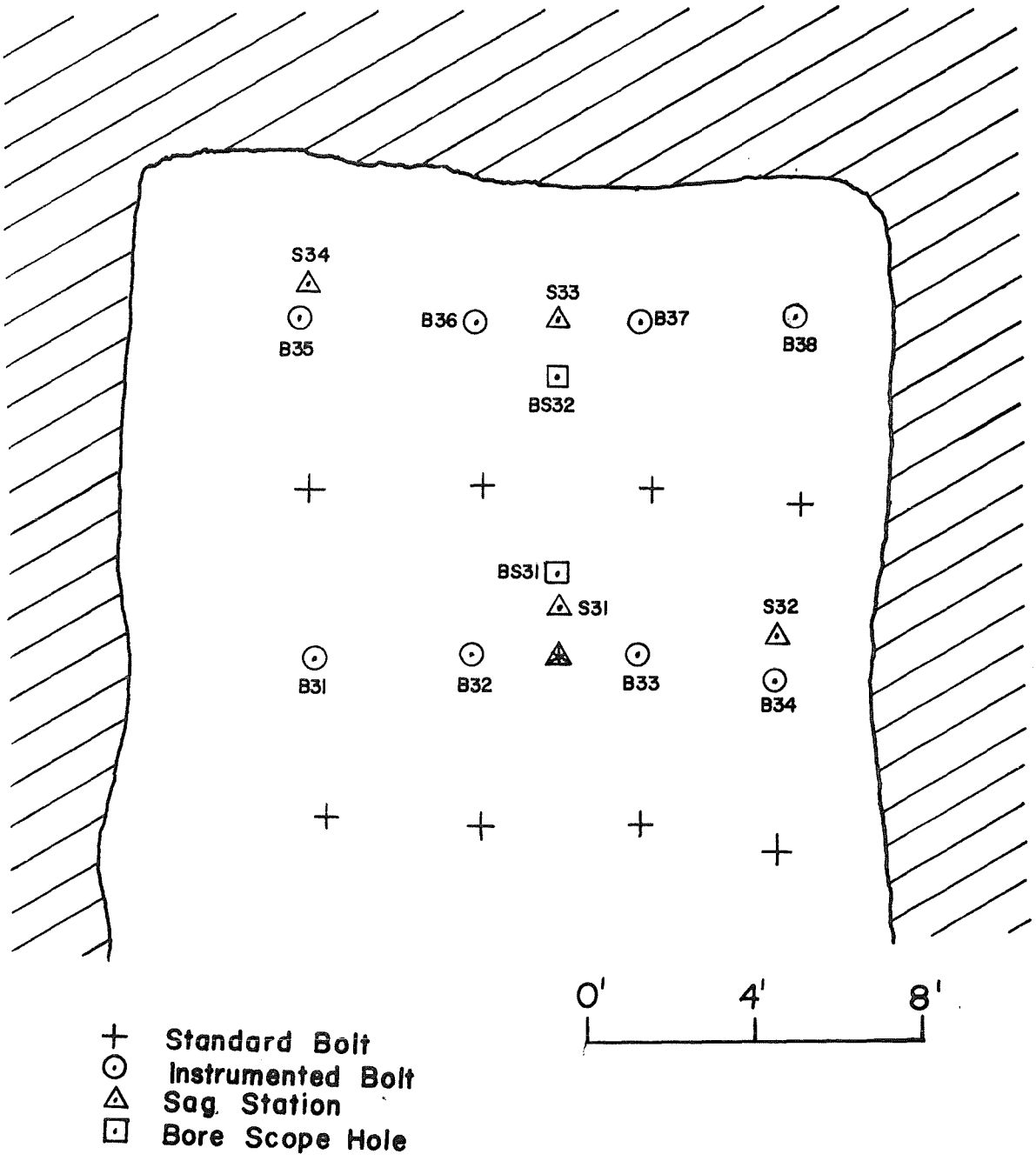

Fig. 6-9 Plan View of Test Site 2, Mine 3, in Shale Roof Showing Location of Instrumentation.

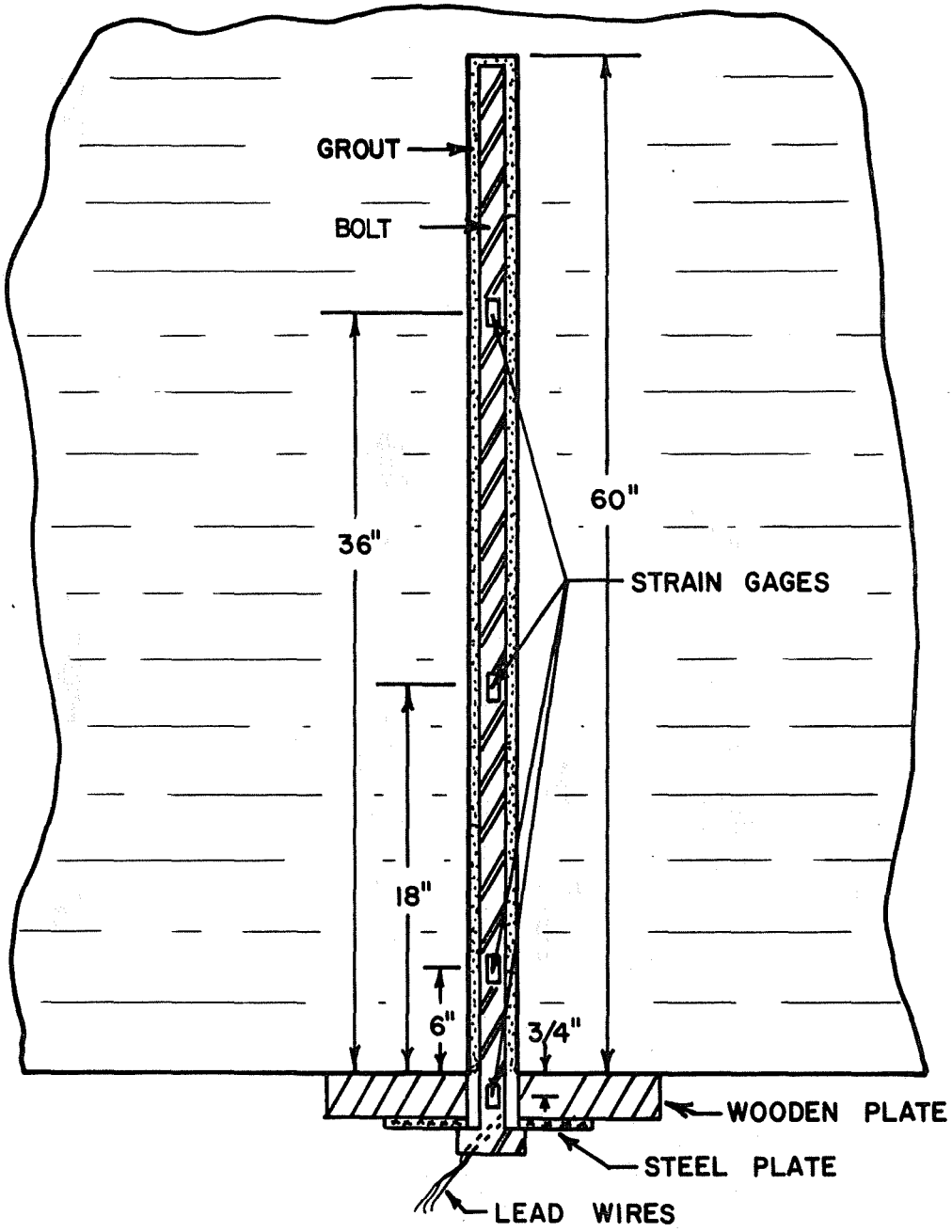

Fig. 6-10 Instrumented Roof Bolt After Installation. (Dimensions given are for Mine 1)

Strain and sag station readings were taken within one hour after installation and at least once more in the following 12-hour period. Readings were taken at one to two-week intervals thereafter until the test was completed.

Results and Discussion

The six test sites provided data useful in gaining a better understanding of how full-column resin-grouted roof bolts react to various loadings. Although it is not possible at this point to predict the response of grouted bolts to all loading conditions, several interesting observations were made at each site which should be applicable to mines having similar geologic conditions and roof bolt geometries. Among these observations are the presence of installation induced stresses, compressive bolts stresses, and relationships between bolt strain and strata displacements. Detailed bolt load histories are presented in the Third Annual Report (Mine 1) and Appendix B (Mines 2 and 3).

A. Installation Induced Stresses

Strain readings immediately after installation were used to determine the loads induced during bolt installation (Table 6-2). It is evident that the upward thrust of the bolting machine, applied after the grout is thoroughly mixed, is sufficient to cause upward deflection of the roof strata. The bolt load immediately after installation, then, is due to the downward deflection of roof strata which occurs when this thrust is removed.

It was observed that the installation load was not confined to the bearing plate region of the bolt but also often occurs at points farther up the bolts. The variability of installation load from mine to mine may be due to differences in applied thrust and differences in strata stiffness. The weak shale roof in Mine 1 apparently deflected more readily than did the limestone roof, thus a greater installation induced load was noted. A great deal of load variability was noted within each test site of Mine 2. This may be due to either equipment malfunctions or inconsistencies on the part of equipment operators.

B. Load Distribution Along Bolt

It was evident in each mine that great variability in bolt load should be expected within any given mine. An extreme case of this was seen in Mine 1. The strain and displacement histories of Test Sites 1 and 2 provide some interesting information. Bolts in limestone roof rock (Site 2) experienced strains not exceeding about 250 μ in./in., whereas those in shale roof rock (Site 1) had strain magnitudes as great as 3,500 μ in./in. (Figs. 6-13 and 6-14). Three bolts in Site 1 were elongated beyond the yield strain. The mine map (Fig. 6-15) indicates that the two sites are only 70 ft apart; yet the geologic and, hence, bolt loading conditions are much different. This observation has practical significance in that standard roof bolting patterns, which may be determined from test site data, must be capable of supporting the maximum expected load under the worst geologic conditions.

Table 6-2. Installation-Induced Bolt Loads

Mine Number	Roof Rock	Average Installation Load, lb.
1	Shale	3100
	Limestone	2400
2	Shale with Sand Stringers	1750
3	Shale with Sand Stringers	2590

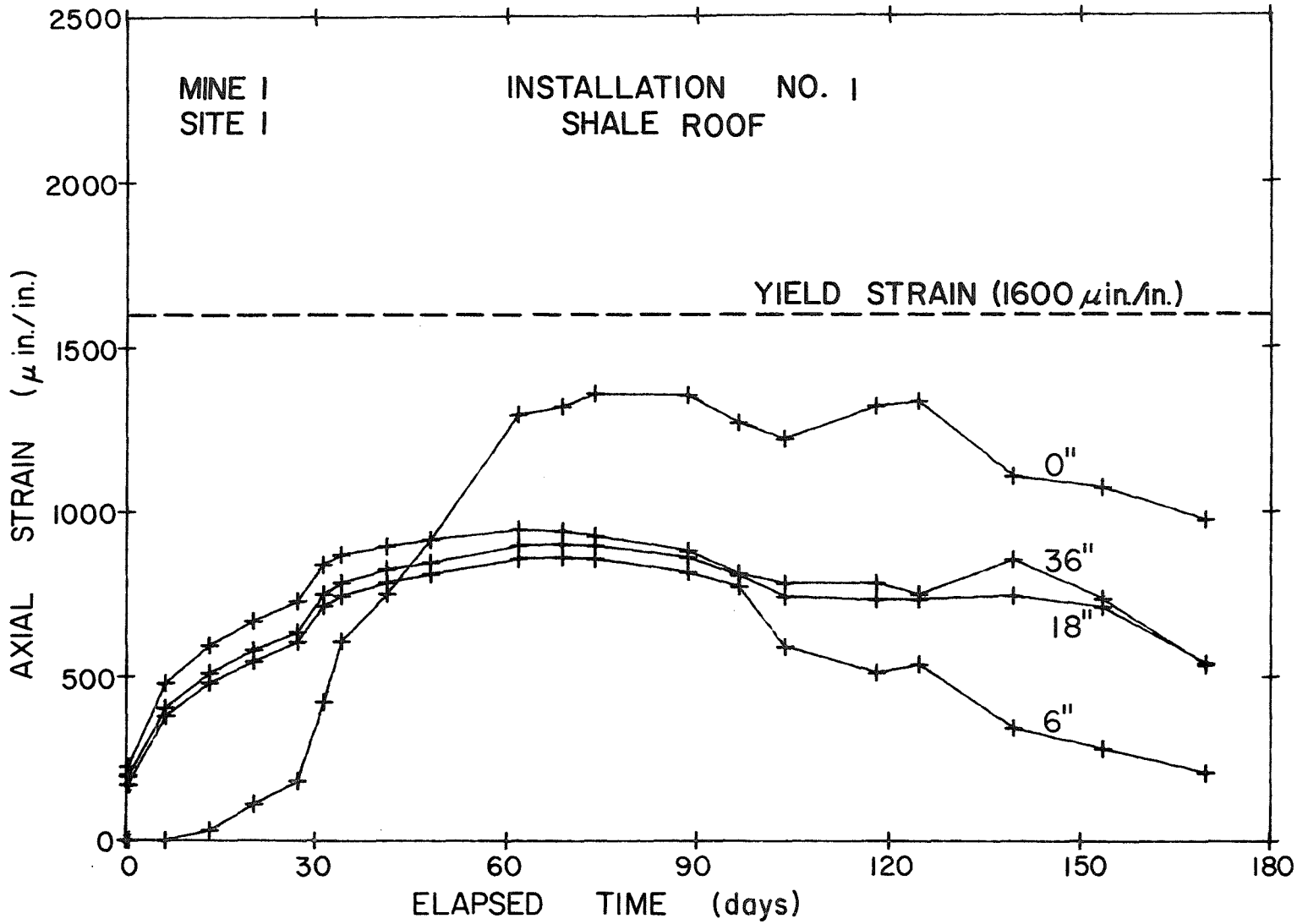

Fig. 6-13 Axial Strain Versus Elapsed Time at Each of Four Gage Locations, Installation No. 1, Shale Roof.

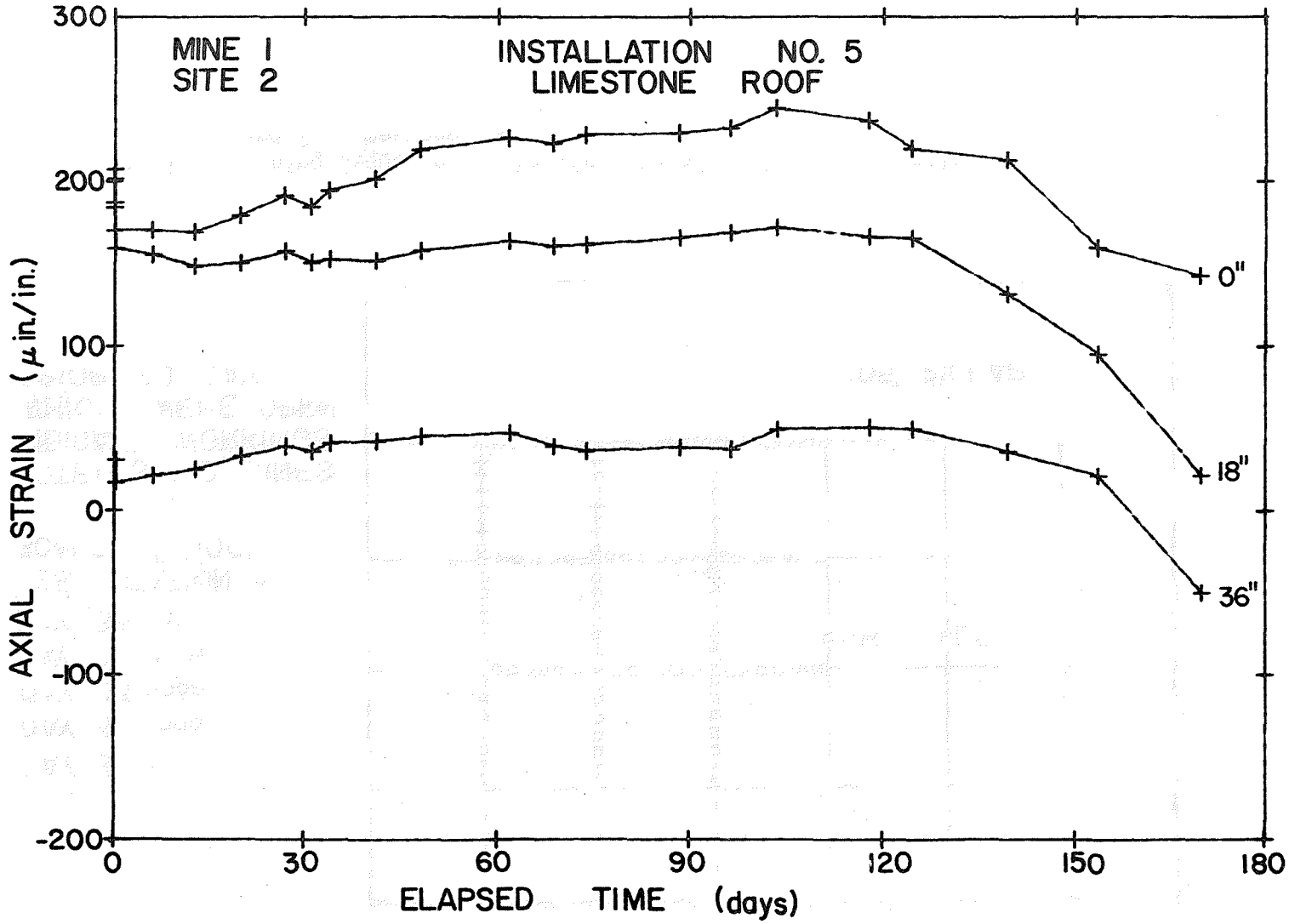

Fig. 6-14 Axial Strain versus Elapsed Time at Each of Three Gage Locations, Installation No. 5, Limestone Roof.

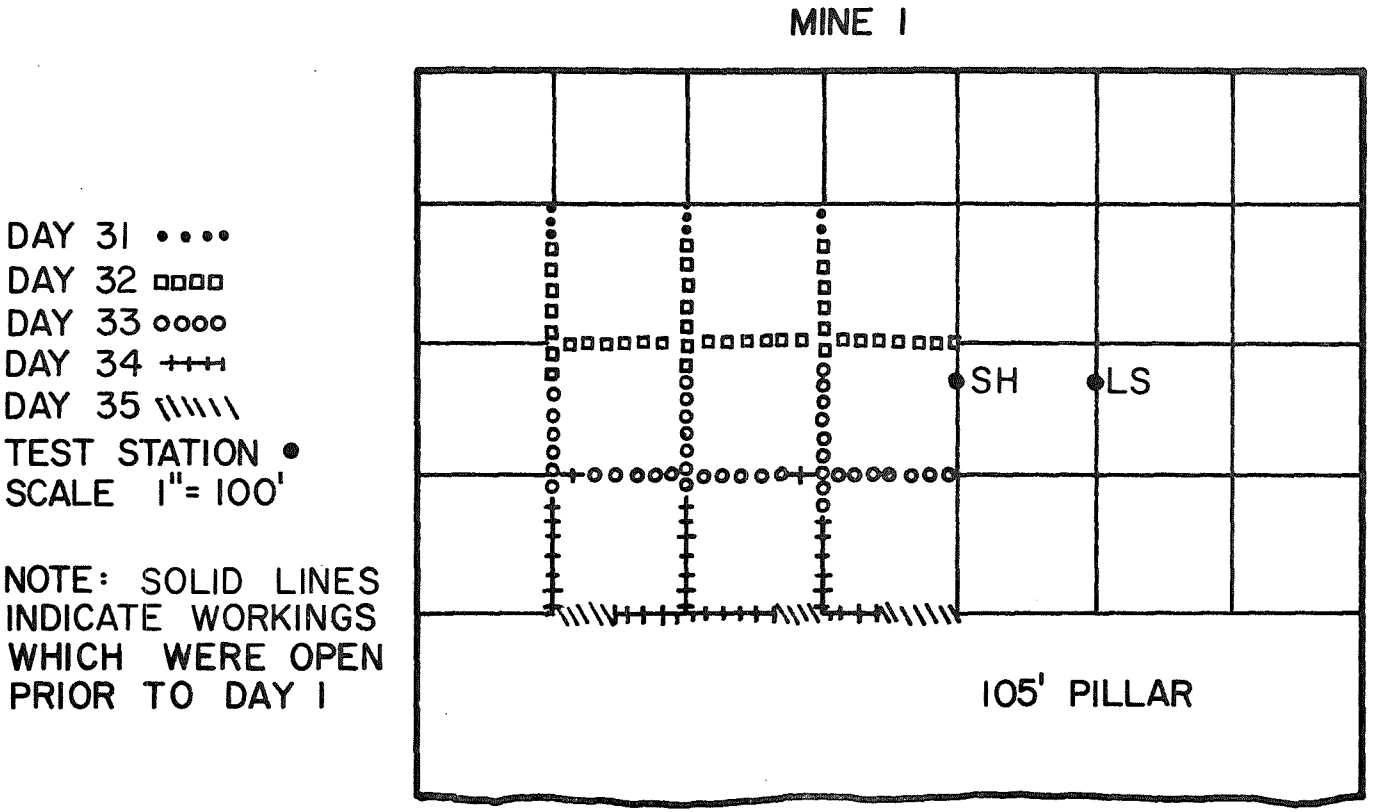

Fig. 6-15 Mining Sequence in the Vicinity of Test Site 1 (shale roof) and 2 (limestone roof).

The graphs shown in Figs. 6-16 to 6-18 show the load distributions along each bolt in rows across the opening. The loads are shown immediately after installation and some later time during the test period, generally 90 days. In some cases several of the installations were lost before 90 days so the graphs indicate a lesser time period. Several of the graphs are incomplete showing only two or three test points due to gage or leadwire damage which most often occurred during installation. The maximum bolt load may exist at any point along the bolt (Figs. 6-16 to 6-18). Since the bolt is anchored along its entire length, only a small section of the bolt close to a strata separation experiences high loading. This phenomenon explains the inherent high axial stiffness of full-column grouted bolts. Also, bolt loads may decrease with time at some locations. This would occur when first a lower stratum moved downward, elongating the bolt, and then some upper stratum moved downward, relieving some of the tension in the section of bolt between the two strata while producing tensile loads further up the bolt. Time-dependent behavior noted in the laboratory studies also effects load decreases.

Also of interest is the occurrence of compressive loads in some of the bolts (Figs. 6-16 to 6-18). Such compressive loading was surprising when first observed; however, it was later noted that similar compressive loadings had been recorded on resin-grouted bolts in the White Pine mine (Refs. 13, 14, and 15). Dave (Ref. 4) showed with the finite element method (Fig. 6-19) that the lower part of a grouted bolt is in tension while the upper part is in compression when gravity was "turned on" for his models, and that the load distribution was shifted to more compressive when the rock was later allowed to progressively fail in tension.

Compressive loads may also be generated in the bolts under certain conditions of deflection history of the roof strata. As mining progresses, the support of the immediate roof is removed, allowing some initial strata deflection. If the roof rock is very weak, a roof fall may occur. On the other hand, a fairly competent strata will deflect downward slightly without failing. This deflection may be elastic or may involve the separation of strata. After these movements have occurred, the bolts are installed, thus securing the relative location of each stratum of the bolted sequence. Compressive bolt loads may now develop if the upper strata begin to move downward at a greater rate than the lower strata as mining in the area progresses or as deterioration of the structure continues.

The sag-station data (Fig. 6-20) from Mine 1, Site 1, with a shale roof indicate that there was a considerable amount of relative vertical movement between strata, and that the deflections were not "well behaved". The deflections in Fig. 6-20 were measured relative to an anchor 15 ft above the roof line, and one would expect decreasing deflections as he goes from 12 in. to 72 in. on the curves in Fig. 6-20. The curves do not show this progression; in fact, the 48-in. horizon even moved upward relative to the 15-ft anchor point. With this type of vertical movement occurring in the roof strata one can explain bolt loading histories of compression or alternate tension and compression. It is important to realize that where compressive bolt loads develop, the upper strata are pushing down on the lower strata, thereby contributing to the forces inducing roof failure.

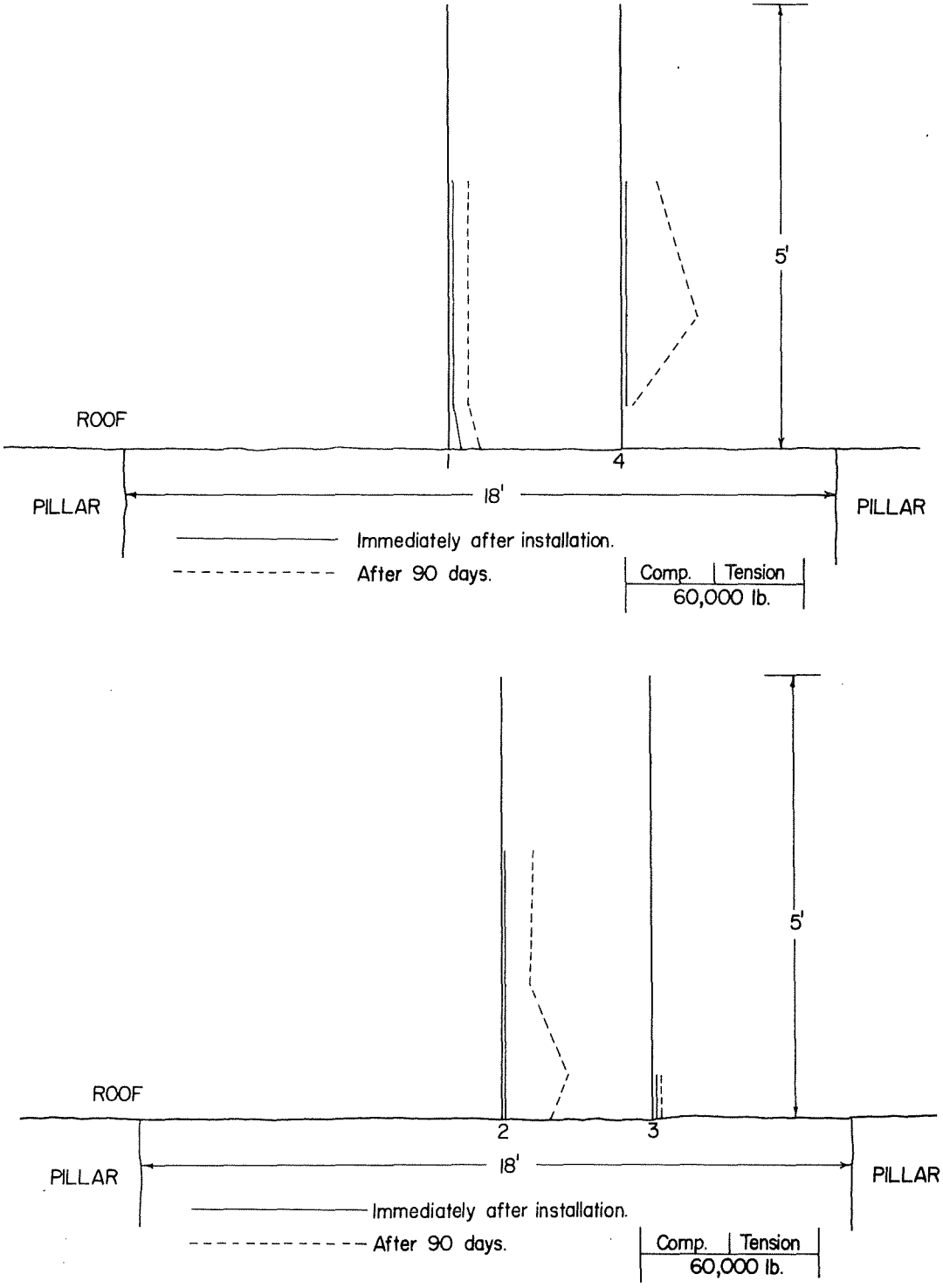

Fig. 6-16a Bolt Load Distributions, Mine 1, Test Site 1.

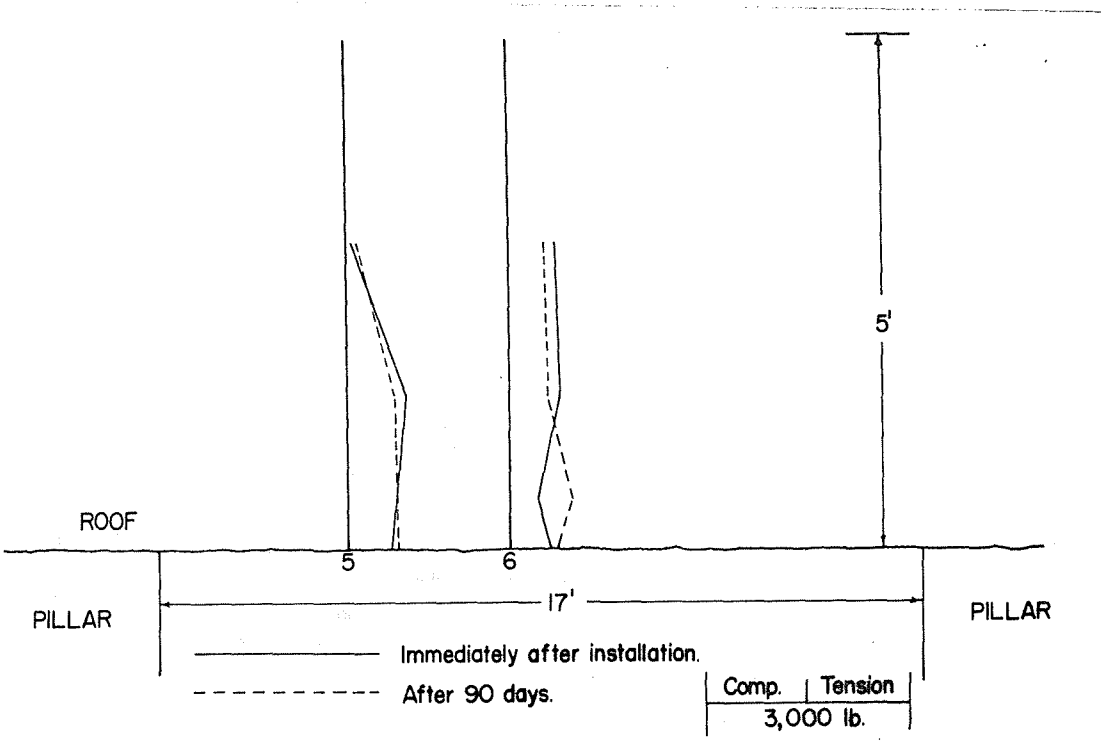

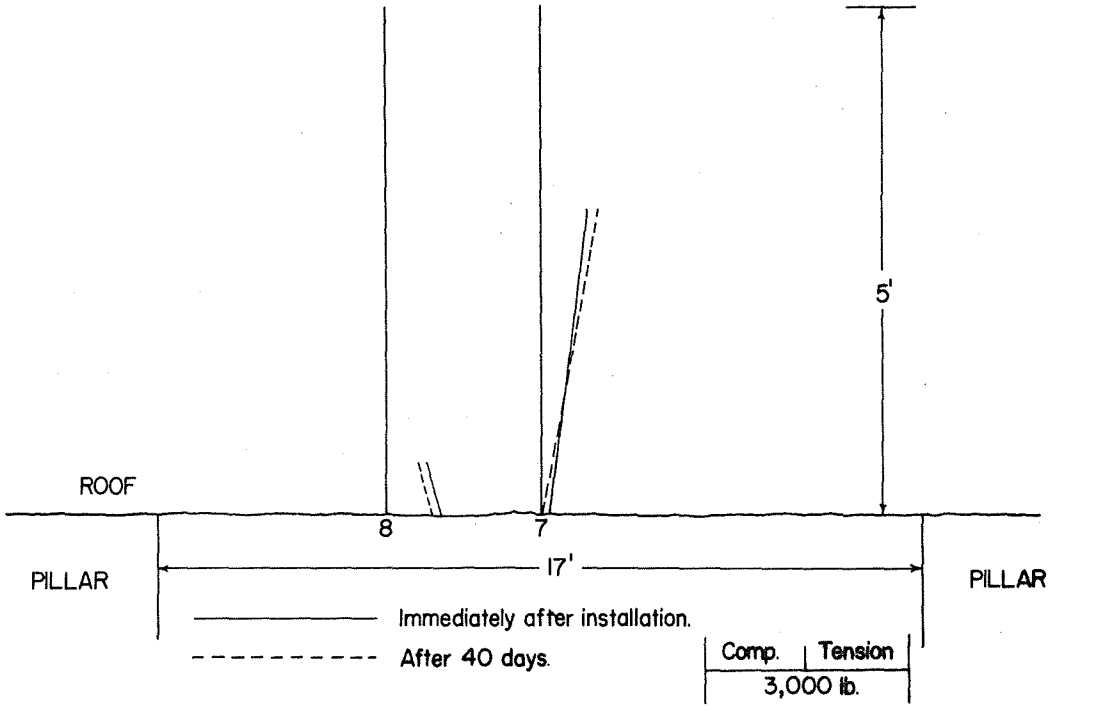

Fig. 6-16b Bolt Load Distributions, Mine 1, Test Site 2.

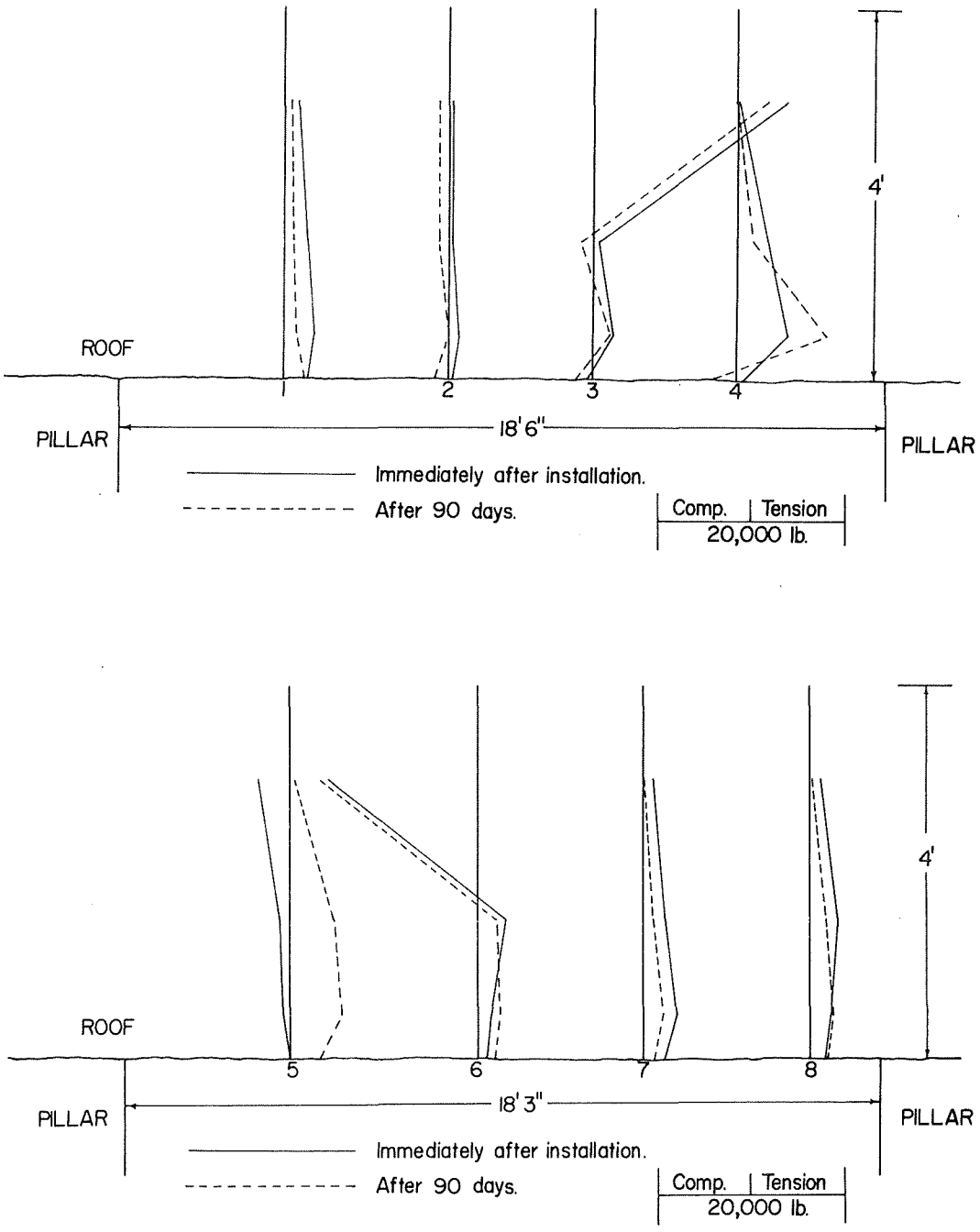

Fig. 6-17a Bolt Load Distributions, Mine 2, Test Site 1.

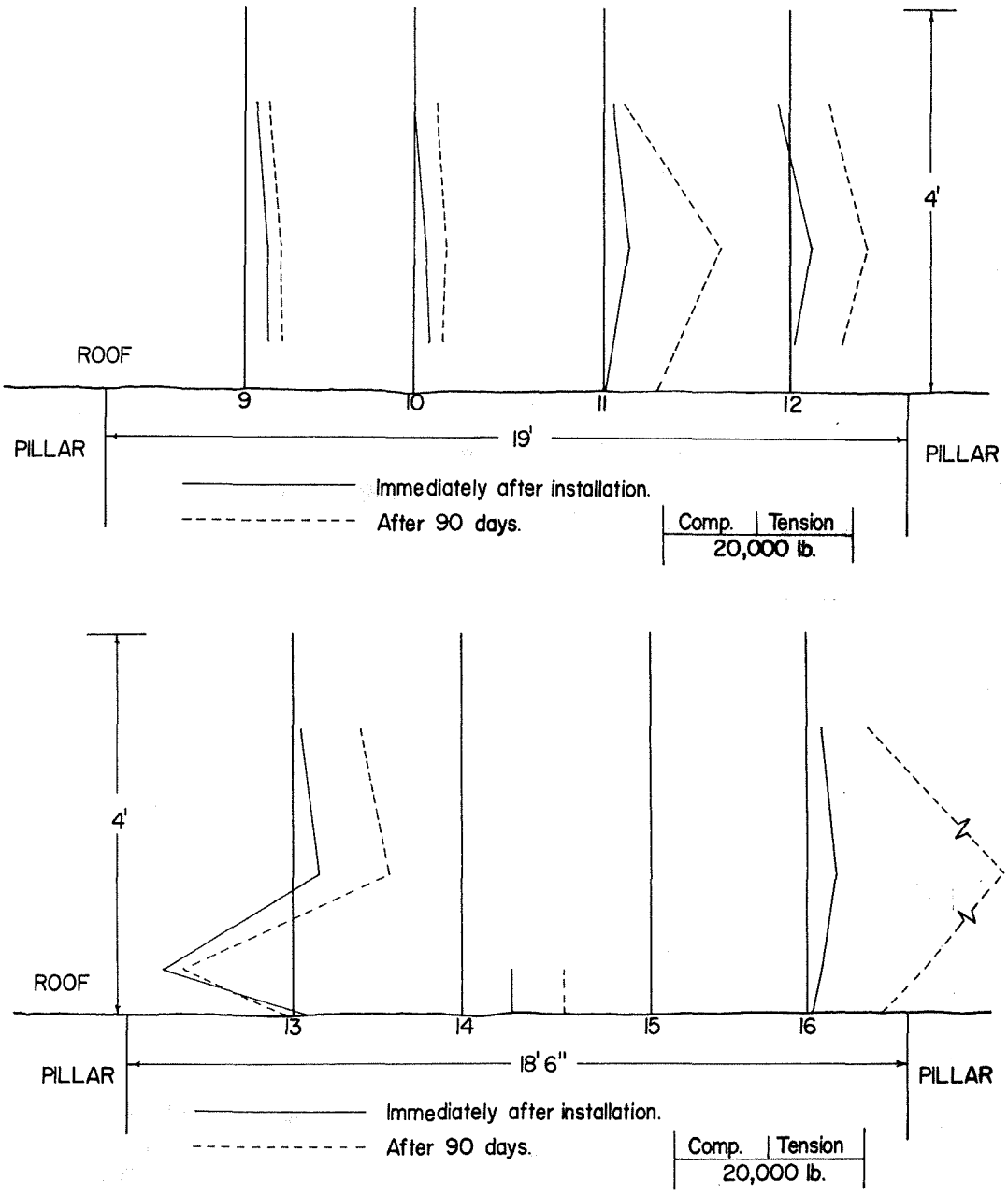

Fig. 6-17b Bolt Load Distributions, Mine 2, Test Site 2.

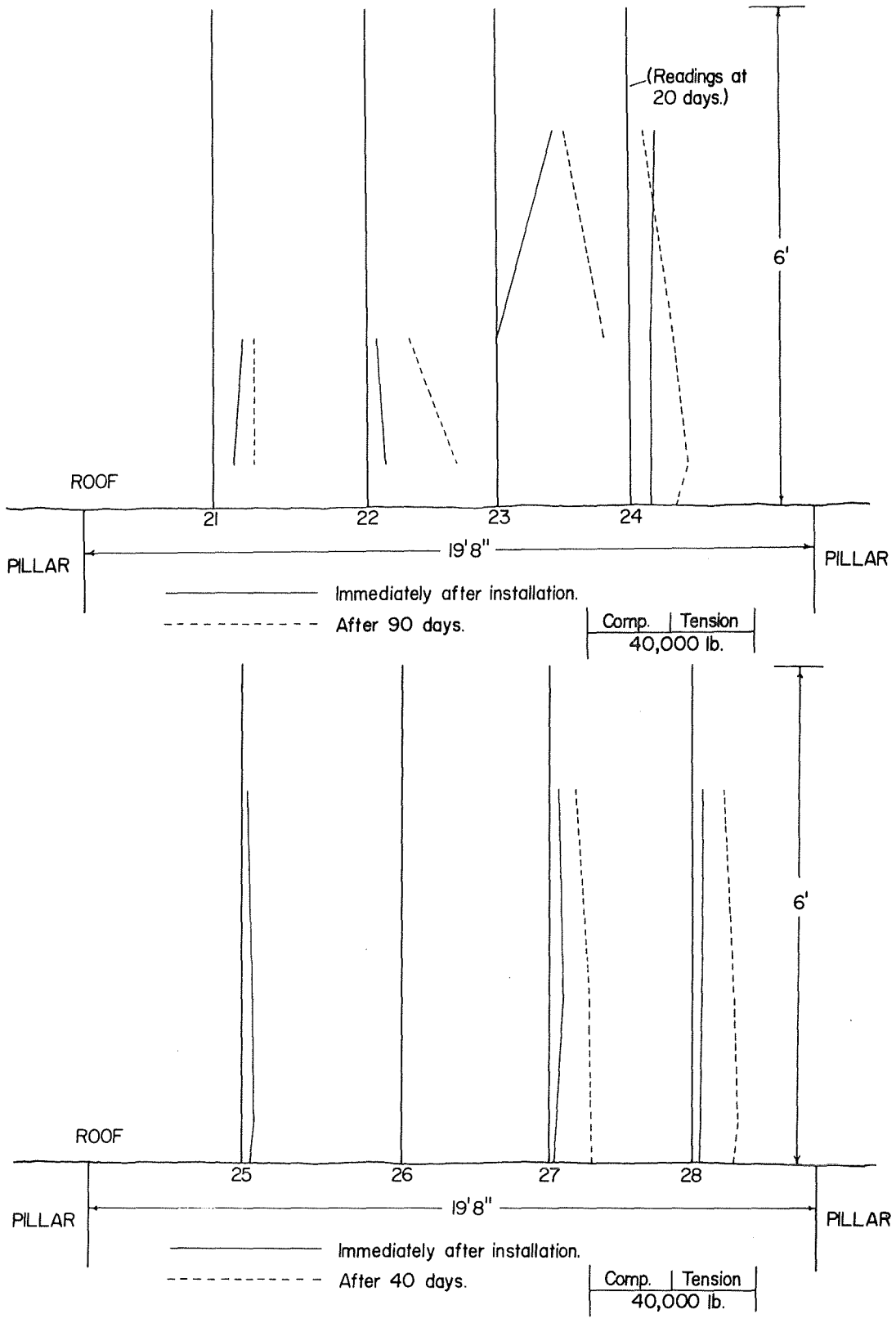

Fig. 6-18a Bolt Load Distributions, Mine 3, Test Site 1.

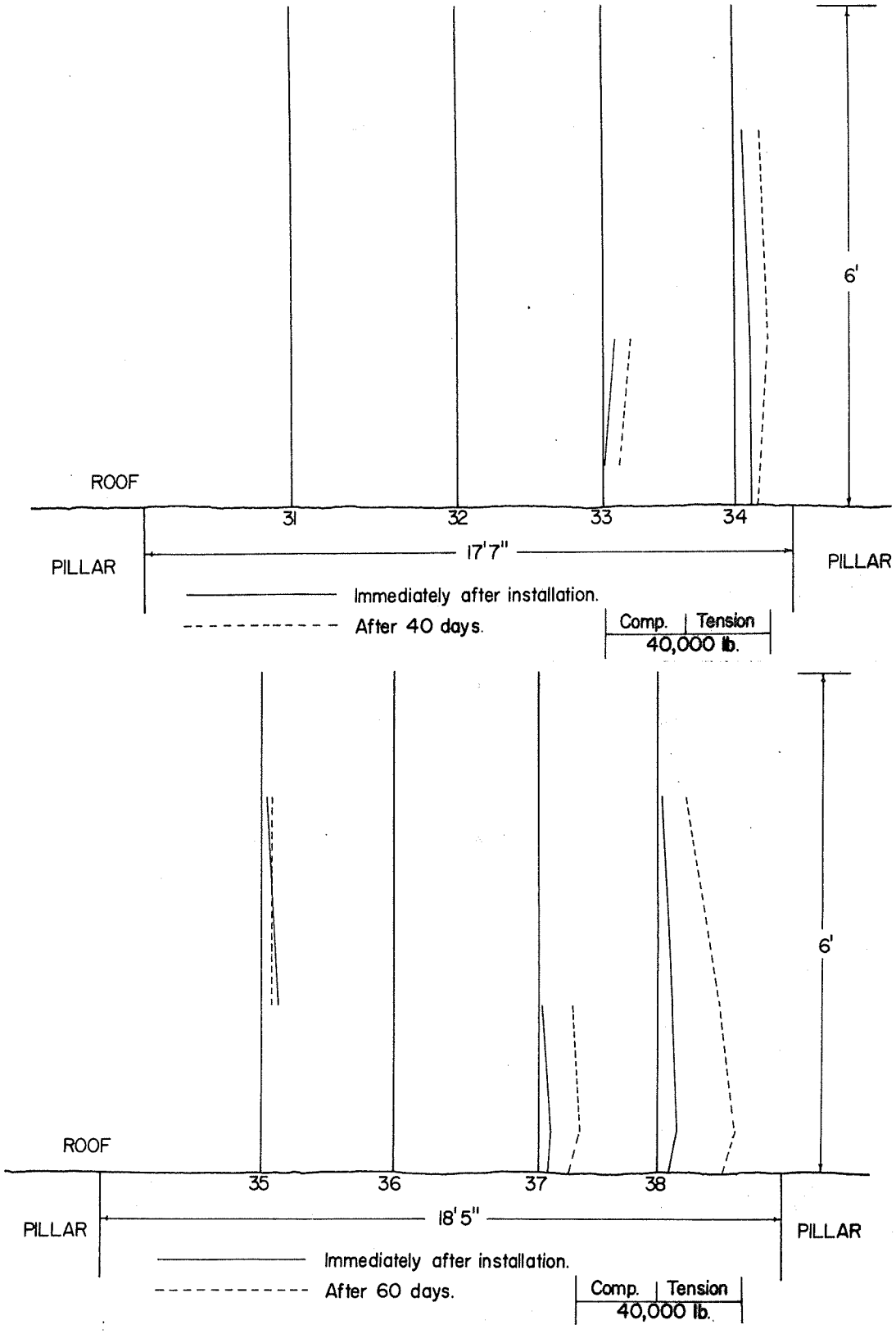

Fig. 6-18b Bolt Load Distributions, Mine 3, Test Site 2.

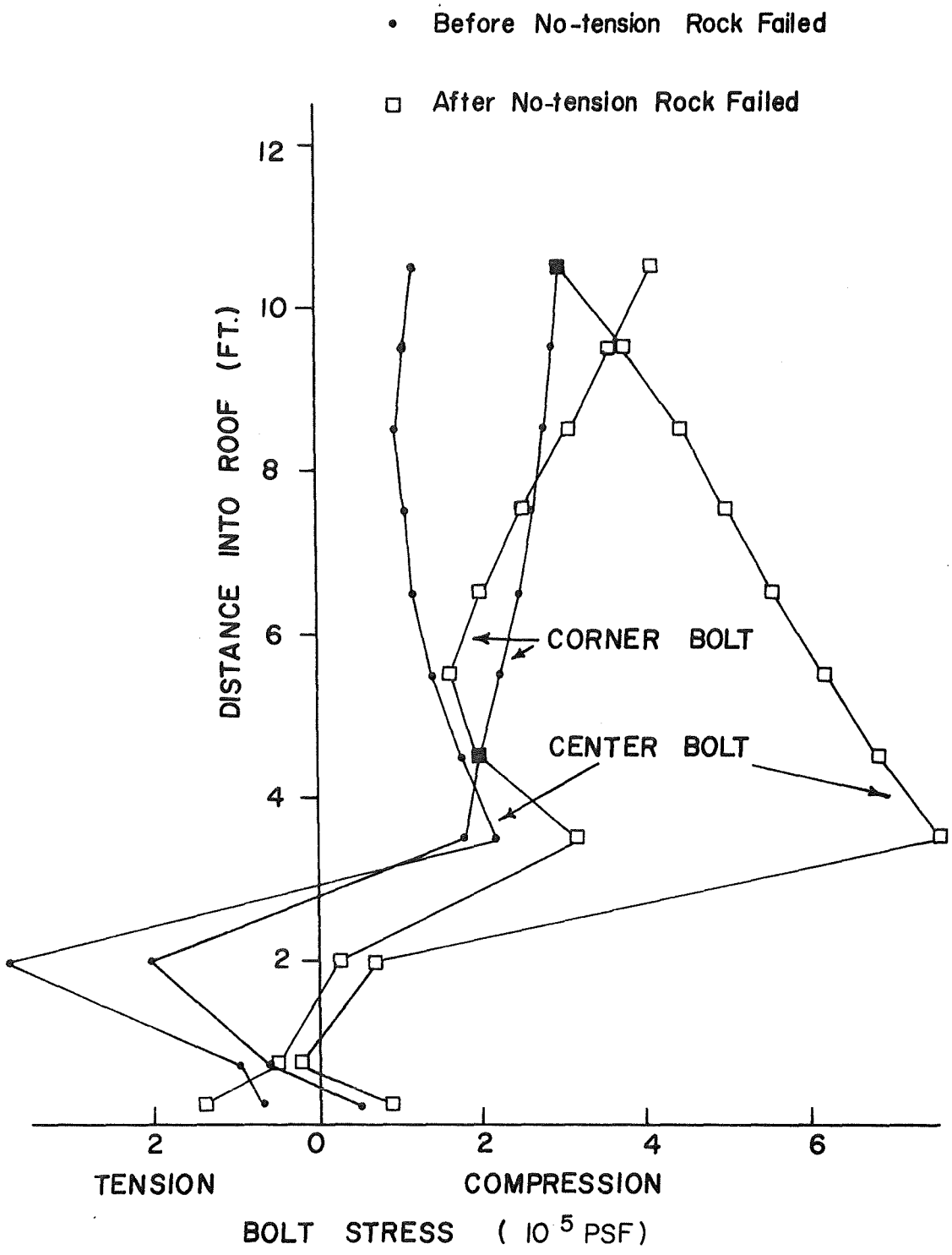

Fig. 6-19 Stresses Along the Length of Bolts (after Dave).

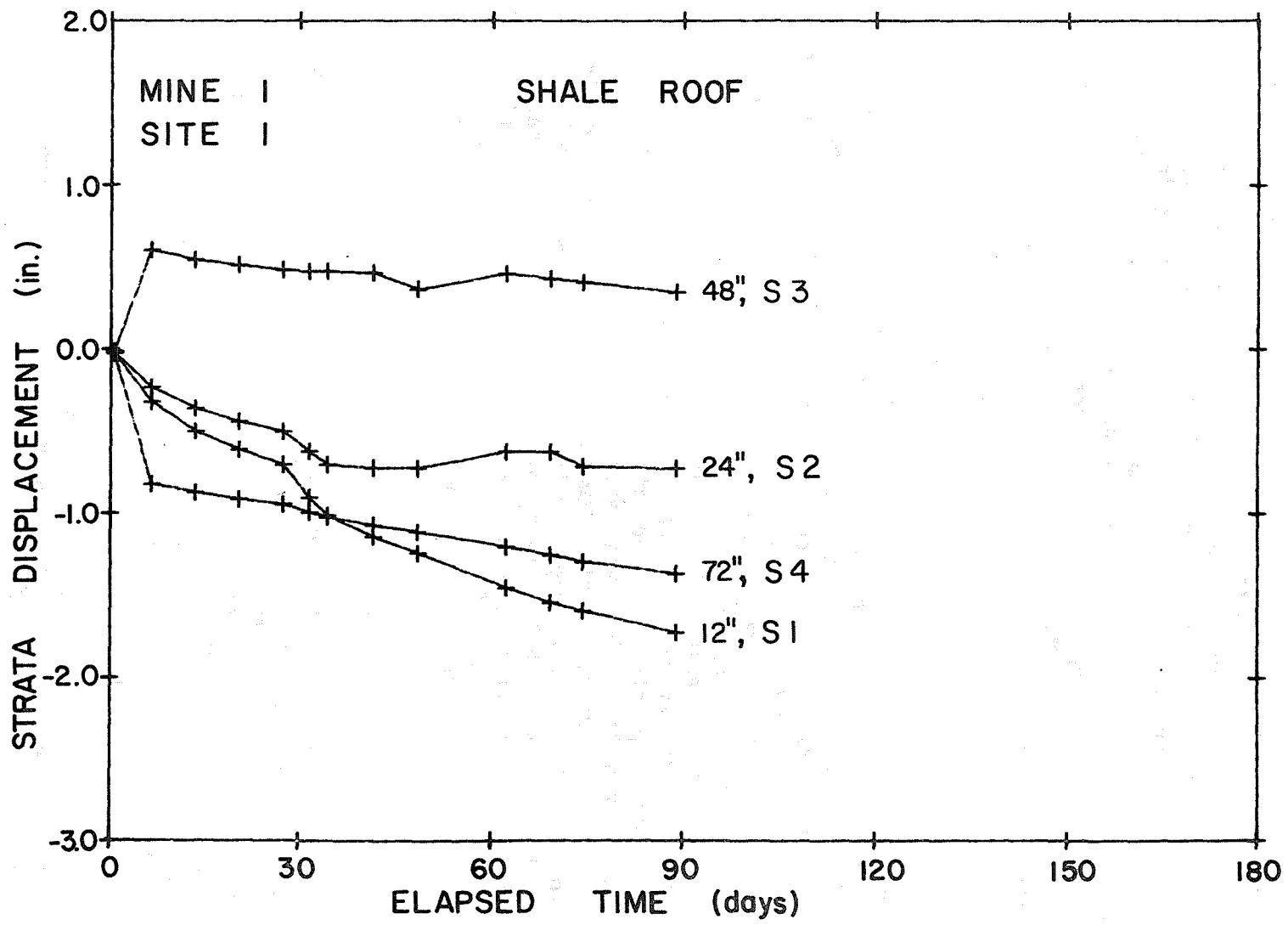

Fig. 6-20 Strata Displacement versus Elapsed Time at each of Four Horizons, Shale Roof.

The influence of the mining sequence on strata movements and bolt loads was observed in each mine (Figs. 6-13, 6-21, 6-22). Mine 1 will be used as an example because mining activity did not progress in the area immediately after instrumentation. The effects of mining should, therefore, be better separated from other strata movements. The area near Test Site 1 in Mine 1 was mined out 30 days subsequent to installation of the instrumentation (Fig. 6-15). Large increases in bolt strain (Fig. 6-13) and strata displacement (Fig. 6-20) were noted in the next set of readings. This is reasonable behavior since the shale roof of this site was supported by the adjacent unmined region at the time of instrumentation. Much of this support was then removed as nearby rooms were opened resulting in increased strata displacements and bolt loads.

C. Bolt Strain and Strata Displacement Relationships

The preceding discussion brought out the observations that either compressive or tensile loads may occur in grouted bolts and that the distribution of load is not constant the entire length of the bolt. Because of the mechanism of load transfer from the bolt to the surrounding rock, the only condition producing uniform bolt strain would be uniform loading of each incremental length of bolt. It is apparent that such loading conditions do not exist (Figs. 6-16 to 6-18). Therefore it is not possible to measure the strain at some point along a bolt and relate it to the average vertical strata strain between the adjacent sag-station anchor points. Note how this situation differs from the loading of a conventional bolt with anchorage at some horizon. Here, all vertical strata displacements between the head of the bolt and the anchor would produce some average strain in the strata which would be equal to the increase in bolt strain, assuming bolt strain and sag-station readings were taken at essentially the same location in plan view. The result of this difference in mode of load application is that the full-column grouted bolt is much more resistant to strata separation than is the conventional bolt.

D. Relationship of Bolt Load to Apparent Support Requirements

As noted previously, the loads in resin-grouted bolts immediately after installation were relatively small, being on the order of one ton. These loads remained small throughout the test period for all bolts in Site 2 of Mine 1 with limestone roof (Fig. 6-16b) and some of the bolts in Sites 1 and 2 in both Mine 2 and Mine 3, all with shale roof (Figs. 6-17 and 6-18). High bolt loads were not expected in the limestone roof at Site 2 of Mine 1 because of the apparent good condition of the roof in this intersection.

A borescope hole was drilled at midspan in each row of instrumented bolts in Mines 2 and 3. These holes were inspected a few hours after bolt installation and at the end of the test period. The logs given in Appendix B indicate that fracturing of the roof did occur up to a distance of 29 in. above the roof line in Site 2 of Mine 2 (Fig. B-2). The roof at this location appeared unstable as it bulged downward in the middle of the room due to undulations in the shale bedding. A horizontal crack intersected the bulge part of the way around. The workers were predicting that the room would fall within a few days or

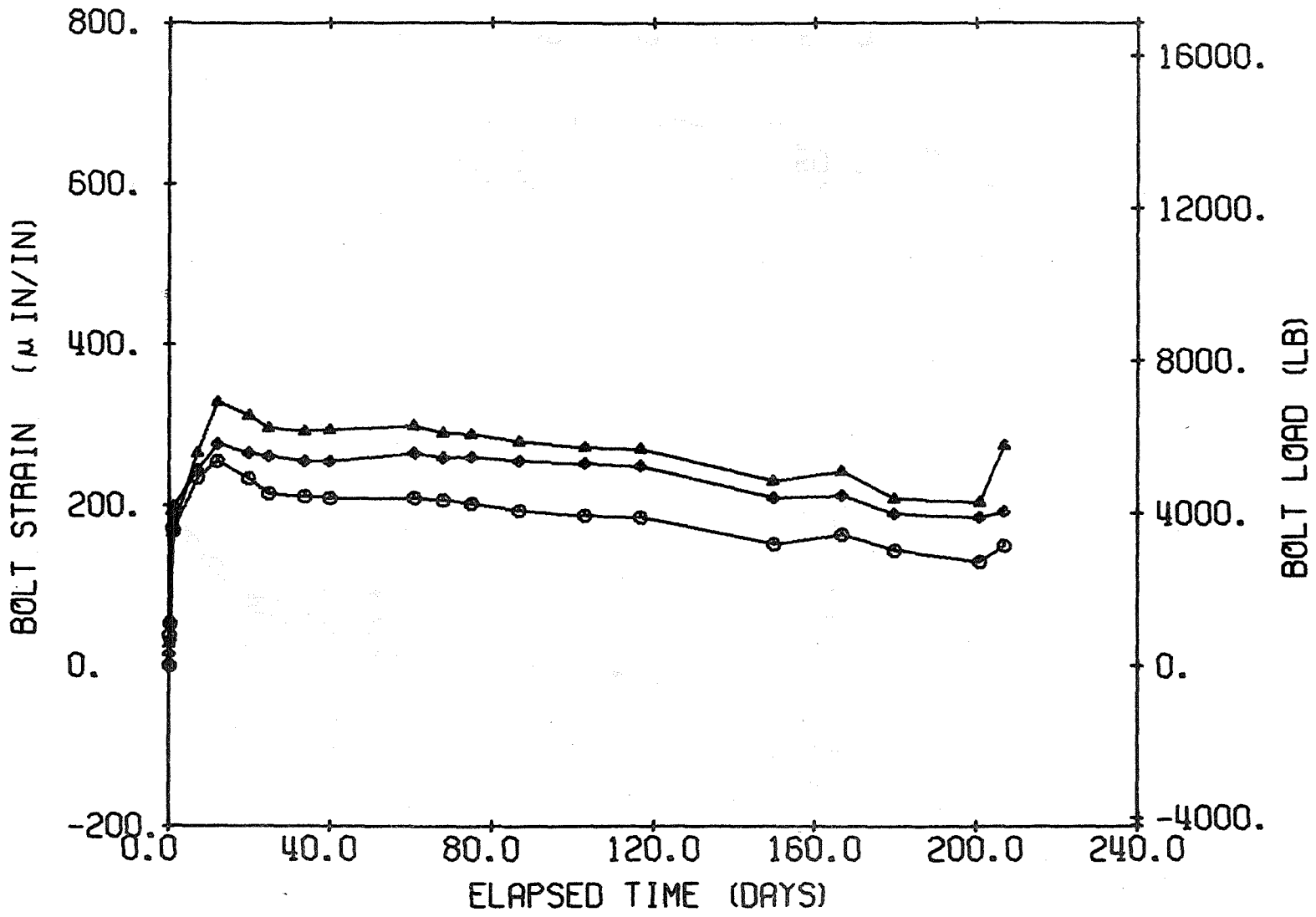

Fig. 6-21 BOLT NUMBER 12 IN MINE NO. 2.
1 IN. BAR IN 1-3/8 IN. HOLE DUPONT RESIN

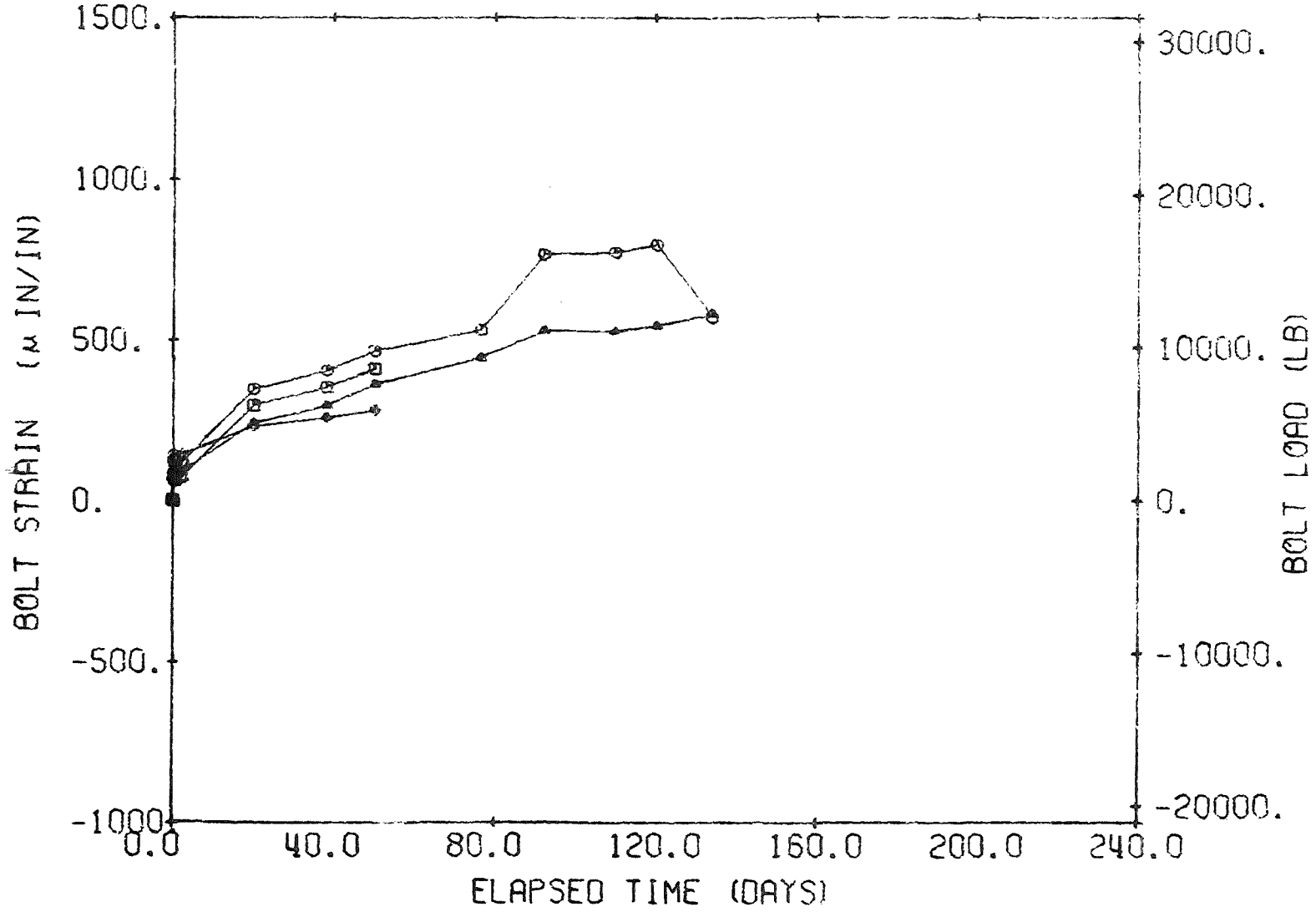

Fig. 6-22 BOLT NUMBER 28 IN MINE NO. 3.
1 IN. BAR IN 1-3/8 IN. HOLE, DUPONT RESIN

weeks. The instrumentation showed, however, that the room was relatively stable in that the bolt loads did increase (Fig. 6-17b) somewhat, but except for one point in Bolt No. 16, were well below the yield load of 50,500 lb. The roof sag relative to an anchor point 15 ft above the roof was less than 0.1 in. during the entire test (Figs. B-24 through B-27 in Appendix B). Visual inspection of the test site at the end of the test period, several months later also indicated little additional deterioration of the roof. The borescope readings taken at the end of the test period also indicated no additional fractures or strata separations. This particular site is an excellent example of a bad roof condition which was quite probably stabilized by the roof bolt system.

Even in this area though some of the bolts carried but little load, while a few of them experienced significant loading. This substantiates the requirement for a systematic bolting pattern since at present there is no way to selectively say which bolts will hold up the critical areas in the roof and which are just there but not contributing to the roof support.

Conclusions

This field study of the behavior of full-column resin-grouted bolts under geologic loadings produced the following findings.

1. The practice of installing instrumented rock bolts and sag stations to evaluate the effectiveness of a bolting pattern provides data useful in selecting adequate roof support measures.

2. Installation of bolts commonly produces an initial tensile bolt load on the order of one ton.

3. The load distribution along a grouted bolt is nonuniform due to the nonuniform nature of loading following installation and the load transfer mechanism present with full-column anchorage.

4. Compressive loads may occur in a bolt given certain strata displacement histories. These loads may tend to weaken the lower roof strata, possibly inducing roof failure.

5. Strains in fully-grouted bolts cannot be directly related to vertical strata displacements because of complex strain distributions along the bolts and uncertainty of the location of the points (or zones) of load application to the bolt.

Chapter VII

Roof Bolt Design Criteria

Introduction

The modern practice of rock bolting, first introduced in the early 1950's, is now a primary method of roof control in underground coal mines. A variety of bolt configurations has been developed, most of which provide adequate ground control if installed and maintained properly and if used only where favorable conditions exist. No one support system developed to date can be used successfully in all economic, geologic, and mining environments. On the other hand, each system will perform satisfactorily under certain circumstances.

The problem facing the mine engineer, and the thrust of this discussion, is the determination of the most effective roof support system for a given situation. Guidelines are given here to assist the mine engineer in selecting the type, length, orientation, and spacing of roof bolts to provide the safest, most cost-effective primary support system for his mine. Though by no means the final words in roof control design criteria, this discussion does present a critical assessment of the most definitive, current research in roof support theory and practice related to multiple openings in bedded deposits having horizontal or near-horizontal orientations. Among the sources of information used in this assessment are publications from industrial and governmental sources, field information from mine personnel, and the findings of four years of research under the current contract.

Current Theory and Practice

The engineering design of any structure is based on the geometric size and shape of the structure, the material properties, and the magnitudes and orientations of applied loads. The existing design criteria are not based on a direct knowledge of applied loads and rock failure mechanisms, as they should be, but instead are very broad guidelines based on industry-wide observations. They, therefore, tend to be quite conservative and often unnecessarily expensive due to overdesign. Design restrictions are provided (Ref. 16) for beambuilding and suspension, two commonly accepted modes of roof support. Since no indication of the applicability of these two modes is given, it is required that the mine engineer and MESA personnel determine which mode of support is to be used, often with little knowledge of actual roof failure mechanisms. Past practice and an examination of the character of the immediate roof may be the only input used in constructing a roof control plan.

Current design practice is as likely to produce an underdesigned, unsafe mine as an overdesigned, costly support system. Although neither of these alternatives is acceptable, it must be recognized that a certain degree of overdesign and underdesign will exist because of the wide variability of conditions in a mine. Current theories and practices will be assessed within the context of this variability.

A. Continuous Beam Theory

Some of the earliest rock bolt research was performed by Panek (Refs. 6, 17, 18). Using laboratory model studies, he was able to develop the concept of reinforcing factors for conventional bolts. The underlying assumptions of the model studies must be understood and, more important, must be satisfied in the prototype if this analysis is to be used with confidence in roof support selection.

1. The immediate roof consists of a sequence of continuous, homogeneous, elastic beds of any thickness, density, or modulus with no interbed bonding.

2. The roof plate is approximated as one or more beams clamped at both ends and supported on a rigid base. The term rigid is used here to denote a base (pillar) which allows much smaller deflections than occur in the roof rock. A pillar with a Young's modulus of 2 to 10 times that of the roof rock would qualify the base as rigid. These conditions are not commonly encountered in bituminous coal mines.

3. Bolts are installed vertically in straight rows and are tensioned so normal compressive loading occurs along all or part of the interfaces between beds.

4. Material properties of the bolts do not affect reinforcement; only bolt tension is important. Perfect anchorage is assumed (nuts and washers were used on both ends of the bolts in model tests).

5. The ratio of bolt diameter to hole diameter does not affect the degree of reinforcement.

6. All bolts terminate in the immediate roof. This simulates anchorage in the uppermost bed of the sequence being supported. Therefore, the studies are evaluating only how the immediate roof can be made to support itself rather than how it can be supported by some massive and more competent upper stratum.

7. Gravitational loading is assumed. Horizontal stresses of tectonic origin are neglected.

Two modes of support were analyzed. First, frictional support is that degree of reinforcement resulting from the increased frictional resistance between beds caused by the increased normal loads on the beds produced by the roof bolts. Panek used regression analysis of model study data to determine the relationship between bolting and strata parameters and the ratio of the decrease in maximum bending strain, $\Delta\varepsilon_f$, due to frictional effects and the maximum bending strain of the unbolted strata (Ref. 19).

$$\frac{\Delta\varepsilon_f}{\varepsilon_{nfs}} = -0.265(bL)^{-1/2}\left(NF_b\left(\frac{\frac{h}{t}-1}{\gamma}\right)\right)^{1/3}; \qquad (7\text{-}1)$$

where

b = spacing of rows of bolts,

L = roof span,

N = number of bolts per row,

F_b = bolt tension,

h = bolt length,

t = lamina thickness, and

γ = unit weight of lamina

Units must be chosen so the right hand side of the equation is unitless. For a sequence of beds of variable thickness and unit weight, average values of these properties may be used. The reinforcement factor, RF, may now be defined as

$$RF = \frac{1}{1 + \frac{\Delta\varepsilon_f}{\varepsilon_{nfs}}} \tag{7-2}$$

or

$$RF = \frac{\varepsilon_{nfs}}{\varepsilon_f} \tag{7-3}$$

where

ε_{nfs} = maximum bending strain with no friction or suspension,

$\varepsilon_f = \varepsilon_{nfs} + \Delta\varepsilon_f$ = maximum bending strain in the bolted model (friction effect only), and

$\Delta\varepsilon_f$ = the change in bending strain due to the frictional effect of bolting.

Combining Eqs. (7-1) and (7-2) provides a design equation which is represented by the nomograph in Fig. 7-1, in which γ has the value of 0.09 lb/in.^{3}.

A certain degree of support by suspension results if all beds of the bolted sequence are not of equal flexural rigidity, i.e., if either or both the thickness or Young's modulus varies between beds. Suspension here applies to the support of more flexible strata by stiffer strata, all of which are contained in the bolted sequence. Panek found that the effects of suspension had a multiplicative, though small, effect on reinforcement.

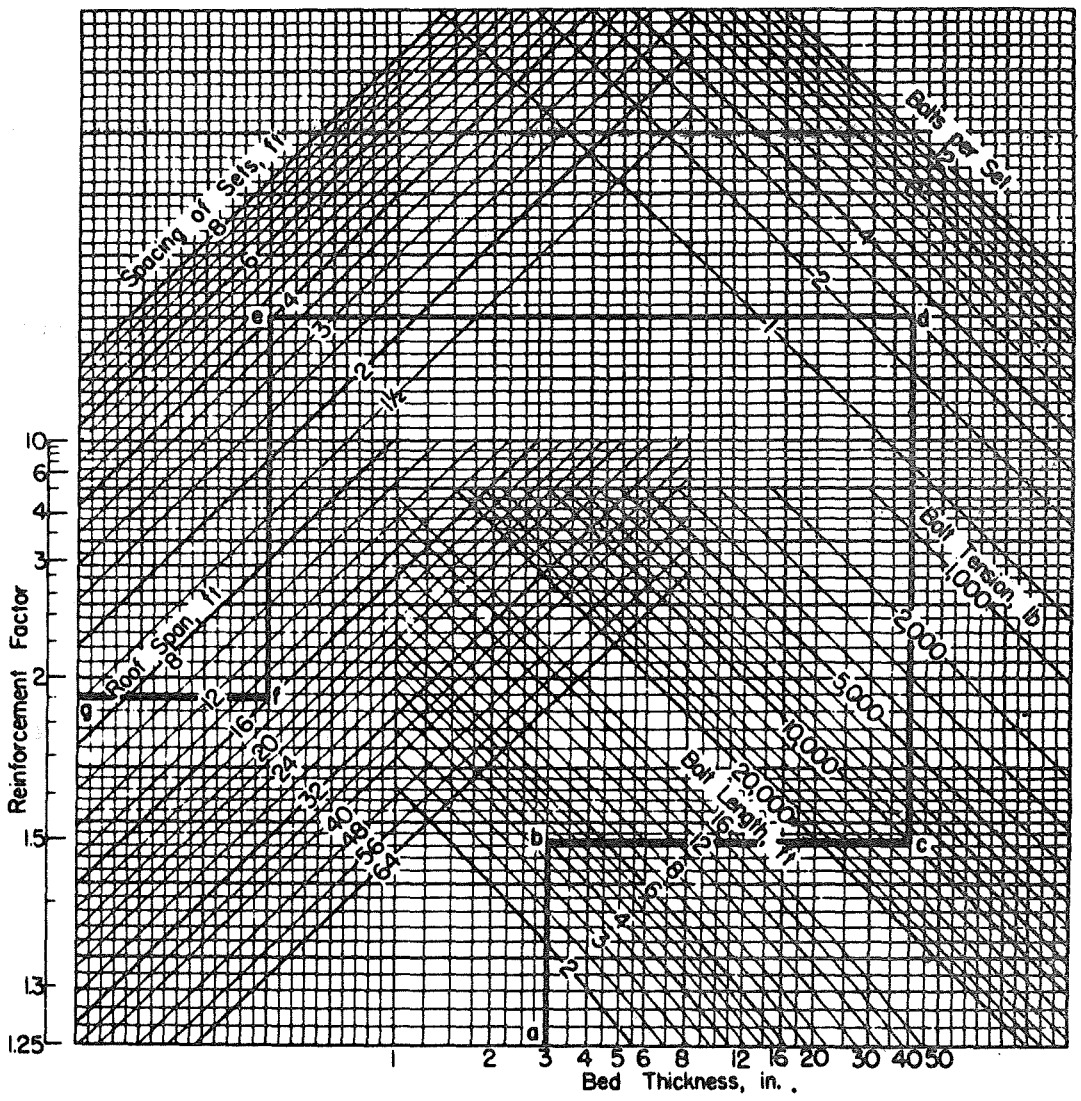

Fig. 7-1 Roof-bolting Design Chart for Friction Effect, (after Panek).

The maximum bending stress with bolts installed in a sequence of beds providing reinforcement by friction and suspension; σ_{fs}, was found to be given by

$$\sigma_{fs} = \sigma_{nfs} \left(1 + \frac{\Delta\sigma_f}{\sigma_{nfs}}\right)\left(1 + \frac{\Delta\sigma_s}{\sigma_{nfs}}\right); \qquad (7\text{-}4)$$

where

σ_{nfs} = maximum bending stress with no friction or suspension effects,

$\Delta\sigma_f = \sigma_f - \sigma_{nfs}$ = change in maximum bending stress due to frictional effects.

$\Delta\sigma_s = \sigma_s - \sigma_{nfs}$ = change in maximum bending stress due to suspension effects.

The value of $\frac{\Delta\sigma_f}{\sigma_{nfs}}$ in Eq. (7-4) is given by

$$\frac{\Delta\sigma_f}{\sigma_{nfs}} = -0.265(bL)^{-1/2} \left(NF_b\left(\frac{\frac{h}{t_{ave}} - 1}{\gamma_{ave}}\right)\right)^{1/3} \qquad (7\text{-}5)$$

The suspension effect was found to be a function of the flexural rigidity of the strata with the ratio $\frac{\Delta\sigma_s}{\sigma_{nfs}}$ given by the equation

$$\frac{\Delta\sigma_s}{\sigma_{nfs}} = \alpha C u_i \qquad (7\text{-}6)$$

where

α = a constant depending on the bolt spacing (Table 7-1a),

C = a constant depending on the number of laminae in a bolted unit (Table 7-1b), and

$$u_i = -1 + \frac{(\gamma_1 t_1/\gamma_i t_i) + (\gamma_2 t_2/\gamma_i t_i) + \ldots + (\gamma_j t_j/\gamma_i t_i)}{(E_1 t_1^3/E_i t_i) + (E_2 t_2^3/E_i t_i) + \ldots + (E_j t_j^3/E_i t_i)} \qquad (7\text{-}7)$$

or for rock strata having equal E_i and γ_i values

$$u_i = \left(t_i^2 \frac{\Sigma t_j}{\Sigma t_j^3}\right) - 1; \qquad (7\text{-}8)$$

Table 7-1a Values of Coefficient, α, for Various Numbers of Bolts per Set.

Bolts per Set	1	2	3	4	5	6	7
α	0.750	0.889	0.938	0.960	0.972	0.980	0.984

Table 7-1b Values of Coefficient, C, for Various Numbers of Strata in a Bolted Sequence

Number of Strata	3	4	5	6	8	10	12
C	0.953	0.900	0.865	0.838	0.800	0.772	0.751

The reinforcement factor in terms of stresses when both friction and suspension effects are included is given by

$$RF = \frac{1}{1 + \frac{\Delta\sigma_{fs}}{\sigma_{nfs}}} \quad \text{where } \Delta\sigma_{fs} = \sigma_{fs} - \sigma_{nfs}. \tag{7-9}$$

Several interesting observations were reported in Panek's work. First, it was found that vertical bolts in a single-member roof unit had no reinforcement effect since no bedding-plane slip was present to be countered. Second, Panek found that untensioned bolts did not contribute to the reinforcement of a bedded sequence. Untensioned bolts were used which fit the hole to close tolerance and also which were actually threaded through the sequence. In both cases washers and nuts were placed on each end of the bolts but were not tightened. Neither case substantially decreased the outer fiber bending strain of the beds. This is in agreement with the empirical equation (7-1). However, the drill steel bolts used in Hydrostone strata may not accurately model mild steel bolts, perhaps surrounded by low modulus resin grout, employed in coal mine roof control.

Panek is careful to point out that bolted multimember beams seldom behave like a single-member beam having the same total thickness as the multimember sequence (Ref. 17). The model studies showed that some of the very short multimember spans acted like single-member beams to the point where the shearing forces overcame the frictional strength along the bedding planes after which they, too, responded like a sequence of independent beams. Further, the bolted unit did not exhibit a single neutral axis but had bending strains opposite in sign on the upper and lower surfaces of each layer. In models loaded to failure, each beam cracked at the ribs and at midspan, verifying the locations of maximum bending stresses in each beam of the sequence. Substantial decreases in bending stresses indicate the useful action of bolts in supporting the immediate roof.

Experiments with photoelastic materials subjected to uniform distributed loads were conducted by Tsur-Lavie and Van Ham (Ref. 20) to determine the reinforcing effects of oblique bolts on roof strata. Test geometry differed from that described above in that stresses and Young's moduli were scaled since one g gravitational loads were employed rather than centrifugal loads. Oblique bolting was found to give larger reinforcing factors than did vertical bolting. This result is misleading, however, since the upper anchor point was commonly located in the clamped abutment of the model where displacements would be essentially zero. Thus, both upper and lower anchor points were not located in the supported sequence, as they were in Panek's studies. Similar oblique-bolting experiments produced the result that oblique bolts were more effective in supporting a sequence with one or more layers of soft material. It is apparent that a soft, mud-like layer would not possess any significant frictional resistance with or without either vertical or oblique bolts. Here again, the oblique bolts were effective due to the location of the upper anchor point. The primary contribution to roof stability

is probably due to the suspension effect of the bolted strata from the stable abutments. It should also be noted that oblique bolts may adversely effect roof stability if the beams are jointed rather than continuous since the horizontal components of bolt tension may tend to open up vertical cracks in the roof.

B. Cracked Beam Studies

Recent research by Wright (Ref. 21) considers the design of support for bedded roof strata intersected by one or more vertical joints. This is a valuable extension of the continuous beam studies since mine roof rock is commonly jointed and fractured. Earlier observations (Refs. 22, 23, 24, 25, 26) indicated that a cracked beam may support itself, provided lateral pressure is exerted on the beam. Also noted was that relatively little upward force was required to maintain the integrity of the cracked beam.

Three possible modes of failure were recognized. First, a cracked beam may fail by sliding downward along two joints leading to collapse of the roof. Second, crushing of rock at points of high horizontal compressive stress may permit rotation of roof blocks. Third, thin beams may buckle under combined vertical and horizontal loads.

Finite element modeling with rigid abutments and common material properties was used to validate the results of physical modeling for prototype structures. Open joints were defined as elements having a very low Young's modulus, commonly 1 psi in the single beam models. Closed joints had a modulus value similar to that of the rest of the model, typically 10^6 psi. Multiple beam models employed slip elements between beds to eliminate the large displacements associated with compressing a layer of material having a very low elastic modulus. The center of the mine opening was taken as a vertical plane of symmetry. The beams were gravity loaded and an initial horizontal force was applied to simulate an in-situ horizontal stress field.

Physical modeling using limestone blocks and bricks was employed to more economically evaluate the general response of various beam geometries to vertical and horizontal loads. Several assumptions are implicit in the test results obtained using physical models.

1. The immediate roof consists of one or more layers of jointed rock with no interbed bonding.

2. The roof plate is approximated by one or more beams supported only by horizontal thrust forces (flat arch action). No clamping or pillar support is present. A vertical joint exists at each abutment.

3. Bolts are installed vertically in straight rows and are tensioned to some scaled value (typically 208 lb, 156 lb, or 104 lb). No bolts are used in the single layer model.

4. Perfect bolt anchorage is assumed and bolt tension is scaled (nuts and washers were used on both ends of the bolts).

5. The ratio of bolt diameter to hole diameter is such that the direct shear resistance component of the bolt is present only at very large strata displacements.

6. All bolts terminate in the immediate roof.

7. Bolts are installed so as to bind blocks together in the vertical plane only. That is, vertical joints are continuous from top to bottom of the bolted sequence and are not intersected by bolts.

8. Both gravity load and a partial uniformly distributed load are applied.

Several observations were made from model study data. Buckling was the common mode of failure when the predicted deflection of the beam, based on material properties and beam dimensions, exceeded 14 to 15 percent of the beam thickness. Although design equations were not developed to predict the load carried by roof bolts supporting multilayered roofs, a valuable observation was made. It was found that if a support is installed at the centerline of a single cracked beam after small deflection of the beam has occurred (say one percent of the beam thickness), the support will carry one half of any additional applied load with the other half going to the abutments. At much larger initial deflections, more load is transferred to the abutments. This describes the action of flat arches under load. Some crossover initial deflection probably exists which determines which mode of support loading will occur but this has not been investigated to date.

Wright (Ref. 21) proceeds to develop a set of design equations for a single cracked beam from his finite element results. These equations then form the basis for the more complicated analysis of multiple cracked beams.

The design equations for a single cracked beam which follow are based on the geometry shown in Fig. 7-2. The sketch is a free body diagram of the left half of a beam containing three vertical cracks, one at each abutment and one at midspan. The various quantities are defined as follows:

A = length of moment arm of couple produced by T

L = span of opening

Q = total uniformly distributed transverse load per unit width of beam

T = horizontal thrust per unit width of beam

$V = \frac{Q}{2}$ = vertical shear force at abutment

a = distance between point of application of resultant thrust T and bottom of beam at abutment

c = distance between point of application of resultant thrust T and top of beam at midspan

d = vertical deflection at midspan

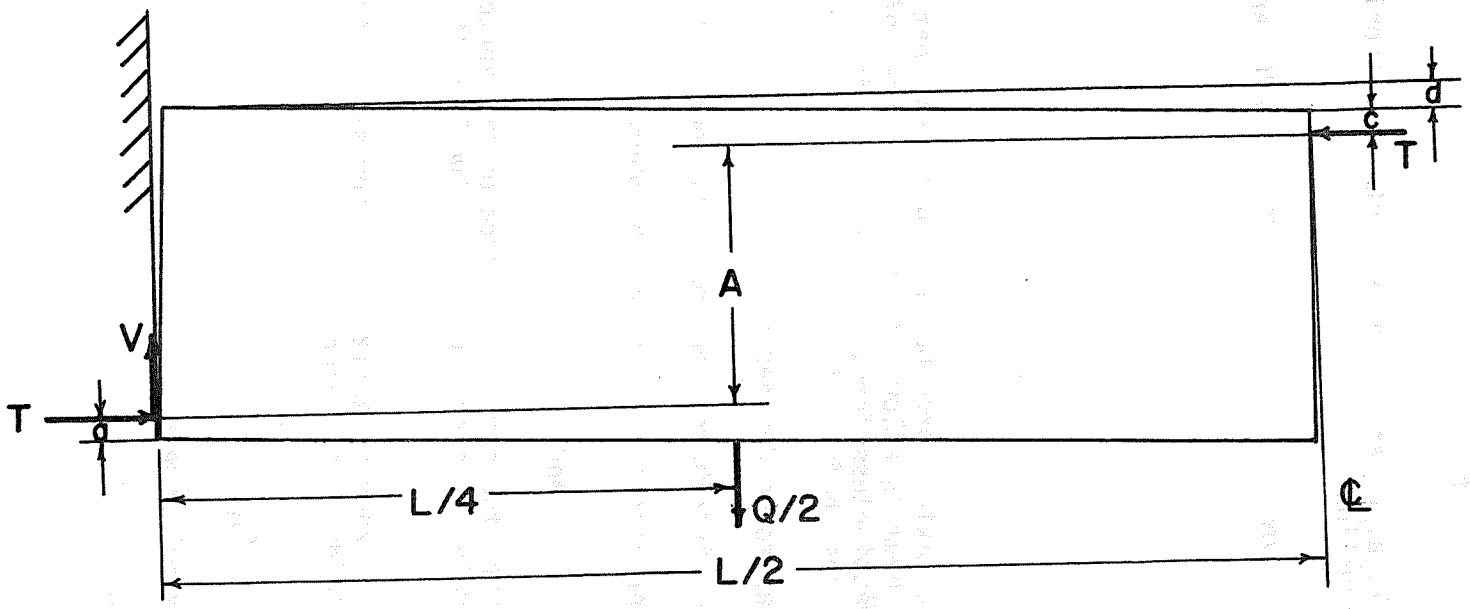

Fig. 7-2 Diagram of the Forces Acting on the Left Half of a Cracked Beam, (after Wright)

Equilibrium considerations for the beam in some displaced position (Fig. 7-2) require that

$$A = \frac{QL}{8T} \tag{7-10}$$

The quantities A, L, Q, T, a, c, and d are put into dimensionless form by the following transformations

$$\overline{A} = A/D;\ \overline{L} = L/D;\ \overline{Q} = Q/DE;\ \overline{T} = T/DE;\ \overline{a} = a/D;\ \overline{c} = c/D;\ \text{and}$$
$$\overline{d} = d/D \tag{7-11}$$

where

D = depth of beam

E = Young's modulus

An initial horizontal axial force per unit width of beam is assumed to be present before the beam is allowed to deflect. This initial force is denoted by P. In dimensionless form, $\overline{P} = P/DE$. This force simulates the horizontal in-situ stress before mining.

Additional quantities to be defined are

q = Q/L = transverse distributed load per unit length of the beam

p = P/D = initial horizontal pressure on the abutments

In dimensionless form, $\overline{p} = p/E$ and $\overline{q} = q/E$.

It should be noted that the horizontal force on the abutments will change from its initial value P to some greater value T as the transverse load Q is increased.

The assumption of a triangular horizontal compressive stress distribution on the abutments leads to the equation

$$\sigma_{max} = \frac{2T}{3a} \tag{7-12}$$

where σ_{max} = maximum flexural stress.

In dimensionless form

$$\overline{\sigma}_{max} = \sigma_{max}/E = \frac{2\overline{T}}{3\overline{a}} \tag{7-13}$$

The design equations based on the finite element analysis of the section of the beam shown in Fig. 7-2 are written so that the vertical loading pressure q and the initial horizontal pressure p are input as

known quantities. The modulus E is also presumed to be known so that $\bar{q}$ and $\bar{p}$ can be determined. The thickness of the cracked beam D is considered to be known and a span L is assumed. Thus $\bar{P}$ and $\bar{Q}$ can be calculated from equations stated above.

The moment arm $\bar{A}$ is first approximated by an equation developed from the finite element method for cracked beams at very low values of transverse load $\bar{Q}$ (hence negligible deflection). This value, denoted by $\bar{A}_o$, is given by

$$\bar{A}_o = \frac{.44\bar{L} + 2.4}{.44\bar{L} + 3.4} \tag{7-14}$$

Curve fitting of the finite element data resulted in the following equations for thrust $\bar{T}$ and deflection $\bar{d}$:

1. For low values of deflection ($\bar{d} < .002$)

$$\bar{T}_o = \frac{1}{4}\frac{\bar{P}}{\bar{A}_o} + \left(\bar{P}^2 \left(1 - \frac{1}{4\bar{A}_o}\right)^2 + \frac{\bar{L}^2}{64\bar{A}_o^2}\left(\bar{Q} - \frac{2\bar{P}}{\bar{L}}\right)^2\right)^{1/2} \tag{7-15}$$

$$\bar{d}_o = \frac{\bar{P}\bar{L}^2}{16} + 1.2\,\bar{A}_o\bar{L}^{1.78}\left((\bar{T} - \bar{P} + b_o)^2 - b_o^2\right)^{1/2} \tag{7-16}$$

where

$$b_o = \frac{0.115\,\bar{P}\,\bar{L}^{0.22}}{\bar{A}_o}$$

2. For high values of deflections ($\bar{d} > .002$). Values of $\bar{T}_o$ and $\bar{d}_o$ are calculated as above. Then a new value of A_i is determined by subtracting the deflection $\bar{d}_o$ from $\bar{A}_o$, and $\bar{A}_i$ is then used to calculate a new value of $\bar{T}$. Thus

$$\bar{A}_i = \bar{A}_o - \bar{d}_o \tag{7-17}$$

$$\bar{T}_i = \frac{1}{4}\frac{\bar{P}}{\bar{A}_i} + \left(\bar{P}^2 \left(1 - \frac{1}{4\bar{A}_i}\right)^2 + \frac{\bar{L}^2}{64\bar{A}_i^2}\left(\bar{Q} - \frac{2\bar{P}}{\bar{L}}\right)^2\right)^{1/2} \tag{7-18}$$

$$\bar{d}_i = \frac{\bar{P}\,\bar{L}^2}{16} + 1.2\,\bar{A}_o\bar{L}^{1.78}\left((\bar{T}_i - \bar{P} + b_o)^2 - b_o^2\right)^{1/2} \qquad (7\text{-}19)$$

$$\bar{A}_{i+1} = \bar{A}_o - \bar{d}_i \qquad (7\text{-}20)$$

The iteration process is thus continued until the values of $\bar{T}$ and $\bar{d}$ converge to the desired accuracy.

After the final value of $\bar{T}$ has been determined, a more accurate value of $\bar{A}$ is determined from the equation

$$\bar{A} = \frac{\bar{L}\,\bar{Q}}{8\bar{T}} \qquad (7\text{-}21)$$

The value of $\bar{a}$ is then determined from the equation

$$\bar{a} = 0.294 - 0.294\bar{A} \qquad (7\text{-}22)$$

With the values of $\bar{T}$ and $\bar{a}$ now determined, the maximum stress $\bar{\sigma}_{max}$ may be determined from the equation

$$\bar{\sigma}_{max} = \frac{2}{3}\frac{\bar{T}}{\bar{a}} \qquad (7\text{-}23)$$

The resulting factor of safety would then be

$$SF = \frac{\text{compressive strength of rock}}{\sigma_{max}} \qquad (7\text{-}24)$$

where

$$\sigma_{max} = E\,\bar{\sigma}_{max}$$

Often in design practice, one would like to know what is the maximum span for a given roof situation which can be tolerated without exceeding some predetermined factor of safety. This critical span could be determined by several applications of the preceding design equations using different values for the span. Wright (Ref. 21) has already done this and has presented the results in the form of design tables for different values of allowable working stresses

$\bar{\sigma} = 500 \times 10^{-6}$, 1000×10^{-6}, 2000×10^{-6}, 3000×10^{-6}, and 4000×10^{-6}

as given in Table 7-2. The values of $\bar{p}$ and $\bar{q}$ are again presumed to be known so that the applicable values can be selected in Table 7-2. The maximum allowable span $\bar{L}$, and the corresponding thrust $\bar{T}$ and deflection $\bar{d}$ may then be read directly from the design table.

Table - 7-2a. Design Table for Single Beam with Cracks
$\bar{\sigma} = 500 \times 10^{-6}$

$\bar{q}$ ($\times 10^{-6}$) / $\bar{p}$ ($\times 10^{-6}$)	0.25	0.5	1.0	2.0	5.0	10.0	20.0
0.00	$\bar{L}$ = 22.7 $\bar{T}$ = 17.50* $\bar{d}$ = .0050 α_1 = 64.2 α_2 = 72.6 Crushing	17.3 20.66 .0036 66.8 75.3 Crushing	13.2 24.50 .0026 70.1 78.5 Crushing	10.0 28.74 .0018 74.20 82.6 Crushing	6.8 34.30 .0011 81.4 89.80 Crushing	5.1 39.55 .0007 87.8 90^0	3.7 42.74 .0004 90^0 90^0
50.0	$\bar{L}$ = 38.2 $\bar{T}$ = 64.54 d = .0229 α_1 = 59.24 α_2 = 67.7 Crushing	27.1 64.92 .0121 61.0 69.4 Crushing	19.2 65.50 .0064 63.35 71.8 Crushing	13.6 66.29 .0034 66.6 75.0 Crushing	8.7 68.34 .0016 72.7 81.1 Crushing	6.2 70.06 .0009 78.9 87.30 Crushing	4.4 71.53 .0005 86.6 90^0
100.0	$\bar{L}$ = 42.0 $\bar{T}$ = 106.94 $\bar{d}$ = .0294 α_1 = 57.8 α_2 = 66.2 Crushing	29.7 106.95 .0150 59.0 67.4 Crushing	21.0 107.14 .0077 60.6 69.0 Crushing	14.8 107.30 .0040 62.9 71.3 Crushing	9.4 108.11 .0017 67.3 75.7 Crushing	6.6 108.25 .0009 72.0 80.4 Crushing	4.7 109.25 .0005 78.3 86.7 Crushing
150.0	$\bar{L}$ = 39.1 $\bar{T}$ = 150.55 $\bar{d}$ = .0196 α_1 = 56.9 α_2 = 65.3 Crushing	27.6 150.54 .0098 57.6 66.1 Crushing	19.5 150.55 .0049 58.71 67.1 Crushing	13.8 150.59 .0025 60.2 68.7 Crushing	8.7 150.61 .0010 63.2 71.7 Crushing	6.2 150.75 .0005 66.6 75.1 Crushing	4.4 150.86 .0003 71.3 79.7 Crushing

Table - 7-2b. Design Table for Single Beam with Cracks

$\overline{\sigma} = 1000 \times 10^{-6}$

$\overline{p}$ ($\times 10^{-6}$) \ $\overline{q}$ ($\times 10^{-6}$)	0.25	0.5	1.0	2.0	5.0	10.0	20.0
0.0	$\overline{L}$ = 31.4	23.3	17.6	13.3	9.1	6.8	5.1
	$\overline{T}$ = 33.33	37.06	42.90	49.88	60.06	68.69	79.16
	$\overline{d}$ = .0174	.0112	.0077	.0053	.0032	.0021	.0014
	α_1 = 61.7	63.9	66.6	69.9	75.8	81.3	87.8
	α_2 = 70.2 Crushing	72.4 Crushing	75.0 Crushing	78.4 Crushing	84.2 Crushing	89.8 Crushing	90
50.0	$\overline{L}$ = 47.4	33.2	23.5	16.7	10.8	7.8	5.6
	$\overline{T}$ = 87.71	85.26	85.58	87.12	92.15	97.28	102.00
	$\overline{d}$ = .0621	.0304	.0160	.0086	.0042	.0024	.0014
	α_1 = 58.9	60.6	62.8	65.9	71.3	76.9	83.8
	α_2 = 67.3	69.0	71.3	74.3	79.8	85.3	90^o
	Crushing	Crushing	Crushing	Crushing	Crushing	Crushing	
100.0	$\overline{L}$ = 54.9	38.4	27.1	19.2	12.1	8.7	6.2
	$\overline{T}$ = 136.27	131.46	130.65	131.44	132.51	136.82	140.20
	$\overline{d}$ = .1031	.0483	.0245	.0129	.0054	.0031	.0017
	α_1 = 57.9	59.2	60.9	63.3	67.9	72.6	78.9
	α_2 = 66.3 Crushing	67.6 Crushing	69.4 Crushing	71.7 Crushing	76.3 Crushing	81.1 Crushing	87.3 Crushing
150.0	$\overline{L}$ = 58.3	41.1	29.0	20.5	13.0	9.2	6.5
	$\overline{T}$ = 177.85	174.1	173.04	173.23	174.76	176.22	177.71
	$\overline{d}$ = .1231	.0590	.0296	.0152	.0065	.0034	.0018
	α_1 = 57.3	58.4	59.8	61.8	65.5	69.9	75.1
	α_2 = 65.8	66.8	68.2	70.2	74.0	78.1	83.5
	Crushing	Crushing	Crushing	Crushing	Crushing	Crushing	Crushing

Table - 7-2b. (continued)

$\bar{p}$ (x 10^{-6}) \ $\bar{q}$ (x 10^{-6})	0.25	0.5	1.0	2.0	5.0	10.0	20.0
200.0	$\bar{L}$ = 59.4	42.5	29.7	21.0	13.3	9.4	6.6
	$\bar{T}$ = 217.16	214.99	214.44	214.56	215.46	216.29	216.54
	$\bar{d}$ = .1240	.0604	.0305	.0156	.0066	.0034	.0017
	α_1 = 57.0	57.8	59.0	60.6	63.8	67.3	72.0
	α_2 = 65.4	66.2	67.4	69.0	72.2	75.7	80.4
	Crushing	Crushing	Crushing	Crushing	Crushing	Crushing	Crushing
250.0	$\bar{L}$ = 58.5	41.4	29.3	20.7	13.1	9.3	6.5
	$\bar{T}$ = 257.43	256.68	256.54	256.58	256.99	257.69	257.38
	$\bar{d}$ = .1081	.0535	.0271	.0138	.0057	.0030	.0015
	α_1 = 56.6	57.3	58.3	59.6	62.3	65.2	69.2
	α_2 = 65.1	65.7	66.7	68.0	70.7	73.7	77.6
	Crushing	Crushing	Crushing	Crushing	Crushing	Crushing	Crushing
300.0	$\bar{L}$ = 55.3	39.1	27.6	19.5	12.4	8.7	6.2
	$\bar{T}$ = 301.25	301.16	301.11	301.12	301.32	301.22	301.51
	$\bar{d}$ = .0789	.0394	.0197	.0099	.0041	.0020	.0011
	α_1 = 56.3	56.9	57.6	58.7	60.9	63.2	66.6
	α_2 = 64.7	65.3	66.1	67.1	69.3	71.7	75.1
	Crushing	Crushing	Crushing	Crushing	Crushing	Crushing	Crushing

Table - 7-2c. Design Table for Single Beam with Cracks.
$\bar{\sigma} = 2000 \times 10^{-6}$

$\bar{p}$ ($\times 10^{-6}$) \ $\bar{q}$ ($\times 10^{-6}$)	0.25	0.5	1.0	2.0	5.0	10.0	20.0
0.0	$\bar{L}$ = 53.3	44.3	25.2	18.2	12.4	9.2	6.9
	$\bar{T}$ = 109.14	151.83	88.18	92.57	109.61	123.15	141.67
	$\bar{d}$ = .1494	.1485	.0308	.0177	.0103	.0066	.0045
	α_1 = 58.5	59.20	63.1	66.1	70.8	75.5	81.0
	α_2 = 66.9	67.6	71.6	74.6	79.2	83.9	89.4
	Mode=Buckling	Buckling	Crushing	Crushing	Crushing	Crushing	Crushing/Sliding
50.0	$\bar{L}$ = 56.6	46.4	29.7	20.9	13.5	9.9	7.2
	$\bar{T}$ = 128.32	170.16	129.17	127.58	134.62	146.64	158.02
	$\bar{d}$ = .1499	.1487	.0457	.0234	.0111	.0069	.0042
	α_1 = 58.2	58.9	61.6	64.3	69.1	73.7	79.5
	α_2 = 66.6	67.3	70.0	72.7	77.5	82.1	87.9
	Mode=Buckling	Buckling	Crushing	Crushing	Crushing	Crushing	Crushing
100.0	$\bar{L}$ = 58.9	48.1	34.1	23.8	15.1	10.8	7.8
	$\bar{T}$ = 154.14	193.91	183.80	177.07	179.10	184.97	194.99
	$\bar{d}$ = .1497	.1493	.0722	.0346	.0149	.0084	.0049
	α_1 = 57.7	58.6	60.3	62.7	66.9	71.3	76.8
	α_2 = 66.2	67.0	68.7	71.1	75.3	79.7	85.2
	Mode=Buckling	Buckling	Crushing	Crushing	Crushing	Crushing	Crushing
150.0	$\bar{L}$ = 60.5	49.4	37.1	25.8	16.3	11.6	8.3
	$\bar{T}$ = 186.24	222.02	233.99	223.02	222.87	227.10	234.27
	$\bar{d}$ = .1499	.1496	.0961	.0442	.0185	.0100	.0056
	α_1 = 57.3	58.2	59.5	61.6	65.4	69.3	74.5
	α_2 = 65.8	66.6	68.0	70.0	73.8	77.8	82.9
	Mode=Buckling	Buckling	Crushing	Crushing	Crushing	Crushing	Crushing

Table - 7-2c. (continued)

$\bar{P}$ ($\times 10^{-6}$) \ $\bar{q}$ ($\times 10^{-6}$)	0.25	0.5	1.0	2.0	5.0	10.0	20.0
200.0	$\bar{L}$ = 61.6	50.3	39.0	27.3	17.2	12.2	8.7
	$\bar{T}$ = 223.36	253.55	277.7	267.36	265.49	268.35	274.15
	$\bar{d}$ = .1496	.1481	.1123	.0524	.0214	.0114	.0062
	α_1 = 57.0	57.9	59.0	60.8	64.2	67.8	72.6
	α_2 = 65.4	66.3	67.5	69.3	72.6	76.2	81.0
	Mode=Buckling	Buckling	Crushing	Crushing	Crushing	Crushing	Crushing
250.0	$\bar{L}$ = 62.4	51.1	40.4	28.3	17.9	12.7	9.0
	$\bar{T}$ = 264.44	289.76	319.71	308.89	307.78	310.35	313.78
	$\bar{d}$ = .1489	.1486	.1246	.0578	.0238	.0126	.0067
	α_1 = 56.7	57.5	58.6	60.2	63.3	66.6	71.0
	α_2 = 65.1	66.0	67.1	68.7	71.7	75.0	79.4
	Mode=Buckling	Buckling	Crushing	Crushing	Crushing	Crushing	Crushing
300.0	$\bar{L}$ = 63.2	51.8	41.3	29.1	18.4	13.0	9.2
	$\bar{T}$ = 308.72	329.32	359.17	350.77	349.31	350.33	352.90
	$\bar{d}$ = .50	.150	.1309	.0622	.0254	.0131	.0069
	α_1 = 56.5	57.3	58.3	59.8	62.5	65.5	69.6
	α_2 = 64.9	65.7	66.7	68.2	70.9	73.9	78.0
	Mode=Buckling	Buckling	Crushing	Crushing	Crushing	Crushing	Crushing
350.00	$\bar{L}$ = 63.8	52.3	41.8	29.5	18.7	13.2	9.3
	$\bar{T}$ = 354.79	370.86	397.42	390.78	390.11	390.68	391.66
	$\bar{d}$ = .1495	.1496	.1319	.0633	.0260	.0133	.0068
	α_1 = 56.3	57.0	58.0	59.3	61.8	64.6	68.4
	α_2 = 64.7	65.5	66.4	67.8	70.3	73.0	76.8
	Mode=Buckling	Buckling	Crushing	Crushing	Crushing	Crushing	Crushing

Table - 7-2d. Design Table for Single Beam with Cracks.

$\overline{\sigma} = 3000 \times 10^{-6}$

$\overline{p}$ ($\times 10^{-6}$) \ $\overline{q}$ ($\times 10^{-6}$)	0.25	0.5	1.0	2.0	5.0	10.0	20.0
0.0	$\overline{L}$ = 53.3	44.3	36.9	23.9	15.0	11.1	8.2
	$\overline{T}$ = 109.14	151.83	212.77	162.91	160.06	177.91	198.07
	$\overline{d}$ = .1494	.1485	.1492	.0516	.0214	.0136	.0086
	α_1 = 58.5	59.2	60.0	63.4	68.2	72.3	77.5
	α_2 = 66.9	67.6	68.4	71.8	76.6	80.8	85.9
	Mode=Buckling	Buckling	Buckling	Crushing	Crushing	Crushing	Crushing
50.0	$\overline{L}$ = 56.6	46.4	38.2	25.3	15.8	11.5	8.4
	$\overline{T}$ = 128.32	170.16	230.33	186.20	180.86	193.86	210.48
	$\overline{d}$ = .1499	.1487	.1490	.0541	.0217	.0131	.0080
	α_1 = 58.2	58.9	59.7	62.7	67.3	71.5	76.8
	α_2 = 66.6	67.3	68.2	71.2	75.8	89.0	85.2
	Mode=Buckling	Buckling	Buckling	Crushing	Crushing	Crushing	Crushing
100.0	$\overline{L}$ = 58.9	48.1	39.3	28.1	17.3	12.4	8.9
	$\overline{T}$ = 154.14	193.91	251.39	241.39	225.64	233.34	243.74
	$\overline{d}$ = .1497	.1493	.1484	.0752	.0276	.0155	.0088
	α_1 = 57.7	58.6	59.5	61.6	65.9	69.9	75.1
	α_2 = 66.2	67.0	67.9	70.1	74.3	78.3	83.5
	Mode=Buckling	Buckling	Buckling	Crushing	Crushing	Crushing	Crushing
150.0	$\overline{L}$ = 60.5	49.4	40.3	30.3	18.6	13.2	9.5
	$\overline{T}$ = 186.24	222.02	227.18	295.36	272.42	275.51	287.46
	$\overline{d}$ = .1499	.1496	.1494	.0967	.0340	.0181	.0104
	α_1 = 57.3	58.2	59.2	60.9	64.7	68.5	73.3
	α_2 = 65.8	66.6	67.6	69.3	73.1	76.9	81.7
	Mode=Buckling	Buckling	Buckling	Crushing	Crushing	Crushing	Crushing

Table - 7-2d. (continued)

$\bar{q}$ ($\times 10^{-6}$) / $\bar{p}$ ($\times 10^{-6}$)	0.25	0.5	1.0	2.0	5.0	10.0	20.0
200.0	$\bar{L}$ = 61.6	50.3	41.1	31.9	19.7	13.9	9.9
	$\bar{T}$ = 223.36	253.55	305.43	343.89	319.09	318.72	325.70
	$\bar{d}$ = .1496	.1481	.1495	.1143	.0404	.0208	.0114
	α_1 = 57.0	57.8	58.9	60.3	63.8	67.3	71.9
	α_2 = 65.4	66.3	67.3	68.7	72.2	75.7	80.3
	Mode=Buckling	Buckling	Buckling	Crushing	Crushing	Crushing	Crushing
250.0	$\bar{L}$ = 62.4	51.1	41.7	33.2	20.5	14.5	10.3
	$\bar{T}$ = 264.44	289.76	335.77	390.59	361.77	361.91	367.30
	$\bar{d}$ = .1489	.1486	.1483	.1303	.0451	.0233	.0125
	α_1 = 56.7	57.5	58.6	59.9	63.1	66.3	70.7
	α_2 = 65.1	66.0	67.0	68.3	71.5	74.7	79.1
	Mode=Buckling	Buckling	Buckling	Crushing	Crushing	Crushing	Crushing
300.0	$\bar{L}$ = 63.2	51.8	42.2	34.1	21.2	15.0	10.6
	$\bar{T}$ = 308.72	329.32	369.17	431.58	404.71	404.40	406.88
	$\bar{d}$ = .150	.1499	.1473	.1404	.0496	.0256	.0133
	α_1 = 56.5	57.3	58.3	59.5	63.5	65.5	69.6
	α_2 = 64.9	65.7	66.7	68.0	70.9	73.9	78.0
	Mode=Buckling	Buckling	Buckling	Crushing	Crushing	Crushing	Crushing
350.0	$\bar{L}$ = 63.8	52.3	42.8	34.8	21.8	15.4	10.9
	$\bar{T}$ = 354.79	370.86	407.19	470.65	447.43	445.86	448.73
	$\bar{d}$ = .1495	.1496	.1499	.1476	.0537	.0273	.0143
	α_1 = 56.3	57.0	58.0	59.2	62.0	64.8	68.7
	α_2 = 64.7	65.5	66.4	67.7	70.4	73.2	77.1
	Mode=Buckling	Buckling	Buckling	Crushing	Crushing	Crushing	Crushing

Table - 7-2e. Design Table for Single Beam with Cracks.

$\bar{\sigma} = 4000 \times 10^{-6}$

$\bar{p}$ ($\times 10^{-6}$) \ q ($\times 10^{-6}$)	0.25	0.5	1.0	2.0	5.0	10.0	20.0
0.0	$\bar{L}$ = 53.3 $\bar{T}$ = 109.14 $\bar{d}$ = .1494 α_1 = 58.5 α_2 = 66.9 Mode=Buckling	44.3 151.83 .1485 59.2 67.6 Buckling	36.9 212.77 .1492 60.0 68.4 Buckling	30.7 297.58 .1491 60.9 69.3 Buckling	18.0 233.33 .0438 65.9 74.4 Crushing	12.8 236.58 .0236 70.1 78.6 Crushing	9.4 259.04 .0146 75.0 83.4 Crushing
50.0	$\bar{L}$ = 56.6 $\bar{T}$ = 128.32 $\bar{d}$ = .1499 α_1 = 58.2 α_2 = 66.6 Mode=Buckling	46.4 170.16 .1487 58.9 67.3 Buckling	38.2 230.33 .1490 59.7 68.2 Buckling	31.5 314.66 .1488 60.7 69.2 Buckling	18.3 242.81 .0406 65.7 74.1 Crushing	13.1 249.73 .0225 69.7 78.1 Crushing	9.6 271.94 .0139 74.5 82.9 Crushing
100.0	$\bar{L}$ = 58.9 $\bar{T}$ = 154.14 $\bar{d}$ = .1497 α_1 = 57.7 α_2 = 66.2 Mode=Buckling	48.1 193.91 .1493 58.6 67.0 Buckling	39.3 251.39 .1484 59.5 67.9 Buckling	32.2 333.85 .1479 60.5 68.9 Buckling	19.6 286.49 .0484 64.7 73.1 Crushing	13.8 283.88 .0248 68.7 77.1 Crushing	10.0 301.04 .0146 73.6 81.8 Crushing
150.0	$\bar{L}$ = 60.5 $\bar{T}$ = 186.24 $\bar{d}$ = .1499 α_1 = 57.3 α_2 = 65.8 Mode=Buckling	49.4 222.02 .1496 58.2 66.6 Buckling	40.3 277.18 .1494 59.2 67.6 Buckling	32.9 357.83 .1489 60.3 68.7 Buckling	20.8 333.57 .0572 63.9 72.3 Crushing	14.6 327.28 .0286 67.6 76.0 Crushing	10.4 334.89 .0156 72.3 80.7 Crushing

Table - 7-2e (continued)

$\bar{p}$ ($\times 10^{-6}$) \ $\bar{q}$ ($\times 10^{-6}$)	0.25	0.50	1.0	2.0	5.0	10.0	20.0
200.0	$\bar{L}$ = 61.6 $\bar{T}$ = 223.36 $\bar{d}$ = .1496 α_1 = 57.0 α_2 = 65.4 Mode=Buckling	50.3 253.55 .1481 57.8 66.3 Buckling	41.1 305.43 .1495 58.9 67.3 Buckling	33.5 383.47 .1493 60.0 68.4 Buckling	21.9 382.63 .0670 63.2 71.6 Crushing	15.3 371.02 .0324 66.7 75.1 Crushing	10.9 378.38 .0176 71.1 79.5 Crushing
250.0	$\bar{L}$ = 62.4 $\bar{T}$ = 264.4 $\bar{d}$ = .1489 α_1 = 56.7 α_2 65.1 Mode=Buckling	51.1 289.76 .1486 57.5 66.0 Buckling	41.7 335.77 .1483 58.6 67.0 Buckling	34.0 410.51 .1489 59.7 68.2 Buckling	22.8 429.17 .0757 62.6 71.0 Crushing	15.9 414.09 .0360 65.9 74.3 Crushing	11.3 419.45 .0193 70.1 78.5 Crushing
300.0	$\bar{L}$ = 63.2 $\bar{T}$ = 308.72 $\bar{d}$ = .150 α_1 = 56.5 α_2 = 64.9 Mode=Buckling	51.8 329.32 .1799 57.3 65.7 Buckling	42.2 369.17 .1473 58.3 66.7 Buckling	34.4 438.82 .1476 59.5 67.9 Buckling	23.5 472.04 .0825 62.1 70.5 Crushing	16.5 459.95 .0402 65.2 73.6 Crushing	11.7 463.18 .0212 69.2 77.6 Crushing
350.0	$\bar{L}$ = 63.8 $\bar{T}$ = 354.79 $\bar{d}$ = .1495 α_1 = 56.3 α_2 = 64.7 Mode=Buckling	52.3 370.86 .1496 57.0 65.5 Buckling	42.8 407.19 .1499 58.0 66.4 Buckling	34.8 470.65 .1476 59.2 67.7 Buckling	24.2 517.48 .0903 61.7 70.1 Crushing	16.9 499.85 .0425 64.6 73.0 Crushing	12.0 503.50 .0225 68.4 76.8 Crushing

The values of α_1, in Table 7-2, are the dips of joints along which sliding failure will occur if the coefficient of friction on the joint surfaces is 0.7. The values of α_2 are the dips when the coefficient of friction is 0.5. The predicted type of failure (buckling, crushing, or sliding) is given on the bottom line in each square in Table 7-2.

It should be noted that the previous analysis applied to a single cracked roof beam with no roof bolts installed. Its usefulness in roof design would therefore be limited to determining the maximum safe span for a single unsupported cracked beam in the immediate roof.

Wright (Ref. 21) then proceeds to modify and extend the preceding theory for single cracked beams to apply to multiple cracked beams. The suspension and friction effects are considered separately.

The suspension effect is assumed to be present when a thick or rigid bed is overlain by thinner (less rigid) beds so that the upper beds apply a certain amount of load to the bottom bed. The deflection of all beds is equal. Suspension may also occur if thinner beds are suspended from a thicker overlying bed by roof bolts. The roof bolts are presumed to be tensioned sufficiently so that the underlying thin beds are pulled up into contact with each other and with the upper thick bed. Again, the deflections of each beam at midspan, d, will all be equal so that

$$d_1 = d_2 = d_i = d_n \tag{7-25}$$

Further, the bedding planes are assumed to be frictionless. The total vertical load on all beams together is

$$\sum_{i=1}^{n} q_i = \sum_{i=1}^{n} \gamma_i D_i + w \tag{7-26}$$

where q_i = vertical distributed load per unit length of bed i that will cause a deflection d_i.

γ_i = unit weight of bed

w = uniformly distributed load from above per unit length of beam

D_i = depth of the i^{th} bed

The values of q_i for the various beds are not known initially because of the complex interactions taking place between the beams. The solution consists of treating each of the interacting beds or separate beds which are subject to the conditions stated in Eqs. (7-25, 7-26). The single cracked beam theory previously outlined is applied to each beam; however, at the outset the load q_i is not known for each beam since its value depends in part on the interaction pressures between the beams.

The interaction problem may be solved by making a plot of deflection d versus load q for each bed in the sequence. The span L is known or assumed so that L may be calculated for each bed. The dimensionless horizontal load $\overline{P}$ is also assumed to be known for each bed. The values of d_i

for various values of q_i would be determined by the use of Eqs. (7-15) through (7-20) for each bed. Proper dimensional transformations must, of course, be applied in the use of the equations.

From the plots of d versus q for each bed, one must find a line of constant deflection d along which the summation of all the q's for all the beds equals w plus the summation of all the unit weights times depths as stated in Eq. (7-26).

Once the final values of q_i, d_i and T_i are determined for each beam then Eqs. (7-21) through (7-24) may be employed to determine the factor of safety for compressive failure of each beam in the sequence.

Wright recommends that if the value of $\bar{d}$ exceeds the buckling value in a particular bed, then that bed should probably be treated as a dead load. Also, if compressive failure occurs in a particular bed, it also should be treated as a dead load.

The friction effects in bolted multiple cracked beams analyzed by Wright (Ref. 21) are caused by the increased normal stresses on the bedding planes which increase the frictional resistance along these planes. The coefficient of interbed friction is not zero in this case as it was in the previous discussion on the suspension effect in cracked beams.

In a bolted sequence of beams with interbed friction, there may be shear failure along one or more bedding planes. Therefore, a major problem in the analysis is to determine which bedding planes in a particular sequence will fail. The roof bolts are tensioned to produce an average uniform pressure b.

Slippage is assumed to occur along the entire length of the bedding planes considered. Partial slippage is assumed to have a negligible effect on the behavior. The total shearing force on a bedding plane directed from the abutment to midspan acts in a horizontal direction since deflections are assumed to be small. It is further assumed that the total shearing force H is the same for each of the bedding planes along which slippage occurs. Also, the frictional resistance is that due to bolt tension only; interactions between beds by suspension are neglected.

The total horizontal frictional force on a bedding plane located a distance y above the bottom surface of a bolted sequence of cracked beams (Fig. 7-3) can be determined from equilibrium considerations of the portion of the beam below the plane y. This horizontal force is, in fact, equal to the difference between the areas of the two horizontal stress distributions below plane y as shown in Fig. 7-3. If the stress distributions are linear the total shear force on the y plane is given by

$$\text{Shear Force} = T\left(1 - \frac{(3a - y)^2}{9a^2} - \frac{(y + 3c - D)^2}{9c^2}\right) \qquad (7\text{-}27)$$

if $3a > y$ and $y + 3c > D$. If either of these conditions are not met, the second and/or third terms in the brackets should be set equal to zero.

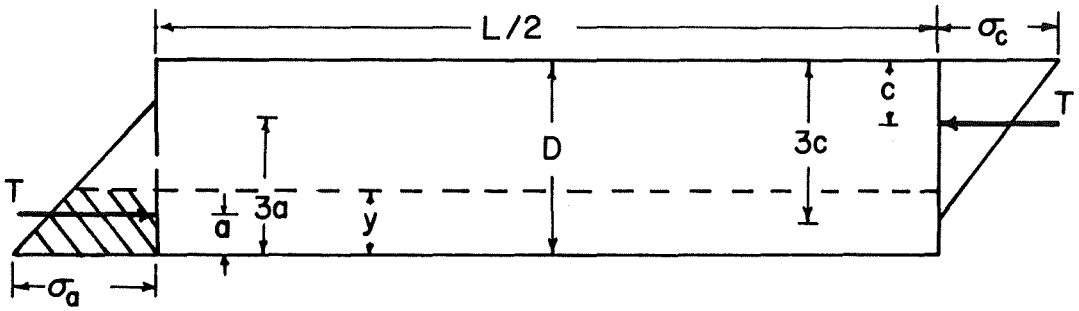

Fig. 7-3 Distribution of Horizontal Stress, σ_x, on Vertical Cracks at the Abutment and Center of the Left Half of a Cracked Beam (after Wright)

The maximum shear resistance H along bedding plane y due to an average normal bolt pressure b and the interaction pressure between beds I is

$$H = \frac{\mu L}{2}(b + I) \qquad (7\text{-}28)$$

where μ = coefficient of friction

Slippage will occur along the bed whenever the shear force given by Eq. (7-27) exceeds the maximum shear resistance H given by Eq. (7-28). This criterion is expressed as

$$T\left(1 - \frac{(3a - y)^2}{9a^2} - \frac{(y + 3c - D)^2}{9c^2}\right) > \frac{\mu L}{2}(b + I) = H \qquad (7\text{-}29)$$

Fig. 7-4 depicts the left half of a three-layered, bolted, cracked beam sequence and the forces acting on each member. Equilibrium considerations for n beds similar to the n = 3 case in Fig. 7-4 yield the following set of equations

$$T_1 A_1 = \frac{Q_1 L}{8} - Hc_1$$

$$T_i A_i = \frac{Q_i L}{8} - HD_i \qquad i = 2, 3, \ldots n\text{-}1 \qquad (7\text{-}30)$$

$$T_n A_n = \frac{Q_n L}{8} - Ha_n$$

The design procedure is to select a bolting pattern for a given cracked roof and to determine the resulting factor of safety for this plan. If this factor of safety is not acceptable, then other bolting patterns are analyzed until an acceptable one is found. The following input information must be known or assumed at the outset: span (L), depth of beam or beams (D), Young's modulus (E), initial axial force per unit width of beam (P), total uniformly distributed transverse load per unit width of beam (Q), and uniform normal pressure exerted by bolts (b).

The following steps outline the method of solution.

1. First assume that the entire bolted sequence acts like a solid beam of depth D and then calculate an approximate value of $\overline{T}$ by Eqs. (7-14) and (7-15). Determine T from $\overline{T}$ and calculate H from Eq. (7-28). The interaction pressure I in Eq. (7-28) is presumed to be zero.

2. Determine $\overline{A}$ from Eq. (7-21) and $\overline{a}$ from Eq. (7-22). Then calculate A and a.

3. Check for the possibility of sliding along each bedding plane in the bolted sequence using Eq. (7-29). The value of c in Eq. (7-29) is equal to D - A - a where D in this case is the depth of the entire bolted

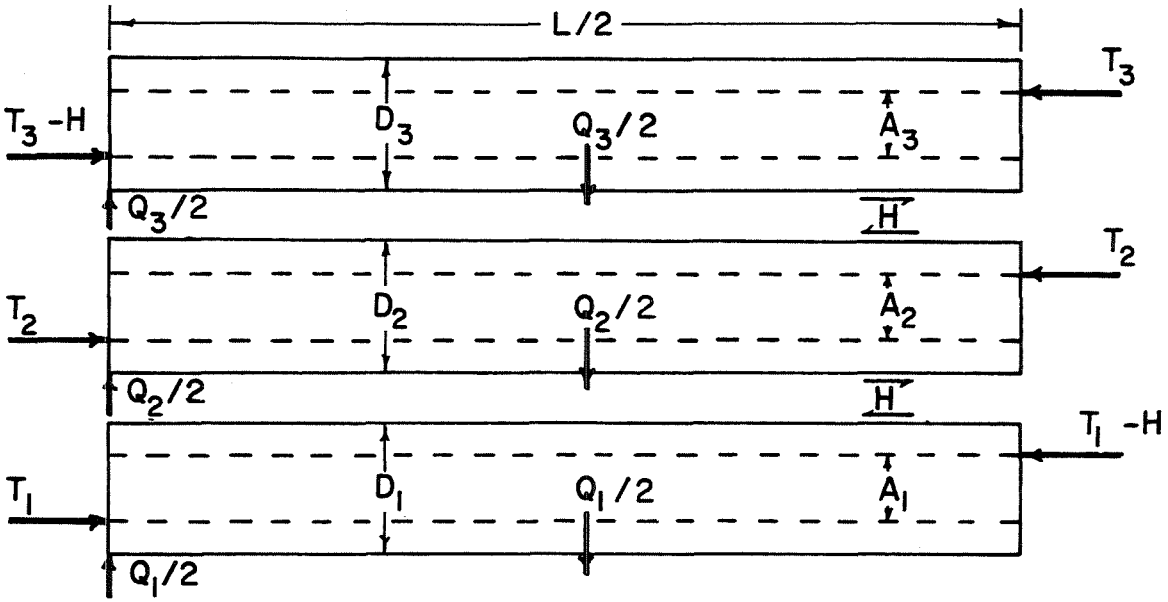

Fig. 7-4 Forces Acting on Left Half of a Three-Layer Cracked Beam with Frictional Resisting Forces, H, Acting on the Bedding Planes. (after Wright)

sequence. The value of y is the vertical distance to each bedding plane measured from the bottom surface of the bottom bed (Fig. 7-3). All bedding planes are checked for sliding one at a time. If sliding does occur, assume that it occurs along that bedding plane having the greatest shear force.

4. Then proceed to analyze the bolted sequence as a two-member beam, each member having its own depth D. Steps 1 and 2 are applied to both the upper and lower members. Additional checks as in Step 3 are made for sliding for any bedding planes which may be present in either of the two members. If sliding is again predicted along one or more bedding planes, the plane with the highest shear force is selected as the one to fail and the sequence is then considered as three (or possibly four) members which can be subsequently analyzed as single beams, each possibly still containing a bedding plane. Continue to check for sliding along beds, one by one, using the values of a_1 and c_1 or a_m and c_m, or a_n and c_n in Eq. (7-29) as appropriate.

5. The procedure described in the previous steps is continued until all of the possible slippage planes have been evaluated to determine which will fail (slip) and which will not. During this process first approximations for $\bar{T}$ and T will be determined for each bed or sequence of beds acting as a solid unit.

6. Calculate the thrust at the abutment for each middle solid unit, and the top solid unit, T_m. Calculations have shown that the abutment thrust on the bottom bed T_1 equals the thrust T for a single layer without the shear resistance H on top. The thrust at the abutment for each middle solid unit and the top solid unit, T_m, is now approximated more accurately with the equation

$$(T_m)_i = T_i - H;\ i = 2, 3, \ldots n \tag{7-31}$$

where T_i is the first approximation to the thrust on the i^{th} bed determined in Step 5.

The total thrust on all beds, T_t, is then determined with the following equation

$$T_t = T_1 + \sum_{i=2}^{n} (T_m)_i \tag{7-32}$$

7. Determine an average thrust T_a on each solid unit as follows

$$(T_a)_i = \frac{D_i T_t}{\sum_{i=1}^{n} D_i} \tag{7-33}$$

where D_i = thickness of the i^{th} solid unit.

Use this average thrust T_a in Eq. 7-16 to determine the dimensionless deflection $\bar{d}$ for each bed. If the deflection $\bar{d}$ is less than 0.01 for

a particular bed, then the average thrust for that bed is sufficiently accurate for that bed. If, however, the value of $\bar{d}$ is greater than 0.01, subtract $\bar{d}$ from $\bar{A}_o$ as in Eq. (7-17) and calculate a new value for $\bar{T}$ for that bed with Eq. (7-18). A new value of $\bar{d}$ is then determined for the bed with Eq. (7-19). This new deflection $\bar{d}$ is then compared with that used in the previous iteration. If the two values are not close together, then one or more additional iterations with Eqs. (7-18), (7-19), and (7-20) must be made. This procedure is followed for each solid unit in the sequence until a final value of T is found for each unit. One must then go back to Eq. (7-32) and determine a new value for T_t. If this new value is significantly different from the one previously calculated in Step 6, a new average thrust must be calculated for each beam with Eq. (7-33). The procedure in Step 7 following Eq. (7-33) is repeated until a final stable value of T_t is found.

8. If the final value of $\bar{d}$ for any of the beams as determined in Step 7 is 0.15 or greater, a buckling type of failure of that beam can be expected.

9. The factor of Safety F.S., for sliding of the entire bolted sequence at the abutments can now be determined from the equation

$$F.S. = \frac{\text{Maximum Resistive Force}}{\text{Driving Force}} = \frac{T\mu}{\frac{Q}{2}} = \frac{2T\mu}{Q} \qquad (7\text{-}34)$$

10. The maximum compressive stress at the abutment in the bottom solid unit can be determined since the thrust $\bar{T}$, is now known. Eq. (7-23), along with Eqs. (7-21) and (7-22), are used to determine $\bar{\sigma}_{max}$. The factor of safety for compressive failure is finally given by Eq. (7-24).

After the foregoing ten steps have been completed, the engineer must judge whether or not the failure possibilities indicated in Steps 8, 9, and 10 are acceptable. If not, the bolting plan can be modified by varying the average normal bolting pressure b and reworking the problem until a suitable bolting plan is finally arrived at.

Failure possibilities may be judged in part from the safety factors applied in the design process. Wright suggests the use of a safety factor as low as 1.5 provided input data is good and only single member beams are considered. For multiple beds the safety factor against buckling should be increased to about 2.5 or so. Factors of safety against compressive failure are recommended to be at least 4.0 and 5.0, for single and multiple layer roofs, respectively. The large safety factors reflect the degree of uncertainty involved in the design process. The more accurately input properties model those of the real roof, the smaller the safety factors may be.

C. Suspension from Competent Strata

One of the easiest modes of roof support to understand is the suspension of a finite volume of rock from a thick, competent layer of overlying rock. The volume may be well defined. For example, a thin layer of coal and shale is frequently left to protect continuous miner teeth from abrading against a limestone or sandstone strata. Also, a relatively thick layer of

weak material may be left simply because removal of the layer would require excessive clean-up costs or would produce excessive ash content, if mined with the coal. The zone of weak material may, on the other hand, be poorly defined. Rock materials, frequently possessing little or no tensile strength, have been observed to progressively fail until a stable arch configuration is attained (Ref. 27). Finite element studies (Ref. 4) have shown that the geometry of these arches is a function of the stress field around the opening. Since these stress fields are generally unknown, the extent of the volume of rock requiring support is also unknown.

The suspension concept is based on several simplifying assumptions.

1. The volume of supported rock (the immediate roof) may assume any size or shape. The overlying rock used as the bolt-anchorage horizon is a massive, competent material which exhibits essentially no deflection under loading from the supported volume.

2. The supported zone does not interact with the pillars or the roof rock outside the supported zone although this zone may be delineated from a knowledge of pillar, roof, and stress field parameters.

3. Bolts are installed vertically or at some angle on a regular square-grid pattern or some other pattern, as required.

4. Bolts may be tensioned or untensioned but must be located far enough into the competent strata that no loss of anchorage occurs either with time or with loading by the supported volume of rock.

5. The supported volume is gravity loaded.

If the volume of rock to be supported is a well defined beam-like layer (Fig. 7-5a), the following simple equation may be applied to solve for either bolt load, and hence required bolt strength, or bolt spacing (Ref. 19).

$$W_b = \frac{\gamma t B L}{n_1 n_2} \tag{7-35}$$

where

W_b = load per bolt,

n_1 = number of rows of bolts included within length L,

n_2 = number of bolts included within width B,

γ = unit weight of rock,

t = thickness of layer,

B = width of layer measured from center point to center point between supports (bolt or pillar),

L = length of layer supported, measured from center point to center point between supports

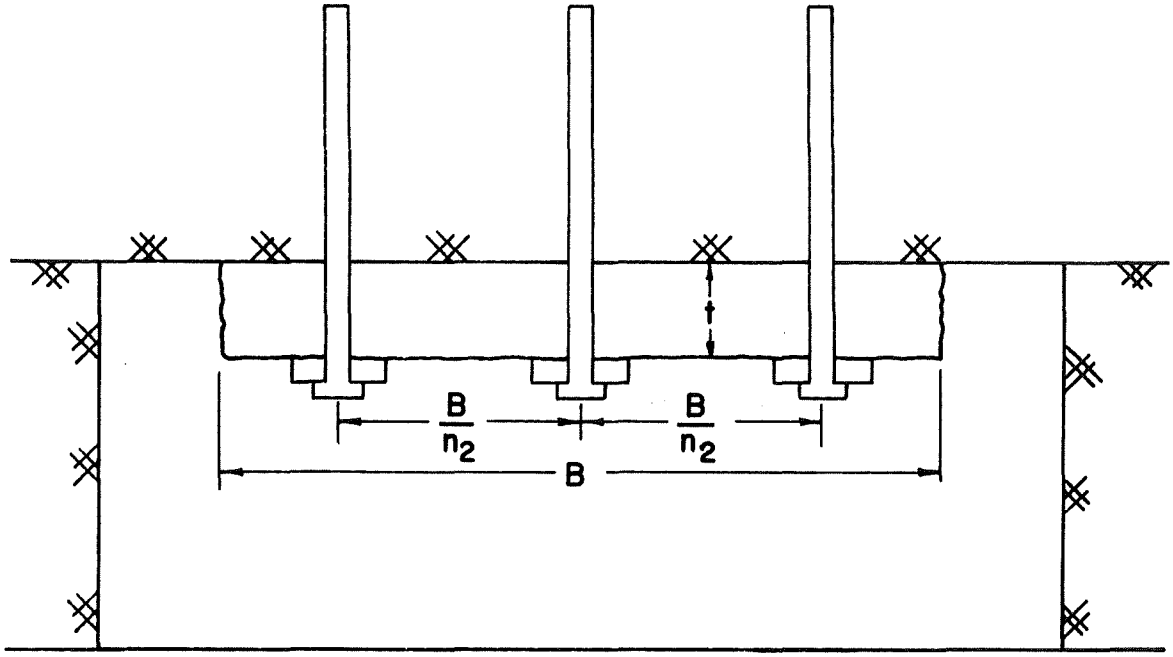

Fig. 7-5a Support of Competent Layer Independent of Pillars.

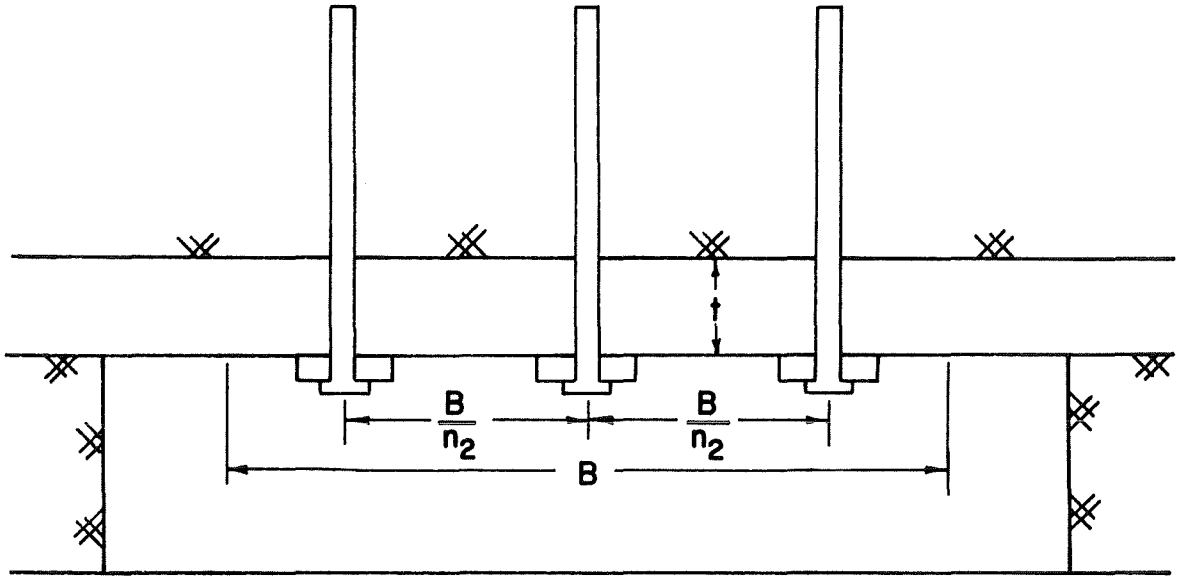

Fig. 7-5b Support of Competent Layer with Constrained Ends

The case illustrated in Fig. 7-5b in which each pillar contributes the equivalent of one half of the load carried by each bolt W_b can also be analyzed by Eq. (7-35).

The principle used here is a simple one. It is considered that the weight of a finite zone of weak material must be completely supported by rock bolts or other means. If the geometry and extent of that zone can be delineated, it is possible to determine the length, diameter, and spacing of bolts required to suspend the zone from a more competent strata. This suspending action need not be restricted to the support of competent, beam-like layers but may be applied to the suspension of any zone of weak rock. A zone of highly fractured ground may be bounded on its upper surface by a massive competent strata (Fig. 7-6). Steel channels, wooden lagging, or wire mesh may be required to prevent the fractured material from falling out from between the bolts, but the basic suspension effect employed is the same as with the more competent layers. Likewise, arch-shaped zones of fractured rock may be suspended by bolts having anchor points outside the fractured zone. The phenomenon of arch formation is discussed in Chapter 2 (page 44) in terms of progressive failure of no-tension rock and is discussed further in a following section of this chapter.

D. Keying of Blocks

Where there exists no beam-like roof structure or where an upper competent layer is either not present or is located too far above the roof line, keying of blocks of jointed rock may produce an effective forms of roof control. The principle involved is to some degree similar to that used in suspension. The bolts are required by some means to support a finite zone of material intersected by joints and fractures. Bolts may act to increase the normal forces between blocks and thus increase the shear resistance along a joint. The bolts may also contribute directly to increasing the shear resistance along planes which they intersect.

The assumptions used in this model are as follows (Fig. 7-7).

1. The immediate roof consists of a zone of rock, possibly of variable thickness, intersected by joints, fractures, and slickenside surfaces.

2. Bolts may be installed vertically in a regular pattern or may be installed at oblique angles so as to cross the prominent discontinuities at some angle.

3. Bolts are tensioned so the key blocks remain in contact with the rest of the roof. Perfect anchorage is required since any loss of tension would be reflected in decreased normal and shear components of resistance to movements.

4. Loading of the supported zone is a result of gravity forces only. No loads due to free-field stresses are considered.

Large underground openings and tunnels often present situations in which individual blocks may be analyzed for failure conditions by sliding wedge techniques (Ref. 28) common in soil and rock mechanics engineering. Multiple openings such as are present in coal mines present a more complex design problem. The size, variability, and uncertainty of the problem

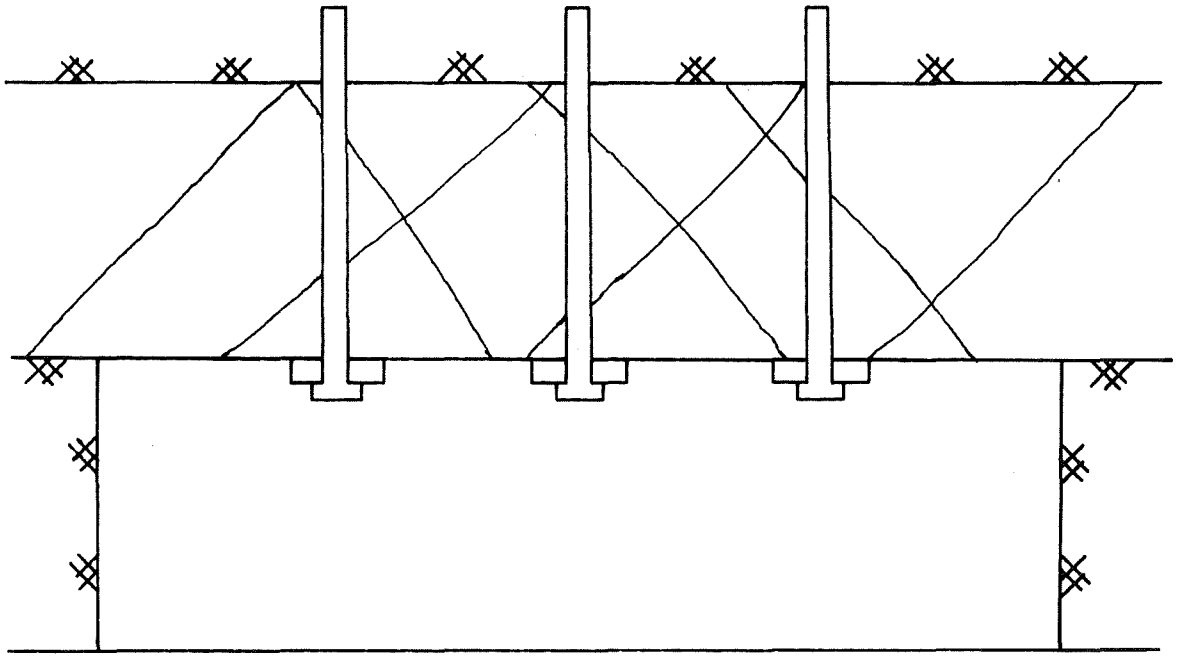

Fig. 7-6 Support of Highly Fractured Rock from a Competent Strata

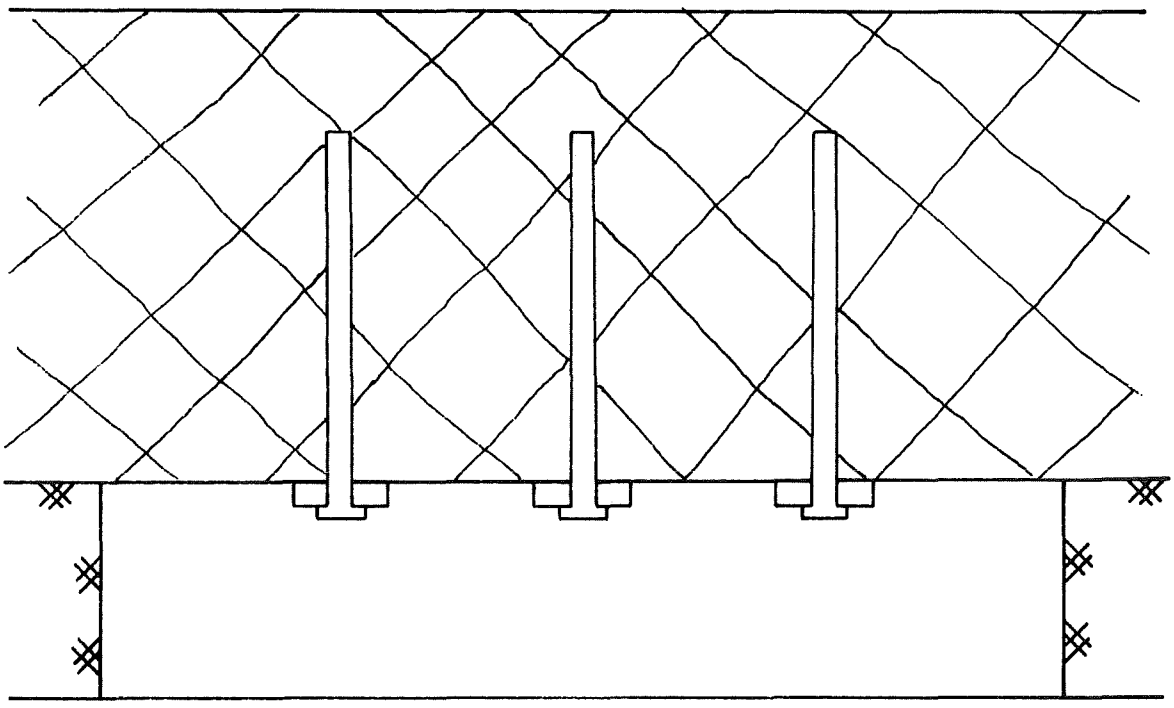

Fig. 7-7 Keying Support of Highly Fractured Rock

usually precludes the use of simple calculations in treating the situation shown in Fig. 7-7. Computer techniques, particularly interactive computer graphics, are helpful in obtaining solutions when this roof geometry is encountered.

Some helpful guidelines for applying the keying concept were developed in conjunction with the Snowy Mountain hydroelectric project (Ref. 29). A series of model experiments using fine (<3/16 in.) crushed rock, plastic rods, or marbles to model fractured rock and scale-size rock bolts resulted in the following relationship between the clear space, S, between bolt washers and the mean particle size, M, of supported material.

$$F = \frac{S}{M} \leq 3.0; \qquad (7\text{-}36)$$

Under these conditions, even a mass of glass marbles could be stabilized. At F = 4.0, the marble mass would always collapse but crushed rock could often be supported. The Code of Federal Regulations discussed in a later section of this chapter also considers this ratio when broken ground is encountered.

E. Arch Formation and Control

The formation of arch- or dome-shaped failure surfaces has been observed in model studies (Refs. 21, 30) and in the field (Ref. 14). In addition, finite element studies (Refs. 2, 3) indicate that this mode of failure should be common in rock materials possessing little or no tensile strength. Both low-angle and high-angle arches have been found to be stable roof configurations, depending on the in-situ stress conditions present.

Continuous and cracked beams are stable under moderate horizontal end loads. These end loads, the model equivalent of a lateral stress field, act to form a flat arch which is resistant to progressive failure as may be induced by increasing vertical loads. In the absence of the end loads, cracked beams would fail under their own weights so positive support is required to link the fractured zone to a more massive, stable region. Likewise, large end loads may buckle thin beds. Thin members may be bolted together to effectively counter this tendency to buckle (Ref. 21). Increasing the roof span also reduces the likelihood of failure by buckling since this reduces the stress concentration factors in the roof. Increasing the major axis of the opening in the horizontal direction when high horizontal stresses are present aligns the opening more favorably relative to the major stress field.

Low-angle and high-angle arches have been observed to occur as a result of a number of different stress field configurations. In general, arches may be the result of shear failure of the roof or may be the expression of progressive tensile or buckling failure of roof rock. The former may occur where a massive roof layer is subjected to high compressive stresses. The stratum is unable to flex downward, thereby relieving some of the stress. The angle of the resulting shear failure is related to the relative magnitudes of the principal stresses (Figs. 7-8a, 7-8b). The low-angle failure may be stabilized by bolting the potential failure zone to a massive upper strata. The high-angle failure cannot usually be controlled by bolting.

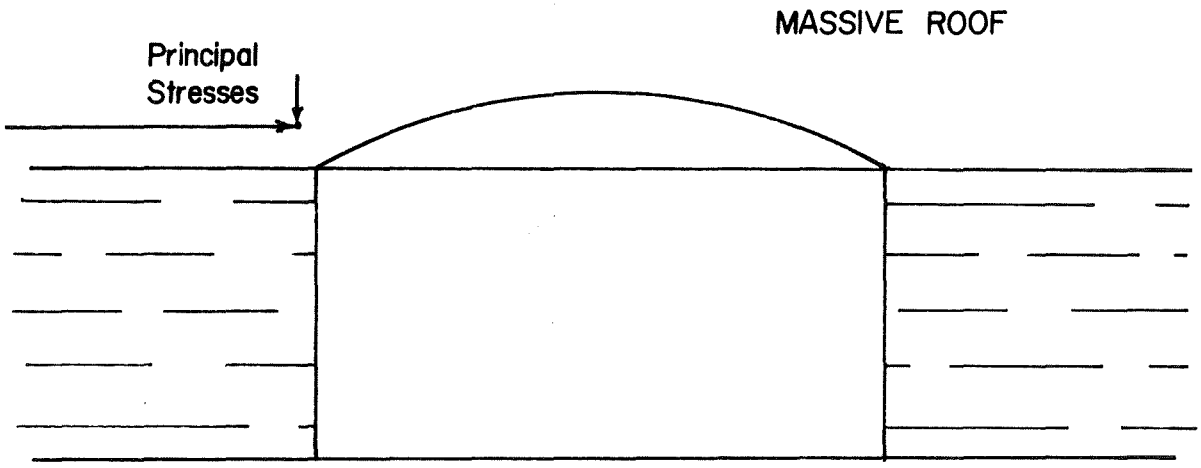

Fig. 7-8a Low-Angle Arch Failure in Massive Roof, High Lateral Stresses

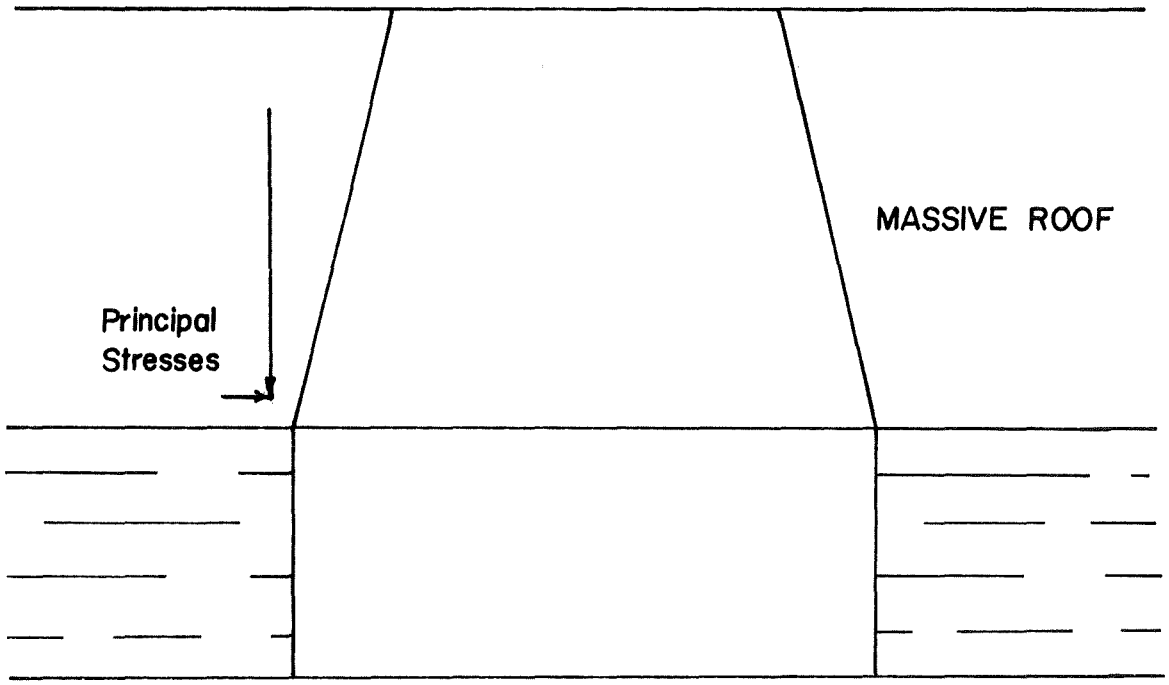

Fig. 7-8b High-Angle Arch Failure in Massive Roof, High Vertical Stresses.

Timbers or steel sets and crossmembers are often required to support the failed mass. The mechanisms of failure are quite different, however, and careful observation will enable the engineer to ascertain which type of failure has occurred. Since the shear-induced falls are generally the result of high stresses in more massive rock units, evidence of shearing movements such as gouge material and striations are often present. The contour of the arch is also relatively smooth and continuous (Fig. 7-8). Arches formed by the progressive tensile failure of thin strata exhibit evidence of the rock falling out along pre-existing fractures, slickenside surfaces, and newly created tensile fractures. The resulting dome or arch usually has an irregular contour broken by bedding planes and other discontinuities (Fig. 7-9). This geometry favors stabilization by bolting to a massive upper strata or anchoring inclined bolts over the abutments, if these are stable. Bolting into the abutments in areas of low or tensile horizontal stresses may be detrimental, however, to overall roof control since the required angling of the bolts may produce more tensile stresses in the roof. The recently introduced roof trusses have been shown to be effective in supporting the roof under these conditions (Ref. 31).

Finite element analyses have been instrumental in examining the relative effects of stress fields on mine opening stability (Refs. 3 and 4). The influence of the lateral stress field on the formation of tensile regions in the roof has been examined. It is apparent (Fig. 7-10) that as the magnitude of the lateral stress decreases, the extent of the tensile region increases substantially. This is of practical significance since mine roof rock is commonly jointed and fractured. It is, therefore, unable to support tensile loads. Finite element analyses of a zero-tensile-strength rock mass subjected to low lateral stresses shows the same arch-shaped failure profile observed in the field (Fig. 7-11). This entire region would require support if roof failure was to be avoided.

Tensile zone analysis alone is not sufficient to describe support requirements. The high-lateral-stress case (Fig. 7-10), for example, has a relatively small tensile region but stress analysis in Chapter II of this report shows the octahedral shear stresses to be twice as great as those for the low lateral stress case. This situation favors low-angle shear failure rather than tensile failure.

The finite element studies described in Chapter II also indicate that bolts have little effect on stresses and deflections in massive roof rock. As more bedding planes were added to the model, the bolts played an increasingly important role in reducing strata deflections when the rock possessed some tensile strength. The analyses of zero-tensile-strength materials with low lateral stresses predicted failure regions which included the anchorage horizons of the bolts. Therefore the bolts would contribute to roof stability only inasmuch as a keying effect was occurring.

Studies of mine roof intersected by nonvertical joints shows the tendency of blocks of rock defined by the joints to be pushed downward (causing failure) by high lateral stresses. Bolts installed so as to intersect these joints contribute substantially to the stability of the roof.

The information about arch formation obtained from field observations, model studies, and finite element analyses should be applicable to a wide range of mining conditions. Since a number of complex factors are involved,

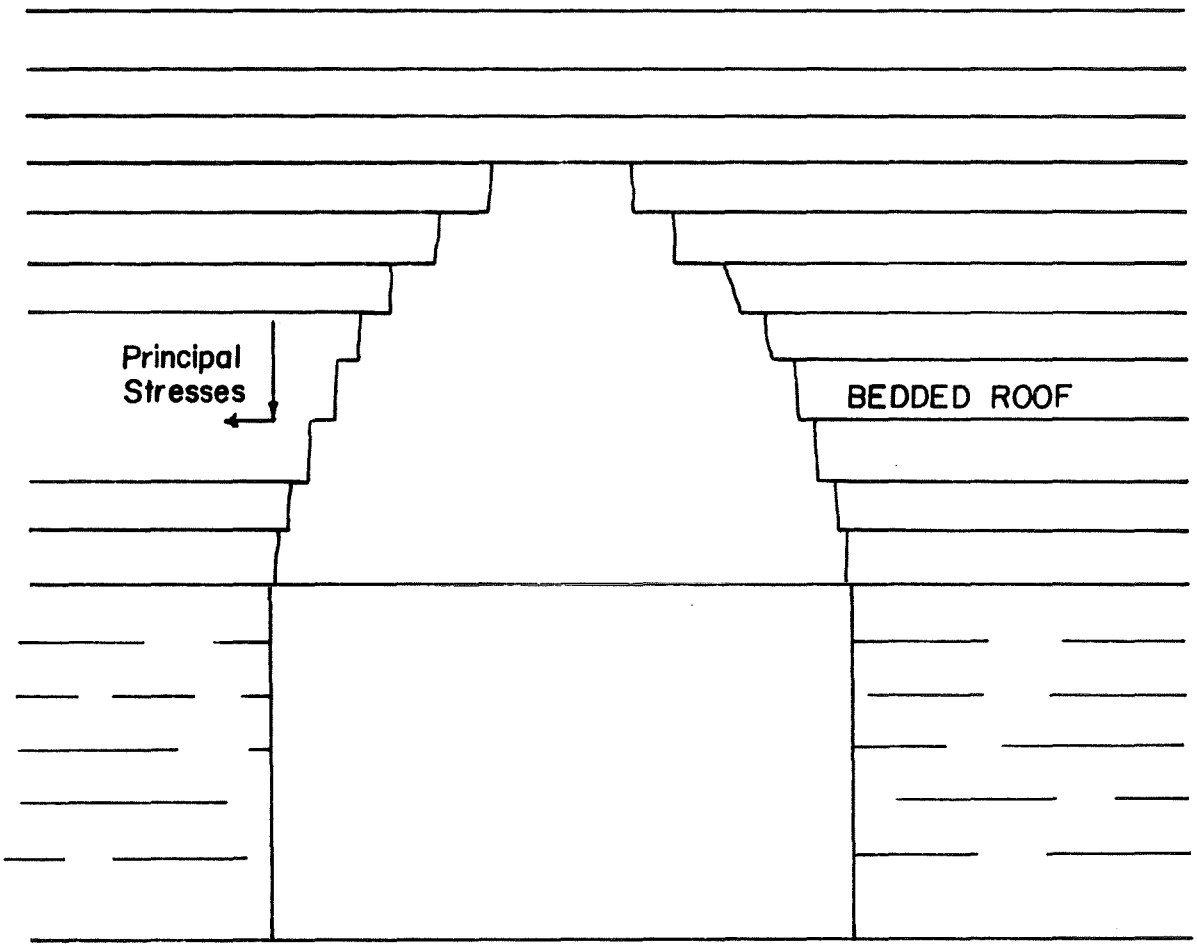

Fig. 7-9 Arch Failure in Bedded Roof, Tensile Lateral Stresses

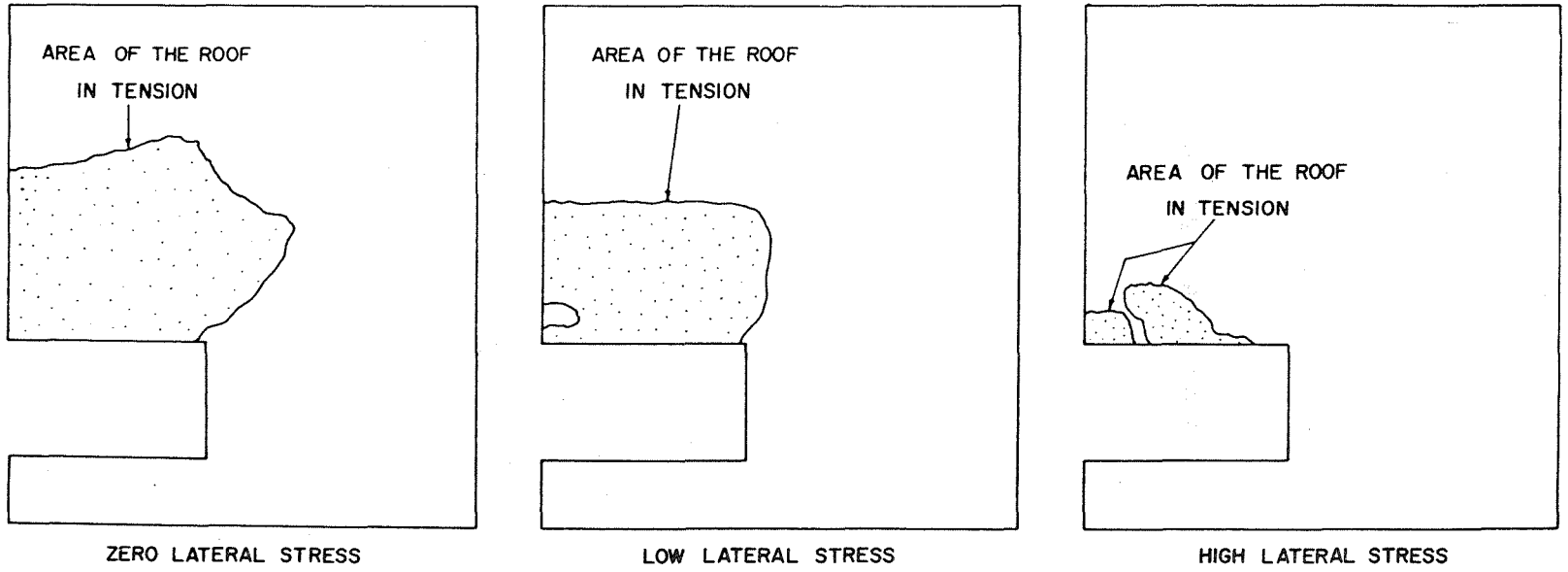

Fig. 7-10 Effect of Lateral Stress on the Area of Roof in Tension for Two Bedding Planes and No Bolts

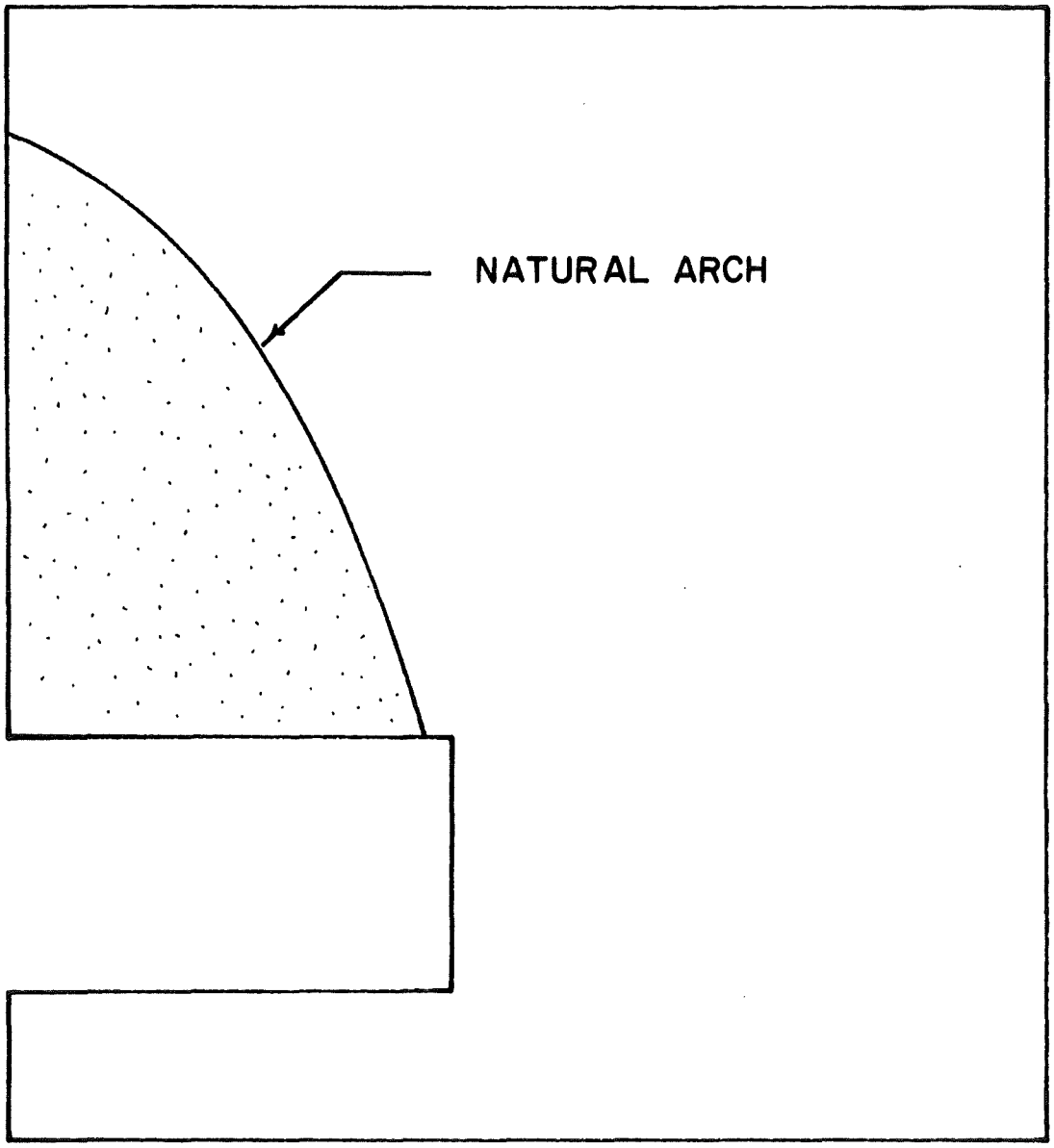

Fig. 7-11 Arch Failure in Rock Possessing No Tensile Strength, Low Lateral Stresses

no simple formulae have been developed to date to aid in the design process. Careful analysis coupled with sound engineering judgment should allow the available observations to be applied to current roof control problems. It is essential that, in applying these observations, the underlying assumptions of each analysis or observation be compatible with those present in the problem at hand.

F. Code of Federal Regulations Requirements

Drawing on current practice and early rock bolt research, the Federal government has established legal guidelines for coal mine roof support requirements. These are presented in Title 30 (Mineral Resources) of the Code of Federal Regulations and will be given here in abbreviated form for the purpose of comparison with the research already presented.

For situations favoring support of beam-like strata, bolts are to be installed on no more than 5-ft centers and within 5 ft of the ribs and face, the bolts being at least 20 in. long. Bolts employed to suspend weak rock from a competent strata should be anchored at least 12 in. into the strong bed.

In broken ground, bolt length should be at least twice the bolt spacing or at least three times the average joint spacing, whichever is greater. These should be tensioned to 60 to 80 percent of their yield strength. Highly fragmented ground should be bolted in such a manner that the space between anchor plates not exceed three times the mean particle size, unless wire mesh is employed.

Additional regulations are also given to specify support requirements using resin bolts (all the above information applies to conventional bolts, only), timber sets, and mixed forms of support. Material properties and quality control testing procedures are also outlined.

Although it is uncertain how much these regulations have improved the general support given mine roof rock, it is evident from injury statistics that mine safety has been improved since the introduction of the regulations in 1969. Overdesign of support systems has probably increased as a result of the Code, primarily because any approach with the degree of generality present in the Code allows for the worst possible situations expected in any coal mine. As with several of the previously discussed theories, the Code does not account for such important factors as in-situ stresses, moisture effects, and the presence of underclay. The broad, conservative approach used is largely responsible for the successful application of the guidelines under a variety of mining conditions.

Field Considerations in Support Selection

Each roof support mechanism described thus far has associated with it certain design assumptions. Before the engineer can select the proper support mechanism and the consequent type and density of support, the field conditions must be determined. A support mechanism compatible with the field conditions may then be selected.

Support requirements are influenced by a variety of factors. For ease of discussion these are grouped under the headings geologic, bolting, and operational parameters. Some factors may be related to more than one of these groups.

A. Geologic Parameters

The geology of a typical coal mining operation is usually complex and highly variable throughout the mine. Included under this heading are rock properties, premining and post-mining stresses, joint and fault frequency and character, anchorage capacity (which is also a bolting parameter), support stiffness requirements as related to strata stiffness, and rock moisture sensitivity. Many of these parameters are design constraints which cannot be altered but which must be designed around. Rock properties, joint data, and bolt anchorage characteristics are measurable quantities; however, the cost of the measurements is often more than what the mining company can afford or is willing to spend. These quantities, when determined, form a minimum basis upon which the engineering design of the roof support system can be made. Moisture sensitivity of certain shales is becoming much better understood (Refs. 27, 32) and, although not usually determined prior to the beginning of mining activity, can be recognized by experienced personnel. Proper countermeasures such as the application of sealants or the use of conditioning chambers can then be employed.

The effects of stress fields have been studied using finite element techniques (Ref. 4) and field observations (Refs. 27, 33). Only cracked beam theory and the arch control theory discussed previously recognize the importance of these stresses and use them in the analysis and design procedures. Research personnel are largely restricted in their work in this area by the lack of adequate equipment for making the large quantity of stress measurements necessary to develop a relationship between field stresses and support requirements.

Probably the least understood of the geologic parameters is the influence of the relative stiffness of roof strata and support materials on support selection. Intuitive reasoning supported by field studies (Ref. 7) indicates that there exists an optimum resistance to strata displacements which a support system should provide. More research is necessary to quantify the matching of strata and support stiffnesses but two examples point out the importance of such matching. First, consider the installation of high stiffness full-column grouted bolts in squeezing ground. After an initial rapid load increase with little strata deflection, the bolts would break, allowing the entire supported volume to collapse. Yieldable bolts or friction rock stabilizers would be more applicable here. The second example deals with the attempt to support highly fractured rock with a low stiffness system such as those just mentioned. Such a system may allow sufficient movements to reduce the frictional resistance between blocks of rock to the point where any keying action would be lost. Deterioration of the roof would then occur. Stiff supports would, on the other hand, maintain block-to-block contact pressures and would thus help the roof to support itself.

Several of the roof control theories discussed relied on some type of beam action. The pertinent design equations required a knowledge of beam thickness in this application. Drill core, and borescope inspections can be used to locate the upper and lower bounds of a geologic unit, mud seams, or other discontinuities which would delineate the thicknesses of the layers constituting the immediate roof. Layer thickness is not so easily obtained if a layer of crossbedded sandstone or shale is encountered. Here, planes of weakness may occur every few inches or even every few hundredths of an inch. Since these materials would also commonly be discontinuous in

horizontal extent, it could be reasoned that beams, as such, do not exist. The question of beam thickness becomes an academic one since some mode of support other than beam-building would be required to support the roof. Judgment must be used when considering roof materials which are not clearly either competent enough to be called beams or weak and fractured enough to require complete suspension.

B. Bolting Parameters

Bolt material properties and installation geometries as well as load loss, creep, and shock loading effects are well documented in the literature (Refs. 2, 3, 10, 34). In addition, each of these items is directly or indirectly treated in the Code of Federal Regulations. Problems arise in design, however, because the required magnitude and orientation of supporting forces is generally only vaguely known. This reduces the design procedure to educated guessing at bolt length and diameter since not even the geometry of the zone requiring support is known. This lack of knowledge carries with it the requirement that large safety factors be applied to calculations, thus producing overdesigned support systems in many cases. A knowledge of the interaction between geologic and bolting parameters is required if adequate support systems are to be designed.

Field conditions must be adequately modeled by the underlying assumptions of a proposed roof support theory if that theory is to accurately predict support requirements. The foregoing discussion of the most common theories should aid the engineer in selecting a support concept which is compatible with conditions in a particular section of roof. The safety factor must be increased if the assumptions do not accurately reflect mine conditions. The amount of increase is a matter of judgment, based largely on experience.

Another consideration in assigning a required factor of safety is the anticipated life of the opening. Safety factors should be larger in longer lived openings for two reasons. First, none of the theories considers the effects of secondary phenomena such as rock and bolt-anchor creep, cyclic moisture effects on roof rock, and so on. Second, longer lived openings are often haulageways, airways, or other important areas in which a roof fall would be a much greater problem than it would be in the average section, infrequently traveled by men and equipment.

C. Operational Parameters

Operational parameters are those associated with mining methods, life of the various openings, and cost considerations. Direct costs of roof support are a major concern of the mine manager so an attempt is usually made to trim material and labor costs whenever possible. Too often little thought goes into the secondary costs associated with bolting such as cleanup, resupport, damage to equipment, and injuries resulting from inadequate support. Likewise, the cost of overdesign due to the absence of adequate, accurate data is not accounted for.

Currently the rule of thumb approach is used in determining the additional support requirements of certain areas in the mine such as haulageways and large intersections (Ref. 35). Case study data compiled by a leading manufacturer of rock bolts indicate that considerably more money can be invested in providing adequate support in these areas while the total costs

of bolting remain the same or decrease slightly due to reduced secondary costs. The problem of determining in advance of use how much better support type B is than support type A is substantial and has not yet been solved completely. This relationship between the relative support capabilities of various roof control systems and roof failure probabilities associated with each support type is a primary concern in the evaluation of the costs and safety aspects of roof support.

Conclusion and Example Problems

It should be apparent now that the common roof support theories cover a wide range of possible mining and geologic conditions. Each concept is applicable to certain situations, depending on the assumptions of the model. The arch concept and the Code of Federal Regulations have the greatest potential for application to all mining environments. The former requires finite element modeling and is for that reason probably the most difficult and expensive design tool presented here. The Code is, on the other hand, much easier to use but has associated with it a greater likelihood for overdesign. All of the concepts discussed require a knowledge of certain material properties and of the configuration of the zone to be supported. A set of example problems are presented here to familiarize the reader with several of the roof support theories.

Problem 7-1, Frictional Support of Continuous Beams

Drill core records indicate that the first 4 ft of roof consists of a series of shaley limestone layers about 3 in. thick. Above these is a massive layer of black limestone. Equipment size and available materials favor the use of the following parameters.

L = 16 ft = roof span,

N = 3 = bolts per row

B = 4 ft = row spacing (square grid)

t = 3 in. = layer thickness

h = 4 ft = bolt length

F_b = 10,000 lb = bolt tension on 5/8-in. diameter grade-40 steel.

Using Fig. 7-1 the reinforcing factor is found to be 1.9. Now find the maximum bending strain for the unbolted condition.

$$\varepsilon_{max} = \frac{\gamma L^2}{2Et}$$

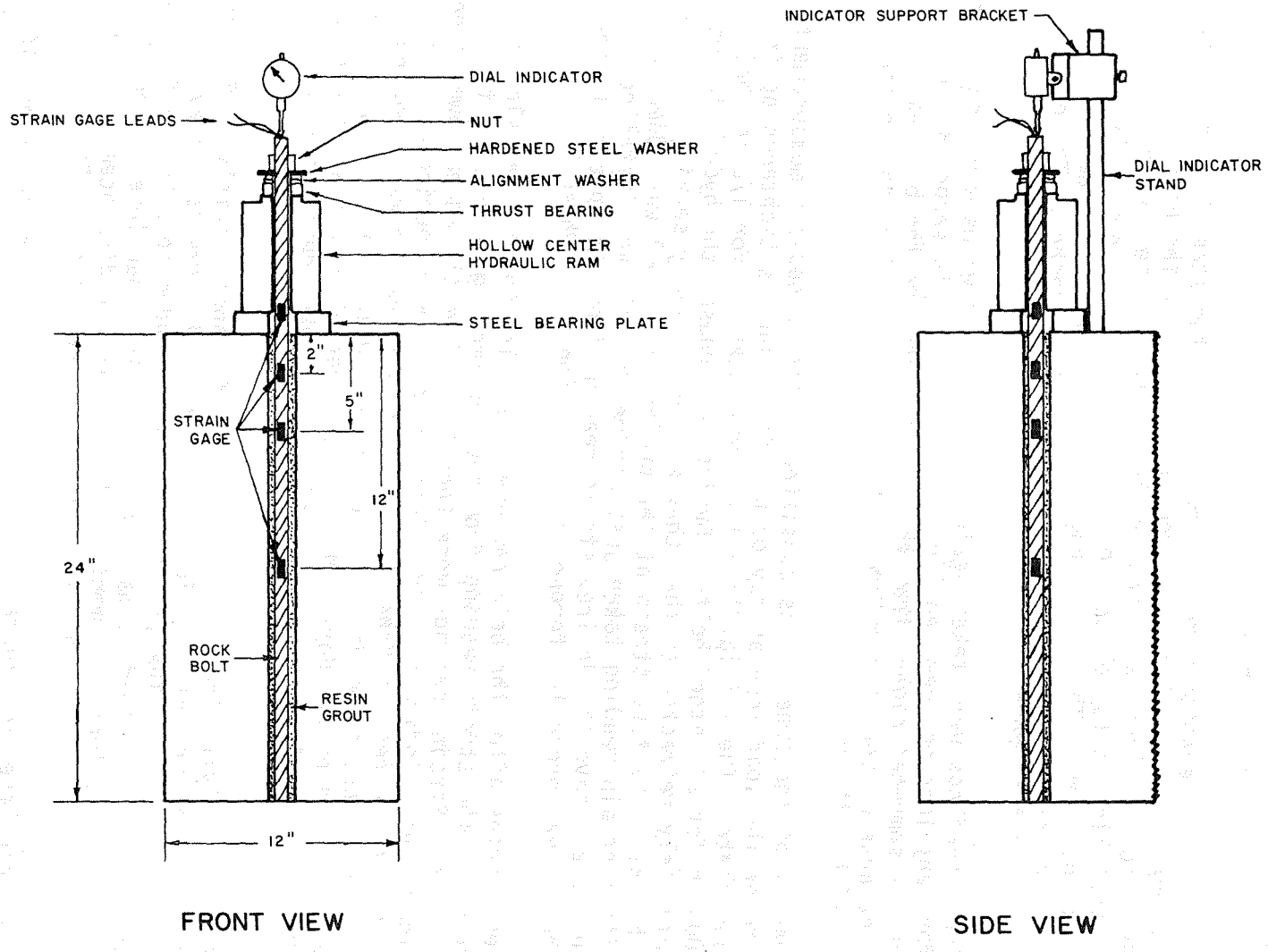

Fig. 5-4 Creep Test Installation Showing Strain-Gage Locations and Dial Indicator

whereas for Groups 6-11 the bolt was first pushed through the resin to the bottom of the hole with a pneumatic impact hammer and then rotated with the electric drill. Total mixing time after insertion of the bar was 30-40 sec for Celtite resin and 10-20 sec for Fasloc resin. Thorough mixing was rapidly followed by hardening of the grout as was noted by an increase in torque on the drill.

The drill and adaptor were then removed and the steel bearing plate and hollow ram were installed over the exposed end of the bolt. A thrust bearing, spherical alignment washer, hardened steel washer, and nut were installed on top of the loading ram which was completely retracted at this time. The strain gage leads were then resoldered to the cable and the dial indicator and bracket were attached. The dial indicator was set to zero.

Strain readings were taken again as soon as the wires were connected, but before any load had been applied to the bolt. This second set of readings was somewhat higher than the set taken before the bolt was installed because of the temperature increase resulting from the chemical reaction within the resin.

Phase I of the creep tests consisted of load bleed-off measurements to determine the load loss as may occur after a nut is tightened against a bearing plate. The initial load level was 4,000 lb for 1/2-in. bolts and 8,000 lb for all other bolts. During this phase, the hydraulic rams were completely retracted so that they were effectively serving as rigid spacer blocks. The true strain at the proper load level was added to the initial strain reading taken just before the bolt was installed. This sum, then, gave the desired strain reading from the uppermost gage when the nut was properly torqued at the beginning of Phase I.

Ten minutes after the bolt had been installed the nut was slowly torqued until the strain reading from the uppermost gage reached the proper value. Strain readings were then taken from the three lower gages and from the dial indicator. Additional readings were periodically recorded during the rest of Phase I. The time interval between readings was 10 minutes just after installation and was gradually increased to one day over a period of two days. Much of the load bleed off which did occur was during the first day so more readings were taken during that early period.

Phase I, a load bleed-off test, lasted for approximately 40-60 days. For Phase II pressure was applied to the hydraulic rams to achieve the initial load levels. (The 1/2-in. bolts were loaded to 3,540 lb instead of 4,000 lb due to a loading malfunction). These load levels were then maintained for at least one month. The strains and displacements were recorded periodically on the same schedule as described in Phase I.

The load level was increased to 5,890 lb on 1/2-in. bolts and 16,000 lb on the other bolts for Phase III. This load increase was accomplished stepwise in 2,000 lb increments with the dial indicator being read after each load increment. The axial pullout stiffness of each bar could then be evaluated after a correction for the stretch in that portion of the bar within the hollow ram was made. After the desired load level was

reached, the strains and displacements were again recorded at increasing time intervals ranging from ten minutes to one day for approximately one month.

Phase I - Load Bleed Off

Phase I testing began with the previously described installation of resin-grouted bolts and was in effect for 40-60 days. Decreases in load and bolt pullout were measured and recorded through the test period. This data was used to generate graphs depicting bolt strain as a function of time and load distribution along the bolts.

A. Load Bleed Off

A substantial loss of initially applied load was noted for all installations. This phenomenon is easily seen in the example graph (Fig. 5-5). Two important relations can be obtained from the graphs. First, the tensioning of the bar has progressively less effect deeper in the grout column. This is in general agreement with the elastic time-independent solution which assumed perfect bonding at the grout-rock and grout-bolt interfaces as described by Haas, et al., (Ref. 1). The grout serves as a medium for stress transfer from the bolt to the rock around it. Second, the bleed off slows to a negligible rate or ceases completely after approximately four days.

To quantify the amount of load bleed off, the percentages of load remaining ten minutes, one hour, one day, one week, and one month after installation were determined for each group of installations (Table 5-2). Comparing Groups 1, 7, and 11 with Groups 2, 6, and 10, respectively, it can be seen that the Celtite systems have somewhat more favorable bleed-off properties, showing 11 to 26 percent less load loss one month after installation. Groups 8 and 9 were not compared because the Anna shale was so weak the full load of 8,000 lb could not be applied. Thus, a quantitative comparison with the other installations would not be meaningful.

A comparison of Groups 2 and 5 indicates that bolt size, of itself, has some effect on load bleed-off characteristics. In these groups, bolt size and hole diameter were altered in such a way that annulus size was constant at 1/4 in. with the same resin type being used in each configuration. The 1/2-in. bolt lost 6.5 to 18.6 percent more load at various times during the test than did the 7/8-in. bolt.

Groups 1 and 3 had the same hole diameter and type of resin but different bolt sizes. Group 3, with the smaller bolt, had a slightly greater grout annulus than Group 1. Here, Group 1 shows up to seven percent less load loss than Group 3. Additional tests would be necessary to determine whether the smaller bolt size or larger grout annulus was responsible for the greater load bleed-off rate. Groups 3 and 4 cannot reasonably be compared for the effect of annulus size with constant bolt diameter since different bolt and resin types are utilized in the tests. These comparisons indicate that perhaps a combination of annulus size and grout/bolt contact area controls the load bleed-off characteristics of the systems.

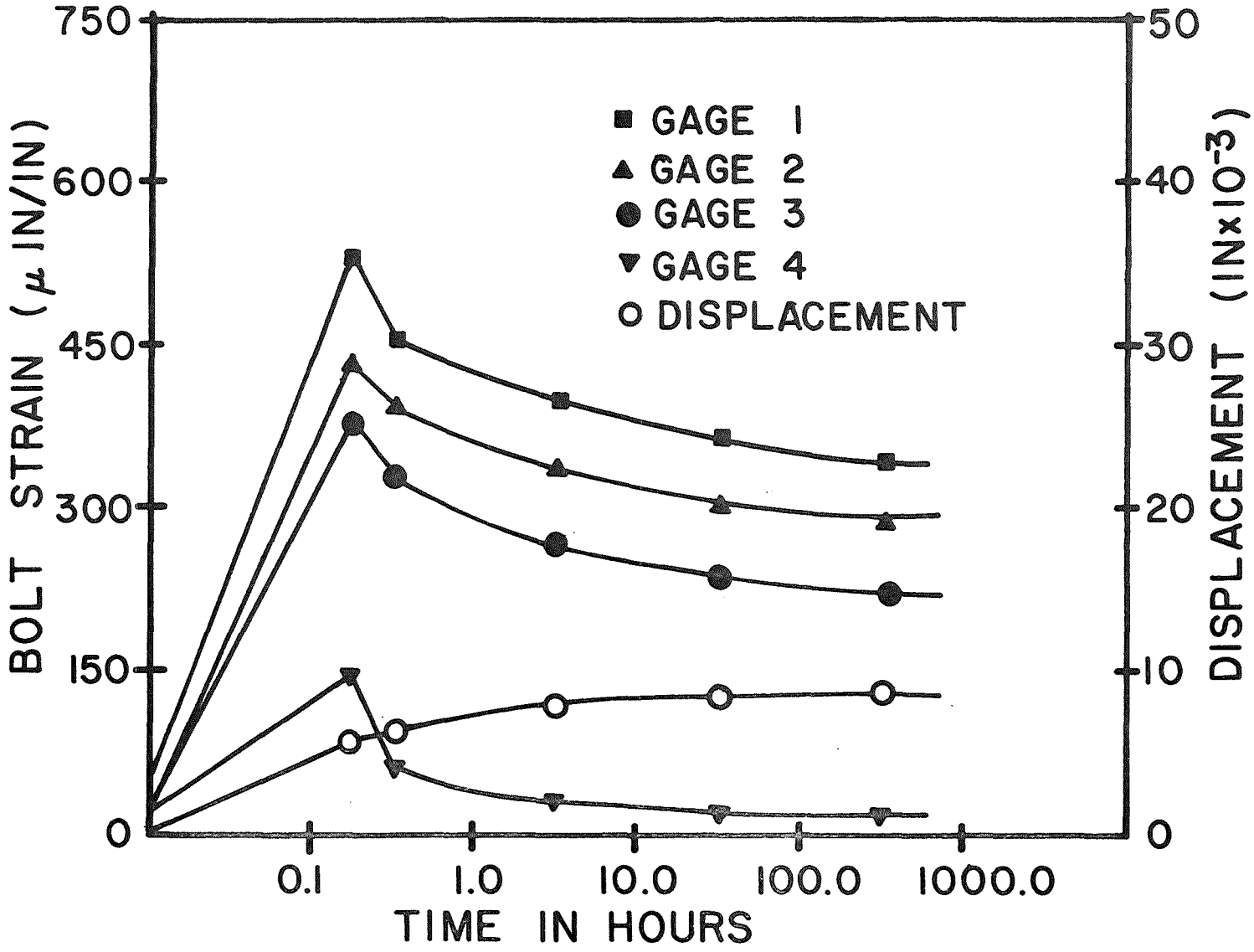

Fig. 5-5 Example of Loss of Load with Time.

Table 5-2

Group Averages of the Percentage of Load Remaining in the Rock Bolt at Various Times (Phase I Rock Bolt Creep Tests).

Installation Description					Average Percent Load Remaining After				
Group Number	Resin Type	Rock Type	Hole Diameter (in.)	Bolt Diameter (in.)	10 Minutes	1 Hour	1 Day	1 Week	1 Month
1	Celtite	Limestone	1 3/8	7/8	91.8	84.5	71.8	67.3	68.5
2	Fasloc	Limestone	1 3/8	7/8	83.1	78.9	67.1	59.9	57.0
3	Celtite	Limestone	1 3/8	3/4	92.2	77.7	67.9	63.4	63.0
4	Fasloc	Limestone	1	3/4	83.3	73.5	60.0	54.2	50.5
5	Fasloc	Limestone	1	1/2	76.6	63.8	48.3	42.3	38.4
6	Fasloc	Limestone	1	3/4	88.5	83.2	72.2	67.6	64.2
7	Celtite	Limestone	1	3/4	94.9	91.5	85.3	82.7	80.8
8	Fasloc	Anna Shale	1	3/4	77.7	63.9	42.9	21.1	14.1
9	Celtite	Anna Shale	1	3/4	82.2	74.3	62.5	56.7	52.5
10	Fasloc	Interbedded Shale	1	3/4	86.9	79.5	68.2	64.2	60.3
11	Celtite	Interbedded Shale	1	3/4	95.5	93.5	89.6	88.4	86.6

It would seem reasonable that rock type would influence the bleed off characteristics of rock bolt installations. It is evident from comparing Groups 6 and 7 with Groups 8 and 9 and Groups 10 and 11 that the weak, highly fractured Anna shale was much less able to support the applied bolt load than were the limestone and interbedded shale.

Load bleed off is not peculiar to resin-grouted bolts. A similar phenomenon in mechanically anchored bolts was reported by Stefanko (Ref. 10). Stefanko examined the mechanisms of load loss and found that retightening aided in restoring and maintaining the required bolt tension. An extension of this research to resin-grouted bolts produced some interesting results. In this study, three groups of instrumented resin-grouted bolts were installed in blocks of limestone rock. The first group (A) consisted of four bolts installed in an approved manner and immediately loaded to 8,000 lb by torqueing a nut on the end of the bolt. The second group (B) consisted of two bolts which were installed, loaded, and subsequently reloaded by torqueing after an initial one-month load bleed-off phase. The third group (C) consisted of two bolts which were installed but not initially loaded. The resin was allowed to cure without load on the bolts for ten days, after which the bolts were loaded to 8,000 lb by torqueing (Table 5-3). Grade 40 7/8-in. diameter reinforcing bars with Celtite resin were placed in 1 3/8-in. holes for all eight installations.

A comparison of Groups A and B indicates the benefits obtained from retorqueing bolts subsequent to installation. It has been hypothesized (Ref. 3) that reloading was effective in reducing the load bleed off because the newly mixed grout, though hard to the touch, was not fully cured and thus could deform in a viscous manner when subjected to loading. The data obtained from Groups A and C tend to nullify this line of reasoning. The load bleed off of these groups was very similar throughout the experiment with the remaining loads after one month, differing by only 2.4 percent (Table 5-4). The load bleed-off mechanism associated with resin-grouted bolts is probably very similar to that of mechanical bolts. It is probable that some initial "seating in" at the resin-rock and resin-bolt interfaces is necessary before loads can be maintained by the bolt. This requirement may be a result of grout shrinkage or of readjustments in stress due to localized material failures at areas of stress concentrations.

Analysis of the data obtained from Group C indicated a relative compressive stress developed in the bolt which increased with increasing distance into the grout. Table 5-5 shows the total compressive strain at each gage location. Since the end of the bolt was free and the uppermost gage was outside the grout column, it may be concluded that the apparent compressive strain in this gage was due to thermal effects of the curing resin. Subtracting this strain from the strains at other gage locations provides an approximate measure of the shrinkage induced strains in the bolts.

It is clear now that substantial load bleed off occurs in resin-grouted bolts with the magnitude of the bleed off being dependent on the installation configuration. There is some question, however, as to whether or not initial and subsequent torqueing or loading of the resin-grouted bolts is necessary and beneficial in roof control applications. An examination of the theory and philosophy of full column resin-grouted bolting as a means of ground control should answer this question.

Table 5-3 Description of Test Installations

Group	Bolt Numbers	Nominal Bar Dia.	Nominal Hole Dia.	Resin Type	Loaded
A	CL1-CL4	7/8 in.	1 3/8 in.	Celtite	Immediately
B	CL10,Cl12	7/8 in.	1 3/8 in.	Celtite	Reloaded
C	CL25,CL26	7/8 in.	1 3/8 in.	Celtite	After 10 days

Table 5-4 Percentage of Load Remaining on the Bolt at Various Times After Installation

Group	Percentage of Load Remaining After				
	10 Minutes	1 hour	1 day	1 week	1 month
A	91.8	84.5	71.8	67.3	68.5
B	99.4	99.1	95.9	92.3	86.9
C	92.7	85.6	77.5	75.0	70.9

Table 5-5 Variation in Strain During Curing of Resin With No Applied Load (After 1 day)

Bolt Number	Depth of Gage Into Grout Column			
	0 in.	2 in.	5 in.	12 in.
CL25	-13μ in./in.	-21μ in./in.	-24μ in./in.	-44μ in./in.
CL26	-11	-20	-20	-28
Average	-12	-20	-22	-36

1. As was previously mentioned, theoretical and laboratory analyses indicate that the load induced at the end of a grouted bolt is transferred into the rock so that at 16 in. within the grout column virtually no load is present in the bolt. This would indicate that only surface loose is supported by the loading and that the loading has little effect on holding weak strata together if the bedding planes are, say, greater than 16 in. from the hole collar.

2. The laboratory test loadings were achieved by tightening a nut at the threaded end of a bolt. Another means of inducing load in the bolt is to apply the full thrust of the bolting machine upward against the bolt subsequent to mixing and prior to resin setup. This action compresses the strata and, after the resin is set and the bolter removed, induces tension in the bolt. According to Nitzsche and Haas (Ref. 11) loading the bolt in this manner would tend to hold weak strata together should a separation or plane of weakness occur between the ends of the grout column. It should also be noted, however, that if the upper end of the grout column occurs at or very near a plane of weakness, the compression induced by the bolting machine in the lower beds would produce a tensile force in the rock near the upper end of the bolt after the thrust was removed. The tensile force need not be large to produce failure along a plane of weakness so detrimental effects may occur as a result of using this method of installation. This mode of loading (applying thrust while resin sets) is also subject to bleed-off characteristics similar to those already described but there is no way of retightening this system after load bleed-off occurs because a head forged integral with the bolt, instead of a nut, is employed. Therefore, surface loose may not be given adequate support.

3. The practice of tightening grouted bolts may be a "throwback" from mechanical bolting procedures. In the latter, tensioning is necessary to remove some of the stretch from the system; stretch is present to a much lesser degree in the grouted bolts as will be shown in subsequent sections of this chapter. The tensioning also served to seat the anchor of the mechanical bolt, another action which is unnecessary with grouted bolts.

4. The grouted system is self-tightening and is advertised as such by some manufacturers. Should a bedding separation, joint, or other discontinuity begin to widen, tension is induced in the bolt providing the needed resistance to separation. Here again, this action is much different from the action of the mechanical bolt in a similar situation. In the latter, resistance to the separation is generated over the length of the bolt rather than over a few inches of effected length as in the grouted case. Under the same load a much greater elongation is allowed in the mechanical system, an action which allows further weakening of the strata.

5. If surface loose is to be supported, some preloading of the bolt would be beneficial to maintain control of surface material. This load need not be great, but only enough to support the weight of the immediate roof without allowing sag of a magnitude which would cause cracking and subsequent deterioration of the roof. For example, if bolts were installed on four-foot centers and six inches of coal were left below a fairly competent shale or limestone roof, the amount of material needing immediate support would be (4 ft) by (4 ft) by (0.5 ft) by

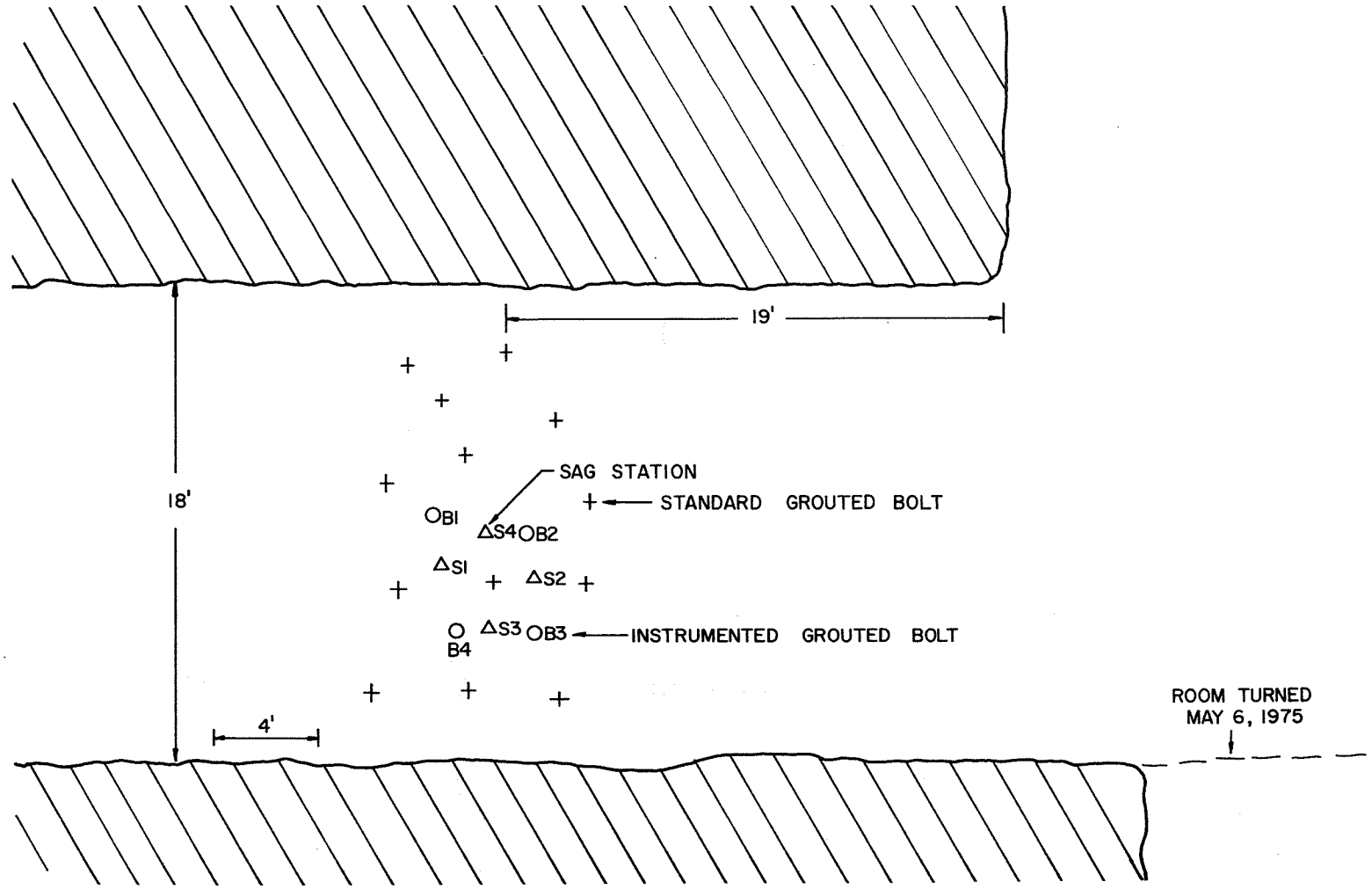

Fig. 6-4 Plan View of Test Site 1, Mine 1, in Shale Roof Showing Location of Instrumentation

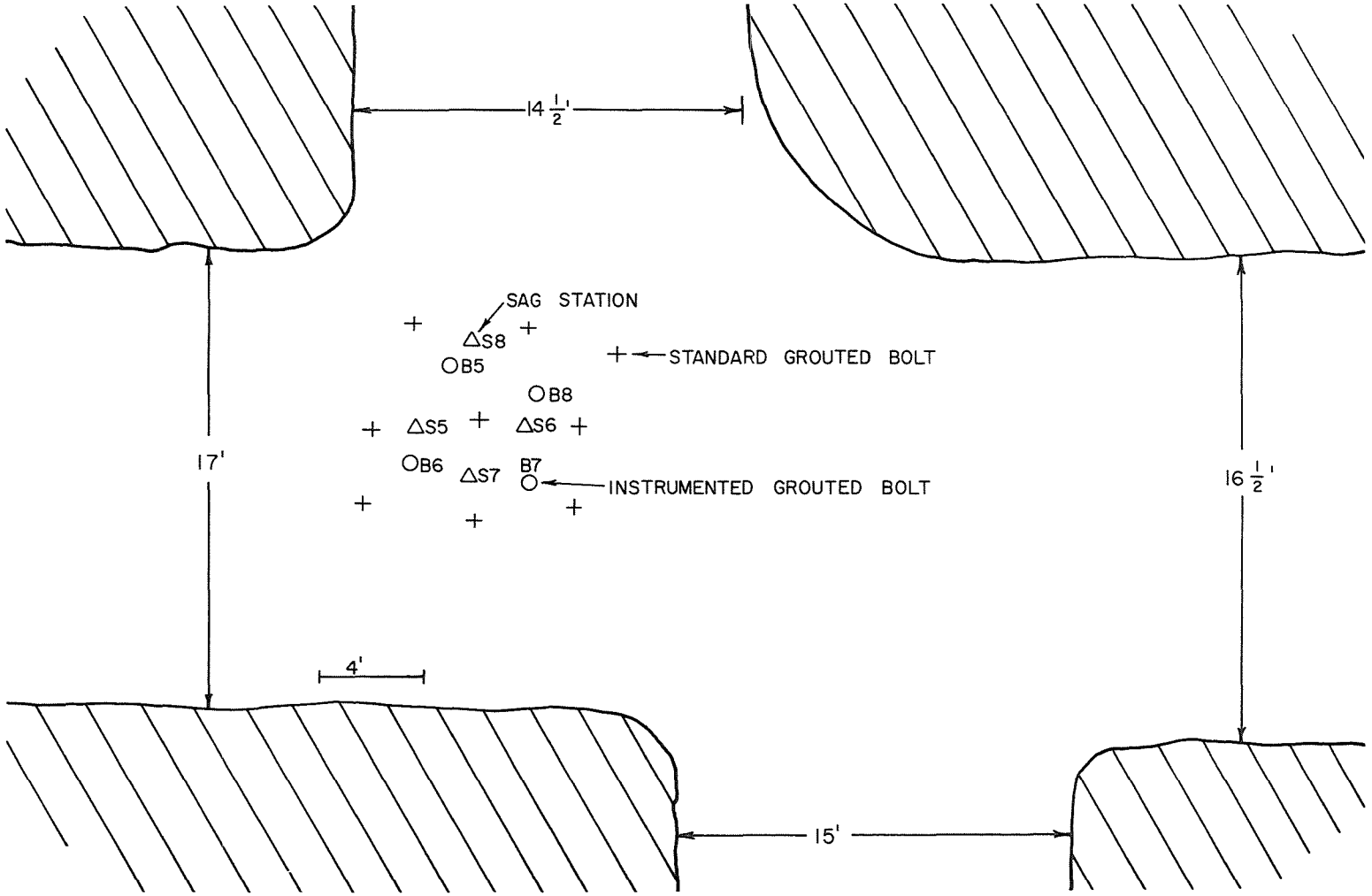

Fig. 6-5 Plan View of Test Site 2, Mine 1, in Limestone Roof Showing Location of Instrumentation.

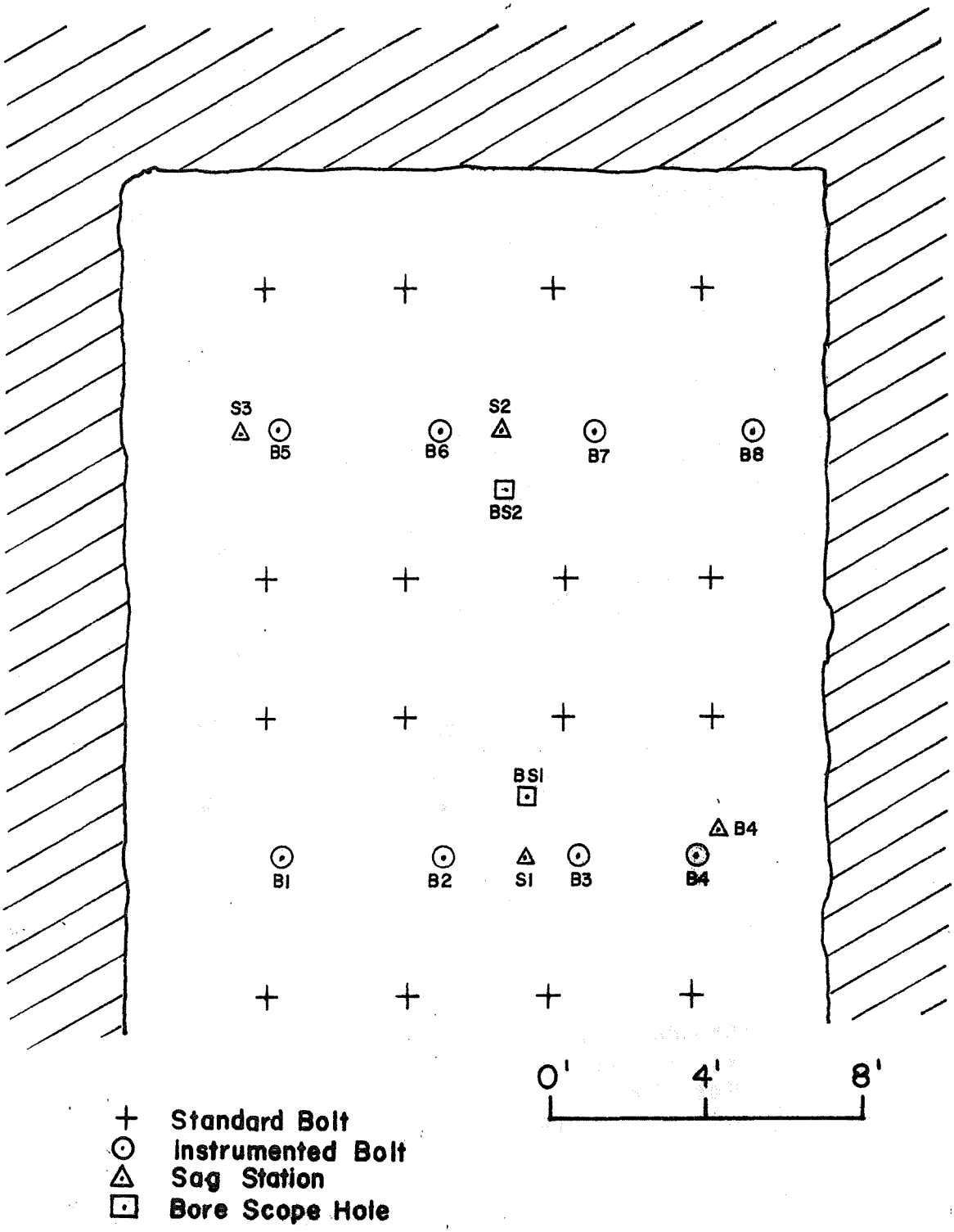

Fig. 6-6 Plan View of Test Site 1, Mine 2, in Shale Roof Showing Location of Instrumentation.

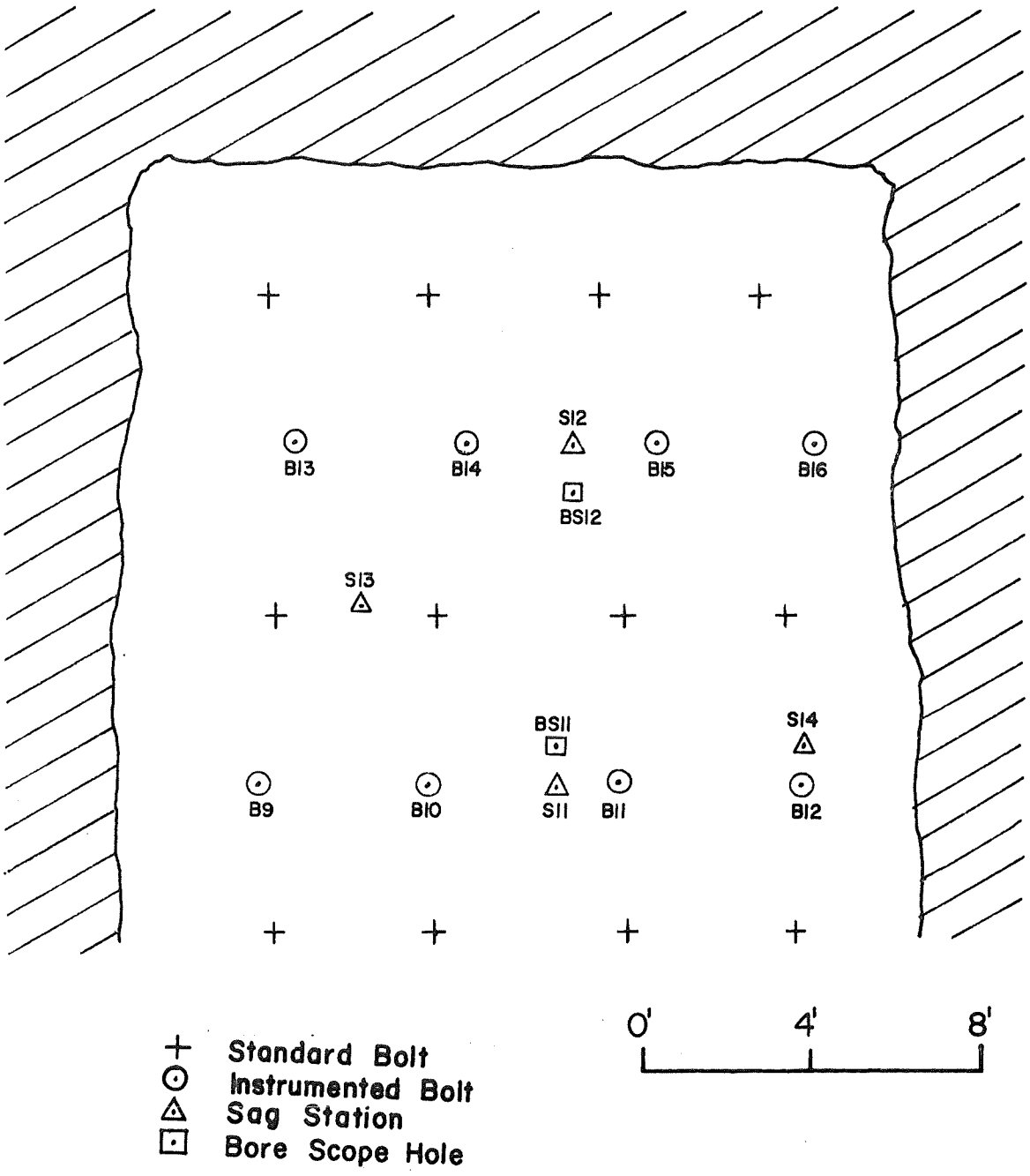

Fig. 6-7 Plan View of Test Site 2, Mine 2, in Shale Roof Showing Location of Instrumentation.

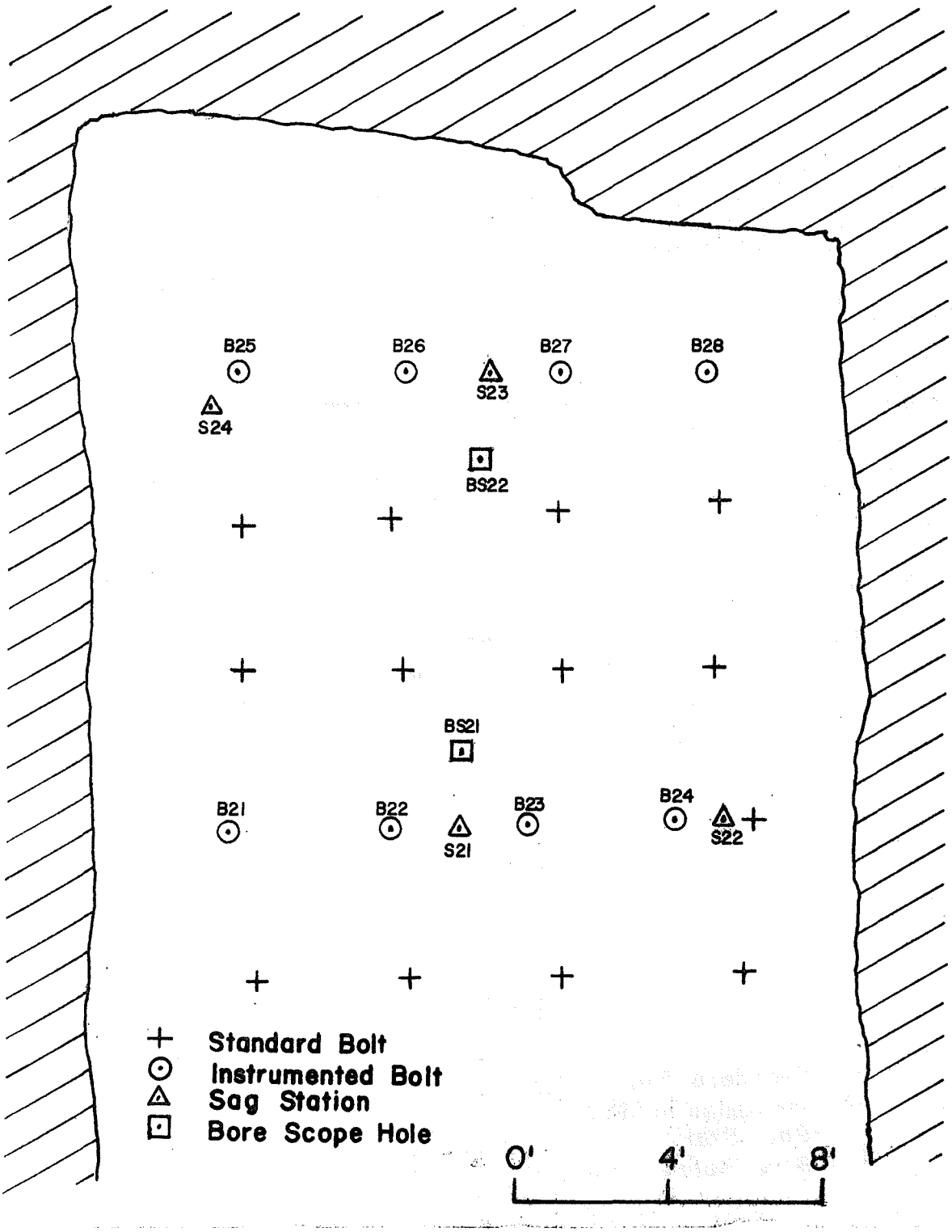

Fig. 6-8 Plan View of Test Site 1, Mine 3, in Shale Roof Showing Location of Instrumentation.

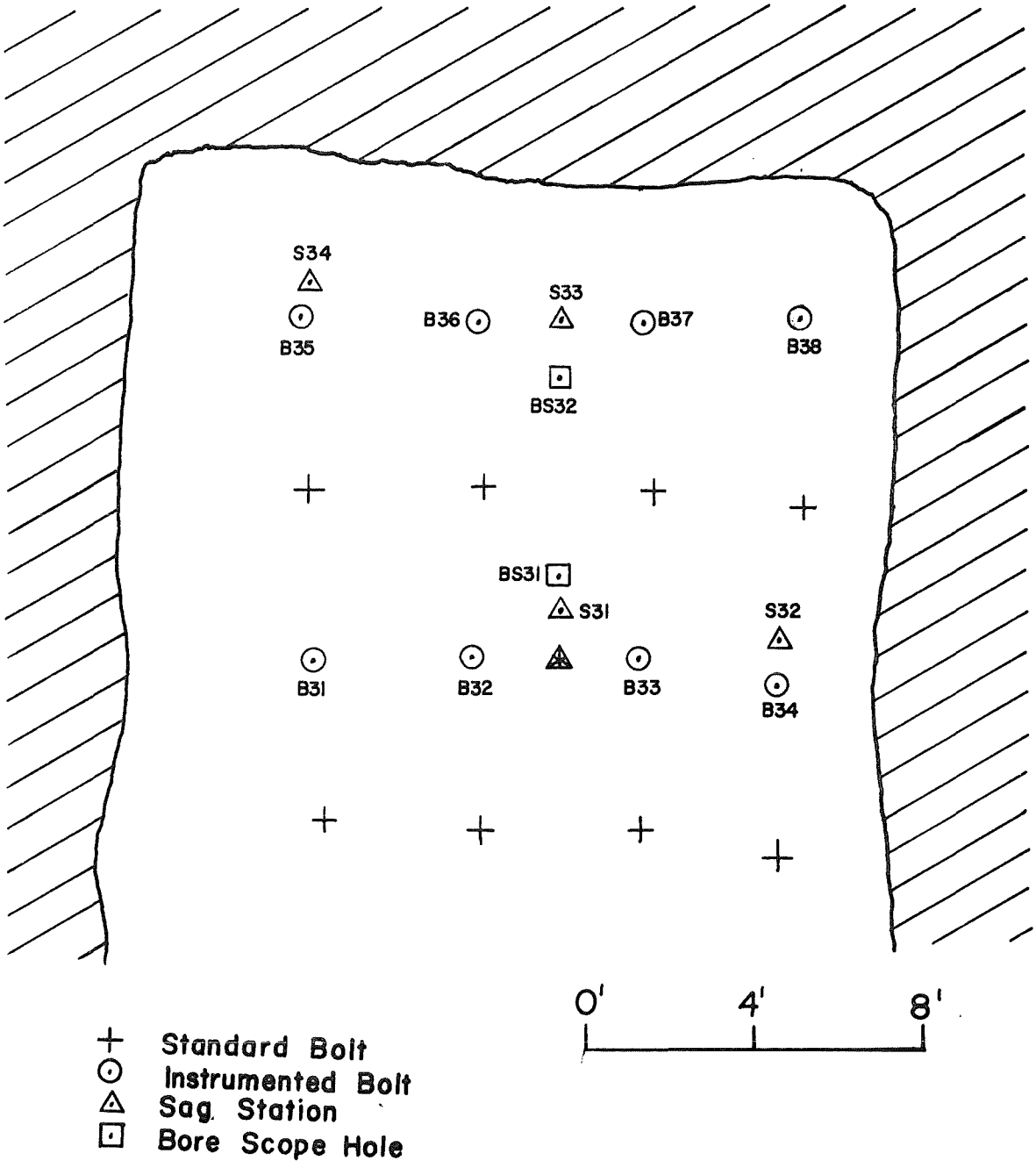

Fig. 6-9 Plan View of Test Site 2, Mine 3, in Shale Roof Showing Location of Instrumentation.

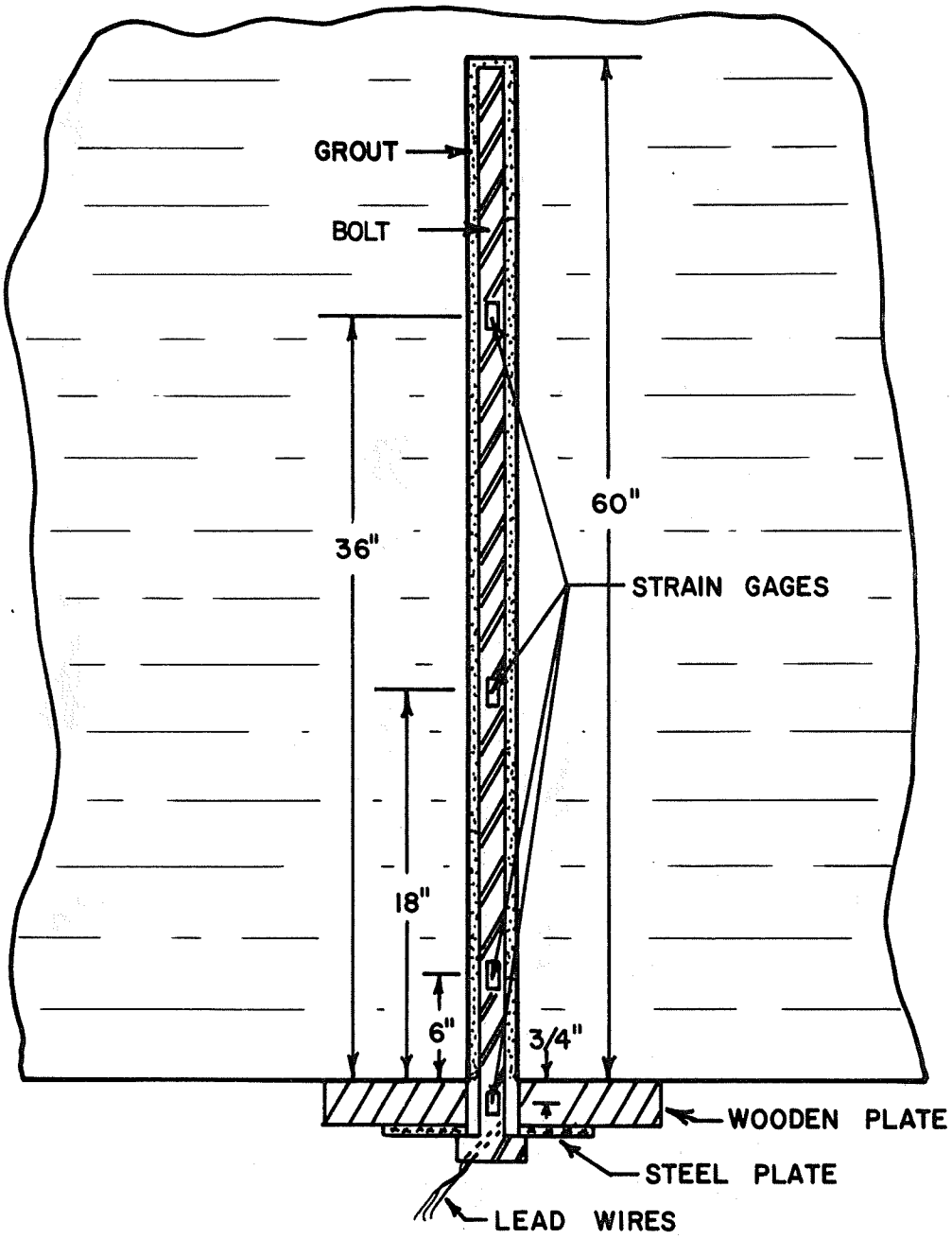

Fig. 6-10 Instrumented Roof Bolt After Installation. (Dimensions given are for Mine 1)

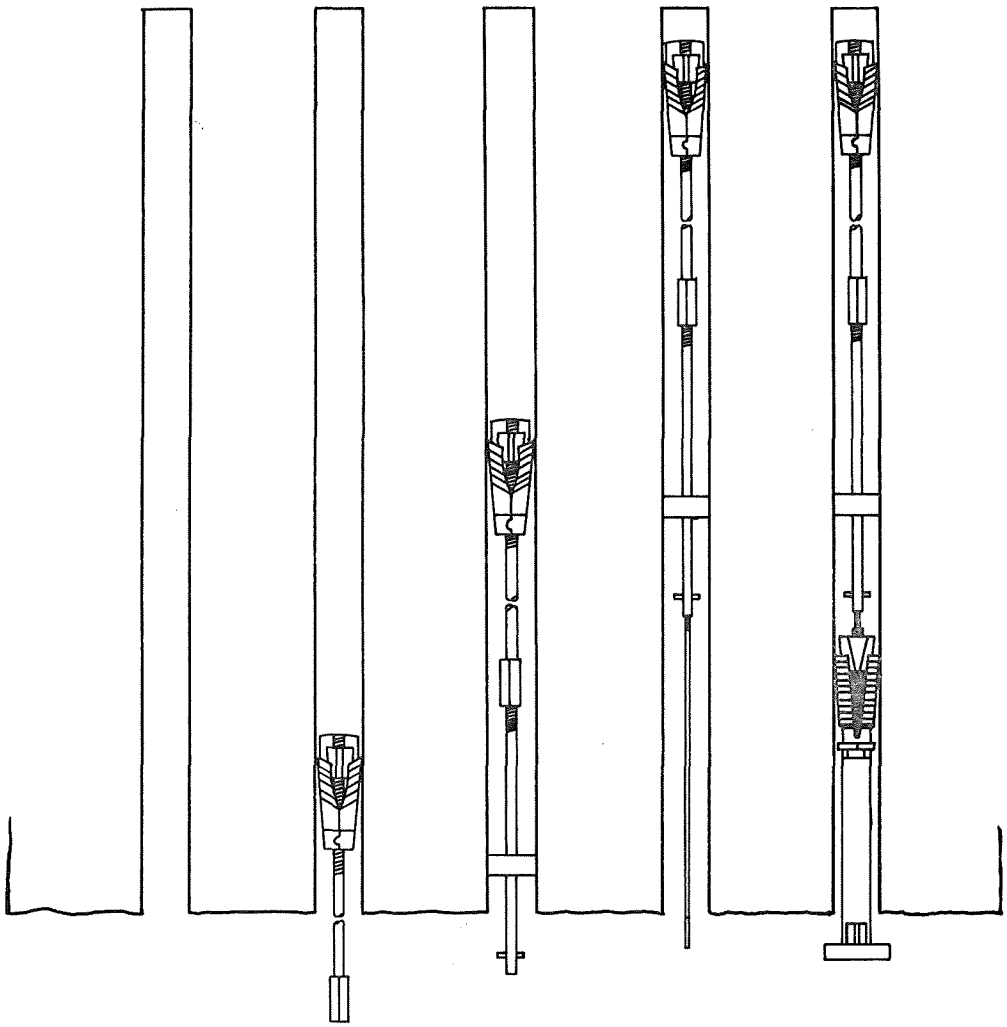

NOT TO SCALE

Fig. 6-11 Five Step Procedure for Installing a Roof Sag Indicator.

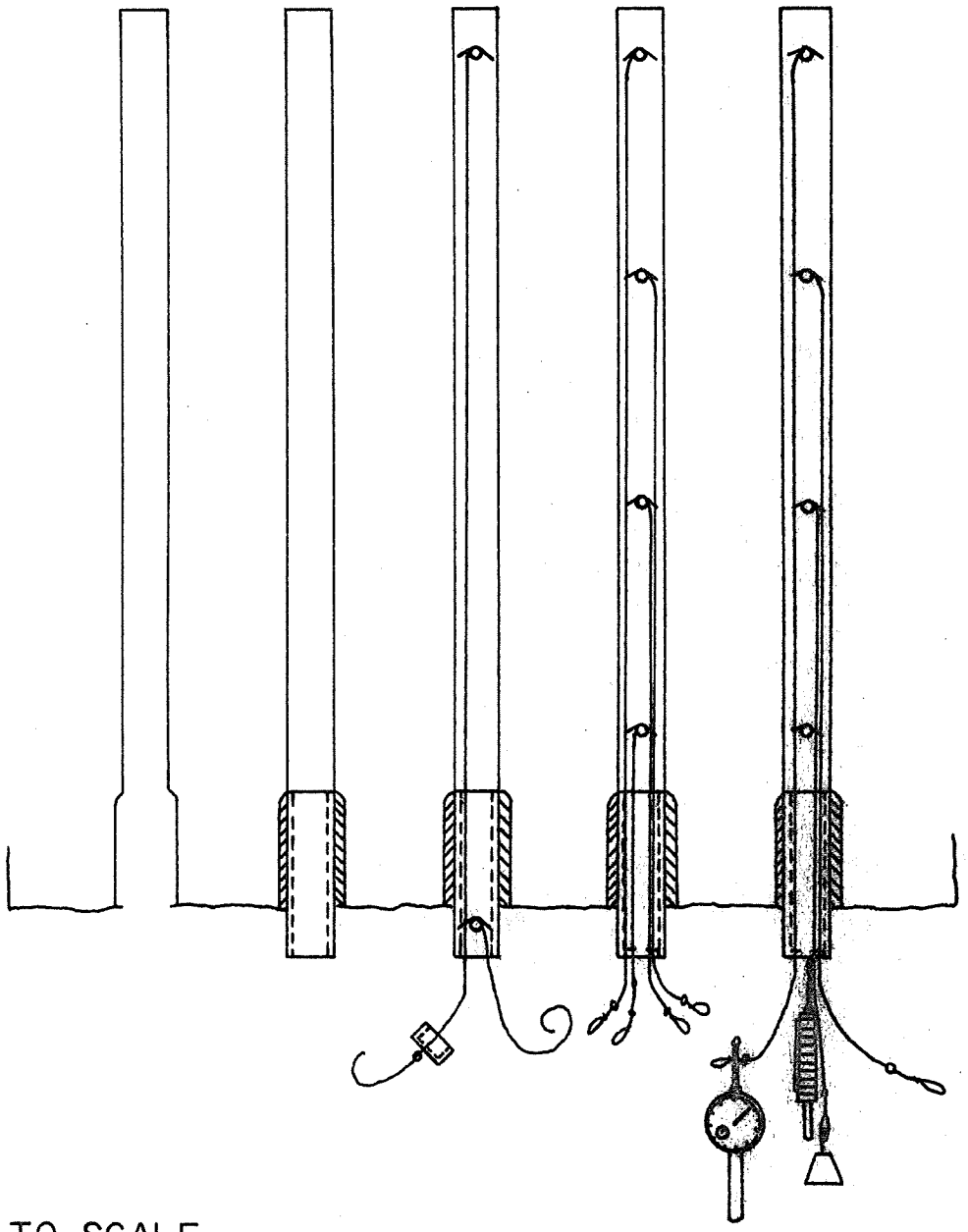

Fig. 6-12 Five-Step Procedure for Installing MESA Wire-Type Roof Sag Indicator.

Strain and sag station readings were taken within one hour after installation and at least once more in the following 12-hour period. Readings were taken at one to two-week intervals thereafter until the test was completed.

Results and Discussion

The six test sites provided data useful in gaining a better understanding of how full-column resin-grouted roof bolts react to various loadings. Although it is not possible at this point to predict the response of grouted bolts to all loading conditions, several interesting observations were made at each site which should be applicable to mines having similar geologic conditions and roof bolt geometries. Among these observations are the presence of installation induced stresses, compressive bolts stresses, and relationships between bolt strain and strata displacements. Detailed bolt load histories are presented in the Third Annual Report (Mine 1) and Appendix B (Mines 2 and 3).

A. Installation Induced Stresses

Strain readings immediately after installation were used to determine the loads induced during bolt installation (Table 6-2). It is evident that the upward thrust of the bolting machine, applied after the grout is thoroughly mixed, is sufficient to cause upward deflection of the roof strata. The bolt load immediately after installation, then, is due to the downward deflection of roof strata which occurs when this thrust is removed.

It was observed that the installation load was not confined to the bearing plate region of the bolt but also often occurs at points farther up the bolts. The variability of installation load from mine to mine may be due to differences in applied thrust and differences in strata stiffness. The weak shale roof in Mine 1 apparently deflected more readily than did the limestone roof, thus a greater installation induced load was noted. A great deal of load variability was noted within each test site of Mine 2. This may be due to either equipment malfunctions or inconsistencies on the part of equipment operators.

B. Load Distribution Along Bolt

It was evident in each mine that great variability in bolt load should be expected within any given mine. An extreme case of this was seen in Mine 1. The strain and displacement histories of Test Sites 1 and 2 provide some interesting information. Bolts in limestone roof rock (Site 2) experienced strains not exceeding about 250 μ in./in., whereas those in shale roof rock (Site 1) had strain magnitudes as great as 3,500 μ in./in. (Figs. 6-13 and 6-14). Three bolts in Site 1 were elongated beyond the yield strain. The mine map (Fig. 6-15) indicates that the two sites are only 70 ft apart; yet the geologic and, hence, bolt loading conditions are much different. This observation has practical significance in that standard roof bolting patterns, which may be determined from test site data, must be capable of supporting the maximum expected load under the worst geologic conditions.

Table 6-2. Installation-Induced Bolt Loads

Mine Number	Roof Rock	Average Installation Load, lb.
1	Shale	3100
	Limestone	2400
2	Shale with Sand Stringers	1750
3	Shale with Sand Stringers	2590

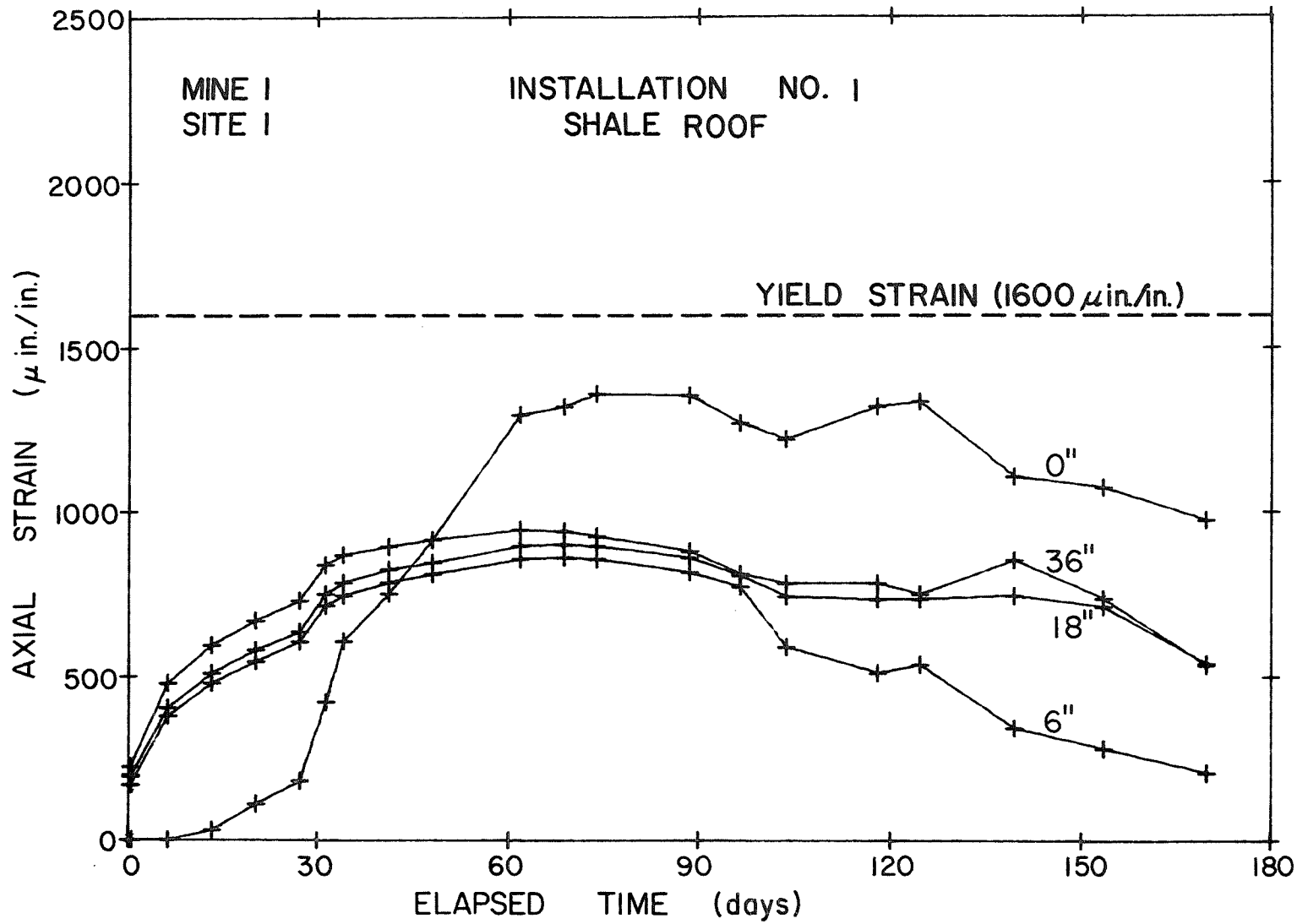

Fig. 6-13 Axial Strain Versus Elapsed Time at Each of Four Gage Locations, Installation No. 1, Shale Roof.

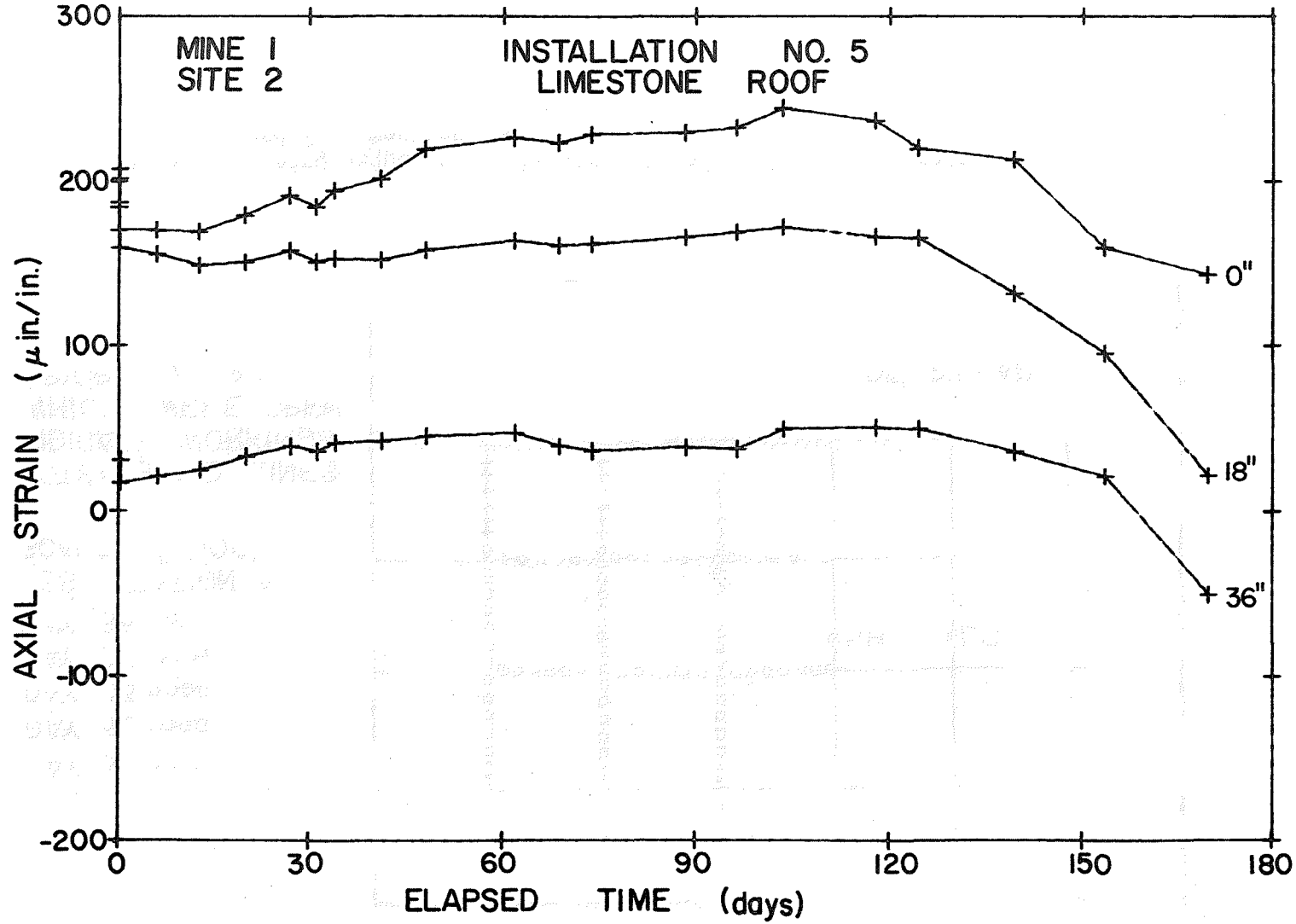

Fig. 6-14 Axial Strain versus Elapsed Time at Each of Three Gage Locations, Installation No. 5, Limestone Roof.

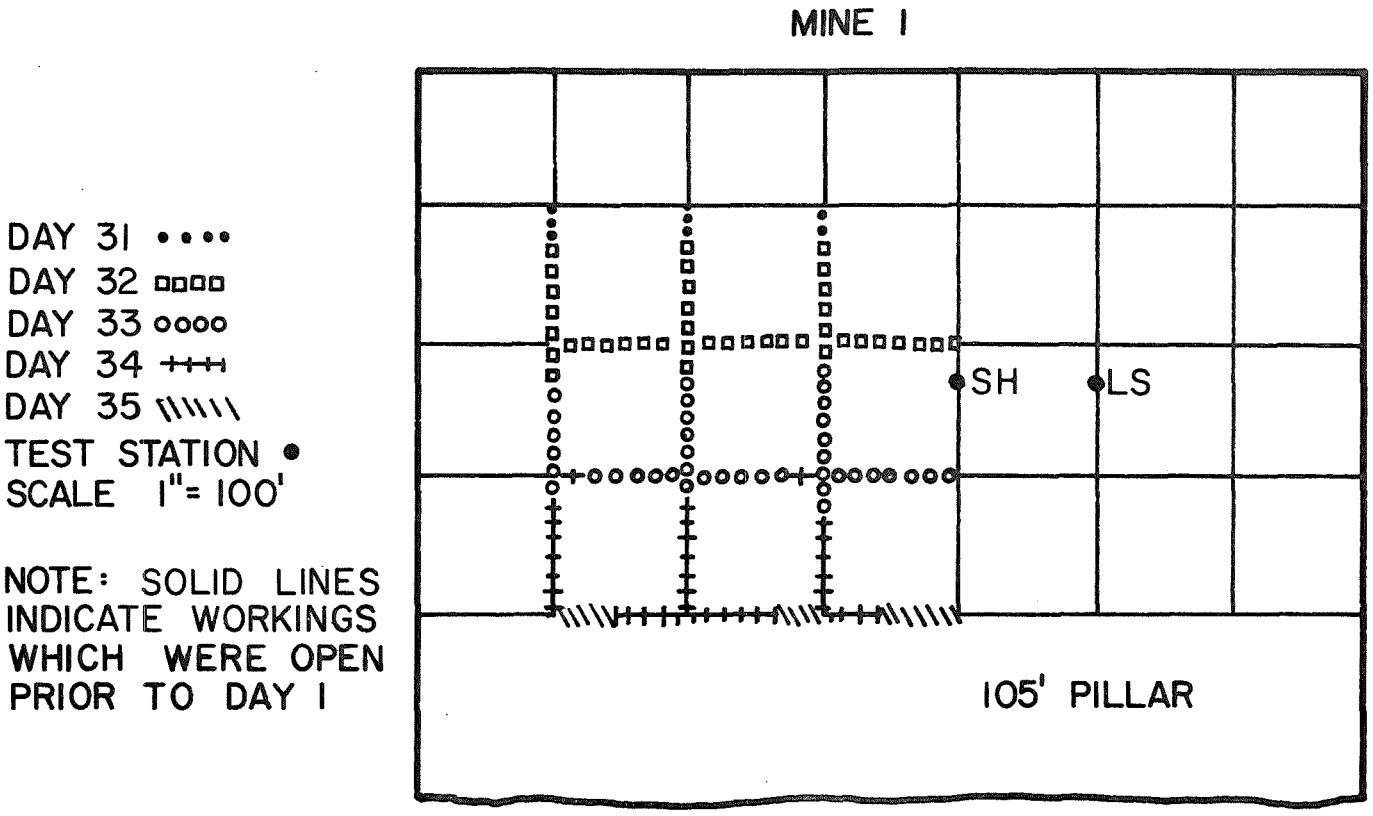

Fig. 6-15 Mining Sequence in the Vicinity of Test Site 1 (shale roof) and 2 (limestone roof).

Laboratory tests on a representative sample gave

$$\gamma = 155 \text{ lb/ft}^3$$

$$E = 2.5 \times 10^6 \text{ psi}$$

$$\varepsilon_{ult} = 400 \ \mu\text{in./in.}$$

so

$$\varepsilon_{max} = \frac{(155 \text{ lb/ft}^3)(16 \text{ ft})^2(1 \text{ ft}/12 \text{ in.})}{2(2.5 \times 10^6 \text{ psi})(3 \text{ in.})}$$

$$\varepsilon_{max} = 220 \ \mu\text{in./in.} = \varepsilon_{nfs}$$

From Eq. (7-3)

$$RF = \frac{\varepsilon_{nfs}}{\varepsilon_f}$$

$$\varepsilon_f = \frac{220 \ \mu\text{in./in.}}{1.9} = 116 \ \mu\text{in./in.}$$

The safety factor may now be calculated:

$$SF = \frac{\varepsilon_{ult}}{\varepsilon_f} = \frac{400}{116}$$

$$SF = 3.45$$

which should be adequate. Note that the strength of the rock was not used directly in obtaining the beam relations leading to the design chart in Fig. 7-1. A trial and error type solution is required to find a value of ε_f which is sufficiently less than the failure strain of the material.

Problem 7-2, Frictional and Suspension Support of Continuous Beams

Suppose now that in Problem 7-1 a layer of shaley limestone 2 ft thick was included in the sequence. The thinner strata would be suspended from the thick layer. From Eq. (7-6)

$$\frac{\Delta\sigma_s}{\sigma_{nfs}} = \alpha C u_i$$

where, from Eq. (7-8)

$$u_i = \left(t_i^2 \ \frac{\sum t_j}{\sum t_j^3} \right) - 1$$

Calculations can be made for the 2-ft thick layer and for one 3-in. thick layer since all eight 3-in. layers will experience the same stresses.

$$u_{24} = (24)^2 \left(\frac{48}{14{,}040}\right) - 1$$

$$u_{24} = 0.969$$

$$u_3 = (3)^2\left(\frac{48}{14{,}040}\right) - 1$$

$$u_3 = -0.969$$

From Tables 7-1a and 7-1b, find $\alpha = 0.938$ and $C = 0.786$ by linear interpolation.

$$\left(\frac{\Delta\sigma_s}{\sigma_{nfs}}\right)_{24} = (0.938)(0.786)(+0.969) = +0.714$$

$$\left(\frac{\Delta\sigma_s}{\sigma_{nfs}}\right)_{3} = (0.938)(0.786)(-0.969) = -0.714$$

Now, from Problem 7-1,

$$\frac{\Delta\sigma_f}{\sigma_{nfs}} = \frac{\Delta\varepsilon_f}{\varepsilon_{nfs}} = -0.473$$

$$\sigma_{nfs} = \frac{\gamma L^2}{2t_i} = \frac{(155\ \text{lb/ft}^3)(16\ \text{ft})^2(1\ \text{ft}/12\ \text{in.})}{2t_i}$$

$$\left(\sigma_{nfs}\right)_{24} = 68.9\ \text{psi}$$

$$\left(\sigma_{nfs}\right)_{3} = 551\ \text{psi}$$

$$\left(\sigma_{fs}\right)_{24} = (68.9)(1-0.473)(1+0.714) = 62.2\ \text{psi}$$

$$\left(\sigma_{fs}\right)_{3} = (551)(1-0.473)(1-0.714) = 83.0\ \text{psi}$$

In this case, the combined effects of friction and suspension decreased the stresses in the thick bed to about 90 percent of the unbolted values. The thin beds were aided much more with stresses being reduced to 15 percent of the unbolted values.

Problem 7-3, Support of a Single Cracked Beam

A 3-ft thick layer of sandstone is overlain by 2 ft of badly fractured shale and mudstone. Laboratory tests show

$E = 2.5 \times 10^6$ psi = Young's modulus of sandstone

$\gamma = 145$ lb/ft^3 = unit weight of sandstone

$\gamma = 160$ lb/ft^3 = unit weight of shale

$C_o = 10{,}000$ psi = compressive strength of sandstone

$\mu = 0.5$ = joint frictional coefficient

The beam-like sandstone layer is loaded vertically by the shale material. Vertical abutment cracks plus several joints at midspan dipping from 75° to 90° from the horizontal are encountered. A factor of safety against crushing of 4.0 will be used since material properties are quite well known.

$$\sigma_{allow} = \frac{C_o}{SF} = \frac{10{,}000}{4.0} = 2{,}500 \text{ psi}$$

$$\bar{\sigma}_{allow} = \frac{\sigma_{allow}}{E} = \frac{2{,}500}{2.5 \times 10^6} = 1{,}000 \times 10^{-6}$$

The vertical load is

$$\bar{q} = \frac{\Sigma q}{E} = \frac{(145 \text{ lb/ft}^3)(3 \text{ ft}) + (160 \text{ lb/ft}^3)(2 \text{ ft})}{(2.5 \times 10^6 \text{ psi})(144 \text{ in.}^2/\text{ft}^2)}$$

$$\bar{q} = 2.10 \times 10^{-6}, \text{ say } 2.0 \times 10^{-6}$$

The horizontal in-situ stress, p, is believed to be nearly zero so

$$\bar{p} = \frac{p}{E} = 0$$

From Table 7-2b, obtain

$\overline{L}$ = 13.3, so

$L = \overline{L}\, D = (13.3)(3) = 40$ ft = span length, also

$\overline{d}$ = 0.0053 which is well below the buckling stage, and

$\alpha_1 = 69.9° < 75°$ indicates sliding is not a problem.

The proposed design should be adequate.

Problem 7-4, Suspension of Incompetent Rock

A 4-ft thick layer of badly fractured shale overlain by a massive bed of limestone is encountered. Joint spacing varies from 3 in. to 12 in. so wire mesh will be used between the roof and the bearing plates. Bolt loads will be distributed by 6-in. by 6-in. steel plates bearing against 2-in. thick hardwood boards. Opening width is 16 ft and the zone to be supported is 24 ft long.

$\gamma = 160$ lb/ft^3 = unit weight of shale

L = 24 ft = length of supported zone

B = 16 ft = width of supported zone

t = 4 ft = thickness of supported zone

Bolts 6 ft long and 5/8 in. in diameter are available. These are high strength bolts with 40,000 psi yield strength. Determine the bolt spacing required to have the bolt load, W_b, be less than two-thirds the yield load of the bolts.

$$W_{yp} = \sigma_{yp} \cdot A = (40{,}000 \text{ psi})\left(\frac{\pi}{4}\right)(5/8)^2$$

W_{yp} = 12,272 lb

$W_{allow} = 2/3\ W_{yp}$ = 8,181 lb

Try four-foot spacing, i.e., 3 bolts per row and 5 rows of bolts.

From Eq. (7-35)

$$W_b = \frac{(160 \text{ lb/ft}^3)(4 \text{ ft})(16 \text{ ft ft})(24 \text{ ft})}{(4)(5)}$$

$$W_b = 12{,}288 \text{ lb, exceeds criteria}$$

Reduce spacing by introducing one more bolt per row and one more row of bolts.

$$W_b = \frac{245{,}760 \text{ lb}}{(5)(6)}$$

$$W_b = 8{,}192 \text{ lb, which is sufficiently close to meeting criteria}$$

Spacing between rows is

$$S_{row} = \frac{24 \text{ ft}}{6} = 4 \text{ ft}$$

Spacing between bolts is

$$S_{bolts} = \frac{16}{5} = 3.2 \text{ ft}$$

A total of 24 bolts is required.

Problem 7-5, Support by Keying Action

Alter the conditions in Problem 7-4 to consider the design of support for the opening if the fractured zone extended upward, say, 20 ft. Use mesh, bearing plates, and bolts to the same specifications but alter bolt spacing to reflect the design criterion given as Eq. (7-36). Mean joint spacing is 9 in.

$$F = \frac{S}{M} \leq 3.0$$

$$S \leq (3.0)(9 \text{ in.})$$

$$S \leq 27 \text{ in. where S is the clear space between bearing plates}$$

Bolt spacing is S + 6 = 33 in. in each direction. This would require 5 bolts per row and about 9 rows of bolts for a total of 45 bolts. Even spacing would result in 32 in. between bolts.

Problem 7-6, Application of the Code of Federal Regulation to Highly Fractured Rock

A 20-ft thick zone of highly fractured shale with a mean joint spacing of 9 in. is encountered as in Problem 7-5. The first criterion is that clear space between bearing plates not exceed three times the mean particle size. This produces the 32 in. spacing calculated in Problem 7-5. Additional criteria are used to determine bolt length.

$$l_1 \geq 2(S_b)$$

$$l_1 \geq 2(32 \text{ in.}) = 64 \text{ in. minimum bolt length}$$

$$l_2 \geq 3(M)$$

$$l_2 \geq 3(9 \text{ in.}) = 27 \text{ in. minimum bolt length}$$

The greater of the two, l_1, is selected and 6-ft long bolts would be used. Other criteria state that these bolts should be tensioned to 60 to 80 percent of their yield strength.

REFERENCES

1. Haas, C.J., Clark, G.B., and Nitzsche, R.N., "An Investigation of the Interactions of Rock and Types of Rock Bolts for Selected Loading Conditions," First Annual Rept., U.S. Bur. Mines Contract No. H-0122110, 1974.

2. Haas, C.J., Keith, H.D., Nitzsche, R.N., Dave, J., Hoffmann, R.L., and Patrick, W.C., "An Investigation of the Interaction of Rock and Types of Rock Bolts for Selected Loading Conditions," Second Annual Rept., U.S. Bur. Mines Contract No. H-0122110, 1975.

3. Haas, C.J., Davis, R.L., Keith, H.D., Dave, J., Patrick, W.C., and Strosnider, J.R., "An Investigation of the Interaction of Rock and Types of Rock Bolts for Selected Loading Conditions," Third Annual Rept., U.S. Bur. Mines Contract No. H-0122110, 1976.

4. Dave, J., "Finite Element Investigation of Bolted Mine Roof Structures," Ph.D. Dissertation, U. of Mo.-Rolla, 1976.

5. Ghaboussi, J., Wilson, E.L., and Isenberg, J., "Finite Element for Rock Joints and Interfaces," J. of Soil Mech. and Found. Div., ASCE, pp. 833-848, October 1973.

6. Panek, L.A., "The Combined Effects of Friction and Suspension in Bolting Bedded Mine Roof," U.S. Bur. Mines Rept. Inv., RI 6139, 1962.

7. Scott, J.J., "Friction Rock Stabilizers and Their Application to Ground Control Problems," paper presented at Fall Meeting, Soc. Min. Engrs. of AIME, Acapulco, Mexico, 1974.

8. Byars, E.F., and Snyder, R.D., Engineering Mechanics of Deformable Bodies, International Press, Pa., p. 371, 1966.

9. Horino, F.G., Duvall, W.I., and Brady, B.T., "The Use of Rock Bolts or Wire Rope to Increase the Strength of Fractured Model Pillars," U.S. Bur. Mines Rept. Inv., RI 7568, 1971.

10. Stefanko, R., "New Look of Long-Term Anchorage: Key to Roof Bolt Efficiency," Min. Eng., pp. 55-59, May 1962.

11. Nitzsche, R.N., and Haas, C.J., "Installation Induced Stresses for Grouted Roof Bolts," Intl. J. Rock Mech. and Min. Sci., Vol. 13, No. 1, pp. 17-24, 1976.

12. Dunham, R.K., "Some Aspects of Resin Anchored Rock Bolting," Tunnels and Tunnelling, pp. 376-385, July 1973.

13. Bennett, G.H., and Herrick, J.D., "Evaluation of Resin and Mechanical Roof Bolting Systems for Strata-Bound Deposits," Final Rept., U.S. Bur. Mines Contract No. H-0230016, 1974.

14. Maher, J., "Comparison of Uniform Four-foot Length, Fully-Grouted Resin Roof Bolts and Alternating Four- and Six-foot Length, Fully-Grouted Resin Roof Bolts," Final Rept., U.S. Bur. Mines Contract No. H-0242029, 1975.

15. Gerdeen, J.C., Snyder, V., and Viegelahn, G.L., "Strain-Gaged Resin-Grouted Roof-Bolt Load Measurements," Soc. for Exp. Stress Analysis, Preprint, Spring Meeting, Maryland, 1976.

16. U.S. Code of Federal Regulations, Title 30 (Mineral Resources), 1976.

17. Panek, L.A., "Principles of Reinforcing Bedded Mine Roof with Bolts," U.S. Bur. Mines Rept. Inv., RI 5156, 1956.

18. Panek, L.A., "Design of Bolting Systems to Reinforce Bedded Mine Roof," U.S. Bur. Mines Rept. Inv., RI 5155, 1956.

19. Obert, L., and Duvall, W.I., Rock Mechanics and the Design of Structures in Rock, John Wiley and Sons, Inc., New York, Chap. 20, 1967.

20. Tsur-Lavie, Y., and Van Ham, F., "The Reinforcement Factor Obtained in Sedimentary Roof Layers by Means of Perpendicular and Oblique Roof Bolts," Israel J. of Technology, Vol. 7, No. 5, 1969.

21. Wright, F.D., "Design of Roof Bolt Patterns for Jointed Rock," Final Rept., U.S. Bur. Mines Grant No. G-0111162,1974.

22. Bucky, P.B., "Effect of Approximately Vertical Cracks on Behavior of Horizontally Lying Roof Strata," Trans. AIME, Vol. 109, pp. 212-229, 1934.

23. Evans, W.H., "The Strength of Undermined Strata," Trans. Inst. of Min. and Met., Vol. 50, pp. 475-500, 1941.

24. Mohr, F., "Rock Pressure and Support," Mine and Quarry Engr., pp. 227-230, June 1956.

25. Haycocks, C., "Mechanics of the Voussoir Arch as Applied to Block Caving," Thesis, Missouri School of Mines and Metallurgy, 1962.

26. Wright, F.D., "Arching Action in Cracked Roof Beams," Sec. 29, Fifth Intl. Strata Control Conf., London, 1972.

27. Aughenbaugh, N.B., and Bruzewski, R.F., "Failure of Roofs in Coal Mines," Final Rept., U.S. Bur. Mines Contract No. H-0232057, 1976.

28. Hoek, E., and Bray, J.W., Rock Slope Engineering, Inst. of Min. and Met., London, 309 pages, 1974.

29. Lang, T.A., "Rock Bolting Speeds Snowy Mountains Project," Civ. Engr., pp. 40-42, February 1958.

30. Stephansson, O., "Stability of Single Openings in Horizontally Bedded Rock," Engr. Geol. Vol. 5, pp. 5-71, 1971.

31. Kmetz, W.J., "Roof Trusses Support Problem Strata," Coal Age, pp. 64-68, January 1970.

32. Hylbert, D.K., "Developing Geological Structural Criteria for Predicting Unstable Mine Roof Rocks," Annual Report, U.S. Bur. Mines Contract No. H-0133018, 1974.

33. Patrick, W.C., and Aughenbaugh, N.B., "Classification of Roof Falls in Coal Mines," paper presented at Fall Meeting, Soc. Min. Engrs. of AIME, St. Louis, Mo., 1977.

34. Parsons, E.W., and Osen, L., "Load Loss from Rock-Bolt Anchor Creep," U.S. Bur. Mines Rept. Inv., RI 7220, 1969.

35. Manula, C.B., Mozumdar, B., and Jeng, D.K., "A Master Environmental Control and Mine System Design Simulator for Underground Coal Mining, Vol. IV, Roof Support Subsystem," Final Rept., U.S. Bur. Mines Grant No. G-0111808, 1974.

APPENDIX A

Computer Program for the Analysis

of

Split-Sets

A listing of the computer program used for the analysis of Split-Set Roof Bolts is presented in this appendix. Ample comment cards have been used to provide better understanding of the program's functions. A description of the required input data has also been provided.

INPUT INSTRUCTIONS

Card 1 Format (12 I5)

Col.	Program Variable	Description
1-5	ERCNT	No. of "interference fit" (ER) values to be given (9 or less)
6-10	RSCNT	No. of "Radius Ratio" (R*) values to be given (10 or less)
11-15	MCNT	No. of "Strain Hardening" (M) values to be given (2 or less)
16-20	ACNT	No. of "Angle" (alpha) values to be given (2 or less)
21-25	PL0	PL01 initializes, and terminates all of the following Plot segments. It must be set to one to produce any plots.
26-30	PL01	Set to 1 to plot a family of ER curves on ETA vs Epsilon for each R*, Alpha and M. Title is "Fig. ___ Strain Distribution Through Split-Set Wall"
31-35	PL02	Set to 1 to plot a family of R* curves on ETA vs Epsilon for each ER, Alpha and M. Title is "Fig. ___ Strain Distribution through Split-Set Wall"
36-40	PL03	Set to 1 to plot a family of ER curves on ETA vs Sigma for each R*, Alpha and M.
41-45	PL04	Set to 1 to plot a family of R* curves on F* vs. ER for each Alpha and M. Title is "Fig. ___ Split-Set Insertion Force--Variable Wall Thickness"
46-50	PL05	
51-55	PL06	Set to 1 to plot a family of ER curves, normal and Shear, vs θ for each R*, Alpha and M. Title is "Fig. ___ Surface Loading on a Split-Set After Installation.

Col.	Program Variable	Description
56-60	PL07	Set to 1 to plot a family of ER curves on F* vs R* for each Alpha and M. Title is "Fig. ___ Split-Set Insertion Force--Variable Interference"

END OF CARD 1

Second Card(s):
Input all the interference (ER) values, (limit 9)
one value per card, Format F8.6

Third Card(s):
Input all the Radius Ratio (R*) values, (limit 10)
one value per card, Format F8.6

Fourth Card(s):
Input all the Strain Hardening Coefficients (m), (limit 2)
one value per card, Format F8.6

Fifth Card(s):
Input all the Alphas (α_s)* values, (limit 2)
one value per card, Format F8.6

Sixth Card(s):
Input coefficient of friction (f) value, (limit 1)
Format F8.6

The ER's are dimensionless interference fits

$$ER = \varepsilon_R = \frac{R_i - R}{R\varepsilon_o}$$

The R*'s are dimensionless wall thicknesses

$$R^* = R/t$$

---

*Note: α_s has only been assigned values in the range of 155° to 165°, thus values outside this range may give convergence problems.

```
C                                                                       00000100
C     INPUT INSTRUCTIONS                                                00000200
C     CARD 1  IS 1215                                                   00000300
C     READ ERCNT,RSCNT,MCNT,ACNT,THEN THE 8 PLOT CONTROL VALUES         00000400
C                                                                       00000500
C     ERCNT IS THE NO. OF ER VALUES                                     00000600
C     RSCNT IS THE NO. OF RSTAR VALUES                                  00000700
C     MCNT IS THE NO. OF STRAIN HARDENING COEFF.                        00000800
C     ACNT IS THE NO OF ALPHA VALUES                                    00000900
C                                                                       00001000
C     IF PLO* IS 0 NOT GENERATED IF NOT 0 THEN IS GENERATED             00001100
C     PLO INITIALIZES THE PLOTS                                         00001200
C     PLO1 PLOTS ER ON R* VS M                                          00001300
C     PLO2 PLOTS R* ON ER VS M                                          00001400
C     WILL PLOT ONLY THE VALUES FOR THE LAST XM VALUE  PLO3             00001500
C     PLO3 PLOTS ON S VS ETA                                            00001600
C     PLO4 PLOTS F ON F* VS ER                                          00001700
C     PLO5 PLOTS F ON F* VS R*                                          00001800
C     PLO6 PLOTS P* AND T* VS THETA                                     00001900
C     PLO7 PLOTS ER ON F* VS R*                                         00002000
C                                                                       00002100
C     ALL THE FOLLOWING ARE E8.6 WITH ONE VALUE PER CARD                00002200
C     ALL THE ER VALUES       LIMIT IS 4                                00002300
C     ALL THE RSTAR VALUES    LIMIT IS 10                               00002400
C     ALL THE STRAIN HARDENING COEFF.     M VALUES     LIMIT IS 2       00002500
C     ALL THE ALPHA VALUES IN DEGREES  LIMIT 2                          00002600
C       ONE FRICTIONAL COEFF.                                           00002700
C                                                                       00002800
C     ALL VALUES ARE TO BE READ IN,IN AN INCREASING ORDER EXCEPT ALPHA  00002900
C     WHICH SHOULD BE IN A DECREASING ORDER                             00003000
C                                                                       00003100
C     THAT IS ALL                                                       00003200
C                                                                       00003300
C     ******************************************************************00003400
C                                                                       00003500
C                                                                       00003600
C     ******************************************************************00003700
C     *                                                                 *00003800
C     *   DESCRIPTION OF VARIABLES -                                    *00003900
C     *                                                                 *00004000
C     *   S      = STRESS                                               *00004100
C     *   E      = TOTAL STRAIN                                         *00004200
C     *   EP     = PLASTIC STRAIN                                       *00004300
C     *   ETA    = DISTANCE FROM CENTROID.                              *00004400
C     *   XM     = STRAIN HARDENING EXPONENT                            *00004500
C     *   RSTAR  = RADIUS                                               *00004600
C     *   ER     = RADIAL STRAIN                                        *00004700
C     *   MSTAR  = MOMENT AT ANY SECTION                                *00004800
```

```
C      *   FSTAR = INSERTATION FORCE                                          *00004900
C      *                                                                      *00005000
C      *   ALL OF THE ABOVE ARE NONDIMENSIONAL VARIABLES.                     *00005100
C      *                                                                      *00005200
C      ************************************************************************00005300
C                                                                             00005400
       IMPLICIT REAL*8(A-H,O-Y)                                               00005500
       REAL*8 MSTAR,NSTAR,NT                                                  00005600
       REAL XINCR,XMIN,XMAX                                                   00005700
       INTEGER ERCNT,RSCNT,MCNT,ACNT                                          00005800
       COMMON    E(41),EP(41),S(41),ETA(41),ER(9),RSTAR(10),XM(2),            00005900
      2 DUMEP(41),ESAVE(9,41,10),FSTAR(  2),F   ,ALPHA(2),SSAVE(10,9,41),00006000
      3 XXEP(41),RALPHA(2),C6(2)    ,FSAVE(  2,9,10)                         00006100
       COMMON/PRINT/DD(6,6)                                                   00006200
       COMMON/CCOM/ASTAR(6)                                                   00006300
       COMMON/AT/KONT,KOUNT,KUNT                                              00006400
       DIMENSION BS(2)                                                        00006500
       DIMENSION Q(6),ZX(41),ZY(41)                                           00006600
       DIMENSION ZC(5,9)                                                      00006700
       COS(X)=DCOS(X)                                                         00006800
       SIN(X)=DSIN(X)                                                         00006900
       ABS(X)=DABS(X)                                                         00007000
       ALOG(X)=DLOG(X)                                                        00007100
       SQRT(X)=DSQRT(X)                                                       00007200
       THIC=.033                                                              00007300
       ALEN=10.                                                               00007400
       BINCR=1.0                                                              00007500
       B=110.                                                                 00007600
       BETA=1.9198                                                            00007700
       NSTAR=.0025/(ALEN*THIC)                                                00007800
       NSTAR=-NSTAR                                                           00007900
       ASTAR(1)=1.                                                            00008000
       ASTAR(2)=1.                                                            00008100
       ASTAR(3)=1.                                                            00008200
       ASTAR(4)=1.                                                            00008300
       ASTAR(5)=NSTAR                                                         00008400
C      TST=0.                                                                 00008500
       DO 700 I=1,41                                                          00008600
       EP(I)=0.0E0                                                            00008700
       DUMEP(I)=0.0E0                                                         00008800
   700 CONTINUE                                                               00008900
C                                                                             00009000
C      MACHINE DEPENDENT I/O DEVICES.  'IN' IS INPUT. 'IO' IS OUTPUT.         00009100
       IN=5                                                                   00009200
       IO=6                                                                   00009300
C                                                                             00009400
       READ(IN,1) ERCNT,RSCNT,MCNT,ACNT,PLC,PLO1,PLO2,PLO3,PLO4,PLO5,PLO600009500
      2,PLO7                                                                  00009600
```

```
    1 FORMAT(16I5)                                                          00009700
      IF(PLO.NE.0) WRITE(IO,108)                                            00009800
      IF(PL01.NE.0) WRITE(IO,101)                                           00009900
      IF(PL02.NE.0) WRITE(IO,102)                                           00010000
      IF(PL03.NE.0) WRITE(IO,103)                                           00010100
      IF(PL04.NE.0) WRITE(IO,104)                                           00010200
C     IF(PL05.NE.0) WRITE(IO,105)                                           00010300
      IF(PL05.NE.0) PL07=1.                                                 00010400
      PL05=0.                                                               00010500
      IF(PL06.NE.0) WRITE(IO,106)                                           00010600
      IF(PL07.NE.0) WRITE(IO,107)                                           00010700
  108 FORMAT(' PLOT INITIALIZED')                                           00010800
  101 FORMAT(' PLOT OF ER ON R* VS M')                                      00010900
  102 FORMAT(' PLOT OF R* ON ER VS M')                                      00011000
  103 FORMAT(' PLOT OF ER ON S VS ETA')                                     00011100
  104 FORMAT(' PLOT OF F ON F* VS ER')                                      00011200
C 105 FORMAT(' PLOT OF F ON F* VS R*')                                      00011300
  106 FORMAT(' PLOT OF P* AND T* VS THETA')                                 00011400
  107 FORMAT(' PLOT OF ER ON F* VS R*')                                     00011500
C                                                                           00011600
CC    DECLARE NUMBER OF POINTS. ***                                         00011700
      NPOINT=41                                                             00011800
C                                                                           00011900
CC    DECLARE SENSITIVITY. ***                                              00012000
      DELTA=0.001                                                           00012100
      ETAMIN=-1.0                                                           00012200
      ETAMAX=1.0                                                            00012300
      XMIN=-25.0                                                            00012400
      XMAX=25.0                                                             00012500
      XINCR=1.                                                              00012600
C     KSW=0                                                                 00012700
CC                                                                          00012800
CC    DECLARE MAXIMUM NUMBER OF ITERATIONS. ***                             00012900
      MAXIT=80                                                              00013000
      MAXIIT=30                                                             00013100
      MAXIT=30                                                              00013200
      MAXIIT=35                                                             00013300
      KBB=0                                                                 00013400
      KB=0                                                                  00013500
      KBK=0                                                                 00013600
      PI=3.14159265358979323846                                             00013700
C                                                                           00013800
CC   ...'PLTKEY' IS INDICATOR OF MAXIMUM ALLOWABLE ACCURACY TO BE           00013900
C    ... PLOTTED.                                                           00014000
      PLTKEY=1.0E-2                                                         00014100
C                                                                           00014200
CC     READ INPUT VALUES. ***                                               00014300
      READ(IN,3,END=5000)(ER(I),I=1,ERCNT)                                  00014400
```

```
    3 FORMAT(E8.6)                                                          00014500
      READ(IN,3)(RSTAR(I),I=1,RSCNT),(XM(I),I=1,MCNT)                       00014600
C                                                                           00014700
C     ECHO-CHECK INPUT VALUES. ***                                          00014800
      WRITE(IO,5)                                                           00014900
    5 FORMAT('1',T40,'*INPUT VALUES*'//T10,'ER',T26,'R*',T42,'M'/)          00015000
      I=0                                                                   00015100
    7 I=I+1                                                                 00015200
      K=0                                                                   00015300
      IF (I .GT. ERCNT) GO TO 8                                             00015400
      WRITE(IO,11) ER(I)                                                    00015500
      K=K+1                                                                 00015600
    8 IF (I .GT. RSCNT) GO TO 9                                             00015700
      IF (K .LE. 0) WRITE(IO,15)                                            00015800
      K=K+1                                                                 00015900
      WRITE(IO,12) RSTAR(I)                                                 00016000
    9 IF (I .GT. MCNT) GO TO 10                                             00016100
      IF (K .LE. 0) WRITE(IO,15)                                            00016200
      K=K+1                                                                 00016300
      WRITE(IO,13) XM(I)                                                    00016400
      GO TO 7                                                               00016500
   10 IF (K) 17,17,7                                                        00016600
   11 FORMAT(' ',T5,F10.4)                                                  00016700
   12 FORMAT('+',T21,F10.4)                                                 00016800
   13 FORMAT('+',T37,F10.4)                                                 00016900
   15 FORMAT(' ')                                                           00017000
C                                                                           00017100
   17 READ(IN,3)(ALPHA(I),I=1,ACNT), F                                      00017200
C                                                                           00017300
      IF(ACNT.EQ.2) WRITE(IO,4) ALPHA(1),ALPHA(2),F                         00017400
    4 FORMAT(' ','VALUES FOR ALPHA ARE ',2F7.2/' VALUES FOR F ARE ',        00017500
     $       1F6.2)                                                         00017600
      IF(ACNT.EQ.1) WRITE(IO,6) ALPHA(1),F                                  00017700
    6 FORMAT(' ','VALUES FOR ALPHA ARE ',1F7.2/' VALUES FOR F ARE ',        00017800
     2  1F6.2)                                                             00017900
C     LOAD THE ARRAY 'ETA'. ***                                             00018000
      ETA(1)=ETAMIN                                                         00018100
C     ..CALCULATE INCREMENT OF ETA....                                      00018200
C                                                                           00018300
      EINCR=ABS(ETAMAX-ETAMIN)/(NPOINT-1)                                   00018400
      DO 18 I=2,NPOINT                                                      00018500
      ETA(I)=ETA(I-1)+EINCR                                                 00018600
      IF ((ABS(ETA(I))) .LT. 1.0E-8) ETA(I)=0.0                             00018700
   18 CONTINUE                                                              00018800
C                                                                           00018900
C     CONVERT DEGREES TO RADIANS. ***                                       00019000
      DO 19 KL=1,ACNT                                                       00019100
      RALPHA(KL)=ALPHA(KL)*PI/180.0                                         00019200
```

```
   19 CONTINUE                                                          00019300
C                                                                       00019400
      LINE=2                                                            00019500
      NPAGE=0                                                           00019600
      CALL HEADER(IO,NPAGE)                                             00019700
      IF(PLO) 21,20,21                                                  00019800
   21 CONTINUE                                                          00019900
C                                                                       00020000
CC                                                                      00020100
C     INITIALIZE PLOTTER ROUTINES. ***                                  00020200
C                                                                       00020300
      IPEN=1                                                            00020400
      IPEN=2                                                            00020500
      CALL PEN$(IPEN)                                                   00020600
      CALL PENPOS('FOR DAVIS BY BARNHART',21,0)                         00020700
C                                                                       00020800
CC    BEGIN ITERATION PROCESS. ***                                      00020900
C                                                                       00021000
      XMIN=0.                                                           00021100
      XMAX=0.                                                           00021200
   20 DO 600 I=1,MCNT                                                   00021300
      DO 500 K=1,RSCNT                                                  00021400
      DO 491 J=1,ERCNT                                                  00021500
      DO 491 IA=1,ACNT                                                  00021600
      WRITE(IO,15)                                                      00021700
      WRITE(IO,23) ER(J),RSTAR(K),XM(I)                                 00021800
   23 FORMAT(1X,'ER=',F10.4,5X,'R*=',F10.4,5X,'M=',F10.4)               00021900
      LINE=LINE+1                                                       00022000
      IF(LINE.LT.50) GO TO 24                                           00022100
      CALL HEADER (IO,NPAGE)                                            00022200
      LINE=2                                                            00022300
   24 CONTINUE                                                          00022400
      Z=-1.0+RSTAR(K)*ALOG((RSTAR(K)+ .5)/(RSTAR(K)-.5))                00022500
C                                                                       00022600
      B=60.0                                                            00022700
      BINCR=10.0                                                        00022800
      BETA=B*PI/180.0                                                   00022900
C     REINITIALIZE INTEGRAL TO ZERO.                                    00023000
      X=0.0E0                                                           00023100
   30 BSTART=B                                                          00023200
      BBETA=0.0                                                         00023300
      KB=-6                                                             00023400
      KBK=0                                                             00023500
      BETA2=0.                                                          00023600
      KUNT=0                                                            00023700
   29 KONT=0                                                            00023800
   28 KOUNT=0                                                           00023900
C                                                                       00024000
```

```
   22 DO 100 L=1,NPOINT                                                  00024100
      ACCRCY=DELTA                                                       00024200
   25 E(L)=(ER(J)-2.*NSTAR-.5*X)*(Z/(Z+1.0))*(1.0+(1.0/Z*ETA(L)/         00024300
     2   (2.*RSTAR(K)+ETA(L))))+.5*X+NSTAR                              00024400
C     TEST NEW VALUE OF 'E' AND CALCULATE 'S'.                          00024500
      IF (E(L) .GT. 1.0) GO TO 50                                        00024600
      IF (E(L) .LT. -1.0) GO TO 60                                       00024700
C                                                                        00024800
C     WE GET HERE IF 'E' IS BETWEEN -1 AND 1.                            00024900
      S(L)=E(L)                                                          00025000
      EP(L)=E(L)                                                         00025100
      GO TO 90                                                           00025200
C                                                                        00025300
C     WE GET HERE WHEN 'E' IS GREATER THAN 1.                            00025400
   50 S(L)=XM(I)*(E(L)-1.0)+1.0                                          00025500
      EP(L)=(1.0-XM(I))*(E(L)-1.0)                                       00025600
      GO TO 90                                                           00025700
C                                                                        00025800
C     WE GET HERE WHEN 'E' IS LESS THAN -1.                              00025900
   60 S(L)=XM(I)*(E(L)+1.0)-1.0                                          00026000
      EP(L)=(1.0-XM(I))*(E(L)+1.0)                                       00026100
C                                                                        00026200
C     PATHS REJOIN HERE. ***                                             00026300
   90 CONTINUE                                                           00026400
  100 CONTINUE                                                           00026500
C     CALCULATE NEW VALUE OF INTEGRAL. ***                               00026600
      X=SIMPSN(EP,ETAMIN,ETAMAX,NPOINT-1)                                00026700
C                                                                        00026800
      DO 150 LL=1,NPOINT                                                 00026900
      IF ((ABS(E(LL))) .LE. 1.0) GO TO 150                               00027000
      GO TO 180                                                          00027100
  150 CONTINUE                                                           00027200
      ACC=0.0                                                            00027300
      GO TO 240                                                          00027400
C                                                                        00027500
CC                                                                       00027600
C ***************************************************************      00027700
C *                C O N V E R G E N C E   C H E C K            *      00027800
C ***************************************************************      00027900
C                                                                        00028000
C         THIS ROUTINE TESTS FINAL CONVERGENCE FOR VARIABLE 'EP'.        00028100
C     IF CONVERGENCE IS NOT ACHIEVED, CONTROL IS PASSED BACK TO          00028200
C     THE CALCULATION ROUTINE.                                           00028300
C                                                                        00028400
  180 IF (KOUNT) 220,220,190                                             00028500
  190 IF(0.999-XM(I)) 220,220,191                                        00028600
  191 DO 200 N=1,NPOINT                                                  00028700
      IF((ABS((EP(N)-DUMEP(N))/DUMEP(N))).LE. DELTA) GO TO 200           00028800
```

```
C      CONVERGENCE NOT MET.  RETAIN PRESENT VALUES AND RECALCULATE. ***   00028900
       GO TO 220                                                          00029000
  200  CONTINUE                                                           00029100
       GO TO 240                                                          00029200
C                                                                         00029300
C *** SAVE PRESENT POINTS. ***                                            00029400
  220  KOUNT=KOUNT+1                                                      00029500
       IF (KOUNT-MAXIT) 225,235,235                                       00029600
  225  DO 230 KK=1,NPOINT                                                 00029700
       DUMEP(KK)=EP(KK)                                                   00029800
  230  CONTINUE                                                           00029900
       GO TO 22                                                           00030000
C                                                                         00030100
C      THIS LOOP IS ENTERED AFTER THE MAXIMUM NUMBER OF ITERATIONS        00030200
C      HAVE BEEN REACHED.  CALCULATE THE ACCURACY AND PRINT OUT RESULTS.  00030300
  235  DO 237 L=1,NPOINT                                                  00030400
       IF(DUMEP(L).EQ.0.) GO TO 237                                       00030500
       ACC=ABS((EP(L)-DUMEP(L))/DUMEP(L))                                 00030600
       ACCRCY=ACC                                                         00030700
  237  CONTINUE                                                           00030800
C                                                                         00030900
  240  CONTINUE                                                           00031000
       DO 92 IC=1,NPOINT                                                  00031100
       XXEP(IC)=ETA(IC)*EP(IC)                                            00031200
   92  CONTINUE                                                           00031300
       XNEW=SIMPSN(XXEP,ETAMIN,ETAMAX,NPOINT-1)                           00031400
       MSTAR=4.*RSTAR(K)*(ER(J)-2*NSTAR-0.5*X)*(Z/(Z+1.0))-XNEW           00031500
C                                                                         00031600
       NT=NSTAR                                                           00031700
       CALL LINEQ(5,      ER(J),RSTAR(K),BETA,MSTAR,RALPHA(IA))           00031800
       NSTAR=ASTAR(5)                                                     00031900
        KONT=KONT+1                                                       00032000
       IF(NT.EQ.0) GO TO 80                                               00032100
       IF(KONT-MAXIT) 91,93,93                                            00032200
   91  AC=0.                                                              00032300
       IF(ABS((NSTAR-NT)/NT).LE.DELTA) GO TO 94                           00032400
       GO TO 28                                                           00032500
   80  IF(KONT-MAXIT) 28,83,83                                            00032600
   83  AC=ABS(NSTAR)                                                      00032700
       GO TO 94                                                           00032800
   93  AC=ABS((NSTAR-NT)/NT)                                              00032900
   94  CONTINUE                                                           00033000
       Q(1)=F     *SIN(RALPHA(IA))-COS(RALPHA(IA))                        00033100
       Q(2)=BETA**4.*SIN(BETA)+12.*BETA*BETA*SIN(BETA)                    00033200
       Q(2)=-Q(2)                                                         00033300
       Q(3)=-ASTAR(4)*SIN(BETA)+ASTAR(1)*BETA*BETA*SIN(BETA)+ASTAR        00033400
      2     (2)*(BETA**3.*COS(BETA)-3.*BETA*BETA*SIN(BETA))+ASTAR(3)      00033500
      3     *BETA*COS(BETA)                                               00033600
```

```
      Q(4)=F     *COS(RALPHA(IA))+SIN(RALPHA(IA))                                00033700
      Q(5)=         -  BETA**4.*COS(BETA)-12.*BETA*BETA*COS(BETA)                00033800
      Q(6)=           ASTAR(4)*(1.-COS(BETA))+ASTAR(1)*          BETA*BETA      00033900
     2*COS(BETA)-ASTAR(2)*(3.*BETA*BETA*COS(BETA)+BETA**3.*SIN(BETA))           00034000
     3         -ASTAR(3)*          BETA*SIN(BETA)-ASTAR(5)/RSTAR(K)             00034100
      FSTAR(    IA)=(Q(3)-Q(6)*Q(2)/Q(5))/(Q(1)-Q(4)*Q(2)/Q(5))                 00034200
      C6(IA)=(Q(3)-FSTAR(    IA)*Q(1))/Q(2)                                     00034300
      C4=ASTAR(1)+12.*C6(IA)                                                    00034400
      C3=ASTAR(2)-4.*C6(IA)                                                     00034500
      C1=ASTAR(3)+6.*C3-2.*C4+24.*C6(IA)                                        00034600
      C2=ASTAR(4)-C1+6.*C3-2.*C4+24.*C6(IA)                                     00034700
      C2=-C2                                                                    00034800
      BETA=       (C1/2.)*(C1/2.)+C3*((MSTAR-4.*F     *FSTAR(    IA)          00034900
     2*RSTAR(K)*RSTAR(K)-4.*NSTAR*RSTAR(K))/(4.*RSTAR(K)*RSTAR(K)))             00035000
      BETA=ABS(BETA)                                                            00035100
       BETA=SQRT(BETA)                                                          00035200
      BETA=( BETA-C1/2)/(C3/2)                                                  00035300
      IF(BETA.GE.0.) GO TO 87                                                   00035400
      BETA=  (BETA*C3/2+C1/2)                                                   00035500
      BETA=(-BETA-C1/2)/(C3/2)                                                  00035600
C     WRITE(IO,184)                                                           00035700
C184  FORMAT('  - ROOT USED')                                                  00035800
      IF(BETA.GE.0.) GO TO 87                                                   00035900
C     WRITE(IO,188)                                                           00036000
C188  FORMAT('  SQUARE NEG.')                                                 00036100
 87   CONTINUE                                                                 00036200
      BETA=ABS(BETA)                                                            00036300
      BETA=SQRT(BETA)                                                           00036400
      KUT=KUNT+1                                                                00036500
       BETAB=BETA*180./PI                                                       00036600
      IF(KUT.LT.MAXIIT+2) GO TO 242                                             00036700
       IF(LINE.LT.47) GO TO 181                                                 00036800
      CALL HEADER (IO,NPAGE)                                                    00036900
      LINE=2                                                                    00037000
181   CONTINUE                                                                 00037100
      WRITE(IO,185)(II,ASTAR(II),II=1,5)                                        00037200
185   FORMAT(5X,5(5X,'ASTAR(',I1,')=',1PE10.3))                                 00037300
      WRITE(IO,186)                                    C1,C2,C3,C4,C6(IA)       00037400
186   FORMAT(5X,'C1=',1PE10.3                                                   00037500
     2,5X,'C2=',1PE10.3,5X,'C3=',1PE10.3,5X,'C4=',1PE10.3,5X,'C6=',             00037600
     31PE10.3)                                                                  00037700
      WRITE(IO,183) NSTAR                                                       00037800
183   FORMAT(10X,' N VALUE IS',1PE10.3)                                         00037900
      WRITE(IO,187) B                                                           00038000
187   FORMAT(10X,'B=',1PE20.13)                                                 00038100
      WRITE(IO,89) BETAB,KONT,KUT,KOUNT                                         00038200
 89   FORMAT(10X,' BETA=',1PE20.13,9X,' KONT =',I3 ,10X,'KUNT-',I3 ,10X,00038300
     2'KOUNT=',I3 //)                                                           00038400
```

```
      LINE=LINE+7                                                       00038500
  242 CONTINUE                                                          00038600
  241 ACA=0.                                                            00038700
  244 CONTINUE                                                          00038800
      FSTAR(   IA)=2.*F    *(C2*BETA+C4*BETA**3./3+C6(IA)*BETA**5.      00038900
     2   /5.+FSTAR(   IA))                                            00039000
      FSAVE(   IA,J,K)=FSTAR(   IA)                                     00039100
C                                                                       00039200
C     OUTPUT RESULTS.  ***                                              00039300
C                                                                       00039400
      IF(KUT.LT.MAXIIT) GO TO 27                                        00039500
  126 WRITE(IO,89) BETAB,KONT,KUT,KOUNT                                 00039600
      WRITE(IO,26)                                                      00039700
   26 FORMAT(/T7,'E',T19,'EP',T31,'ER',T43,'S',T55,'R*',T67,'ETA',      00039800
     2 T79,'Z*',T90,'M',T102,'ACCURACY')                                00039900
      LINE=LINE+1                                                       00040000
      IF(LINE.LT.50) GO TO 27                                           00040100
      CALL HEADER(IO,NPAGE)                                             00040200
      LINE=2                                                            00040300
   27 CONTINUE                                                          00040400
      DO 250 L=1,NPOINT                                                 00040500
      IF( KUT.LT.MAXIIT) GO TO 250                                      00040600
      WRITE(IO,245)E(L),EP(L),ER(J),S(L),RSTAR(K),ETA(L),Z,XM(I),ACCRCY 00040700
  245 FORMAT(' ',10F12.4)                                               00040800
      LINE=LINE+1                                                       00040900
  251 IF(L-NPOINT)248,246,248                                           00041000
  246 CONTINUE                                                          00041100
      ACA=BINCR                                                         00041200
      WRITE(IO,247) MSTAR,(F                ),(FSTAR(   IA)           ), 00041300
     2C6(IA)    ,ALPHA(IA)    ,AC,ACA                                   00041400
C                                                                       00041500
C******  FORMAT CHANGES NEEDED FOR FCNT                                 00041600
C                                    # FOR FCNT        # FOR FCNT      00041700
  247 FORMAT(' ***MSTAR=',E12.4,'   F=',1F10.6,3X,' F*=',1F10.6,        00041800
     23X,'C6*=',F10.6,3X,'ALPHA=',F6.1,'   AC=',F10.6,'  ACA=',E10.3)   00041900
      LINE=LINE+1                                                       00042000
  248 IF (LINE .LT. 50) GO TO 250                                       00042100
      CALL HEADER(IO,NPAGE)                                             00042200
      LINE=2                                                            00042300
  250 CONTINUE                                                          00042400
C                                                                       00042500
      DO 260 MMM=1,NPOINT                                               00042600
      SSAVE(K,J,MMM)=S(MMM)                                             00042700
  260 CONTINUE                                                          00042800
      IF(PLO) 261,262,261                                               00042900
  261 CONTINUE                                                          00043000
      CALL INCRE(XMIN,XMAX,XINCR,NPOINT,E)                              00043100
  262 CONTINUE                                                          00043200
```

```
      DO 270 LL=1,NPOINT                                                00043300
      ESAVE(J,LL,K)=E(LL)                                               00043400
  270 CONTINUE                                                          00043500
      IF(KUNT.GT.MAXIIT) GO TO 274                                      00043600
      IF(KBK.EQ.1) GO TO 300                                            00043700
      IF(BETA-BBETA) 271,273,272                                        00043800
  271 B=B-BINCR                                                         00043900
C     IF(BETA2.LT.BETA) B=B-BINCR                                       00044000
      KB2=2                                                             00044100
      BINCR=BINCR*0.1                                                   00044200
      KBB=1+KBB                                                         00044300
  272 CONTINUE                                                          00044400
      KB2=KB2-1                                                         00044500
      IF(KB2.NE.1) BETA2=BBETA                                          00044600
      BBETA=B*PI/180.                                                   00044700
      IF(BBETA.GT.BETA) GO TO 278                                       00044800
      KBK=1                                                             00044900
      B=B-BINCR*0.1                                                     00045000
      BINCR=BINCR*0.1                                                   00045100
      GO TO 276                                                         00045200
  278 CONTINUE                                                          00045300
      B=B+BINCR                                                         00045400
      BBETA=BETA                                                        00045500
      IF(KB2.EQ.1) BBETA=BETA2                                          00045600
      KBB=KBB+1                                                         00045700
      IF(KBB.LE.4) GO TO 276                                            00045800
      KBB=0                                                             00045900
      KB=0                                                              00046000
  276 CONTINUE                                                          00046100
      IF(KB.GE.1) GO TO 264                                             00046200
      IF(KUNT-4) 264,264,265                                            00046300
  265 IF(B-BSTART) 266,266,264                                          00046400
  266 B=BSTART-25.                                                      00046500
      BETA=B*PI/180.                                                    00046600
      BBETA=0.0                                                         00046700
      KB=KB-6                                                           00046800
      BINCR=10.                                                         00046900
      IF(KB.LT.-10) GO TO 400                                           00047000
      GO TO 30                                                          00047100
  264 KB=KB+1                                                           00047200
      BETA=B*PI/180.                                                    00047300
      NSTAR=-0.003012048                                                00047400
      KUNT=KUNT+1                                                       00047500
      IF(MAXIIT-KUNT)274,274,29                                         00047600
  273 WRITE(IO,275)                                                     00047700
  275 FORMAT('      BETA HAS CONVERGED')                                00047800
      KUNT=MAXIIT+1                                                     00047900
      GO TO 126                                                         00048000
```

```
  274 CONTINUE                                                          00048100
      B=110.                                                            00048200
      BETA=1.9198                                                       00048300
      BBETA=0.0                                                         00048400
      BETA2=0.0                                                         00048500
      BINCR=10.                                                         00048600
      GO TO 400                                                         00048700
  300 CONTINUE                                                          00048800
C     WRITE(IO,305) BINCR                                               00048900
C 305 FORMAT(10X,1PE13.6)                                               00049000
      BBETA=B*PI/180.                                                   00049100
      IF(BBETA-BETA) 310,273,320                                        00049200
  310 B=B-BINCR                                                         00049300
      GO TO 276                                                         00049400
  320 B=B+BINCR*0.9                                                     00049500
      BINCR=BINCR*0.1                                                   00049600
      GO TO 276                                                         00049700
C                                                                       00049800
  400 CONTINUE                                                          00049900
      ZC(1,J)=C6(1)                                                     00050000
      ZC(2,J)=C1                                                        00050100
      ZC(3,J)=C2                                                        00050200
      ZC(4,J)=C3                                                        00050300
      ZC(5,J)=C4                                                        00050400
  491 CONTINUE                                                          00050500
C                                                                       00050600
CC    PLOTS P* AND T* VS THETA                                          00050700
C                                                                       00050800
      IF(PL06) 490,493,490                                              00050900
  490 DO 492 JJ=1,ERCNT                                                 00051000
      J=ERCNT+1-JJ                                                      00051100
      Z=ER(J)                                                           00051200
      CALL PL3(ZC(1,J),ZC(2,J),ZC(3,J),ZC(4,J),ZC(5,J),JJ,Z)            00051300
      CALL SYM(1.,5.6,.14,'F=',0,2)                                     00051400
      Z=F                                                               00051500
      CALL NUM(1.4,5.6,.14,Z     ,0,2)                                  00051600
      CALL SYM(1.,5.4,.14,'R*=',0,3)                                    00051700
      Z=RSTAR(K)                                                        00051800
      CALL NUM(1.4,5.4,.14,Z         ,0,2)                              00051900
      CALL SYM(1.,5.2,.14,' M=',0,3)                                    00052000
      Z=XM(I)                                                           00052100
      CALL NUM(1.4,5.2,.14,Z     ,0,2)                                  00052200
      CALL SYM(1.,5.,.14,'ALPHA=',0,6)                                  00052300
      Z=ALPHA(IA)                                                       00052400
      CALL NUM(1.8,5.,.14,Z         ,0,0)                               00052500
      CALL SYM(-0.7,5.0,0.14,'SURFACE LOAD INTENSITY',-90.0,23)         00052600
      CALL SYM(2.8,-0.4,0.14,'ANGULAR POSITION',0.,16)                  00052700
      CALL SYM(0.5,-0.6,0.14,'FIG      SURFACE LOADING ON A SPLIT-SET AF00052800
```

```
     2TER INSTALLATION',0.0,58)                                                00052900
  492 CONTINUE                                                                 00053000
      CALL ENDPLT                                                              00053100
  493 CONTINUE                                                                 00053200
C                                                                              00053300
      ZTAMIN=ETAMIN                                                            00053400
      ZTAMAX=ETAMAX                                                            00053500
C     PLOT FOR R* VS M PL01                                                    00053600
      IF(PL01) 401,499,401                                                     00053700
  401 CALL INCR(XMIN,XMAX,XINCR)                                               00053800
      ZINCR=EINCR                                                              00053900
      CALL STPLOT(XMIN,XMAX,ZTAMIN,ZTAMAX,XINCR,ZINCR,NPOINT)                  00054000
      CALL SYM(-2.35,3.3,0.14, 'OUTSIDE SURFACE',0.0,15)                       00054100
      CALL SYM(-2.35,3.1,0.14,'OF SPLIT-SET',0.0,12)                           00054200
      CALL SYM(0.1,-3.3,0.14,'INSIDE SURFACE OF SPLIT-SET',0.0,27)             00054300
      DO 402 J=1,FRCNT                                                         00054400
      DO 403 LL=1,NPOINT                                                       00054500
      ZY(LL)=ETA(LL)                                                           00054600
  403 ZX(LL)=ESAVE(J,LL,K)                                                     00054700
      CALL XYPLT(ZX,ZY,NPOINT,1,-1)                                            00054800
      CALL SYM(XSTOIN(ZX(NPOINT)),YSTOIN(ZTAMAX)+0.035,0.07,'ER=',90.,3)00054900
      Z=FR(J)                                                                  00055000
      CALL NUM(XSTOIN(ZX(NPOINT)),YSTOIN(ZTAMAX)+.35,.07,Z     ,90.,3)         00055100
  402 CONTINUE                                                                 00055200
      CALL NEWPLT(5.5,5.,10.)                                                  00055300
      CALL SYM(4.0,0.0,0.35,44,0.0,-1)                                         00055400
      CALL SYM(0.0,4.1,0.35,45,0.0,-1)                                         00055500
      CALL SYM(-3.0,2.5,0.175,'R*=',0.0,3)                                     00055600
      Z=RSTAR(K)                                                               00055700
      CALL NUM(-2.5,2.5,0.175,Z        ,0.0,3)                                 00055800
      CALL SYM(-3.0,2.3,0.175,'M=',0.0,2)                                      00055900
      Z=XM(I)                                                                  00056000
      CALL NUM(-2.6,2.3,0.175,Z      ,0.0,1)                                   00056100
      CALL SYM(-3.0,2.1,0.175, 'F=',0.0,2)                                     00056200
      Z=F                                                                      00056300
      CALL NUM(-2.6,2.1,0.175,Z,0.0,1)                                         00056400
      CALL SYM(-3.0,-4.0,0.14,'FIG      STRAIN DISTRIBUTION THROUGH SPLI00056500
     2T-SET WALL',0.0,51)                                                      00056600
      CALL ENDPLT                                                              00056700
      XMIN=0.                                                                  00056800
      XMAX=0.                                                                  00056900
  499 CONTINUE                                                                 00057000
  500 CONTINUE                                                                 00057100
C                                                                              00057200
C     PLO FOR ER VS M   PL02                                                   00057300
      IF(PL02) 501,599,501                                                     00057400
  501 CONTINUE                                                                 00057500
C                                                                              00057600
```

```
      DO 570 LL=1,ERCNT                                                 00057700
      CALL NEWPLT(5.5,5.0,10.0)                                         00057800
      CALL SYM(-3.0,-4.0,0.14,'FIG      STRAIN DISTRIBUTION THROUGH SPLI00057900
     2T-SET WALL',0.0,51)                                               00058000
      CALL SYM(-3.0,2.5,0.175,'ER=',0.0,3)                              00058100
      Z=ER(LL)                                                          00058200
      CALL NUM(-2.5,2.5,0.175,Z     ,0.0,3)                             00058300
      CALL SYM(-3.0,2.3,0.175,'M=',0.0,2)                               00058400
      Z=XM(I)                                                           00058500
      CALL NUM(-2.6,2.3,0.175,Z     ,0.0,1)                             00058600
      CALL SYM(-3.0,2.1,0.175,  'F=',0.0,2)                             00058700
      Z=F                                                               00058800
      CALL NUM(-2.6,2.1,0.175,Z,0.0,1)                                  00058900
      CALL SYM(4.0,0.0,0.35,44,0.0,-1)                                  00059000
      CALL SYM(0.0,4.1,0.35,45,0.C,-1)                                  00059100
C                                                                       00059200
C     LOOP TO PLOT 'E' VS. 'ETA' VARYING RSTAR AND HOLDING              00059300
C     'ER' CONSTANT.                                                    00059400
C                                                                       00059500
      DO 550 JJ=1,RSCNT                                                 00059600
      DO 549 MM=1,NPOINT                                                00059700
  549 E(MM)=ESAVE(LL,MM,JJ)                                             00059800
      CALL INCRE(XMIN,XMAX,XINCR,NPOINT,E)                              00059900
  550 CONTINUE                                                          00060000
      CALL INCR(XMIN,XMAX,XINCR)                                        00060100
      CALL STPLOT(XMIN,XMAX,ZTAMIN,ZTAMAX,XINCR,ZINCR,NPOINT)           00060200
      DO 565 JJ=1,RSCNT                                                 00060300
      DO 540 MM=1,NPOINT                                                00060400
      ZY(MM)=ETA(MM)                                                    00060500
      ZX(MM)=ESAVE(LL,MM,JJ)                                            00060600
  540 CONTINUE                                                          00060700
C                                                                       00060800
      CALL XYPLT(ZX,ZY,NPOINT,1,-1)                                     00060900
      CALL SYM(XSTOIN(ZX(NPOINT)),YSTOIN(ZTAMAX)+0.035,0.07,'R*=',90.,3)00061000
      Z=RSTAR(JJ)                                                       00061100
      CALL NUM(XSTOIN(ZX(NPOINT)),YSTOIN(ZTAMAX)+.35,.07,Z,90.,3)       00061200
  565 CONTINUE                                                          00061300
      CALL SYM(-2.35,3.3,0.14, 'OUTSIDE SURFACE',0.0,15)                00061400
      CALL SYM(-2.35,3.1,0.14,'OF SPLIT-SET',0.0,12)                    00061500
      CALL SYM(0.1,-3.3,0.14,'INSIDE SURFACE OF SPLIT-SET',0.0,27)      00061600
      CALL ENDPLT                                                       00061700
      XMIN=0.                                                           00061800
      XMAX=0.                                                           00061900
  570 CONTINUE                                                          00062000
C                                                                       00062100
  599 CONTINUE                                                          00062200
      CALL PL2(RSCNT,ERCNT,I,PLO5,PLO4,FSAVE,ER,RSTAR,XM,ALPHA,F)       00062300
      Z=F                                                               00062400
```

```
      IF(PLC7) 590,600,590                                                    00062500
  590 CALL PL4(ACNT,RSCNT,ERCNT,I,FSAVE,XM,ALPHA,RSTAR,ER,MCNT,Z)             00062600
C     PL4 PLOTS ER ON F* VS R*                                                00062700
  600 CONTINUE                                                                00062800
C                                                                             00062900
      IF(PL03) 601,5000,601                                                   00063000
  601 CONTINUE                                                                00063100
C                                                                             00063200
C     LOOP TO PLOT GRAPHS OF 'S' VS. 'ETA'. ***                               00063300
C                                                                             00063400
      DO 650 I=1,MCNT                                                         00063500
      DO 650 II=1,RSCNT                                                       00063600
      CALL NEWPLT(5.5,5.0,10.0)                                               00063700
      CALL SYM(1.0,-1.5,0.175,'R*=',0.0,3)                                    00063800
      Z=RSTAR(II)                                                             00063900
      CALL NUM(2.0,-1.5,0.175,Z          ,0.0,3)                              00064000
      CALL SYM(1.,-1.75,0.175,'ALPHA=',0.,6)                                  00064100
      Z=ALPHA(ACNT)                                                           00064200
      CALL NUM(2.,-1.75,0.175,Z              ,0.,0)                           00064300
      CALL SYM(1.0,-2.0,0.175,'M=',0.0,2)                                     00064400
      Z=XM(I)                                                                 00064500
      CALL NUM(2.0,-2.0,0.175,Z      ,0.0,1)                                  00064600
      CALL SYM(1.0,-2.25,0.175,'F=',0.0,2)                                    00064700
        Z=F                                                                   00064800
      CALL NUM(2.0,-2.25,0.175,Z,0.0,1)                                       00064900
      CALL SYM(-3.1,-3.5,0.14,'FIG      STRESS DISTRIBUTION THROUGH SPLI00065000
     2T-SET WALL',0.0,51)                                                     00065100
      CALL SYM(4.0,0.0,0.35,'S',0.0,1)                                        00065200
      CALL SYM(0.0,4.1,0.35,45,0.C,-1)                                        00065300
      CALL INCRS(XMIN,XMAX,XINCR,ERCNT,NPOINT,II)                             00065400
      CALL STPLOT(XMIN,XMAX,ZTAMIN,ZTAMAX,XINCR,ZINCR,NPOINT)                 00065500
      DO 645 KK=1,ERCNT                                                       00065600
      DO 605 MM=1,NPOINT                                                      00065700
  605 ZY(MM)=ETA(MM)                                                          00065800
      ZA=-1.                                                                  00065900
      DO 630 L=1,NPOINT                                                       00066000
  630 ZX(L)=SSAVE(II,KK,L)                                                    00066100
      DO 640 L=1,NPOINT                                                       00066200
      IF(ZX(L).LT.ZA) GO TO 640                                               00066300
      IF(ZA.GT.0) GO TO 620                                                   00066400
  610 ZX(L)=ZA                                                                00066500
      N=1                                                                     00066600
      CALL LESQUR(L ,ZX,ZY,ZBB,ZB)                                            00066700
      ZY(L)=ZBB*ZX(L)+ZB                                                      00066800
      N=L                                                                     00066900
      ZA=1.                                                                   00067000
      GO TO 640                                                               00067100
  620 IF(ZA.GT.100.) GO TO 640                                                00067200
```

```
      LL=L+2                                                                    00067300
      CALL LESQUR(LL,ZX,ZY,ZBB,ZB)                                              00067400
      ZX(L)=ZA                                                                  00067500
      ZY(L)=ZBB*ZX(L)+ZB                                                        00067600
      NN=L                                                                      00067700
      ZA=5000000.                                                               00067800
  640 CONTINUE                                                                  00067900
      CALL XYPLT(ZX,ZY,NPOINT,1,-1)                                             00068000
      IF(XM(I).LT.0.05) GO TO 645                                               00068100
      CALL SYM(XSTOIN(ZX(NPOINT)),YSTOIN( ZY(NPOINT)),0.07,'ER=',90.,3)         00068200
      Z=ER(KK)                                                                  00068300
      CALL NUM(XSTOIN(ZX(NPOINT)),YSTOIN( ZY(NPOINT))+.4,0.07,Z,90.,2)          00068400
  645 CONTINUE                                                                  00068500
      CALL SYM(-2.35,3.3,0.14, 'OUTSIDE SURFACE',0.0,15)                        00068600
      CALL SYM(-2.35,3.1,0.14,'OF SPLIT-SET',0.0,12)                            00068700
      CALL SYM(0.1,-3.3,0.14,'INSIDE SURFACE OF SPLIT-SET',0.0,27)              00068800
      CALL ENDPLT                                                               00068900
  650 CONTINUE                                                                  00069000
C                                                                               00069100
 5000 CONTINUE                                                                  00069200
C                                                                               00069300
C     TO END PLOTTING                                                           00069400
C                                                                               00069500
      IF(PLO) 5001,5002,5001                                                    00069600
 5001 CALL LSTPLT                                                               00069700
 5002 STOP                                                                      00069800
      END                                                                       00069900
      SUBROUTINE HEADER (IO,N)                                                  00070000
      N=N+1                                                                     00070100
      WRITE(IO,10) N                                                            00070200
   10 FORMAT('1',T40,'* S T R E S S   A N A L Y S I S *',T110,'PAGE ',          00070300
     $ I2/)                                                                     00070400
      RETURN                                                                    00070500
      END                                                                       00070600
      FUNCTION SIMPSN (FUN,A,B,N)                                               00070700
      IMPLICIT REAL*8(A-H,O-Z)                                                  00070800
      DIMENSION FUN(1)                                                          00070900
C     SIMPSON'S RULE INTEGRAL                                                   00071000
C     FUN=ARRAY OF FUNCTION VALUES                                              00071100
C     A=INITIAL VALUE OF X.                                                     00071200
C     B=FINAL VALUE OF X.                                                       00071300
C     N=NUMBER OF INTERVALS, EVEN.                                              00071400
C     EVALUATE INTEGRAL OF FUN(X) FROM                                          00071500
C     X=A TO X=B, USING N INTERVALS.                                            00071600
C                                                                               00071700
C     ENSURE EVEN NUMBER OF INTERVALS.                                          00071800
C                                                                               00071900
 1000 M=(N/2)*2                                                                 00072000
```

```
      IF (M.GE.2) GO TO 1050                                                    00072100
C     CRAZY ENTRY.  RETURN ZERO VALUE.                                          00072200
      SIMPSN=0.0                                                                00072300
      RETURN                                                                    00072400
C                                                                               00072500
C     ENTRY VALID.  SET UP.                                                     00072600
 1050 H=(B-A)/FLOAT(M)                                                          00072700
      EVNSUM=0.0                                                                00072800
      ODDSUM=0.0                                                                00072900
      ENDSUM=FUN(1)+FUN(M+1)                                                    00073000
      IF (M .LT. N) GO TO 1075                                                  00073100
      MMIN1=M-1                                                                 00073200
      GO TO 1080                                                                00073300
 1075 MMIN1=M                                                                   00073400
 1080 J=1                                                                       00073500
C     THIS 'J' IS A SWITCH.  J=1 MEANS AN ODD POINT, J=2 AN EVEN POINT.         00073600
C     NOW BEGIN ITERATION.                                                      00073700
C                                                                               00073800
      DO 1200 I=2,MMIN1                                                         00073900
      GO TO (1101,1102),J                                                       00074000
C     I IS AN ODD POINT.                                                        00074100
 1101 ODDSUM=ODDSUM+FUN(I)                                                      00074200
      J=2                                                                       00074300
      GO TO 1200                                                                00074400
C     I IS AN EVEN POINT.                                                       00074500
 1102 EVNSUM=EVNSUM+FUN(I)                                                      00074600
      J=1                                                                       00074700
C                                                                               00074800
C     PATHS REJOIN HERE.                                                        00074900
 1200 CONTINUE                                                                  00075000
C                                                                               00075100
      SIMPSN=(H/3.0)*(ENDSUM+4.0*ODDSUM+2.0*EVNSUM)                             00075200
 1300 RETURN                                                                    00075300
      END                                                                       00075400
      SUBROUTINE STPLOT(XMIN,XMAX,YMIN,YMAX,XINCR,YINCR,NPOINT)                 00075500
C                                                                               00075600
      XPOSIN=1.4+8*((0.-XMIN)/(XMAX-XMIN))                                      00075700
      CALL NEWPLT(XPOSIN,5.2,10.0)                                              00075800
      CALL ORIGIN(0.0,0.0)                                                      00075900
      CALL XSCALE(XMIN,XMAX,8.0)                                                00076000
      CALL YSCALE(YMIN,YMAX,6.5)                                                00076100
      XINCR=XINCR*5.                                                            00076200
      YINCR=YINCR*5.                                                            00076300
      CALL XAXIS(XINCR)                                                         00076400
      CALL YAXIS(YINCR)                                                         00076500
C                                                                               00076600
C     DO 2 I=1,NPOINT,1                                                         00076700
C     YY=YMIN+FLOAT(I-1)*YINCR                                                  00076800
```

```
C     2 CALL NUM(-.35,YSTOIN(YY)-.035,0.07,YY,0.0,2)                    00076900
        YY=YMIN                                                         00077000
      1 CALL NUM(-0.35,YSTOIN(YY)-0.035,0.07,YY,0.0,2)                  00077100
        YY=YY+YINCR                                                     00077200
        IF(YY-YMAX) 1,1,2                                               00077300
      2 CONTINUE                                                        00077400
        XX=0.                                                           00077500
      3 CALL NUM(XSTOIN(XX)-.035,-0.21,0.07,XX,0.0,2)                   00077600
        XX=XX-1.*XINCR                                                  00077700
        IF(XX.LT.XMIN) GO TO 4                                          00077800
        GO TO 3                                                         00077900
      4 XX=XINCR                                                        00078000
        IF(XX.GT.XMAX) RETURN                                           00078100
      5 CALL NUM(XSTOIN(XX)-.035,-0.21,0.07,XX,0.0,2)                   00078200
        XX=XX+XINCR                                                     00078300
        IF(XX.LE.XMAX) GO TO 5                                          00078400
C                                                                       00078500
        RETURN                                                          00078600
        END                                                             00078700
        SUBROUTINE INCRE(XMIN,XMAX,XINCR,NPOINT,EI)                     00078800
        REAL*8 EI(41)                                                   00078900
        REAL E(41)                                                      00079000
C                                                                       00079100
C       FINDS MIN AND MAX OF E VALUESS                                  00079200
C                                                                       00079300
        DO 10 I=1,NPOINT                                                00079400
        E(I)=EI(I)                                                      00079500
        IF(E(I).LT.XMIN) GO TO 11                                       00079600
        IF(E(I).GT.XMAX) GO TO 12                                       00079700
        GO TO 10                                                        00079800
   11   XMIN=E(I)                                                       00079900
        GO TO 10                                                        00080000
   12   XMAX=E(I)                                                       00080100
   10   CONTINUE                                                        00080200
        RETURN                                                          00080300
        END                                                             00080400
        SUBROUTINE INCR(XMIN,XMAX,XINCR)                                00080500
C                                                                       00080600
C       FINDS INCREMENT FOR PLOTS                                       00080700
C                                                                       00080800
        XMIX=XMAX-XMIN                                                  00080900
        J=0                                                             00081000
        IF(XMIX/10.**J-1) 20,40,30                                      00081100
C       XMIX LESS THAN 1                                                00081200
   20   J=J-1                                                           00081300
        IF(XMIX/10.**J-1) 20,21,22                                      00081400
   21   XINCR=(10.**J)/10.                                              00081500
        GO TO 41                                                        00081600
```

```
   22 CONTINUE                                                          00081700
      IF(XMIX/10.**J-2.0) 21,21,23                                      00081800
   23 XINCR=10.**J                                                      00081900
      GO TO 41                                                          00082000
C     XMIX GREATER THAN 1                                               00082100
   30 J=J+1                                                             00082200
      IF(XMIX/10.**J-1) 32,31,30                                        00082300
   31 XINCR=(10.**J)/10.                                                00082400
      GO TO 41                                                          00082500
   32 IF(XMIX/10.**J-2.0) 31,31,33                                      00082600
   33 XINCR=10.**J                                                      00082700
      GO TO 41                                                          00082800
   40 XINCR=0.1                                                         00082900
   41 XINCR=XINCR*0.1                                                   00083000
      RETURN                                                            00083100
      END                                                               00083200
      SUBROUTINE INCRS (XMIN,XMAX,XINCR,ERCNT,NPCINT,III)               00083300
      IMPLICIT REAL*8(A-H,O-Z)                                          00083400
      COMMON    E(41),EP(41),S(41),ETA(41),ER(9),RSTAR(10),XM(2),       00083500
     2 DUMEP(41),ESAVE(9,41,10),FSTAR(  2),F    ,ALPHA(2),SSAVE(10,9,41),00083600
     3 XXEP(41),RALPHA(2),CISTAR(2),FSAVE(  2,9,10)                     00083700
      REAL XMIN,XMAX,XINCR                                              00083800
      INTEGER ERCNT,RSCNT,MCNT,ACNT                                     00083900
C                                                                       00084000
C     FINDS MIN AND MAX FOR THE 'S' PLOTS                               00084100
C                                                                       00084200
      XMIN=0.                                                           00084300
      XMAX=0.                                                           00084400
      DO 10 II=1,ERCNT                                                  00084500
      DO 10 I=1,NPCINT                                                  00084600
      IF(SSAVE(III,II,I).LT.XMIN) GO TO 11                              00084700
      IF(SSAVE(III,II,I).GT.XMAX) GO TO 12                              00084800
      GO TO 10                                                          00084900
   11 XMIN=SSAVE(III,II,I)                                              00085000
      GO TO 10                                                          00085100
   12 XMAX=SSAVE(III,II,I)                                              00085200
   10 CONTINUE                                                          00085300
      CALL INCR(XMIN,XMAX,XINCR)                                        00085400
      RETURN                                                            00085500
      END                                                               00085600
      SUBROUTINE PL2 (RSCNT,ERCNT,MCNT,PL05,PL04,FSAVE,ERI,RSTARI,XMI,AL00085700
     2PHAI,FI)                                                          00085800
      REAL*8 FSAVE(2,9,10),ERI(9), RSTARI(10),XMI(2),ALPHAI(2) ,FI      00085900
      REAL E(10),ER(9),RSTAR(10),XM(2),ALPHA(2)                         00086000
      INTEGER RSCNT,ERCNT,MCNT                                          00086100
C                                                                       00086200
      F=FI                                                              00086300
      DO 10 I=1,RSCNT                                                   00086400
```

```
   10 RSTAR(I)=RSTARI(I)                                                00086500
      DO 20 I=1,ERCNT                                                   00086600
   20 ER(I)=ERI(I)                                                      00086700
      DO 30 I=1,2                                                       00086800
      XM(I)=XMI(I)                                                      00086900
   30 ALPHA(I)=ALPHAI(I)                                                00087000
C     PLOT FOR F* VS ER  FOR EACH F                                     00087100
      IF(PL04) 101,1001,101                                             00087200
  101 CONTINUE                                                          00087300
      YMAX=FSAVE(  1,ERCNT,1)                                           00087400
      CALL INCR(0.,YMAX,YINCR)                                          00087500
      CALL INCR(0.,ER(ERCNT),XINCR)                                     00087600
      CALL NEWPLT(1.,2.,10.)                                            00087700
      CALL ORIGIN(0.,0.)                                                00087800
      CALL XSCALE(0.,ER(ERCNT),8.)                                      00087900
      CALL YSCALE(0.,YMAX,6.5)                                          00088000
      XINCR=XINCR*5.                                                    00088100
      YINCR=YINCR*10.                                                   00088200
      CALL XAXIS(XINCR)                                                 00088300
      CALL YAXIS(YINCR)                                                 00088400
      XX=0.                                                             00088500
    1 CALL NUM(XSTOIN(XX)-.035,-.21,.07,XX,0.,2)                        00088600
      XX=XX+XINCR                                                       00088700
      IF(XX.LT.ER(ERCNT)) GO TO 1                                       00088800
      YY=0.                                                             00088900
    2 CALL NUM(-.35,YSTOIN(YY),.07,YY,0.,3)                             00089000
      YY=YY+YINCR                                                       00089100
      IF(YY.LT.YMAX) GO TO 2                                            00089200
      DO 1000 K=1,RSCNT                                                 00089300
      DO 5 J=1,ERCNT                                                    00089400
    5 E(J)=FSAVE(  1,J,K)                                               00089500
      CALL XYPLT(ER,E,ERCNT,1,-1)                                       00089600
      CALL SYM(XSTOIN(ER(ERCNT)),YSTOIN(E(ERCNT)),0.07,'R*=',0.,3)      00089700
      F=RSTARI(K)                                                       00089800
      CALL NUM(XSTOIN(ER(ERCNT))+.20,YSTOIN(E(ERCNT)),.07,F    ,0.,2)   00089900
 1000 CONTINUE                                                          00090000
      F=FI                                                              00090100
      CALL SYM(3.0,-0.4,0.14,'INTERFERENCE RATIO (ER)',0.0,23)          00090200
      CALL SYM(-0.8,6.5,0.14,'FIG      SPLIT-SET INSERTION FORCE--VARIAB00090300
     2LE WALL THICKNESS',-90.,59)                                       00090400
      CALL SYM(-0.6,4.0,0.14,'INSERTION FORCE (F*)',-90.,20)            00090500
      CALL SYM(1.,6.6,.14,' F=',0.,3)                                   00090600
      CALL NUM(1.4,6.6,.14,F      ,0.,2)                                00090700
      CALL SYM(1.,6.4,.14,' M=',0.,3)                                   00090800
      CALL NUM(1.4,6.4,.14,XM(MCNT),0.,2)                               00090900
      CALL SYM(1.,6.2,.14,'ALPHA=',0.,6)                                00091000
      CALL NUM(1.8,6.2,.14,ALPHA(1),0.,0)                               00091100
      CALL SYM(8.,0,.14,'ER',0,2)                                       00091200
```

```
      CALL SYM(-.07,6.5,.14,'F*',0,2)                                   00091300
      CALL ENDPLT                                                       00091400
 1001 CONTINUE                                                          00091500
      IF(PL05) 1002,3000,1002                                           00091600
 1002 CONTINUE                                                          00091700
C                                                                       00091800
C     PLOT FOR F* VS R*                                                 00091900
      YMAX=FSAVE(  1,ERCNT,1)                                           00092000
      CALL INCR(0.,YMAX,YINCR)                                          00092100
      CALL INCR(0.,RSTAR(RSCNT),XINCR)                                  00092200
      CALL NEWPLT(1.,2.,10.)                                            00092300
      CALL ORIGIN(0.,0.)                                                00092400
      CALL XSCALE(0.,RSTAR(RSCNT),8.)                                   00092500
      CALL YSCALE(0.,YMAX,6.5)                                          00092600
      CALL XAXIS(XINCR)                                                 00092700
      CALL YAXIS(YINCR)                                                 00092800
      XX=0.                                                             00092900
   11 CALL NUM(XSTOIN(XX),-.21,.07,XX,0.,2)                             00093000
      XX=XX+XINCR*5.                                                    00093100
      IF(XX.LT.RSTAR(RSCNT)) GO TO 11                                   00093200
      YY=0.                                                             00093300
   12 CALL NUM(-.35,YSTOIN(YY),.07,YY,0.,3)                             00093400
      YY=YY+YINCR*5.                                                    00093500
      IF(YY.LT.YMAX) GO TO 12                                           00093600
      DO 2000 J=1,ERCNT                                                 00093700
      DO 25 K=1,RSCNT                                                   00093800
   25 E(K)=FSAVE(  1,J,K)                                               00093900
      CALL SYM(XSTOIN(RSTAR(1)),YSTOIN(E(1)),.07,'ER=',0.,3)            00094000
      F=ERI(J)                                                          00094100
      CALL NUM(XSTOIN(RSTAR(1))+.20,YSTOIN(E(1)),.07,F    ,0.,2)        00094200
      CALL XYPLT(RSTAR,E,RSCNT,1,-1)                                    00094300
 2000 CONTINUE                                                          00094400
      CALL SYM(0.,-.4,.14,' F=',0.,3)                                   00094500
      F=FI                                                              00094600
      CALL NUM(0.4,-.4,.14,F    ,0.,2)                                  00094700
      CALL SYM(0.,-.6,.14,' M=',0.,3)                                   00094800
      CALL NUM(.4,-.6,.14,XM(MCNT),0.,2)                                00094900
      CALL SYM(0.,-.8,.14,'ALPHA=',0.,6)                                00095000
      CALL NUM(.80,-.8,.14,ALPHA(1),0.,0)                               00095100
      CALL SYM(8.,0,.14,'R*',0,2)                                       00095200
      CALL SYM(-.07,6.5,.14,'F*',0,2)                                   00095300
      CALL ENDPLT                                                       00095400
 3000 RETURN                                                            00095500
      END                                                               00095600
      SUBROUTINE PL3(C2STAR,C1,C2,C3,C4,J,ER)                           00095700
      DIMENSION PSTAR(19),TSTAR(19),T(19)                               00095800
      REAL MAX                                                          00095900
C                                                                       00096000
```

```
C      PLOTS P* AND T* VS THETA                                                  00096100
C                                                                                00096200
       DO 1 I=1,19                                                               00096300
     1 T(I) =(I-1.)*10.                                                          00096400
C                                                                                00096500
CC     CALCULATES P* AND T* AND FINDS MAX VALUE FOR PLOTS                        00096600
C                                                                                00096700
       DO 40 L=1,19                                                              00096800
C                                                                                00096900
CC     TH IS THETA IN RADIANS                                                    00097000
C                                                                                00097100
       TH=(L-1.)/18.*3.1415926535                                                00097200
       PSTAR(L)=C2+C4*TH*TH+C2STAR    *TH**4                                     00097300
       TSTAR(L)=C1*TH+C3*TH**3                                                   00097400
       WRITE(6,10) PSTAR(L),TSTAR(L),TH                                          00097500
    10 FORMAT(10X,'PSTAR=',1PE10.3,10X,'TSTAR=',1PE10.3,10X,'THETA=',1PE10     00097600
      20.3)                                                                      00097700
       IF(PSTAR(L).LT.0) PSTAR(L)=0.                                             00097800
       IF(TSTAR(L).LT.0) TSTAR(L)=0.                                             00097900
    40 CONTINUE                                                                  00098000
       IF(J.NE.1) GO TO 52                                                       00098100
       CALL NEWPLT(1.,2.,10.)                                                    00098200
       CALL ORIGIN(0,0)                                                          00098300
       MAX=TSTAR(19)                                                             00098400
       CALL INCR(0.,MAX,YINCR)                                                   00098500
       CALL XSCALE(0,180.,8.)                                                    00098600
       CALL YSCALE(0.,MAX,6.5)                                                   00098700
       CALL XAXIS(45.)                                                           00098800
       YINCR=YINCR*10.                                                           00098900
       CALL YAXIS(YINCR)                                                         00099000
       XX=0.                                                                     00099100
    50 CALL NUM(XSTOIN(XX)-.035,-.21,.07,XX,0.,1)                                00099200
       XX=XX+45.                                                                 00099300
       IF(XX.LE.180.) GO TO 50                                                   00099400
       CALL SYM(8.,-.07,.14,112,0,-1)                                            00099500
       CALL SYM(8.,-.07,.14,96,0,-1)                                             00099600
       YY=0.                                                                     00099700
    51 CALL NUM(-.42,YSTOIN(YY),.07,YY,0.,4)                                     00099800
       YY=YY+YINCR                                                               00099900
       IF(YY.LT.MAX) GO TO 51                                                    00100000
       CALL SYM(XSTOIN(T(3)),YSTOIN(PSTAR(3)),0.07,'NORMAL LOAD (P*)',0.0C0100100
      2,16)                                                                      00100200
       CALL SYM(XSTOIN(T(17))-0.9,YSTOIN(TSTAR(17)),0.07,'SHEAR LOAD (T*)00100300
      2',0.0,15)                                                                 00100400
    52 CONTINUE                                                                  00100500
       CALL SYM(0.05,YSTOIN(PSTAR(1)),0.07,'P* ER=',0.0,6)                       00100600
       CALL NUM(0.41,YSTOIN(PSTAR(1))     ,0.07,ER,0.0,2)                        00100700
C      CALL SYM(8.,YSTOIN(PSTAR(19)),.07,'P*',0,2)                               00100800
```

```
      CALL XYPLT(I,PSTAR,19,1,-1)                                       CC100900
      CALL XYPLT(I,TSTAR,19,1,-1)                                       00101000
      CALL SYM(8.,YSTOIN(TSTAR(19)),.07,'T* ER=',0,6)                   00101100
      CALL NUM(8.36,YSTOIN(TSTAR(19))      ,0.07,ER,0.0,2)              00101200
      RETURN                                                            00101300
      END                                                               00101400
      SUBROUTINE PL4(ACNT,RSCNT,ERCNT,I,FSAVE,XMI,ALPHAI,RSTARI,ERI,    00101500
     2MCNT,ZF)                                                          00101600
      REAL*8 FSAVE(2,9,10),XMI(2),ALPHAI(2),RSTARI(10),ERI(9)           00101700
      REAL E(10),RSTAR(10),ER(9)                                        00101800
      INTEGER ACNT,RSCNT,ERCNT                                          00101900
      DO 5 I=1,10                                                       00102000
    5 RSTAR(I)=RSTARI(I)                                                00102100
      DO 6 I=1,ERCNT                                                    00102200
    6 ER(I)=ERI(I)                                                      00102300
C                                                                       00102400
CC    PLOTS ER ON F* VS R*                                              00102500
C                                                                       00102600
      DO 10 I=1,MCNT                                                    00102700
      DO 10 IA=1,ACNT                                                   00102800
      CALL NEWPLT(1.,2.,10.)                                            00102900
      YMAX=FSAVE(  IA,ERCNT,1)                                          00103000
      CALL INCR(0.,YMAX,YINCR)                                          00103100
      M=RSTAR(1)                                                        00103200
      XX=M                                                              00103300
      CALL INCR(XX       ,RSTAR(RSCNT),XINCR)                           00103400
      CALL ORIGIN(XX,0.)                                                00103500
      CALL XSCALE(XX       ,RSTAR(RSCNT),8.)                            00103600
      CALL YSCALE(0.,YMAX,6.5)                                          00103700
      XINCR=XINCR*5.                                                    00103800
      YINCR=YINCR*10.                                                   00103900
      CALL XAXIS(XINCR)                                                 00104000
      CALL YAXIS(YINCR)                                                 00104100
      CALL SYM(6.,6.0,.14,' M=',0.,3)                                   00104200
      Z=XMI(I)                                                          00104300
      CALL NUM(6.4,6.0,.14,Z     ,0.,2)                                 00104400
      CALL SYM(6.0,5.8,0.14,' F=',0.0,3)                                00104500
      CALL NUM(6.4,5.8,0.14,ZF,0.0,1)                                   00104600
      CALL SYM(6.,5.6,.14,'ALPHA=',0.,6)                                00104700
       Z=ALPHAI(IA)                                                     00104800
      CALL NUM(6.8,5.6,.14,Z          ,0.,0)                            00104900
      CALL SYM(3.0,-0.6,0.14,'RADIUS RATIO (R*)',0.0,17)                00105000
      CALL SYM(-0.8,6.5,0.14,'FIG      SPLIT-SET INSERTION FORCE--VARIAB00105100
     2LE INTERFERENCE',-90.0,57)                                        00105200
      CALL SYM(-0.6,4.0,0.14,'INSERTION FORCE (F*)',-90.,20)            00105300
   11 CALL NUM(XSTOIN(XX)-.035,-.21,.07,XX,0.,2)                        00105400
      XX=XX+XINCR                                                       00105500
      IF(XX.LT.RSTAR(RSCNT)) GO TO 11                                   00105600
```

```
      CALL SYM(8.,0.,.14,'R*',0.,2)                                          00105700
      YY=0.                                                                  00105800
   12 CALL NUM(-.35,YSTCIN(YY),0.07,YY,0.0,3)                                00105900
      YY=YY+YINCR                                                            00106000
      IF(YY.LT.YMAX) GO TO 12                                                00106100
      CALL SYM(-.07,6.5,.14,'F*',0.,2)                                       00106200
      DO 30 J=1,ERCNT                                                        00106300
      DO 20 K=1,RSCNT                                                        00106400
   20 E(K)=FSAVE(  IA,J,K)                                                   00106500
      CALL SYM(XSTOIN(RSTAR(1)),YSTCIN(E(1)),.07,'ER=',0.,3)                 00106600
      CALL NUM(XSTOIN(RSTAR(1))+.4,YSTOIN(E(1)),.07,ER(J),0.,2)              00106700
      CALL XYPLT (RSTAR,E,RSCNT,1,-1)                                        00106800
   30 CONTINUE                                                               00106900
      CALL ENDPLT                                                            00107000
   10 CONTINUE                                                               00107100
      RETURN                                                                 00107200
      END                                                                    00107300
      SUBROUTINE LESQUR(L,S,ETA,BB,B)                                        00107400
C     LEAST SQUARES FIT TO FIND GRAPH CORNERS                                00107500
C     CRAMERS RUL                                                            00107600
      DIMENSION S(1),ETA(1)                                                  00107700
      IF(S(L-1).NE.S(L-2)) GO TO 2                                           00107800
      B=S(L-1)                                                               00107900
      BB=0.                                                                  00108000
      RETURN                                                                 00108100
    2 K=2                                                                    00108200
      X=S(L-1)+S(L-2)                                                        00108300
      XX=S(L-1)*S(L-1)+S(L-2)*S(L-2)                                         00108400
      Y=ETA(L-1)+ETA(L-2)                                                    00108500
      XY=ETA(L-1)*S(L-1)+ETA(L-2)*S(L-2)                                     00108600
      U=XX*K-X*X                                                             00108700
      U=1./U                                                                 00108800
      BB=(XY*K-X*Y)*U                                                        00108900
      B=(XX*Y-XY*X)*U                                                        00109000
      RETURN                                                                 00109100
      END                                                                    00109200
      SUBROUTINE LINEQ (N,  E,R,D,AM,RA)                                     00109300
      IMPLICIT REAL*8(A-H,O-Z)                                               00109400
C     D IS BETA   RA IS ALPHA(S)   AM IS MSTAR   R IS RSTAR    E IS ER       00109500
      COMMON/AT/M,MM,MF                                                      00109600
      COMMON/PRINT/A(6,6)                                                    00109700
      COMMON/BCOM/B(6)                                                       00109800
      COS(X)=DCOS(X)                                                         00109900
      SIN(X)=DSIN(X)                                                         00110000
      ABS(X)=DABS(X)                                                         00110100
      A(1,1)=R*R*((1.+4.*D*RA-4.*D*D)*SIN(2.*D)-(2.*D*COS(2.*D)))            00110200
      A(1,2)=((5.*RA-4.*D)*D**4.)*R*R/5.                                     00110300
      A(1,3)=(3.*RA-2.*D)*D*D*2.*R*R/3.                                      00110400
```

```
 A(1,4)=4.*R*R*(SIN(D)-RA+(RA-D)*COS(D))                                  00110500
 A(1,5)=4.*R*(RA-SIN(RA))                                                 00110600
 B(1)=AM*RA                                                               00110700
 A(2,1)=4.*R*R*(.25*SIN(D)-.25*D*COS(D)-2.*D*COS(D)*COS(D)*COS(D)         00110800
B /3.+2.*SIN(D                                                            00110900
2)*COS(D)*COS(D)/9.+4.*SIN(D)/9.+D*(RA-D)*SIN(2.*D)*(1-COS(D)))          00111000
 A(2,2)=R*R*(.2*D**5.-D**4.*SIN(D)+12.*(D*D-2.)*SIN(D)-4.*D*              00111100
2(D*D-6.)*COS(D)+(RA-D)*D**4.*(1.-COS(D)))                                00111200
 A(2,3)=(D**3.-6.*D*COS(D)-3.*(D*D-2.)*SIN(D)+3.*D*D*(1-COS(D))*          00111300
2(RA-D))/6.*4.*R*R                                                        00111400
 A(2,4)=(2.*SIN(D)-D*1.5-.25*SIN(2.*D)-(1-COS(D))**2.*(RA-D))*4.*R*R      00111500
2R                                                                        00111600
 A(2,5)=4.*R*(RA-2.*SIN(RA)+.5*RA+.25*SIN(2.*RA))                         00111700
 B(2)=AM*(SIN(RA)-RA)                                                     00111800
 B(2)=-B(2)                                                               00111900
 A(3,1)=8.*R*R*((2.-3.*D*SIN(D)*SIN(D)*SIN(D)-2.*COS(D)                   00112000
2-SIN(D)*SIN(D)*COS(D))/9.-D*(RA-D)*SIN(D)*SIN(D)*COS(D))                 00112100
 A(3,2)=R*R*(D**4.*COS(D)-12.*(D*D-2.)*COS(D)-4.*D*(D*D-6.)*SIN(D)-       00112200
224.-D**4.*(RA-D)*SIN(D))                                                 00112300
 A(3,3)=2.*R*R*((D*D-2.)*COS(D)-2.*D*SIN(D)-D*D*(RA-D)*SIN(D)+2.)         00112400
 A(3,4)=4.*R*R*(1.-COS(D)-.5*SIN(D)*SIN(D)+(RA-D)*SIN(D)-(RA-D)*SIN       00112500
2(D)*COS(D))                                                              00112600
 A(3,5)=4.*R*(COS(RA)-1.-.5*RA-.25*SIN(2.*RA)+.5*SIN(RA)**2.)             00112700
 B(3)=AM*(COS(RA)-1.)+E/(3.*R)                                            00112800
 A(4,1)=8.*R*R*(D*SIN(D)*COS(D)*COS(D)*COS(D)*3.- SIN(D)*COS(D) *         00112900
B  SIN(D)*COS(D) *2.-2.-3.*                                               00113000
2D*COS(D)*SIN(D)*SIN(D)*SIN(D)+2.*COS(D))/9.                              00113100
 A(4,2)=R*R*(D**4.-12.*(D*D-2.)-24.*COS(D))                               00113200
 A(4,3)=2.*R*R*(  (D*D-2)    +2.*COS(D))                                  00113300
 A(4,4)=4.*R*R*(COS(D)-1.+.5*D*SIN(D)+.25*SIN(D)+SIN(2.*D)                00113400
2-.5*COS(D)*SIN(D)*SIN(D))                                                00113500
 A(4,5)=4.*R*(SIN(RA)*SIN(D)-COS(D )+COS(RA)*COS(D)-.5*RA-.25*            00113600
2SIN(2.*RA)+.5*SIN(RA)*SIN(RA))                                           00113700
 B(4)=AM*(SIN(D)*SIN(RA)+COS(D)*COS(RA)-COS(D))+E/(3.*R)                  00113800
 A(5,1)=8.*R*R*(3.*D*SIN(RA)*COS(D)*COS(D)*COS(D)-SIN(RA)*SIN(D)*         00113900
8 COS(D)*COS(D)-2.*SIN(RA)*SIN(D)-3.*D*COS(RA)*SIN(D)*SIN(D)*             00114000
2 SIN(D)-COS(RA)*SIN(D)*SI                                                00114100
3N(D)*COS(D)-2.*COS(RA)*COS(D)+2.*COS(RA)+9.*D*(RA-D)*SIN(RA)             00114200
4*SIN(D)*COS(D)*COS(D)-9.*D*(RA-D)*COS(RA)*SIN(D)*SIN(D)*COS(D))/9.       00114300
 A(5,2)=R*R*(D**4.*SIN(RA)*SIN(D)-12.*(D*D-2.)*SIN(RA)*SIN(D)+4.*D        00114400
2*(D*D-6.)*SIN(RA)*COS(D)+D**4.*COS(RA)*COS(D)-12.*(D*D-2.)               00114500
3*COS (RA)*COS(D)-4.*D*(D*D-6.)*COS(RA)*SIN(D)-24.*COS(RA)+D**4.*         00114600
4(RA-D)*SIN(RA)*COS(D)-D**4.*(RA-D)*COS(RA)*SIN(D))                       00114700
 A(5,3)=2.*R*R*(2.*D*SIN(RA)*COS(D)+(D*D-2.)*SIN(RA)*SIN(D)-2.*D*COS      00114800
2S(RA)*SIN(D)+(D*D-2.)*COS(RA)*COS(D)+2.*COS(RA)+D*D*(RA-D)*SIN(RA)       00114900
3*COS(D)-D*D*(RA-D)*COS(RA)*SIN(D))                                       00115000
 A(5,4)=4.*R*R*(COS(RA)-SIN(RA)*SIN(D)-COS(RA)*COS(D)+.5*D*SIN(RA)        00115100
2+.25*SIN(RA)*SIN(2.*D)-.5*COS(RA)*SIN(D)*SIN(D)-(RA-D)*SIN(RA)*          00115200
```

```
     3CCS(D )+(RA-D)*COS(RA)*SIN(D)+(RA-D)*SIN(RA)*COS(D)*COS(D)-(RA-D)  00115300
     4*COS(RA)*SIN(D)*COS(D))                                           00115400
      A(5,5)=4.*R*(1-COS(RA)-.5*RA-.25*SIN(2.*RA)+.5*SIN(RA)*SIN(RA))   00115500
      B(5)=AM*(1.-COS(RA))+E/(3.*R)                                     00115600
C     IF(M .GT.0) GO TO 10                                              00115700
C     MMF=MF+1                                                          00115800
C     WRITE(6,20) MMF,((I,J,A(I,J),J=1,5),I=1,5)                        00115900
C  20 FORMAT(/10X,' KUNT=',I3,5(5X/5(5X,'A(',I1,',',I1,')=',1PE10.3)))  00116000
   10 CONTINUE                                                          00116100
      CALL REDUC(N)                                                     00116200
      CALL BACKED (N)                                                   00116300
      RETURN                                                            00116400
      END                                                               00116500
      SUBROUTINE REDUC(N)                                               00116600
      IMPLICIT REAL*8(A-H,O-Z)                                          00116700
C     REDUCTION OF EQUATIONS BY ELIMINATION                             00116800
      COMMON/PRINT/A(6,6)                                               00116900
      COMMON/BCOM/B(6)                                                  00117000
      NC=0                                                              00117100
      NN=N-1                                                            00117200
      DO 10 K=1,NN                                                      00117300
      KK=K+1                                                            00117400
      DO 10 I=KK,N                                                      00117500
   11 IF(A(K,K).EQ.0) GO TO 30                                          00117600
C     IF A(K,K) IS ZERO WILL CAUSE / BY 0                               00117700
C     REARRANGE ARRAY                                                   00117800
      GO TO 40                                                          00117900
30    LL=K                                                              00118000
      MM=K                                                              00118100
      DO 1 M=MM,N                                                       00118200
1     A(N+1,M)=A(LL,M)                                                  00118300
      B(N+1)=B(LL)                                                      00118400
      DO 2 L=LL,N                                                       00118500
      DO 3 M=MM,N                                                       00118600
3     A(L,M)=A(L+1,M)                                                   00118700
2     B(L)=B(L+1)                                                       00118800
      NC=NC+1                                                           00118900
      IF(NC.LT.100) GO TO 11                                            00119000
      WRITE(6,13)                                                       00119100
   13 FORMAT('  EQUATIONS CAN NOT BE LINEAR AND INDEPENDANT')          00119200
      STOP                                                              00119300
40    DIV=A(I,K)/A(K,K)                                                 00119400
      DO 20 J=KK,N                                                      00119500
20    A(I,J)=A(I,J)-DIV*A(K,J)                                          00119600
      B(I)=B(I)-DIV*B(K)                                                00119700
      NC=0                                                              00119800
10    CONTINUE                                                          00119900
      RETURN                                                            00120000
```

```
      END                                                               00120100
      SUBROUTINE BACKED(N)                                              00120200
      IMPLICIT REAL*8(A-H,O-Z)                                          00120300
C     SOLVE FOR VALUES OF X BY BACKED SUSTITUTION                       00120400
      COMMON/PRINT/A(6,6)                                               00120500
      COMMON/BCOM/B(6)                                                  00120600
      COMMON/CCOM/C(6)                                                  00120700
      C(N+1)=0                                                          00120800
      DO 10 I=1,N                                                       00120900
      VAL=0                                                             00121000
      L=N-I+1                                                           00121100
      A(L,N+1)=0                                                        00121200
      LL=L+1                                                            00121300
      DO 20 J=LL,N                                                      00121400
   20 VAL=VAL+A(L,J)*C(J)                                               00121500
      C(L)=(B(L)-VAL)/A(L,L)                                            00121600
   10 CONTINUE                                                          00121700
      RETURN                                                            00121800
      END                                                               00121900
```

APPENDIX B

FIELD INSTRUMENTATION DATA

Table B-1 lists the dates of installation of instrumented bolts and roof sag stations, the dates of the initial and final borescope readings, and the dates of the end of the test periods for the two test sites in each of the three mines in the field test program.

Table B-1 is followed by graphs showing the borescope data and bolt strain and strata deflection as functions of time. Only data from Mines 2 and 3 are shown since Mine 1 data has been presented elsewhere (Ref. 3, Chapter VI).

Fig. B-1 through B-4: Borescope logs.

Fig. B-5 through B-19: Bolt strain data from Mine 2.

Fig. B-20 through B-27: Strata displacement data from Mine 2.

Fig. B-28 through B-40: Bolt strain data from Mine 3.

Fig. B-41 through B-47: Strata displacement data from Mine 3.

Note: All strata displacements are positive downward. All bolt strains are positive in tension.

Table B-1 Dates of Field Installations, Borescope Readings, and Test Terminations.

Mine No.	Test Site	Dates of Installation		Dates of Borescope Inspection		Termination Date of Test
		Instrumented Bolts	Sag Indicators	Initial	Final	
1	1	April 5, 1975	April 5, 1975	None	None	Nov. 8, 1975
	2	April 5, 1975	April 5, 1975	None	None	Nov. 8, 1975
2	1	Nov. 12, 1976	Nov. 12 and 13, 1976	Nov. 13, 1976	June 7, 1977	June 7, 1977
	2	Nov. 12, 1976	Nov. 12 and 1976	Nov. 13, 1976	June 7, 1977	June 7, 1977
3	1	Feb. 11, 1977	Feb. 11, 1977	Feb. 11, 1977	June 7, 1977	June 7, 1977
	2	Feb. 11, 1977	Feb. 12, 1977	Feb. 11, 1977	June 7, 1977	June 7, 1977

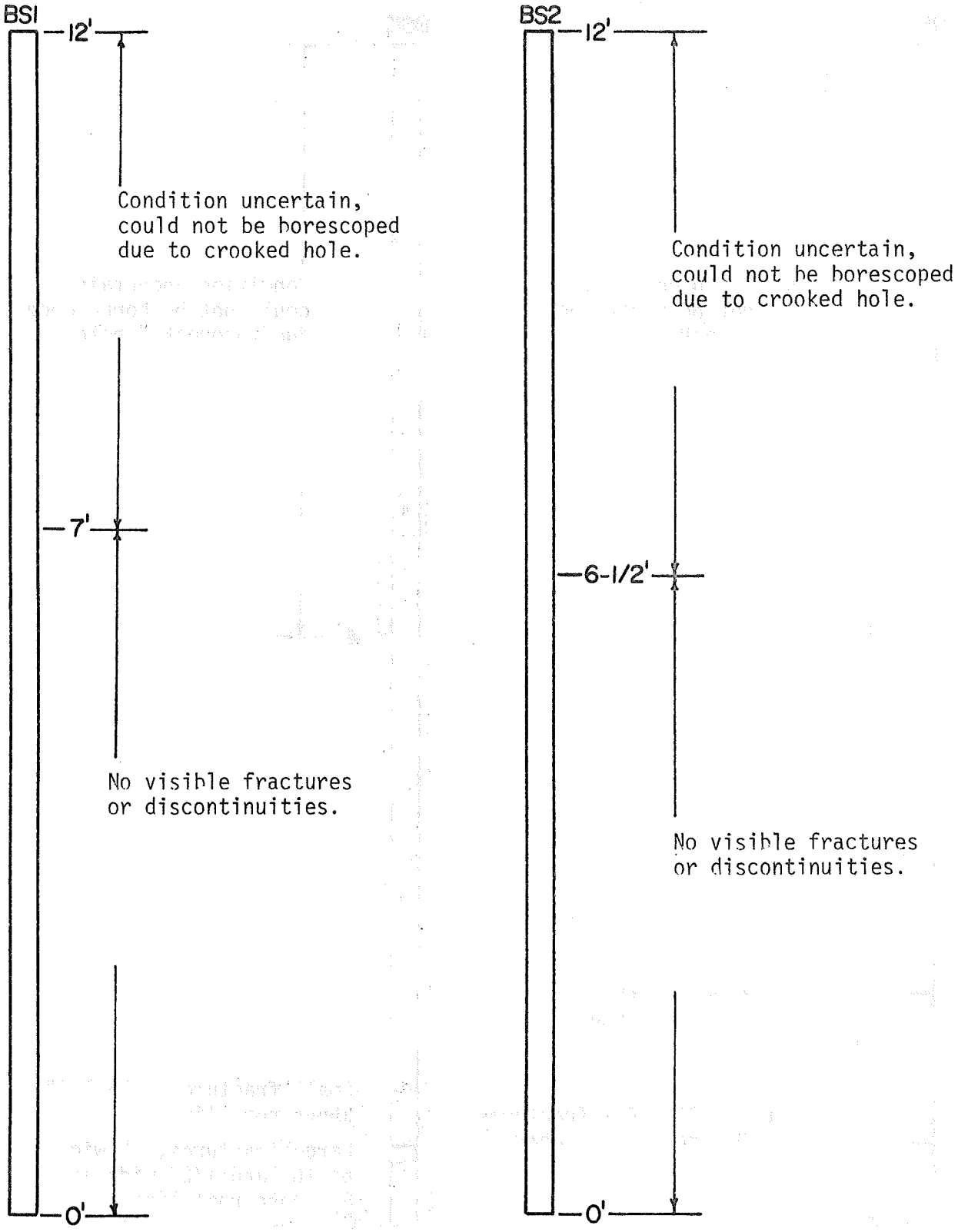

Fig. B-1 Borescope logs at Mine 2, Test site 1.

Note: No visible change during the test period.

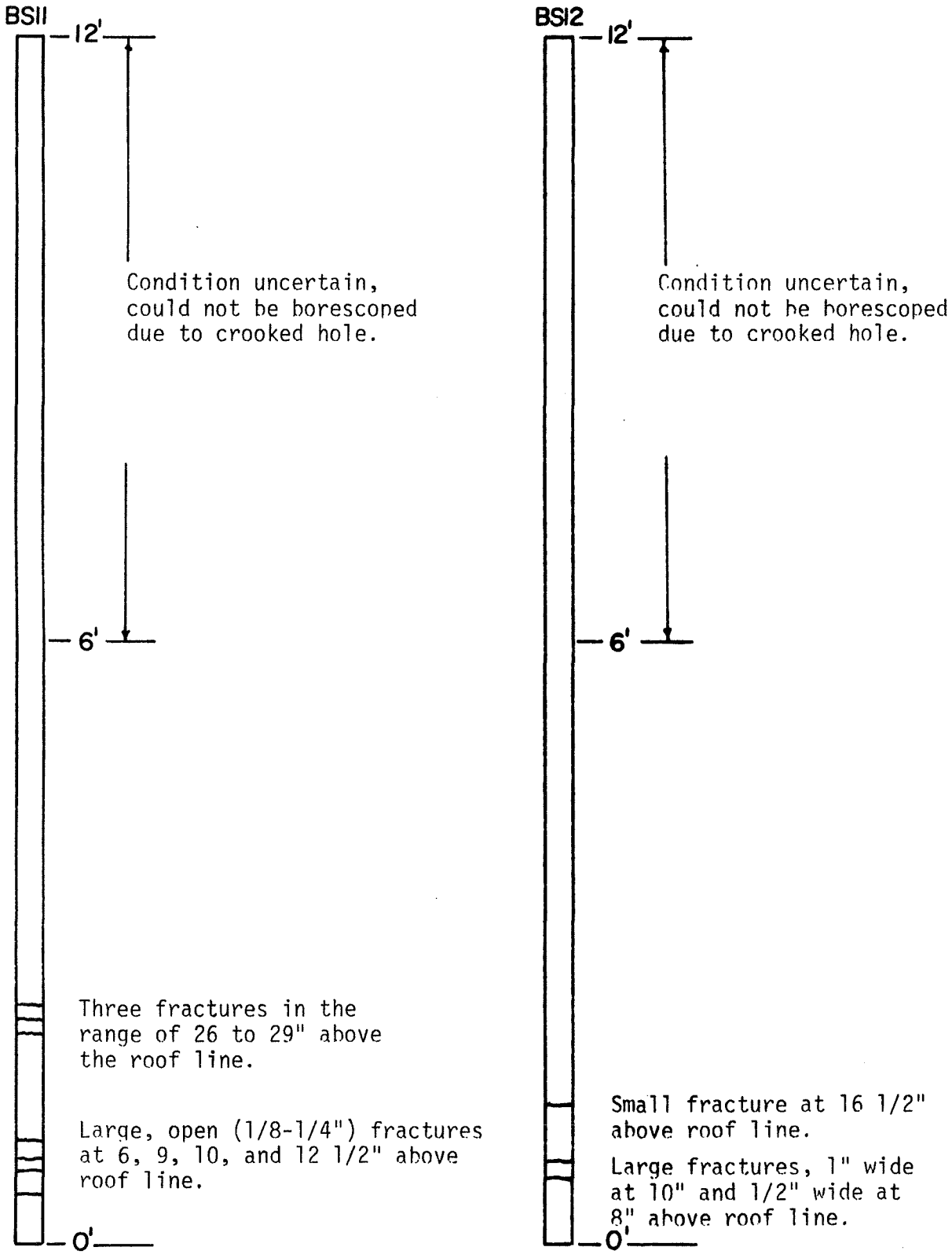

Fig. B-2 Borescope logs at Mine 2, Test site 2.

Note: No visible change during the test period.

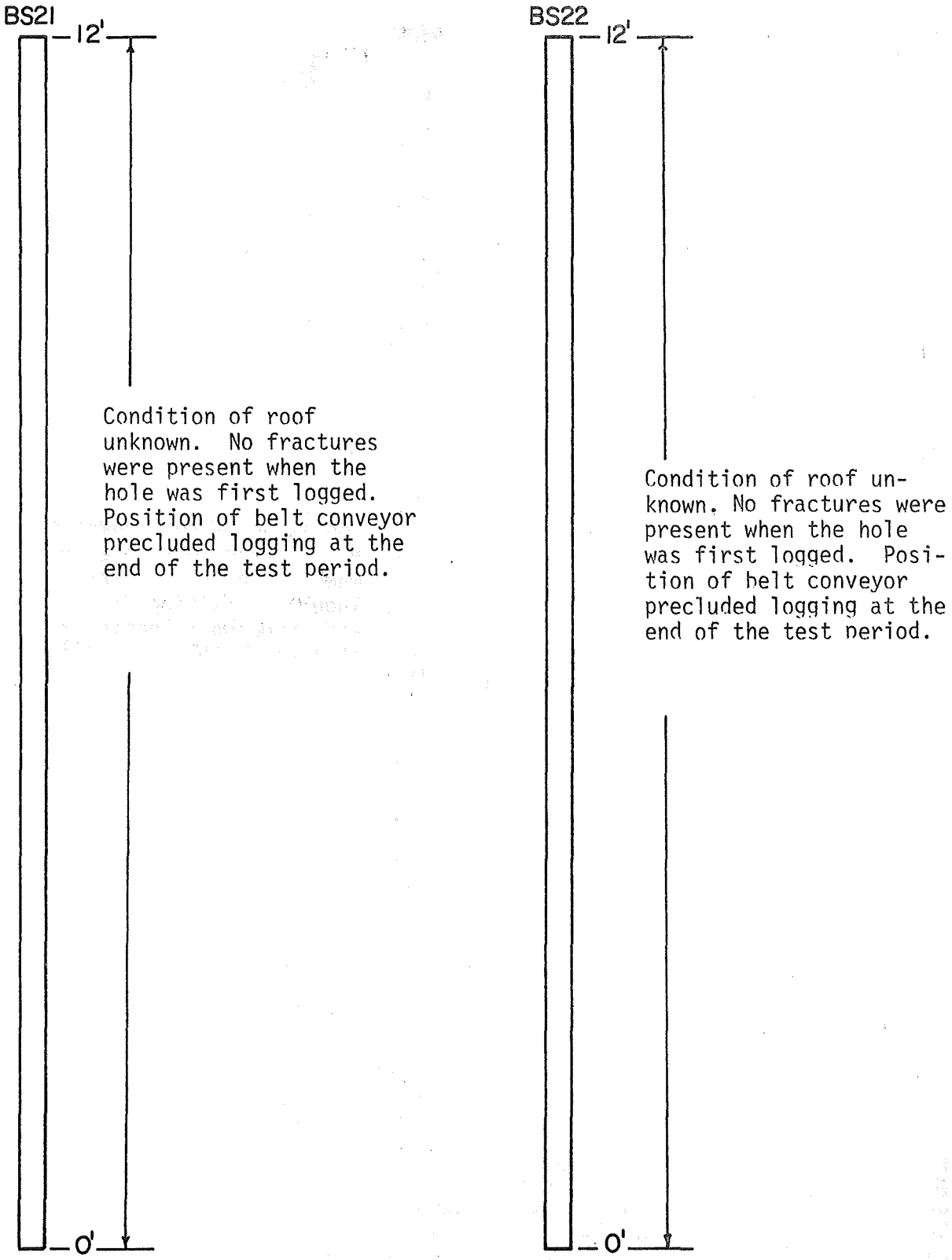

Fig. B-3 Borescope log at Mine 3, Test site 1.

Note: No fractures were visible at time of installation.

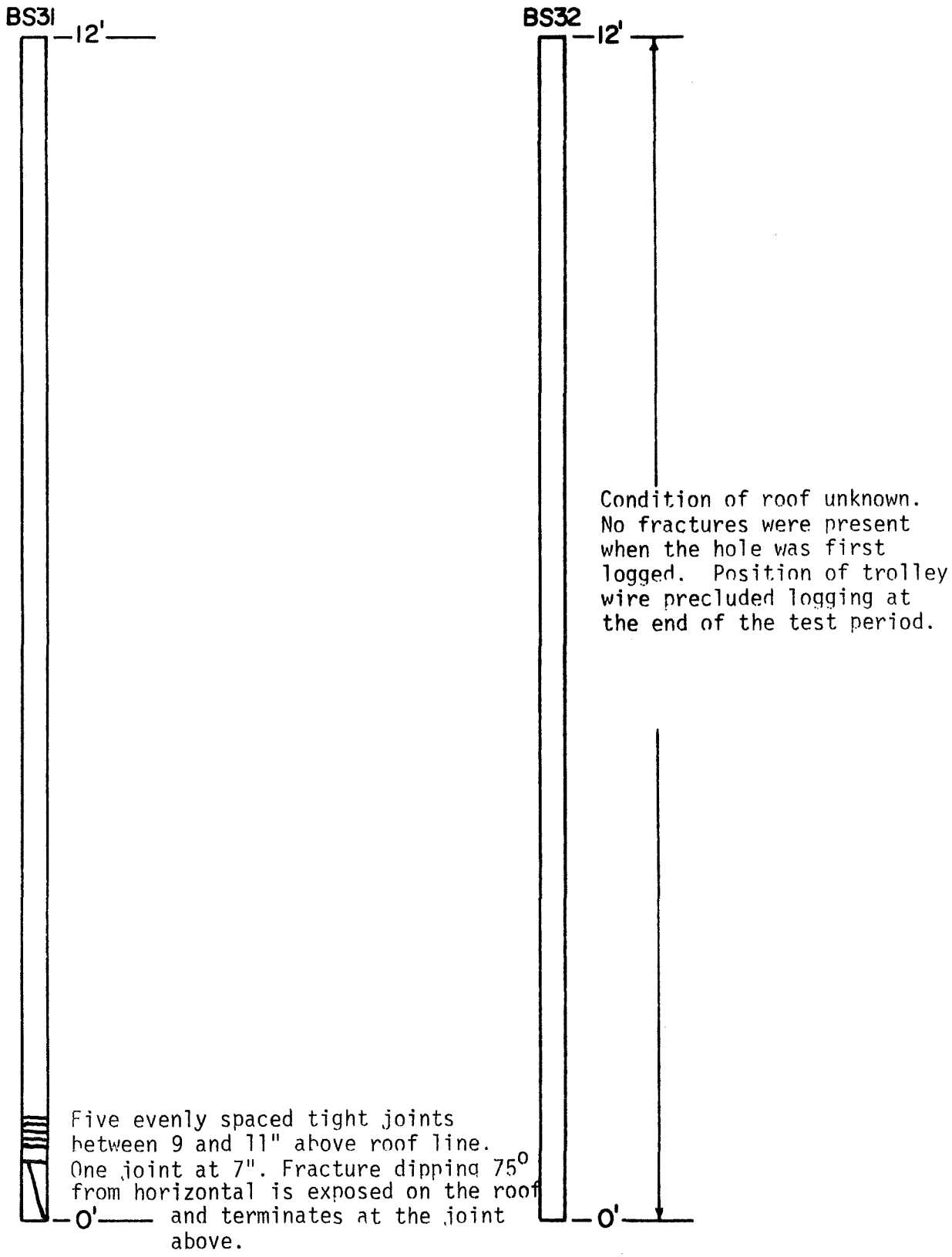

Fig. B-4 Borescope log at Mine 3, Test site 2.

Note: No fractures visible at time of installation.

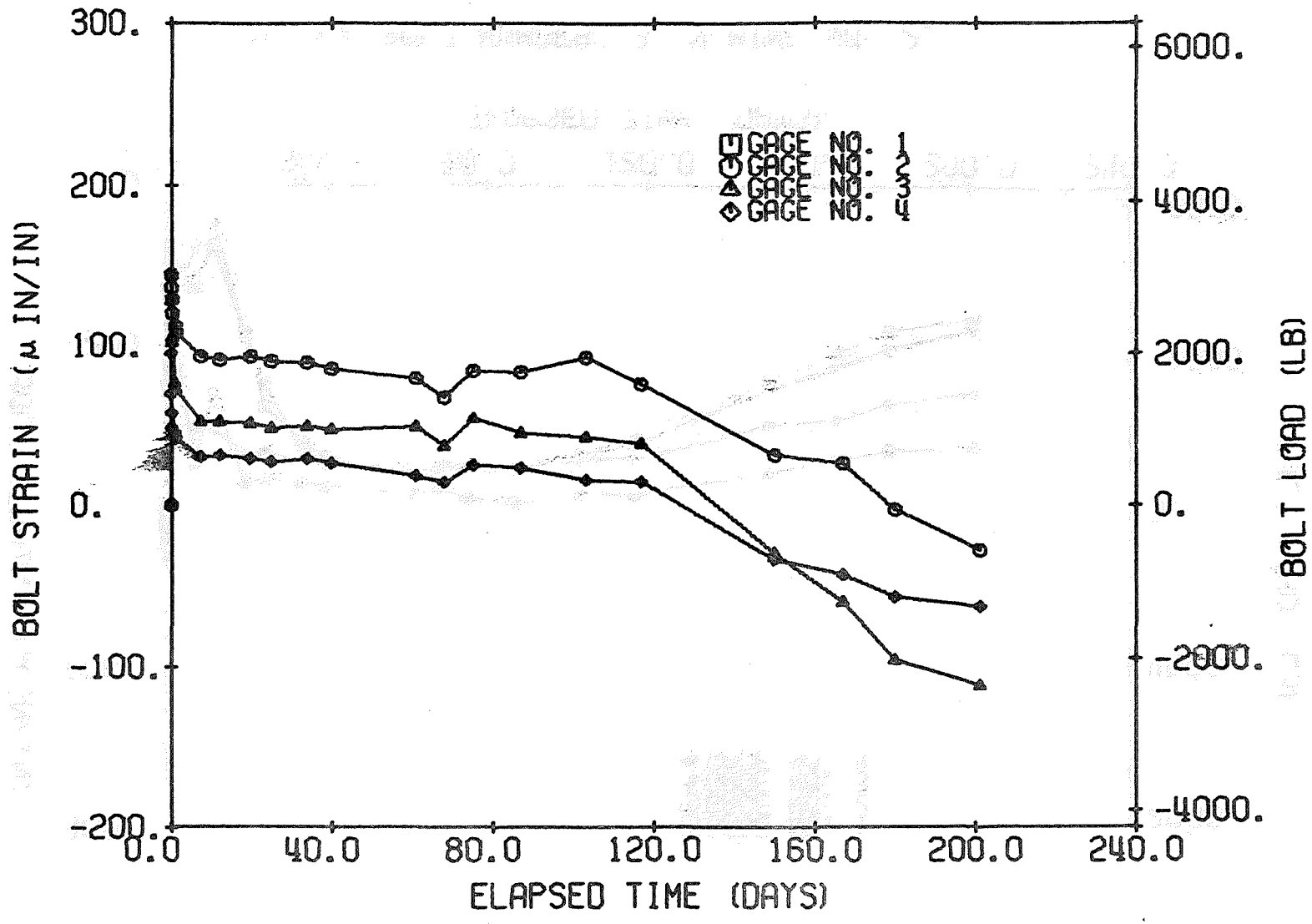

Fig. B-5 BOLT NUMBER 1 IN MINE NO. 2.
1 IN. BAR IN 1-3/8 IN. HOLE DUPONT RESIN

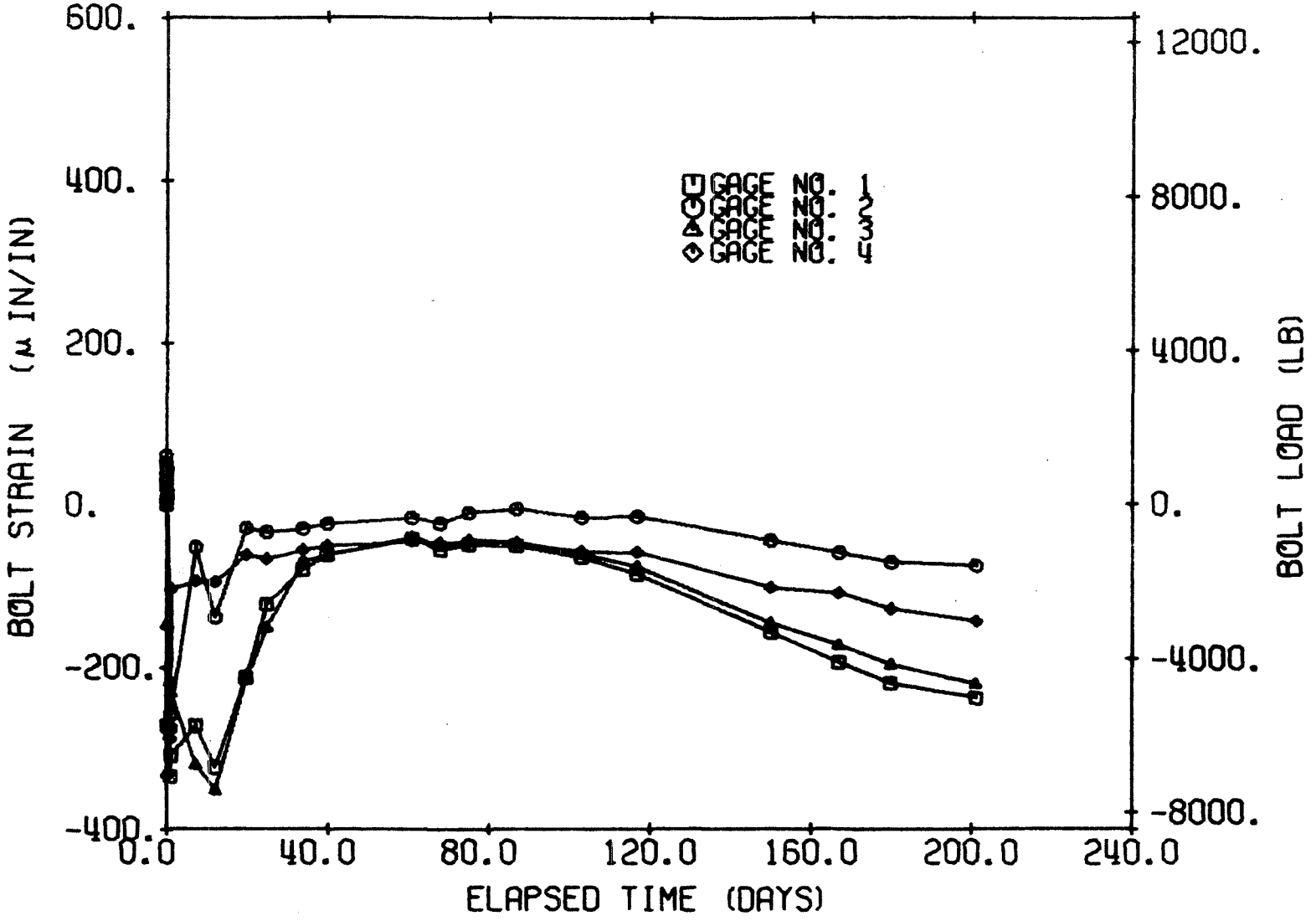

Fig. B-6 BOLT NUMBER 2 IN MINE NO. 2.

1 IN. BAR IN 1-3/8 IN. HOLE DUPONT RESIN

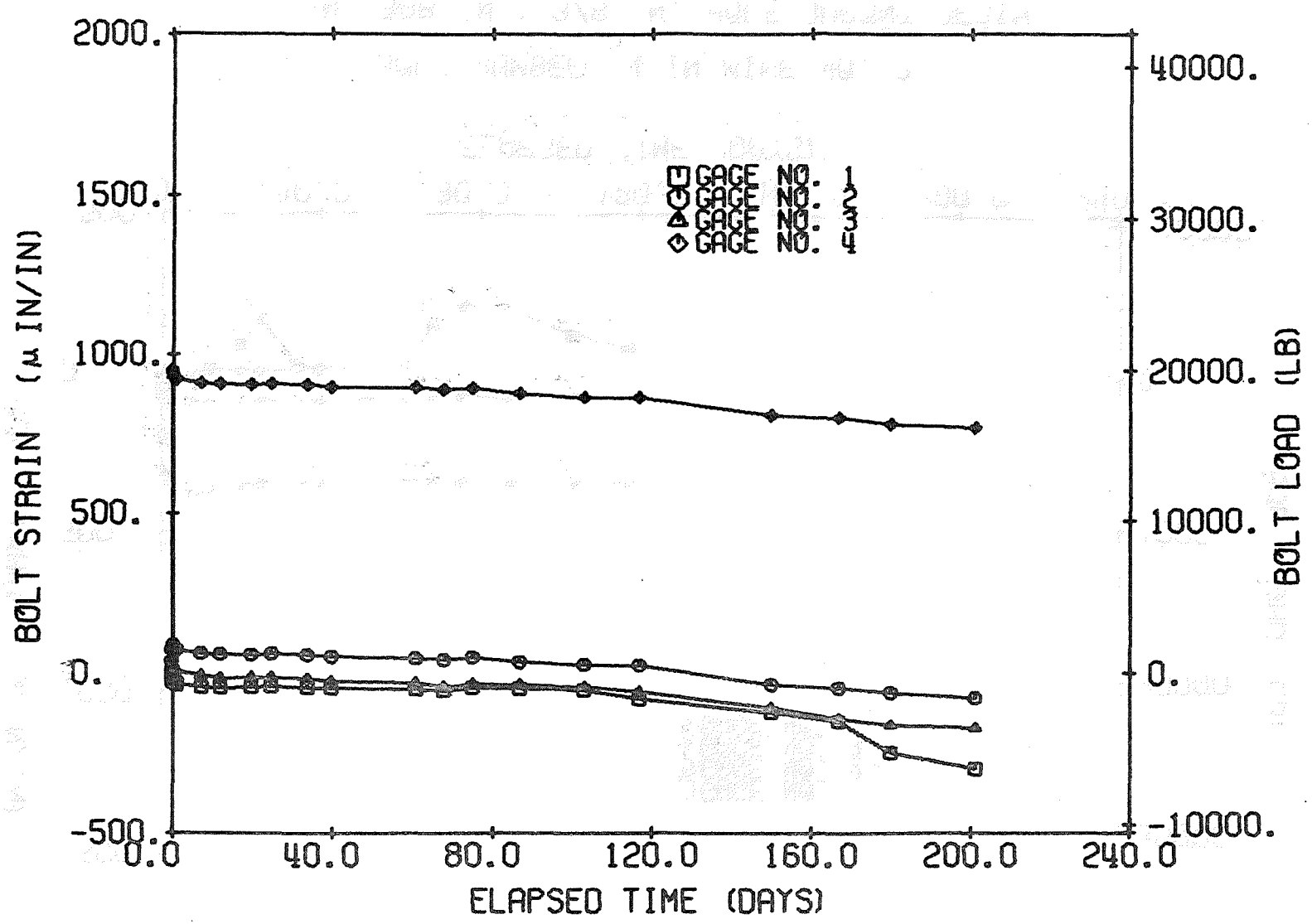

Fig. B-7 BOLT NUMBER 3 IN MINE NO. 2.
1 IN. BAR IN 1-3/8 IN. HOLE DUPONT RESIN

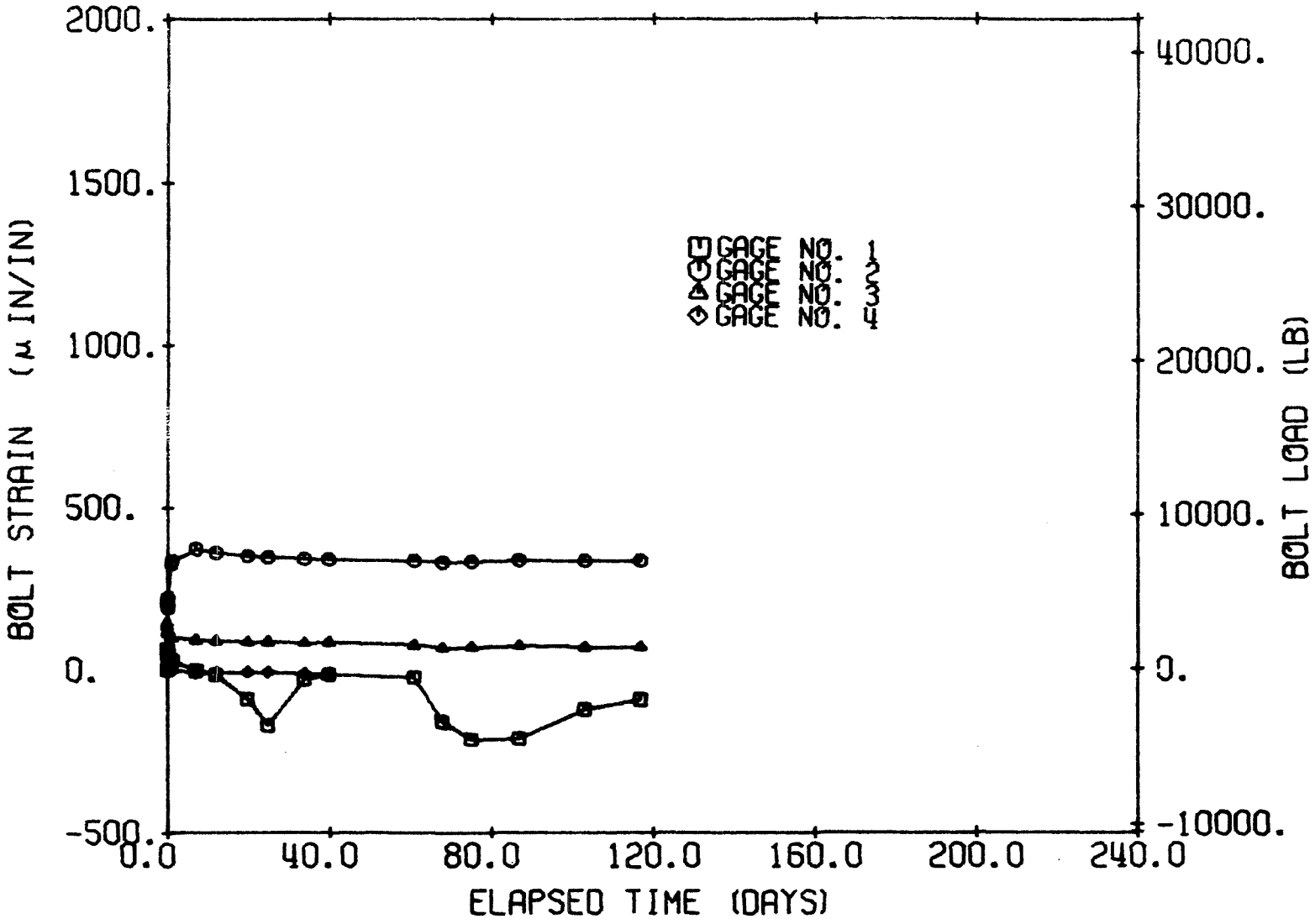

Fig. B-8 BOLT NUMBER 4 IN MINE NO. 2.

1 IN. BAR IN 1-3/8 IN. HOLE DUPONT RESIN

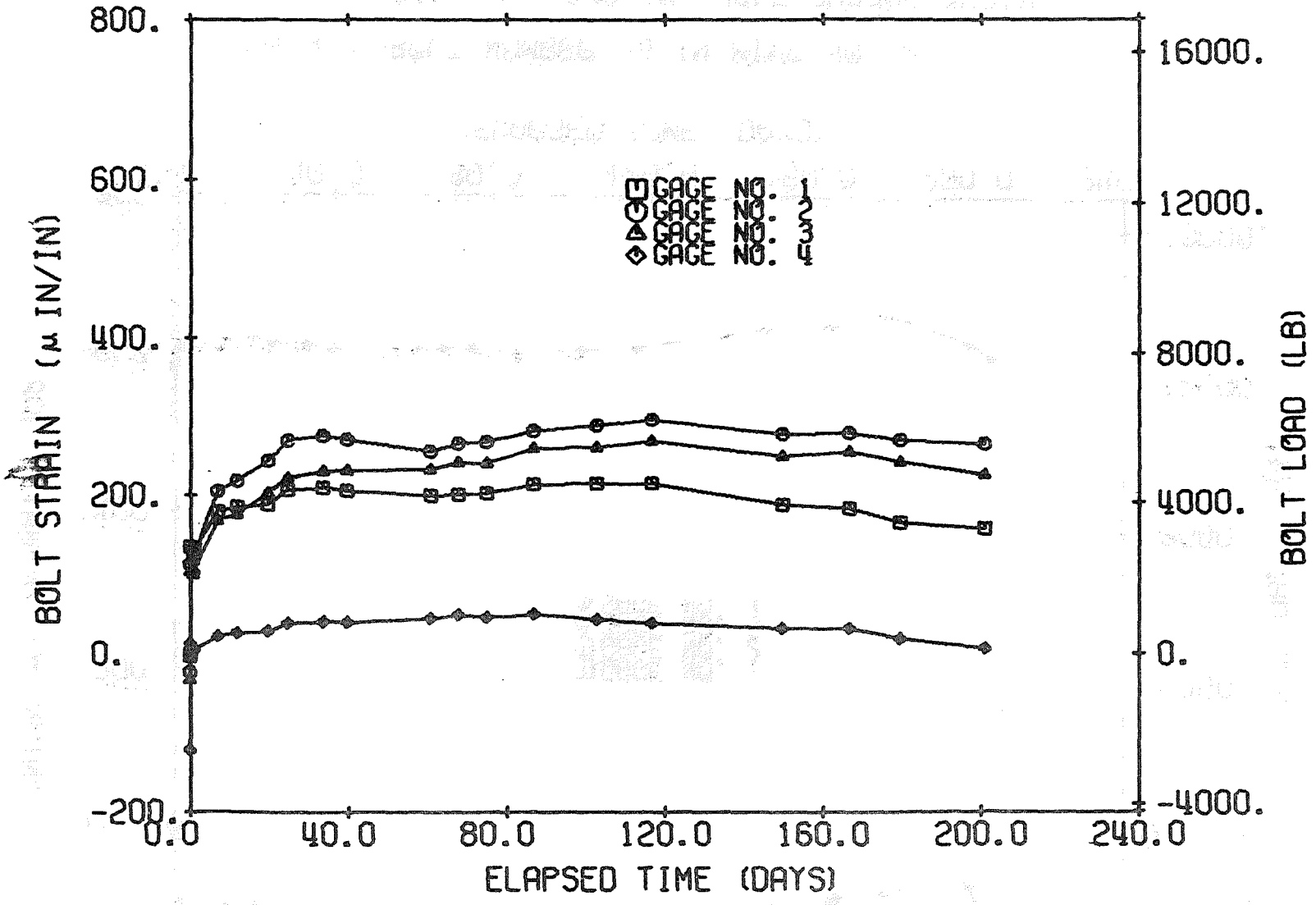

Fig. B-9 BOLT NUMBER 5 IN MINE NO. 2.

1 IN. BAR IN 1-3/8 IN. HOLE DUPONT RESIN

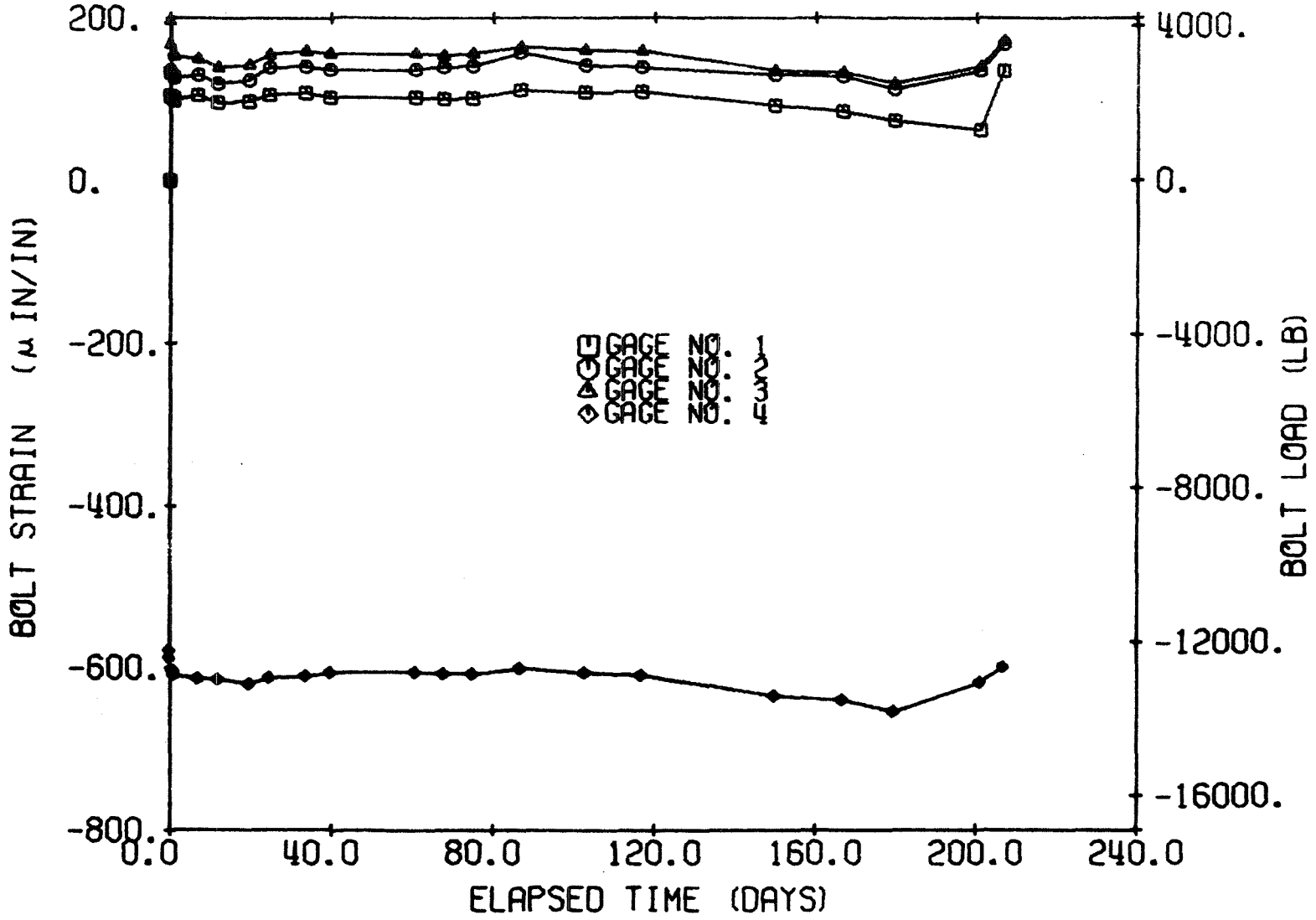

Fig. B-10 BOLT NUMBER 6 IN MINE NO. 2.

1 IN. BAR IN 1-3/8 IN. HOLE DUPONT RESIN

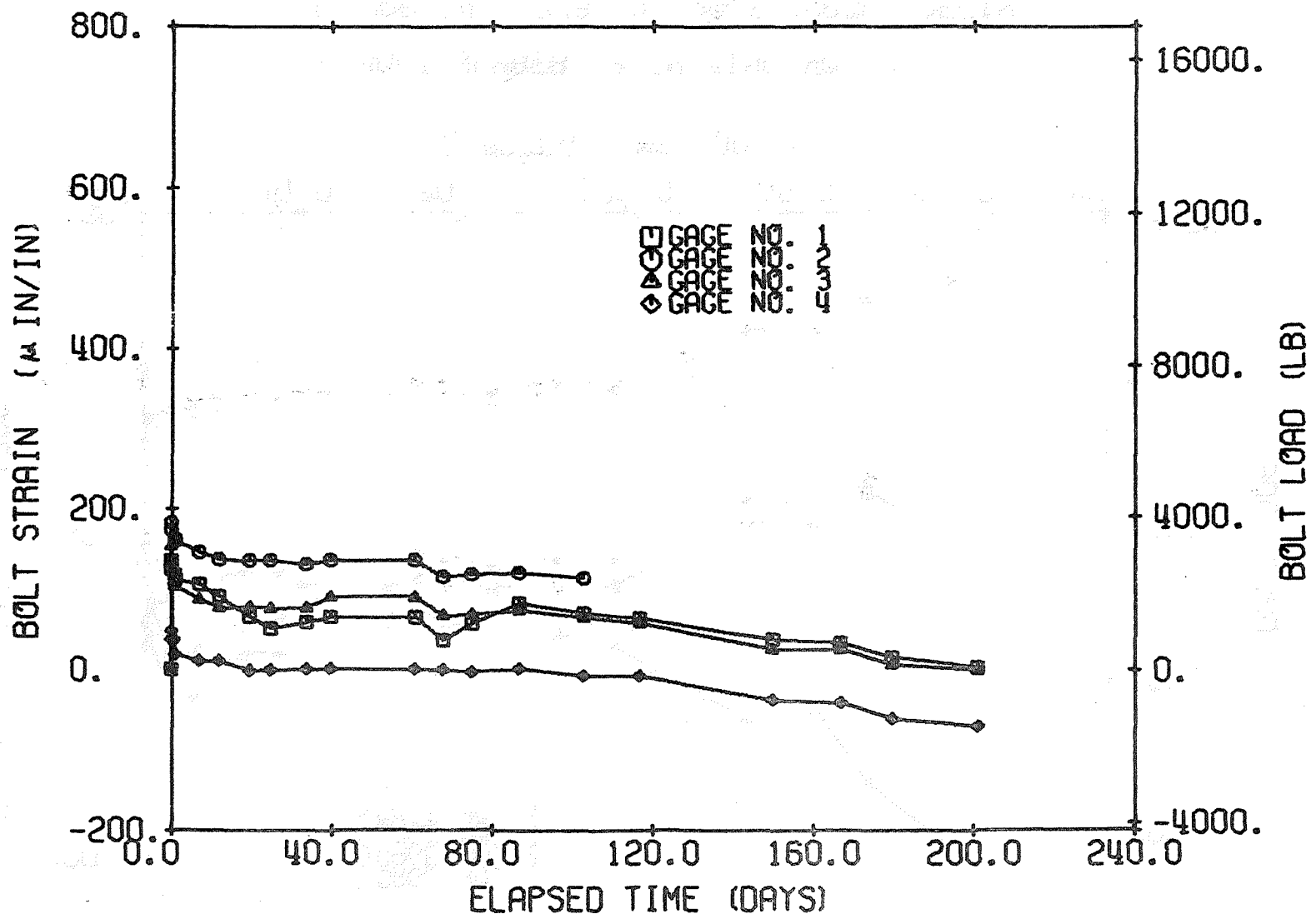

Fig. B-11 BOLT NUMBER 7 IN MINE NO. 2.
1 IN. BAR IN 1-3/8 IN. HOLE DUPONT RESIN

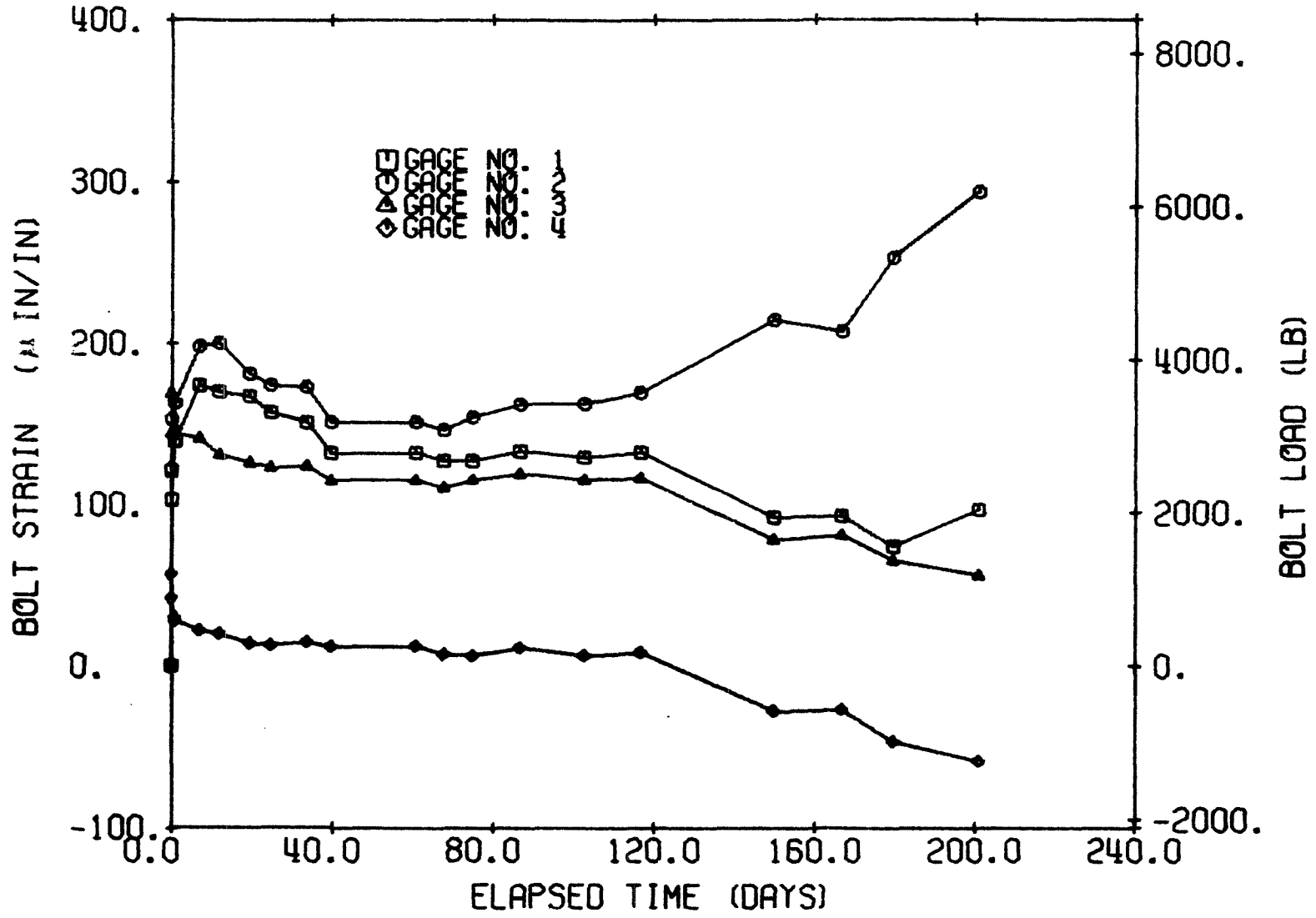

Fig. B-12 BOLT NUMBER 8 IN MINE NO. 2.
1 IN. BAR IN 1-3/8 IN. HOLE DUPONT RESIN

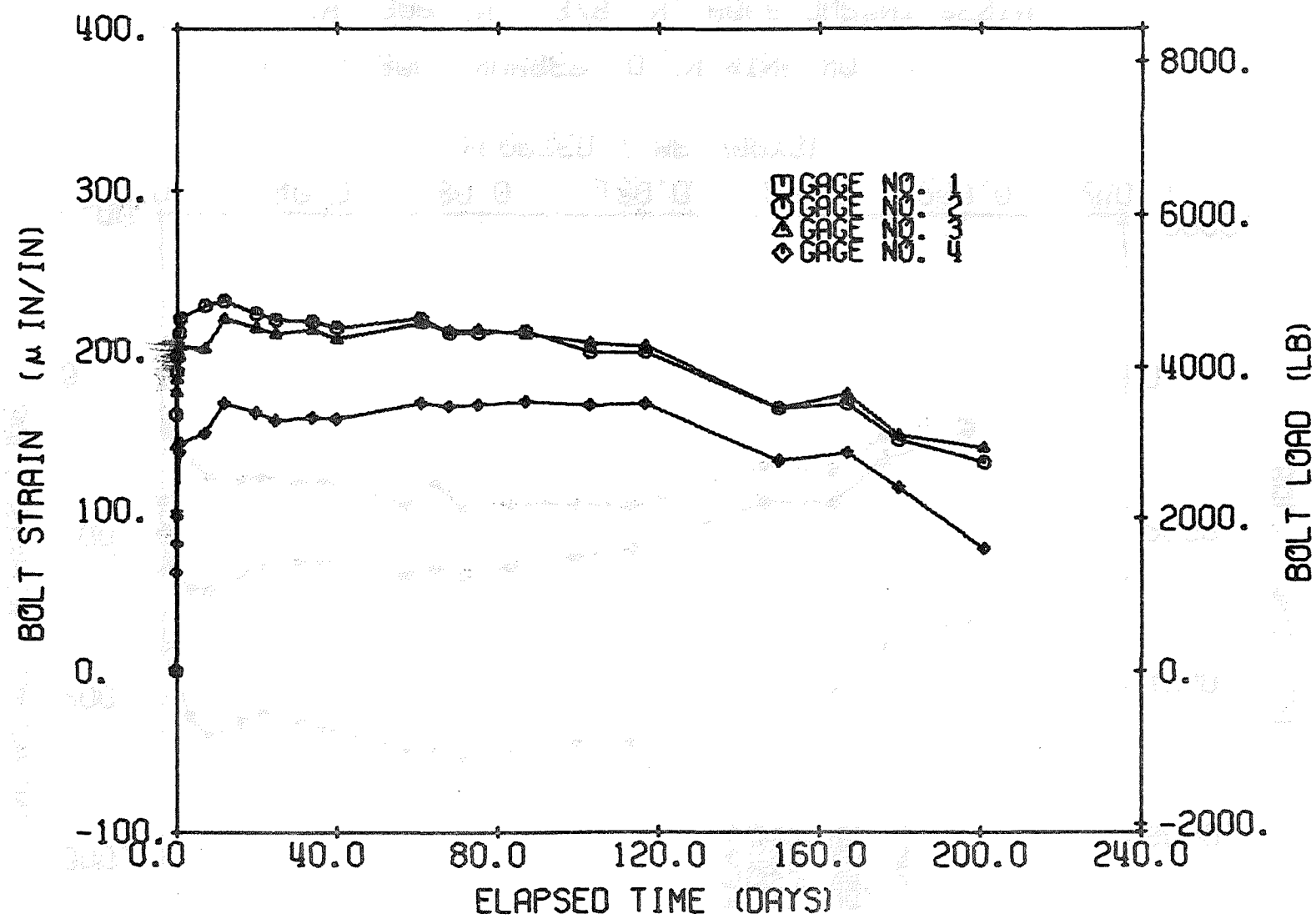

Fig. B-13 BOLT NUMBER 9 IN MINE NO. 2.

1 IN. BAR IN 1-3/8 IN. HOLE DUPONT RESIN

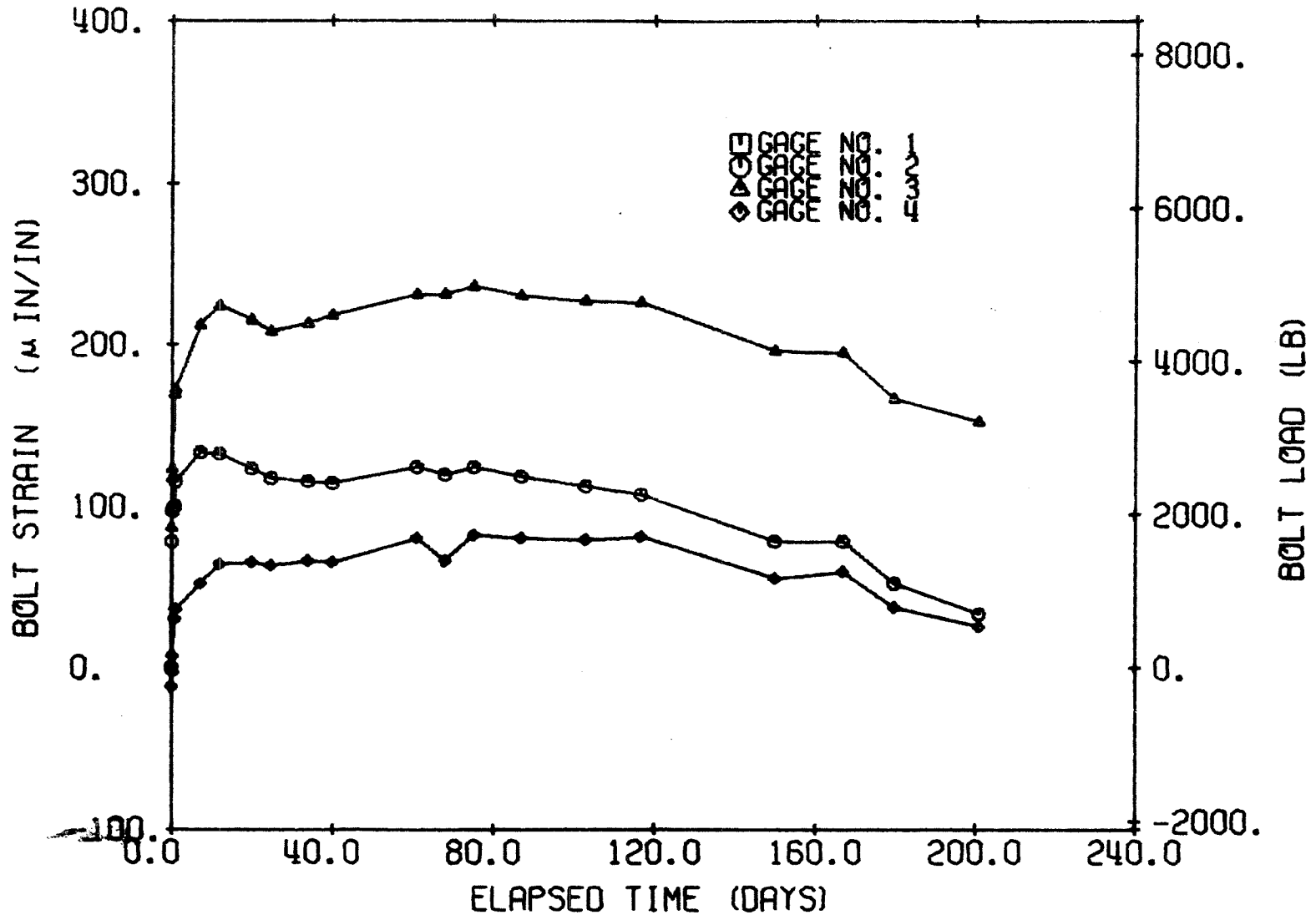

Fig. B-14 BOLT NUMBER 10 IN MINE NO. 2.

1 IN. BAR IN 1-3/8 IN. HOLE DUPONT RESIN

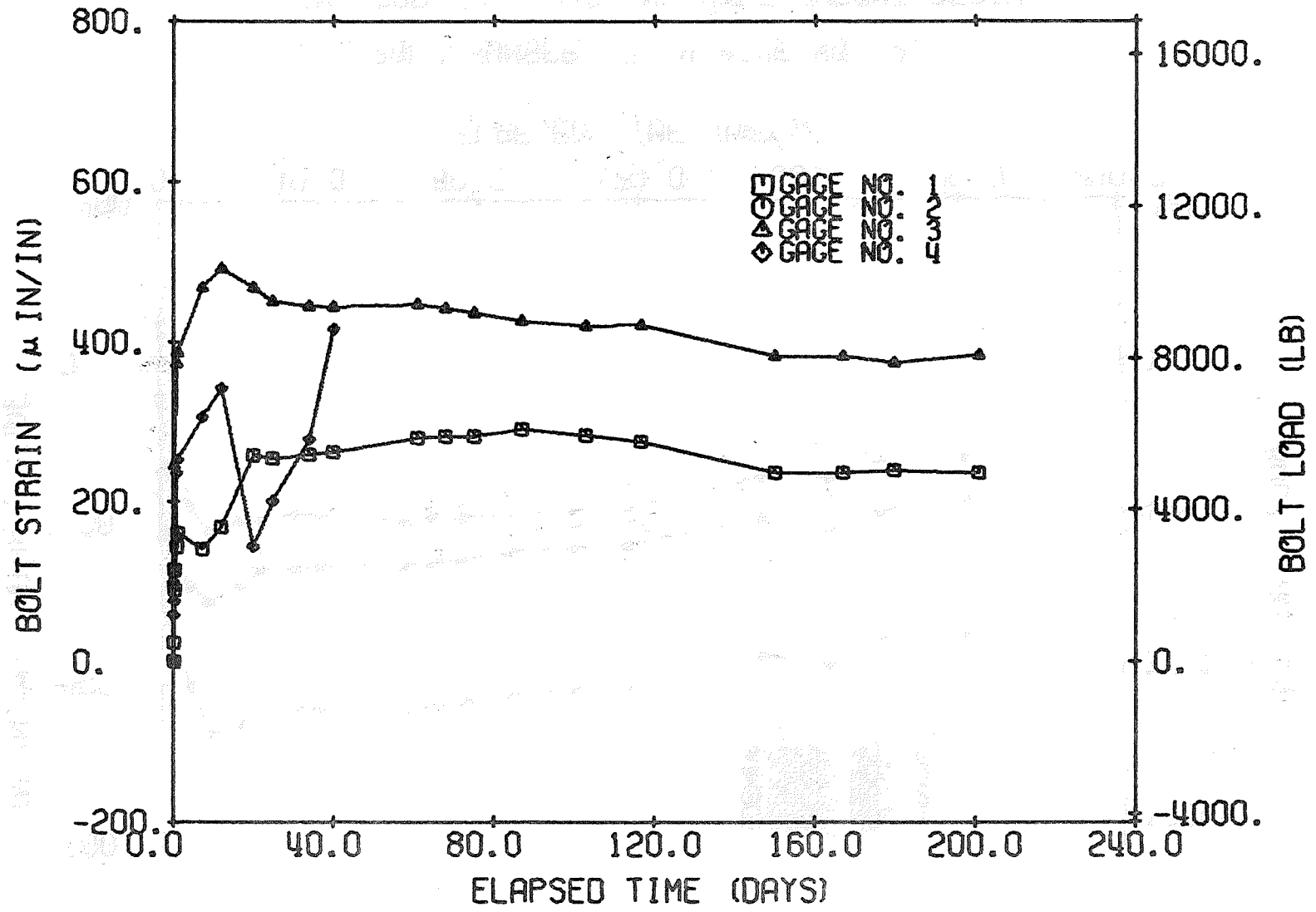

Fig. B-15 BOLT NUMBER 11 IN MINE NO. 2.
1 IN. BAR IN 1-3/8 IN. HOLE DUPONT RESIN

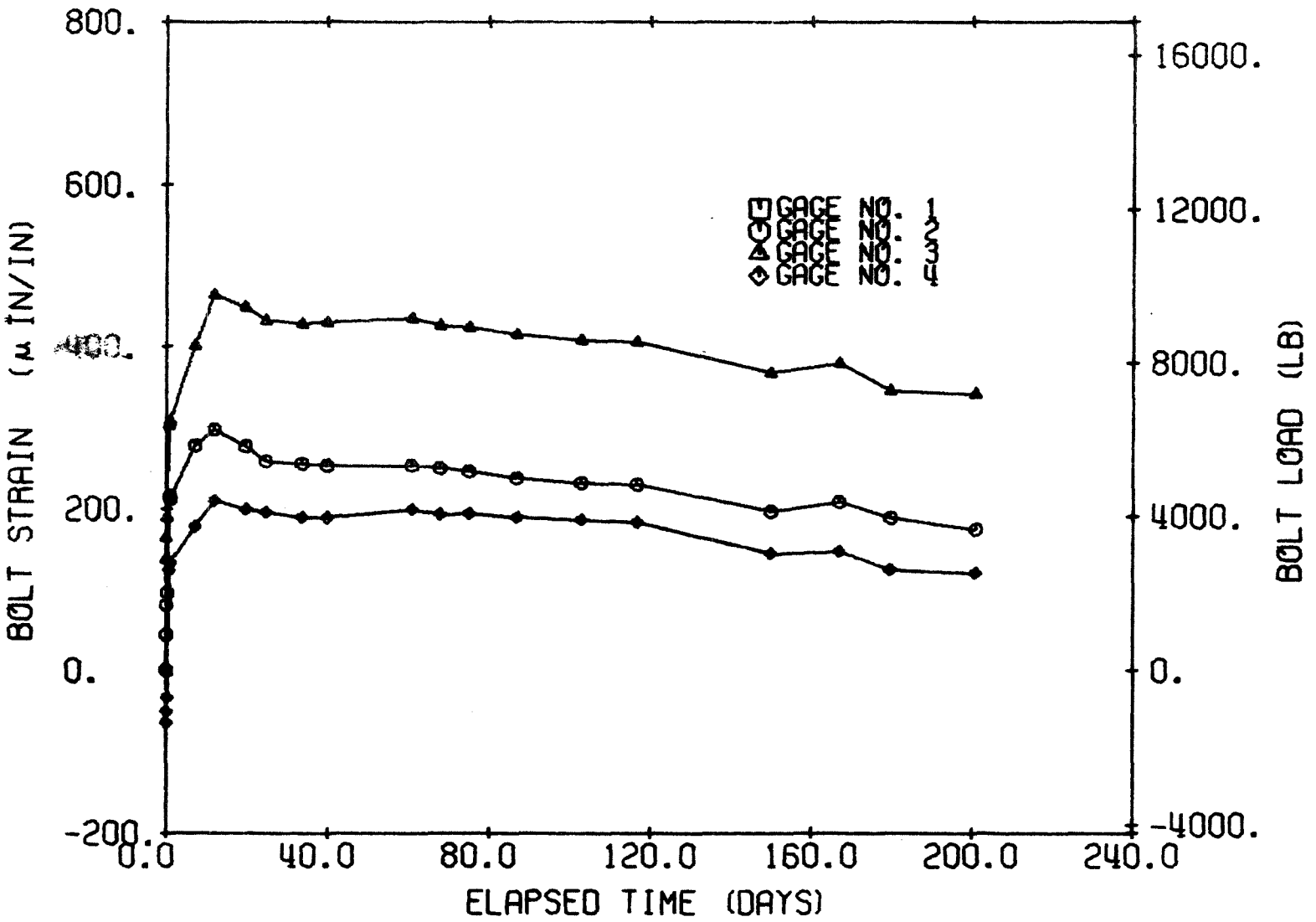

Fig. B-16 BOLT NUMBER 12 IN MINE NO. 2.
1 IN. BAR IN 1-3/8 IN. HOLE DUPONT RESIN

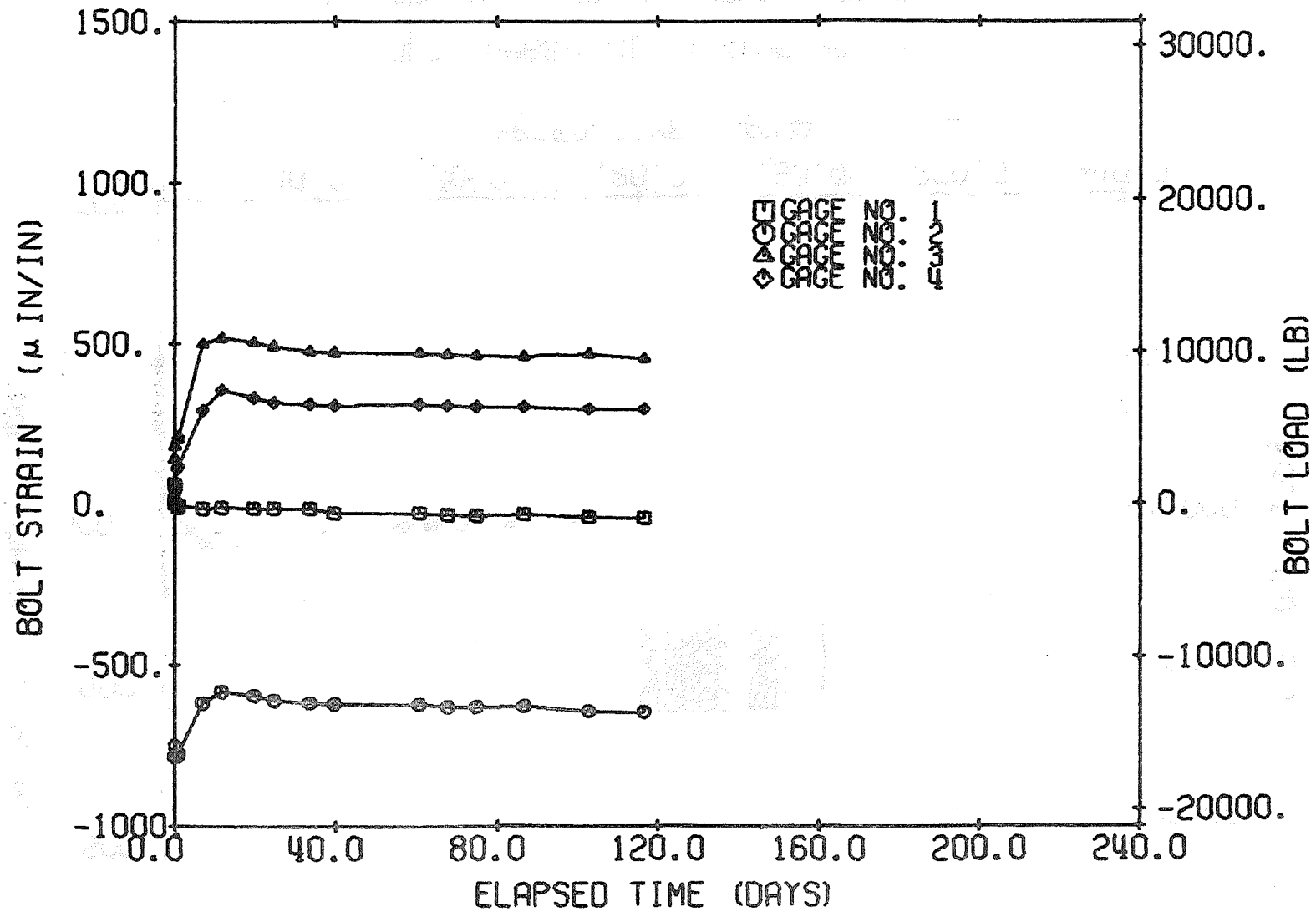

Fig. B-17 BOLT NUMBER 13 IN MINE NO. 2.

1 IN. BAR IN 1-3/8 IN. HOLE DUPONT RESIN

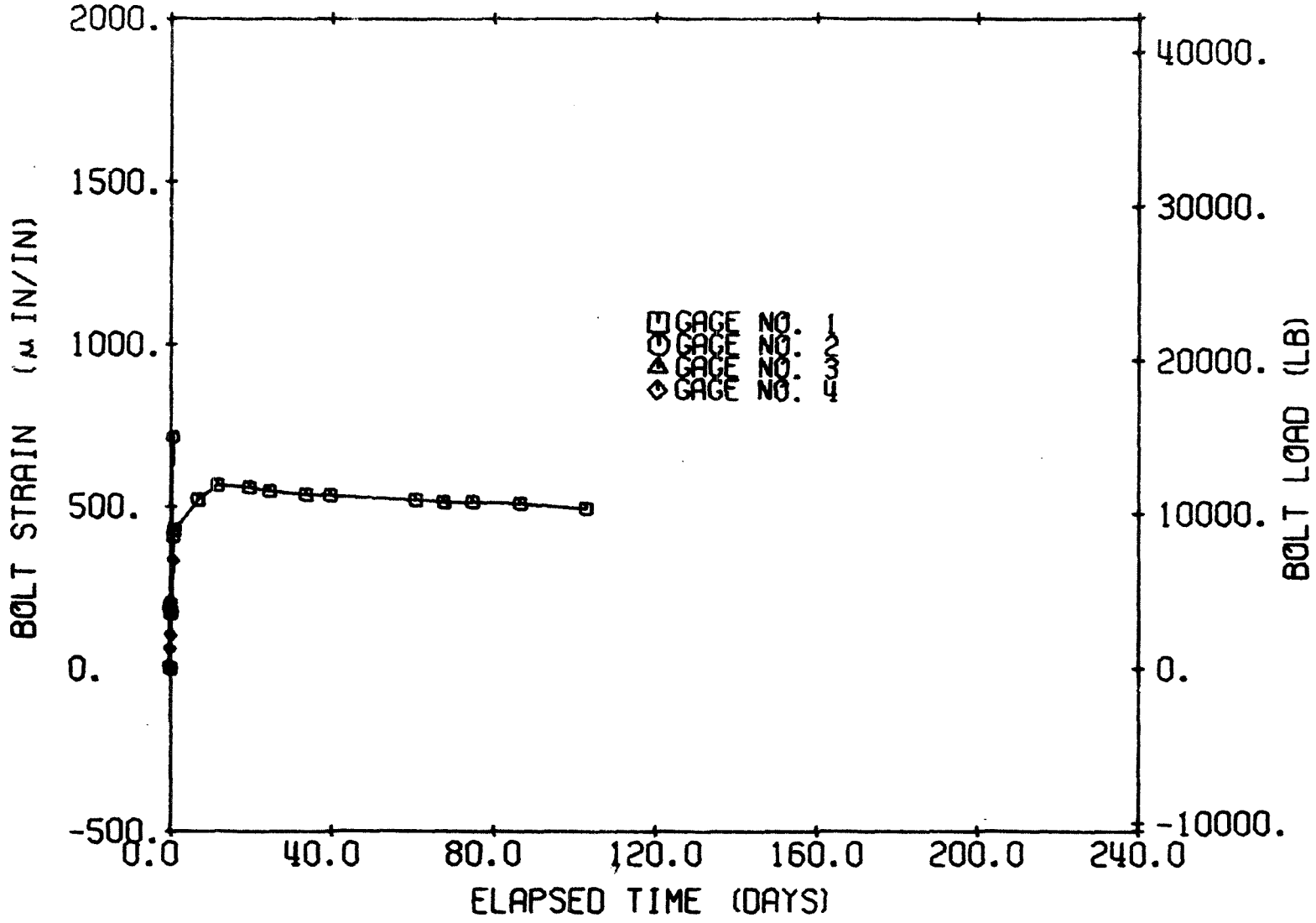

Fig. B-18 BOLT NUMBER 14 IN MINE NO. 2.
1 IN. BAR IN 1-3/8 IN. HOLE DUPONT RESIN

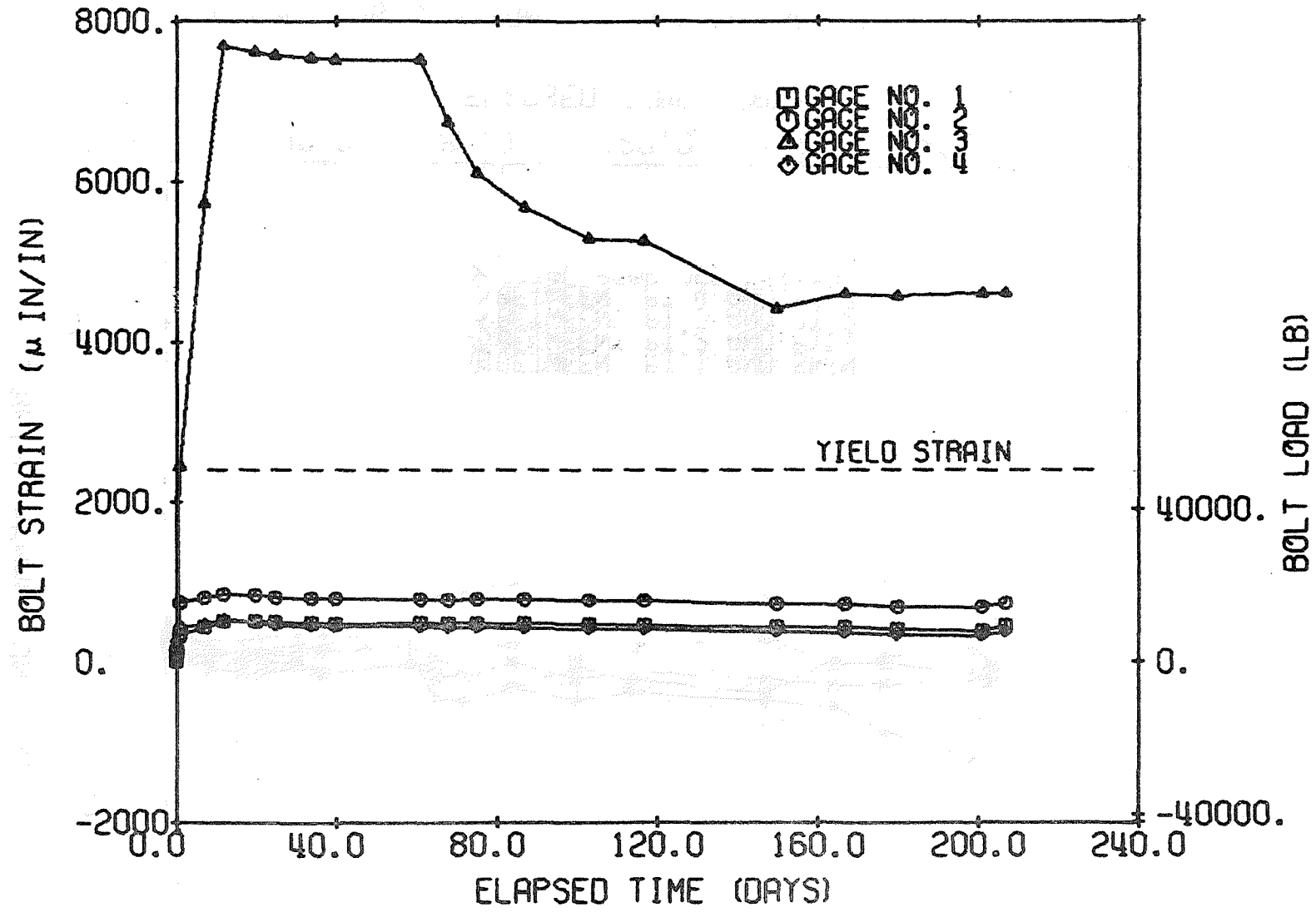

Fig. B-19 BOLT NUMBER 16 IN MINE NO. 2.

1 IN. BAR IN 1-3/8 IN. HOLE DUPONT RESIN

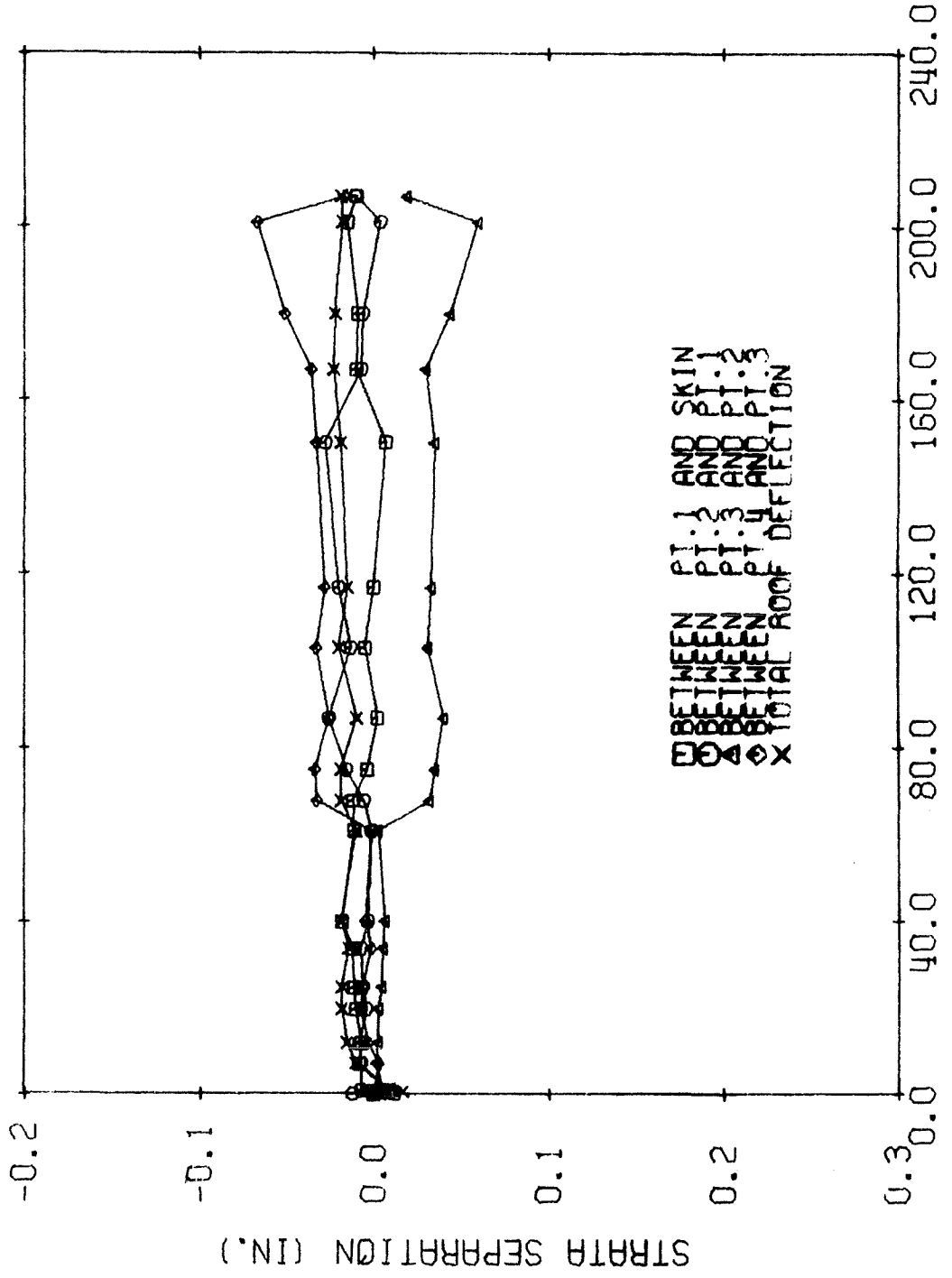

Fig. B-20 SAG STATION 1 IN MINE NO. 2.

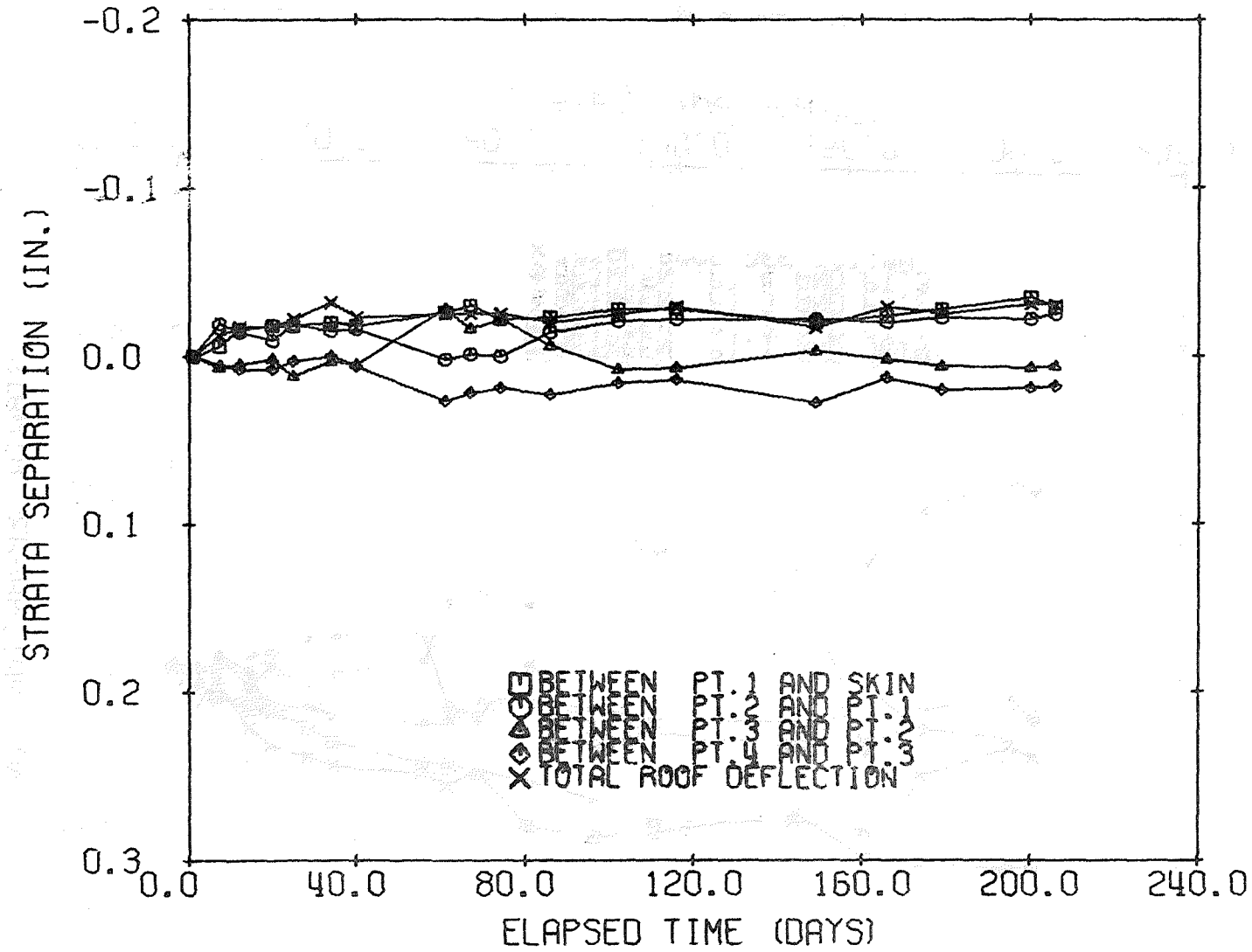

Fig. B-21 SAG STATION 2 IN MINE NO. 2.

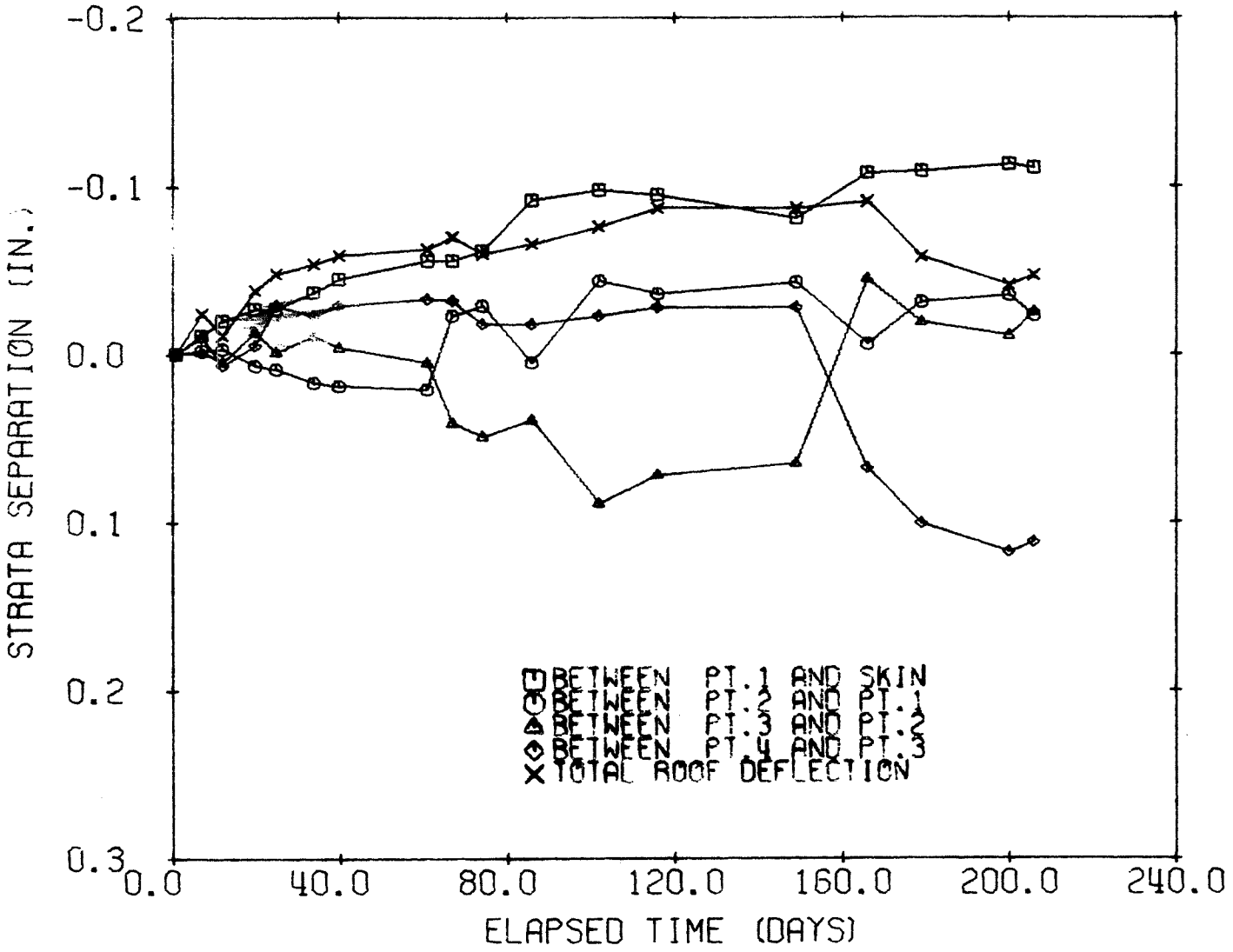

Fig. B-22 SAG STATION 3 IN MINE NO. 2.

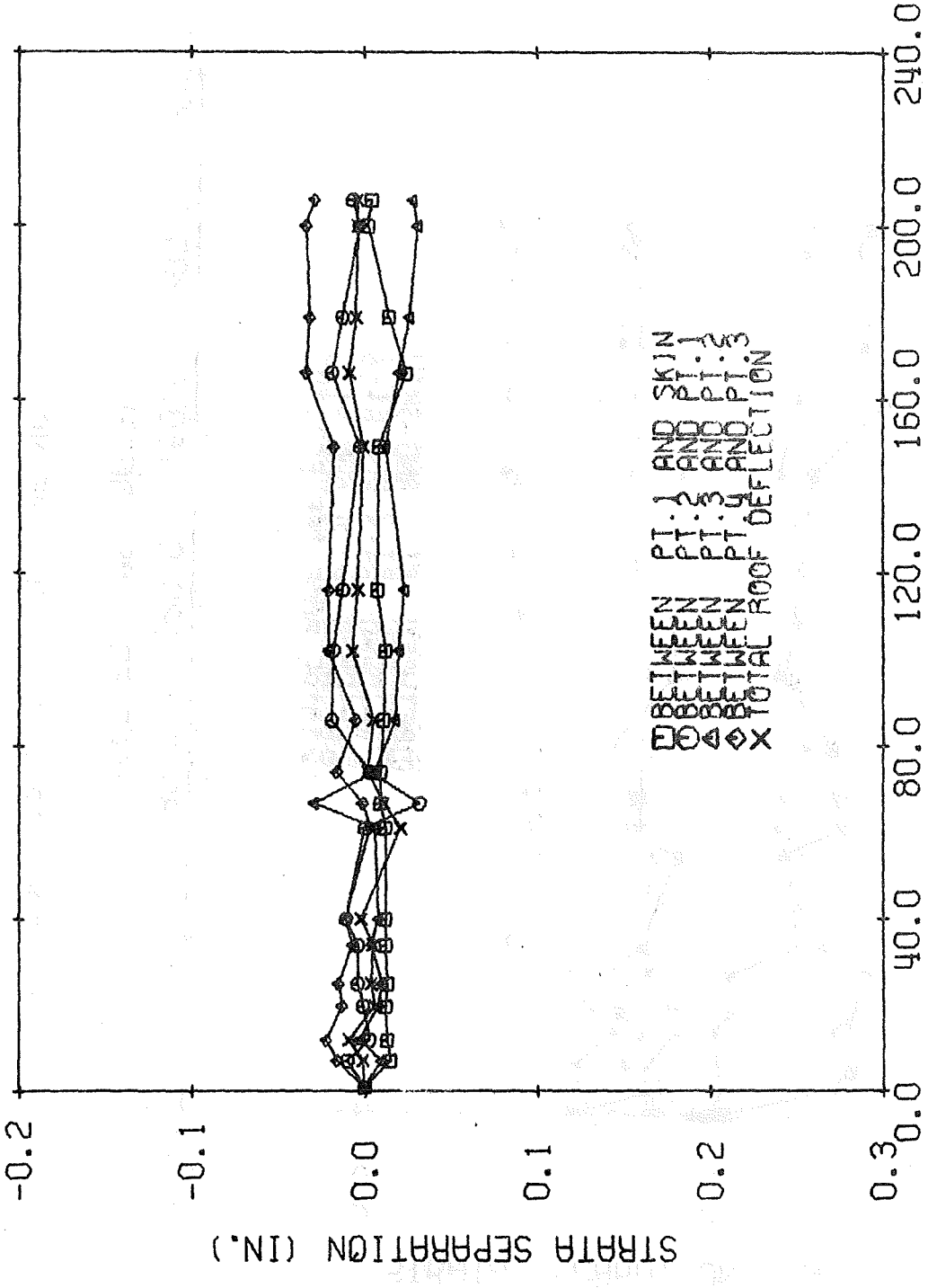

Fig. B-23 SAG STATION 4 IN MINE NO. 2.

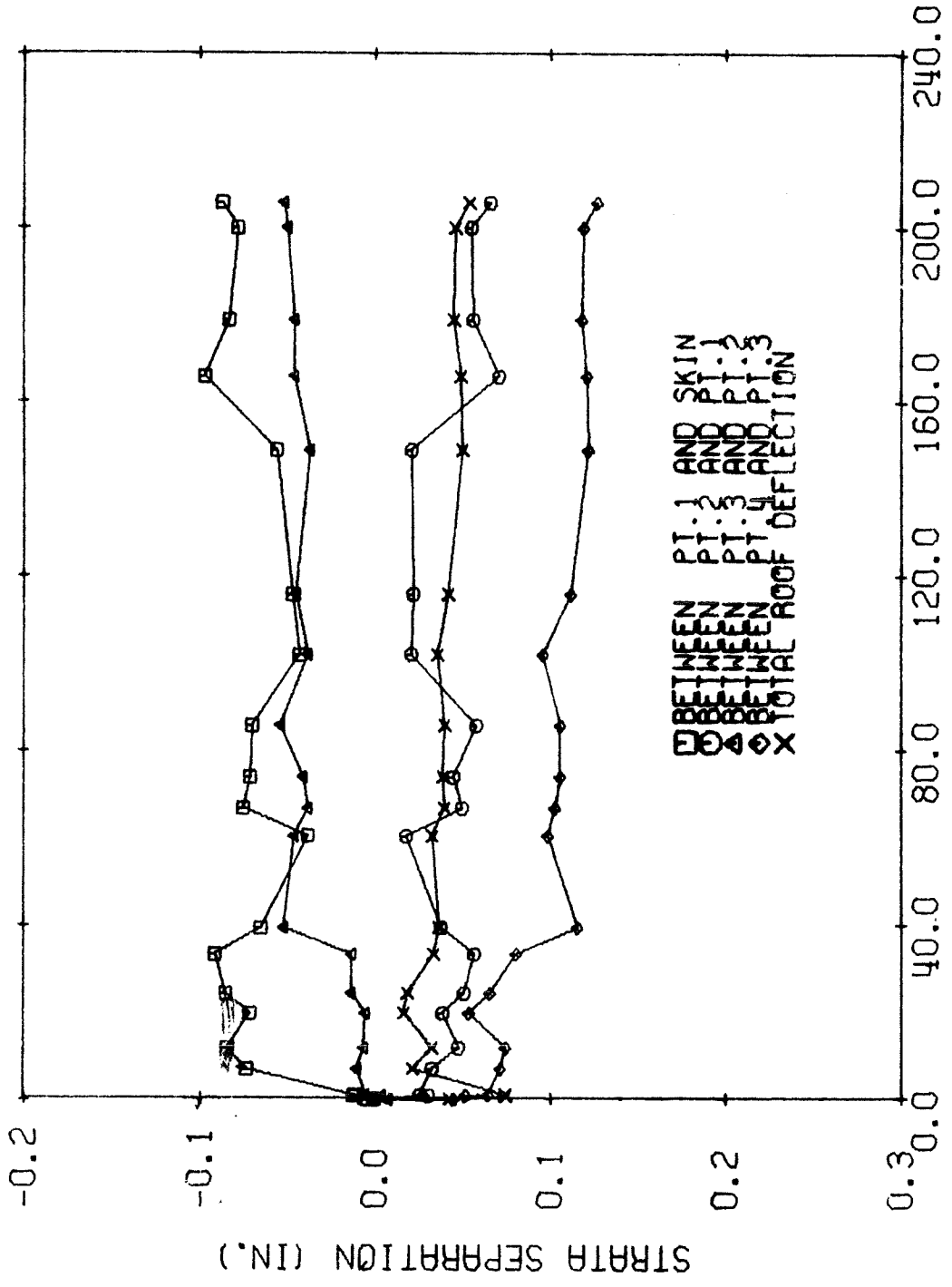

Fig. B-24 SAG STATION 11 IN MINE NO. 2.

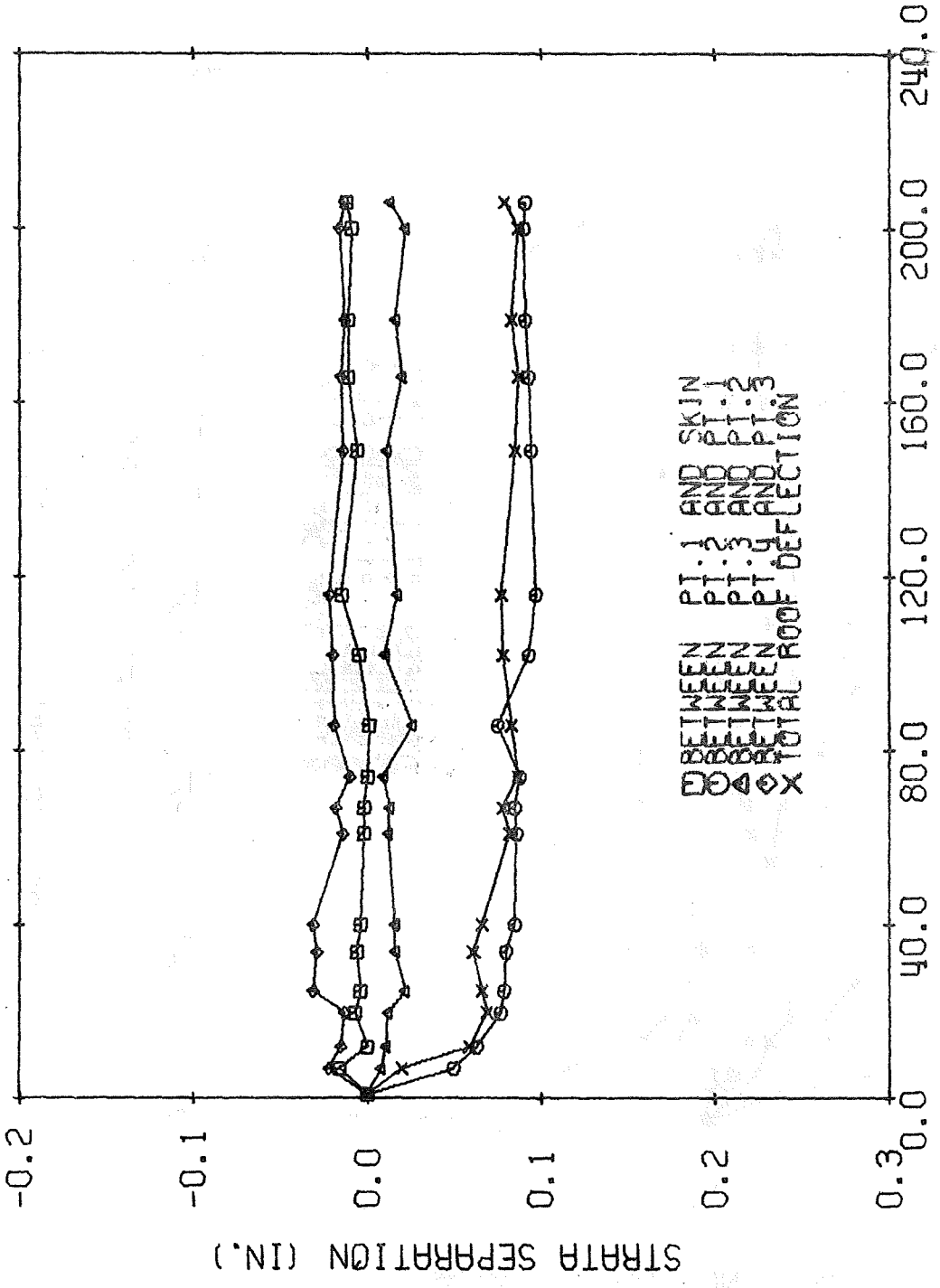

Fig. B-25 SAG STATION 12 IN MINE NO. 2.

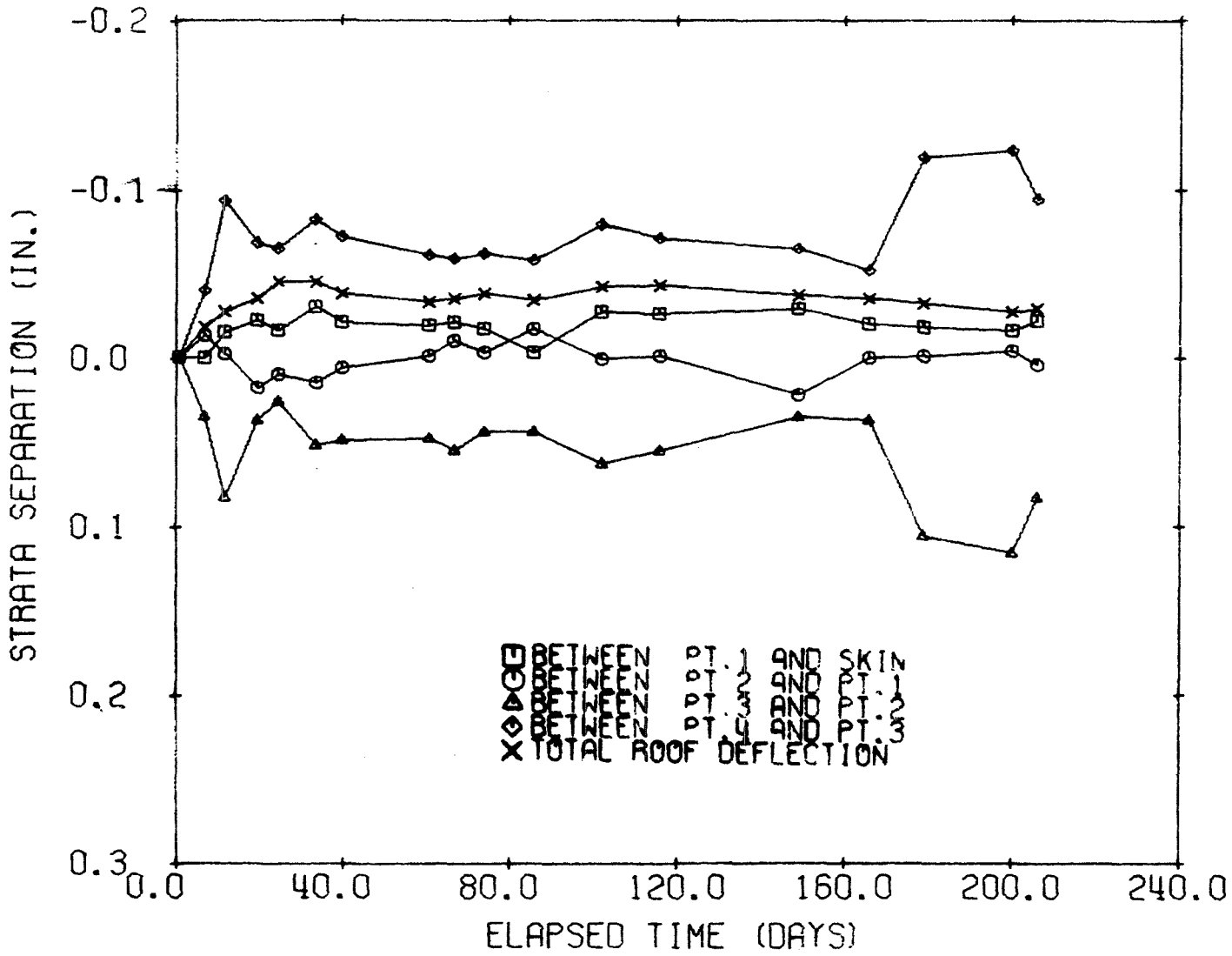

Fig. B-26 SAG STATION 13 IN MINE NO. 2.

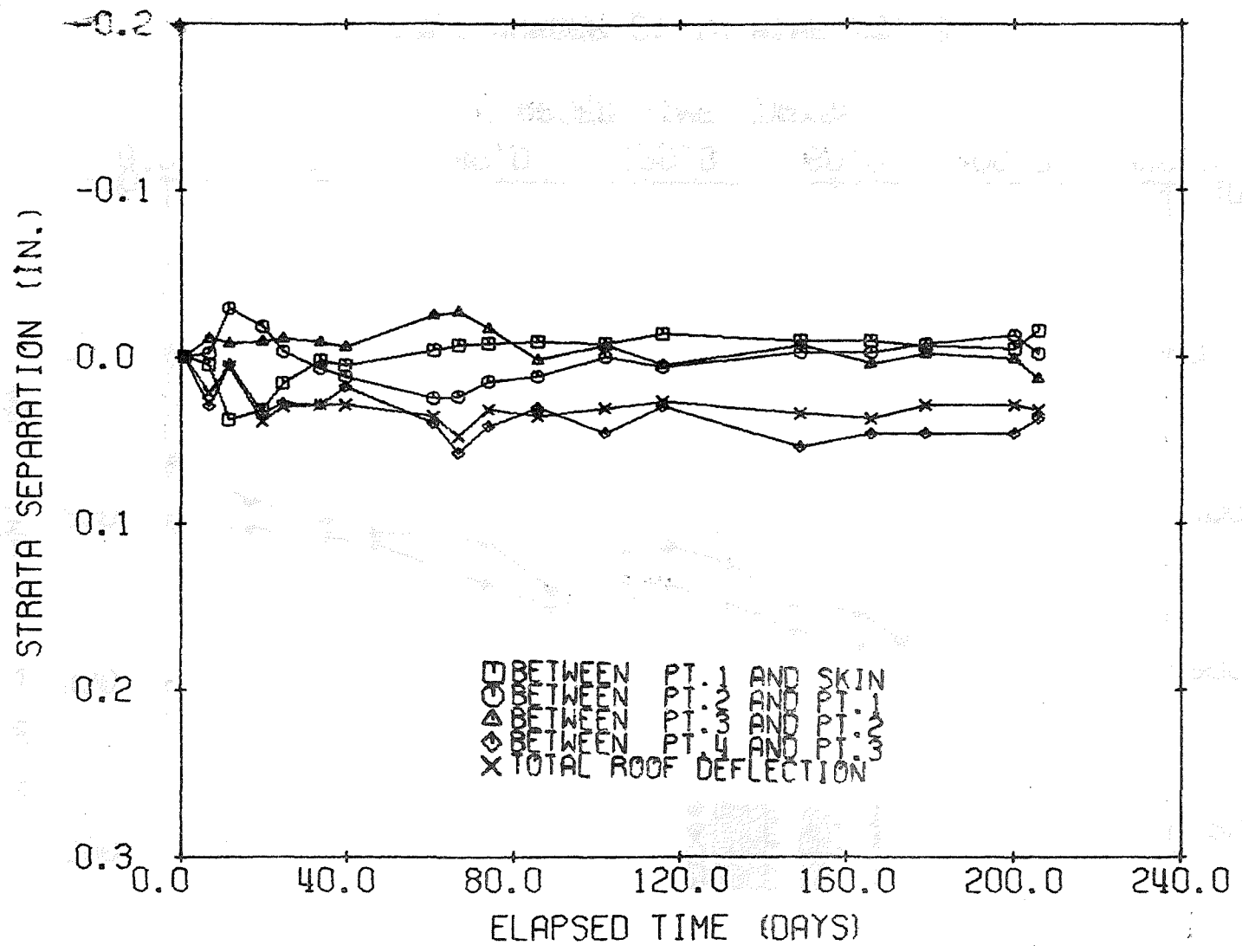

Fig. B-27 SAG STATION 14 IN MINE NO. 2.

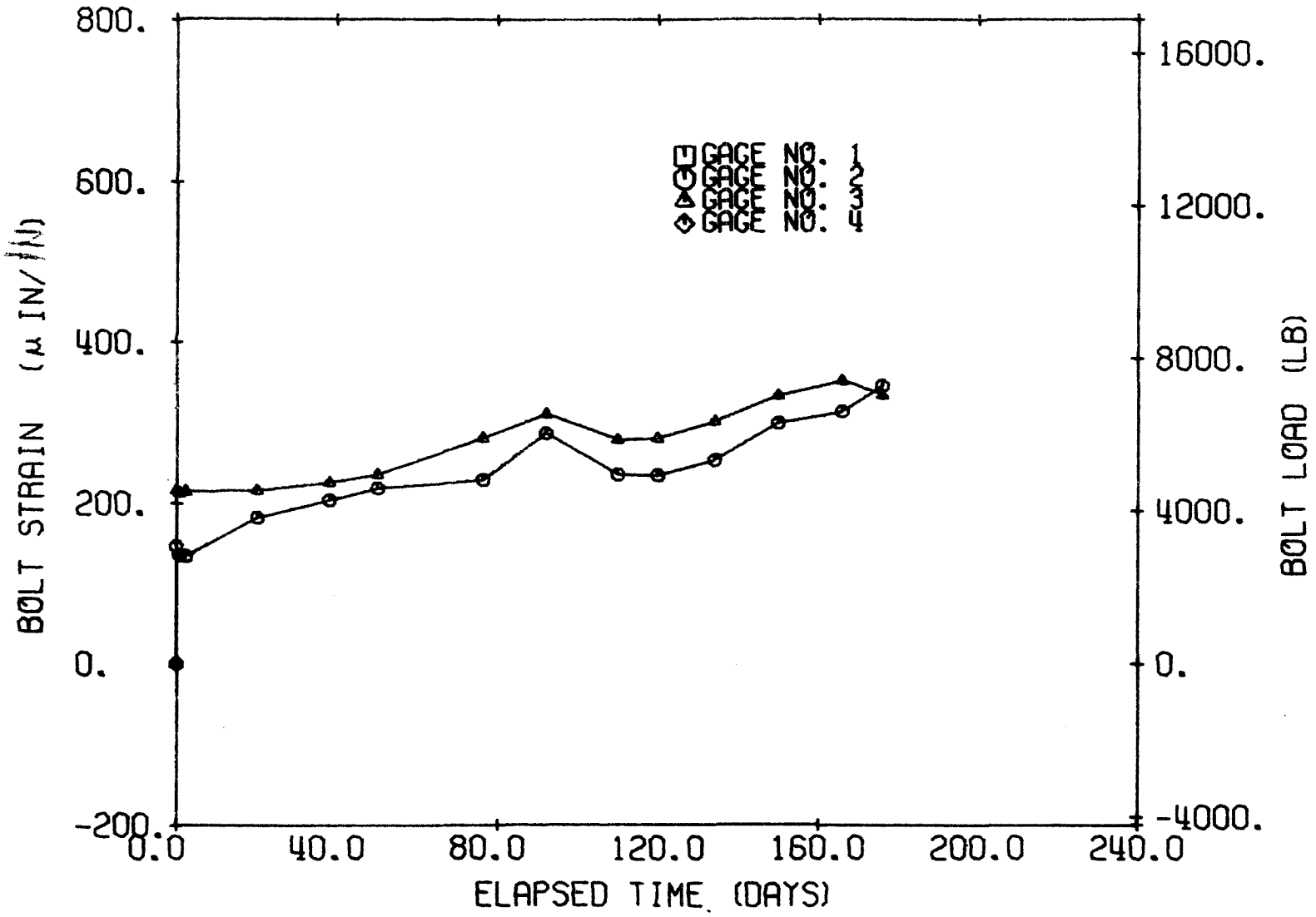

Fig. B-28 BOLT NUMBER 21 IN MINE NO. 3.
1 IN. BAR IN 1-3/8 IN. HOLE DUPONT RESIN

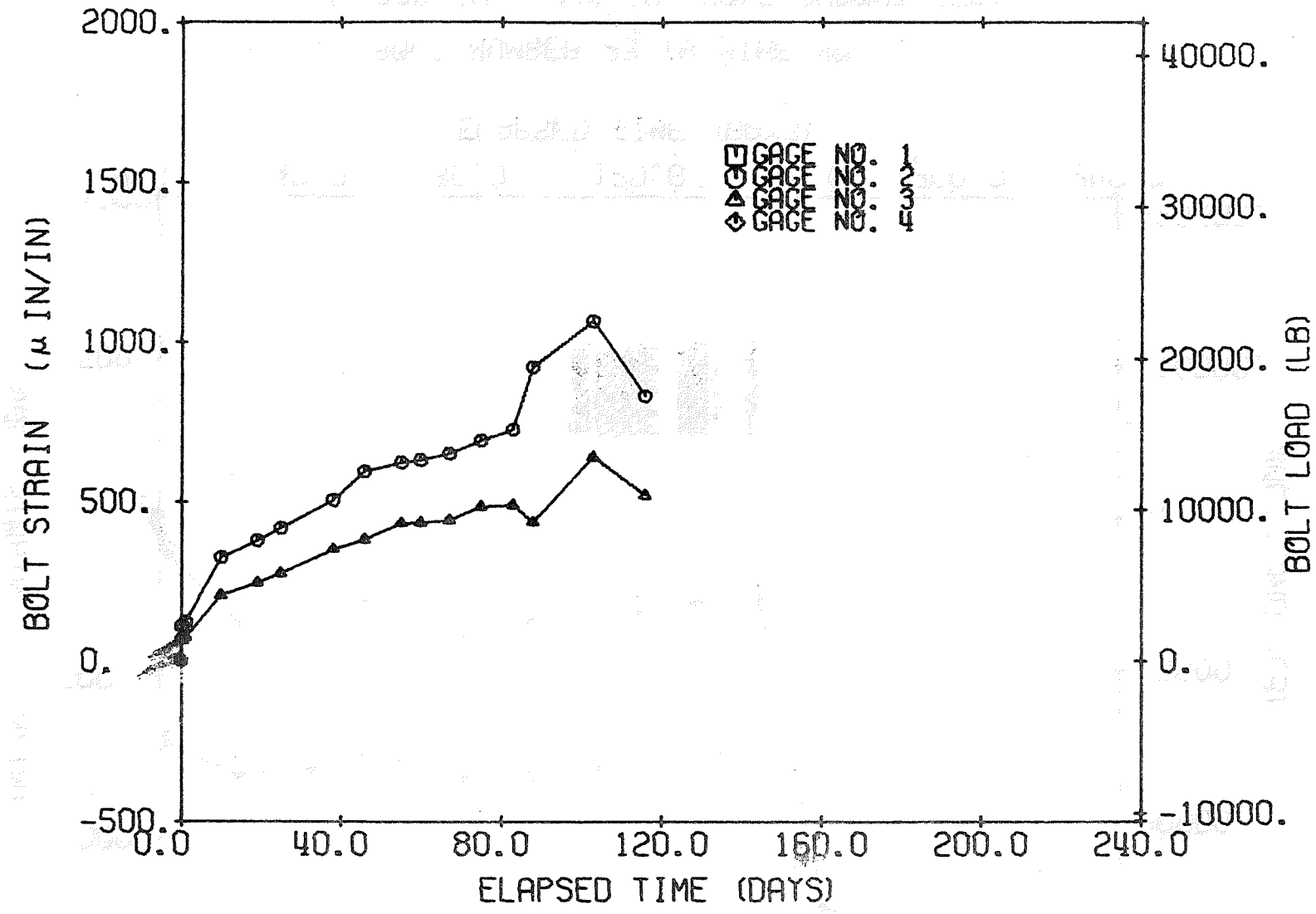

Fig. B-29 BOLT NUMBER 22 IN MINE NO. 3.
1 IN. BAR IN 1-3/8 IN. HOLE DUPONT RESIN

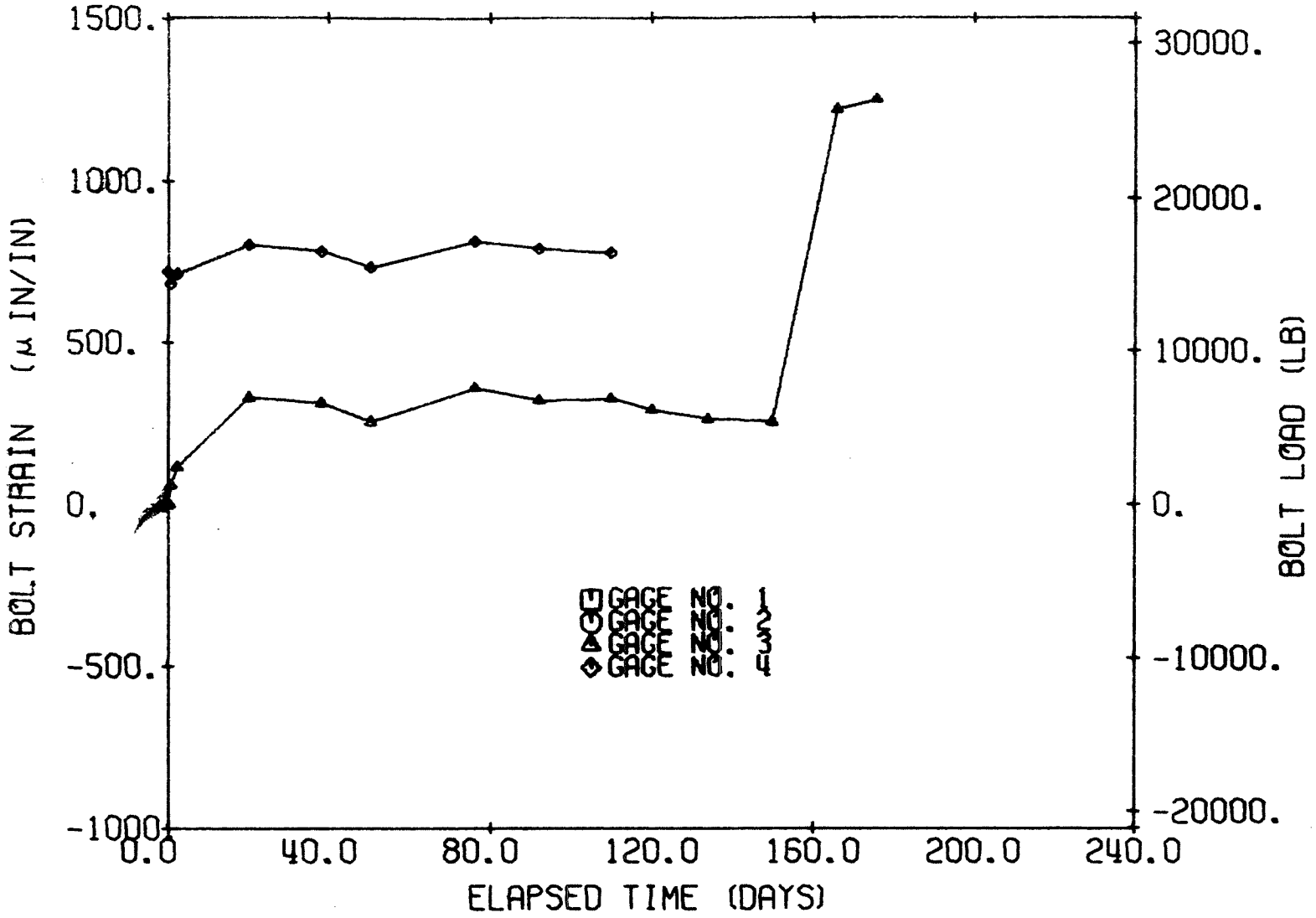

Fig. B-30 BOLT NUMBER 23 IN MINE NO. 3.
1 IN. BAR IN 1-3/8 IN. HOLE DUPONT RESIN

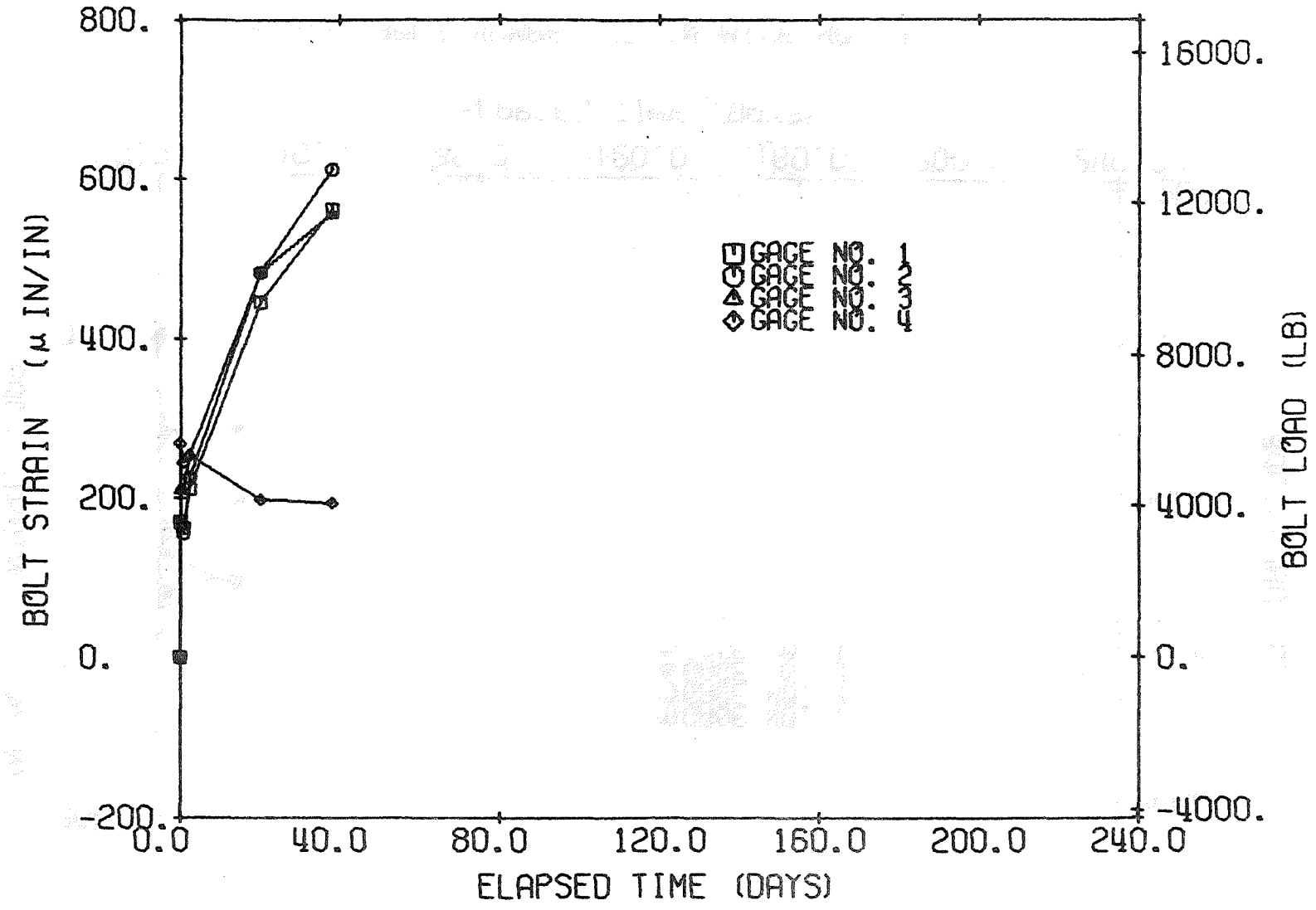

Fig. B-31 BOLT NUMBER 24 IN MINE NO. 3.
1 IN. BAR IN 1-3/8 IN. HOLE DUPONT RESIN

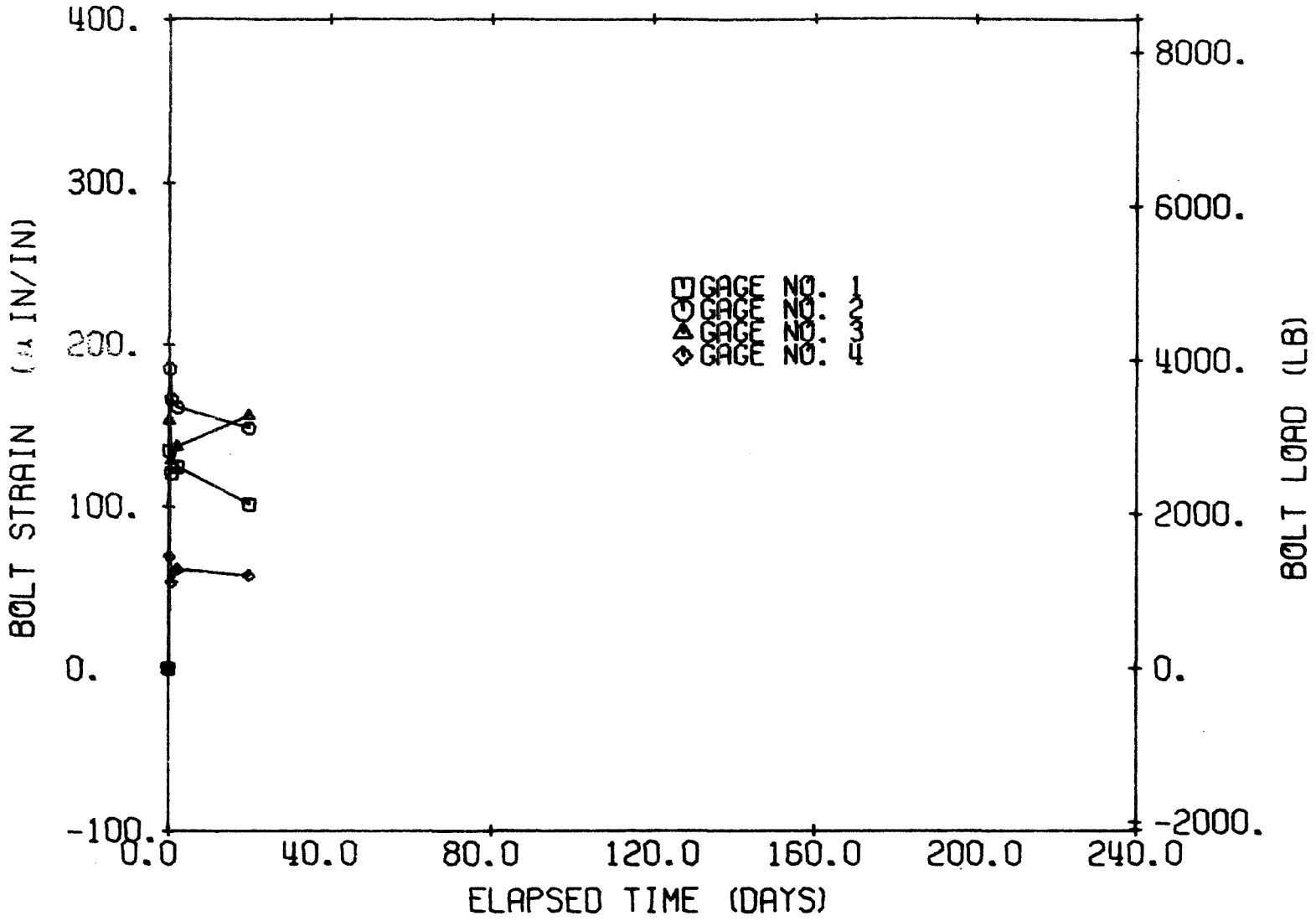

Fig. B-32 BOLT NUMBER 25 IN MINE NO. 3.
1 IN. BAR IN 1-3/8 IN. HOLE DUPONT RESIN

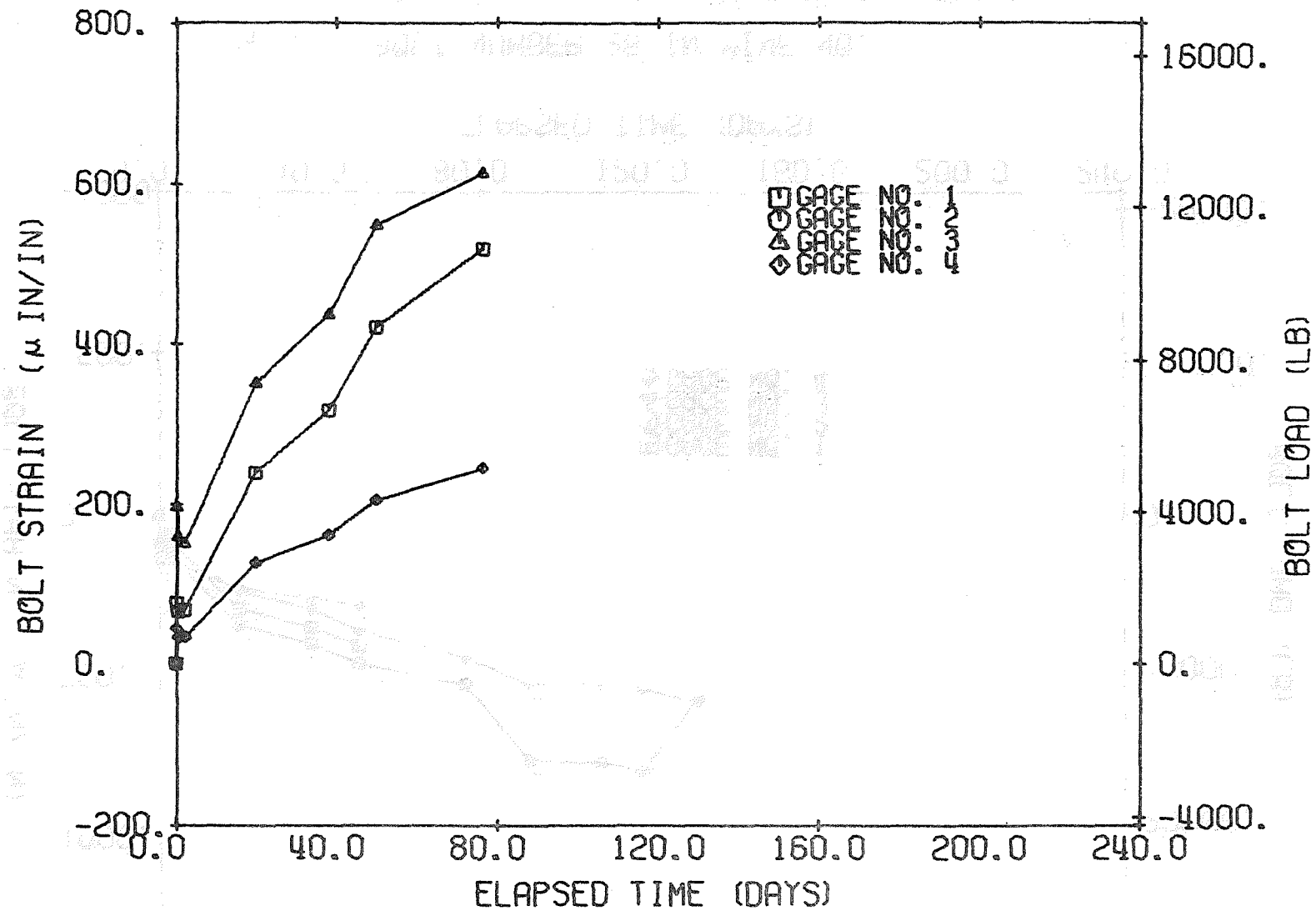

Fig. B-33 BOLT NUMBER 27 IN MINE NO. 3.
1 IN. BAR IN 1-3/8 IN. HOLE DUPONT RESIN

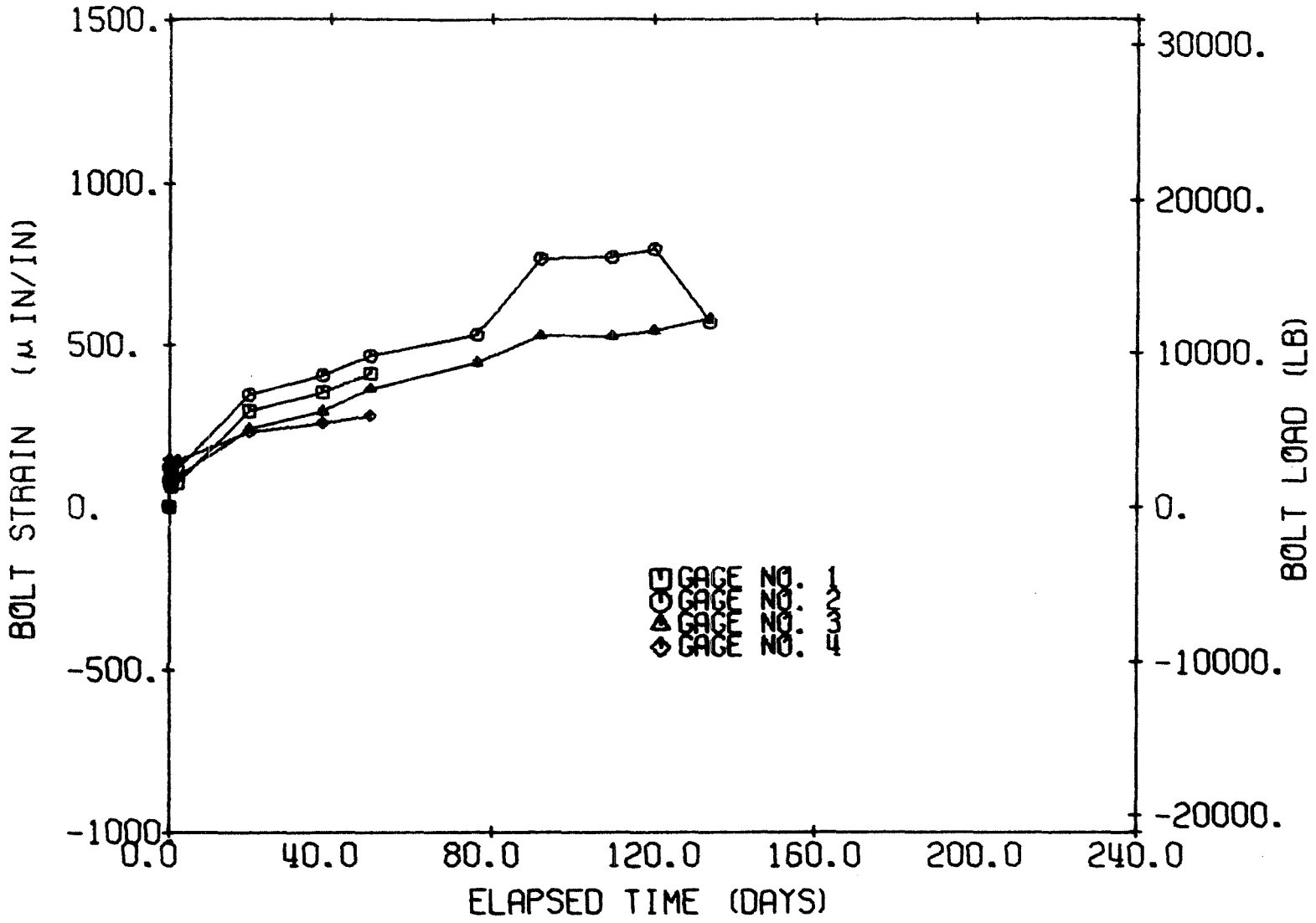

Fig. B-34 BOLT NUMBER 28 IN MINE NO. 3.
1 IN. BAR IN 1-3/8 IN. HOLE DUPONT RESIN

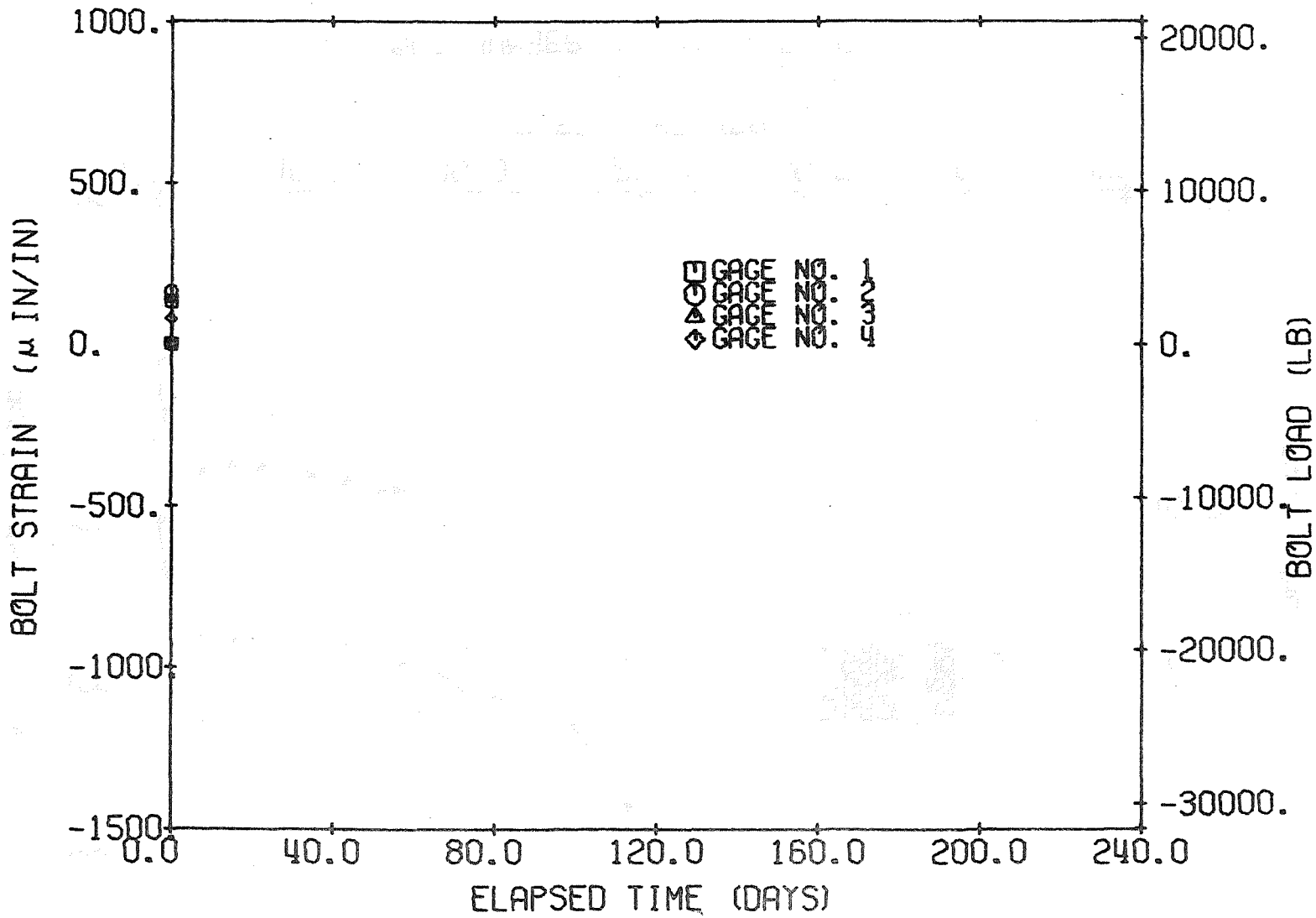

Fig. B-35 BOLT NUMBER 32 IN MINE NO. 3.

1 IN. BAR IN 1-3/8 IN. HOLE DUPONT RESIN

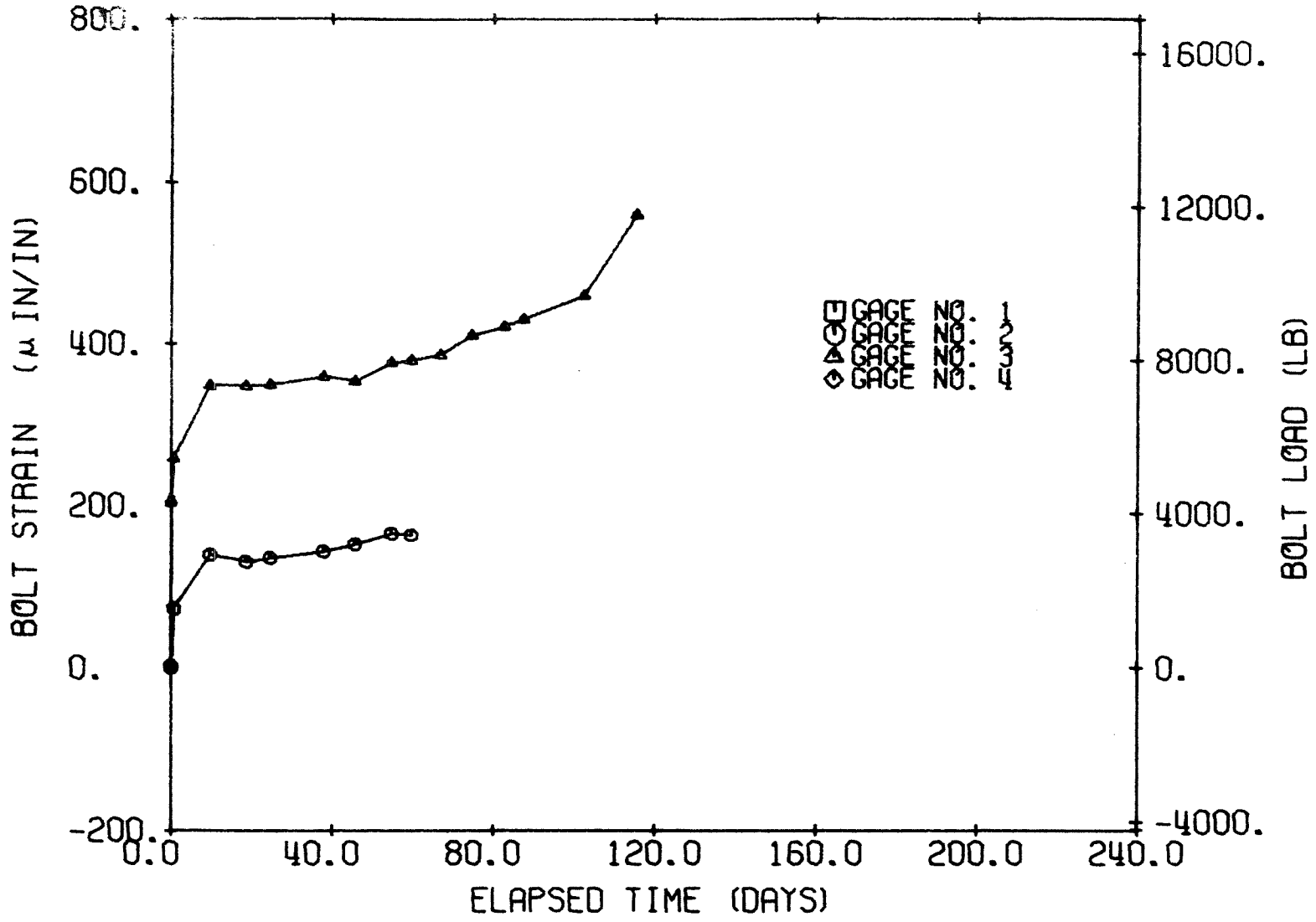

Fig. B-36 BOLT NUMBER 33 IN MINE NO. 3.
1 IN. BAR IN 1-3/8 IN. HOLE DUPONT RESIN

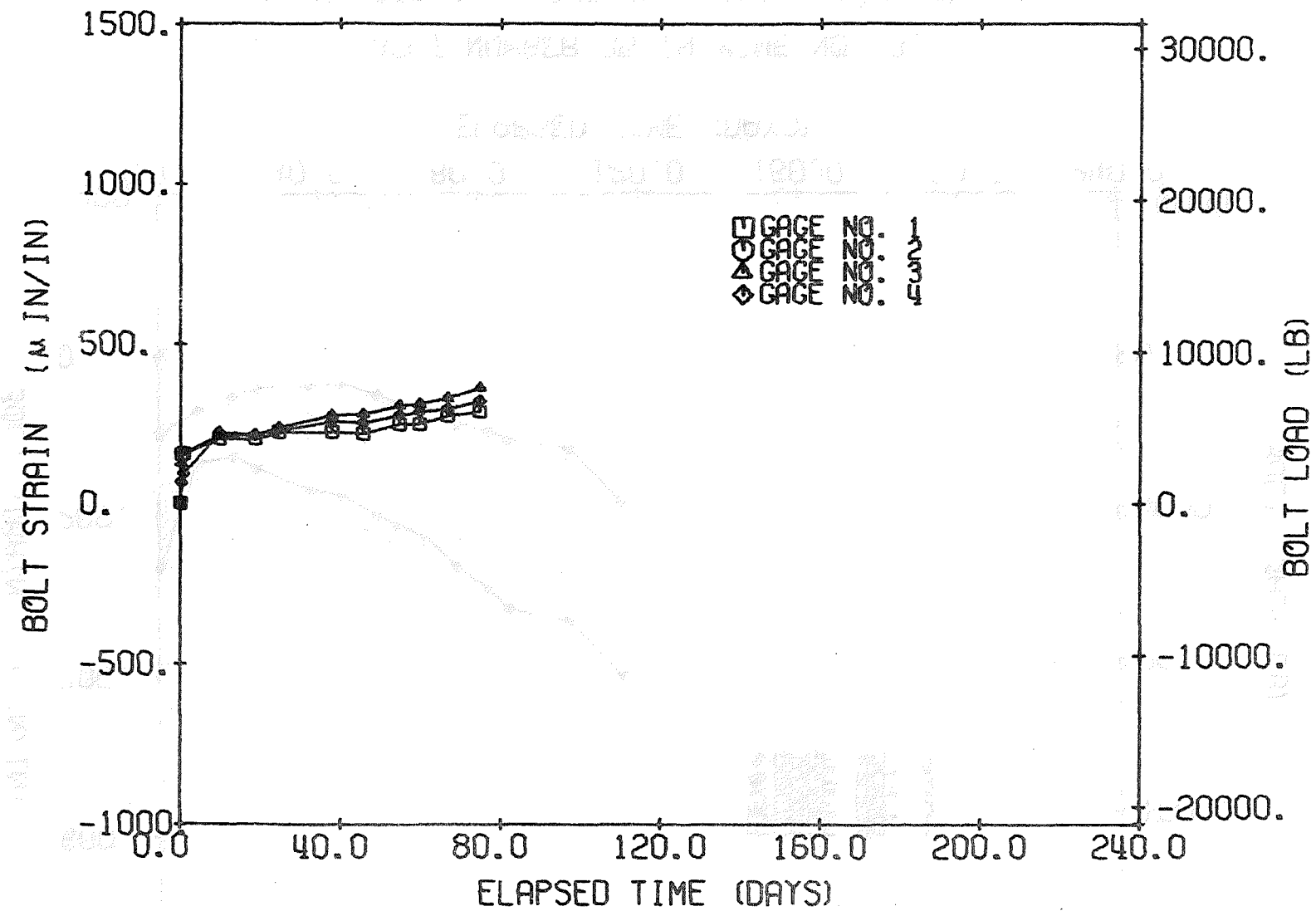

Fig. B-37 BOLT NUMBER 34 IN MINE NO. 3.

1 IN. BAR IN 1-3/8 IN. HOLE DUPONT RESIN

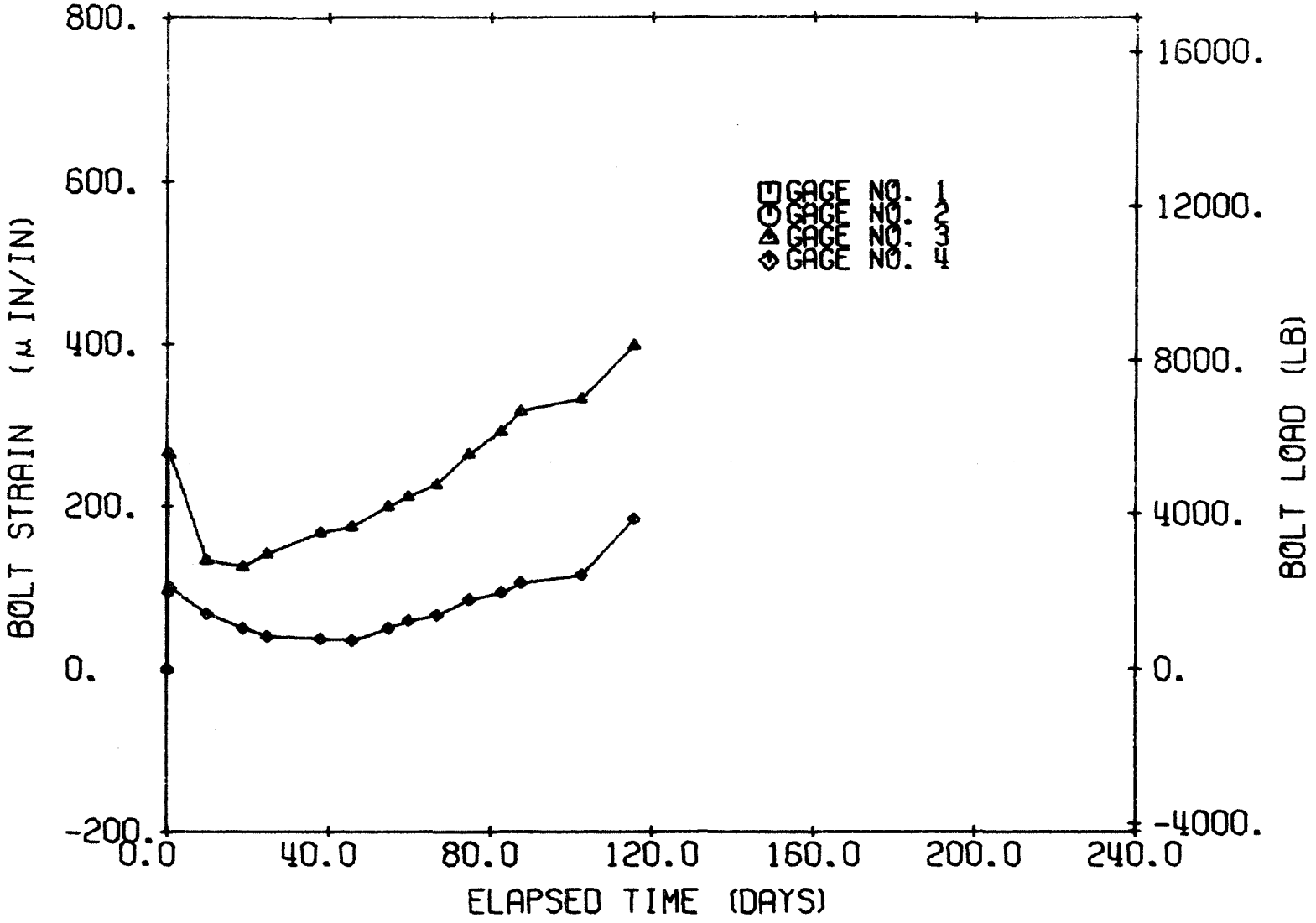

Fig. B-38 BOLT NUMBER 35 IN MINE NO. 3.
1 IN. BAR IN 1-3/8 IN. HOLE DUPONT RESIN

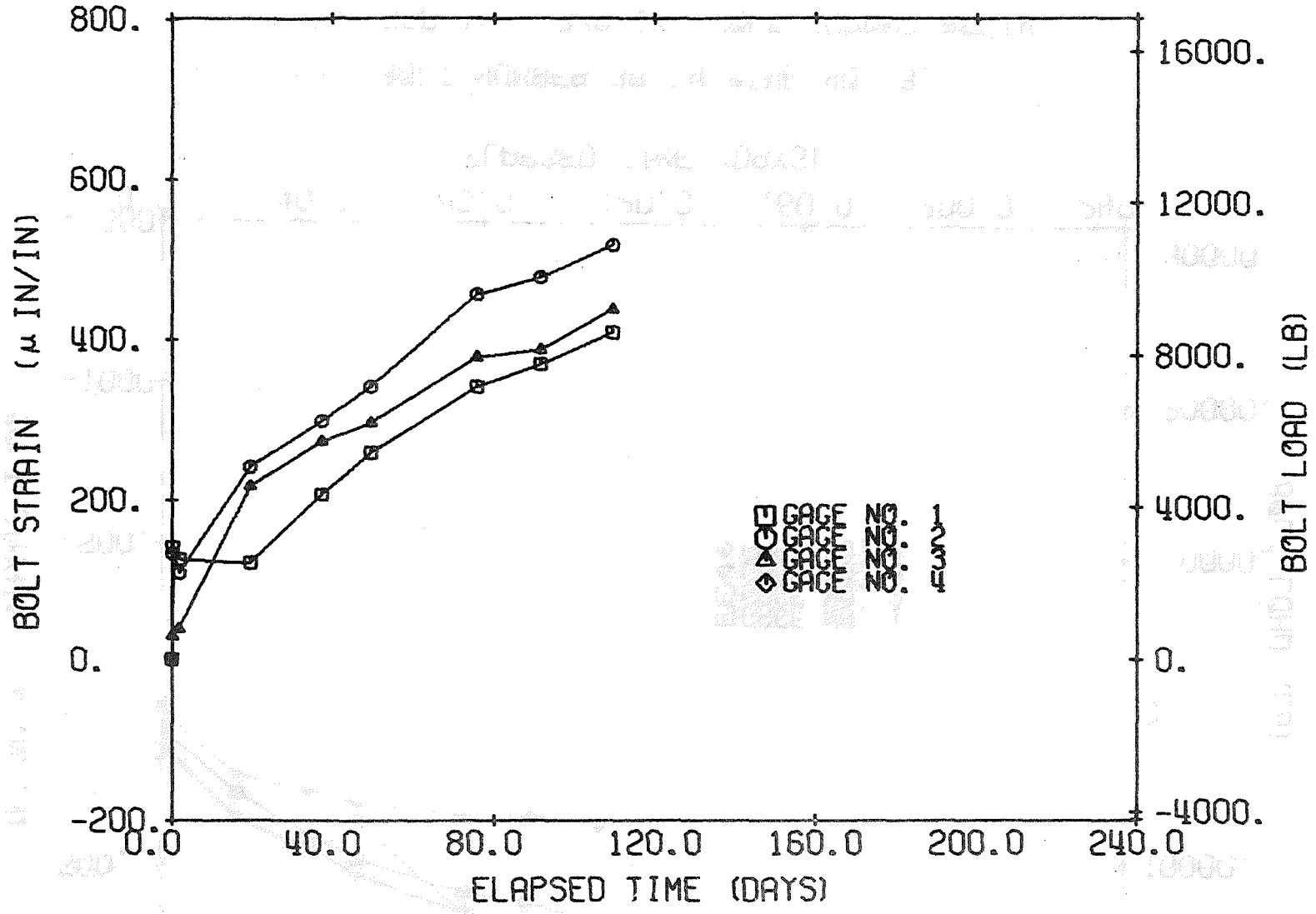

Fig. B-39 BOLT NUMBER 37 IN MINE NO. 3.
1 IN. BAR IN 1-3/8 IN. HOLE DUPONT RESIN

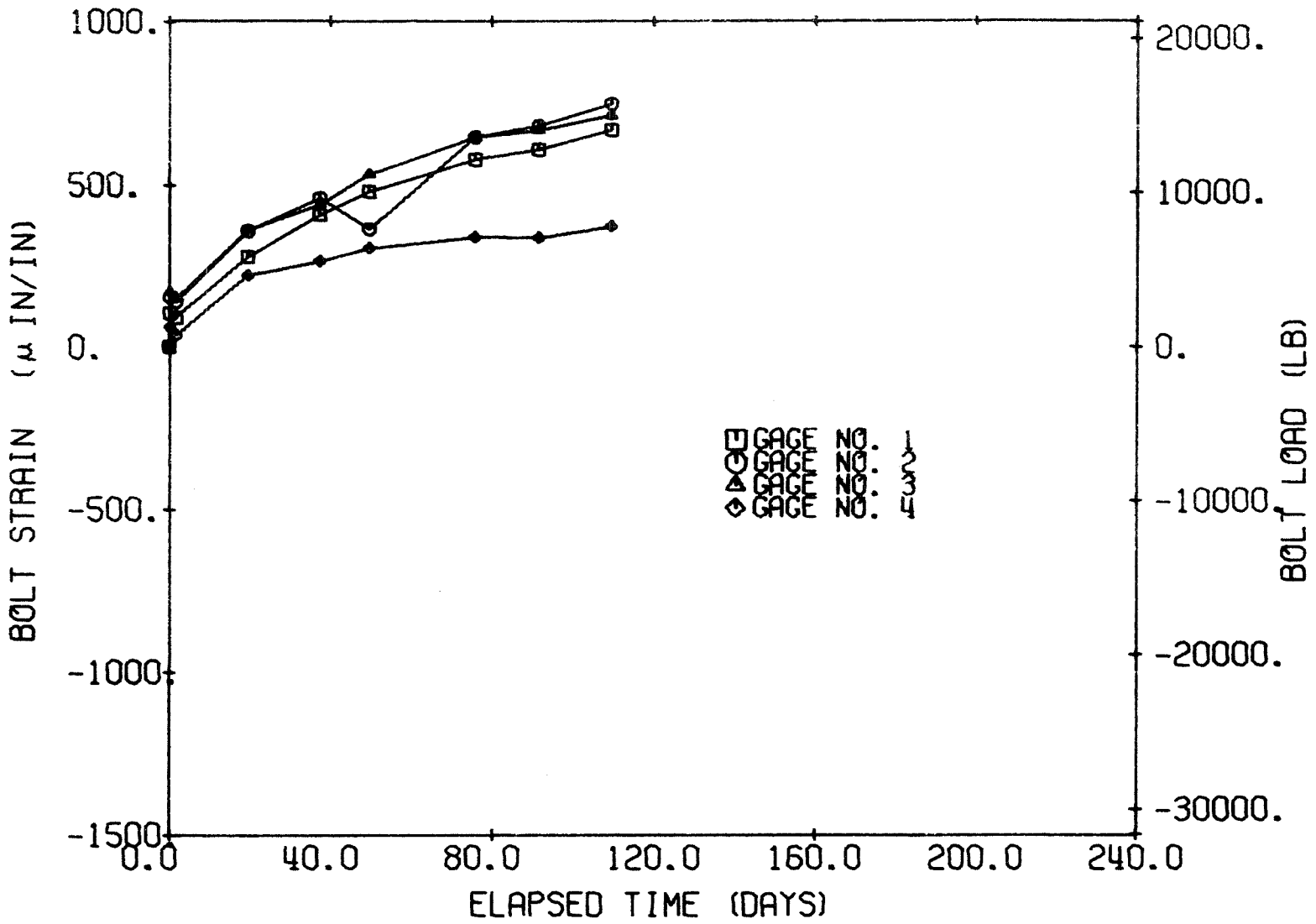

Fig. B-40 BOLT NUMBER 38 IN MINE NO. 3.
1 IN. BAR IN 1-3/8 IN. HOLE DUPONT RESIN

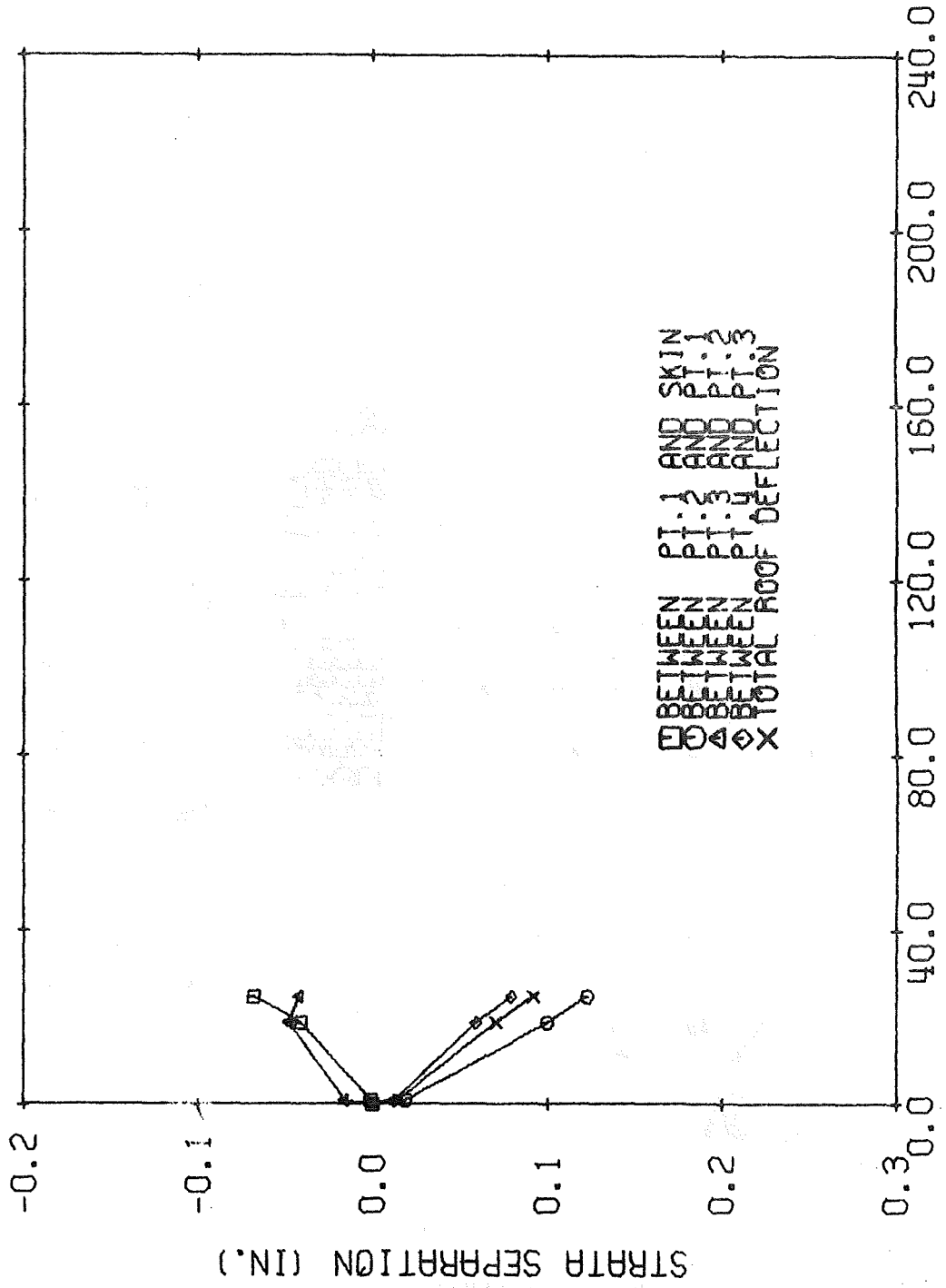

Fig. B-41 SAG STATION 21 IN MINE NO. 3.

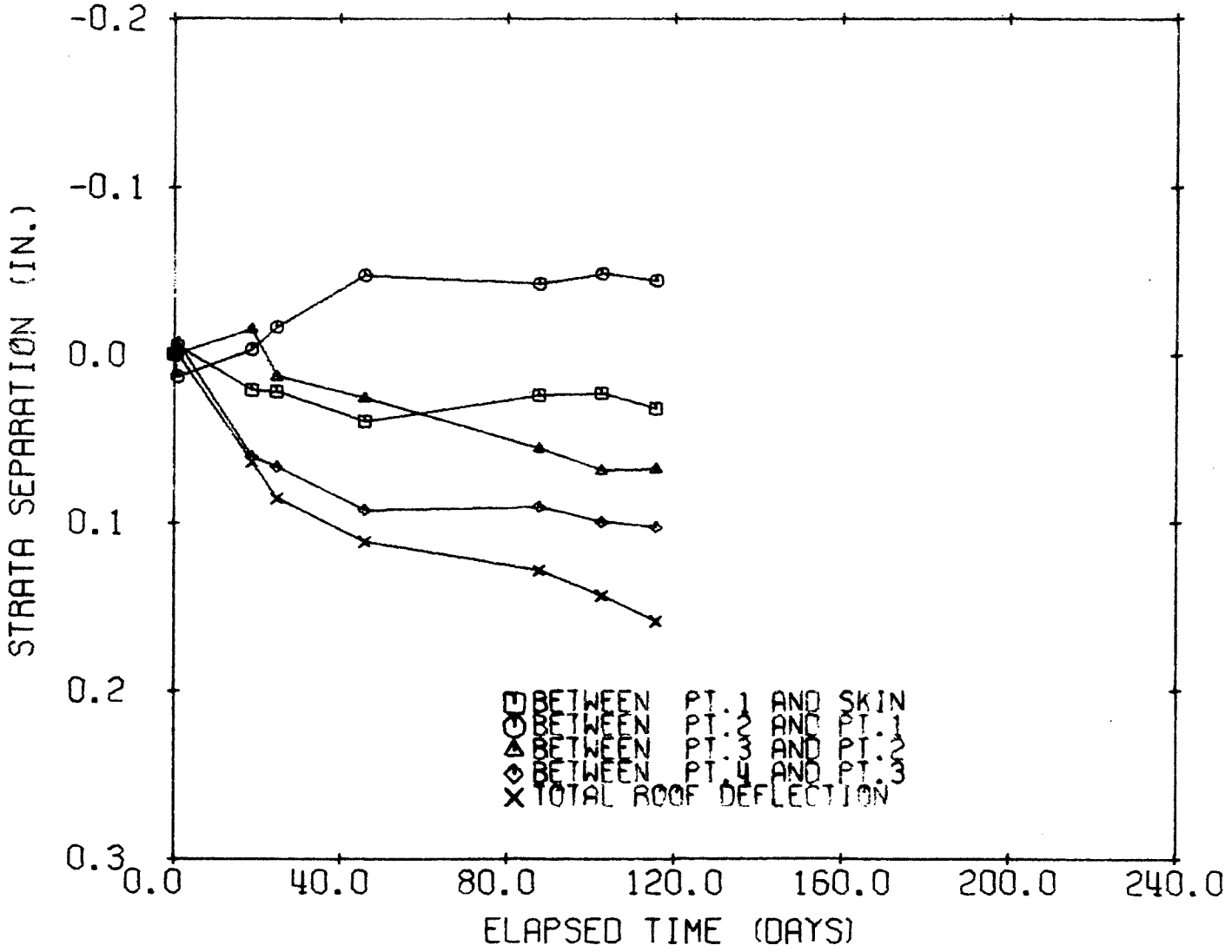

Fig. B-42 SAG STATION 23 IN MINE NO. 3.

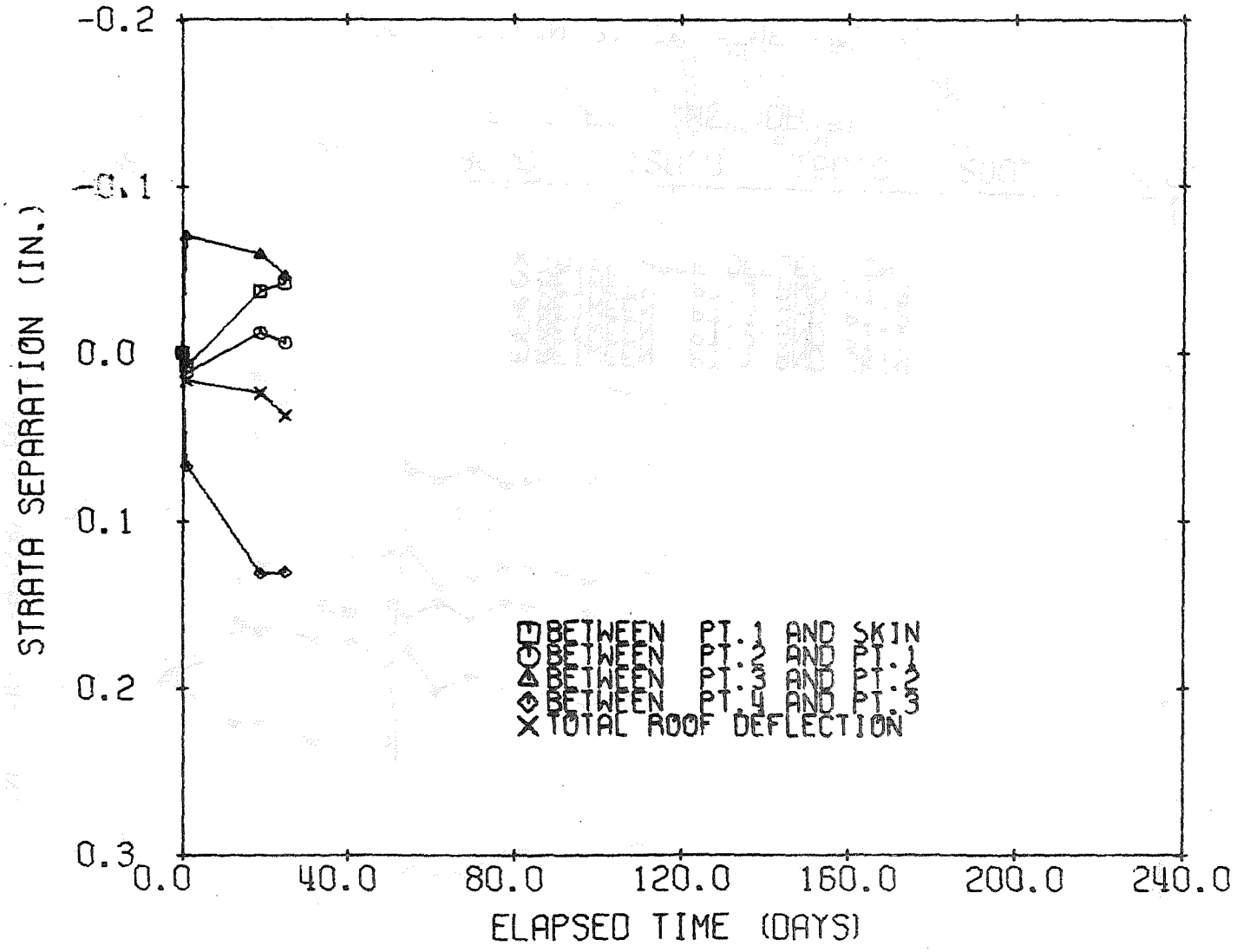

Fig. B-43 SAG STATION 24 IN MINE NO. 3.

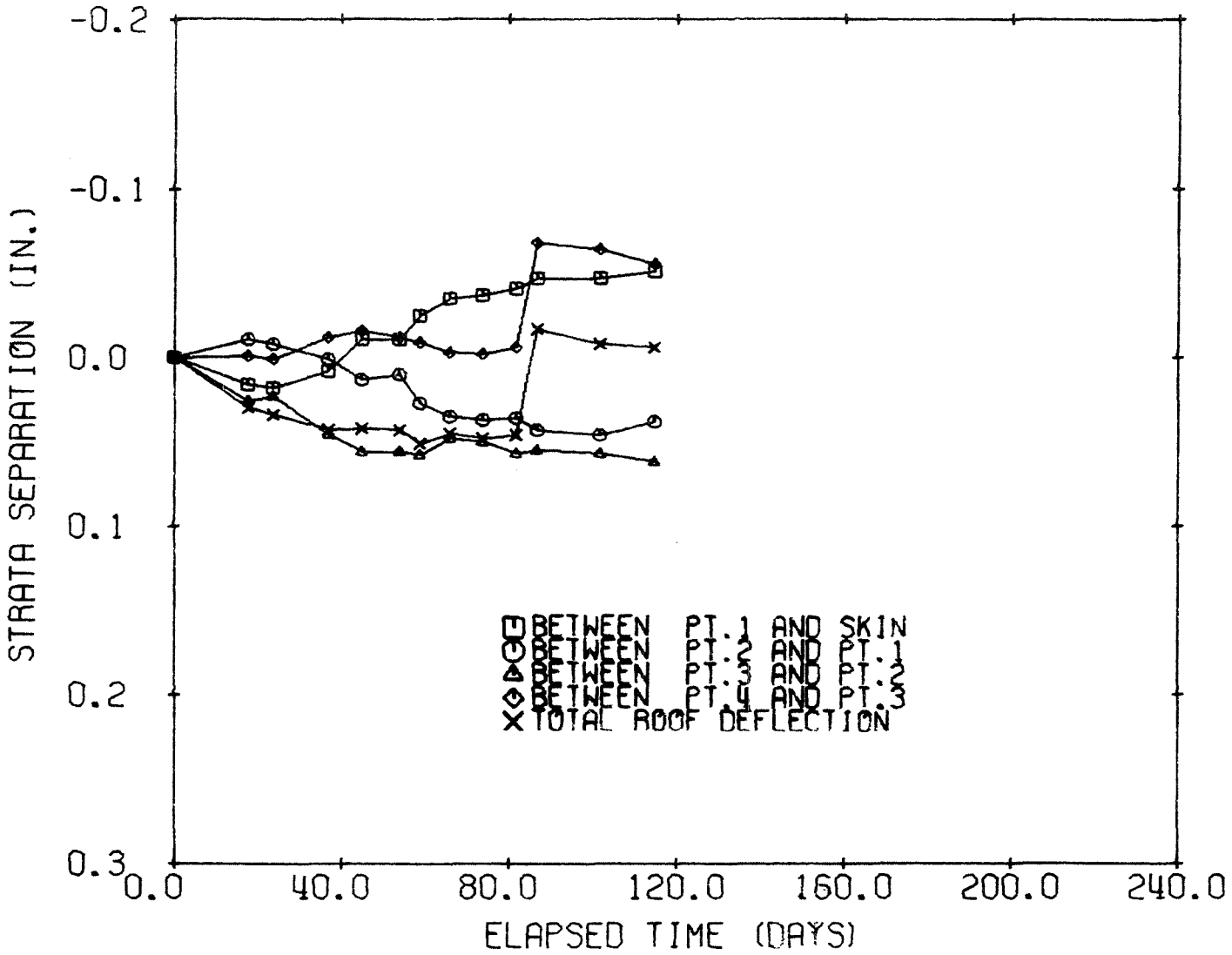

Fig. B-46 SAG STATION 33 IN MINE NO. 3.

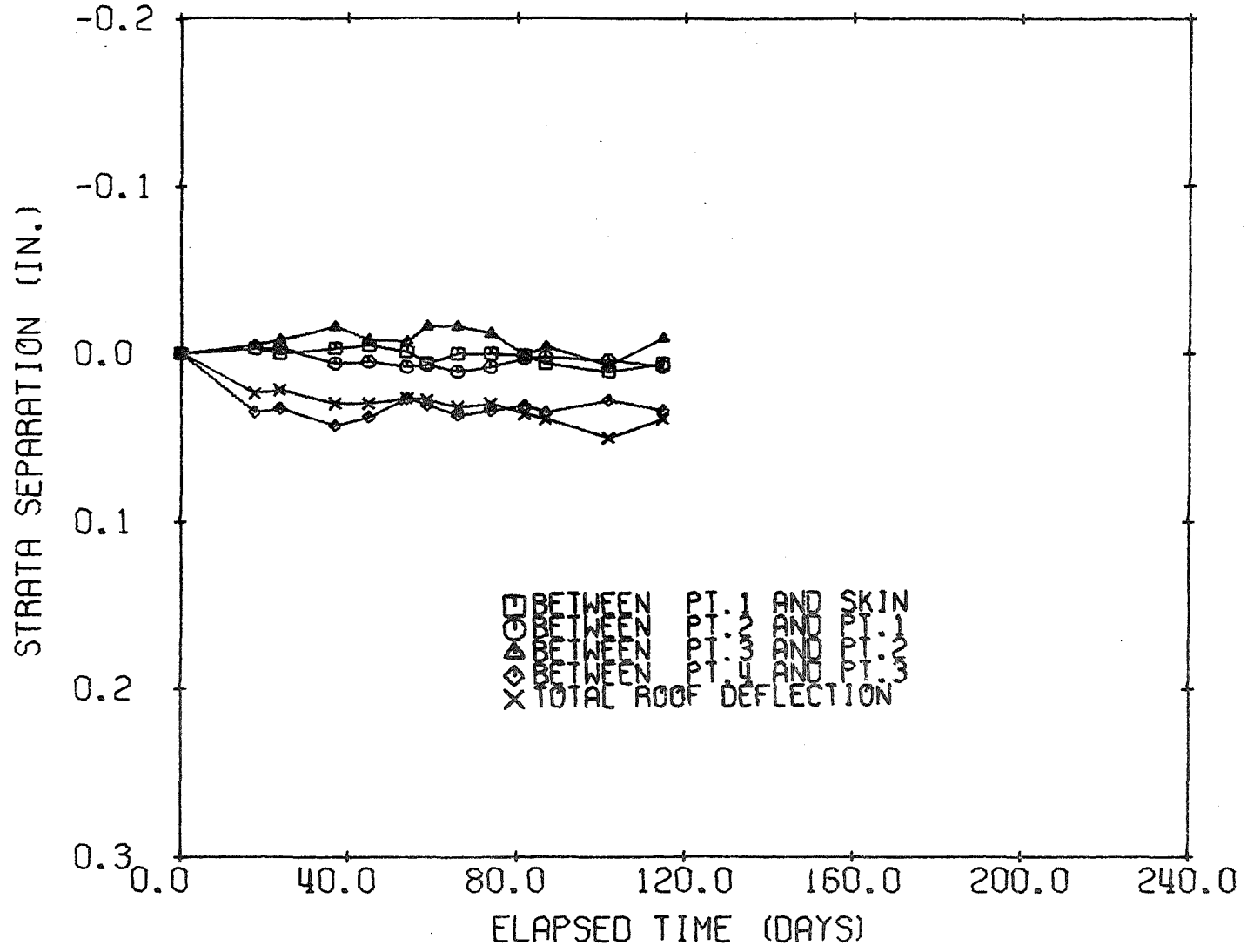

Fig. B-47 SAG STATION 34 IN MINE NO. 3.

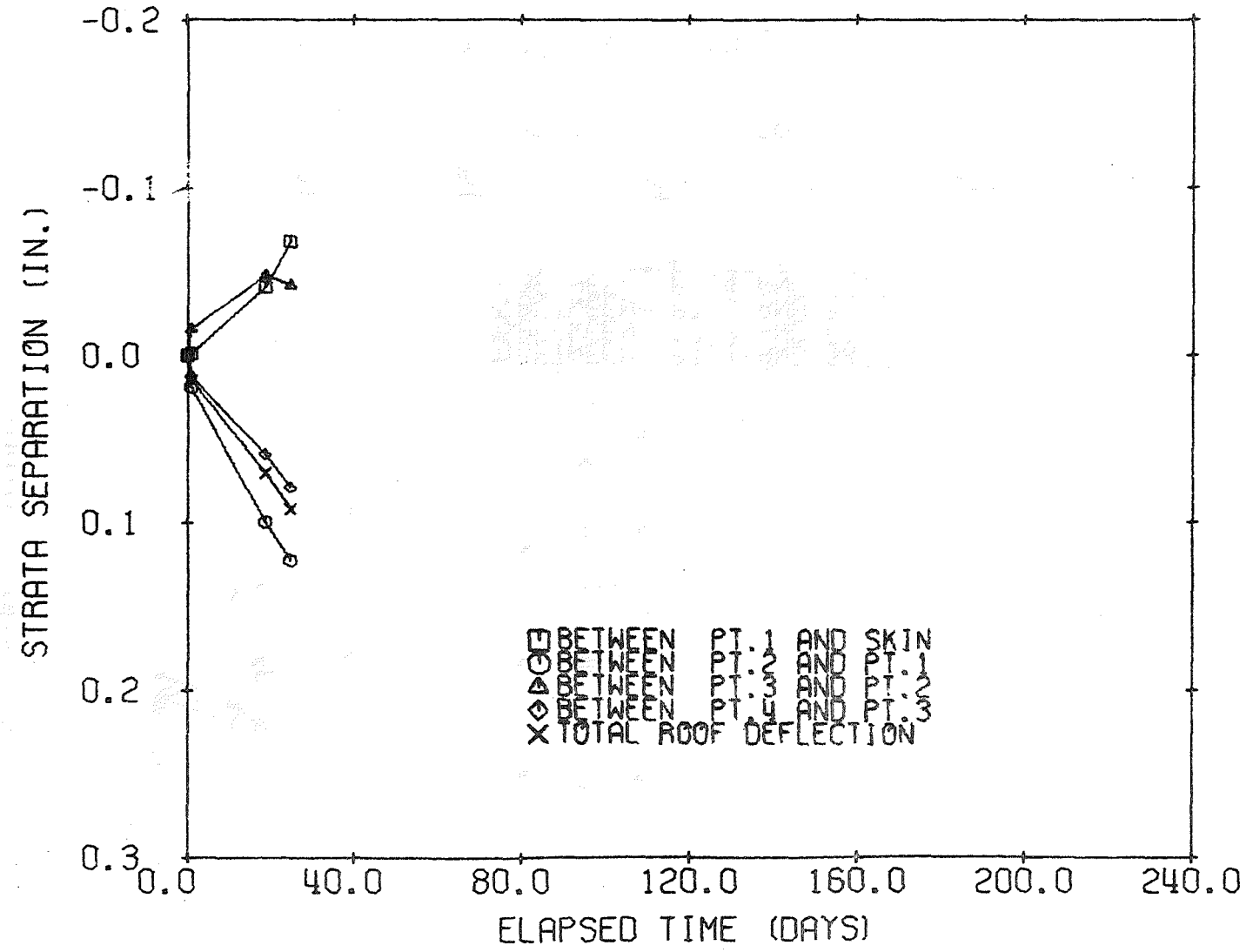

Fig. B-41 SAG STATION 21 IN MINE NO. 3.

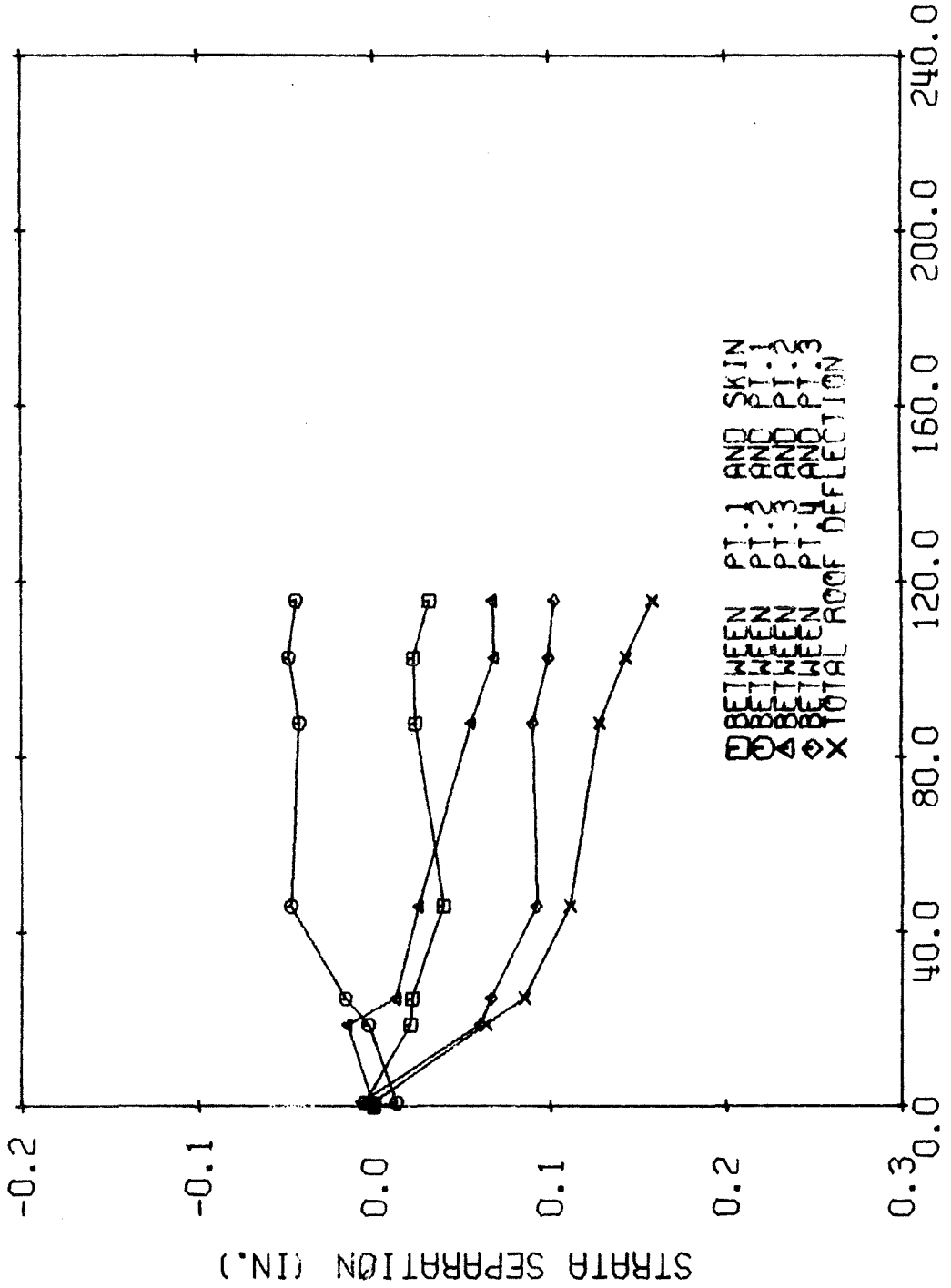

Fig. B-42 SAG STATION 23 IN MINE NO. 3.

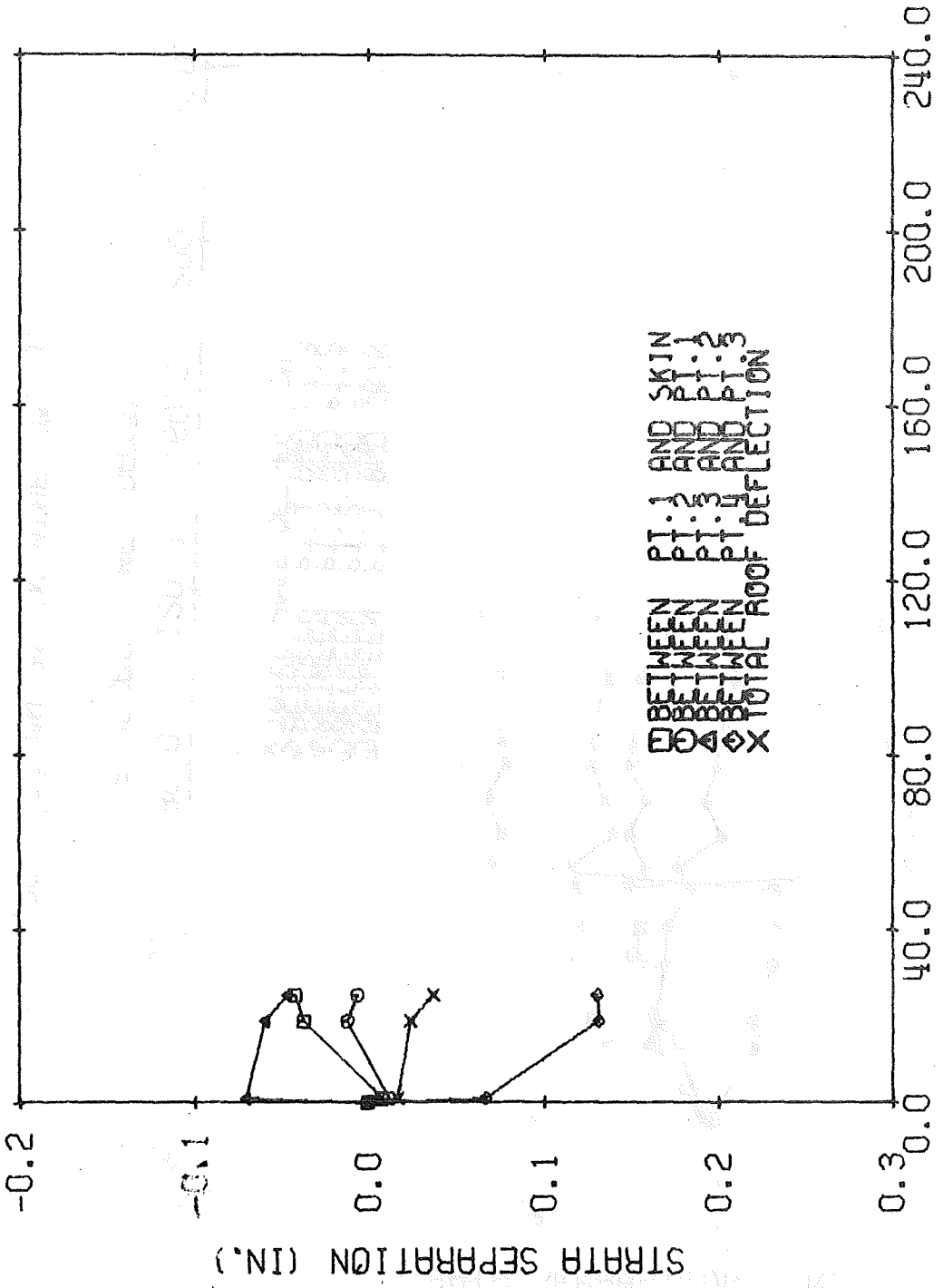

Fig. B-43 SAG STATION 24 IN MINE NO. 3.

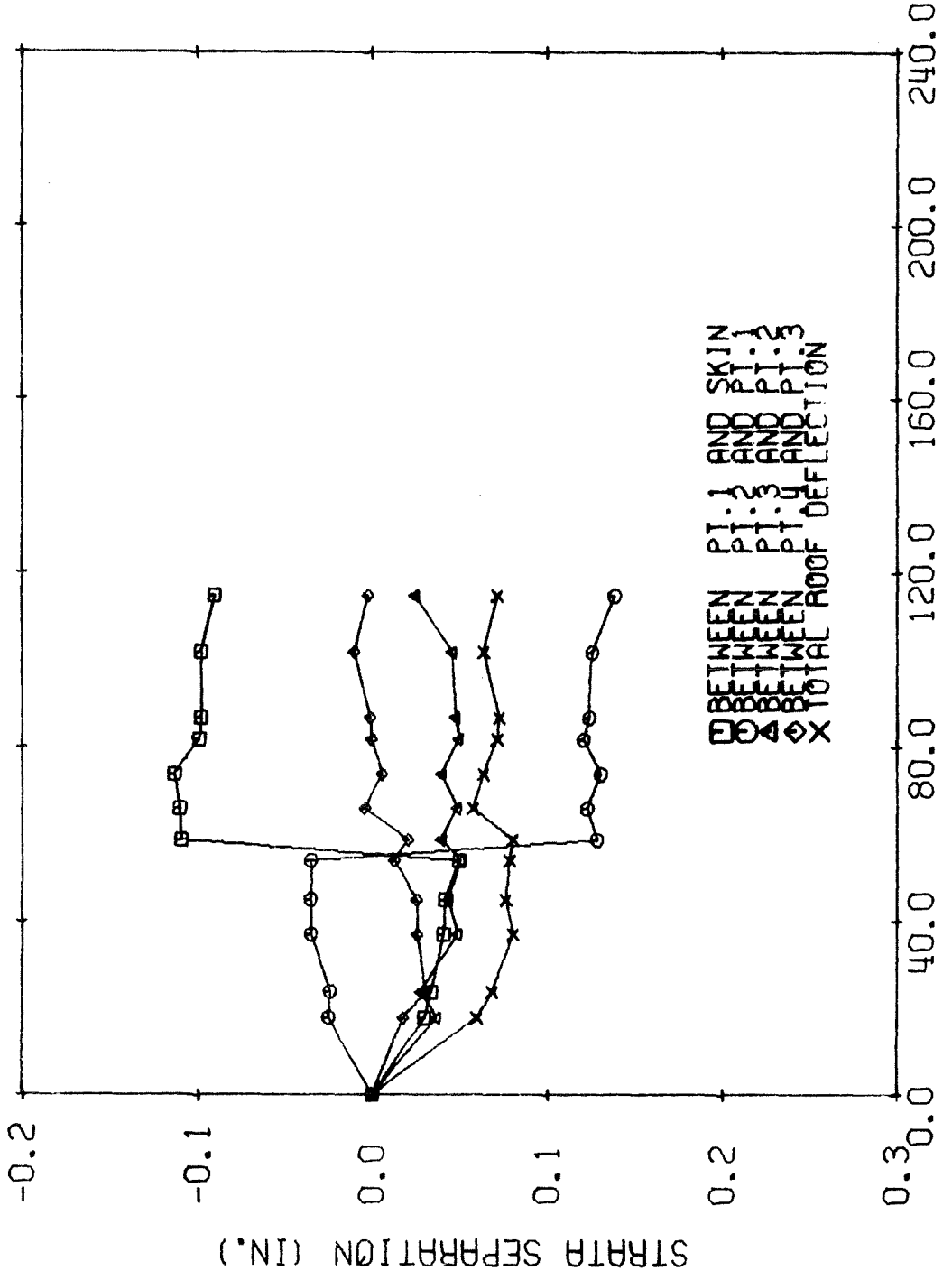

Fig. B-44 SAG STATION 31 IN MINE NO. 3.

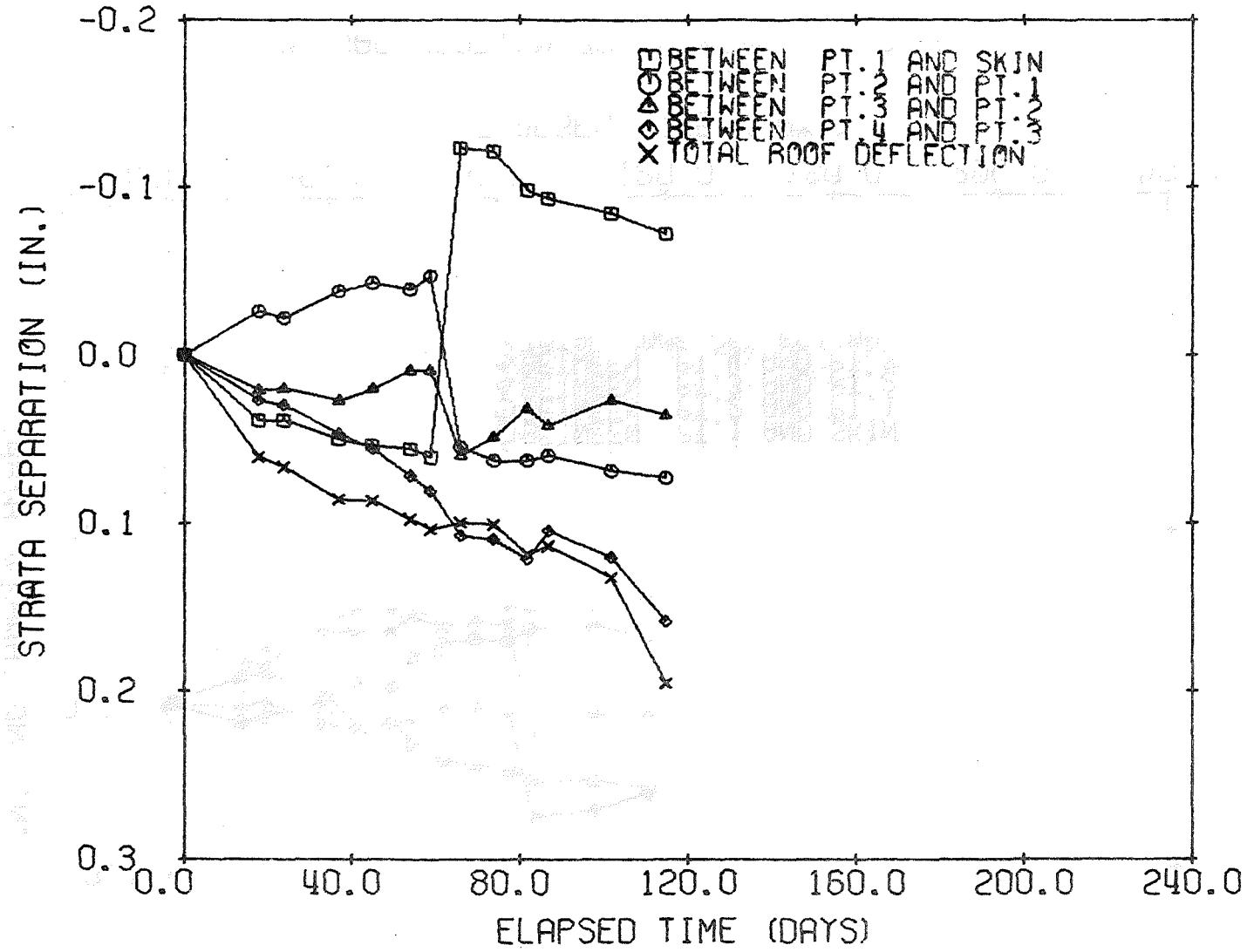

Fig. B-45 SAG STATION 32 IN MINE NO. 3.

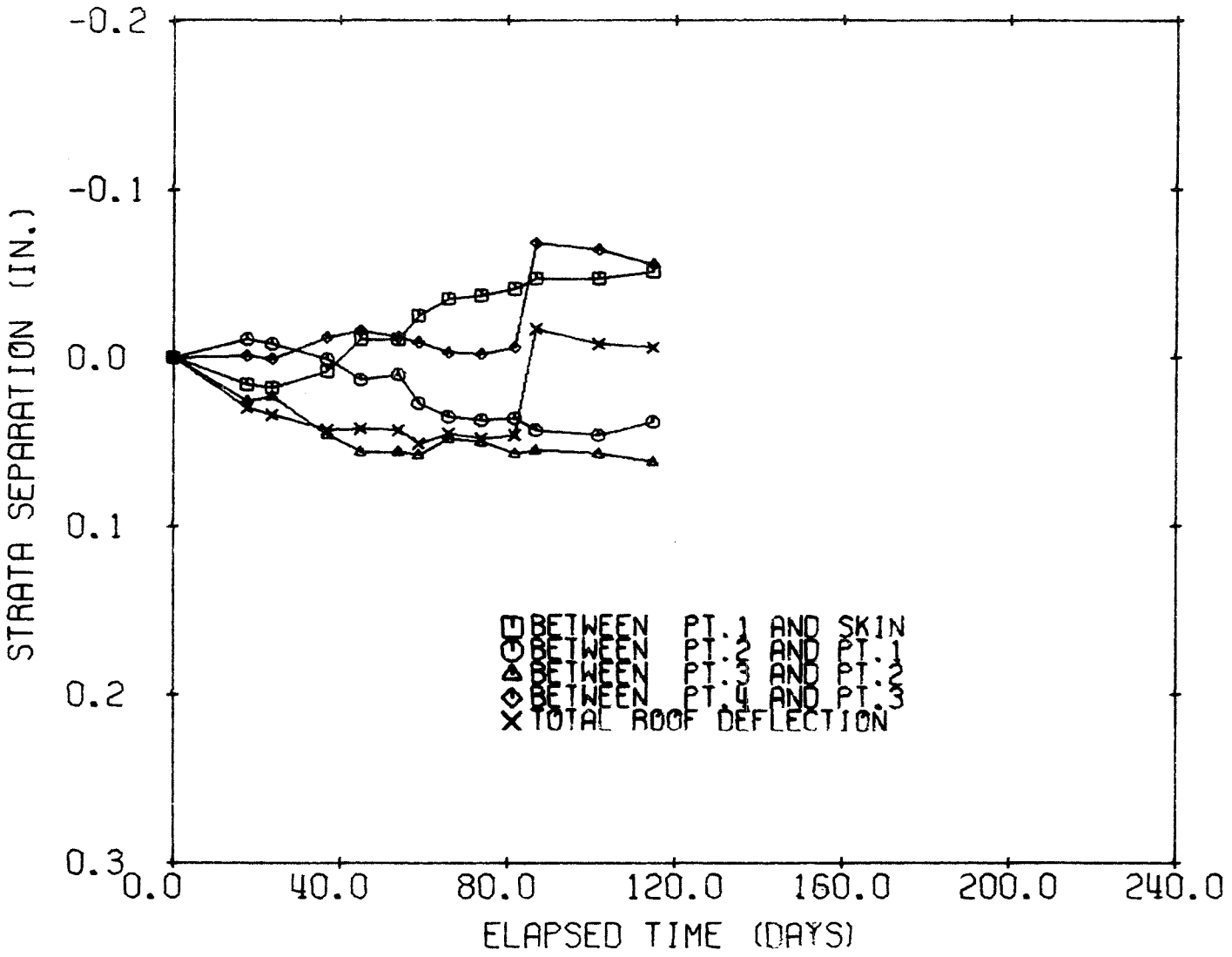

Fig. B-46 SAG STATION 33 IN MINE NO. 3.

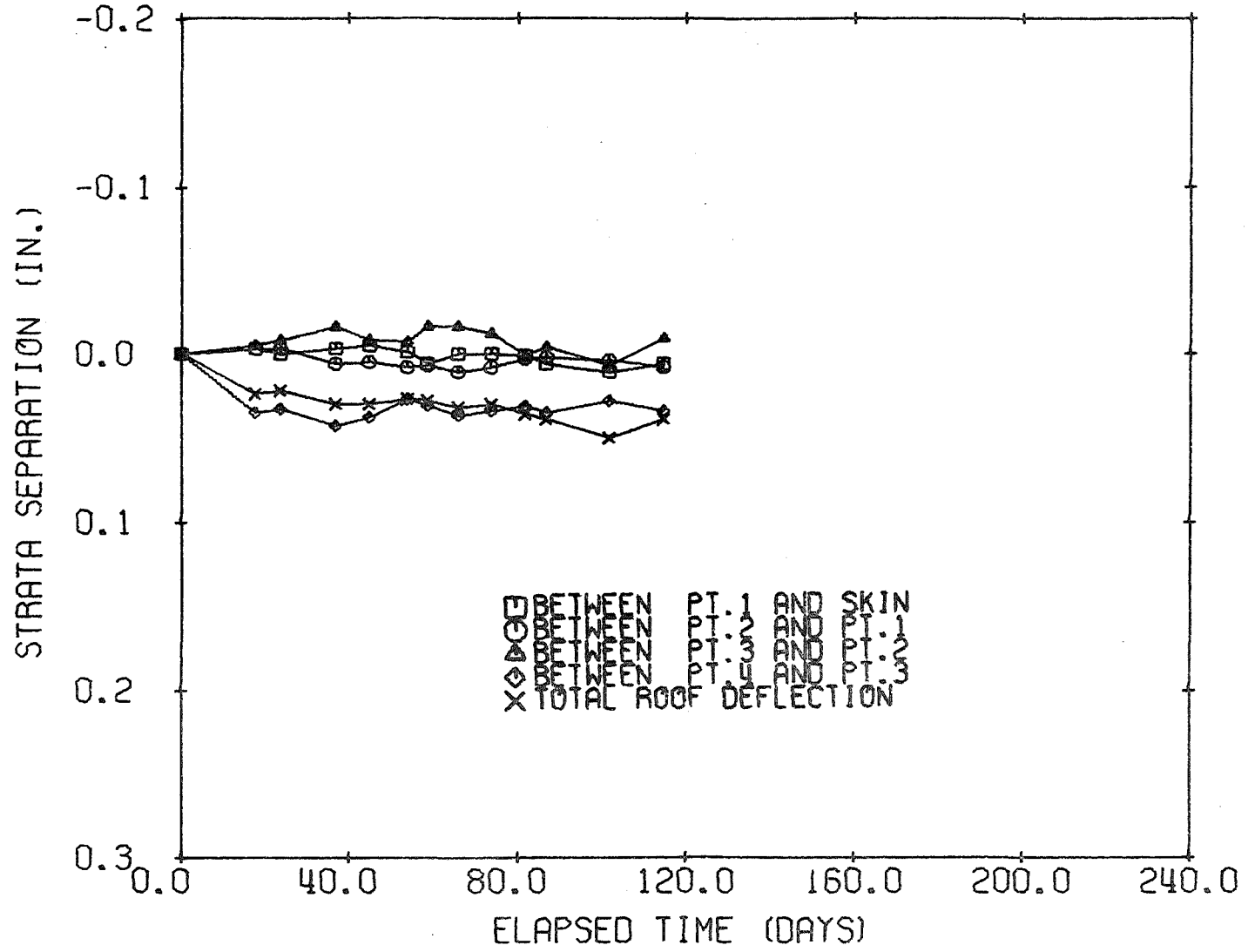

Fig. B-47 SAG STATION 34 IN MINE NO. 3.